교 과 목 414.519 강의록

수 치 선 박 유 체 역 학
- 보 텍 스 방 법 -

COMPUTATIONAL MARINE HYDRODYNAMICS
-VORTEX METHODS-

2015년 8월 15일

서 정 천
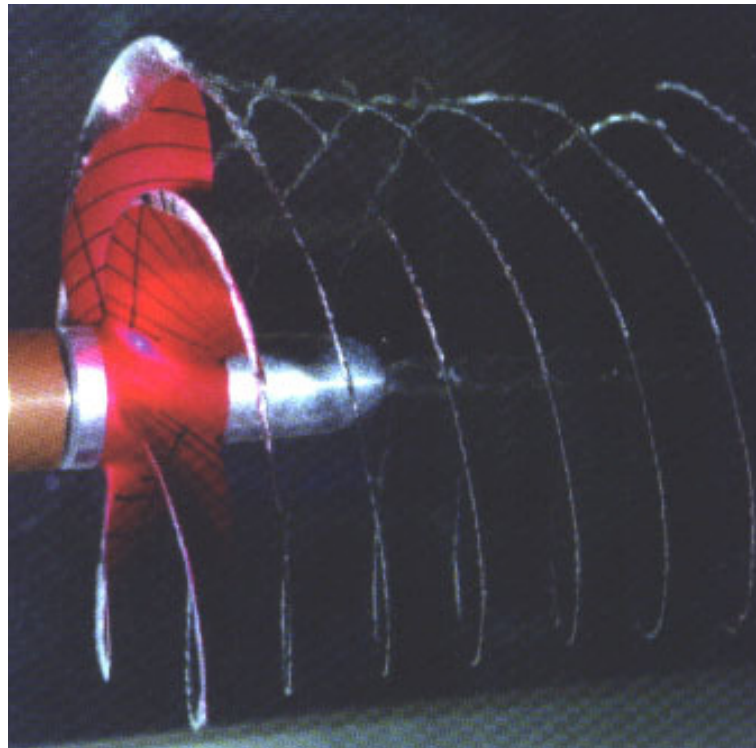
서울대학교 공과대학

조선해양공학과

수 치 선 박 유 체 역 학
- 보 텍 스 방 법 -

COMPUTATIONAL MARINE HYDRODYNAMICS
-VORTEX METHODS-

서 정 천

Contents

List of Figures

List of Tables

0

INTRODUCTION

0.1 Decomposition of Velocity Fields

Vortical flows are observed and conceived in nature. A vortex motion is the rotation of fluid elements. The rotational motion can be characterized by the vorticity $\underline{\omega} = \nabla \times \underline{q}$ where $\underline{q}$ is the fluid velocity. The vortical flow is said to be one of fluid region with relatively high vorticity.

Let us consider two partial diffential equations for $\underline{q}$:

$$\nabla \cdot \underline{q} \;=\; \theta \tag{1}$$

$$\nabla \times \underline{q} \;=\; \underline{\omega} \tag{2}$$

Our problem is to find the velocity field when the local rate of expansion (or compression) θ and the local vorticity (shearing prosess) $\underline{\omega}$ are specified throughout the fluid region with appropriate boundary conditions (and/or initial conditions).

Ignoring actual application of some boundary conditons, we consider 3 sets of differential equations:

$$\left.\begin{array}{rl} \nabla \cdot \underline{u}_\phi & = 0 \\ \nabla \times \underline{u}_\phi & = 0 \end{array}\right\} \tag{3}$$

$$\left.\begin{array}{rl} \nabla \cdot \underline{u}_\omega & = 0 \\ \nabla \times \underline{u}_\omega & = \underline{\omega} \end{array}\right\} \tag{4}$$

$$\left.\begin{array}{rl} \nabla \cdot \underline{u}_\theta & = \theta \\ \nabla \times \underline{u}_\theta & = 0 \end{array}\right\} \tag{5}$$

Then we may write the solution as a linear superposition of their individual solutions:

$$\boxed{\underline{q} = \underline{u}_\phi + \underline{u}_\omega + \underline{u}_\theta} \tag{6}$$

where $\underline{u}_\phi$ is a solenoidal and irrotational component of velocity field, $\underline{u}_\omega$ its rotational component, and $\underline{u}_\theta$ its non-zero divegence component. Note that the last one vanishes by the continuity equation (the principle of mass conservation) in the case of incompressible fluids. [1] The velocity field for an incompressible fluid has the form:

$$\boxed{\underline{q} = \underline{u}_\omega + \underline{u}_\phi} \tag{7}$$

It is well known in vector analysis that any vector function may be written as the sum of two vectors of the Helmholtz decomposition form.

$$\boxed{\underline{q} = \nabla \times \underline{A} + \nabla \phi,} \tag{8}$$

where $\underline{A}$ is '**vector potential (stream function)**' and ϕ is '**scalar potential (velocity potential)**'. [2]

---

[1] In the present course work, we consider only incompressible fluids unless stated otherwise.

[2] Even in the case of compressible fluids, we have the Helmholtz decomposion form; The non-zero divergence component $\underline{u}_\theta$ can be merged into the scalar potential component $\nabla \phi$ since $\underline{u}_\theta$ is irrotational such that $\underline{u}_\theta = \nabla \phi_\theta$ in which ϕ_θ becomes a solution of the Poisson-type equation.

0.2   Outline of Course Work

Our workscope is to construct the solution by numerical implementation based on the vorticity-velocity formulation. The fundamentals in the vorticity-velocity formulation are presented in Chapter 2 and Chapter 6.

Since the physical interpretation of the vorticity dynamics by Lighthill (1963) and Batchelor (1967), the vorticity-velocity formulation is one of candidates for solving Navier-Stokes (N.-S.) equations. The vorticity-velocity formulation is mathematically natural. The inertia force term in the N.-S. equations can be expressed as a Helmholtz decomposition form for which vorticity and pressure become a pair of potentials (Wu & Wu 1993).

The present course work would be focused on the vorticity-velocity formulation for the solution of unsteady incompressible Navier-Stokes equations, with two different numerical methods in a time domain analysis:

(1) Inviscid flow analysis
   The panel method that was well established in the potential flow analysis is explained extensively in Chapter 3 through Chapter 5, and Appendix A and Appendix B. For preliminary studies, we will cover a background about mathematical and fluid basis in Chapter 1 and Chapter 2.

(2) Viscous flow analysis
   The overall basic formulation and some results for simple bodies are presented in Chapter 6 through Chapter 8.

   (a) Eulerian finite volume method
      An integral approach is used, in conjunction with a finite volume scheme for solving the vorticity transport equation. The integral approach reflects the global coupling when imposed the boundary condition for vorticity at a solid surface. Mathematical identity for a vector or scalar field is used.

   (b) Lagrangian vortex particle method
      The main difference would be the discrete (particle) representation of the vorticity field. The main feature in the numerical scheme is

of a combination of the particle method and the boundary integral method (panel method). We also deal with the vortex-in-cell method as a hybrid method.

1

VECTOR ANALYSIS

1.1 Introduction

We will be concerned with both scalar and vector functions, in the form of fields as well as parametric description of curves in space. Because the laws governing

physical processes are independent of coordinate systems, vector notation is ideally suited for expressing these laws.

A scalar is often called a zero-order tensor and a vector is a first-order tensor. In addition to them, we shall use even more complicated quantities called tensors. We will use both dyads, or second-order tensors which have a 3×3 matrix form and are described by 9 scalar variables. A special third-order tensor called the alternating tensor ϵ_{ijk} will be frequently used in these notes.

1.1.1 Definition of domain

Some terms related to a domain are defined as follows, but we would not use the mathematical meaning rigorously. [1]

(1) Open ball: Set of points $\underline{x}$ inside ball of radius a centered at the origin, such that $|\underline{x}| < a$.

(2) Closed ball: Set of points such that $|\underline{x}| \leqq a$.

(3) Sphere: Set $|\underline{x}| = a$.

(4) Disk: 2-dimesional concept of the ball.

(5) Circle: 2-dimensional concept of the sphere.

(6) Open set D: For $\underline{x} \in D$, some sufficiently small ball centered at $\underline{x}$ belongs to D.

(7) Boundary B of open set D: For $\underline{x} \notin D$, if every open ball centered at $\underline{x}$ contains a point of D.

(8) Closure of D: Open set D plus boundary B.

(9) Connected: Each pair of points in D can be connected by a curve lying entirely in D.

---

[1] See, e.g., Stakgold, I. (1979), *Green's Functions and Boundary Value Problems*, John Wiley & Sons Inc. and Aris, R. (1962), *Vectors, Tensors and the Basic Equations of Fluid Mechanics*, Prentice Hall, p 44.

(10) Domain: Open connected set, such as an open ball. The union of two disjoint open balls is not a domain.

(11) Simply connected domain: Any all closed curves in domain D can be shrunk into a point in D without leaving D. The curves are called 'reducible'. For example, domain between concentric spheres is simply connected, but donut-shaped domain is not.

(12) Region: Domain plus all or part of boundary. Sometimes, the terms 'domain' and 'region' are used without distinction.

(13) Closed surface: A surface which lies within a bounded region of space and has an inside and an outside. The Klein bottle shown in Figure **1.1** has no inside or outside. Also there are some surfaces that do not have two sides. The Mobius strip is the known example of these surfaces.

(14) Smooth surface: A part of a surface is called 'smooth' if the normal to the surface varies continuously over that part. Some surfaces are made up of a number of subregions which are smooth and are called 'piecewise smooth'.
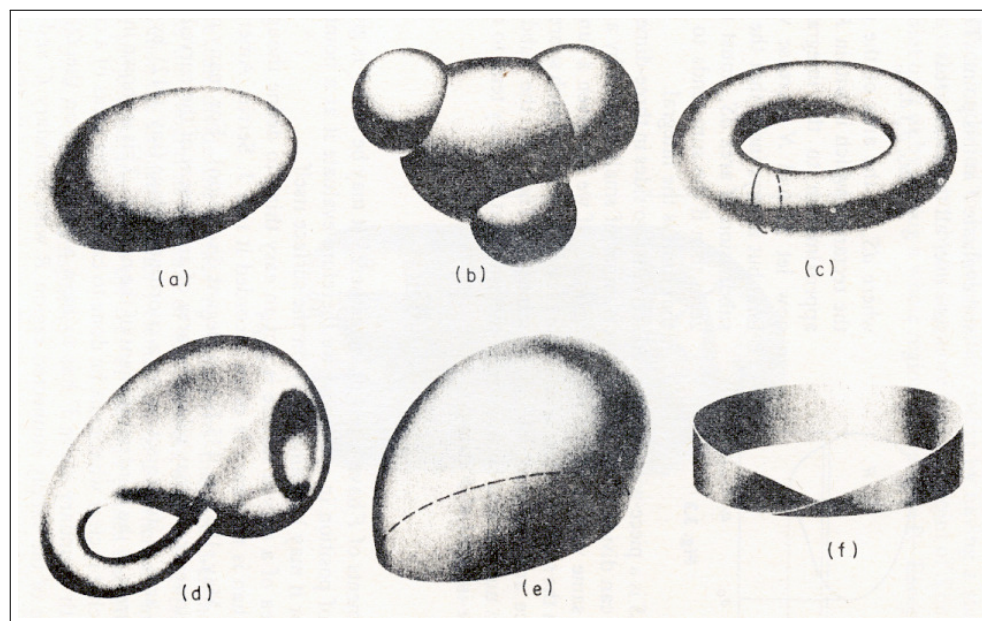
Figure **1.1** Types of surfaces: (a) a smooth closed surface; (b) a piecewise smooth surface; (c) a surface that is not simple connected; (d) a surface that is not closed: Klein bottle; (e) a hemisphere: (f) Mobius strip. From Aris (1962), p. 45.

1.1.2   Fundamental function analysis

A scalar field f is defined in a region D of two- or three-dimensional space with the property that the value of f varies from point to point in D. Some concepts and analysis for scalar functions are listed below.

(1) If $\lim_{x \to c} f(x) = f(c)$, the function $f(x)$ is said to be continuous at the point $x = c$.

(2) The base of natural logarithm is denoted by e, where $e = \lim_{n \to \pm\infty} \left(1 + \dfrac{1}{n}\right)^n$ $= 2.7182818285 \cdots$. One often writes $\ln(x)$ for $\log_e x$.

(3) By using the Euler formula $e^{i\theta} = \cos\theta + i \sin\theta$, the real sine and cosine function can be combined into a single function.

(4) A definite integral of a function $f(x)$ which exists on the interval $a \leq x \leq b$, can be defined by the limiting process in the sense of Riemann sum: namely,

$$\int_a^b f(x)\,dx = \lim_{N \to \infty} \sum_{i=1}^{N} f\left(a + i\,\frac{b-a}{N}\right) \frac{b-a}{N} \qquad (1.1)$$

(5) For function of one variable, the rule for change of variable in a definite integral is

$$\int_{x_1}^{x_2} f(x)\,dx = \int_{u_1}^{u_2} f(x(u))\,\frac{dx}{du}\,du \qquad (1.2)$$

where we assume $f(x)$ and $f(x(u))$ are continuous in the range of integration and $x = x(u)$ is continuous and its derivative is continuous for $u_1 \leq u \leq u_2$.

(6) For functions of two variables, the integral becomes

$$\int_{S_{xy}} f(x,y)\,dx\,dy = \int_{S_{uv}} f(x(u,v),\, y(u,v))\,|J|\,du\,dv, \qquad (1.3)$$

where Jacobian $J \equiv \dfrac{\partial(x,y)}{\partial(u,v)} = \dfrac{\partial x}{\partial u}\frac{\partial y}{\partial v} - \dfrac{\partial x}{\partial v}\frac{\partial y}{\partial u}.$

(7) For $f(x,t)$ and $\dfrac{\partial f}{\partial t}$ in a region $S_{xt}, \quad a(t) \le x \le b(t), t_1 \le t \le t_2,$

$$\frac{d}{dt} \int_{a(t)}^{b(t)} f(x,t)\,dx = f\left[b(t),t\right]\,b'(t) - f\left[a(t),t\right]\,a'(t) + \int_{a(t)}^{b(t)} \frac{\partial f}{\partial t}\,dx$$

(1.4)

This relationship is called Leibnitz's rule. The corresponding expression for the integral over a two or three dimensional region is called Reynolds transport theorem, which will be derived later.

(8) Dirac delta functions

Dirac delta function is defined as the sense of generalized functions:

$$\int_{-\infty}^{\infty} \delta(t)\,dt = 1$$

(1.5)

Also, the derivative of the unit-step function:

$$\frac{dU(t)}{dt} = \delta(t)$$

(1.6)

The definite integral of Dirac delta function:

$$\int_{a}^{b} \delta(t)\,dt = \begin{cases} 1 & \text{if } a < 0 < b \\ 0 & \text{otherwise} \end{cases}$$

(1.7)

Dirac delta function is combined with a regular function:

$$\int_{a}^{b} g(t)\,\delta(t)\,dt = g(0) \int_{a}^{b} \delta(t)\,dt$$

(1.8)

(9) Fourier transforms

For $f(x)$ periodic with period $2L$, then $f(x)$ can be expressed in a Fourier Series

$$f(x) = \frac{a_0}{2} + \sum_{n=1}^{\infty} \left[a_n \cos\left(\frac{n\pi x}{L}\right) + b_n \sin\left(\frac{n\pi x}{L}\right) \right]$$

(1.9)

where

$$a_n = \frac{1}{L} \int_0^{2L} f(x) \cos\left(\frac{n\pi x}{L}\right) dx, \quad b_n = \frac{1}{L} \int_0^{2L} f(x) \sin\left(\frac{n\pi x}{L}\right) dx \tag{1.10}$$

The Fourier transform of a function and its inverse transform:

$$F(\omega) = \int_{-\infty}^{\infty} f(t) e^{-i\omega t} dt \tag{1.11}$$

$$f(t) = \frac{1}{2\pi} \int_{-\infty}^{\infty} F(\omega) e^{i\omega t} d\omega \tag{1.12}$$

(10) The Laplace transform:

$$F(s) = \int_0^{\infty} f(t) e^{-st} dt \tag{1.13}$$

$$f(t) = \frac{1}{2\pi i} \int_{a-i\infty}^{a+i\infty} F(s) e^{st} ds \tag{1.14}$$

1.2 Vector Calculus

1.2.1 Definition of vector quantity

The simplest physical vector quantity is a *line vector*, that is, a linear displacement.

Now we investigate how a line vector is transformed from one coordinate system to another. Vector quantities are those that transform the same way independent of coordinate systems taken.

Consider two rectangular Cartesian coordinate systems rotated with respect to one another. Let a_{11}, a_{21}, a_{31} denote the direction cosines of the x_1' axis, with respect to the x_1, x_2, x_3 axes, respectively. Let a_{12}, a_{22}, a_{32} denote those of x_2', and a_{13}, a_{23}, a_{33} those of x_3'. [2]

---

[2] a_{ij} represents the cosine of the angle between the x_i and x_j' axes.
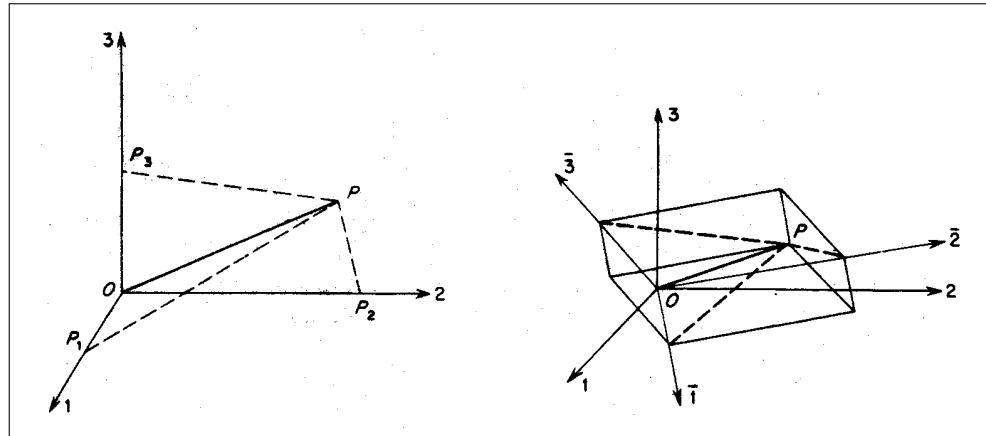
Figure **1.2** Two Cartesian coordinate systems rotated with respect to one another. From Aris (1962), p. 9.

Then, to find the coordinates of a point $P(x, y, z)$ in the primed system, note that in moving a distance x_1 along the x_1 axis you move $a_{11} x_1$ along x_1', $a_{12} x_1$ along x_2', and $a_{13} x_1$ along x_3'; etc. Hence, the new coordinates of P are

$$
\begin{aligned}
x_1' &= a_{11} x_1 + a_{21} x_2 + a_{31} x_3 \\
x_2' &= a_{12} x_1 + a_{22} x_2 + a_{32} x_3 \\
x_3' &= a_{13} x_1 + a_{23} x_2 + a_{33} x_3
\end{aligned}
\tag{1.15}
$$

Also, if we transform from x_1', x_2', x_3' to x_1, x_2, x_3 by a similar calculation, we find

$$
\begin{aligned}
x_1 &= a_{11} x_1' + a_{12} x_2' + a_{13} x_3' \\
x_2 &= a_{21} x_1' + a_{22} x_2' + a_{23} x_3' \\
x_3 &= a_{31} x_1' + a_{32} x_2' + a_{33} x_3'
\end{aligned}
\tag{1.16}
$$

Then we express Eqs. (1.15) and (1.16) in a summation notation:

$$
x_i' = \sum_{j=1}^{3} a_{ji} x_j \quad \text{for} \quad i = 1, 2, 3
\tag{1.17}
$$

$$
x_i = \sum_{j=1}^{3} a_{ij} x_j' \quad \text{for} \quad i = 1, 2, 3
\tag{1.18}
$$

A *vector* is defined as a set of three numbers u_1, u_2, u_3, referred to a coordinate system x_1, x_2, x_3, having the property that when transferred to the x_1', x_2', x_3' system the corresponding quantities are given by

$$u_i' = \sum_{j=1}^{3} a_{ji}\, u_j \quad \text{for} \quad i = 1, 2, 3 \tag{1.19}$$

This is really the same as our earlier definition in terms of a line vector, because Eqs. (1.17) and (1.18) are the transformation formulas for a line vector.

It is clear that, to test whether a physical quantity is a vector quantity, one must have a definition that permits examination of its transformation formula. Let us consider two simple examples.

(1) First, consider velocity of a point $P(x_1, x_2, x_3)$. The components of this quantity along the three axes are $\dfrac{dx_1}{dt}, \dfrac{dx_2}{dt}$, and $\dfrac{dx_3}{dt}$. Calculating the velocity in the primed system, we find

$$\frac{dx_i'}{dt} = \frac{d}{dt} \sum_{j=1}^{3} a_{ji}\, x_j = \sum_{j=1}^{3} a_{ji}\, \frac{dx_j}{dt}. \tag{1.20}$$

This has exactly the form required by Eq. (1.19). Hence the velocity of a point is a vector quantity.

(2) Next, consider the set of numbers $\dfrac{\partial u}{\partial x_i}$ where u is a scalar function $u(x_1, x_2, x_3)$. We see how $\dfrac{\partial u}{\partial x_i'}$ is expressed in terms of $\dfrac{\partial u}{\partial x_i}$:

$$\frac{\partial u}{\partial x_i'} = \sum_{j=1}^{3} \frac{\partial u}{\partial x_j} \frac{\partial x_j}{\partial x_i'} = \sum_{j=1}^{3} \frac{\partial u}{\partial x_j}\, a_{ji} \quad \text{from Eq. (1.18).} \tag{1.21}$$

Hence $\dfrac{\partial u}{\partial x_i}$ is a vector. It is actually a gradient of the scalar function.

1.2.2 Symbol of vectors

In these notes, we denote vectors by underlined symbols and scalar numbers by ordinary symbols. In particular, let us define three *unit vectors*, $\underline{i}, \underline{j}$, and $\underline{k}$, each having unit magnitude and being directed along x, y, and z axes of a rectangular cartesian coordinate system respectively. For general curvilinear coordinate systems, we denote the corresponding unit base vectors as $\underline{e}_1, \underline{e}_2$, and $\underline{e}_3$.

We can write an expression for any vector $\underline{a}$ as the sum of its components; i.e.

$$\underline{a} = a_1\,\underline{i} + a_2\,\underline{j} + a_3\,\underline{k}. \tag{1.22}$$

For instance, the position vector $\underline{x}$, denoting the displacement of any point from the origin, is [3]

$$\underline{x} = x\,\underline{i} + y\,\underline{j} + z\,\underline{k}. \tag{1.23}$$

In this case we write the distance of $\underline{x}$ from the origin as $r \equiv |\underline{x}| \equiv \sqrt{x^2 + y^2 + z^2}$. We also denote the distance between two position vectors by r.

Let the three coordinates of a rectangular Cartesian system be called x_1, x_2, and x_3. Then, for a vector whose corresponding components are a_1, a_2, and a_3, we write simply a_n instead of writing down all components and unit vectors, where the subscript is understood to take the values 1, 2, and 3. Thus a vector is recognized by the presence of a subscript; a scalar by the absence of a subscript. This notation of vector (tensor) analysis is the simplest one when we perform vector operations with the least memory work.

1.2.3 Basic unit tensors

In general, in a 3-dimensional space a tensor of order (rank) m has 3^m components,

$$\tau_{ij\cdots k}\,\underline{e}_i\,\underline{e}_j\,\cdots\,\underline{e}_k \quad \text{for} \quad i, j, \cdots k = 1, 2, 3 \tag{1.24}$$

---

[3]$\underline{r}$ is also used for $\underline{x}$ herein.

1.2.3.1 Kronecker delta tensor

The most useful tensor of order 2 is the unit tensor, denoting by doubly-underlined upper-cased bold face:

$$\underline{\underline{I}} = \delta_{ij} \, \underline{e}_i \, \underline{e}_j \qquad (1.25)$$

with Kronecker delta δ_{ij} being defined by

$$\delta_{ij} = 1 \;\text{ if }\; i = j; \quad \delta_{ij} = 0 \;\text{ if }\; i \neq j \qquad (1.26)$$

The contraction (inner product) of 2 unit tensors gives

$$\underline{\underline{I}} \cdot \underline{\underline{I}} = \delta_{ij} \, \delta_{jk} = \delta_{ik} = \underline{\underline{I}} \qquad (1.27)$$

The double contraction of 2 unit tensors (denoted by a colon) gives

$$\underline{\underline{I}} : \underline{\underline{I}} = \delta_{ij} \, \delta_{ji} = \delta_{ii} = d \qquad (1.28)$$

where d is the dimension of the space that we dealt with; e.g., $d = 3$ in 3-dimesions.

1.2.3.2 Permutation tensor

As another example, the important tensor of order 3 is the permutation (alternating) tensor:

$$\underline{\underline{\underline{E}}} = \epsilon_{ijk} \, \underline{e}_i \, \underline{e}_j \, \underline{e}_k \qquad (1.29)$$

where ϵ_{ijk} are the Cartesian components of permutation symbol:

$$\left. \begin{array}{rl} \epsilon_{ijk} &= 0 \quad\;\; \text{if any } i, j, k \text{ equal} \\ \epsilon_{ijk} &= 1 \quad\;\; \text{if } (ijk) = (123), (231), (312) \\ \epsilon_{ijk} &= -1 \quad \text{if } (ijk) = (132), (213), (321). \end{array} \right\} \qquad (1.30)$$

1.2.3.3   Multiplication of basic tensors

We can easily see that the following formulas for δ_{ij} and ϵ_{ijk} holds from their definitions:

$$\delta_{ii} = 3, \tag{1.31}$$

$$\delta_{ij}\, u_{klmi} = u_{klmj}, \tag{1.32}$$

$$\delta_{ij}\, \epsilon_{ijk} = 0, \tag{1.33}$$

The permutation tensor is used for cross (vector) product of vectors. If we need more than one cross products, the multiplication of two permutation tensors is involved. Let us start with the rule of vector product: [4]

$$\epsilon_{ijk} = \underline{e}_i \cdot (\underline{e}_j \times \underline{e}_k) = \begin{vmatrix} \underline{e}_i \cdot \underline{e}_1 & \underline{e}_i \cdot \underline{e}_2 & \underline{e}_i \cdot \underline{e}_3 \\ \underline{e}_j \cdot \underline{e}_1 & \underline{e}_j \cdot \underline{e}_2 & \underline{e}_j \cdot \underline{e}_3 \\ \underline{e}_k \cdot \underline{e}_1 & \underline{e}_k \cdot \underline{e}_2 & \underline{e}_k \cdot \underline{e}_3 \end{vmatrix} = \begin{vmatrix} \delta_{i1} & \delta_{i2} & \delta_{i3} \\ \delta_{j1} & \delta_{j2} & \delta_{j3} \\ \delta_{k1} & \delta_{k2} & \delta_{k3} \end{vmatrix} \tag{1.34}$$

From Eq. (1.34), the product of two permutation tensors is written as

$$\epsilon_{ijk}\, \epsilon_{mnl} = \begin{vmatrix} \begin{bmatrix} \delta_{i1} & \delta_{i2} & \delta_{i3} \\ \delta_{j1} & \delta_{j2} & \delta_{j3} \\ \delta_{k1} & \delta_{k2} & \delta_{k3} \end{bmatrix} \begin{bmatrix} \delta_{m1} & \delta_{m2} & \delta_{m3} \\ \delta_{n1} & \delta_{n2} & \delta_{n3} \\ \delta_{l1} & \delta_{l2} & \delta_{l3} \end{bmatrix} \end{vmatrix} = \begin{vmatrix} \delta_{im} & \delta_{in} & \delta_{il} \\ \delta_{jm} & \delta_{jn} & \delta_{jl} \\ \delta_{km} & \delta_{kn} & \delta_{kl} \end{vmatrix} \tag{1.35}$$

Contraction with respect to k, l (i.e., $k = l$) yields

$$\epsilon_{ijk}\, \epsilon_{mnk} = \delta_{im}\, \delta_{jn} - \delta_{in}\, \delta_{jm} \tag{1.36}$$

Making the contraction with respect to j, n and continuing again give

$$\epsilon_{ijk}\, \epsilon_{mjk} = \delta_{im}\, \delta_{jj} - \delta_{ij}\, \delta_{jm} = 3\, \delta_{im} - \delta_{im} = 2\, \delta_{im} \tag{1.37}$$

$$\epsilon_{ijk}\, \epsilon_{ijk} = 2\, \delta_{ii} = 6 \tag{1.38}$$

---

[4]We will follow the procedure in the text, Wu, J.-Z, Ma, H.-Y. and Zhou, M.-D. (2006), *Vorticity and Vortex Dynamics*, Springer, pp. 697–698.

The corresponding formulas in a 2-dimensional space are given by

$$\epsilon_{ij3}\,\epsilon_{mn3} = \begin{vmatrix} \delta_{im} & \delta_{in} \\ \delta_{jm} & \delta_{jn} \end{vmatrix} = \delta_{im}\,\delta_{jn} - \delta_{in}\,\delta_{jm} \tag{1.39}$$

$$\epsilon_{ij3}\,\epsilon_{mj3} = \delta_{im}\,\delta_{jj} - \delta_{ij}\,\delta_{jm} = 2\,\delta_{im} - \delta_{im} = \delta_{im} \tag{1.40}$$

$$\epsilon_{ij3}\,\epsilon_{ij3} = 2 \tag{1.41}$$

1.2.3.4   Example of permutation tensor

A special example of the permutation tensor can be observed in definition of vorticity: [5]

$$\underline{\omega} = \omega_i = \nabla \times \underline{q} = \epsilon_{ijk}\frac{\partial q_k}{\partial x_j} = \epsilon_{ijk}\frac{1}{2}\left(\frac{\partial q_k}{\partial x_j} - \frac{\partial q_j}{\partial x_k}\right) = \frac{1}{2}\,\epsilon_{ijk}\,\Omega_{jk} \tag{1.42}$$

where $\Omega_{jk} \equiv \left(\dfrac{\partial q_k}{\partial x_j} - \dfrac{\partial q_j}{\partial x_k}\right)$ is a spin(rotational) tensor. Also it is easily seen that, by multiplying the above equation by ϵ_{lmi} and using Eq. (1.34),

$$\epsilon_{lmi}\,\omega_i = \epsilon_{lmi}\frac{1}{2}\epsilon_{ijk}\,\Omega_{jk} = \frac{1}{2}(\delta_{lj}\,\delta_{mk} - \delta_{lk}\,\delta_{jm})\,\Omega_{jk} = \frac{1}{2}(\Omega_{lm} - \Omega_{ml}) = \Omega_{lm} \tag{1.43}$$

from which we have

$$\Omega_{ij} = \epsilon_{ijk}\,\omega_k. \tag{1.44}$$

The inner product of a vector $\underline{a}$ and an antisymmetric tensor $\underline{\underline{\Omega}}$ becomes

$$\underline{a}\cdot\underline{\underline{\Omega}} = a_i\,\epsilon_{ijk}\,\omega_k = \underline{\omega}\times\underline{a}, \quad \underline{\underline{\Omega}}\cdot\underline{a} = \epsilon_{ijk}\,\omega_k\,a_j = \underline{a}\times\underline{\omega}. \tag{1.45}$$

If the relative velocity $\underline{v}$ of any two points is $\underline{\underline{\Omega}}\cdot\underline{x}$ where $\underline{x}$ is the relative position vector of the two points, then the motion is due to a rigid body rotation. Here $\underline{\underline{\Omega}}$ relates to the angular velocity.

---

[5] See Aris, R. (1962), *Vectors, Tensors and the Basic Equations of Fluid Mechanics*, Prentice Hall, p. 25 and Wu, J.-Z, Ma, H.-Y. and Zhou, M.-D. (2006), *Vorticity and Vortex Dynamics*, Springer, p. 698.

Similarly, we also have

$$\nabla \cdot \underline{\underline{\Omega}} = \frac{\partial}{\partial x_i} \left(\epsilon_{ijk} \, \omega_k \right) = -\nabla \times \underline{\omega}. \tag{1.46}$$

Such relations between vorticity $\underline{\omega}$ and the spin tensor $\underline{\underline{\Omega}}$ are useful to deduce the physical interpretation in vortex dynamics that will be described in more detail in Chapter 6.

1.2.4 Multiplication of vectors

1.2.4.1 Scalar product

The *scalar product* of two vectors $\underline{a}$ and $\underline{b}$ is defined as the scalar number given by the product of their scalar magnitudes and the cosine of the angle between them: $\underline{a} \cdot \underline{b} = a \, b \, \cos(\underline{a} \cdot \underline{b})$ or $\underline{a} \cdot \underline{b} = a_1 \, b_1 + a_2 \, b_2 + a_3 \, b_3$. According to the notation of Kronecker delta tensors, it becomes $\underline{a} \cdot \underline{b} = \delta_{ij} \, a_i \, b_j = a_i \, b_i$, where summation convention has been used.

1.2.4.2 Vector product

The *vector product* of two vectors $\underline{a}$ and $\underline{b}$ is defined as a vector whose direction is perpendicular to both $\underline{a}$ and $\underline{b}$ and whose magnitude is the product of their magnitudes and the sine of the angle between them; i. e., $\underline{c} = \underline{a} \times \underline{b}; \quad w = a \, b \, \sin(\underline{a}, \, \underline{b})$.

To determine the expression for $\underline{a} \times \underline{b}$ in terms of Cartesian components, we may write by cyclic substitution of subscripts as an aid to memory; in a form of tensor-notation, $\underline{a} \times \underline{b} = \epsilon_{ijk} \, a_j \, b_k$.

1.2.4.3 Scalar triple product

The *scalar triple product*, $\underline{a} \cdot (\underline{b} \times \underline{c})$, is a scalar number having a value equal to the volume of the parallelepiped erected on $\underline{a}, \underline{b}$, and $\underline{c}$. This may be expressed as,

using the alternating tensor, $\underline{a} \cdot (\underline{b} \times \underline{c}) = a_i \, \epsilon_{ijk} \, b_j \, c_k$. Obviously, the parentheses used here are unnecessary and we see $\underline{a} \cdot \underline{b} \times \underline{c} = \underline{a} \times \underline{b} \cdot \underline{c} = \underline{b} \cdot \underline{c} \times \underline{a}$ etc.

1.2.4.4 Vector triple product

The *vector triple product*, $\underline{a} \times (\underline{b} \times \underline{c})$, is expressed in terms of components in the plane of $\underline{b}$ and $\underline{c}$:

$$\underline{a} \times (\underline{b} \times \underline{c}) = (\underline{a} \cdot \underline{c}) \, \underline{b} - (\underline{a} \cdot \underline{b}) \, \underline{c} \tag{1.47}$$

This can be easily verified by using the basic formula for the alternating tensor listed above:

$$\underline{a} \times (\underline{b} \times \underline{c}) = \epsilon_{mli} \, a_l \, \epsilon_{ijk} \, b_j \, c_k = (\delta_{mj} \, \delta_{lk} - \delta_{mk} \, \delta_{lj}) \, a_l \, b_j \, c_k = a_k \, b_j \, c_k - a_j \, b_j \, c_k. \tag{1.48}$$

Combining the above results one finds

$$\underline{a} \times (\underline{b} \times \underline{c}) + \underline{b} \times (\underline{c} \times \underline{a}) + \underline{c} \times (\underline{a} \times \underline{b}) = 0 \tag{1.49}$$

1.2.5 Vector derivatives

1.2.5.1 Gradient: ∇u

Consider a scalar function $u = u(x, y, z)$ that is differentiable and has continuous derivatives. Let us define the gradient of u at x, y, z as the limiting value of a certain surface integral over a surface surrounding the point x, y, z, as follows

$$\nabla u \equiv \lim_{\triangle V \to 0} \frac{1}{\triangle V} \oint_S u \, \underline{n} \, dS \tag{1.50}$$

where S is the area enclosing the volume $\triangle V$, dS is the element of area, and $\underline{n}$ is the unit vector normal to the surface at each point of the surface integration.
[6]

---

[6] $\int_S \cdots dS$ and $\oint_S \cdots dS$ are the symbolism to indicate that the integration is over, respectively, an open surface and a closed surface.

Now we can take $\triangle V$ very small, in the form of a cube, say, with sides $\triangle x, \triangle y, \triangle z$. Then, neglecting second-order quantities, $\triangle V = \triangle x \triangle y \triangle z$, and

$$\int_S u\,\underline{n}\,dS \approx -u\,\underline{i}\,\triangle y\,\triangle z - u\,\underline{j}\,\triangle x\,\triangle z - u\,\underline{k}\,\triangle x\,\triangle y$$

$$+ \left(u + \frac{\partial u}{\partial x}\triangle x \right)\underline{i}\,\triangle y\,\triangle z + \left(u + \frac{\partial u}{\partial y}\triangle y \right)\underline{j}\,\triangle x\,\triangle z$$

$$+ \left(u + \frac{\partial u}{\partial z}\triangle z \right)\underline{k}\,\triangle x\,\triangle y \tag{1.51}$$

$$\approx \left\{ \frac{\partial u}{\partial x}\underline{i} + \frac{\partial u}{\partial u}\underline{j} + \frac{\partial u}{\partial z}\underline{k} \right\} V \tag{1.52}$$

Hence, in limit,

$$\nabla u = \underline{i}\,\frac{\partial u}{\partial x} + \underline{j}\,\frac{\partial u}{\partial y} + \underline{k}\,\frac{\partial u}{\partial z} \tag{1.53}$$

We recognize this as the vector. Another symbol often used for ∇u is grad u. In a form of tensor notation, it is $\dfrac{\partial u}{\partial x_i}$.

1.2.5.2 Divergence: $\nabla \cdot \underline{v}$

Consider now a *vector function*, $\underline{v} = \underline{v}(x, y, z) \equiv v_1\,\underline{i} + v_2\,\underline{j} + v_3\,\underline{k}$, where v_1, v_2, and v_3 are all scalar functions of x, y, z, having continuous derivatives. We define

$$\nabla \cdot \underline{v} = \lim_{\triangle V \to 0} \frac{1}{\triangle V} \oint_S \underline{n} \cdot \underline{v}\,dS \tag{1.54}$$

Now, by calculating for a small cubical volume, you can easily confirm the following equality:

$$\nabla \cdot \underline{v} = \frac{\partial v_1}{\partial x} + \frac{\partial v_2}{\partial y} + \frac{\partial v_3}{\partial z} \tag{1.55}$$

Another symbol used for $\nabla \cdot \underline{v}$ is div $\underline{v}$. In a form of tensor notation, it is $\dfrac{\partial v_i}{\partial x_i}$.

1.2.5.3 Curl: $\nabla \times \underline{v}$

We define the curl of a vector

$$\nabla \times \underline{v} \equiv \lim_{\triangle V \to 0} \frac{1}{\triangle V} \oint_S \underline{n} \times \underline{v} \, dS \qquad (1.56)$$

and find, by considering a small cube, that

$$\nabla \times \underline{v} = \left(\frac{\partial v_3}{\partial y} - \frac{\partial v_2}{\partial z} \right) \underline{i} + \left(\frac{\partial v_1}{\partial z} - \frac{\partial v_3}{\partial x} \right) \underline{j} + \left(\frac{\partial v_2}{\partial x} - \frac{\partial v_1}{\partial y} \right) \underline{k} \qquad (1.57)$$

or, to assist the memory, purely symbolically we write

$$\nabla \times \underline{v} = \begin{vmatrix} \underline{i} & \underline{j} & \underline{k} \\ \dfrac{\partial}{\partial x} & \dfrac{\partial}{\partial y} & \dfrac{\partial}{\partial z} \\ v_1 & v_2 & v_3 \end{vmatrix} \qquad (1.58)$$

Another symbol used for curl $\underline{v}$ is $\nabla \times \underline{v}$. In a form of tensor notation, it is $\epsilon_{ijk} \dfrac{\partial v_k}{\partial x_j}$.

1.2.5.4 Laplacian: $\nabla^2 u$

The Laplacian of a scalar function $u(x, y, z)$ is defined as

$$\nabla^2 u \equiv \nabla \cdot (\nabla u) = \frac{\partial^2 u}{\partial x^2} + \frac{\partial^2 u}{\partial y^2} + \frac{\partial^2 u}{\partial z^2} \qquad (1.59)$$

By analogy, the Laplacian of a vector function is the vector whose rectangular Cartesian components are the Laplacian of the vector's corresponding components [7]

$$\nabla^2 \underline{v} = \underline{i} \, \nabla^2 v_1 + \underline{j} \, \nabla^2 v_2 + \underline{k} \, \nabla^2 v_3 \qquad (1.60)$$

---

[7] We must do more work to find its expression in a non-Cartesian system.

1.2.5.5   Differential operator: ∇

From the original definition of grad u, we can deduce that the differential du is given by the formula, in rectangular Cartesian coordinates,

$$du = \frac{\partial u}{\partial x}\,dx + \frac{\partial u}{\partial y}\,dy + \frac{\partial u}{\partial z}\,dz = d\underline{\ell} \cdot \nabla u \qquad (1.61)$$

where $d\underline{\ell}$ is any directed line (vector) element. This means that du is the increment of u corresponding to a position increment $d\underline{\ell}$.

Similarly, for a vector function $\underline{v}(x, y, z)$,

$$
\begin{aligned}
d\underline{v} &\equiv \underline{i}\,dv_1 + \underline{j}\,dv_2 + \underline{k}\,dv_3 \\
&= \left(dx\,\frac{\partial}{\partial x} + dy\,\frac{\partial}{\partial y} + dz\,\frac{\partial}{\partial z} \right) \left(\underline{i}\,v_1 + \underline{j}\,v_2 + \underline{k}\,v_3 \right) \\
&= d\underline{\ell} \cdot \nabla \underline{v} \qquad\qquad\qquad\qquad\qquad\qquad (1.62)
\end{aligned}
$$

In all of the formulas above, we consider the symbol ∇ as representing a *vector operator* $\underline{i}\,\dfrac{\partial}{\partial x} + \underline{j}\,\dfrac{\partial}{\partial y} + \underline{k}\,\dfrac{\partial}{\partial z}$. If you treat this operator as a vector, with the appropriate vector-multiplication signs, you get the right result. Equations (1.61) and (1.62) are independent of the choice of coordinate system. As will be seen later on, the expressions for *div, grad, curl,* etc. in a more general curvilinear system do not bear much resemblance to one another.

1.2.5.6   Directed derivative

Equations (1.61) and (1.62) lead immediately to the formulas for the *directed derivative* in the direction of a given vector $\underline{s} \equiv s_1\,\underline{i} + s_2\,\underline{j} + s_3\,\underline{k}$ in rectangular Cartesian coordinate:

$$\frac{\partial u}{\partial s} = \underline{e}_s \cdot \nabla u \qquad (1.63)$$

$$\frac{\partial \underline{v}}{\partial s} = \underline{e}_s \cdot \nabla \underline{v} \qquad (1.64)$$

Again we have defined a new vector operator: $\underline{e}_s \cdot \nabla = \dfrac{s_1}{s}\dfrac{\partial}{\partial x} + \dfrac{s_2}{s}\dfrac{\partial}{\partial y} + \dfrac{s_3}{s}\dfrac{\partial}{\partial z}$, where s is the magnitude of $\underline{s}$.

1.2.6 Expansion formulas

The following formulas are of general utility. Let ϕ denote any differentiable scalar function of x, y, z, and $\underline{u}, \underline{v}$ and $\underline{w}$ any such vector functions.

$$\nabla \cdot (\phi\,\underline{u}) = \underline{u} \cdot \nabla\phi + \phi\,\nabla \cdot \underline{u} \tag{1.65}$$

$$\nabla \times (\phi\,\underline{u}) = (\nabla\phi) \times \underline{u} + \phi\,\nabla \times \underline{u} \tag{1.66}$$

$$\nabla \cdot (\underline{v} \times \underline{w}) = \underline{w} \cdot \nabla \times \underline{v} - \underline{v} \cdot \nabla \times \underline{w} \tag{1.67}$$

$$\nabla \times (\underline{v} \times \underline{w}) = \underline{w} \cdot \nabla\underline{v} + \underline{v}\nabla \cdot \underline{w} - \underline{w}\nabla \cdot \underline{v} - \underline{v} \cdot \nabla\underline{w} \tag{1.68}$$

$$\nabla(\underline{v} \cdot \underline{w}) = \underline{v} \cdot \nabla\underline{w} + \underline{w} \cdot \nabla\underline{v} + \underline{v} \times (\nabla \times \underline{w}) + \underline{w} \times (\nabla \times \underline{v}) \tag{1.69}$$

$$\nabla \cdot (\nabla \times \underline{v}) = 0 \tag{1.70}$$

$$\nabla \times (\nabla\,\phi) = 0 \tag{1.71}$$

$$\nabla \times (\nabla \times \underline{v}) = \nabla(\nabla \cdot \underline{v}) - \nabla^2\underline{v} \tag{1.72}$$

Operation on the position vector $\underline{x} = x_1\,\underline{i} + x_2\,\underline{j} + x_3\,\underline{k}$ whose magnitude is denoted by $r = |\underline{x}| = \sqrt{\underline{x} \cdot \underline{x}}$, with a constant vector $\underline{a}$, is illustrated as follows:

$$\nabla r = \underline{x}/r \tag{1.73}$$

$$\nabla \cdot \underline{x} = 3 \tag{1.74}$$

$$\nabla \times \underline{x} = 0 \tag{1.75}$$

$$\nabla r^n = n\,r^{n-2}\,\underline{x} \tag{1.76}$$

$$\nabla \cdot (r^n\,\underline{x}) = (n+3)\,r^n \tag{1.77}$$

$$\nabla \times (r^n\,\underline{x}) = 0 \tag{1.78}$$

$$\nabla^2(r^n) = n(n+1)\,r^{n-2} \tag{1.79}$$

$$\nabla \cdot (\underline{a} \times \underline{x}) = 0 \tag{1.80}$$

$$\nabla (\underline{a} \cdot \underline{x}) = \underline{a} \tag{1.81}$$

$$\nabla \times (\underline{a} \times \underline{x}) = 2\,\underline{a} \tag{1.82}$$

$$\nabla \cdot (\underline{a} \times \nabla r) = 0 \tag{1.83}$$

$$\nabla \cdot (r\,\underline{a}) = (\underline{x} \cdot \underline{a})/r \tag{1.84}$$

$$\nabla \times (r\,\underline{a}) = (\underline{x} \times \underline{a})/r \tag{1.85}$$

1.3   Integral Theorems

1.3.1   Divergence theorem

Let u and $\underline{v}$ denote arbitrary scalar and vector functions of x, y, z as before. These are assumed to be defined, continuous, and single-valued in a certain region of space, and, moreover, that their first derivatives with respect to $x, y,$ and z satisfy the same requirements.

Now consider the surface integral $\oint_S u\,\underline{n}\,dS$, carried over any closed surface S within the region, enclosing a volume V, where $\underline{n}$ is the unit normal vector directed outward. It is clear that, if the volume V is subdivided into small volume V_i, this integral equals the sum of all the integrals $\oint_{S_i} u\,\underline{n}\,dS$ taken over the small surfaces S_i. Since integration over neighboring elements will cancel one another, and only the integration over the outside will remain:

$$\oint_S u\,\underline{n}\,dS = \sum \oint_{S_i} u\,\underline{n}\,dS \tag{1.86}$$

But, in the limit, the surface integral over the small surface become $\nabla u\,dV$, according to our definition of the gradient, Eq. (1.50), and the summation becomes a volume integration:

$$\oint_S u\,\underline{n}\,dS = \int_V \nabla u\,dV \tag{1.87}$$

In particular, if $u = const.$, Eq. (1.87) becomes

$$\oint_S \underline{n} \, dS = 0. \tag{1.88}$$

It means that the integral of vectorial surface element over a closed surface must vanish.

If u is taken as a negative of static pressure acting on a body submerged fully into a fluid (i.e., $u = -p = \rho g z$, where z is vertically upward coordinate), the force acting on the body is

$$\underline{F} = \oint_S (-p) \, \underline{n} \, dS = \int_V \nabla(\rho \, g \, z) \, dV = \int_V (\rho \, g \, \underline{k}) \, dV = \rho \, g \, V \, \underline{k} \tag{1.89}$$

This relation is well known as the Archimedes principle for buoyancy force of a submerged body.

By entirely analogous reasoning, using the definitions of the divergence and curl, we have

$$\oint_S \underline{n} \cdot \underline{v} \, dS = \int_V \nabla \cdot \underline{v} \, dV \tag{1.90}$$

and

$$\oint_S \underline{n} \times \underline{v} \, dS = \int_V \nabla \times \underline{v} \, dV \tag{1.91}$$

Equation (1.90) is known as the divergence theorem, or Gauss theorem. If we take $\underline{v}$ as fluid velocity, Eqs. (1.90) and (1.91) become, respectively,

$$\oint_S \underline{n} \cdot \underline{v} \, dS = \int_V \theta \, dV \tag{1.92}$$

and

$$\oint_S \underline{n} \times \underline{v} \, dS = \int_V \underline{\omega} \, dV \tag{1.93}$$

These equations show that the velocity components over boundary are directly related with the field distribution of expansion (or compressing process) and vorticity in fluid region.

The three types of the theorem above can be unified by a general form:

$$\oint_S (\underline{n} * f)\, dS = \int_V (\nabla * f)\, dV \tag{1.94}$$

where $*$ denotes one of differential operator, scalar product and vector product, and f is a scalar or vector function depending on the choice.

As an example, take $\underline{f} = \nabla u$ to yield

$$\int_V \nabla^2 u\, dV = \int_V \nabla \cdot (\nabla u)\, dV = \oint_S \underline{n} \cdot \nabla u\, dS = \oint_S \frac{\partial u}{\partial n}\, dS \tag{1.95}$$

where $\partial u / \partial n$ is the directed derivative in the outward direction as defined in Eq (1.63).

1.3.2 Stokes theorem

Let us apply Eq. (1.50) for definition of ∇u to a very small volume element of a thin disk with uniform height $\triangle h$ and base area $\triangle S$. Its volume then becomes $\triangle S\ \triangle h$. Consider the product of ∇u with the outward unit normal vector to the upper surface $\underline{n}_u$. Then it is not difficult to prove that,

$$\underline{n}_u \times \nabla u \approx \underline{n}_u \times \frac{1}{\triangle V} \oint_S u\, \underline{n}\, dS \approx \frac{1}{\triangle S} \oint_C u\, d\underline{\ell} \tag{1.96}$$

where C is the small contour that forms the boundary of $\triangle S$. The line integral in Eq. (1.96) is taken in the direction that would advance a right-hand screw in the $\underline{n}$ direction.

Now consider a volume element with the uniform thin height and an arbitrary base surface S. If this volume is subdivided into very small volume V_i with the same height, the above product in an integral sense can be expressed as the sum of all the integrals taken over the small line integrals:

$$\int_S \underline{n} \times \nabla u\, dS = \lim_{V_i \to 0} \sum \oint_{C_i} u\, d\underline{\ell} \tag{1.97}$$

Since the line integration over neighboring contour elements will cancel one another, and only the integration over the outside contour will remain:

$$\int_S \underline{n} \times \nabla u \, dS = \oint_C u \, d\underline{\ell} \tag{1.98}$$

With this knowledge, two more important transformation theorems follow:

$$\int_S \underline{n} \cdot \nabla \times \underline{v} \, dS = \oint_C \underline{v} \cdot d\underline{\ell} \tag{1.99}$$

$$\int_S (\underline{n} \times \nabla) \times \underline{v} \, dS = \oint_C d\underline{\ell} \times \underline{v} \tag{1.100}$$

The first of these is known as *Stokes theorem.* [8]

If u is constant, Eq. (1.98) becomes

$$0 = \oint_C u \, d\underline{\ell} \tag{1.101}$$

and if $\underline{v} = \underline{x}$, Eq. (1.100) becomes, since $(\underline{n} \times \nabla) \times \underline{x} = -2\,\underline{n}$,

$$\int_S \underline{n} \, dS = \frac{1}{2} \oint_C \underline{x} \times d\underline{\ell}. \tag{1.102}$$

If we consider $\underline{v}$ as fluid velocity, we have the well-known relation between vorticity flux through an open surface and circulation along the boundary of the surface:

$$\int_S \underline{n} \cdot \underline{\omega} \, dS = \oint_C \underline{v} \cdot d\underline{\ell} \tag{1.103}$$

By analogous reasoning, we have used the relationship,

$$\underline{n} \cdot \nabla \times \underline{v} \approx \frac{1}{S} \oint_C \underline{v} \cdot d\underline{\ell} \tag{1.104}$$

The conditions on u and $\underline{v}$ are analogous to those imposed above; that is, the functions and their first derivations must be finite, continuous, and single-valued

---

[8]For rigorous proof, see Arfken, G. (1970), *Mathematical Methods for Physicists*, 2nd ed., Academic Press, pp. 51–53.

in the region. The surface S enclosed by the contour C need not be flat; $\underline{n}$ is normal to S at every point, and the direction of C is chosen as described above.

The unified form of Stokes theorem may be written by,

$$\int_S (\underline{n} \times \nabla) * f \, dS = \oint_C d\underline{\ell} * f \tag{1.105}$$

1.3.3   Volume integrals of a vector

Using integration by parts, we can express the integration of $f(x)$ by the moment of $f'(x)$:

$$\int_a^b f(x) \, dx = b \, f(b) - a \, f(a) - \int_a^b x \, f'(x) \, dx \tag{1.106}$$

In a similar fashion to this one-dimensional formula, a surface or volume integral can be cast to the integrals of the first moment of the derivative of f plus boundary integrals.

With $d = 2, 3$ being the space dimesion and $\underline{x}$ the position vector, we find the vector expansion formulas:

$$
\begin{aligned}
\nabla \cdot (\underline{f} \, \underline{x}) &= \underline{f} + \underline{x} \, (\nabla \cdot \underline{f}) & (1.107) \\
\nabla \cdot (\underline{x} \, \underline{f}) &= d \, \underline{f} + \underline{x} \cdot \nabla \underline{f} & (1.108) \\
\nabla (\underline{x} \cdot \underline{f}) &= \underline{f} + \underline{x} \cdot \nabla \underline{f} + \underline{x} \times (\nabla \times \underline{f}) & (1.109) \\
\underline{x} \times (\underline{n} \times \underline{f}) &= \underline{n} \, (\underline{f} \cdot \underline{x}) - (\underline{n} \cdot \underline{x}) \, \underline{f}, & (1.110)
\end{aligned}
$$

From the volume integral for Eq. (1.107), we apply the divergence theorem to find an identity:

$$\int_V \underline{f} \, dV = - \int_V \underline{x} \, (\nabla \cdot \underline{f}) \, dV + \oint_S \underline{x} \, (\underline{n} \cdot \underline{f}) \, dS \tag{1.111}$$

Another form of Eq. (1.111) can be provided as follows.
First, subtracting Eq. (1.109) from Eq. (1.108) yields

$$\nabla \cdot (\underline{x} \, \underline{f}) - \nabla (\underline{x} \cdot \underline{f}) = (d - 1) \, \underline{f} - \underline{x} \times (\nabla \times \underline{f}) \tag{1.112}$$

Now we take volume integrals of this equation and apply the divergence theorem to find another identity, using Eq. (1.110):

$$
\begin{aligned}
\int_V \underline{f}\, dV &= \frac{1}{d-1} \int_V \underline{x} \times (\nabla \times \underline{f})\, dV + \frac{1}{d-1} \int_V \left\{ \nabla \cdot (\underline{x}\, \underline{f}) - \nabla(\underline{f} \cdot \underline{x}) \right\}\, dV \\
&= \frac{1}{d-1} \int_V \underline{x} \times (\nabla \times \underline{f})\, dV + \frac{1}{d-1} \oint_S \left\{ (\underline{n} \cdot \underline{x})\, \underline{f} - \underline{n}\, (\underline{f} \cdot \underline{x}) \right\}\, dS \\
&= \frac{1}{d-1} \int_V \underline{x} \times (\nabla \times \underline{f})\, dV - \frac{1}{d-1} \oint_S \underline{x} \times (\underline{n} \times \underline{f})\, dS \qquad (1.113)
\end{aligned}
$$

We note that the left-hand side of Eq. (1.112) and Eq. (1.113) is independent of the choice of the origin of $\underline{x}$, so must be the right-hand side.

1.3.3.1 Volume integral of first moment

We can also cast the first vector moment $\underline{x} \times \underline{f}$ to the second moments of $\nabla \times \underline{f}$:

$$
2 \int_V \underline{x} \times \underline{f}\, dV = -\int_V x^2 (\nabla \times \underline{f})\, dV + \oint_S x^2\, \underline{n} \times \underline{f}\, dS \qquad (1.114)
$$

$$
\int_V \underline{x} \times \underline{f}\, dV = \int_V \underline{x} \left\{ \underline{x} \cdot (\nabla \times \underline{f}) \right\}\, dV - \oint_S \left\{ (\underline{n} \times \underline{f}) \cdot \underline{x} \right\} \underline{x}\, dS \qquad (1.115)
$$

$$
3 \int_V \underline{x} \times \underline{f}\, dV = \int_V \underline{x} \times \left\{ \underline{x} \times (\nabla \times \underline{f}) \right\}\, dV - \oint_S \underline{x} \times \left\{ \underline{x} \times (\underline{n} \times \underline{f}) \right\}\, dS
$$
$$
\qquad (1.116)
$$

To derive Eq. (1.114) and Eq. (1.115), we have used the following relations and then applied the divergence theorem:

$$
\begin{aligned}
\nabla \times (x^2 \underline{f}) &= \nabla(x^2) \times \underline{f} + x^2 \nabla \times \underline{f} \\
&= 2\, \underline{x} \times \underline{f} + x^2 \nabla \times \underline{f} \qquad (1.117) \\
\nabla \cdot (\underline{f} \times \underline{x}\, \underline{x}) &= \nabla \cdot (\underline{f} \times \underline{x})\, \underline{x} + \underline{f} \times \underline{x} \\
&= \underline{x} \left\{ \underline{x} \cdot (\nabla \times \underline{f}) \right\} + \underline{f} \times \underline{x} \qquad (1.118) \\
(\underline{n} \times \underline{f}) \cdot \underline{x} &= \underline{n} \cdot (\underline{f} \times \underline{x}) \qquad (1.119)
\end{aligned}
$$

Equation (1.116) is the sum of Eq. (1.114) and Eq. (1.115) by aid of the relation $\underline{x} \times (\underline{x} \times \underline{a}) = \underline{x}\, (\underline{x} \cdot \underline{a}) - x^2\, \underline{a}$.

1.3.4   Surface integrals of a vector

The corresponding transformation rule on surface integral is, since $(\underline{n} \times \nabla) \times (\phi\,\underline{x}) = (\underline{n} \times \nabla\phi) \times \underline{x} - (d-1)\phi\,\underline{n}$,

$$\int_S \phi\,\underline{n}\,dS = -\frac{1}{d-1}\int_S \underline{x} \times (\underline{n} \times \nabla\phi)\,dS + \frac{1}{d-1}\oint_C \phi\,\underline{x} \times d\underline{x} \quad (1.120)$$

and for $d = 3$, the integral of tangent vector becomes

$$\int_S \underline{n} \times \underline{f}\,dS = -\int_S \underline{x} \times \{(\underline{n} \times \nabla) \times \underline{f}\}\,dS + \oint_C \underline{x} \times (d\underline{x} \times \underline{f}) \quad (1.121)$$

Equation (1.120) is a special case of Eq. (1.113) with $\underline{f} = \nabla\phi$. Here we apply the divergence theorem for a volume integral, in which the closed boundary surface can be regarded as being composed of two open surfaces (S_1 and S_2):

$$\int_{S_1+S_2} \phi\,\underline{n}\,dS = -\frac{1}{d-1}\int_{S_1+S_2} \underline{x} \times (\underline{n} \times \nabla\phi)\,dS \quad (1.122)$$

Then the surface integral over the first surface S_1 can be expressed in terms of integrals over the second part of the closed surface:

$$\begin{aligned}
\int_{S_1} \phi\,\underline{n}\,dS = {} & -\frac{1}{d-1}\int_{S_1} \underline{x} \times (\underline{n} \times \nabla\phi)\,dS \\
& -\frac{1}{d-1}\int_{S_2} \underline{x} \times (\underline{n} \times \nabla\phi)\,dS - \int_{S_2} \phi\,\underline{n}\,dS \quad (1.123)
\end{aligned}$$

Use of the relation $(\underline{n} \times \nabla) \times (\phi\,\underline{x}) = (\underline{n} \times \nabla\phi) \times \underline{x}) - (d-1)\,\phi\,\underline{n}$ for the integral over the second surface makes us to have

$$\begin{aligned}
\int_{S_1} \phi\,\underline{n}\,dS = {} & -\frac{1}{d-1}\int_{S_1} \underline{x} \times (\underline{n} \times \nabla\phi)\,dS + \frac{1}{d-1}\int_{S_2} (\underline{n} \times \nabla) \times (\phi\,\underline{x})\,dS \\
= {} & -\frac{1}{d-1}\int_{S_1} \underline{x} \times (\underline{n} \times \nabla\phi)\,dS + \frac{1}{d-1}\oint_{-C_2} d\underline{x} \times (\phi\,\underline{x}) \\
= {} & -\frac{1}{d-1}\int_{S_1} \underline{x} \times (\underline{n} \times \nabla\phi)\,dS + \frac{1}{d-1}\oint_{C_2} (\phi\,\underline{x}) \times d\underline{x} \quad (1.124)
\end{aligned}$$

by applying the Stokes theorem for the second integral.

Proof of Eq. (1.121)

According to the associated vector expansion formulas, we have

$$
\begin{aligned}
(\underline{n} \times \nabla) \times (\underline{f} \times \underline{x}) &= \epsilon_{pil}\, \epsilon_{ijk}\, n_j\, \frac{\partial}{\partial x_k}(\epsilon_{lmn}\, f_m\, x_n) \\
&= \epsilon_{lpi}\, \epsilon_{lmn}\, \epsilon_{ijk}\, n_j \left(\frac{\partial f_m}{\partial x_k}\, x_n + f_m\, \delta_{kn} \right) \\
&= (\delta_{pm}\, \delta_{in} - \delta_{pn}\, \delta_{im}) \left(\epsilon_{ijk}\, n_j\, \frac{\partial f_m}{\partial x_k}\, x_n + \epsilon_{ijk}\, n_j\, f_m\, \delta_{kn} \right) \\
&= \epsilon_{ijk}\, n_j\, \frac{\partial f_m}{\partial x_k}\, x_i - \epsilon_{ijk}\, n_j\, \frac{\partial f_i}{\partial x_k}\, x_n + \epsilon_{ijk}\, n_j\, f_m\, \delta_{ki} - \epsilon_{ijk}\, n_j\, f_i \\
&= \underline{x} \cdot (\underline{n} \times \nabla \underline{f}) - \{(\underline{n} \times \nabla) \cdot \underline{f}\}\, \underline{x} + \underline{n} \times \underline{f} \qquad (1.125)
\end{aligned}
$$

and, with a similar manipulation,

$$
\begin{aligned}
(\underline{n} \times \nabla) \times \underline{f} \times \underline{x} &= \underline{x} \cdot (\underline{n} \times \nabla \underline{f}) - (\underline{n} \times \nabla \underline{f}) \cdot \underline{x} & (1.126) \\
(\underline{n} \times \nabla)(\underline{f} \cdot \underline{x}) &= (\underline{n} \times \nabla \underline{f}) \cdot \underline{x} + \underline{n} \times \underline{f} & (1.127) \\
(\underline{n} \times \nabla) \cdot (\underline{f}\, \underline{x}) &= \{(\underline{n} \times \nabla) \cdot \underline{f}\}\, \underline{x} - \underline{n} \times \underline{f} & (1.128)
\end{aligned}
$$

Now, adding Eqs. (1.125) and (1.128) and subtracting Eqs. (1.126) and (1.127) from its result, we have

$$
\begin{aligned}
&(\underline{n} \times \nabla) \times (\underline{f} \times \underline{x}) + (\underline{n} \times \nabla) \cdot (\underline{f}\, \underline{x}) - (\underline{n} \times \nabla) \times \underline{f} \times \underline{x} - (\underline{n} \times \nabla)(\underline{f} \cdot \underline{x}) \\
&= -\underline{n} \times \underline{f} \qquad (1.129)
\end{aligned}
$$

We then take a surface integral for Eq. (1.129) and use Stokes theorem to yield

$$
\begin{aligned}
&\oint_C d\underline{x} \times (\underline{f} \times \underline{x}) + \int_S \underline{x} \times \{(\underline{n} \times \nabla) \times \underline{f}\}\, dS - \oint_C d\underline{x}\, (\underline{f} \cdot \underline{x}) + \oint_C d\underline{x} \cdot (\underline{f}\, \underline{x}) \\
&= -\int_S \underline{n} \times \underline{f}\, dS \qquad (1.130)
\end{aligned}
$$

Rearranging this equation, we provide Eq. (1.121):

$$
\begin{aligned}
\int_S \underline{n} \times \underline{f}\, dS &= -\oint_C \left\{ \underline{f}\,(\underline{x} \cdot d\underline{x}) - \underline{x}\,(\underline{f} \cdot d\underline{x}) \right\} - \int_S \underline{x} \times \left\{ (\underline{n} \times \nabla) \times \underline{f} \right\} dS \\
&\quad + \oint_C d\underline{x}\,(\underline{f} \cdot \underline{x}) - \oint_C d\underline{x} \cdot (\underline{f}\,\underline{x}) \\
&= \oint_C \underline{x} \times (d\underline{x} \times \underline{f}) - \int_S \underline{x} \times \left\{ (\underline{n} \times \nabla) \times \underline{f} \right\} dS \qquad (1.131)
\end{aligned}
$$

∎∎∎

1.3.4.1   Surface integrals of first moment

The surface integrals of the first moment $\underline{x} \times \underline{n}\phi$ and $\underline{x} \times (\underline{x} \times \underline{f})$ can also be transformed to the following alternative forms: [9]

$$
\int_S \underline{x} \times \underline{n}\,\phi\, dS = \frac{1}{2} \int_S x^2\, \underline{n} \times \nabla\phi\, dS - \frac{1}{2} \oint_C x^2\,\phi\, dl \quad (1.132)
$$

$$
\begin{aligned}
\int_S \underline{x} \times \underline{n}\,\phi\, dS &= -\int_S \underline{x} \left\{ \underline{x} \cdot (\underline{n} \times \nabla\phi) \right\} dS \\
&\quad + \oint_C \phi\,\underline{x}\,(\underline{x} \cdot d\underline{x}) \qquad (1.133)
\end{aligned}
$$

$$
\begin{aligned}
\int_S \underline{x} \times \underline{n}\,\phi\, dS &= -\frac{1}{3} \int_S \underline{x} \times \left\{ \underline{x} \times (\underline{n} \times \nabla\phi) \right\} dS \\
&\quad + \frac{1}{3} \oint_C \phi\,\underline{x} \times (\underline{x} \times d\underline{x}) \qquad (1.134)
\end{aligned}
$$

$$
\begin{aligned}
\int_S \underline{x} \times (\underline{n} \times \underline{f})\, dS &= \int_S \underline{\underline{S}} \cdot \left\{ (\underline{n} \times \nabla) \times \underline{f} \right\} dS \\
&\quad - \oint_C \underline{\underline{S}} \cdot (d\underline{x} \times \underline{f}) \qquad (1.135)
\end{aligned}
$$

where $\underline{\underline{S}}$ is the second order tensor depending only on $\underline{x}$:

$$
\underline{\underline{S}} = \frac{1}{2}\,x^2\,\underline{\underline{I}} - \underline{x}\,\underline{x} \quad \text{or} \quad S_{ij} = \frac{1}{2}\,x^2\,\delta_{ij} - x_i\,x_j \qquad (1.136)
$$

Equation (1.133) is obtained from applying the Stokes' theorem to the sur-

---

[9] See Wu, J.-Z, Ma, H.-Y. and Zhou, M.-D. (2006), *Vorticity and Vortex Dynamics*, Springer, p. 702.

face integrals of the following identity:

$$
\begin{aligned}
(\underline{n} \times \nabla) \cdot (\phi \, \underline{x} \, \underline{x}) &= \underline{n} \cdot \{\nabla \times (\phi \, \underline{x} \, \underline{x})\} = n_i \left\{ \epsilon_{ijk} \frac{\partial}{\partial x_j} (\phi \, x_k \, x_l) \right\} \\
&= n_i \left\{ \epsilon_{ijk} \frac{\partial \phi}{\partial x_j} x_k \, x_l + \phi \, \epsilon_{ijk} \, x_k \, \delta_{jl} \right\} \\
&= n_i \left\{ \epsilon_{ijk} \frac{\partial \phi}{\partial x_j} x_k \, x_l + \phi \, \epsilon_{ilk} \, x_k \right\} \\
&= \underline{n} \cdot (\nabla \phi \times \underline{x}) \, \underline{x} - \phi \, \underline{n} \times \underline{x} \\
&= \{\underline{n} \times \nabla \phi) \cdot \underline{x}\} \, \underline{x} + \underline{x} \times (\phi \, \underline{n}) \qquad (1.137)
\end{aligned}
$$

Note that Eq. (1.134) is obtained from a linear combination of Eq. (1.132) and Eq. (1.133).

1.4   Curvilinear Coordinates on Lines and Surfaces

We are used to encounter Cartesian components in vector and tensor analysis. In some situations, local curvilinear coordinates along a line or surface are more convenient, especially when they orthogonal. Therefore they are as intrinsic as possible, with an arbitrarily moving origin thereon. [10]

1.4.1   Intrinsic line frame

If we are interested in the flow behavior along a smooth line C with arc length element ds, say a streamline or a vortex line, the intrinsic coordinate system with origin $O(\underline{x})$ on C has three orthonormal basis vectors: the tangent vector $\underline{t} = \dfrac{\partial \underline{x}}{\partial s}$, the binormal $\underline{b} = \underline{t} \times \underline{n}$, and the principal normal $\underline{n}$ (toward the center of curvature), see Figure **1.3** .

---

[10]Most of material covered in this section has been taken from
(1) Kreyszig, E. (2006), *Advanced Engineering Mathematics*, 9th ed., Wiley, pp. 397-398,
(2) Wu, J.-Z, Ma, H.-Y. and Zhou, M.-D. (2006), *Vorticity and Vortex Dynamics*, Springer, pp. 705-712,
(3) Farin G. & Hansford D. (2000), *The Essentials of CAGD*, A K Peters, Natick, MA, pp. 119-121, and
(4) Farin G. (2002), *Curves and Surfaces for CAGD-A Practrical Guide*, 5th ed., Morgan Kaufmann Publishers, pp. 181-187, 419-421.
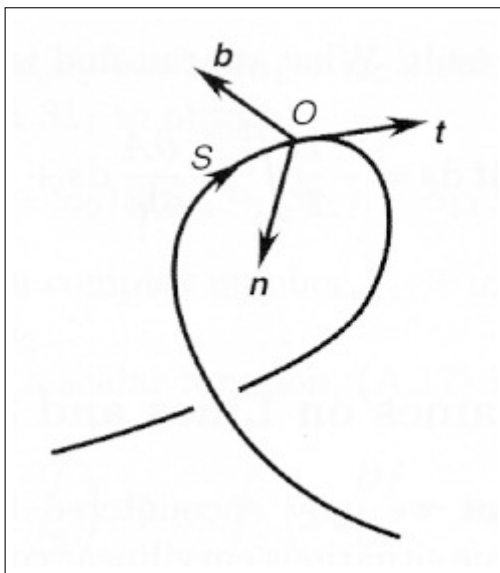
Figure 1.3 Intrinsic 3 orthonomal basis vectors along a curve in a local curvilinear coordinate system. From Wu, Ma and Zhou (2006), p. 706.

Three axes $\underline{t}$, $\underline{b}$ and $\underline{n}$ are defined as

$$\underline{t}(s) = \frac{\partial \underline{x}}{\partial s} \bigg/ \left| \frac{\partial \underline{x}}{\partial s} \right| \tag{1.138}$$

$$\underline{b}(s) = \left(\frac{\partial \underline{x}}{\partial s} \times \frac{\partial^2 \underline{x}}{\partial s^2} \right) \bigg/ \left| \frac{\partial \underline{x}}{\partial s} \times \frac{\partial^2 \underline{x}}{\partial s^2} \right| \tag{1.139}$$

$$\underline{n}(s) = \underline{b} \times \underline{t} \tag{1.140}$$

The plane spanned by the point $\underline{x}$, $\underline{t}$, and $\underline{n}$ is called the **osculating plane**. The planes spanned by $(\underline{x}, \underline{t}, \underline{b})$ and $(\underline{x}, \underline{b}, \underline{n})$ are called, respectively, the **rectifying plane** and the **normal plane**. [11]

The key of using this frame is to know how the basis vectors change their directions as s varies. This is given by the 'Frenet-Serret formulas', form the entire basis of spatial curve theory in classical differential geometry:

$$\frac{\partial \underline{t}}{\partial s} = \kappa \, \underline{n}, \quad \frac{\partial \underline{n}}{\partial s} = -\kappa \, \underline{t} + \tau \, \underline{b}, \quad \frac{\partial \underline{b}}{\partial s} = -\tau \, \underline{n} \tag{1.141}$$

---

[11](1) The equation of the osculating plane is $det \left[\underline{y} - \underline{x}, \frac{\partial \underline{x}}{\partial s}, \frac{\partial^2 \underline{x}}{\partial s^2} \right] = 0$, where $\underline{y}$ denotes any point on the plane.

(2) A curve C in a surface is a *geodesic* of the surface if the second derivative $\left(\frac{\partial^2 \underline{x}}{\partial s^2} \right)$ of the position vector of C is always normal to the surface. (See O'Neill (1966), p. 228 or Aris (1962), p. 201).

where κ and τ are the curvature and torsion of C, respectively. The curvature radius is $r_c = 1/\kappa$ with $d\,r = -d\,n$. A formula for the curvature is given by

$$\kappa(s) = \frac{\left| \frac{\partial \underline{x}}{\partial s} \times \frac{\partial^2 \underline{x}}{\partial s^2} \right|}{\left| \frac{\partial \underline{x}}{\partial s} \right|^3} \tag{1.142}$$

A point where the curvature changes sign is called *inflection points*. The torsion measures how much a curve deviates from a plane curve, i.e., it is the curvature of the projection of C onto the $(\underline{n}, \underline{b})$ plane (i.e., the normal plane). Similarly, a formula for the torsion is given by

$$\tau(s) = \frac{det \left[\frac{\partial \underline{x}}{\partial s}, \frac{\partial^2 \underline{x}}{\partial s^2}, \frac{\partial^3 \underline{x}}{\partial s^3} \right]}{\left| \frac{\partial \underline{x}}{\partial s} \times \frac{\partial^2 \underline{x}}{\partial s^2} \right|^2} \tag{1.143}$$

The Taylor expansion of $\underline{x}(s + \triangle s)$ can be written as

$$\begin{aligned}
\underline{x}(s + \triangle s) &= \underline{x}(s) + \triangle s\,\underline{t} + \frac{1}{2}\kappa\,\triangle s^2\,\underline{n} \\
&\quad - \frac{1}{6}\kappa^2\,\triangle s^3\,\underline{t} + \frac{1}{6}\kappa'\,\triangle s^3\,\underline{n} + \frac{1}{6}\kappa\,\tau\,\triangle s^3\,\underline{b} \\
&\quad + \cdots
\end{aligned} \tag{1.144}$$

For 2-D curves only, the slope κ' is given by, [12]

$$\frac{d\kappa}{ds} = \frac{det \left[\frac{\partial \underline{x}}{\partial s}, \frac{\partial^3 \underline{x}}{\partial s^3} \right]}{\left| \frac{\partial \underline{x}}{\partial s} \right|^4} - 3 \left(\frac{\partial \underline{x}}{\partial s} \right) \left(\frac{\partial^2 \underline{x}}{\partial s^2} \right) \frac{det \left[\frac{\partial \underline{x}}{\partial s}, \frac{\partial^2 \underline{x}}{\partial s^2} \right]}{\left| \frac{\partial \underline{x}}{\partial s} \right|^6} \tag{1.145}$$

Now, let the differential distance form O along the directions of $\underline{n}$ and $\underline{b}$ be

---

[12] See Farin G. (2002), *Curves and Surfaces for CAGD-A Practrical Guide*, 5th ed., Morgan Kaufmann Publishers, p. 421.

dn and db, respectively. Then

$$\nabla = \underline{t}\,\frac{\partial}{\partial s} + \underline{n}\,\frac{\partial}{\partial n} + \underline{b}\,\frac{\partial}{\partial b} \tag{1.146}$$

It involves curves along $\underline{n}$ and $\underline{b}$ directions, for which the Frenet-Serret formulas can be applied to complete the gradient operation.

1.4.1.1   Example: Propeller pitch helix

Let us consider the constant-pitch helix of a propeller blade. The position vector is expressed as, by converting a cylindrical coordinates (r, θ, x) into the Cartersian coordinates,

$$\underline{x}(\theta) = r\,\theta\,\tan\phi\,\underline{i} + r\cos\theta\,\underline{j} + r\sin\theta\,\underline{k} \tag{1.147}$$

where ϕ is the constant pitch angle. Simple calculations yield

$$\frac{\partial \underline{x}}{\partial \theta} = r\tan\phi\,\underline{i} - r\sin\theta\,\underline{j} + r\cos\theta\,\underline{k} \tag{1.148}$$

$$\frac{\partial^2 \underline{x}}{\partial \theta^2} = -r\cos\theta\,\underline{j} - r\sin\theta\,\underline{k} \tag{1.149}$$

$$\frac{\partial \underline{x}}{\partial \theta} \times \frac{\partial^2 \underline{x}}{\partial \theta^2} = -r^2\cos\theta\tan\phi\,\underline{k} + r^2\tan\phi\sin\theta\,\underline{j} + r^2\,\underline{i} \tag{1.150}$$

from which the curvature becomes

$$\kappa = \frac{r^2(1 + \tan^2\phi)^{1/2}}{r^3(1 + \tan^2\phi)^{3/2}} = \frac{\cos^2\phi}{r} \tag{1.151}$$

The radius of curvature is given by $r_c = \dfrac{1}{\kappa} = \dfrac{r}{\cos^2\phi}$. The center of the *osculating circle* is, in the direction of the normal vector $\underline{n}$,

$$\underline{x}_c = \underline{x} + r_c\,\underline{n} \tag{1.152}$$

By developing of such an osculating circle onto a (2-D) plane, we can take two end points of the circular arc with the radius r_c that correspond to, respectively, the leading edge and the trailing edge of the blade section.

By assembling the corresponding two end points of the osculating circular arcs for pitch helices at other radial positions, we can produce a developed outline of the propeller blade. In general, the corresponding radii of curvature might be different each other.

1.4.1.2 Example: Streamline intrinsic frame

For example, if C is a streamline such that $\underline{u} = q\,\underline{t}$, then the divergence of the velocity becomes

$$\nabla \cdot \underline{u} = \frac{\partial q}{\partial s} + q\,\nabla \cdot \underline{t} = \frac{\partial q}{\partial s} + q\left(\underline{n} \cdot \frac{\partial \underline{t}}{\partial n} + \underline{b} \cdot \frac{\partial \underline{t}}{\partial b}\right) \qquad (1.153)$$

Similarly, the curl operation for $\underline{t}$ is

$$\nabla \times \underline{t} = \left(\underline{n} \times \frac{\partial \underline{t}}{\partial n} + \underline{b} \times \frac{\partial \underline{t}}{\partial b}\right) + \kappa\,\underline{b} \qquad (1.154)$$

Here, since $|\underline{t}| = 1$, it follows that

$$\underline{n} \cdot \left(\underline{n} \times \frac{\partial \underline{t}}{\partial n} + \underline{b} \times \frac{\partial \underline{t}}{\partial b}\right) = \underline{t} \cdot \frac{\partial \underline{t}}{\partial b} = \frac{1}{2}\frac{\partial |\underline{t}|^2}{\partial b} = 0 \qquad (1.155)$$

$$\underline{b} \cdot \left(\underline{n} \times \frac{\partial \underline{t}}{\partial n} + \underline{b} \times \frac{\partial \underline{t}}{\partial b}\right) = -\underline{t} \cdot \frac{\partial \underline{t}}{\partial n} = -\frac{1}{2}\frac{\partial |\underline{t}|^2}{\partial b} = 0 \qquad (1.156)$$

The first term of $\nabla \times \underline{t}$ in (1.154) must be along the $\underline{t}$ direction, with the magnitude known as the 'torsion of neighboring vector lines'.

$$\xi \equiv \underline{t} \cdot (\nabla \times \underline{t}) = \underline{b} \cdot \frac{\partial \underline{t}}{\partial n} - \underline{n} \cdot \frac{\partial \underline{t}}{\partial b} \qquad (1.157)$$

Using this notation we obtain

$$\nabla \times \underline{t} = \xi\,\underline{t} + \kappa\,\underline{b} \qquad (1.158)$$

This result enables us to derive the vorticity expression in the streamline

intrinsic frame

$$\underline{\omega} = \nabla \times (q\,\underline{t}) = \nabla q \times \underline{t} + q\,\nabla \times \underline{t} = \nabla q \times \underline{t} + q\,\xi\,\underline{t} + q\,\kappa\,\underline{b} \qquad (1.159)$$

The first term of this equation is

$$(\nabla q) \times \underline{t} = \frac{\partial q}{\partial b}\,\underline{n} - \frac{\partial q}{\partial n}\,\underline{b} \qquad (1.160)$$

so we obtain

$$\underline{\omega} = q\,\xi\,\underline{t} + \frac{\partial q}{\partial b}\,\underline{n} + \left(q\,\kappa - \frac{\partial q}{\partial n}\right)\underline{b} \qquad (1.161)$$

Thus, $\xi = 0$ if $\underline{\omega} \cdot \underline{u}\,(= q^2\,\xi) = 0$.

1.4.2   Curvilinear orthogonal coordinates

We will have need for the expressions of several vector differential operators in terms of curvilinear orthogonal coordinates. [13] Suppose x_1, x_2, x_3 are mutually orthogonal curvilinear coordinates.

1.4.2.1   Line element

When the line-element vector in the orthogonal system is expressed in terms of a scalar multiple, the scalar multiple is usually written h_i and is called a scale factor:

$$d\underline{s} = (h_1\,dx_1, h_2\,dx_2, h_3\,dx_3) \qquad (1.162)$$

where $h_1 = h_1(x_1, x_2, x_3) = \left|\dfrac{\partial \underline{s}}{\partial x_1}\right| = \left\{\left(\dfrac{\partial s_1}{\partial x_1}\right)^2 + \left(\dfrac{\partial s_2}{\partial x_1}\right)^2 + \left(\dfrac{\partial s_3}{\partial x_1}\right)^2\right\}^{1/2}$ etc.

The base vectors, $\dfrac{\partial \underline{s}}{\partial x_i}$, is then expressed in terms of the scale factor and a

---

[13] For example, expressions for the related common differentials in spherical, cylindrical and polar coordinate systems are found in Batchelor, G. K. (1967), *An Introduction to Fluid Dynamics*, Cambridge University Press, Cambridge, pp. 598–603.

unit vector, e.g.

$$\frac{\partial \underline{s}}{\partial x_1} = h_1(x_1, x_2, x_3) \, \underline{e}_1(x_1, x_2, x_3) \tag{1.163}$$

For example, if we take spherical coordinates $x_1 = r, x_2 = \theta$, and $x_3 = \phi$ where ϕ is the azimuthal angle about the axis $\theta = 0$, the line element is $d\underline{s} = (dr, \, r \, d\theta, \, r \sin \theta \, d\phi)$; hence the scale factors $h_1 = 1, h_2 = r, h_3 = r \sin \theta$.

If we take cylindrical coordinates $x_1 = \rho, x_2 = \phi$, and $x_3 = z$ where ϕ is the azimuthal angle about the axis $\rho = 0$, the line element is $d\underline{s} = (d\rho, \rho \, d\phi, dz)$; hence the scale factors $h_1 = 1, h_2 = \rho, h_3 = 1$.
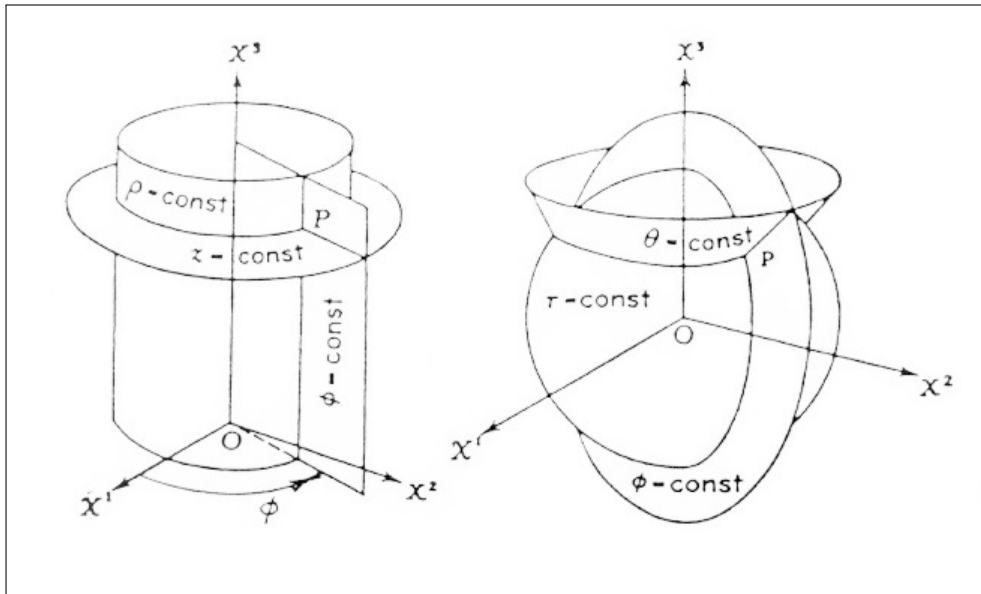
Figure 1.4 Cylindrical and spherical coordinate systems. From Brockett(Lecture note NA520, 1988), p.1-30a.

The scalar differential arc length, denoted by ds is determined from

$$\begin{aligned} ds^2 &= d\underline{s} \cdot d\underline{s} = \left(\frac{\partial \underline{s}}{\partial x_i} \, dx_i \right) \cdot \left(\frac{\partial \underline{s}}{\partial x_j} \, dx_j \right) \\ &= h_i \, h_j \, dx_i \, dx_j \, \underline{e}_i \cdot \underline{e}_j \end{aligned} \tag{1.164}$$

When the unit base vectors are orthogonal, this expression reduces to the simple form

$$ds^2 = h_1^2 \, dx_1^2 + h_2^2 \, dx_2^2 + h_3^2 \, dx_3^2 \tag{1.165}$$

By the triple scalar product, the volume element can be obtained from the elemental arc length vectors:

$$dV = \pm \left(\frac{\partial \underline{s}}{\partial x_1} dx_1 \right) \cdot \left(\frac{\partial \underline{s}}{\partial x_2} \times \frac{\partial \underline{s}}{\partial x_3} dx_2 \, dx_3 \right) \qquad (1.166)$$

where the $\pm$ sign is necessary to provide a positive element of volume. For an orthogonal coordinate system, with $\dfrac{\partial \underline{s}}{\partial x_1} = h_1 \underline{e}_1$, etc, the volume element is

$$dV = h_1 \, h_2 \, h_3 \, dx_1 \, dx_2 \, dx_3 \qquad (1.167)$$

since $\underline{e}_1 \cdot (\underline{e}_2 \times \underline{e}_3) = \pm 1$. Multiplication of the scale factors corresponds to the Jacobian $J = h_1 \, h_2 \, h_3$.

1.4.2.2 Gradient (∇u)

We have the formula $du = d\underline{s} \cdot \nabla u$, which is completely general. Also in any coordinate system, we have

$$du = \frac{\partial u}{\partial x_1} \, dx_1 + \frac{\partial u}{\partial x_2} \, dx_2 + \frac{\partial u}{\partial x_3} \, dx_3 \qquad (1.168)$$

Equating these two relations gives

$$\frac{\partial u}{\partial x_1} \, dx_1 + \frac{\partial u}{\partial x_2} \, dx_2 + \frac{\partial u}{\partial x_3} \, dx_3 = h_1 \, dx_1 \, (\nabla u)_1 + h_2 \, dx_2 \, (\nabla u)_2 + h_3 \, dx_3 \, (\nabla u)_3 \qquad (1.169)$$

Now dx_1, dx_2, dx_3 are completely arbitrary; hence this equation can be true only if their coefficients are equal. Thus

$$\nabla u = \left(\frac{1}{h_1} \frac{\partial u}{\partial x_1}, \frac{1}{h_2} \frac{\partial u}{\partial x_2}, \frac{1}{h_3} \frac{\partial u}{\partial x_3} \right) \qquad (1.170)$$

1.4.2.3 Divergence $(\nabla \cdot \underline{v})$

For this operator we return to the original definition; thus, denoting by v_1, v_2, v_3 the components of $\underline{v}$ in the 1, 2, 3 directions at any point,

$$
\begin{aligned}
\nabla \cdot \underline{v} \approx\ & (h_1\, h_2\, h_3\, \triangle x_1\, \triangle x_2\, \triangle x_3)^{-1} \\
& \left\{ -v_1\, h_2\, h_3\, \triangle x_2\, \triangle x_3 - v_2\, h_3\, h_1\, \triangle x_3\, \triangle x_1 - v_3 h_1 h_2 \triangle x_1 \triangle x_2 \right. \\
& + \left[v_1\, h_2\, h_3 + \frac{\partial}{\partial x_1}(v_1\, h_2\, h_3)\, \triangle x_1 \right] \triangle x_2\, \triangle x_3 \\
& + \left[v_2\, h_3\, h_1 + \frac{\partial}{\partial x_2}(v_2\, h_3\, h_1)\, \triangle x_2 \right] \triangle x_3\, \triangle x_1 \\
& + \left. \left[v_3\, h_1\, h_2 + \frac{\partial}{\partial x_3}(v_3\, h_1\, h_2)\, \triangle x_3 \right] \triangle x_1\, \triangle x_2 \right\} \\
=\ & \frac{1}{h_1\, h_2\, h_3} \left\{ \frac{\partial}{\partial x_1}(h_2\, h_3\, v_1) + \frac{\partial}{\partial x_2}(h_3\, h_1\, v_2) + \frac{\partial}{\partial x_3}(h_1\, h_2\, v_3) \right\}
\end{aligned}
$$

$$(1.171)$$

1.4.2.4 Curl $(\nabla \times \underline{v})$

Apply Stoke's Theorem to one face of the element of a cube, say the 1-3 face:

$$
\begin{aligned}
\int_S \underline{n} \cdot \nabla \times \underline{v}\, dS &= \oint_C \underline{v} \cdot d\underline{s} \\
&= v_1\, h_1\, \triangle x_1 - v_3\, h_3\, \triangle x_3 \\
&\quad + \left[v_3\, h_3 + \frac{\partial}{\partial x_1}(v_3\, h_3)\, \triangle x_1 \right] \triangle x_3 - \left[v_1\, h_1 + \frac{\partial}{\partial x_3}(v_1\, h_1)\, \triangle x_3 \right] \triangle x_1 \\
&= \left[\frac{\partial}{\partial x_1}(h_3\, v_3) - \frac{\partial}{\partial x_3}(h_1\, v_1) \right] \triangle x_1\, \triangle x_3
\end{aligned}
$$

$$(1.172)$$

But also

$$
\int_S \underline{n} \cdot \nabla \times \underline{v}\, dS \approx -h_1\, h_3\, \triangle x_1\, \triangle x_3\, (\nabla \times \underline{v})_2
$$

$$(1.173)$$

Thus, by cyclic substitution,

$$
\begin{aligned}
(\nabla \times \underline{v})_2 &= \frac{1}{h_3\, h_1} \left[\frac{\partial}{\partial x_3}(h_1\, v_1) - \frac{\partial}{\partial x_1}(h_3\, v_3) \right] \\
(\nabla \times \underline{v})_3 &= \frac{1}{h_1\, h_2} \left[\frac{\partial}{\partial x_1}(h_2\, v_2) - \frac{\partial}{\partial x_2}(h_1\, v_1) \right] \\
(\nabla \times \underline{v})_1 &= \frac{1}{h_2\, h_3} \left[\frac{\partial}{\partial x_2}(h_3\, v_3) - \frac{\partial}{\partial x_3}(h_2\, v_2) \right]
\end{aligned}
\tag{1.174}
$$

or, symbolically

$$
\nabla \times \underline{v} = \frac{1}{h_1\, h_2\, h_3}
\begin{vmatrix}
h_1\, \underline{i}_1 & h_2\, \underline{i}_2 & h_3\, \underline{i}_3 \\
\dfrac{\partial}{\partial x_1} & \dfrac{\partial}{\partial x_2} & \dfrac{\partial}{\partial x_3} \\
h_1\, v_1 & h_2\, v_2 & h_3\, v_3
\end{vmatrix}
\tag{1.175}
$$

For example, if we take spherical coordinates $x_1 = r$, $x_2 = \theta$, and $x_3 = \alpha$ where α is the azimuthal angle about the axis $\theta = 0$,

$$
\begin{aligned}
\nabla \times \underline{v} &= \frac{\underline{e}_r}{r \sin\theta} \left\{ \frac{\partial(v_\alpha\, \sin\theta)}{\partial\theta} - \frac{\partial v_\theta}{\partial\alpha} \right\} \\
&+ \frac{\underline{e}_\theta}{r} \left\{ \frac{1}{\sin\theta} \frac{\partial v_r}{\partial\alpha} - \frac{\partial(r\, v_\alpha)}{\partial r} \right\} \\
&+ \frac{\underline{e}_\alpha}{r} \left\{ \frac{\partial(r\, v_\theta)}{\partial r} - \frac{\partial(r\, v_r)}{\partial\theta} \right\}
\end{aligned}
\tag{1.176}
$$

1.4.2.5   Laplacian ($\nabla^2 u$)

For $\nabla^2 u$, we simply employ Eqs. (1.170) and (1.171) above:

$$
\begin{aligned}
\nabla^2 u = \nabla \cdot (\nabla u) = \\
\frac{1}{h_1\, h_2\, h_3} \left\{ \frac{\partial}{\partial x_1}\left(\frac{h_2\, h_3}{h_1} \frac{\partial u}{\partial x_1} \right) + \frac{\partial}{\partial x_2}\left(\frac{h_3\, h_1}{h_2} \frac{\partial u}{\partial x_2} \right) + \frac{\partial}{\partial x_3}\left(\frac{h_1\, h_2}{h_3} \frac{\partial u}{\partial x_3} \right) \right\}
\end{aligned}
\tag{1.177}
$$

The most convenient way to write out $\nabla^2 \underline{v}$ is by use of expansion formula

Eq. (1.72):

$$\nabla^2 \underline{v} = \nabla(\nabla \cdot \underline{v}) - \nabla \times (\nabla \times \underline{v}) \tag{1.178}$$

which can be expanded by use of formulas, Eqs. (1.170), (1.171), and (1.175).

1.4.2.6 Convection term $(\underline{u} \cdot \nabla \underline{v})$

This useful vector appears in the Navier-Stokes equation when we write the time rate of flow momentum in Eulerian description sense. Performing very complicated procedure but straightforward manipulation, we arrive at the following result:

$$
\begin{aligned}
(\underline{u} \cdot \nabla \underline{v})_1 &= \frac{1}{h_1}\left[u_1 \frac{\partial v_1}{\partial x_1} + u_2 \frac{\partial v_2}{\partial x_1} + u_3 \frac{\partial v_3}{\partial x_1} \right. \\
&\quad \left. + \frac{1}{h_2}(u_1 v_2 - u_2 v_1)\frac{\partial h_1}{\partial x_2} + \frac{1}{h_3}(u_1 v_3 - u_3 v_1)\frac{\partial h_1}{\partial x_3} \right] \\
&\quad - \frac{u_2}{h_1 h_2}\left[\frac{\partial(h_2 v_2)}{\partial x_1} - \frac{\partial(h_1 v_1)}{\partial x_2} \right] + \frac{u_3}{h_3 h_1}\left[\frac{\partial(h_1 v_1)}{\partial x_3} - \frac{\partial(h_3 v_3)}{\partial x_1} \right]
\end{aligned}
\tag{1.179}
$$

$$
\begin{aligned}
(\underline{u} \cdot \nabla \underline{v})_2 &= \frac{1}{h_2}\left[u_1 \frac{\partial v_1}{\partial x_2} + u_2 \frac{\partial v_2}{\partial x_2} + u_3 \frac{\partial v_3}{\partial x_2} \right. \\
&\quad \left. + \frac{1}{h_3}(u_2 v_3 - u_3 v_2)\frac{\partial h_2}{\partial x_3} + \frac{1}{h_1}(u_2 v_1 - u_1 v_2)\frac{\partial h_2}{\partial x_1} \right] \\
&\quad - \frac{u_3}{h_2 h_3}\left[\frac{\partial(h_3 v_3)}{\partial x_2} - \frac{\partial(h_2 v_2)}{\partial x_3} \right] + \frac{u_1}{h_1 h_2}\left[\frac{\partial(h_2 v_2)}{\partial x_1} - \frac{\partial(h_1 v_1)}{\partial x_2} \right]
\end{aligned}
\tag{1.180}
$$

$$
\begin{aligned}
(\underline{u} \cdot \nabla \underline{v})_3 &= \frac{1}{h_3}\left[u_1 \frac{\partial v_1}{\partial x_3} + u_2 \frac{\partial v_2}{\partial x_3} + u_3 \frac{\partial v_3}{\partial x_3} \right. \\
&\quad \left. + \frac{1}{h_1}(u_3 v_1 - u_1 v_3)\frac{\partial h_3}{\partial x_1} + \frac{1}{h_2}(u_3 v_2 - u_2 v_3)\frac{\partial h_3}{\partial x_2} \right] \\
&\quad - \frac{u_1}{h_3 h_1}\left[\frac{\partial(h_1 v_1)}{\partial x_3} - \frac{\partial(h_3 v_3)}{\partial x_1} \right] + \frac{u_2}{h_2 h_3}\left[\frac{\partial(h_3 v_3)}{\partial x_2} - \frac{\partial(h_2 v_2)}{\partial x_3} \right]
\end{aligned}
\tag{1.181}
$$

1.5   Tensors of Second Order

For example, let us consider a stress tensor that is a key quantity in continuum mechanics. [14] A stress is a force per unit area, in which force and an element of area are vectors. The area element have to specify both its magnitude and the direction of its normal. If $\underline{F}$ denotes the force and $\underline{S}$ is the area element, the stress tensor $\underline{\underline{T}}$ might be thought of as $\underline{F}/\underline{S}$. This quotient of two vectors cannot be defined, but rather we can define $\underline{F}$ as $\underline{S} \cdot \underline{\underline{T}}$. The stress tensor at a point $\underline{\underline{T}}$ becomes a newly physical quantity associated with two directions. In fact, it needs 9 numbers to specify the stress tensor in a reference system corresponding to the 9 possible combinations of 2 base vectors.

A <u>second-order tensor</u> is a set of nine numbers τ_{ij}, having the property that when transferred from the x_1, x_2, x_3 system to the x'_1, x'_2, x'_3 system the corresponding quantities are given by

$$\tau'_{ij} = \sum_{k=1}^{3} \sum_{\ell=1}^{3} a_{ki} \, a_{\ell j} \, \tau_{k\ell}, \quad \text{for} \quad i, j = 1, 2, 3 \qquad (1.182)$$

1.5.1   Dyadic products

Much of our work can be simplified if we extend our definitions of vector multiplication to include the *dyadic product $\underline{u}\,\underline{v}$*. For our purpose, this need only be defined by the relations

$$\begin{aligned}
(\underline{u}\,\underline{v}) \cdot \underline{w} &\equiv \underline{u}\,(\underline{v} \cdot \underline{w}) \\
\underline{w} \cdot (\underline{u}\,\underline{v}) &\equiv (\underline{w} \cdot \underline{u})\,\underline{v}
\end{aligned} \qquad (1.183)$$

Actually the dyadic product $\underline{u}\,\underline{v}$ is a special form of *second-order tensor*; it can easily be seen to satisfy the definition of such a tensor. This definition may be stated as follows, with reference to the x_i and x'_i coordinate systems.

In the case of $\underline{u}\,\underline{v}$, of course, the nine numbers involved are the products $u_i\,v_j\,(i, j = 1, 2, 3)$.

---

[14]See Aris, R. (1962), *Vectors, Tensors and the Basic Equations of Fluid Mechanics*, Prentice Hall, p. 5.

Let us consider some examples:

(1) For $\nabla(\underline{u} \cdot \underline{v})$, using dyadic notation, $\nabla(\underline{u} \cdot \underline{v}) = (\nabla \underline{u}) \cdot \underline{v} + (\nabla \underline{v}) \cdot \underline{u}$.

(2) Laplacian $\nabla^2 \underline{v} = \nabla \cdot (\nabla \underline{v})$.

(3) When we define $(\underline{u}\,\underline{v}) \times \underline{w} \equiv \underline{u}(\underline{v} \times \underline{w})$ and $\underline{w} \times (\underline{u}\,\underline{v}) \equiv (\underline{w} \times \underline{u})\underline{v}$, these are obviously dyadics.

(4) If ϕ is any dyadic product, $\phi \cdot (\underline{a} \times \underline{b}) = (\phi \times \underline{a}) \cdot \underline{b}$.

(5) Let us look at the more important example. Let u_i be a vector, and consider the set of nine numbers $\partial u_i / \partial x_j$. This is easily shown to be a second-order tensor. It might be represented by the symbol *grad* $\underline{u}$ or $\nabla \underline{u}$.

1.5.2   Gradient of a vector

Now, consider the gradient of a vector, $\nabla \underline{u}$, which is involved into the convection and the diffusion terms of the Navier-Stokes equations.
The velocity change at a point $d\underline{u}$ is

$$d\underline{u} = (d\underline{x} \cdot \nabla)\,\underline{u} \tag{1.184}$$

The gradient of a vector is defined by, in a similar fashion to the gradient of a scalar,

$$\nabla \underline{u} = \lim_{V \to 0} \frac{1}{V} \oint_S \underline{n}\,\underline{u}\,dS = \frac{\partial u_j}{\partial x_i} \tag{1.185}$$

In a rectangular Cartesian coordinate system, the gradient of a vector $\underline{u} = u_1\,\underline{i} + u_2\,\underline{j} + u_3\,\underline{k}$ is

$$\nabla \underline{u} = \frac{\partial u_1}{\partial x_1}\,\underline{i}\,\underline{i} + \frac{\partial u_2}{\partial x_1}\,\underline{i}\,\underline{j} + \frac{\partial u_3}{\partial x_1}\,\underline{i}\,\underline{k} + \cdots \text{ similar 6 terms} \tag{1.186}$$

In general orthogonal curvilinear coordinates, the gradient of a vector $\underline{u} = u_1 \, \underline{e}_1 + u_2 \, \underline{e}_2 + u_3 \, \underline{e}_3$, is [15]

$$
\begin{aligned}
\nabla \underline{u} \; = \;\; & \frac{1}{h_1} \left(\frac{\partial u_1}{\partial x_1} + \frac{u_2}{h_2} \frac{\partial h_1}{\partial x_2} + \frac{u_3}{h_3} \frac{\partial h_1}{\partial x_3} \right) \underline{e}_1 \, \underline{e}_1 + \frac{1}{h_1} \left(\frac{\partial v_2}{\partial x_1} - \frac{v_1}{h_2} \frac{\partial h_1}{\partial x_2} \right) \underline{e}_1 \, \underline{e}_2 \\
& + \frac{1}{h_1} \left(\frac{\partial v_3}{\partial x_1} - \frac{v_1}{h_3} \frac{\partial h_1}{\partial x_3} \right) \underline{e}_1 \, \underline{e}_3 + \cdots \text{ similar 6 terms} \qquad (1.187)
\end{aligned}
$$

If the vector $\underline{v}$ is a velocity vector in the field of fluid mechanics, this is often resolved into a symmetric and antisymmetric form:

$$
\begin{aligned}
\nabla \underline{v} \; = \;\; & \frac{1}{2} \left[(\nabla \underline{v} + \nabla \underline{v}^T) + (\nabla \underline{v} - \nabla \underline{v}^T) \right] \\
= \;\; & \frac{1}{2} \, def(\underline{v}) + \frac{1}{2} \, rot(\underline{v}) \qquad (1.188)
\end{aligned}
$$

where, if we consider a second-order tensor to be a 3×3 matrix, the superscript T stand for transpose of the matrix which is the operation described by interchanging the rows and columns of the matrix. The first term is called the *strain rate tensor*, having 6 independent components. It represents (i) normal strain rate and (ii) shear strain rate which cause stress in fluid.

The second term is called the *spin tensor* or *vorticity tensor* $\underline{\underline{\Omega}}$, having only off-diagonal components. It represents rigid body rotation of a fluid element.

1.6   Transport Theorem

We will have need for the rate of change of an integral taken over a volume moving through a field

$$
\frac{d}{dt} \int_{V(t)} F(\underline{x}, t) \, dV \qquad (1.189)
$$

where $F(\underline{x}, t)$ may be a scalar, vector or tensor variable. We assume the path of points in $V(t)$ are known:

$$
\underline{x} = \underline{x}(\underline{\xi}, t) \qquad (1.190)
$$

---

[15]For details, see Milne-Thomson, L. M. (1968), *Theoretical Hydrodynamics*, Fifth edition, Macmillan, London, pp. 62–66 and Batchelor, G. K. (1967), *An Introduction to Fluid Dynamics*, Cambridge University Press, Cambridge, pp. 598–603.

where $\underline{\xi}$ is the initial point of $\underline{x}$. Hence we can invert the integral to the $\underline{\xi}$ variable:

$$\int_{V(t)} F(\underline{x}, t)\, dV = \int_{V(0)} F^*(\underline{\xi}, t)\, J\, d\xi_1\, d\xi_2\, d\xi_3 \qquad (1.191)$$

where Jacobian J is written as

$$J = \frac{\partial(x_1,\, x_2,\, x_3)}{\partial(\xi_1,\, \xi_2,\, \xi_3)} = \epsilon_{ijk} \frac{\partial x_1}{\partial \xi_i} \frac{\partial x_2}{\partial \xi_j} \frac{\partial x_3}{\partial \xi_k} \qquad (1.192)$$

and the integrand

$$F^*(\underline{\xi}, t) = F\left\{\underline{x}(\underline{\xi}, t), t\right\} \qquad (1.193)$$

Hence

$$\frac{d}{dt} \int_{V(0)} F^*(\underline{\xi}, t)\, J\, d\xi_1\, d\xi_2\, d\xi_3 = \int_{V(0)} \left(\frac{\partial F^*}{\partial t} J + F^* \frac{\partial J}{\partial t}\right) d\xi_1\, d\xi_2\, d\xi_3$$
$$(1.194)$$

Now

$$\frac{\partial J}{\partial t} = \epsilon_{ijk} \frac{\partial}{\partial t}\left(\frac{\partial x_1}{\partial \xi_i} \frac{\partial x_2}{\partial \xi_j} \frac{\partial x_3}{\partial \xi_k}\right) \qquad (1.195)$$

$$\frac{\partial}{\partial t}\left(\frac{\partial x_1}{\partial \xi_i}\right) = \frac{\partial}{\partial \xi_i}\left(\frac{\partial x_1}{\partial t}\right) = \frac{\partial v_1}{\partial \xi_i} \qquad (1.196)$$

If $v_1 = v_1(x_1,\, x_2,\, x_3)$,

$$\frac{\partial v_1}{\partial \xi_i} = \frac{\partial v_1}{\partial x_j} \frac{\partial x_j}{\partial \xi_i} \qquad (1.197)$$

Since $\epsilon_{ijk} \dfrac{\partial v_1}{\partial x_2} \dfrac{\partial x_2}{\partial \xi_i} \dfrac{\partial x_2}{\partial \xi_j} \dfrac{\partial x_3}{\partial \xi_k}$ and similar terms are zero, the non-zero terms

$$\epsilon_{ijk}\left(\frac{\partial v_1}{\partial x_1} \frac{\partial x_1}{\partial \xi_i} \frac{\partial x_2}{\partial \xi_j} \frac{\partial x_3}{\partial \xi_k} + \frac{\partial v_2}{\partial x_2} \frac{\partial x_1}{\partial \xi_i} \frac{\partial x_2}{\partial \xi_j} \frac{\partial x_3}{\partial \xi_k} + \frac{\partial v_3}{\partial x_3} \frac{\partial x_1}{\partial \xi_i} \frac{\partial x_2}{\partial \xi_j} \frac{\partial x_3}{\partial \xi_k}\right) \qquad (1.198)$$

remain. So

$$\frac{\partial J}{\partial t} = (\nabla \cdot \underline{v})\, J \qquad (1.199)$$

where $\underline{v}$ is the velocity of the point $\underline{x}$. Hence

$$\int_{V(0)} \left(\frac{\partial F^*}{\partial t} + F^* \nabla \cdot \underline{v} \right) J \, d\xi_1 \, d\xi_2 \, d\xi_3 = \int_{V(t)} \left[\left(\frac{\partial F^*}{\partial t} \right)_{\underline{\xi}=const} + F^* \nabla \cdot \underline{v} \right] dV \tag{1.200}$$

Now

$$\left. \frac{\partial F^*}{\partial t} \right|_{(\underline{\xi}=const)} = \left. \frac{F \left\{ \underline{x}(\underline{\xi}, t), t \right\}}{\partial t} \right|_{\underline{\xi}} = \frac{\partial F}{\partial t} + \frac{\partial \underline{x}}{\partial t} \cdot \nabla F = \frac{\partial F}{\partial t} + \underline{v} \cdot \nabla F \tag{1.201}$$

Hence

$$\frac{d}{dt} \int_{V(t)} F \, dV = \int_V \left[\frac{\partial F}{\partial t} + \nabla \cdot (\underline{v} \, F) \right] dV \tag{1.202}$$

or

$$\boxed{\frac{d}{dt} \int_{V(t)} F \, dV = \int_{V(t)} \frac{\partial F}{\partial t} \, dV + \oint_{S(t)} \underline{n} \cdot (\underline{v} \, F) \, dS} \tag{1.203}$$

We can apply this relation at any instant in time.

The first integral implies rate of change in volume and the second one rate of change associated with motion of surface bounding volume. [16] It is noted that this is similar to Leibnitz's rule for an integral over one dimensional region:

$$\frac{d}{dt} \int_{a(t)}^{b(t)} f(x, t) \, dx = \int_{a(t)}^{b(t)} \frac{\partial f}{\partial t} \, dx + f[b(t), t] \, b'(t) - f[a(t), t] \, a'(t) \tag{1.204}$$

We can apply extensively the transport theorem to the case that there is a discontinuity interface Σ within a volume V. [17] The volume V is considered to be composed of two volumes V_1 and V_2 divided by an internal surface Σ. V is a material volume but as Σ moves with arbitrary velocity $\underline{u}$ and across it F suffers a discontinuity, F_1 and F_2 being its values on either side. If $\underline{\nu}$ is the normal to Σ in the direction form V_1 to V_2, Eq. (1.203) may be generalized to

$$\frac{d}{dt} \int_{V(t)} F \, dV = \int_{V(t)} \frac{\partial F}{\partial t} \, dV + \oint_{S(t)} \underline{n} \cdot (\underline{v} \, F) \, dS + \oint_{\Sigma(t)} \underline{\nu} \cdot (\underline{u} \, F) \, dS \tag{1.205}$$

---

[16] See Newman, J. N. (1977), *Marine Hydrodynamics*, MIT Press, for depicted interpretation.

[17] Refer to Aris, R. (1962), *Vectors, Tensors and the Basic Equations of Fluid Mechanics*, Prentice Hall, p. 86.

1.7   Moving Coordinate Systems

1.7.1   Velocity due to rigid body rotation

Suppose a rigid body rotates about an axis through the origin of a coordinate system with an angular velocity $\underline{\omega} = \omega\,\underline{n}$, where the direction of the axis is given by a unit vector $\underline{n}$ and ω is the magnitude of the angular velocity (see Figure **1.5**). [18]
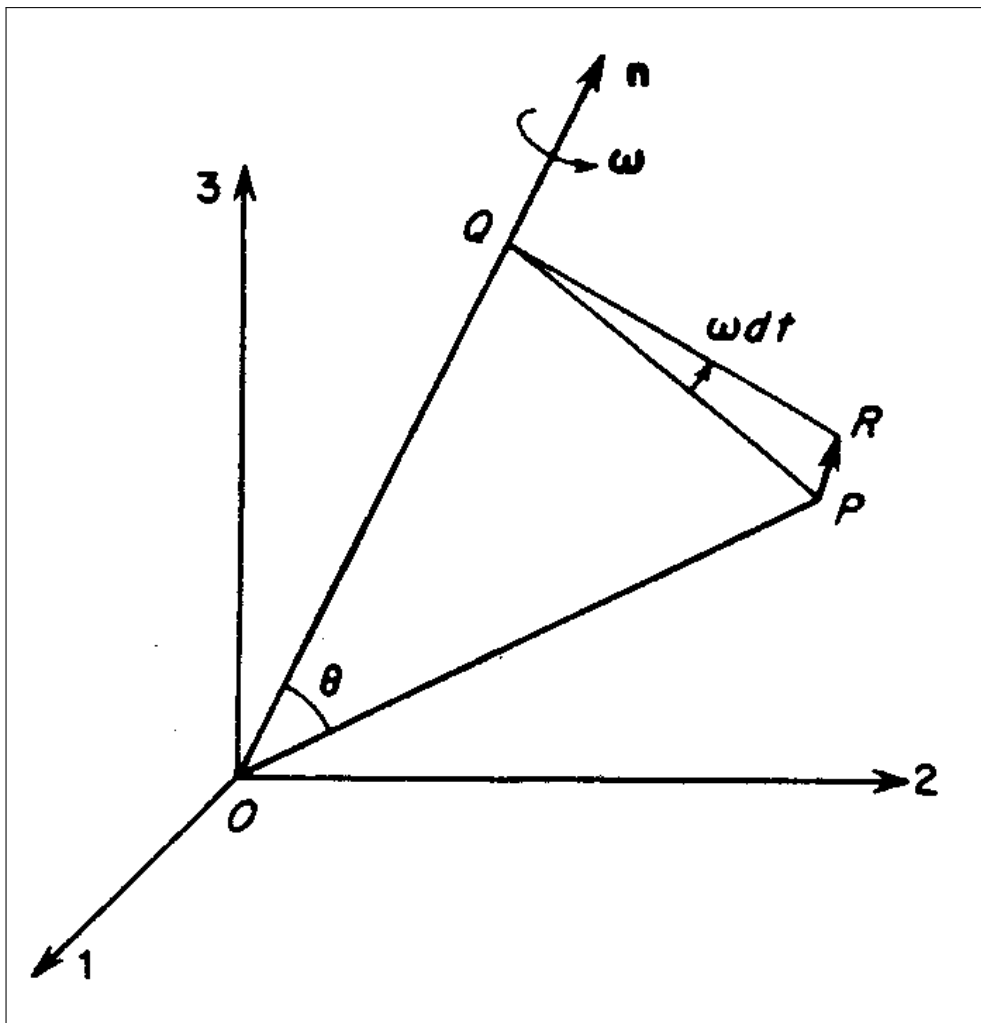
Figure 1.5 Rotation of a rigid body. From Aris (1962), p. 17.

Let P be any point in the body at position $\underline{x}$. Then $\underline{n} \times \underline{x}$ is a vector in the direction of PR of which magnitude is $|\underline{x}| \sin\theta$. However, $|\underline{x}| \sin\theta = PQ$ is the

---

[18]The description herein is based on Aris, R. (1962), *Vectors, Tensors and the Basic Equations of Fluid Mechanics*, Prentice Hall, p. 17.

perpendicular distance from P to the axis of rotation. In a small interval of time δt, the radius PQ moves through an angle $\omega \, \delta t$ and hence P moves through a distance $(PQ) \, \omega \, \delta t$.

It follows that the small short distance PR is a vector $\delta \underline{x}$ perpendicular to the plane of OP and the axis of rotation:

$$\delta \underline{x} = (\underline{n} \times \underline{x}) \, \omega \, \delta t = (\underline{\omega} \times \underline{x}) \, \delta t \qquad (1.206)$$

Dividing both sides by δt and taking the limit $\delta t \to 0$ provide the velocity of the point P. Thus the linear velocity $\underline{v}$ of the point $\underline{x}$ due to a rotation $\underline{\omega}$ is

$$\underline{v} = \underline{\omega} \times \underline{x} \qquad (1.207)$$

This result can be directly applied to moving coordinate systems. Details are given in the following subsection.

1.7.2   Transformations of moving coordinates

Let us introduce two coordinate systems: one system fixed to space and the other moving relative to the space-fixed system. The moving (the unprimed) coordinate system is supposed to be in motion of both translation and rotation relative to the space-fixed (the unprimed) system. Then the position vector $\underline{x}'$ defined in the space-fixed system is related to the position vector $\underline{x}$ defined in the moving system as follows:

$$\underline{x}' = \underline{x} + \underline{R} \qquad (1.208)$$

where $\underline{R}$ is the distance vector between the origins of two coordinate systems. (See figure **1.6**)

Because of the relative motion, time-derivative will appear different to observers in the two coordinate systems. For example, a vector that is constant in either system would seem to vary with time to an observer fixed in the other system. We can write the relationship between the derivative(d'/dt) observed in the space-fixed system and the derivative(d/dt) observed in the moving system,
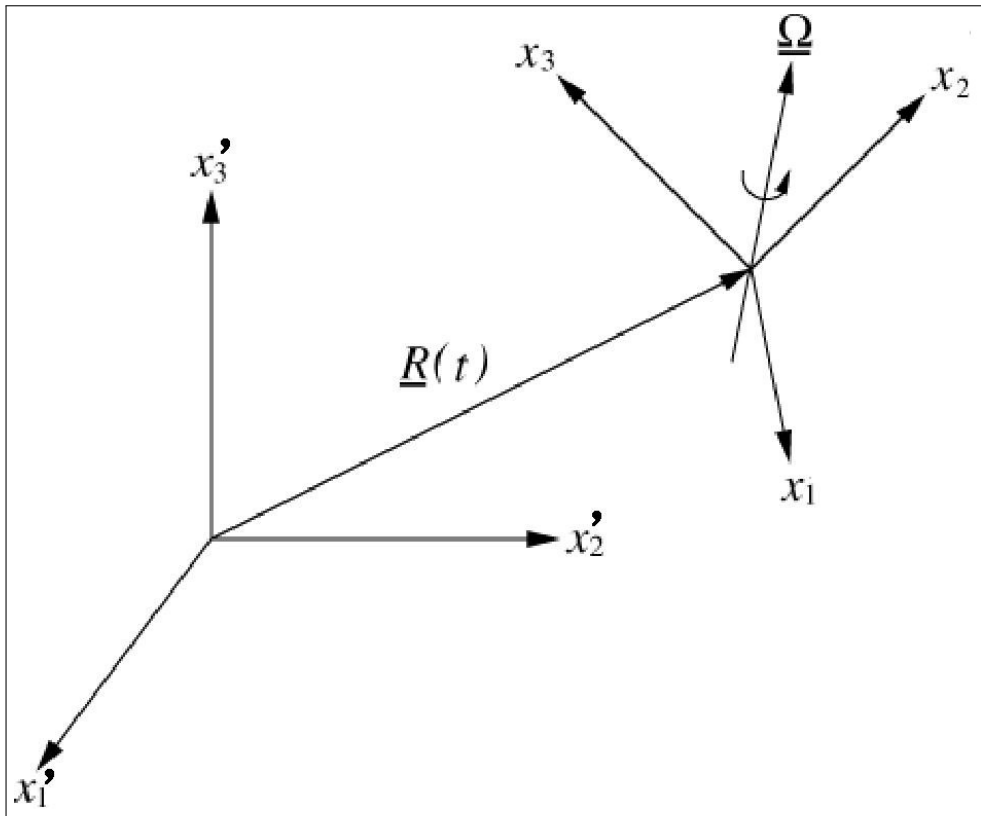
Figure **1.6** Moving coordinate system.

for an arbitrary vector:

$$\frac{d\underline{A}'}{dt} = \frac{d\underline{A}}{dt} + \underline{\Omega} \times \underline{A} \tag{1.209}$$

where $\underline{\Omega}$ is the vector angular velocity of the moving system. The last term in Eq. (1.209) implies a rotation of a rigid body. [19]

If this formula is applied to the special case of the position vector $\underline{x}$ given in Eq. (1.208), we have the velocity:

$$\underline{q}' = \underline{q} + \underline{\Omega} \times \underline{x} + \dot{\underline{R}} \tag{1.210}$$

where $\dot{\underline{R}}$ represents the translation velocity of the moving frame. Therefore this equation implies that the absolute velocity is the sum of the velocity($\underline{q}$) measured by an observer in the moving system and the frame velocity of the moving system ($\underline{\Omega} \times \underline{x} + \dot{\underline{R}}$).

---

[19]See 김 형 종 (1999), 미적분학, 총 2권, 서울대학교 출판부, pp. 317–318, and Aris, R. (1962), *Vectors, Tensors and the Basic Equations of Fluid Mechanics*, Prentice Hall, p. 17.

In a similar manner, we can obtain the relation between acceleration vectors by making use of the general rule Eq. (1.209):

$$\underline{a}' \equiv \frac{d'^2\underline{x}'}{dt^2} = \underline{a} + 2\,\underline{\Omega} \times \underline{q} + \frac{d\underline{\Omega}}{dt} \times \underline{x} + \underline{\Omega} \times (\underline{\Omega} \times \underline{x}) + \underline{\ddot{R}} \qquad (1.211)$$

Here we have written $d\underline{\Omega}/dt$ instead of $d'\underline{\Omega}/dt$ because $\underline{\Omega}$ is a vector that is always the same in both systems.

The first term of Eq. (1.211) ($\underline{a}$) is the acceleration viewed in the moving system. The second is the *Coriolis acceleration*, which depends on the velocity in the moving system. The meaning of the third term is not clear. The fourth term is the generalized centripetal acceleration, since

$$|\underline{\Omega} \times (\underline{\Omega} \times \underline{x})| = \Omega^2\,\underline{x}\,\sin(\underline{\Omega}, \underline{x}) \qquad (1.212)$$

It is noted that, if we consider the self-rotation of earth with constant angular speed, this term becomes a form of gradient of a scalar function and its effect was already included in gravitational acceleration for treatment as a body force term of the momentum equations.

1.8   Mathematical Identities

1.8.1   Green's scalar identity

If $\underline{u} = \psi\nabla\phi$ in Eq. (1.90), we obtain Green's first identity:

$$\int_V \left[\psi\nabla^2\phi + \nabla\psi \cdot \nabla\phi\right]\,dV \;=\; \oint_S \psi\,\underline{n} \cdot \nabla\phi\,dS \qquad (1.213)$$

And if $\underline{u} = \phi\nabla\psi$, use Eq. (1.90) and add the result to Green's first identity, we obtain Green's second(scalar) identity:

$$\int_V \left[\psi\nabla^2\phi - \phi\nabla^2\psi\right]\,dV \;=\; \oint_S \left[\psi\frac{\partial\phi}{\partial n} - \phi\frac{\partial\psi}{\partial n}\right]\,dS \qquad (1.214)$$

where $\underline{n} \cdot \nabla \phi = \dfrac{\partial \phi}{\partial n}$. For these relations to be valid, ϕ and ψ must be continuous in the volume and on the surface and the second derivatives must be continuous within the volume while on the surface only the first derivatives need be continuous. [20]

As an practical application, an arbitrary scalar field defined in a volume V can be represented in terms of integrals over the enclosing surfaces plus an integral of $\nabla^2 \phi$ over the volume.

From the expansion formulas, we see that $\dfrac{1}{|\underline{x}|} = \dfrac{1}{|\underline{r}|} = \dfrac{1}{r}$ satisfies Laplace's equation: $\nabla^2 \left(\dfrac{1}{r} \right) = 0$ if $\underline{r} \neq 0$. Similarly $\nabla^2 \left(\dfrac{1}{|\underline{y} - \underline{x}|} \right) = 0$ for $\underline{y}$ a constant vector. Since $\nabla^2 \left(\dfrac{1}{|\underline{y} - \underline{x}|} \right)$ does not exist at $\underline{x} = \underline{y}$, we exclude this point from the volume by surrounding it with a sphere.
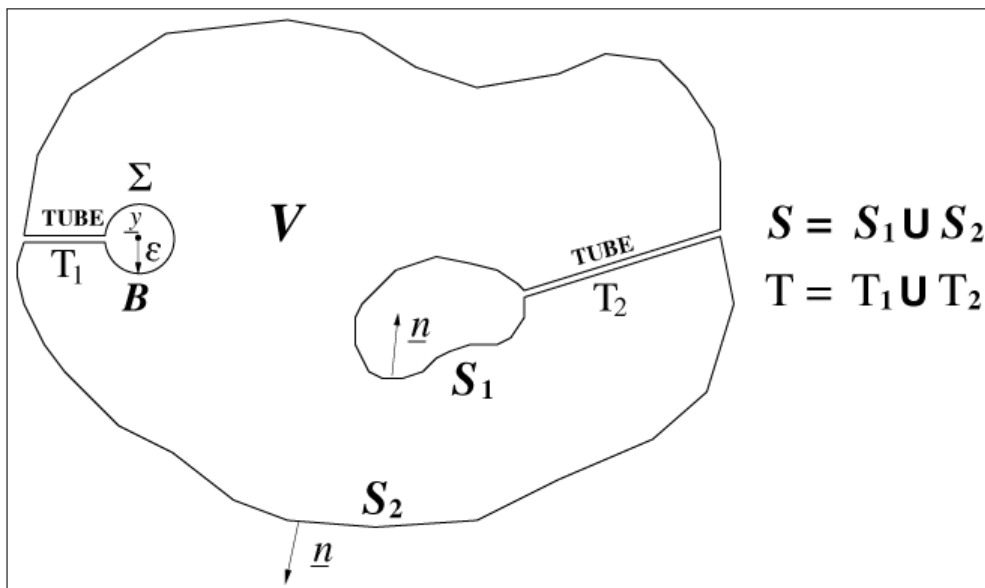
Figure 1.7 Two-dimensional drawing of a simply connected region for deriving the scalar identity.

---

[20]More detailed explanation can be found in mathematical texts, e.g., Kreyszig, E. (1993), *Advanced Engineering Mathematics*, Seventh ed.,Wiley, pp. 553–554.

Hence if we take $\psi = \dfrac{1}{|\underline{y} - \underline{x}|}$, Green's second identity becomes:

$$\oint_{S+T+\sum(\underline{y},\epsilon)} \left[\frac{\underline{n} \cdot \nabla \phi}{|\underline{y} - \underline{x}|} - \phi \, \underline{n} \cdot \nabla \frac{1}{|\underline{y} - \underline{x}|} \right] dS = \int_{V-B(\underline{y},\epsilon)} \left[\frac{1}{|\underline{y} - \underline{x}|} \nabla^2 \phi \right] dV$$

$$(1.215)$$

where $B(\underline{y}, \epsilon)$ is a sphere of radius ϵ centered at $\underline{y}$ and bounded by Σ.

In this application, the surface is in three-dimensional space and the integration variable is $\underline{x}$. We illustrate the situation with a two-dimensional drawing as shown in Figure **1.7** . Integrations over the small tubes joining Σ and S_2, and S_1 and S_2 vanish by continuity of ϕ.

On the surface Σ surrounding the point $\underline{y}$, as shown in Figure **1.8** for an enlarged view, we have

$$\underline{y} - \underline{x} = -\epsilon \, \underline{e}_r \tag{1.216}$$

$$\underline{n} = -\underline{e}_r \tag{1.217}$$

$$dS = (\epsilon \, d\theta)(\epsilon \sin \theta \, d\alpha) \tag{1.218}$$

$$\phi(\underline{x}) = \phi(\underline{y}) + \epsilon \left. \frac{\partial \phi}{\partial r} \right|_{\underline{y}} + \cdots \tag{1.219}$$

$$\nabla \frac{1}{|\underline{y} - \underline{x}|} = \frac{(\underline{y} - \underline{x})}{|\underline{x} - \underline{y}|^3} = -\frac{\epsilon \, \underline{e}_r}{\epsilon^3} \tag{1.220}$$

where $\underline{e}_r$ is the unit vector in the radial direction. Hence the integration for the surface Σ and the small ball B becomes, respectively,

$$\oint_\Sigma \left[\frac{\underline{n} \cdot \nabla \phi}{|\underline{y} - \underline{x}|} - \phi \, \underline{n} \cdot \nabla \frac{1}{|\underline{y} - \underline{x}|} \right] dS$$

$$= -\phi(\underline{y}) \int_0^{2\pi} d\alpha \int_0^\pi \left[\epsilon^2 \frac{\underline{e}_r \cdot (\epsilon \, \underline{e}_r)}{\epsilon^3} \sin \theta \right] d\theta + O(\epsilon)$$

$$= -4\pi \, \phi(\underline{y}) + O(\epsilon) \tag{1.221}$$

and

$$\int_B \left[\nabla^2 \phi \frac{1}{|\underline{y} - \underline{x}|} \right] dV = \nabla^2 \phi \big|_{\underline{y}} \left(O(\epsilon^2) \right) \tag{1.222}$$
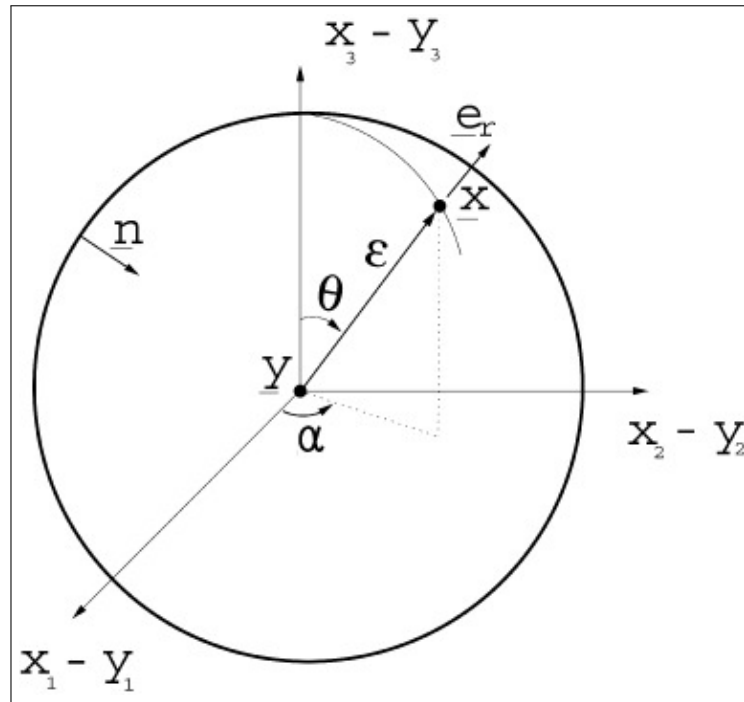
Figure **1.8** Small sphere region containing a singular point.

Hence, taking the limit as $\epsilon \to 0$, we find

$$\boxed{\phi(\underline{y}) = \frac{1}{4\pi} \oint_S \left[\frac{\underline{n} \cdot \nabla \phi}{|\underline{y} - \underline{x}|} - \phi \frac{\underline{n} \cdot (\underline{y} - \underline{x})}{|\underline{y} - \underline{x}|^3} \right] dS - \frac{1}{4\pi} \int_V \frac{\nabla^2 \phi}{|\underline{y} - \underline{x}|} dV} \quad (1.223)$$

If the point $\underline{y}$ had been outside V, the left-hand side would have been zero.

For a two-dimensional field, $\psi = \ln \frac{1}{\sqrt{x_1^2 + x_2^2}}$ in Green's second identity and a similar expression is obtained.

1.8.2 Uniqueness of scalar identity

Let us consider the uniqueness of this integral representation. If another scalar field, say $\phi'(\underline{x})$ had the same value of $\nabla^2 \phi$ in V and the same value of ϕ or $\underline{n} \cdot \nabla \phi$ on S, then we could construct a third solution which had $\nabla^2 \phi'' = 0$ in V, and either $\phi'' = 0$ or $\underline{n} \cdot \nabla \phi''$ on S. If $\phi = \psi = \phi''$ in Green's first identity,

then

$$\int_V \left[\phi'' \, \nabla^2 \phi'' + \nabla \phi'' \cdot \nabla \phi'' \right] dV = \oint_S \left[\phi'' \, \underline{n} \cdot \nabla \phi'' \right] dS \qquad (1.224)$$

and this reduces to only

$$\int_V \nabla \phi'' \cdot \nabla \phi'' \, dV = 0 \qquad (1.225)$$

Since $(\nabla \phi)^2$ is always greater than or equal to zero, the only solution is

$$\nabla \phi'' \cdot \nabla \phi'' = 0 \qquad (1.226)$$

This requires that ϕ'' be at most a constant. If ϕ were specified on the boundary, the constant is zero. If $\underline{n} \cdot \nabla \phi$ is specified on the boundary, ϕ is uniquely determined by the integral to within a constant. It is important to recognize that our expression for ϕ is in terms of ϕ and $\underline{n} \cdot \nabla \phi$ and the above consideration shows we need specify only one of these on the boundary. Hence to find the unknown on the boundary, one must first solve an integral equation.

Also we have assumed that the field boundaries are fixed. If they were to depend on the field, then special conditions must be specified to insure the solution is unique. In addition to this uniqueness, we should also consider the far-field behavior of ϕ as the distance r goes to infinity. [21]

1.8.3 Type of boundary conditions

(1) Dirichlet boundary condition (1st type)
   The Dirichlet (or first type) boundary condition is perhaps the easiest one to understand. When we solve a differential equation, we put specified values on the boundary of the domain where a solution needs to take. For example, when Poisson equation such as $\nabla^2 \psi = -\omega$ for stream function ψ and vorticity ω is satisfied in a domain Ω, the Dirichlet boundary condition

---

[21]Detailed consideration may be found in Batchelor, G. K. (1967), *An Introduction to Fluid Dynamics*, Cambridge University Press, Cambridge.

takes the form $\psi(\underline{x}) = f(\underline{x})$ on the boundary $\partial\Omega$, where $f(\underline{x})$ is a known function defined on the boundary.

(2) Neumann boundary condition (2nd type)

The Neumann (or second type) boundary condition specifies the values that the derivative of a solution is to take on the boundary of the domain, when imposed on an ordinary or a partial differential equation. For example, for Laplace equation $\nabla^2\phi = 0$ which we will present later on, the Neumann boundary condition takes the form $\dfrac{\partial\phi(\underline{x})}{\partial n} = g(\underline{x})$. Here, n denotes the (typically exterior) normal to the boundary and g is a given scalar function.

(3) Robin boundary condition (3rd type)

The Robin (or third type) boundary condition is a type of hybrid boundary condition; it is a linear combination of Dirichlet and Neumann boundary conditions, namely, it is a specification of a linear combination of the values of a function and the values of its derivative on the boundary of the domain. Robin boundary conditions are a weighted combination of Dirichlet boundary conditions and Neumann boundary conditions, such as $a\,\phi + b\,\dfrac{\partial\phi}{\partial n} = h(\underline{x})$ where a and b are non-zero constants or functions more generally. Robin boundary conditions are commonly used in solving Sturm-Liouville problems (Stakgold, 1986). These boundary conditions should not be confused with mixed boundary conditions, which are boundary conditions of different types specified on different subsets of the boundary.

(4) Mixed boundary condition

The mixed boundary condition for a partial differential equation implies that different types of boundary condition are used on different parts of the boundary. For example, in partial sheet cavity problems for a hydrofoil, if ϕ is a solution to Laplace equation on a fluid domain and the boundary is divided into two portions of cavity and non-cavity, one would impose a Dirichlet boundary condition on the cavity portion and a Neumann boundary condition on the non-cavity portion.

(5) Cauchy boundary condition

A Cauchy boundary condition imposed on an ordinary differential equation or a partial differential equation specifies both the values a solution of a differential equation is to take on the boundary of the domain and the normal derivative at the boundary. It corresponds to imposing both a Dirichlet and a Neumann boundary condition.

Cauchy boundary conditions can be understood from the theory of second order, ordinary differential equations, where to have a particular solution one has to specify the value of the function and the value of the derivative at a given initial or boundary point.

For a second order partial differential equation, we now need to know the value of the function at the boundary, and its normal derivative in order to solve the partial differential equation.

When the variable is specially time, Cauchy conditions can also be called initial value conditions.

1.8.4 Vector identity

Another identity involving vectors can be constructed from divergence theorems for a vector and a dyadic. In the third divergence theorem given by Eq. (1.91), let the vector be $\underline{u} \times \underline{v}$, then

$$\int_V [\nabla \times (\underline{u} \times \underline{v})] \, dV = \oint_S [\underline{n} \times (\underline{u} \times \underline{v})] \, dS \qquad (1.227)$$

According to the expansion formula on vector triple products, we know

$$\begin{aligned}
\underline{n} \times (\underline{u} \times \underline{v}) &= (\underline{n} \times \underline{u}) \times \underline{v} + (\underline{v} \times \underline{n}) \times \underline{u} \\
&= (\underline{n} \times \underline{u}) \times \underline{v} - \underline{v}(\underline{n} \cdot \underline{u}) + \underline{n}(\underline{u} \cdot \underline{v}) \qquad (1.228)
\end{aligned}$$

Hence

$$\oint_S [\underline{n} \times (\underline{u} \times \underline{v})] \, dS = \oint_S [(\underline{n} \times \underline{u}) \times \underline{v} - (\underline{n} \cdot \underline{u}) \underline{v} + \underline{n}(\underline{u} \cdot \underline{v})] \, dS \quad (1.229)$$

These integrals can be rearranged by the divergence theorem:

$$\oint_S [(\underline{n} \times \underline{u}) \times \underline{v}] \, dS = \int_V [\nabla \times (\underline{u} \times \underline{v}) + \nabla \cdot (\underline{u}\,\underline{v}) - \nabla(\underline{u} \cdot \underline{v})] \, dV$$
(1.230)

Now adding the results of the divergence theorem for a dyadic $\underline{u}\,\underline{v}$ to both sides:

$$\oint_S (\underline{n} \times \underline{u}) \times \underline{v} + (\underline{n} \cdot \underline{u})\,\underline{v}] \, dS$$
$$= \int_V [\nabla \times (\underline{u} \times \underline{v}) + 2\,\underline{v}\,(\nabla \cdot \underline{u}) + 2\,\underline{u} \cdot \nabla\underline{v} - \nabla(\underline{u} \cdot \underline{v})] \, dV$$
(1.231)

Using the expansion formulas

$$\nabla \times (\underline{u} \times \underline{v}) = \underline{v} \cdot \nabla\underline{u} + \underline{u}\,(\nabla \cdot \underline{v}) - \underline{v}\,(\nabla \cdot \underline{u}) - \underline{u} \cdot \nabla\underline{v} \quad (1.232)$$
$$\nabla(\underline{u} \cdot \underline{v}) = \underline{v} \cdot \nabla\underline{u} + \underline{v} \times (\nabla \times \underline{u}) + \underline{u} \times (\nabla \times \underline{v}) + \underline{u} \cdot \nabla\underline{v}$$
(1.233)

and subtracting one from the other, we obtain

$$\nabla \times (\underline{u} \times \underline{v}) - \nabla(\underline{u} \cdot \underline{v}) = \underline{u}\,(\nabla \cdot \underline{v}) - \underline{v}\,(\nabla \cdot \underline{u}) - 2\,\underline{u} \cdot \nabla\underline{v}$$
$$-\underline{v} \times (\nabla \times \underline{u}) - \underline{u} \times (\nabla \times \underline{v})$$
(1.234)

Hence

$$\oint_S [(\underline{n} \times \underline{u}) \times \underline{v} + (\underline{n} \cdot \underline{u})\,\underline{v}] \, dS$$
$$= \int_V [\underline{v}\,(\nabla \cdot \underline{u}) + \underline{u}\,(\nabla \cdot \underline{v}) - \underline{u} \times (\nabla \times \underline{v}) - \underline{v} \times (\nabla \times \underline{u})] \, dV$$
(1.235)

This is called vector identity.

An arbitrary vector field can be represented by this vector identity by choos-

ing

$$\underline{v} = \nabla \frac{1}{|\underline{y} - \underline{x}|} = \frac{(\underline{y} - \underline{x})}{|\underline{y} - \underline{x}|^3} \quad \text{for } \underline{y} \text{ fixed} \tag{1.236}$$

For which, we have

$$\left. \begin{array}{r} \nabla \times \underline{v} = 0 \\[2mm] \nabla \cdot \underline{v} = 0 \end{array} \right\} \quad \text{for } \underline{x} \neq \underline{y} \tag{1.237}$$

Hence for $\underline{y}$ not in V, Eq. (1.235) becomes, without any restriction,

$$\oint_S \left[(\underline{n} \times \underline{u}) \times \frac{(\underline{y} - \underline{x})}{|\underline{y} - \underline{x}|^3} + (\underline{n} \cdot \underline{u}) \frac{(\underline{y} - \underline{x})}{|\underline{y} - \underline{x}|^3} \right] dS$$

$$= \int_V \left[\frac{(\underline{y} - \underline{x})}{|\underline{y} - \underline{x}|^3} (\nabla \cdot \underline{u}) - \frac{(\underline{y} - \underline{x})}{|\underline{y} - \underline{x}|^3} \times (\nabla \times \underline{u}) \right] dV \tag{1.238}$$

For the case when $\underline{y}$ is in V, $\left(\dfrac{1}{|\underline{y} - \underline{x}|} \right)$ becomes singular as $\underline{y}$ tends to $\underline{x}$. The point $\underline{y}$ can be excluded from V by surrounding it with a sphere of radius ϵ centered at $\underline{y}$, as shown in Fig. **1.7** . This sphere plus any other surfaces inside V can be connected to the exterior surface by small tubes to make all the surfaces continuous and the region remains simply connected, in the same manner as for the scalar identity.

The vector identity applies to the region V as defined with the exclusions:

$$\oint_{S+T+\sum(y,\epsilon)} \left[(\underline{n} \times \underline{u}) \times \frac{(\underline{y} - \underline{x})}{|\underline{y} - \underline{x}|^3} + (\underline{n} \cdot \underline{u}) \frac{(\underline{y} - \underline{x})}{|\underline{y} - \underline{x}|^3} \right] dS$$

$$= \int_{V-B} \left[\frac{(\underline{y} - \underline{x})}{|\underline{y} - \underline{x}|^3} (\nabla \cdot \underline{u}) - \frac{(\underline{y} - \underline{x})}{|\underline{y} - \underline{x}|^3} \times (\nabla \times \underline{u}) \right] dV \tag{1.239}$$

Integrations over the small tubes T_1 and T_2 vanish by continuity as they become increasingly small.

On the surface Σ surrounding the point $\underline{y}$ (see Figure **1.8**):

$$\underline{y} - \underline{x} = -\epsilon\,\underline{e}_r \tag{1.240}$$

$$\underline{n} = -\underline{e}_r \tag{1.241}$$

$$dS = (\epsilon\,d\theta)\,(\epsilon\,\sin\theta\,d\phi) \tag{1.242}$$

$$\frac{(\underline{y} - \underline{x})}{|\underline{x} - \underline{y}|^3} = \frac{-\epsilon\,\underline{e}_r}{\epsilon^3} \tag{1.243}$$

where $\underline{e}_r$ is the unit vector in the radial direction. Furthermore,

$$\underline{u}|_{\Sigma} = \underline{u}(\underline{y}) + (\underline{x} - \underline{y}) \cdot \nabla\underline{u} + \cdots = \underline{u}(\underline{y}) + O(\epsilon) \tag{1.244}$$

$$(\underline{n} \times \underline{u}) \times (\underline{y} - \underline{x}) = \epsilon\,(-\underline{e}_r \times \underline{u}) \times (-\underline{e}_r) = \epsilon\,\{\underline{u} - \underline{e}_r(\underline{u} \cdot \underline{e}_r)\} \tag{1.245}$$

$$(\underline{n} \cdot \underline{u})\,(\underline{y} - \underline{x}) = \epsilon\,(\underline{e}_r \cdot \underline{u})\,\underline{e}_r \tag{1.246}$$

Hence,

$$\oint_{\Sigma} \left[(\underline{n} \times \underline{u}) \times \frac{(\underline{y} - \underline{x})}{|\underline{y} - \underline{x}|^3} + (\underline{n} \cdot \underline{u}) \frac{(\underline{y} - \underline{x})}{|\underline{y} - \underline{x}|^3} \right] dS$$

$$= \underline{u}(\underline{y}) \int_0^{2\pi} d\alpha \int_0^\pi \frac{\epsilon^3 \sin\theta\,d\theta}{\epsilon^3} + O(\epsilon)$$

$$= 4\pi\,\underline{u}(\underline{y}) + O(\epsilon) \tag{1.247}$$

And for $\epsilon \to 0$,

$$4\pi\,\underline{u}(\underline{y}) = -\oint_S \left[(\underline{n} \times \underline{u}) \times \frac{(\underline{y} - \underline{x})}{|\underline{y} - \underline{x}|^3} + (\underline{n} \cdot \underline{u}) \frac{(\underline{y} - \underline{x})}{|\underline{y} - \underline{x}|^3} \right] dS_x$$

$$+ \lim_{\epsilon \to 0} \int_{V - B(\underline{y},\epsilon)} \left[\frac{(\underline{y} - \underline{x})}{|\underline{y} - \underline{x}|^3} (\nabla \cdot \underline{u}) - \frac{(\underline{y} - \underline{x})}{|\underline{y} - \underline{x}|^3} \times (\nabla \times \underline{u}) \right] dV_x \tag{1.248}$$

This is a representation of $\underline{u}$ in terms of both components on the boundary, the normal component $\underline{n} \cdot \underline{u}$, and the tangential component, $\underline{n} \times \underline{u}$, plus the divergence and the curl integrated over the field.

If $\underline{u}$ is divided into two components after interchanging the variables $\underline{x}$ and

$\underline{y}$, Eq. (1.248) is rewritten as

$$
\begin{aligned}
4\pi \underline{u} \;=\;& \underline{u}_1 + \underline{u}_2 & (1.249) \\
\underline{u}_1(\underline{x}) \;=\;& +\fint_V \frac{(\underline{x}-\underline{y})}{|\underline{x}-\underline{y}|^3}(\nabla \cdot \underline{u})\, dV_y - \oint_S (\underline{n}\cdot\underline{u})\frac{(\underline{x}-\underline{y})}{|\underline{x}-\underline{y}|^3}\, dS_y & (1.250) \\
\underline{u}_2(\underline{x}) \;=\;& -\fint_V \frac{(\underline{x}-\underline{y})}{|\underline{x}-\underline{y}|^3} \times (\nabla \times \underline{u})\, dV_y - \oint_S (\underline{n}\times\underline{u}) \times \frac{(\underline{x}-\underline{y})}{|\underline{x}-\underline{y}|^3}\, dS_y & \\
& & (1.251)
\end{aligned}
$$

where the bar through the integral sign indicates the limit integration.

1.8.5   Integral expression of Helmholtz decomposition

For a vector field $\underline{u}$ given in a domain V, we define a vector $\underline{F}$ by

$$
\underline{F}(\underline{x}) = -\int_V G(\underline{x}-\underline{y})\,\underline{u}(\underline{y})\, dV_y \tag{1.252}
$$

where $G(\underline{r})$ is the fundamental solution (Green function) of Poisson equation

$$
\nabla^2 G(\underline{r}) = \delta(\underline{r}). \tag{1.253}
$$

For example, $G(\underline{r}) = -\dfrac{1}{4\pi|\underline{r}|}$ in 3-D dimesional free space.

By Eqs. (1.252) and (1.253) and the definition of the Dirac delta function, we have

$$
-\nabla^2 \underline{F} = -\int_V \delta(\underline{x}-\underline{y})\,\underline{u}(\underline{y})\, dV_y = \underline{u}(\underline{x}) \tag{1.254}
$$

According to Eq. (1.72),

$$
\underline{u}(\underline{x}) = -\nabla^2 \underline{F} = -\nabla(\nabla \cdot \underline{F}) + \nabla \times (\nabla \times \underline{F}) \tag{1.255}
$$

By comparing this expression with the Helmholtz decomposition form $\underline{u} = \nabla\phi + \nabla \times \underline{A}$, the scalar and the vector potentials are simply given by

$$
\phi = -\nabla \cdot \underline{F}, \quad \underline{A} = \nabla \times \underline{F} \tag{1.256}
$$

We can then perform the integration of Eq. (1.252) to yield

$$
\begin{aligned}
\phi = -\nabla \cdot \underline{F} \;&=\; \int_V \nabla \cdot \left\{ G(\underline{x} - \underline{y})\, \underline{u}(\underline{y}) \right\} dV_y \\
&=\; \int_V \nabla G(\underline{x} - \underline{y}) \cdot \underline{u}(\underline{y})\, dV_y \\
&=\; -\int_V \nabla_y G(\underline{x} - \underline{y}) \cdot \underline{u}(\underline{y})\, dV_y \\
&=\; -\int_V \left\{ \nabla_y \cdot (G\,\underline{u}) - G\,\nabla_y \cdot \underline{u} \right\} dV_y \\
&=\; -\oint_S G\,\underline{n} \cdot \underline{u}\, dS_y + \int_V G\,\theta\, dV_y
\end{aligned}
\qquad (1.257)
$$

$$
\begin{aligned}
\underline{A} = \nabla \times \underline{F} \;&=\; -\int_V \nabla \times \left\{ G(\underline{x} - \underline{y})\, \underline{u}(\underline{y}) \right\} dV_y \\
&=\; -\int_V \nabla G(\underline{x} - \underline{y}) \times \underline{u}(\underline{y})\, dV_y \\
&=\; \int_V \nabla_y G(\underline{x} - \underline{y}) \times \underline{u}(\underline{y})\, dV_y \\
&=\; \int_V \left\{ \nabla_y \times (G\,\underline{u}) - G\,\nabla_y \times \underline{u} \right\} dV_y \\
&=\; \oint_S G\,\underline{n} \times \underline{u}\, dS_y - \int_V G\,\underline{\omega}\, dV_y
\end{aligned}
\qquad (1.258)
$$

Here we denote the gradient operator with respect to the integration variables $\underline{y}$ by ∇_y so that $\nabla G = -\nabla_y G$. Equations (1.257) and (1.258) provide the mathematical background of the Helmholtz decomposition for any vector field. Therefore the irrotational vector $\nabla\phi$ and the solenoidal vector $\nabla \times \underline{A}$ can be expressed in terms of dilatation and vorticity, respectively:

$$
\nabla\phi \;=\; -\oint_S (\underline{n} \cdot \underline{u})\, \nabla G\, dS_y + \int_V \theta\, \nabla G\, dV_y
\qquad (1.259)
$$

$$
\nabla \times \underline{A} \;=\; -\oint_S (\underline{n} \times \underline{u}) \times \nabla G\, dS_y + \int_V \underline{\omega} \times \nabla G\, dV_y
\qquad (1.260)
$$

Note that we have dropped the subscript y in ∇G for brevity, and hence it denotes the operator with respect to the integration variables $\underline{y}$. This result is the

same as the expression of the vector identity Eqs. (1.250) and (1.251) derived in the previous subsection.

1.8.6 Green functions

When other surfaces can be included in the problem of the Laplace equation (more generally other partial differential equations, not necessarily the Laplace equation) that governs flow fields, additional boundary conditions are imposed. Then the Green function is often taken instead of the elementary function for computational advantage.

(1) Green fuction is defined as an elementary singularity plus another non-singular component that satisfies Laplace equation as well as boundary contions on the other surfaces.

(2) What is left unsatisfied is boundary conditions on a body.

(3) Scalar (velocity potential) at $\underline{x}$ in terms of a distribution of elementary singularities $\psi = \dfrac{1}{|\underline{x} - \underline{y}|}$. When we add a function (say $H(\underline{x}, \underline{y})$) that also satisfies the Laplace equation and is not singular within the field to ψ, identity is unchanged except that we have a modified singularity element. It is necessary but not easy to find a function H with the following properties.

(4) If there were surfaces near a body, construct new singularity element $G(\underline{x}, \underline{y})$ with $\nabla^2 G = 0$ and such that

   (a) G satifies given boundary conditions on non-body surfaces

   (b) G contains elementary singularity element (say $\dfrac{1}{|\underline{x} - \underline{y}|}$) to give the field point value $\phi(\underline{x})$

   (c) G results in integral equation over only the body surface.

(5) The formulation is as follows

$$G(\underline{x}, \underline{y}) = \frac{1}{|\underline{x} - \underline{y}|} + H(\underline{x}, \underline{y}) \qquad (1.261)$$

where $H(\underline{x}, \underline{y})$ is non-singular for all $\underline{x} \in V$, $\nabla^2 H = 0$ and

$$\phi \, \underline{n} \cdot \nabla G - G \, \underline{n} \cdot \nabla \phi = 0 \quad \text{on} \quad \text{S} \neq \text{S}_\text{B} \tag{1.262}$$

(6) For a simple example, if a wall is aligned with onset flow, H is image of elementary singularity.

1.8.7 Uniqueness of vector identity

To examine uniqueness of the solution as before, suppose that vectors $\underline{u}_1$ and $\underline{u}_2$ satisfy $\nabla \cdot \underline{u}_1 = \nabla \cdot \underline{u}_2$ and $\nabla \times \underline{u}_1 = \nabla \times \underline{u}_2$ in V. Then the difference vector $\underline{u}_3 = \underline{u}_1 - \underline{u}_2$ satisfies $\nabla \cdot \underline{u}_3 = 0$ and $\nabla \times \underline{u}_3 = 0$ in V. The condition that the curl and divergence of $\underline{u}_3$ are both zero is necessary and sufficient to establish that $\underline{u}$ is the gradient of a scalar function P which satisfies Laplace's equation:

$$\underline{u}_3 = \nabla P \tag{1.263}$$
$$\nabla^2 P = 0 \tag{1.264}$$

Green's first identity, Eq. (1.213),

$$\int_V \left[\psi \nabla^2 \phi + \nabla \psi \cdot \nabla \phi \right] dV = \oint_S \psi \, \underline{n} \cdot \nabla \phi \, dS \tag{1.265}$$

with $\psi = \phi = P$ reduces to

$$\int_V \underline{u}_3 \cdot \underline{u}_3 \, dV = \oint_S P \, \underline{n} \cdot \underline{u}_3 \, dS \tag{1.266}$$

If the normal component of the two solution vector is specified equal on the boundary, then $\underline{n} \cdot \underline{u}_3 = 0$ on S and hence

$$\int_V \underline{u}_3 \cdot \underline{u}_3 \, dV = 0 \tag{1.267}$$

Since $\underline{u}_3 \cdot \underline{u}_3$ is always greater than or equal to zero, the only possible solution is

$$\underline{u}_3 = 0 \tag{1.268}$$

When the boundary condition uniquely defines the normal component of the vector, Eq. (1.249) represents a unique representation of an arbitrary vector and no information need be given about the tangential component of the vector.

1.8.8 Classification of vector fields

We have noted two distinct types of vector field; 'solenoidal' and 'irrotational'. Apart from these types, several other types of fields have been named. [22]
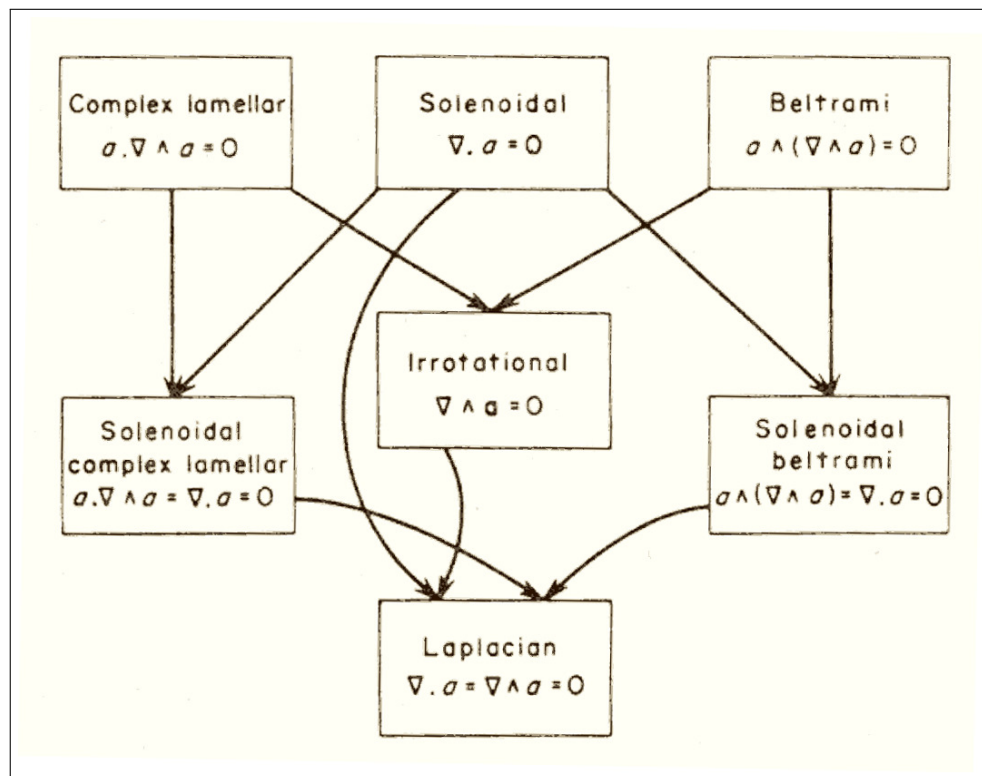
Figure 1.9 Classification of vector fields. From Aris (1962), p. 64.

(1) Laplacian: A field which is both solenoidal and irrotational is called Laplacian. It is the gradient of a potential function. The potential function is taken to be either scalar or vectorial.

(2) Complex lamellar: The condition for a field to be 'complex lamellar' is $\underline{a} \cdot (\nabla \times \underline{a}) = 0$. This field is orthogonal to its curl if $\nabla \times \underline{a} \neq 0$. The

---

[22]See Aris, R. (1962), *Vectors, Tensors and the Basic Equations of Fluid Mechanics*, Prentice Hall, p. 64.

name 'lamellar' is also applied to an irrotational vector field $\nabla \times \underline{a} = 0$. The 'lamellar' is therefore a special case of the 'complex lamellar'.

(3) Beltrami: The field is parallel to its curl, i.e, $\underline{a} \times (\nabla \times \underline{a}) = 0$. As a special case, if its curl is proportional to the original vector $\underline{a}$ with a contant (i.e., $\nabla \times \underline{a} = k\,\underline{a}, \quad \nabla k = 0$), it is called 'Trkalian'.

The relations between these types are shown in a schematic diagram (Figure **1.9**). If a field is both a complex lamellar and Beltrami field, it is irrotational if $\underline{a} \neq 0$.

1.9 Improper Integrals

1.9.1 Examples

Most of integrals involved in physics are well defined as a limit of a Rieman sum for which integrand and range of integration are well behaved. [23] Several types of integrals occur in hydrodynamic problems that involve quantities that tend to infinity. Some of these integrals have meaning in the classical mathematical sense that the integral is to be interpreted as a limit process, but a some additional insight is also required. Two general types of integrals are of concern:

(1) those with a range of integration that tends to infinity and

(2) those that have integrands that are singular at points within the range of integration.

As an example of the second type of improper integral, suppose $f(x)$ has singularities at the start of the range and at an intermediate point x_0 within the range of integration, then the definition of the improper integral of $f(x)$ is

$$\int_a^b f(x)\,dx = \lim_{a_1,b_1,c_1 \to 0} \left[\int_{a+a_1}^{x_0-b_1} f(x)\,dx + \int_{x_0+c_1}^b f(x)\,dx \right] \qquad (1.269)$$

---

[23] See, e.g., Kaplan, W. (1952), *Advanced Calculus*, Addison-Wesley.

if it exist.

Such an interpretation of the integral does not always exist. The improper integral $\int_1^\infty \frac{dx}{x}$ has an infinite range of integration but no singularities in the integrand over the range of integration. It is to be interpreted as

$$\lim_{R\to\infty}\left[\int_1^R \frac{dx}{x}\right] = \lim_{R\to\infty}\left[\ln(R)\right] \to \infty \qquad (1.270)$$

and thus does not produce a finite value. Hence the integral is both improper and unbounded, even the integrand is well behaved over the range of integration.

Meanwhile, the integrand of $\int_0^1 \frac{dx}{\sqrt{x}}$ is singular at $x = 0$. Hence we interpret it as

$$\lim_{\epsilon\to0}\int_\epsilon^1 \frac{dx}{\sqrt{x}} = \lim_{\epsilon\to0}\left[2 - \sqrt{\epsilon}\right] = 2, \qquad (1.271)$$

and hence it exists by construction. We say the integral is convergent improper.

1.9.2   Principal value integrals

There are a class of improper integrals that are fundamental to investigations of the flow about bodies. These are Principal Value Integrals and are defined with some aspect of symmetry relative to the infinities involved. For integrals with infinite limits this may be

$$(P.V.)\int_{-\infty}^\infty f(x)\,dx \equiv \fint_{-\infty}^\infty f(x)\,dx = \lim_{R\to\infty}\int_{-R}^R f(x)\,dx \qquad (1.272)$$

and for integrals with integrands that are singular at points within the range of integration, say at the point x_0 such that $\lim_{x\to x_0} f(x) \to \infty$,

$$(P.V.)\int_a^b f(x)\,dx \equiv \fint_a^b f(x)\,dx = \lim_{\epsilon\to0}\left[\int_a^{x_0-\epsilon} f(x)\,dx + \int_{x_0+\epsilon}^b f(x)\,dx\right] \qquad (1.273)$$

Some integrals have both an infinite range of integration and singularities in

the integrand at some points. They may exist in the principal-value sense by cancelling the positive and negative values around the singularities.

A specific form of an improper integral, with a well-behaved numerator and specific singular denominator, called a Cauchy Principal Value Integral is defined in the same manner. In application, we will arrive at such integrals when a form of the general solution for the flow about a body(obtained with sources, sinks, dipoles or vortices distributed over the body surface) is derived for the case that a field point approaches the body surface. However we will treat the limiting process in such a way that not only is the Cauchy Principal Value Integral obtained but a local contribution from the excluded region is defined.

In the previous section, we have already treated two cases for which an improper integral was evaluated for the representation of scalar and vector field values in terms of surface and volume integrals. For the case with a singular point in the field, a small sphere around the point excluded it from the field. The sphere had constant radius so the integral is a principal-value one with the symmetry appropriate for such integrals. Such an approach is similar to the classical mathematical one in the sense that we saw the integrand had a singular point after we selected the specific form of the function(i.e., Green function satisfying $\nabla^2 G(\underline{x}, \underline{y}) = \delta(\underline{x} - \underline{y})$) [24] to put into an identity and we found a way to define a finite value for the expression obtained. It is, however, worthy to note that exclusion of the singular point for the scalar function $\phi(\underline{y})$ as a principal value in the previous section is not required in potential flow theory. The exclusion need be only as defined for an improper integral. In our later treatment of the values as a field point tends to a surface point, we will find some integrals are principal-value ones and some are simply improper.

---

[24]The function is of a form $1/r$, which can be also obtained by taking Fourier transform of this equation.

2

BASIS OF FLUID FLOWS

2.1   Introduction

In this chapter, basic concepts and analysis for fluid flow are listed below and will not be presented in detail. Detailed and fundamental explanation can be found in some hydrodynamics texts.

2.1.1   Basic definitions

While solid can be in stable equilibrium under shear stress oblique to the surface separating any two parts, fluid cannot be in stationary equilibrium. [1] Resistance to rate of shear deformation from viscosity gives rise to drag for bodies. We can easily recognize that such shear stresses do exist in fluids: e.g., consider how the fluid in a rotating circular vessel takes on the rotating motion of the vessel eventually.

Other observed properties of fluids are:

(1) resistance to volumetric compression and tension in general,

(2) no shape or preferred orientation,

---

[1] For detailed information on difference and similarity among various fields in continuum mechanics and their historical background, see the article: 이승준 (1992), "재료역학과 고체역학: 유체역학자의 관점에서", 대한 조선학회지, 제29권, 제3호.
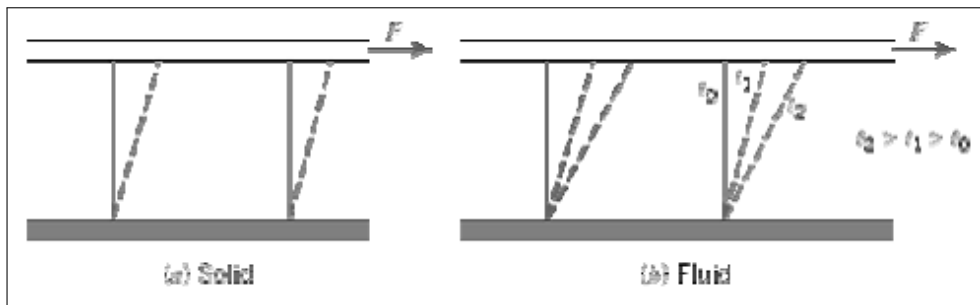
Figure **2.1** Behavior of a solid and a fluid, under the action of constant shear force. (left) solid; (right) fluid. From Fox et al. (2004).

(3) homogeneous matter in general, and

(4) has mass.

There are two kinds of fluids depending on bulk elasticity(compressibility): [2]

(1) liquid forms a free surface(density $\rho \approx 0$ above free surface), and

(2) gas expands to fill container.

With the principal types of fluid flow and their associated phenomena, it is possible to make up practically any flow combination in nature, even the complex system around a moving ship: potential flow pattern, viscosity of fluid, turbulent flow, separation of flow, cavitation, wave making, vortex motion and flow-induced sound.

Such flow phenomena can be characterized by several principal effects which constitute the basis for important relationships in the form of non-dimensional numbers: velocity effects, acceleration effects, force effects, inertia effects, gravity effects, viscosity, elastic effects, surface tension effects.

2.1.2 Assumptions and axioms

We assume that the fluid is <u>continuous</u> and <u>homogeneous</u> in structure. Actually this is not so since matter is ultimately made up of molecules and atoms, but in

---

[2]On the mechanism of formation of liquid and vapor, see Brennen, C. (1995), *Cavitation and Bubble Dynamics*, Oxford University Press, pp. 1–6.

many applications the dimensions we are concerned with are large compared to the molecular structure, and the smallest sample of fluid that concerns us contains a very great number of molecules(i.e., number of about $2.687 \times 10^7/\mu^3$). In such cases, the properties of any sample are the average values over many molecules, and the approximation of a continuum is found to be acceptable and useful.

Nevertheless, results obtained on the assumption of a continuum may be erroneous whenever the molecular structure dimensions are relatively large. For example, at very high altitudes (low pressures), the molecular spacing is so great that air is not even approximately a continuum in its contact with a body the size of an airplane wing. Failures of the continuum assumption occur probably in the cases of that body size compares with molecular dimensions (e.g., a very small body in a fluid) or with distances between molecules (e.g., a body in a rarefied gas).

Other acceptable and useful assumptions are those as follows:

(1) that physical laws are independent of the coordinate system used to express them (frame indifference).

(2) that natural laws are independent of the dimensions of physical quantities that occur in the expressions (dimensional homogeneity),

(3) that derivations of physical quantities with respect to space and time exist to the required order (smoothness of quantities), and

(4) that the present motion is a function of its history and not the future (memory of history).

Newton's laws of motion are derived from rigid body mechanics. Our use of these laws are based on continuum hypothesis. We postulate that mass, momentum and energy are conserved: Conservation of mass, Conservation of momentum, Conservation of energy. Since these notes tend to deal mostly with incompressible flows, we do not examine the conservation of energy.

2.1.3 Description of fluid motion

Although one of our assumption on a fluid is that it is a continuum and does not consist of discrete particles, we introduce the term "fluid particles," such as, "velocity of a particle," etc, to identify simply an infinitesimal portion or sample of the fluid by mathematically tagging it. There are two common ways of representing equations to describe a fluid flow.

2.1.3.1 Lagrangian description

We may take the tag to be the initial position, denoted by $\underline{\xi}(a, b, c)$. Let a, b, c denote the coordinates of any fluid particle at the time $t = 0$. Let x, y, z denote the coordinates of the same particle at time t. Then the flow geometry is completely specified if we know $x = x(a, b, c, t)$, $y = y(a, b, c, t)$, $z = z(a, b, c, t)$. These give the trajectories of various particles.

The <u>pathline</u> of a particle is the curve $\underline{x} = \underline{x}(\underline{\xi}, t)$, where $\underline{x}$ is the position vector. The velocity is $\underline{q}(a, b, c, t) = \partial \underline{x}/\partial t$ and the acceleration is $\partial \underline{q}/\partial t = \partial^2 \underline{x}/\partial t^2$. Any other physical quantities would be given by a function, say, $f = f(a, b, c, t)$. This description is called Lagrangian, material, or convective description of motion.

2.1.3.2 Eulerian description

Instead of following individual particles as above, in Eulerian description we fix our attention on a point in space, x, y, z. Consider any property of the fluid, for example, the density ρ, and calculate its differential:

$$\rho = \rho(x, y, z, t) \tag{2.1}$$

$$d\rho = \frac{\partial \rho}{\partial x} dx + \frac{\partial \rho}{\partial y} dy + \frac{\partial \rho}{\partial z} dz + \frac{\partial \rho}{\partial t} dt = d\underline{\ell} \cdot \nabla \rho + \frac{\partial \rho}{\partial t} dt \tag{2.2}$$

For any given particle as it moves along, dx, dy, dz are not independent; in fact, $dx = u\, dt, dy = v\, dt$, and $dz = w\, dt$, i.e., $d\underline{\ell} = \underline{q}\, dt$, where $\underline{q}(x, y, z, t)$ is the

velocity. Thus, the rate of change of the density of a particle is

$$\frac{d\rho}{dt} = \frac{\partial\rho}{\partial t} + u\frac{\partial\rho}{\partial x} + v\frac{\partial\rho}{\partial y} + w\frac{\partial\rho}{\partial z} = \frac{\partial\rho}{\partial t} + \underline{q}\cdot\nabla\rho \tag{2.3}$$

2.1.4 Particle tracing lines

In the previous subsection, the material and spatial descriptions of the flow were described. Below we list some additional prerequisites.

(1) Local derivative

The time rate of change of a flow quantity at a fixed point $\underline{x}$ is given by

$$\left.\frac{\partial}{\partial t}\right|_{\underline{x}=\text{const}} \tag{2.4}$$

The flow is then called <u>steady</u> if the first term vanishes, that is, it does not vary with time.

(2) Material derivative

We use the symbol $\dfrac{D}{Dt}$ for this type of derivative, sometimes called the "convective or material derivative":

$$\frac{D}{Dt} \equiv \frac{\partial}{\partial t} + \underline{q}\cdot\nabla \tag{2.5}$$

The time rate of change of a flow quantity following a particle is given by

$$\left.\frac{\partial}{\partial t}\right|_{\underline{\xi}=\text{const}} \equiv \frac{D}{Dt} \tag{2.6}$$

The velocity of a particle is the material derivative of the position vector of the particle:

$$\underline{q}^*(\underline{\xi},t) = \left.\frac{\partial\underline{x}}{\partial t}\right|_{\underline{\xi}} = \frac{D\underline{x}}{Dt} = \underline{q}(\underline{x},t) \tag{2.7}$$

This can be applied to any fluid property including vector properties. The

acceleration of a particle, for example, is

$$\frac{D\underline{q}}{Dt} \equiv \frac{\partial \underline{q}}{\partial t} + \underline{q} \cdot \nabla \underline{q} \tag{2.8}$$

A similar description for the evolution of the material line element [3] is

$$\frac{D(d\underline{\xi})}{Dt} = d\underline{q} = dx_j \frac{\partial \underline{q}}{\partial x_j} = d\underline{x} \cdot \nabla \underline{q}. \tag{2.9}$$

If $F(\underline{x}, t)$ is some property of the flow field, then

$$\frac{\partial F}{\partial t}\bigg|_{\underline{\xi}} = \frac{\partial F}{\partial t}\bigg|_{\underline{x}} + \underline{q} \cdot \nabla F \tag{2.10}$$

(3) Streamlines

A streamline is defined as a line everywhere parallel to velocity $\underline{q}$. Namely, the tangent of the streamline at each point is parallel to the fluid velocity at that point. We can produce a streamline by taking a short time exposure picture of a flow for which numerous particles have been tagged. We try to trace out curves on the photograph such that each curve is tangent to the velocity vector at a point.

Let the fluid velocity be denoted by the vector $\underline{q}$; then $\underline{q} = \underline{q}(x, y, z, t) = (u, v, w)$. Differential equations for streamlines are

$$\frac{dx}{u} = \frac{dy}{v} = \frac{dz}{w}. \tag{2.11}$$

If $\underline{x}(\sigma)$ (σ parameter) describes the position vector of a streamline, then $\dfrac{d\underline{x}}{d\sigma}$ is tangent to a streamline and parallel to the velocity at $\underline{x}(\sigma)$. Hence we can express the differential equation for streamlines in terms of the parameter σ:

$$\frac{d\underline{x}}{d\sigma} \times \underline{q}(\underline{x}(\sigma), t) = 0, \quad \text{or} \quad \frac{d\underline{x}}{d\sigma} \propto \underline{q}(\underline{x}(\sigma), t) \tag{2.12}$$

---

[3]A material line is a line composed of the same fluid particles in a moving fluid. Similarly a material surface and a material volume are, respectively, a surface and a volume composed of the same particles. A material surface may be a bounding surface and every impenetrable bounding surface must be a materialsurface.

(4) Streaklines

At time t, a streakline through a fixed point $\underline{y}$ is the curve traced out by particles each of which have gone through $\underline{y}$ since time $t_0 < t$. (Typically $t_0 = 0$.) Physically we construct a streakline by making (or tagging) all particles that pass a point, e.g., by continuously emitting dye at that point. The dye trail marks the streakline.

A particle is on the streakline at time of observation t if it had been at $\underline{y}$ at time s where s lies in the inteval $t_0 \leq s \leq t$. The material coordinates fo the particle that went through $\underline{y}$ at s are $\underline{\xi} = \underline{\xi}(\underline{y}, t)$. At time t, the particle is at the spatial position

$$\underline{x} = \underline{x}\left(\underline{\xi}(\underline{y}, s), t\right) \tag{2.13}$$

where $\underline{y}$ and t are to be assigned and s varies from t_0 to t to trace out the streakline.

For steady flows, a pathline, a streamline and a streakline coincide.

2.1.4.1   Example of particle tracing lines

(1) Velocity field

The concepts of various flow lines may be illustrated by the 2-D case for which the particle velocity is considered to be

$$\underline{q}^*(\underline{\xi}, t) = \xi_1 \underline{i} + \xi_2 e^t \underline{j} \tag{2.14}$$

This means that at the initial time $t_0 = 0$ the particle velocity is equal to the position vector: $\underline{q}^*(\underline{\xi}, 0) = \underline{\xi}$, and as time proceeds from $t = 0$, the horizontal component of the velocity remains unchanged but the vertical velocity component grows exponentially with time.

(2) Pathlines

The <u>pathline</u> of the particle that was initially at $\underline{\xi}$ is the curve

$$\underline{x} = \underline{\xi} + \int_0^t \underline{q}^*(\underline{\xi}, t)\, dt = \xi_1(1 + t)\,\underline{i} + \xi_2\, e^t\, \underline{j} \tag{2.15}$$

Spatial coordinates and material coordinates can be related:

$$x_1 = \xi_1\,(1+t), \qquad x_2 = \xi_2\,e^t \tag{2.16}$$

This is the parametric representation of the pathline. Eliminate the parameter t from the equation to find the <u>pathline</u> in the (x_1, x_2) plane:

$$x_2 = \xi_2\,e^{(x_1/\xi_1 - 1)} \tag{2.17}$$

The inverse of the pathline is the relation obtained by solving for $\underline{\xi}(\underline{x}, t)$

$$\underline{\xi} = \frac{x_1}{(1+t)}\,\underline{i} + \frac{x_2}{e^t}\,\underline{j} \tag{2.18}$$

With the inverse of the pathlines known, the spatial description of the velocity vector can be constructed:

$$
\begin{aligned}
\underline{q}(\underline{x}, t) &= \underline{q}^*(\underline{\xi}(x, t), t) \\
&= \frac{x_1}{(1+t)}\,\underline{i} + \frac{x_2}{e^t}\,e^t\,\underline{j} \\
&= \frac{x_1}{(1+t)}\,\underline{i} + x_2\,\underline{j}
\end{aligned}
\tag{2.19}
$$

If the spatial description of the velocity vector were given, the differential equation of the particle pathline would be

$$\frac{\partial \underline{x}\,(\underline{\xi}, t)}{\partial t} = \underline{q}\left(\underline{x}(\underline{\xi}, t), t\right) \tag{2.20}$$

and, if solved, would give the same expressions as above.

(3) Streamlines

We can also use the spatial description of the velocity field to the find the position vector of a streamline, $\underline{x}(\sigma, t)$:

$$
\begin{aligned}
\left.\frac{\partial \underline{x}}{\partial \sigma}\right|_t &= \underline{q}\left(\underline{x}(\sigma), t\right)) \\
&= \frac{x_1(\sigma)}{(1+t)}\,\underline{i} + x_2(\sigma)\,\underline{j}
\end{aligned}
\tag{2.21}
$$

From which we obtain

$$x_1(\sigma) = c_1 \, e^{\frac{\sigma}{(1+t)}} \tag{2.22}$$

$$x_2 = c_2 \, e^{\sigma} \tag{2.23}$$

If we eliminate the parameter σ from these two equations, then in the (x_1, x_2) plane the streamlines are the curves:

$$x_2 = c_2 \, (x_1/c_1)^{(1+t)} \tag{2.24}$$

Note that $x_2 = k \, x_1$ at $t = 0$.

(4) Streaklines

The streaklines are determined by finding the material coordinates of a particle that was a spatial position $\underline{y}$ at some time s. We use the inverse relations for the pathline to define the relationship:

$$\underline{\xi} = \frac{y_1}{(1+s)} \, \underline{i} + \frac{y_2}{e^s} \, \underline{j} \tag{2.25}$$

Hence the streakline is

$$\underline{x}(s) = \frac{y_1}{(1+s)}(1+t) \, \underline{i} + \frac{y_2}{e^s} \, e^t \, \underline{j} \tag{2.26}$$

At $s = t$, these relations give $\underline{x} = \underline{y}$, so that is the location of the particle just passing through the spatial point $\underline{y}$. At $s = 0$, the particle that was previously at $\underline{y}$ for $t = 0$ is to be found. To find the streakline definition for any time, we solve the i component for the relationship between s and the other variables:

$$s = \left(\frac{y_1}{x_1}\right)(1+t) - 1 \tag{2.27}$$

and from the second equation:

$$x_2 = y_2 \, e^{t-(1+t)(y_1/x_1)+1} \tag{2.28}$$

Thus for any particular time t this equation gives the equation of the streakline through the point $\underline{y}$.

Typical flow patterns are illustrated in Figure **2.2** .
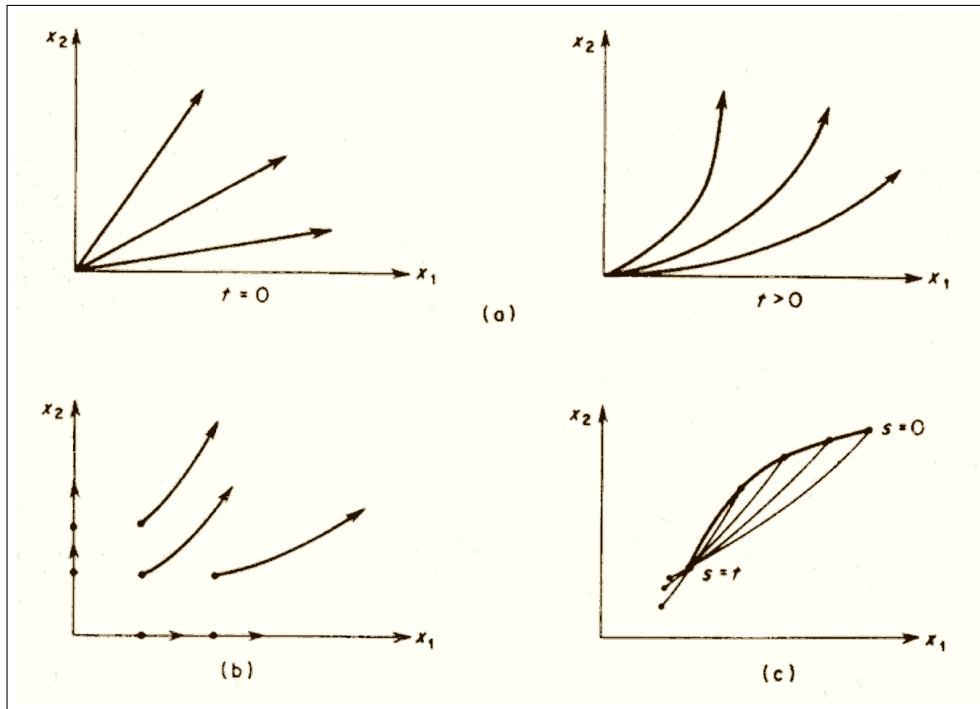
Figure **2.2** Example of various flow lines. (a) streamlines at $t = 0$ and $t > 0$; (b) path lines; (c) streakline. From Aris (1962), p. 82.

2.2   Kinematics

2.2.1   Continuity

Consider an arbitrary volume $V(t)$ enclosed in a material surface $S(t)$. A material surface is always composed of the same fluid particles. As the volume moves through space it experiences deformation although the mass within the volume remains constant. The mass enclosed within $V(t)$ is given by, in an integral form for density ρ,

$$\int_{V(t)} \rho \, dV \tag{2.29}$$

where the integration is over the region of space occupied by V at time t. Since the mass of the material volume is constant, the time derivation of this expres-

sion is zero:

$$\frac{d}{dt} \int_{V(t)} \rho \, dV = 0 \tag{2.30}$$

Using the (Reynolds) transport theorem, one obtains

$$\int_{V(t)} \left[\frac{\partial \rho}{\partial t} + \nabla \cdot (\rho \, \underline{q}) \right] dV = 0. \tag{2.31}$$

This is the integral form of the continuity equation. Since the volume taken is arbitrary, the integrand must be zero at all points within V:

$$\frac{\partial \rho}{\partial t} + \nabla \cdot (\rho \, \underline{q}) = 0. \tag{2.32}$$

This is the spatial or Eulerian description of the continuity equation. The above derivation of the continuity equation was from the system analysis point of view for which the mass within a deformable bounding surface is constant. Meanwhile, it is common to also use control volume analysis, for which one consider an arbitrary fixed volume V enclosed in a surface S. Let $\underline{n}$ be the outward unit normal vector. The mass of fluid in V is $\int_V \rho \, dV = m$, say. If m increases it means that fluid has entered through S:

$$\frac{dm}{dt} = - \int_S \rho \, \underline{n} \cdot \underline{q} \, dS \tag{2.33}$$

and by the "divergence theorem", this surface integral is equal to

$$- \int_V \nabla \cdot (\rho \, \underline{q}) \, dV, \tag{2.34}$$

V being a fixed volume, we can write

$$\frac{dm}{dt} = \int_V \frac{\partial \rho}{\partial t} \, dV \tag{2.35}$$

Hence, for arbitrary choice of V, we have

$$\int_V \frac{\partial \rho}{\partial t} \, dV = - \int_V \nabla \cdot (\rho \, \underline{q}) \, dV. \tag{2.36}$$

The only way that these integrals can be equal for any and every choice of V is that their integrands be equal; thus we obtain the *General Equation of Continuity*:

$$\frac{\partial \rho}{\partial t} + \nabla \cdot (\rho \, \underline{q}) = 0 \qquad (2.37)$$

Noting that $\nabla \cdot (\rho \, \underline{q}) = \underline{q} \cdot \nabla \rho + \rho \nabla \cdot \underline{q}$, this equation can be expressed, in an alternative form, as

$$\frac{D\rho}{Dt} + \rho \nabla \cdot \underline{q} = 0 \qquad (2.38)$$

There are two important special cases:

(1) Steady motion

Since, for steady motion, all partial derivatives $\partial(\ )/\partial t$ vanish, Eq. (2.37) becomes

$$\nabla \cdot (\rho \, \underline{q}) = 0 \qquad (2.39)$$

(2) Incompressible flow

If the density of every particle is constant, $D\rho/Dt = 0$, and Eq. (2.38) gives us

$$\nabla \cdot \underline{q} = 0 \qquad (2.40)$$

Vector fields with this property are called solenoidal. Most of our work will deal with incompressible fluid. It is to be noted that this is correct whether the fluid is steady or not, and moreover it applies to the case of an inhomogeneous fluid, such as a stratified liquid, in which ρ varies throughout the fluid, provided each particle is incompressible.

2.2.2   Vorticity, circulation, and velocity potential

2.2.2.1   Vorticity

The vector function $\nabla \times \underline{q}$, where $\underline{q}(x, y, z, t)$ is the velocity of the fluid, is called the <u>vorticity</u>. Its components are occasionally represented by the symbols

ξ, η, ζ; namely, in rectangular Cartesian coordinates

$$\xi = \frac{\partial w}{\partial y} - \frac{\partial v}{\partial z}, \quad \eta = \frac{\partial u}{\partial z} - \frac{\partial w}{\partial x}, \quad \zeta = \frac{\partial v}{\partial x} - \frac{\partial u}{\partial y} \tag{2.41}$$

To give a physical feature of the meaning of vorticity, it is often said that $\nabla \times \underline{q}$ is twice the angular-velocity vector of the fluid particle. Since the particle is being deformed continually, perhaps we should say the average angular velocity at a point.

2.2.2.2   Vortex line and vortex tube

A vortex line is a curve which is tangent at each point to the vorticity at the point. It is analogous to the stream line. Its differential equation is $dx/\xi = dy/\eta = dz/\zeta$ where the Cartesian component of $\underline{\omega}$ are ξ, η, ζ.

Since the divergence of any curl of a vector must be zero, a continuity equation $\nabla \cdot \underline{\omega}$ for $\underline{\omega}$ must be invoked especially in the case that the vorticity field is itself to be sought with independence of the velocity field. The condition $\nabla \cdot \underline{\omega} = 0$ can be thought of as meaning that vortex lines do not begin nor end in the fluid. We call a tube whose walls are made up of vortex lines a vortex tube. (The analogous tube made up of streamlines would be called a stream tube.)

2.2.2.3   Circulation and vorticity flux

We classify flows as irrotational and rotational, depending on whether $\nabla \times \underline{q}$ is or is not everywhere zero. The irrotational type will be found to be rather common, for sound physical reasons, and will occupy a considerable portion of our time.

The line integral

$$\Gamma = \oint_C \underline{q} \cdot d\underline{\ell} \tag{2.42}$$

where $\underline{q}$ is the fluid velocity, taken about any closed curve C in space, is called the circulation about the contour C.

By Stokes theorem, it is clear that the circulation and vorticity are related, for

$$\Gamma = \oint_C \underline{q} \cdot d\underline{\ell} = \int_S \underline{n} \cdot (\nabla \times \underline{q}) \, dS = \int_S \underline{n} \cdot \underline{\omega} \, dS \qquad (2.43)$$

The transformation is only permissible, of course, when $\underline{q}$ is finite and has continuous partial derivatives at each point of S; we may encounter some cases where certain singularities have to be excluded from such processes.

Obviously, if the flow is wholly irrotational, Γ will be zero for every contour. In any case, Γ is zero if C encloses only irrotational portions of the flow.

2.2.2.4 Vortex strength

Again consider the application of Stokes theorem to a cross-section of the vortex tube:

$$\int_\Sigma \underline{n} \cdot \underline{\omega} \, dS = \Gamma = \text{constant along tube} \qquad (2.44)$$

Thus the average vorticity in the cross-section varies inversely as the cross-sectional area. The vorticity becomes very small if the tube spreads out. This is the result of viscosity, for example; the vorticity is dissipated over a wide region.

Suppose, on the other hand, that the tube is necked down; this makes the vorticity large. In the extreme case, we imagine that the tube is contracted to a line. Then the vorticity at this line becomes infinite, but the circulation is still the same, Γ. This is called a vortex filament, or briefly a "vortex", and Γ is its strength.

It is a kind of mathematical approximation to the case where all the vorticity is confined to a tube of relatively small cross-section, as often occurs in nature – for example in a tornado. Outside the core of a tornado, the air is in practically irrotational motion.

The irrotational concentric flow represents the case of a long, straight vortex filament; the singularity at the center is the filament, and there the vorticity is infinite, as predicted. Clearly, a vortex tube or filament, consisting of vortex

lines, cannot begin nor end in the fluid. It can double back on itself in a ring or terminate at a boundary of the fluid.

2.2.2.5 Velocity potential

In regions where the flow is <u>irrotational</u>, the line integral around an entire closed path is the circulation and is zero because the flow is irrotational. This implies that the open line integral $\int q \cdot d\underline{\ell}$ is independent of the path within the regions, but only dependent of the end points of the path. Therefore, choosing A as a fixed point and B as a varying point,

$$\int_{A}^{B(x,y,z)} \underline{q} \cdot d\underline{\ell} = \phi(x, y, z), \tag{2.45}$$

and

$$d\phi = \underline{q} \cdot d\underline{\ell} \tag{2.46}$$

Now we see that $d\phi = d\underline{\ell} \cdot \nabla\phi$ from Eq. (1.61) and hence $d\underline{\ell} \cdot \nabla\phi = \underline{q} \cdot d\underline{\ell}$ for arbitrary choice of $d\underline{\ell}$. This means that

$$\underline{q} = \nabla\phi \tag{2.47}$$

By retracing these steps you will see immediately that this result has nothing to do with the physical meaning of $\underline{q}$. That is, the result Eq. (2.47) will follow for every vector function $\underline{q}$ whose curl is zero. Moreover, the condition $\nabla \times \underline{q} = 0$ is <u>necessary</u>, as well as <u>sufficient</u>, for the result $\underline{q} = \nabla\phi$, because the curl of every gradient is identically zero.

In the case considered here, where $\underline{q}(\underline{x}, t)$ is the fluid velocity, $\phi(\underline{x}, t)$ is called the <u>velocity potential</u>. The surfaces $\phi = $ constant are called *equipotential* surface; thus $\underline{q}$ is the vector perpendicular to these surfaces at every point, and its magnitude is that of derivative $\partial\phi/\partial n$ in the normal direction. These statements are verified by using the relation $d\phi = d\underline{\ell} \cdot \nabla\phi$.

2.2.3 Helmholtz decomposition of a velocity field

The Helmholtz decomposition theorem states that an arbitrary continuously differentiable velocity field can be represented as a combination of solenoidal and irrotational velocity field. [4] Thus for any finite continous velocity field which vanishes at infinity we may find a scalar function (velocity potential) ϕ and a vector potential function (vector stream function) $\underline{A}$ such that

$$q = \nabla\phi + \nabla \times \underline{A} \tag{2.48}$$

To prove this decomposition, we first need the solution of Possion's equation

$$\nabla^2\phi = f(\underline{x}) \tag{2.49}$$

where $f(\underline{x}) = \nabla \cdot q$. We can consider an unsteady velocity field, if necessary, just by adding the time variable.
The solution is provided by the integral [5]

$$\phi(\underline{x}) = -\frac{1}{4\pi}\int_V \frac{f(\underline{\xi})}{r}\,dV_\xi \tag{2.50}$$

where $r = |\underline{x} - \underline{\xi}|$ is the distance from the volumetric element dV_ξ to the point x, y, z. The integration is carried throughout the entire fluid. If f is only defined in a certain region, we may set it equal to zero outside, and if it is defined everywhere we require that it should tend to zero towards infinity.

Now let us return the Helmholtz decomposition form. We have started with the equation $\nabla \cdot q = \nabla^2\phi$ by taking the divegence of the orginal decomposion form, and have derived the solution given by, again,

$$\phi(\underline{x}) = -\frac{1}{4\pi}\int_V \frac{\nabla \cdot q}{r}\,dV_\xi \tag{2.51}$$

Consequently, $q - \nabla\phi$ is a solenoidal since $\nabla \cdot (q - \nabla\phi) = 0$ from $\nabla \cdot q = \nabla^2\phi$.

---

[4]See Aris, R. (1962), *Vectors, Tensors and the Basic Equations of Fluid Mechanics*, Prentice Hall, p. 70.
[5]See Batchelor, G. K. (1967), *An Introduction to Fluid Dynamics*, Cambridge University Press, Cambridge.

Hence we can construct a vector potential function $\underline{A}$ such that

$$q - \nabla\phi = \nabla \times \underline{A} \tag{2.52}$$

which reaches to the Helmholtz decomposition form. In the next subsection, we will deal with the vector potential $\underline{A}$.

Proof of Eq. (2.50)

Consider the gradient of ϕ with respect to $\underline{x}$

$$\nabla_x \phi = +\frac{1}{4\pi} \int_V \frac{f(\underline{\xi})}{r^3}(\underline{x} - \underline{\xi})\, dV_\xi \tag{2.53}$$

Now take integral of $\nabla^2\phi$, where ϕ is given by Eq. (2.50), over an arbitrary volume V enclosed in a closed surface S, and use the divergence theorem:

$$
\begin{aligned}
\int_V \nabla^2\phi\, dV_x &= \oint_S \underline{n} \cdot \nabla\phi\, dS_x \\
&= \oint_S \underline{n} \cdot \left\{ \frac{1}{4\pi} \int_V \frac{f(\underline{\xi})}{r^3}(\underline{x} - \underline{\xi})\, dV_\xi \right\} dS_x \\
&= \int_V f(\underline{\xi})\, dV_\xi \oint_S \frac{\underline{n} \cdot (\underline{x} - \underline{\xi})}{4\pi r^3}\, dS_x
\end{aligned}
\tag{2.54}
$$

Here we have changed the order of integration, since $f(\underline{\xi})$ is the value at the element dV_ξ and is therefore independent of the integration over S. Since $\dfrac{(\underline{x} - \underline{\xi})}{r}$ is a unit vector, $\dfrac{\underline{n} \cdot (\underline{x} - \underline{\xi})\, dS}{r^3}$ is just the solid angle subtended at the point $\underline{\xi}$ by the surface element at the integration point $\underline{x}$. (See Figure 2.3 .)

Now if $\underline{\xi}$ is outside of the volumetric region V, the integral of this solid angle is zero because the contribution from the surface element at $\underline{x}$ is equal and opposite to one from the surface element that is projected extensively on the opposite side of the closed surface. However if $\underline{\xi}$ is inside of the volumetric region V, then the integral is the total solid angle for the closed surface which is equal to 4π.
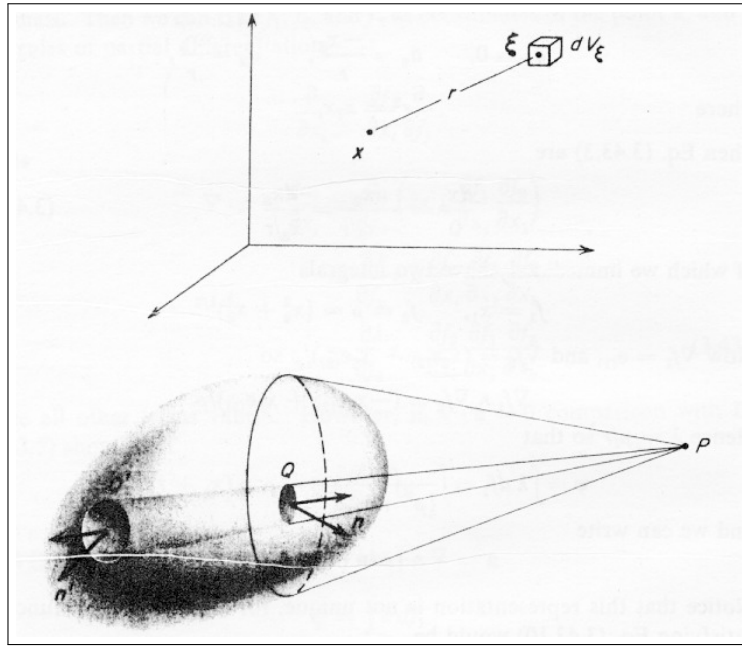
Figure **2.3** Integration region for Poisson's solution of vector fields. From Aris (1962), p. 70.

It follows that

$$\oint_S \frac{\underline{n} \cdot (\underline{x} - \underline{\xi})}{4\pi r^3} \, dS_x = \begin{cases} 1 & \text{if } \underline{\xi} \text{ is inside } V \\ 0 & \text{if } \underline{\xi} \text{ is ouside } V \end{cases} \tag{2.55}$$

Thus the last integral over the whole space of $\underline{\xi}$ has zero integrand outside of V and so may be regarded as the ontegral over V only. Then

$$\int_V \nabla^2 \phi \, dV_x = \int_V f(\underline{x}) \, dV_x \tag{2.56}$$

Since the volume V was arbitrary, this equation reduces to the Poisson's equation (Eq. (2.49)), and Eq. (2.50) gives its solution.

■■■

2.2.4   Velocity field of a vortex: Biot-Savart integral

In order to determine the velocity field of a vortex in an incompressible fluid, we begin with a more general case of rotational flow and later specialize for a vortex filament. Consider incompressible rotational flow in general. The ve-

locity potential does not exist, but, as will be seen later, it may be possible to determine a *vector-potential function* $\underline{A}(x, y, z, t)$, such that

$$q = \nabla \times \underline{A} \tag{2.57}$$

This form has the advantage of satisfying the incompressible equation of continuity identically, for the divergence of every curl is zero. Thus $\underline{A}$ is related to a stream function.

Now we shall try to determine $\underline{A}(x, y, z, t)$ for any given distribution of vorticity $\underline{\omega}(x, y, z, t)$, for then we shall have $\underline{q}(x, y, z, t)$ in terms of the vorticity—a sort of inverse of the relation $\underline{\omega} = \nabla \times \underline{q}$. The relation between $\underline{\omega}$ and $\underline{A}$ is, using Eq. (1.72)

$$\underline{\omega} = \nabla \times (\nabla \times \underline{A}) = \nabla(\nabla \cdot \underline{A}) - \nabla^2 \underline{A} \tag{2.58}$$

This is a differential equation for $\underline{A}$, for given $\underline{\omega}$, and our aim is to obtain a particular integral. We can now assume that $\nabla \cdot \underline{A} = 0$; this does not sacrifice any generality, for we are trying to calculate $\underline{A}$ for given $\underline{\omega}$. If we can succeed in calculating it with this restriction, the problem will be solved. However, we shall have to check our result to verify that the divergence vanishes. With this assumption,

$$\underline{\omega} = -\nabla^2 \underline{A} \tag{2.59}$$

Now Eq. (2.59) is Poisson's equation, and its solution is [6]

$$\underline{A}(x, y, z, t) = \frac{1}{4\pi} \int_V \frac{\underline{\omega}}{r} \, dV \tag{2.60}$$

where $r = |\underline{x} - \underline{\xi}|$ is the distance from the element dV to the point x, y, z, and the integration is carried throughout the entire fluid.

Consequently, the velocity induced by the vorticity distribution is given by

$$\underline{q}(\underline{x}, t) = \nabla \times \underline{A} = \frac{1}{4\pi} \int_V \underline{\omega} \times \frac{(\underline{x} - \underline{\xi})}{|\underline{x} - \underline{\xi}|^3} \, dV \tag{2.61}$$

where the integration variable is $\underline{\xi}$.

[6]See Batchelor, G. K. (1967), *An Introduction to Fluid Dynamics*, Cambridge University Press, Cambridge.

Equation (2.61) is called the *Biot-Savart integral*, by analogy with the expression for the magnetic flux due to a conductor carrying a current. This analogy also leads to the name 'induced velocity' for $\underline{q}$.

To illustrate the use of this result Eq. (2.60), let us calculate the velocity in the field of a vortex filament. That is, let us assume that the vorticity is concentrated in a tube of very small cross-sectional area δS and circulation $\Gamma = \omega\,\delta S$. Then

$$\underline{A} = \frac{1}{4\pi} \int_C \frac{\underline{\omega}}{r} \delta S\,d\ell = \frac{1}{4\pi} \int_C \frac{\Gamma\,\underline{e}_\ell}{r}\,d\ell = \frac{\Gamma}{4\pi} \int_C \frac{d\underline{\ell}}{r} \tag{2.62}$$

where $d\ell$ is an element of length along the filament, $\underline{e}_\ell$ is a unit vector in the direction of the filament, and $d\underline{\ell}$ denotes $\underline{e}_\ell d\ell$. The velocity at $P(x, y, z)$, due to the particular element $d\ell$ is

$$d\underline{q} = \frac{\Gamma}{4\pi} \nabla \times \left(\frac{d\underline{\ell}}{r} \right) = \frac{\Gamma}{4\pi} \nabla \left(\frac{1}{r} \right) \times d\underline{\ell} = -\frac{\Gamma}{4\pi} \frac{\underline{r} \times d\underline{\ell}}{r^3} \tag{2.63}$$

In other words, the velocity due to the filament $d\underline{\ell}$ is directed normal to the plane of $d\underline{\ell}$ and $\underline{r}$, and its magnitude is

$$dq = \frac{\Gamma}{4\pi r^2} \sin\theta\,d\ell \tag{2.64}$$

where θ is defined by the angle between $d\underline{\ell}$ and $\underline{r}$.

Proof of Eq. (2.60)

Consider the integral of $\nabla^2\underline{A}$, where $\underline{A}$ is given by Eq. (2.60), through an arbitrary volume V enclosed in a surface S:

$$\int_V \nabla^2\underline{A}\,dV = \oint_S \underline{n} \cdot \nabla\underline{A}\,dS = \oint_S \underline{n} \cdot \nabla \left(\frac{1}{4\pi} \int_V \frac{\underline{\omega}}{r}\,dV \right) dS \tag{2.65}$$

Since $\underline{\omega}$ is the value at the element dV and is therefore independent of the integration over S, the contribution of the element dV to this integral is

$$\frac{1}{4\pi} \underline{\omega}\,dV \oint_S \underline{n} \cdot \nabla \left(\frac{1}{r} \right) dS = -\frac{1}{4\pi} \underline{\omega}\,dV \oint_S \frac{\underline{n} \cdot \underline{r}}{r^3}\,dS \tag{2.66}$$

The last integral is either zero or 4π, depending on whether dV is inside or outside S, according to the divergence theorem. Thus the contribution of dV is zero if dV is outside V and is $-\underline{\omega}\,dV$ if dV is within V. Consequently, when the integration is taken throughout the fluid, the result is

$$\int_V \nabla^2 \underline{A}\,dV = -\int_V \underline{\omega}\,dV \tag{2.67}$$

and since V is arbitrary, the integrands must be equal.

■■■

Proof of divergence-free $\nabla \cdot \underline{A} = 0$

Next, we must prove that Eq. (2.60) is divergence-free $\nabla \cdot \underline{A} = 0$. Equation (2.60) makes $\underline{A}$ a solution of Eq. (2.59), but not a solution of the differential equation we are trying to solve, Eq. (2.58), unless $\nabla \cdot \underline{A}$ is zero, as has already been mentioned. Therefore take the divergence of Eq. (2.60):

$$\nabla \cdot \underline{A} = \frac{1}{4\pi} \int_V \underline{\omega} \cdot \nabla \left(\frac{1}{r}\right) dV \tag{2.68}$$

But, using an obvious notation, $r = \sqrt{(x-\xi)^2 + (y-\eta)^2 + (z-\zeta)^2}$ and $\nabla_x \left(\frac{1}{r}\right) = -\nabla_\xi \left(\frac{1}{r}\right)$, where ∇_x denotes $\underline{i}\frac{\partial}{\partial x} + \cdots$ etc. and ∇_ξ denotes $\underline{i}\frac{\partial}{\partial \xi} + \cdots$ etc. Moreover,

$$\underline{\omega} \cdot \nabla_\xi \left(\frac{1}{r}\right) = \nabla_\xi \cdot \left(\frac{\underline{\omega}}{r}\right) - \frac{1}{r}\nabla_\xi \cdot \underline{\omega} = \nabla_\xi \cdot \left(\frac{\underline{\omega}}{r}\right) \tag{2.69}$$

Thus, the integral in Eq. (2.68) can be changed to a surface integral of $\underline{n}\cdot\underline{\omega}/r$, by the divergence theorem, and the surface integrated over is the surface enclosing all the areas of rotational flow. But this will be the outer walls of vortex tubes, and on these $\underline{n} \cdot \underline{\omega} = 0$. Hence the divergence is zero as required. [7]

■■■

---

[7]See Lamb, H. (1932), *Hydrodynamics*, Sixth Ed., Dover.

2.3 Dynamics

2.3.1 Forces

Two types of net forces act in flow problems: (1) body forces and (2) surface forces.

2.3.1.1 Body forces

From external source the body force acts throughout volume from afar (e.g., gravity, magnetic attraction). It is convenient to define the net body force as

$$\underline{F}_b(t) = \int_V \underline{F}_B(\underline{x}, t) \, dV \tag{2.70}$$

where $\underline{F}_B(\underline{x}, t)$ is the body force per unit volume acting at a point $\underline{x}$. For gravity $\underline{F}_B = -\rho\, g\, \underline{e}_3$ where $\underline{e}_3$ is the unit vector directed along the upward vertical. Often the body force is defined as the body force per unit mass:

$$\underline{F}_b(t) = \int_V \rho\, \underline{f}(\underline{x}, t) \, dV \tag{2.71}$$

e.g., for gravity $\underline{f}(\underline{x}, t) = -g\, \underline{e}_3$. The torque due to the body force about the spatial point $\underline{x}_0$ is

$$\underline{Q}(t) = \int_V (\underline{x} - \underline{x}_0) \times \underline{F}_B(\underline{x}, t) \, dV \tag{2.72}$$

We will consider only conservative body forces, for which the body force is derived from a scalar potential

$$\underline{F}_B(\underline{x}, t) = -\nabla \Omega(\underline{x}, t) \tag{2.73}$$

For the body force due to gravity, $\Omega = \rho\, g\, x_3$.

2.3.1.2 Surface forces

Internal sources that cancel except at bounding surfaces that have no continuation volume provide an equal but oppositely directed force. Surface force is defined in terms of a stress distribution on the bounding surface

$$\underline{F}_S = \oint_S \underline{\tau}(\underline{x}_s, t)\, dS \tag{2.74}$$

where S bounds V, $\underline{\tau}(\underline{x}_s, t)$ is the stress vector at a point $\underline{x}_s$ on the surface S, with three components. The torque about a field point $\underline{x}_0$ due to the surface force is

$$\underline{Q}(t) = \oint_S (\underline{x}_s - \underline{x}_0) \times \underline{\tau}(\underline{x}_s, t)\, dS \tag{2.75}$$

2.3.1.3 Stress and stress tensor

The stress vector $\underline{\tau}(\underline{x}_s, t)$ is associated with a normal vector to the surface upon which it acts in the sense that if the stresses were in local equilibrium (i.e, no acceleration or other surface forces act), the stress on the one side of a surface(the side denoted by the normal) is equal and oppositely directed as that on the other side (see Figure **2.4**).
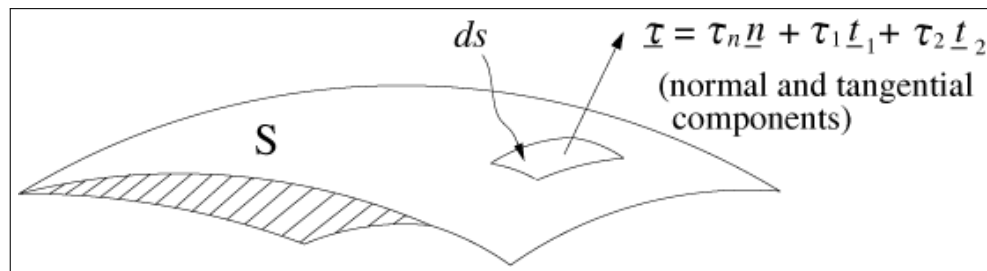
Figure 2.4 Stress vector at surface.

    Let $\underline{n}$ be the normal pointing out of the volume(exterior normal), then $-\underline{n}$ is pointing into the volume(the interior normal), and $\underline{\tau}_{(n)} = -\underline{\tau}_{(-n)}$. This fact leads one to an expressing for the local stress vector as the dot product of the normal(so the equal and opposite property is satisfied) and a dyadic quantity

called the stress tensor of 2nd order

$$\underline{\tau} = \underline{n} \cdot \underline{\underline{\tau}} \tag{2.76}$$

where $\underline{\underline{\tau}}$ is the stress tensor represented with 3 by 3 elements. [8] In three-dimensional Euclidian space, we can write the stress tensor in the dyadic form

$$\underline{\underline{\tau}} = \sum_{i=1}^{3} \sum_{j=1}^{3} \tau_{ij} \, \underline{e}_i \, \underline{e}_j \tag{2.77}$$

where $\underline{e}_i$ and $\underline{e}_j$ are unit base vectors and the scalars τ_{ij} are the physical components of the tensor. Our expression has been with Cartesian coordinates but the same concepts apply to other curvilinear coordinate systems just as well, and definition of the stress tensor components in a system compatible with the geometry is desired.

A fluid is defined as a material that cannot be in stationary equilibrium with applied shear stress. A Newtonian fluid has a resistance to shear deformation that is linearly proportional to the rate of deformation(i.e., proportional to the gradient of velocity), while an ideal(perfect) fluid has no resistance to shear deformation. This linearity can be applied to elastic solids that follow Hooke's law.

Four motions of a fluid particle element are possible: (i) translation, (ii) rotation, (iii) volumetric change, and (iv) squeeze motion. Among them, (iii) and (iv) cause stress in a fluid, while (i) and (ii) represent only rigid body motion for which there will be no stress developed. If there were no deformation(also including rigid body motion), then only a static pressure acts normal to the surface of the volume of interest. The stress vector is simply $\underline{\tau} = -p \, \underline{n}$. Thus the stress tensor $\underline{\underline{\mathbf{T}}} = -p \, \underline{\underline{\mathbf{I}}} = -p \, \delta_{ij}$. The pressure diagram of a fluid is shown in Figure **2.5** .

Combining the above statements leads one to, for a Newtonian fluid,

$$\underline{\underline{\tau}} \equiv \tau_{ij} = -p \, \underline{\underline{\mathbf{I}}} + \mu \left[\nabla \underline{q} + (\nabla \underline{q})^T \right] \tag{2.78}$$

---

[8]Tensors of second order are denoted by using the double under bar $\underline{\underline{\cdot}}$.
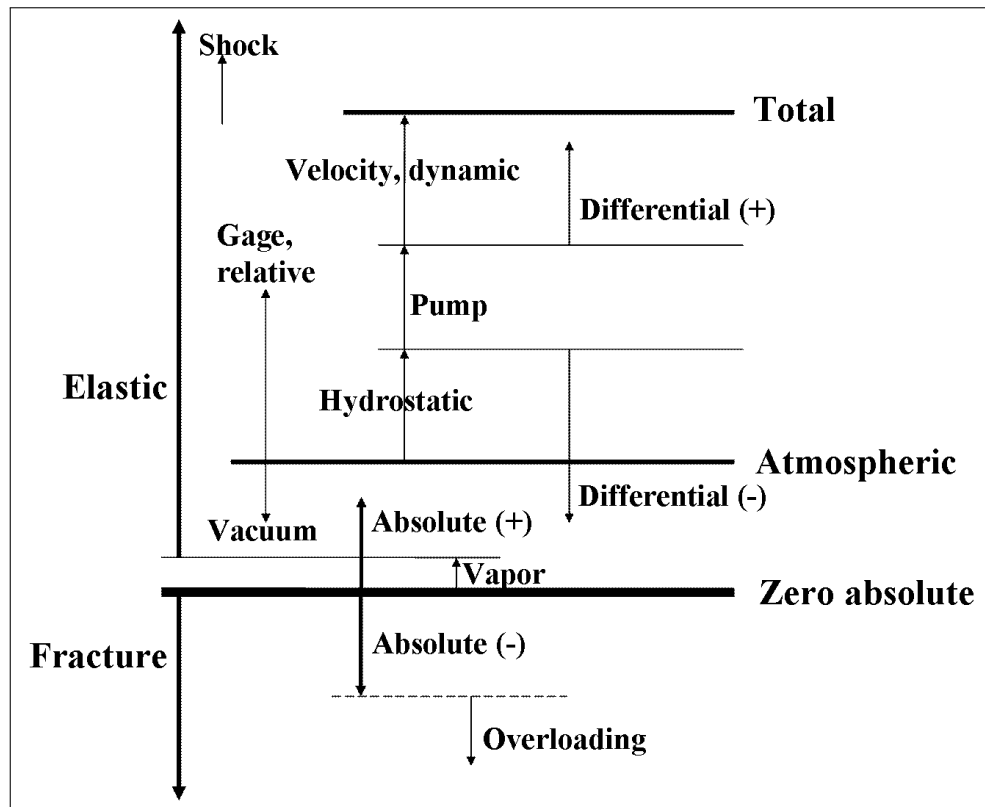
Figure 2.5 Pressure diagram of a fluid.

Here, the proportionality constant μ is called the viscosity coefficient of the
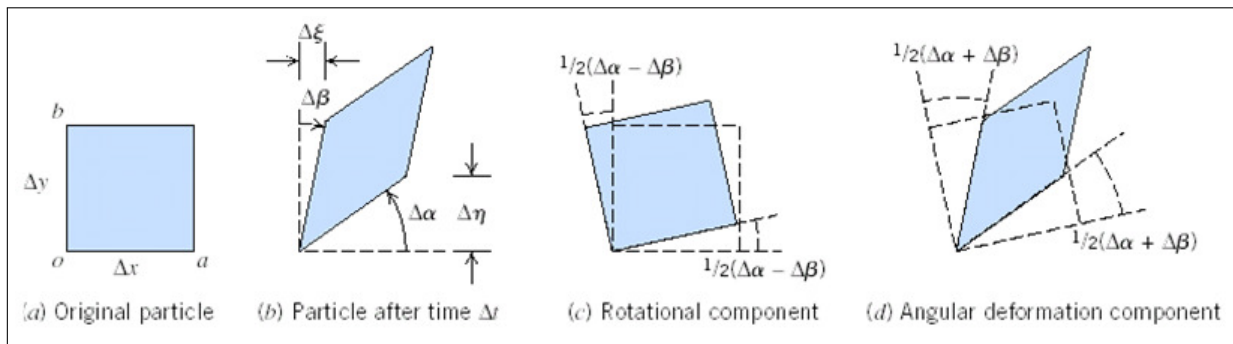
Figure 2.6 Deformation of fluid element in 2-D flows. From Fox, McDonald & Pritchard (2004)

fluid, and the second term is called the viscous stress tensor. The stress tensor is symmetric, i.e., $\tau_{ij} = \tau_{ji}$, because otherwise there will be an unreasonable motion with an infinite speed due to the resultant unbalanced forces acting on an infinitesimal fluid element. Symmetry means that only 6 components are independent (not fully 9). The diagonal terms consist of the divergence of the

velocity vector and (averaged) static pressures, and hence, for an incompressible fluid, are associated with volumetric changes. The off-diagonal terms are associated with the squeeze-like motion.

2.3.2 Example: Stress tensors for low Reynolds number flows

As an example of stress tensors, let us consider low-Reynolds number flow (Stokes flow). [9]
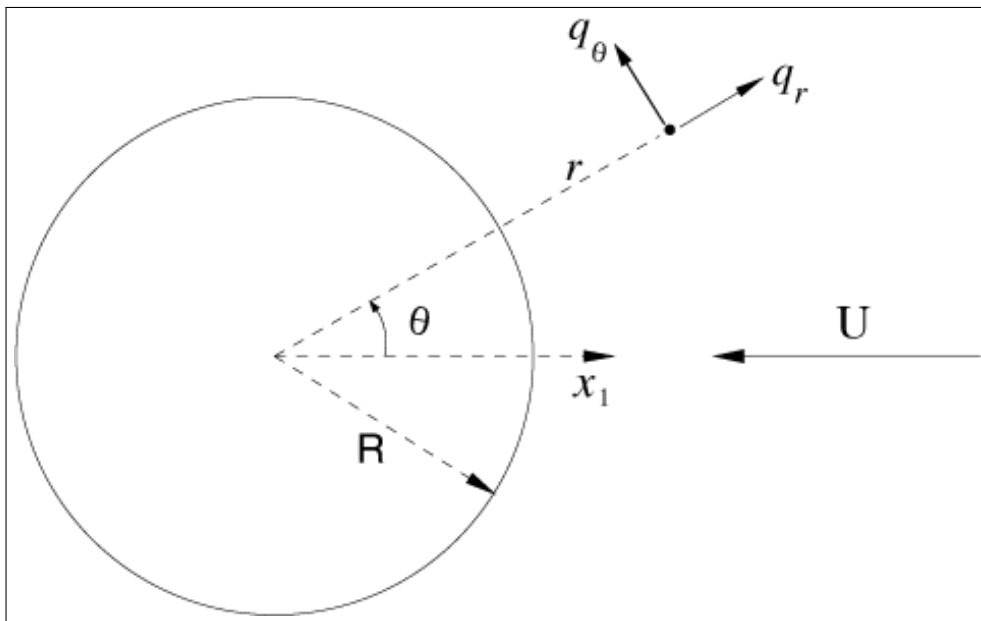
Figure **2.7** Notation for a spherical bubble in uniform flow.

2.3.2.1 Velocity field

The governing equations for such a fluid are, neglecting the inertia terms of the Navier-Stokes equations,

$$\nabla \cdot \underline{u} = 0 \tag{2.79}$$

$$\mu \nabla^2 \underline{u} = \nabla p \tag{2.80}$$

---

[9]See, e.g., Brennen, C. E. (1995), *Cavitation and Bubble Dynamics*, Oxford University Press. and Ton Tran-Cong and J.R. Blake (1984), "General solutions of the Stokes flow equations," *J. of Mathematical Analysis and Applications*, vol. 92, pp. 72–84.

where $\underline{u}$ is the disturbed velocity about a sphere moving in x-axis direction in otherwise fluid at rest. The second equation above physically implies that the pressure gradient balances the viscous force.

The general solution to these equations is given in a form of

$$\underline{u} = \nabla(\underline{r} \cdot \underline{B} + B_o) - 2\underline{B} \tag{2.81}$$

$$p = 2\mu\left(\nabla \cdot \underline{B}\right) \tag{2.82}$$

where $\underline{B}$ and B_0 should satisfy the following conditions, respectively,

$$\nabla^2 \underline{B} = 0, \quad \nabla^2 B_o = 0 \tag{2.83}$$

For Reynolds number values of O(1), the solution for the disturbed velocity field is known to be, by setting $B_x = -3UR/4r$, $B_o = UR^3x/4r^3$, $B_y = B_z = 0$ where U is the moving speed and R is the radius of a sphere,

$$\underline{u} = \left(\frac{3R}{4r} + \frac{R^3}{4r^3}\right)U\,\underline{i} - \left(-\frac{3Rx}{4r^3} + \frac{3R^3x}{4r^5}\right)U\underline{r} \tag{2.84}$$

where $x = r\cos\theta$, $\underline{i} = \underline{e}_r\cos\theta - \underline{e}_\theta\sin\theta$, $\underline{r} = r\,\underline{e}_r$ (see Figure **2.7**).

By introducing a moving frame fixed to the sphere, we can consider equivalently a stream of viscous fluid flows at speed U slowly about a stationary sphere of radius R. Then the relative velocity components for the moving coordinate system are given by, i.e.,

$$\underline{q} = -U\,\underline{i} + \underline{u} \tag{2.85}$$

or

$$q_r = -U\cos\theta + 2\left(\frac{C}{r^3} + \frac{D}{r}\right)\cos\theta \tag{2.86}$$

$$q_\theta = U\sin\theta + \left(\frac{C}{r^3} - \frac{D}{r}\right)\sin\theta \tag{2.87}$$

$$q_\alpha = 0 \tag{2.88}$$

where $C = -UR^3/4$ and $D = +3UR/4$.

The vorticity is

$$\underline{\omega} = \omega \, \underline{e}_\alpha = \left(\frac{1}{r} \frac{\partial (r \, q_\theta)}{\partial r} - \frac{1}{r} \frac{\partial q_r}{\partial \theta} \right) \underline{e}_\alpha = \frac{3}{2} U R \frac{\sin \theta}{r^2} \underline{e}_\alpha \qquad (2.89)$$

The pressure can be obtained from the momentum equation $\nabla p = \mu \nabla^2 \underline{q}$, i.e., $\nabla p = -\mu \nabla \times \underline{\omega}$, using Eqs. (1.176) and (2.89)

$$\frac{\partial p}{\partial r} = -\frac{3\mu \, U R \cos \theta}{r^3}, \quad \frac{1}{r} \frac{\partial p}{\partial \theta} = -\frac{3\mu \, U R \sin \theta}{2r^3}, \qquad (2.90)$$

Integrating with respect to either r or θ, the solution for pressure is known to be

$$p = p_0 + \frac{3}{2} \mu \, R U \frac{\cos \theta}{r^2} \qquad (2.91)$$

where p_0 is a reference pressure at infinity.

2.3.2.2 Stream function approach

Alternatively, we can obtain the same results by introducing the stream function. In terms of spherical polar coordinates (r, θ, α) where α is the azimuth angle about the axis $\theta = 0$ (see Figure 2.7), the flow is of axi-symmetry and then the continuity equation becomes

$$\frac{1}{r^2} \frac{\partial}{\partial r} (r^2 q_r) + \frac{1}{r} \frac{\partial}{\partial \theta} (q_\theta \sin \theta) = 0 \qquad (2.92)$$

Now, we define the stream function $\underline{\Psi} = (0, 0, \psi / r \sin \theta)$ to satisfy the continuity equation automatically, such that $\underline{q} = \nabla \times \underline{\Psi} = \nabla \times \left(\frac{\psi \, \underline{e}_\alpha}{r \sin \theta} \right)$, i.e.,

$$q_r = \frac{1}{r^2 \sin \theta} \frac{\partial \psi}{\partial \theta}, \quad q_\theta = -\frac{1}{r \sin \theta} \frac{\partial \psi}{\partial r} \qquad (2.93)$$

Now we get the equation for the vorticity $\underline{\omega}$ and then for the stream function ψ as follows:

Take the curl of Eq. (2.80) using the expansion formula $\nabla \times (\nabla \times \underline{u}) = \nabla (\nabla \cdot$

$\underline{u}) - \nabla^2 \underline{u}$, we have

$$\nabla \times (\nabla \times (\nabla \times \underline{u})) = 0, \quad \text{i.e.,} \quad \nabla \times (\nabla \times \underline{\omega}) = 0 \qquad (2.94)$$

Consequently, it reduces to $\nabla^2(\nabla^2 \underline{\Psi}) = 0$ where we have used the relation $\nabla^2 \underline{\Psi} = -\underline{\omega}$. Namely, this equation becomes a scalar equation for ψ

$$\left\{ \frac{\partial^2}{\partial r^2} + \frac{\sin \theta}{r^2} \frac{\partial}{\partial \theta} \left(\frac{1}{\sin \theta} \frac{\partial}{\partial \theta} \right) \right\}^2 \psi = 0 \qquad (2.95)$$

Taking the separation of variables for the resulting equation, the stream function would be of a form

$$\psi = \sin^2 \theta \left(\frac{C}{r} + D\,r + E\,r^2 + F\,r^4 \right) \qquad (2.96)$$

Applying the boundary conditions on the sphere surface ($q_r = q_\theta = 0$) and at infinity ($\psi_\infty = -Ur^2 \sin^2 \theta/2$), we obtain $C = -UR^3/4$, $D = +3\,UR/4$, $E = -U/2$, and $F = 0$. The first term and the third term represent the inviscid flow past a sphere, while the second term corresponds to the viscous correction.

2.3.2.3   Stress tensor and drag

From these expressions, the stress tensor is related to rate of strain tensor in a spherical coordinate system. Only 6 components are expressed as:

$$\tau_{rr} = -p + 2\mu \frac{\partial q_r}{\partial r} \qquad (2.97)$$

$$\tau_{r\theta} = \mu \left(\frac{1}{r} \frac{\partial q_r}{\partial \theta} + \frac{\partial q_\theta}{\partial r} - \frac{q_\theta}{r} \right) \qquad (2.98)$$

$$\tau_{r\alpha} = \mu \left(\frac{\partial q_\alpha}{\partial r} + \frac{1}{r \sin \theta} \frac{\partial q_r}{\partial \alpha} - \frac{q_\alpha}{r} \right) \qquad (2.99)$$

$$\tau_{\theta\theta} = -p + 2\mu \left(\frac{1}{r}\frac{\partial q_\theta}{\partial \theta} + \frac{q_r}{r} \right) \tag{2.100}$$

$$\tau_{\theta\alpha} = \mu \left(\frac{1}{r}\frac{\partial q_\alpha}{\partial \theta} - \frac{q_\alpha}{r}\cot\theta + \frac{1}{r\sin\theta}\frac{\partial q_\theta}{\partial \alpha} \right) \tag{2.101}$$

$$\tau_{\alpha\alpha} = -p + 2\mu \left(\frac{1}{r\sin\theta}\frac{\partial q_\alpha}{\partial \alpha} + \frac{q_r}{r} + \frac{q_\theta}{r}\cot\theta \right) \tag{2.102}$$

With the solution for the velocity field, the values of these components are evaluated on the surface of the sphere(i.e., on $r = R$):

$$\tau_{rr} = \tau_{\theta\theta} = \tau_{\alpha\alpha} = -p(R, \theta) \tag{2.103}$$

$$\tau_{r\theta} = \frac{3U}{2R}\mu\sin\theta, \quad \tau_{r\alpha} = \tau_{\theta\alpha} = 0 \tag{2.104}$$

On the surface of the sphere, the normal vector $\underline{n} = \underline{e}_r$(pointing into the fluid from the surface) is taken to find forces acting on the sphere by the fluid). Then, the surface stresses become $\underline{\tau} = \tau_{rr}\,\underline{e}_r + \tau_{r\theta}\,\underline{e}_\theta$ where $\underline{e}_\theta = \sin\theta\,\underline{i} + \cos\theta\,\underline{j}$. The surface force is composed of two components due to the normal and the tangential stress:

$$\underline{F}_S^{(n)} = \oint_S \tau_{rr}\,\underline{e}_r\,dS = 2\pi\mu\,U R\,\underline{i} \tag{2.105}$$

$$\underline{F}_S^{(t)} = \oint_S \tau_{r\theta}\,\underline{e}_\theta\,dS = 4\pi\mu\,U R\,\underline{i} \tag{2.106}$$

Herein we have used the surface element $dS = 2\pi R^2\sin\theta\,d\theta$ for the actual integrations. The total drag of the sphere becomes $D = 6\pi\mu\,U R$ which corresponds to the drag coefficient $C_D = D/(0.5\,\rho\,U^2\pi R^2) = 24/Re$ where Re is the Reynolds number based on the sphere diameter and the speed of the onset flow.

2.3.3 Surface tension

On an interface surface between two fluids (i.e., stratified fluids), the surface tension should be included to satisfy the continuity of the stress across the in-
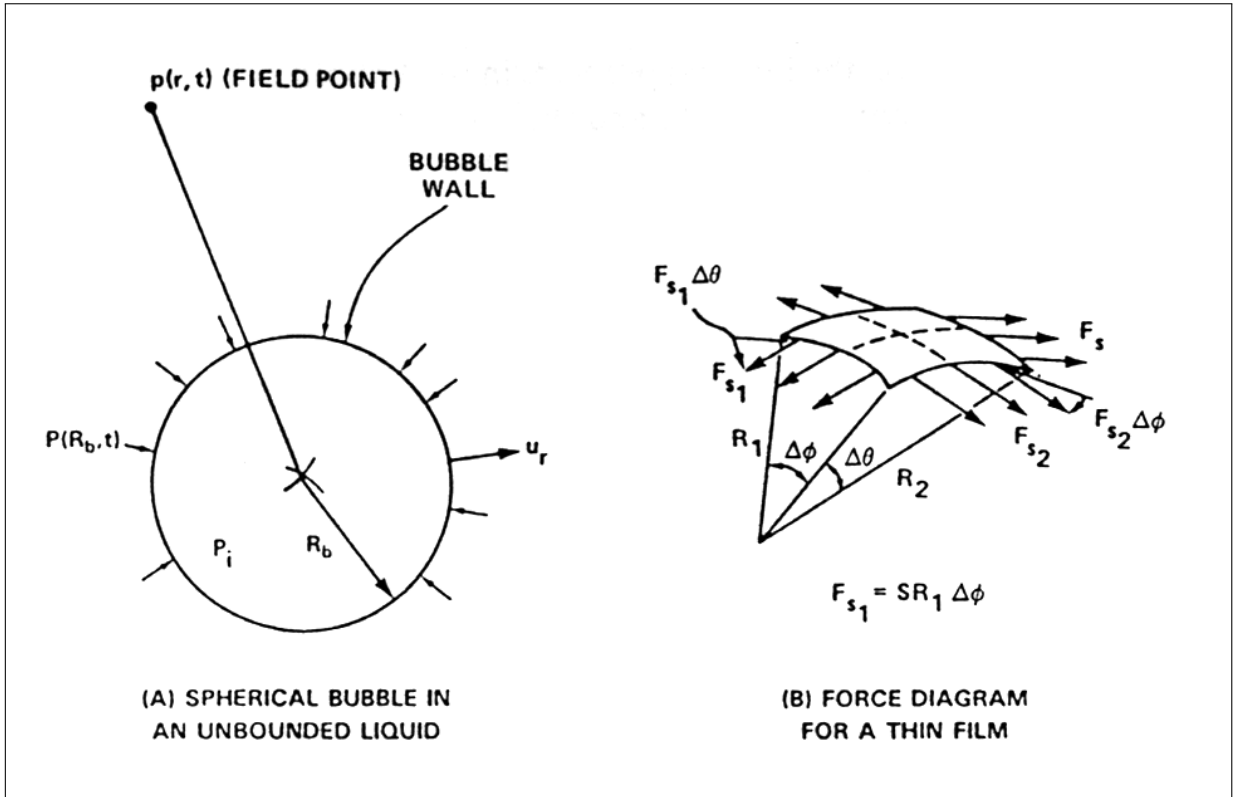
Figure 2.8 Force diagram for a spherical bubble with surface tension.

terface:

$$\underline{n} \cdot (\underline{\underline{\tau}}_i - \underline{\underline{\tau}}_o) = \sigma \left(\frac{1}{R_1} + \frac{1}{R_2} \right) \underline{n} \tag{2.107}$$

where σ is called the surface tension(whose unit is given by force per length), R_1 and R_2 are the principal radii of curvature of the interface, $\underline{n}$ is the normal vector at the interface, and the subscripts i and o refer the two fluid sides of the interface. (See Figure 2.8).

When the two fluids are stationary, only the pressure terms remain in the above relation. From the force equilibrium in the normal direction for a small element of interface,

$$(p_i - p_o)\,(R_1 \triangle\phi)\,(R_2 \triangle\theta) = F_{s_1} \triangle\theta + F_{s_2} \triangle\phi \tag{2.108}$$

where $F_{s_1} = \sigma\,R_1 \triangle\phi$ and $F_{s_2} = \sigma\,R_2 \triangle\theta$. Then,

$$p_i - p_o = \sigma \left(\frac{1}{R_1} + \frac{1}{R_2} \right) \tag{2.109}$$

As a special example, for a stationary spherical droplet(or bubble) of radius R, $p_i - p_o = 2\sigma/R$.

2.3.4 Equations of motion: Navier-Stokes equations

Newton's second law states that the time rate of change of the linear momentum is equal to the applied forces. This statement is also appropriate for continuum matter. Hence for a moving volume $V(t)$ bounded by a material surface $S(t)$, we have (for detailed derivations, refer to texts dealing with fluid mechanics.)

$$\frac{d}{dt}\int_V \rho \, \underline{q} \, dV = \int_V \underline{F}_B \, dV + \int_S \underline{n} \cdot \underline{\underline{\tau}} \, dS \qquad (2.110)$$

For incompressible Newtonian fluids, the corresponding differential form becomes the so-called Navier-Stokes equations:

$$\rho \frac{D\underline{q}}{Dt} = -\nabla p + \underline{F}_B + \mu \, \nabla^2 \underline{q} \qquad (2.111)$$

Alternate forms of the non-linear convective and the viscous term of the Navier-Stokes equations are listed in Gresho (1991). [10]

(1) Alternate form of the convective term, $\underline{q} \cdot \nabla \underline{q}$

    (a) Divergence form : $\nabla \cdot (\underline{q}\,\underline{q}) = \underline{q} \cdot \nabla \underline{q} + \underline{q}\,(\nabla \cdot \underline{q})$

    (b) Advective/convective form : $\underline{q} \cdot \nabla \underline{q} = \dfrac{1}{2}\nabla q^2 - \underline{q} \times (\nabla \times \underline{q})$

    (c) Rotational form : $\underline{\omega} \times \underline{q}$

    (d) Skew-symmetric (transpose of a matrix equals minus the matrix):
$\frac{1}{2}\left[\nabla \cdot (\underline{q}\,\underline{q}) + \underline{q} \cdot \nabla \underline{q}\right] = \underline{q} \cdot \nabla \underline{q} + \dfrac{1}{2}\underline{q}(\nabla \cdot \underline{q})$

(2) Alternate form of the viscous term, $\nabla^2 \underline{q}$

    (a) Stress-divergence form : $\nabla \cdot \left[(\nabla \underline{q}) + (\nabla \underline{q})^T\right] = \nabla^2 \underline{q} + \nabla(\nabla \cdot \underline{q})$

---

[10]Gresho, P. M. (1991), "Incompressible fluid dynamics: some fundamental formulation issues", *Annual Review of Fluid Mechanics*, vol. 23, pp. 413–453.

(b) Div-curl form : $\nabla^2 \underline{q} = \nabla(\nabla \cdot \underline{q}) - \nabla \times (\nabla \times \underline{q})$

(c) Curl form : $-\nabla \times (\nabla \times \underline{q}) = -\nabla \times \underline{\omega}$

2.3.5 Bernoulli equation

The equations of motion for inviscid fluids are called Euler's equations, with dropping the last term of Eq. (2.111). The term $\underline{q} \cdot \nabla \underline{q}$, which occurs in the equations can be transformed by the vector expansion formula:

$$\nabla \left(q^2 \right) = \nabla(\underline{q} \cdot \underline{q}) = 2\,\underline{q} \cdot \nabla \underline{q} + 2\,\underline{q} \times (\nabla \times \underline{q}) \tag{2.112}$$

Thus

$$\underline{q} \cdot \nabla \underline{q} = \frac{1}{2} \nabla \left(q^2 \right) - \underline{q} \times \underline{\omega} \tag{2.113}$$

Eventually an alternate form of the Euler's equation is

$$\frac{\partial \underline{q}}{\partial t} + \underline{\omega} \times \underline{q} = -\frac{1}{\rho} \nabla p + \frac{1}{\rho} \underline{F}_B - \nabla \left(\frac{q^2}{2} \right) \tag{2.114}$$

It is often assumed that the body force $\underline{F}_B$ is derivable from a potential; that is, that it is a conservative force, such as gravity. Then we can write $\underline{F}_B = -\nabla\Omega$, and the equations appear in

$$\frac{\partial \underline{q}}{\partial t} - \underline{q} \times \underline{\omega} = -\nabla \left(\frac{q^2}{2} + \Omega \right) - \frac{1}{\rho} \nabla p \tag{2.115}$$

This is about as far as we can go with complete generality, but the equations can be simplified still further if the fluid is barotropic; that is, if the density ρ depends on the pressure p only: $\rho = \rho(p)$. [11]

Example of this state of affairs are compressible fluids flowing adiabatically ($p \sim \rho^k$) or isothermally ($p \sim \rho$), or, of course, incompressible fluids ($\rho = $ constant). In these cases the term $\dfrac{1}{\rho} \nabla p$ can also be expressed as the gradient of

---

[11]We call a fluid baroclinic if the density does not depend on the pressure.

a function, for consider

$$d\underline{\ell} \cdot \frac{\nabla p}{\rho(p)} = \frac{dp}{\rho(p)} = d \int \frac{dp}{\rho(p)} = d\underline{\ell} \cdot \nabla \int \frac{dp}{\rho(p)} \tag{2.116}$$

Since $d\underline{\ell}$ is arbitrary, $\dfrac{\nabla p}{\rho(p)} = \nabla \displaystyle\int \frac{dp}{\rho(p)}$, and the Euler's equations of motion are reduced to

$$\frac{\partial q}{\partial t} - \underline{q} \times \underline{\omega} = -\nabla \left(\frac{q^2}{2} + \Omega + \int \frac{dp}{\rho} \right) \tag{2.117}$$

There are several important cases in which the Euler's equations of motion can be integrated directly.

(1) Irrotational barotropic flow

In this type of flow $\underline{q}$ is $\nabla \phi$. The left-hand side of Eq. (2.117) becomes simply $\dfrac{\partial}{\partial t}(\nabla \phi)$, and since the time and space derivatives are independent and can be exchanged in order, this is equal to $\nabla \left(\dfrac{\partial \phi}{\partial t} \right)$. Thus

$$\nabla \left(\frac{\partial \phi}{\partial t} + \frac{q^2}{2} + \Omega + \int \frac{dp}{\rho} \right) = 0 \tag{2.118}$$

But when the gradient of a function is zero throughout a region, the function must certainly be constant throughout the region– or rather, since the gradient involves space derivatives only, the function must be constant throughout the region at any instant, but may vary with time. The integrated form is therefore

$$\frac{\partial \phi}{\partial t} + \frac{q^2}{2} + \Omega + \int \frac{dp}{\rho} = C(t) \tag{2.119}$$

Remember that the term $\displaystyle\int \frac{dp}{\rho}$ is just a function of ρ (or p) whose form is known as soon as the particular barotropic law $\rho = \rho(p)$ is specified. For example, the simplest law is that of the incompressible fluid: $\rho =$ constant. Hence the integrated equation for incompressible, frictionless, irrotational,

unsteady flow is

$$\frac{\partial \phi}{\partial t} + \frac{q^2}{2} + \Omega + \frac{p}{\rho} = C(t) \tag{2.120}$$

(2) Steady barotropic motion

For this case we need not assume irrotational flow, and therefore we return to the original form of the Euler's equation of motion, but again assume $\rho = \rho(p)$. The equations then read, for steady flow,

$$\underline{q} \cdot \nabla \underline{q} = -\nabla \left(\int \frac{dp}{\rho} + \Omega \right) \tag{2.121}$$

We shall now show that this can be integrated along individual streamlines; that is, we shall obtain an integral that will tell how the quantities behave along a streamline, but not how they change from streamline to streamline. Let an orthogonal curvilinear coordinate system be defined so that s is measured along a streamline, and r and t normal to it. Then $\underline{q} = (q, 0, 0)$, and $\underline{q} \cdot \nabla \underline{q} = \left(q \dfrac{\partial q}{\partial s}, \cdots, \cdots \right)$ (as may be verified by reference to the formulas in general curvilinear orthogonal coordinates).

Let us substitute this into Eq. (2.121) and then multiply both sides by $\cdot d\underline{s}$:

$$q \frac{\partial q}{\partial s} ds = -\frac{\partial}{\partial s} \left(\int \frac{dp}{\rho} + \Omega \right) ds \tag{2.122}$$

and, integrating along the streamline

$$\frac{1}{2} q^2 + \int \frac{dp}{\rho} + \Omega = C_s \tag{2.123}$$

where C_s is the constant of integration, and we give it the subscript s to emphasize that the constant may vary from streamline to streamline.

Since Eqs. (2.119) and (2.123) must yield the same result in cases of steady, irrotational barotropic flow, we see that the irrotational assumption is equivalent to taking the same constant, C_s, for all streamlines:

$$\frac{1}{2} q^2 + \int \frac{dp}{\rho} + \Omega = \text{constant} \tag{2.124}$$

and finally if this is also <u>incompressible</u>,

$$\frac{1}{2}\rho\, q^2 + p + \rho\,\Omega = \text{constant} \qquad (2.125)$$

This will be recognized as Bernoulli's equation, which is an energy equation, although we obtained it by integration of momentum equations. In fact, Eqs. (2.119), (2.120), and (2.121) are also sometimes called generalized forms of Bernoulli's equation.

2.3.6 Kelvin's theorem

In any flow of a barotropic inviscid fluid, the circulation about any closed path does not vary with time if the contour is imagined to move with the fluid, that is, always to be made up of the same particles. [12] We give here a different proof, which offered more generality. We begin by considering the contour integral $\Gamma = \oint_C \underline{q} \cdot d\underline{\ell}$ where $\underline{q}$ is any vector quantity and C (material contour) is carried by the fluid. Now consider the time derivative of the circulation for a closed curve following the motion:

$$\frac{d\Gamma}{dt} = \frac{d}{dt}\oint_{C(t)} \underline{q}(\underline{x},t) \cdot \underline{s}(\underline{x},t)\, d\ell \qquad (2.126)$$

where $\underline{s}(\underline{x},t)$ is the unit tangent vectors along the integration path of the contour C. This differential is similar to the starting point in our derivation of the Reynolds transport theorem in Chapter 1, but for a moving curve instead of a moving volume. We make the same transformation from spatial ($\underline{x}$) to initial

---

[12] See Lamb, H. (1932), *Hydrodynamics*, sixth ed., Dover.

coordinates $(\underline{\xi})$:

$$
\begin{aligned}
\frac{d\Gamma}{dt} &= \oint_{C(0)} \frac{\partial}{\partial t} \left[\underline{q}^*(\underline{\xi}, t) \cdot \frac{d\underline{x}^*(\underline{\xi}, t)}{d\ell} d\ell \right] \\
&= \oint_{C(0)} \left[\left. \frac{\partial \underline{q}^*}{\partial t} \right|_{\underline{\xi}} \cdot \frac{d\underline{x}^*}{d\ell} + \underline{q}^* \cdot \frac{\partial}{\partial t} \left(\frac{\partial \underline{x}^*(\underline{\xi}, t)}{\partial \xi_j} \frac{d\xi_j}{d\ell} \right) \right] d\ell \\
&= \oint_{C(0)} \left[\left. \frac{\partial \underline{q}^*}{\partial t} \right|_{\underline{\xi}} \cdot \frac{d\underline{x}^*}{d\ell} + \underline{q}^* \cdot \left(\frac{\partial \underline{q}^*(\underline{\xi}, t)}{\partial \xi_j} \frac{d\xi_j}{d\ell} \right) \right] d\ell \\
&= \oint_{C(t)} \left[\frac{D\underline{q}}{Dt} \cdot \underline{s} + \underline{q} \cdot \{ (\underline{s} \cdot \nabla)\underline{q} \} \right] d\ell \\
&= \oint_{C(t)} \left[\frac{D\underline{q}}{Dt} \cdot \underline{s} + \frac{\partial}{\partial \ell} \left(\frac{1}{2} q^2 \right) \right] d\ell \\
&= \oint_{C(t)} \frac{D\underline{q}}{Dt} \cdot \underline{s} \, d\ell \\
&= \oint_{C(t)} \underline{a} \cdot d\underline{\ell} \qquad\qquad (2.127)
\end{aligned}
$$

Now the total (material) derivative term is the LHS of the momentum equation allowing us to put the RHS of the momentum equation into the integral:

$$
\frac{d\Gamma}{dt} = \oint_{C(t)} \left(-\frac{\nabla p}{\rho} + \frac{\underline{F}_B}{\rho} + \nu \nabla^2 \underline{q} \right) \cdot d\underline{\ell} \qquad\qquad (2.128)
$$

For barotropic fluids and conservative body forces, the time rate of change of the circulation reduces to an integral containing only viscous terms since the integral of a gradient about a closed curve is zero:

$$
\frac{d\Gamma}{dt} = \nu \oint_{C(t)} \nabla^2 \underline{q} \cdot d\underline{\ell} \qquad\qquad (2.129)
$$

If the fluid is baroclinic, the circulation can be modified because of the baroclinic generation of vorticity as

$$
\frac{d\Gamma}{dt} = \nu \oint_{C(t)} \nabla^2 \underline{q} \cdot d\underline{\ell} + \int_S \frac{1}{\rho^2} (\nabla \rho \times \nabla p) \cdot d\underline{\ell} \qquad\qquad (2.130)
$$

where the surface integral on the right-hand side is performed over the area bounded by material line. [13]

Every flow that can be produced (without friction) in a barotropic fluid initially at rest, initially in a uniform stream, or initially in any irrotational state, must be an irrotational flow.

2.3.6.1 Viscous diffussion

If we use the vector expansion Eq. (1.72) in Chapter 1 with a solenoidal vector $\underline{q}$ of an incompressible fluid:

$$\nabla^2 \underline{q} = \nabla(\nabla \cdot \underline{q}) - \nabla \times (\nabla \times \underline{q}) = -\nabla \times \underline{\omega} \qquad (2.131)$$

the time derivative of the circulation can be written as:

$$\frac{d\Gamma}{dt} = -\nu \oint_{C(t)} (\nabla \times \underline{\omega}) \cdot d\underline{\ell} \qquad (2.132)$$

In fact, the viscous term on the right-hand side represents the vorticity diffusion that activates the circulation change. We consider a sufficiently thin vortex tube with outward unit normal $\underline{n}$, in which the vortex lines are all parallel. At a point $\underline{x}$ on the side surface S of the tube, let $\underline{e_2} = \underline{\omega}/\omega$ be the unit vector along the vortex line through $\underline{x}$ such that $\underline{e_1} = \underline{e_2} \times \underline{n}$ defines a unit vector tangent to S. Let $\underline{x}$ move along the $\underline{e_1}$-direction around the tube to form a closed line C; see the sketch of Figure **2.9** . $\underline{e_1}$ is actually along the direction of shear stress $\underline{\tau} = \mu \, \underline{\omega} \times \underline{n}$.

---

[13]For details, see Milne-Thomson, L. M. (1968), *Theoretical Hydrodynamics*, fifth edition, Macmillan, London, p. 84.
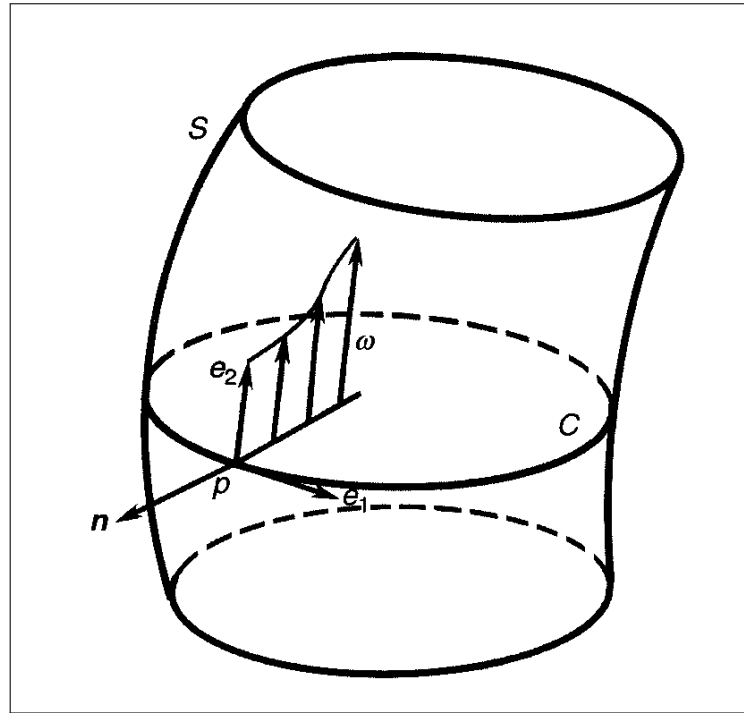
Figure **2.9** Intrinsic frame $\underline{e}_1, \underline{e}_2, \underline{n}$ on the side surface S of a vortex tube. From Wu et al. (2006), p. 139.

For this thin tube, the curvature of S along the tube direction is negligible. It can then be shown that

$$(\nabla \times \underline{\omega}) \cdot d\underline{\ell} = -\underline{e}_2 \cdot \frac{\partial \underline{\omega}}{\partial n} \, d\ell \tag{2.133}$$

and hence Eq. (2.132) yields

$$\frac{d\Gamma}{dt} = \nu \oint_{C(t)} (\underline{\sigma} \cdot \underline{e}_2) \, d\ell \tag{2.134}$$

where $\underline{\sigma} \equiv \nu \, \underline{n} \cdot \nabla \underline{\omega} = \nu \, \dfrac{\partial \underline{\omega}}{\partial n}$. In a 2-D viscous flow, Eq. (2.132) simply becomes

$$\frac{d\Gamma}{dt} = \nu \oint_{C(t)} \frac{\partial \omega}{\partial n} \, d\ell \tag{2.135}$$

where $\nu \, \dfrac{\partial \omega}{\partial n}$ is the vorticity diffusion flux across the contour. $\underline{n}$ is the unit normal outward from the contour.

2.3.6.2 Cases of inviscid flow

Thus when either the kinematic viscosity or the gradient of the vorticity is small, the circulation will be preserved about a curve moving with the fluid. Note that the circulation is not influenced by the pressure or conservative body forces and that if the fluid were inviscid the equation irrespective of the field vorticity. For such flows,

$$\frac{D\Gamma}{Dt} = 0 \tag{2.136}$$

as the theorem states.

Applying this is to the contours that enclose vortex filaments, we see immediately that such vortices do not vary in strength as they move about in any barotropic inviscid fluid. From the theorem above, it becomes clear that if a fluid particle in this type of fluid once has zero vorticity it will always have zero vorticity. For consider a contour surrounding a very small sample of fluid; if ω is zero for this sample, Γ is also zero, and according to the theorem must remain so. But this certainly implies that ω remains zero, since the statement is true for every contour that surround any part of the sample. [14]

2.4   Potential Flows

2.4.1   Laplace equation

We shall devote considerable attention to the study of irrotational motions of incompressible fluids. As we have seen, the irrotational approximation is likely to be valid throughout much of the flow.

Since the equation of continuity is $\nabla \cdot \underline{q}$ and $\underline{q}$ is the gradient of the velocity potential ϕ, the differential equation satisfied by ϕ is Laplace equation:

$$\nabla \cdot (\nabla \phi) = \nabla^2 \phi = 0 \tag{2.137}$$

---

[14]See Kuethe, A. M. and Chow, C.-Y. (1976), *Foundations of Aerodynamics: Bases of Aerodynamic Design*, Wiley, pp. 53–54.

The pressure-velocity relation is given by the integrated dynamical equation:

$$\frac{\partial \phi}{\partial t} + \frac{1}{2} q^2 + \frac{p}{\rho} + \Omega = C(t) \tag{2.138}$$

In a more general case, even if we restrict ourselves to barotropic fluids, we have five dependent variables: u, v, w, p, ρ; and five equations to solve for them:

3 equations of motion, 1 equation of continuity, and 1 equation of state: $\rho = p(\rho)$

We see now that an extreme simplification has been achieved in the irrotational incompressible case, for the equation of state has degenerated to $\rho = $ constant, and we have replaced u, v, w by the velocity potential ϕ, leaving only two unknowns (ϕ and p) and two equations, Eqs. (2.137) and (2.138).

Moreover, Eq. (2.138) has been integrated, and constitutes a formula for calculation of p when Eq. (2.137) has been solved. The only mathematical problem that remains is the solution of Laplace's equation Eq. (2.137), with the appropriate boundary conditions. The most surprising result is that the dynamical equations do not impose any restrictions on the flow. Any solution of the equation of continuity Eq. (2.137) is a possible flow pattern, for some set of boundary conditions. Another statement of this situation is that every *kinematically possible flow* is *dynamically possible*.

It is also important to notice that Eq. (2.137) does not involve t. In a case of unsteady flow, the boundary conditions will vary with time. All that is required is that we solve Laplace's equation with the instantaneous boundary conditions. Another statement of this is that *every unsteady flow pattern* is a *possible steady flow pattern* (and vice versa). Of course, the corresponding pressure will depend on whether the flow is steady or not.

If f satisfies Laplace's equation in a region, then f has no maxima or minima in that region. For any volume V, enclosed in a surface S, lying entirely inside the region:

$$0 = \int_V \nabla^2 f \, dV = \int_V \nabla \cdot \nabla f \, dV = \int_S \underline{n} \cdot \nabla f \, dS = \int_S \frac{\partial f}{\partial n} \, dS \tag{2.139}$$

But if f has a maxima at any point P, we can surely obtain a negative value of $\int_S \dfrac{\partial f}{\partial n}\, dS$ by taking V to enclose P and making it small enough. Similarly we can obtain a positive value by integrating $\dfrac{\partial f}{\partial n}$ around a minimum. Consequently there can be neither.

2.4.2   Kinematic boundary condition

In order to determine the velocity field of a potential flow, we need the boundary condition for velocity on the body surface. For general formulation, we consider a moving boundary here. $\underline{x}$ denotes the position vector of a point on the moving surface, where we take $\underline{\xi}$ as the initial position vector of the point. The velocity of the moving surface is then $\underline{u} = \left.\dfrac{\partial \underline{x}}{\partial t}\right|_{\underline{\xi}}$. The boundary condition on the moving boundary is that the normal component of the fluid velocity must equal the normal velocity of the moving boundary: $\underline{u} \cdot \underline{n} = \underline{U}_B \cdot \underline{n}$.

2.4.2.1   Alternative form

When the moving boundary is specified by a function, $F(\underline{x}, t) = 0$, the boundary condition can be written in an alternate form. Along the path of motion $\underline{x} = \underline{x}(\underline{\xi}, t)$ and the moving surface $F\left\{\underline{x}(\underline{\xi}, t), t\right\} = 0$, the particles are always located at the material surface: $\left.\dfrac{\partial F}{\partial t}\right|_{\underline{\xi}} = 0$. It implies that

$$\frac{\partial F}{\partial t} + \frac{\partial F}{\partial x_i}\left(\frac{\partial x_i}{\partial t}\right)\bigg|_{\underline{\xi}} = 0 \tag{2.140}$$

or

$$\frac{\partial F}{\partial t} + \underline{U}_B \cdot \nabla F = 0 \tag{2.141}$$

The normal vector is defined from the function F as [15]

$$\underline{n} = \frac{\nabla F}{|\nabla F|} \tag{2.142}$$

Then,

$$\frac{\partial F}{\partial t} + \underline{U}_B \cdot \underline{n} \, |\nabla F| = 0 \tag{2.143}$$

Use the condition for the normal components of the velocities of both fluid and surface $\underline{u} \cdot \underline{n} = \underline{U}_B \cdot \underline{n}$, to obtain

$$\frac{\partial F}{\partial t} + \underline{u} \cdot \underline{n} \, |\nabla F| = 0. \tag{2.144}$$

And we find

$$\frac{\partial F}{\partial t} + \underline{u} \cdot \nabla F = 0 \tag{2.145}$$

or

$$\frac{DF}{Dt} = 0 \tag{2.146}$$

This expression is valid for all material surfaces and for any flow conditions, e.g., for unsteady compressible viscous fluids. If F is independent of time, the expression reduces to the simple one: $\underline{u} \cdot \underline{n} = 0$.

But, if we use a relative coordinate system fixed to a moving body to describe the flow field, the influence of the frame velocity of the moving coordinate system should be added. The detailed formulation is given in Chapter 4.

2.4.3 Dynamic boundary condition: Free surface condition

For inviscid fluids in the absence of surface tension, the pressure is continuous across any interface between two fluids. Perhaps the most familiar case is the liquid free surface under the atmospheric air. The boundary condition is that in

---

[15]For scalar field $F(\underline{x})$, we consider a curve $\underline{x}(\sigma)$ on a surface of $F(\underline{x}) = constant$, which is specified with the parameter σ. Then $\dfrac{dF(\underline{x})}{d\sigma} = \dfrac{d\underline{x}(\sigma)}{d\sigma} \cdot \nabla F(\underline{x})$ Because F is constant along the curve $\underline{x}(\sigma)$, $\dfrac{dF}{d\sigma} = 0$. Since $\dfrac{d\underline{x}(\sigma)}{d\sigma}$ is tangent to $\underline{x}(\sigma)$, it requires either that $\nabla F = 0$ or that ∇F is perpendicular to $\dfrac{d\underline{x}(\sigma)}{d\sigma}$ (namely, to $\underline{x}(\sigma)$). Therefore non-zero ∇F is perpendicular to the surface $F = constant$.

the liquid just below the free surface, the pressure is the same as in the air just above the free surface. The atmospheric pressure p_a can generally be taken as a constant. For a liquid free surface that is at rest far ahead of a body whose motion creates disturbances on the free surface, the free surface boundary conditions are $x_3 = \zeta(x_1, x_2, t)$ and $p(x_1, x_2, \zeta, t) = p_a$. The first condition is the kinematic condition which describes the free surface height from $x_3 = 0$ and the second one is dynamic for imposing the atmospheric pressure on the free surface.

For upstream we can expect disturbance-free condition. Hence Bernoulli's equation on the free surface reduces to the expression:

$$\frac{(p - p_a)}{\rho} + g\,\zeta(x_1, x_2, t) + \frac{1}{2}(\nabla\phi)^2 + \frac{\partial\phi}{\partial t} = 0 \qquad (2.147)$$

With $p = p_a$ in this equation, we have a suitable form to derive explicitly the free surface elevation if the velocity potential ϕ is known:

$$\zeta(x_1, x_2, t) = -\frac{1}{g}\left(\frac{\partial\phi}{\partial t} + \frac{1}{2}(\nabla\phi)^2\right) \qquad (2.148)$$

Note that the vortex sheet trailing behind lifting surfaces is another case, about which we will describe in detail in Chapter 4

2.4.4 Examples

2.4.4.1 Flow past a sphere

Let us first consider the steady irrotational flow past a sphere. After the doublet strength μ is replaced in terms of the stream speed U and the radius R of the sphere, as the student can easily verify, the flow is described by

$$\left.\begin{array}{c} \psi = \dfrac{1}{2}U\left(r^2 - \dfrac{R^3}{r}\right)\sin^2\theta; \quad \phi = \dfrac{1}{2}U\left(2r + \dfrac{R^3}{r^2}\right)\cos\theta \\[2ex] q_r = U\left(1 - \dfrac{R^3}{r^3}\right)\cos\theta; \quad q_\theta = -\dfrac{1}{2}U\left(2 + \dfrac{R^3}{r^3}\right)\sin\theta \end{array}\right\} \qquad (2.149)$$

On the sphere, the velocity is given by

$$q_\theta = -\frac{3}{2} U \sin \theta \qquad (2.150)$$

so that there are two stagnation points at $\theta = 0, \pi$, and the maximum local speed is 50% greater than the stream speed. The pressure is given by

$$\frac{p - p_0}{\frac{1}{2} \rho U^2} = 1 - \frac{9}{4} \sin^2 \theta \qquad (2.151)$$

Consequently there can be no force on the sphere.

In describing real-fluid flows, the boundary layer separates from the surface just forward of the equator $\theta = \pi/2$ (in agreement with viscous-fluid theory), and from there back the flow loses its resemblance to perfect-fluid flow. It is clear that the boundary-layer separation is ultimately responsible for the appreciable drag of the sphere.

2.4.4.2 Flow around a circular cylinder

We shall proceed to the consideration of the plane steady irrotational flow around a circular cylinder. In terms of the radius of the cylinder, R, the formulas for this case are

$$\left.\begin{array}{l} \psi = U \left(r - \dfrac{R^2}{r} \right) \sin \theta; \quad \phi = U \left(r + \dfrac{R^2}{r} \right) \cos \theta \\[3mm] q_r = U \left(1 - \dfrac{R^2}{r^2} \right) \cos \theta; \quad q_\theta = -U \left(1 + \dfrac{R^2}{r^2} \right) \sin \theta \end{array}\right\} \qquad (2.152)$$

Thus the maximum surface speed is $2U$ in this case, and the local pressures correspondingly lower than on the sphere. Once more the pressure is distributed symmetrically fore-and-aft, and there is no force on the cylinder.

The boundary conditions satisfied by equation Eq. (2.152) are

$$q_r = 0 \text{ when } r = R, \text{ and } \underline{q} \to U\underline{i} \text{ as } r \to \infty. \qquad (2.153)$$

But these would be just as well satisfied if we were to superimpose a plane

vortex flow about the origin, of any desired strength; namely,

$$\psi = U\left(r - \frac{R^2}{r}\right)\sin\theta - \frac{\Gamma}{2\pi}\ln r \tag{2.154}$$

$$\phi = U\left(r + \frac{R^2}{r}\right)\cos\theta + \frac{\Gamma}{2\pi}\theta \quad (0 \le \theta < 2\pi) \tag{2.155}$$

$$q_r = U\left(1 - \frac{R^2}{r^2}\right)\cos\theta \tag{2.156}$$

$$q_\theta = -U\left(1 + \frac{R^2}{r^2}\right)\sin\theta + \frac{\Gamma}{2\pi r} \tag{2.157}$$

With circulation, the local velocity at the surface becomes $-2U\sin\theta + \Gamma/2\pi R$. Thus the stagnation points have moved to

$$\theta = \sin^{-1}\frac{\Gamma}{4\pi U R} \tag{2.158}$$

provided that $|\Gamma| \le 4\pi U R$. (If $|\Gamma|$ has a greater value, the stagnation points merge and occur in the flow outside the cylinder.)

The fluid pressure on the cylinder is now

$$p = p_0 + \frac{1}{2}\rho U^2 - \frac{1}{2}\rho\left(2U\sin\theta - \frac{\Gamma}{2\pi R}\right)^2 \tag{2.159}$$

and again, we see that there is no force component in the x direction, i.e. no drag. The force component in the y direction is easily computed:

$$Y = -\int_0^{2\pi} p\, R\sin\theta\, d\theta = -\rho U\Gamma \tag{2.160}$$

We see that there is lift on a circular cylinder with circulation. This is obviously related to the so-called 'Magnus effect', which produces lift on a rotating cylinder – in a real fluid, the circulation is produced by the action of viscosity near the spinning cylinder.

3

SINGULARITY DISTRIBUTION METHODS

3.1   General Statements

3.1.1   Techniques for solving Laplace equation

Several specific approaches have been categorized:

(1) Separation of variables
     This is a standard technique but is limited to systems for which separation
     can produce a solution to the Laplace equation. In addition it is desirable
     that the boundary condition can be easily applied, usually that the value of
     one coordinate fixed describes the surface. The 13 curvilinear orthogonal

coordinate systems are known to have suitable properties. [1] Elementary solutions can be found in some texts with this technique. We do not deal with it further herein.

(2) Superposition

Superposition of elementary solutions of the Laplace equation to satisfy the boundary condition. The distributions can be specified to be anywhere inside the body, and this was the approach treated in the undergraduate courses. It is such an important element of fluid mechanics that elementary solutions have been given names: source, sink, vortex, dipole(doublet), etc. For these elementary solutions, several numerical techniques have been formulated employing singularity distributions entirely within the body.

(3) Identity

Identities relating surface distributions of various singularities to field values of the quantity of interest. We have defined two different identities of interest in the vector analysis review: (i) Green's second identity for scalar and (ii) An identity for an arbitrary vector.

Note that (2) and (3) differ in the location of the singularity but not in principle. That is, singularities can be distributed anywhere inside the body, up to and including the surface since it is excluded from the flow field.

Our approach will be to use the identities with a distribution of singularities on the surface since it is convenient for lift, but we will modify the equations extensively.

3.1.2   Preview of singularity methods

(1) The solution in the flow field will be unique.

(2) The location, type, and strength of the singularity elements are not unique.

(3) The strength of the singularity distribution is determined by the body boundary condition.

---

[1]See Morse, P. M. and Feshbach (1953), *Methods of Theoretical Physics*, 2 vols., McGraw-Hill.

(4) We must find expressions valid as the field point approaches the body.

(5) For simple bodies in specified flows, convergence analysis of the numerical solutions is demonstrated by comparison with exact analytic solutions or measured data that are judged to be free of experimental error and significant viscous effects.

(6) It is convenient to divide the surface of the body into sub-elements and make approximations for the integrands to use an intermediate measure for the Riemann-sum definition for definite integral.

(7) The general concept of subdividing the surface into smaller elements is valid in both 2-D and 3-D.

(8) If the flow field were inviscid but rotational, it can be considered the sum of a potential plus a rotational velocity component.

(9) Such an approach can be applied for a general body that has an interior volume and some other special cases.

(10) It is sometimes convenient to work integro-differential formulations of the governing equations with a distribution of singularities for solving the Navier-Stokes equations.

3.1.3   Boundary integral forms

Field values of a quantity of interest (either scalar or vector) may be represented in terms of integrals over the surface bounding the volume of interest plus volume integrals, as shown in Chapter 1. For an irrotational solenoidal field (i.e., a potential field), the volume integrals provide no contribution and then the following expressions are obtained:

Scalar

$$\phi(\underline{x}) = \frac{1}{4\pi} \oint_S \left[\phi(\underline{y}) \frac{\underline{n}(\underline{y}) \cdot (\underline{x} - \underline{y})}{|\underline{x} - \underline{y}|^3} - \underline{n}(\underline{y}) \cdot \nabla \phi(\underline{y}) \frac{1}{|\underline{x} - \underline{y}|} \right] dS_y \qquad \text{in 3-D}$$

$$\tag{3.1}$$

$$\phi(\underline{x}) = \frac{1}{2\pi} \oint_C \left[\phi(\underline{y}) \frac{\underline{n}(\underline{y}) \cdot (\underline{x} - \underline{y})}{|\underline{x} - \underline{y}|^2} - \underline{n}(\underline{y}) \cdot \nabla \phi(\underline{y}) \ln \frac{1}{|\underline{x} - \underline{y}|} \right] d\ell_y \quad \text{in 2-D}$$

$$\tag{3.2}$$

Vector

$$\underline{q}(\underline{x}) = \frac{1}{4\pi} \oint_S \left[\{\underline{n}(\underline{y}) \times \underline{q}(\underline{y})\} \times \frac{(\underline{x} - \underline{y})}{|\underline{x} - \underline{y}|^3} + \underline{n}(\underline{y}) \cdot \underline{q}(\underline{y}) \frac{(\underline{x} - \underline{y})}{|\underline{x} - \underline{y}|^3} \right] dS_y \quad \text{in 3-D}$$

$$\tag{3.3}$$

$$\underline{q}(\underline{x}) = \frac{1}{2\pi} \oint_C \left[\{\underline{n}(\underline{y}) \times \underline{q}(\underline{y})\} \times \frac{(\underline{x} - \underline{y})}{|\underline{x} - \underline{y}|^2} + \underline{n}(\underline{y}) \cdot \underline{q}(\underline{y}) \frac{(\underline{x} - \underline{y})}{|\underline{x} - \underline{y}|^2} \right] d\ell_y \quad \text{in 2-D}$$

$$\tag{3.4}$$

$$\nabla \phi(\underline{x}) = \frac{1}{4\pi} \oint_S \left[\phi(\underline{y}) \left\{ \frac{\underline{n}(\underline{y})}{|\underline{x} - \underline{y}|^3} - 3 \frac{\underline{n}(\underline{y}) \cdot (\underline{x} - \underline{y})}{|\underline{x} - \underline{y}|^5} (\underline{x} - \underline{y}) \right\} \right.$$
$$\left. + \underline{n}(\underline{y}) \cdot \nabla \phi(\underline{y}) \frac{(\underline{x} - \underline{y})}{|\underline{x} - \underline{y}|^3} \right] dS_y \qquad \text{in 3-D} \quad \tag{3.5}$$

$$\nabla \phi(\underline{x}) = \frac{1}{2\pi} \oint_C \left[\phi(\underline{y}) \left\{ \frac{\underline{n}(\underline{y})}{|\underline{x} - \underline{y}|^2} - 2 \frac{\underline{n}(\underline{y}) \cdot (\underline{x} - \underline{y})}{|\underline{x} - \underline{y}|^4} (\underline{x} - \underline{y}) \right\} \right.$$
$$\left. + \underline{n}(\underline{y}) \cdot \nabla \phi(\underline{y}) \frac{(\underline{x} - \underline{y})}{|\underline{x} - \underline{y}|^2} \right] d\ell_y \qquad \text{in 2-D} \quad \tag{3.6}$$

where

(1) $\underline{x} \in V, \underline{x} \notin S$ or C and $\underline{y} \in S$ or C,

(2) derivation of $\nabla \phi$ from ϕ is straight forward, e.g., for Eq. (3.5) in 3-D, use the following expansion:

$$\underline{n} \cdot \nabla \left(\frac{\underline{r}}{|\underline{r}|^3} \right) = \frac{\underline{n}}{|\underline{r}|^3} - 3 \left(\underline{n} \cdot \underline{r} \right) \frac{\underline{x}}{|\underline{r}|^5} \tag{3.7}$$

(3) 2-D forms can be obtained from the 3-D equations by an integration of the third coordinate,

(4) $\underline{n}$ *points out of body and into the field volume,* [2]

(5) these equations are valid for $\nabla^2\phi = 0, \nabla \times \underline{q} = 0, \nabla \cdot \underline{q} = 0$ for $\underline{x} \in V$,

(6) singularities are sources/sinks, vortices, and dipoles centered at $\underline{y}$, a point on the surface bounding V,

(7) and for the surface of the body given by $\underline{s} = \underline{s}(\sigma_1, \sigma_2)$, tangent vectors are $\partial\underline{s}/\partial\sigma_1$ and $\partial\underline{s}/\partial\sigma_2$, and hence we have

$$\underline{n}\, ds = \pm \left(\frac{\partial\underline{s}}{\partial\sigma_1} \times \frac{\partial\underline{s}}{\partial\sigma_2} \right) d\sigma_1\, d\sigma_2 = \pm\, h_1\, h_2\, \underline{e}_{\sigma_1} \times \underline{e}_{\sigma_2}\, d\sigma_1\, d\sigma_2 \quad (3.8)$$

3.1.4   Disturbance flow about a body

We can specify the total velocity vector as the sum of the free-stream velocity plus a vector representing the disturbance introduced by the presence of the body:

$$\underline{q} = \underline{q}_\infty + \underline{u} \tag{3.9}$$

where $\underline{q}_\infty = U\underline{i} + V\underline{j} + W\underline{k}$ is constant and $\underline{u}(\underline{x})$ is disturbance velocity introduced by body (not necessarily small). Also called perturbation velocity. If $\underline{u} = \nabla\phi$, ϕ is the perturbation potential (i.e., it perturbs the well-understood free stream). Now the conditions for the irrotational and solenoidal vector $\underline{q}$ can be applied:

$$\nabla \times \underline{q} = 0 \Rightarrow \nabla \times (\underline{q}_\infty + \underline{u}) = 0 \Rightarrow \nabla \times \underline{u} = 0 \quad \text{for } \underline{x} \in V \tag{3.10}$$

$$\nabla \cdot \underline{q} = 0 \;\Rightarrow \nabla \cdot (\underline{q}_\infty + \underline{u}) = 0 \;\Rightarrow \nabla \cdot \underline{u} = 0 \quad \text{for } \underline{x} \in V \tag{3.11}$$

Hence we can use the vector identity to construct $\underline{u}$. This will be more convenient than $\underline{q}$ for us since $\underline{u} \to 0$ for $|\underline{x}| \to \infty$ and the integration over the surface at $|\underline{y}| \to \infty$ will not contribute to the expression for $\underline{u}$.

---

[2]Note that this orientation for the normal $\underline{n}$ is different from our original derivation and will be used from now on unless stated otherwise.

Now we will prove this argument. Let $\underline{I}$ be the contribution from the region at $|\underline{y}| \to \infty$. Then

$$
\begin{aligned}
I = |\underline{I}| &\leq \left| \frac{1}{4\pi} \oint_{S_\infty} \left[(\underline{n} \times \underline{u}) \times \frac{\underline{x} - \underline{y}}{|\underline{x} - \underline{y}|^3} + (\underline{n} \cdot \underline{u}) \frac{\underline{x} - \underline{y}}{|\underline{x} - \underline{y}|^3} \right] dS_y \right| \\
&\leq \frac{1}{4\pi} \oint_{S_\infty} \left[\frac{|\underline{u}||\underline{x} - \underline{y}|}{|\underline{x} - \underline{y}|^3} + \frac{|\underline{u}||\underline{x} - \underline{y}|}{|\underline{x} - \underline{y}|^3} \right] dS_y \\
&\leq \frac{1}{2\pi} \oint_{S_\infty} \frac{|\underline{u}|}{|\underline{x} - \underline{y}|^2} dS_y
\end{aligned}
\tag{3.12}
$$

If we take the surface far from body to be a sphere:

$$
\underline{y} = \underline{s} = R\,\underline{e}_r \quad (R >> |\underline{x}|)
\tag{3.13}
$$

$$
\frac{\partial \underline{s}}{\partial \theta} = R\,\underline{e}_\theta, \quad \frac{\partial \underline{s}}{\partial \alpha} = R \sin\theta\,\underline{e}_\alpha
\tag{3.14}
$$

$$
|\underline{n}\,dS| = dS = R^2 \sin\theta\,d\theta\,d\alpha \leq R^2\,d\theta\,d\alpha \quad \text{(by Eq. (3.8))}
\tag{3.15}
$$

$$
|\underline{x} - \underline{y}| \to R
\tag{3.16}
$$

Hence

$$
I \leq \frac{1}{2\pi} \oint |\underline{u}|\,d\theta\,d\alpha
\tag{3.17}
$$

So if $|\underline{u}| \to 0$ for $|\underline{y}| \to \infty$, $|\underline{I}| \to 0$ and the only surface that must be considered is that for the body of interest, S_B.

Similar results are found for 2-D flow and for the potential function. [3] Furthermore, if $\underline{u}$ were only bounded for $|\underline{y}| \to \infty$ (i.e. $|\underline{u}| \leq$ constant), then our above arguments are not sufficient to show that the integral over the region at $\underline{y} \to \infty$ is negligible. For both free-surface problems of waves generated by a body on a free surface and the shed vortex sheet behind a lifting body, our inviscid model is one with bounded disturbances at $\underline{y} \to \infty\underline{i}$ (downstream). If we had been more careful with our downstream integral we could have found

---

[3] The potential for 2-D flows has logarithmic far-field behavior. See Batchelor, G. K. (1967), *An introduction to fluid dynamics,* Cambridge University Press, p. 124.

an alternate form over a disk:

$$\oint_A |\underline{u} \cdot \underline{i}| \frac{dS}{|\underline{x} - \underline{y}|} \tag{3.18}$$

where A is a disk downstream. It vanishes for $\underline{y} \to \infty \, \underline{i}$. [4]

3.2   Surface Distributions of Singularity

3.2.1   Interior flow field

We assume our body in the flow field has thickness so that there is also another volume internal to it. (See Figure **3.1**) We consider the disturbance velocity
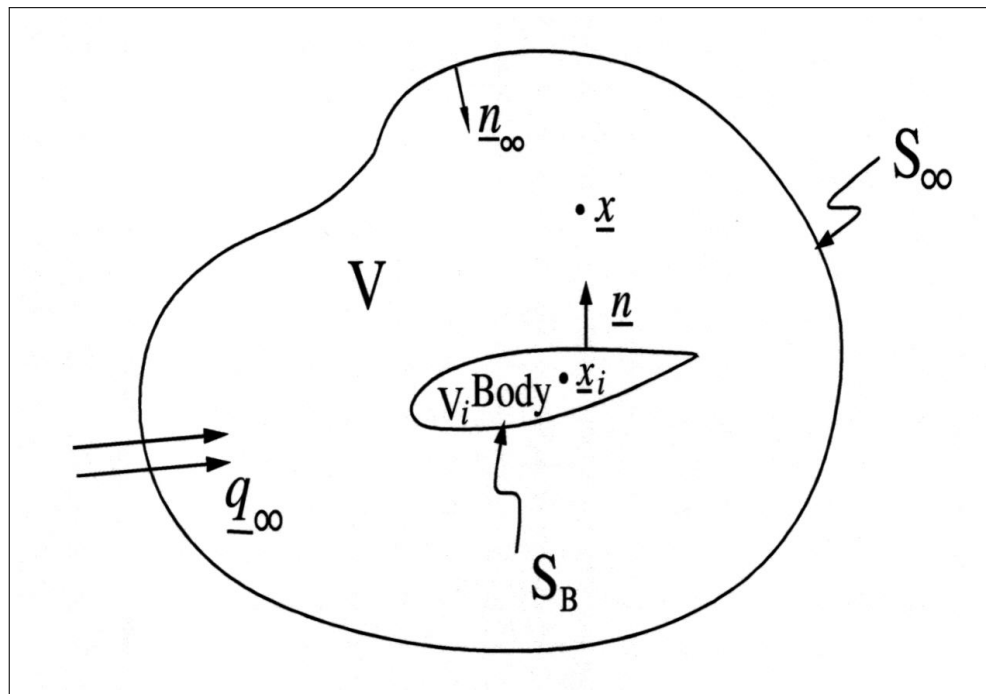
Figure **3.1** Notation for unbounded flow fields.

introduced by the body in an otherwise uniform onset flow, and write it in the form:

$$\underline{u}(\underline{x}) = \frac{1}{4\pi} \oint_{S_B} \left[\{\underline{n} \times \underline{u}\} \times \frac{(\underline{x} - \underline{y})}{|\underline{x} - \underline{y}|^3} + \underline{n} \cdot \underline{u} \frac{(\underline{x} - \underline{y})}{|\underline{x} - \underline{y}|^3} \right] \, dS_y \quad \text{in 3-D} \tag{3.19}$$

---

[4]Brockett, T. E. (1972), "Propeller Perturbation Problems", *NSRDC Report*, no. 3880.

Recall that for our derivation of this equation, we had $\underline{x}$ within V, with the requirement that the region about $\underline{x}$ be excluded from the flow field (and the limit of this excluded region vanishing taken to get the left-hand side). Hence, if $\underline{x}$ were outside V, either exterior to S_∞ or interior to S_B, the LHS would be zero. We are interested in $\underline{x}$ interior S_B. Let this point be $\underline{x}_i$. Then $\underline{u}(\underline{x}_i)$ computed by the above surface integrals would be zero. We say

$$\underline{u}(\underline{x}_i) = 0 \quad \text{for } \underline{x}_i \text{ within } S_B \tag{3.20}$$

We are not really interested in the flow internal to a body but the above property suggests that we may want to think about a flow field consisting of V plus the volume internal to S_B (let's call this V_i) with a surface (S_B) of singularities separating them.

Now let us postulate that the flow inside S_B is also on that satisfies $\nabla \cdot \underline{u}_i = 0 = \nabla \times \underline{u}_i$. Hence we can also represent this flow by a similar distribution of sources and vortices over the inside of S_B. If we keep the same direction of the normal vector $\underline{n}$ at the boundary (i.e., $\underline{n}$ is exterior to S_B) then

$$\underline{u}_i(\underline{x}_i) = -\frac{1}{4\pi} \oint_{S_B} \left[\{\underline{n}(\underline{y}) \times \underline{u}_i(\underline{y})\} \times \frac{(\underline{x}_i - \underline{y})}{|\underline{x}_i - \underline{y}|^3} + \underline{n}(\underline{y}) \cdot \underline{u}_i(\underline{y}) \frac{(\underline{x}_i - \underline{y})}{|\underline{x}_i - \underline{y}|^3} \right] dS_y \tag{3.21}$$

Similar to our observation for $\underline{u}(\underline{x}_i)$, we can state that for a field point outside of V_i the value of the vector $\underline{u}_i$ is zero. In particular, if $\underline{x} \in V$ were the field point, then

$$\underline{u}_i(\underline{x}) = 0 \tag{3.22}$$

Thus if we sum the two equations (3.19) and (3.21) for the vectors $\underline{u}$ and $\underline{u}_i$, we will obtain an expression valid for a point in either V or in V_i. Let us call this more general solution the vector $\underline{u}$:

$$\boxed{\underline{u}(\underline{x}) = \frac{1}{4\pi} \oint_{S_B} \left[\{\underline{n} \times (\underline{u} - \underline{u}_i)\} \times \frac{(\underline{x} - \underline{y})}{|\underline{x} - \underline{y}|^3} + \underline{n} \cdot (\underline{u} - \underline{u}_i) \frac{(\underline{x} - \underline{y})}{|\underline{x} - \underline{y}|^3} \right] dS_y}$$

$$\tag{3.23}$$

where by our construction we have

$$\underline{u}(\underline{x}) = \underline{u} \quad \text{for} \ \ \underline{x} \in V \tag{3.24}$$

$$\underline{u}(\underline{x}_i) = \underline{u}_i \quad \text{for} \ \ \underline{x}_i \in V_i \tag{3.25}$$

We have already noted that our concern is not really the flow internal to the body. Thus we are free to specify this flow as fits our needs. In particular, we can set the value of $\underline{u}_i$ on the boundary to fit arbitrary conditions. Some choices for components of $\underline{u}_i$ on S_B are of particular interest as explained in the following subsections.

3.2.2   Source distributions

We consider the case of $\underline{n} \times (\underline{u} - \underline{u}_i) = 0$ in Eq. (3.23). This implies that the tangential velocity component is continuous across S_B. Then the equation becomes

$$\underline{u}(\underline{x}) = \frac{1}{4\pi} \oint_{S_B} \tau(\underline{y}) \frac{(\underline{x} - \underline{y})}{|\underline{x} - \underline{y}|^3} \, dS_y \tag{3.26}$$

where $\tau = \underline{n} \cdot (\underline{u} - \underline{u}_i)$. The integrand means a distribution of sources having strength τ over S_B. This strength is unknown since we do not know anything about $\underline{n} \cdot \underline{u}_i$, i.e., our choice was to select only the equality of tangential components $\underline{n} \times \underline{u} = \underline{n} \times \underline{u}_i$.

3.2.3   Vortex distributions

We consider the case of $\underline{n} \cdot (\underline{u} - \underline{u}_i) = 0$ in Eq. (3.23). This implies that the normal velocity component is continuous across S_B. Then the equation becomes

$$\underline{u}(\underline{x}) = \frac{1}{4\pi} \oint_{S_B} \underline{\gamma}(\underline{y}) \times \frac{(\underline{x} - \underline{y})}{|\underline{x} - \underline{y}|^3} \, dS_y \tag{3.27}$$

where $\underline{\gamma} = \underline{n} \times (\underline{u} - \underline{u}_i)$. The integrand means a distribution of vortices having strength $\underline{\gamma}$ over S_B. This strength is unknown since $\underline{n} \times \underline{u}_i$ is unknown, i.e., our choice was to select only the equality of normal components $\underline{n} \cdot \underline{u} = \underline{n} \cdot \underline{u}_i$.

This equation is called the Biot-Savart Integral for the velocity induced by a surface distribution of vorticity. Similar forms are available for volume and line distributions of vorticity.

Either source or vortex distribution for $\underline{u}$ can be employed to find the velocity field for flow about a non-lifting body. However we shall see later that vortices are necessary for lifting bodies.

3.2.4   Source and vortex distributions

For 2-D fields, set $\underline{n} \times (\underline{u} - \underline{u}_i) = \gamma_0 \, f(\underline{y})\underline{k}$ where γ_0 is constant and $f(\underline{y})$ is a specified function (often $f(\underline{y}) = 1$). Then the 2-D induced velocity is

$$\underline{u}(\underline{x}) = \frac{1}{2\pi} \oint_{C_B} \tau(\underline{y}) \, \frac{(\underline{x} - \underline{y})}{|\underline{x} - \underline{y}|^2} \, d\ell_y + \frac{\gamma_0}{2\pi} \oint_{C_B} f(\underline{y}) \, \frac{\underline{k} \times (\underline{x} - \underline{y})}{|\underline{x} - \underline{y}|^2} \, d\ell_y \quad \text{in 2-D}$$

(3.28)

where now both the variable source strength $\tau(\underline{y})$ and single constant vortex strength γ_0 are unknown. Such a form is useful for lifting 2-D bodies as we shall discuss later. A similar form may be used for symmetric flow, namely, we may take $\underline{n} \times (\underline{u} - \underline{u}_i) = \gamma_0 \, \underline{e}_t$ where $\underline{e}_t$ is tangent to an axi-symmetric body in the circumferential direction. We can also specify a similar representation in 3-D flow but must be somewhat careful, e.g., for a planar rectangular wing we take $\underline{n} \times (\underline{u} - \underline{u}_i) = \gamma_0(x_3) \, f(x_1) \, \underline{e}_3$ where x_1, x_3, and $\underline{e}_3$ refer to a coordinate system taken.

3.2.5   Remarks for singularity distributions

Similar expressions can be obtained for the scalar potential ϕ. [5] Besides the above 3 types of singularity distribution, We could take $\underline{n} \cdot (\underline{u} - \underline{u}_i) = \tau_0 \, f_1(\underline{y})$ and add this distribution of unknown magnitude τ_0, but fixed form $f_1(\underline{y})$, sources over the boundary S_B to the expression for the Biot-Savart law. This formalism is not as useful in practice as the case in the previous subsection.

---

[5]See Lamb, H. (1932), *Hydrodynamics*, sixth ed., Dover, pp. 59–61. Also see Hunt, B. (1980), "The Mathematical Basis and Numerical Principles of the Boundary Integral Method for Incompressible Potential Flow over 3-D Aerodynamic Configurations," *Numerical Methods in Applied Fluid Dynamics*.

We could have postulated distributions of only the single type of singularity on the boundary to start with since our equations of motion (continuity and Euler equations) apply only within V and not on S_B. This means we are free to distribute singularities anywhere outside V up to and including the boundary of V. Our formal development has confirmed this and also given us explicitly the information that the source distribution produces a flow that has a continuous tangential velocity component at the body surface and the vortex distribution produces a continuous normal velocity distribution across the surface. Since we know certain components are continuous across the boundary we are not surprised to find that the other component will be discontinuous across the boundary.

As we examine the expressions for the field point tending to a body point later on, the specific integrals for satisfying the boundary condition will be derived and the continuity properties just observed will be evident.

3.2.6 Doublet distribution and solid angle

We take a doublet distribution with constant density

$$\frac{1}{4\pi} \int_S \phi \, \underline{n} \cdot \nabla \left\{ \frac{1}{|\underline{x} - \underline{y}|} \right\} \, dS. \tag{3.29}$$

Now consider the volume integral for the region bounded by

(i) the original surface(S) over which the doublet is distributed,

(ii) the spherical surface(S_1) of radius 1 centered at $\underline{x}$, and

(iii) the conical surface(S_c) passing the vertices of the original surface and $\underline{x}$,

$$\int_V \nabla \cdot \nabla \left\{ \frac{1}{|\underline{x} - \underline{y}|} \right\} \, dV. \tag{3.30}$$

See Figure **3.2** for sketch of the integration region.
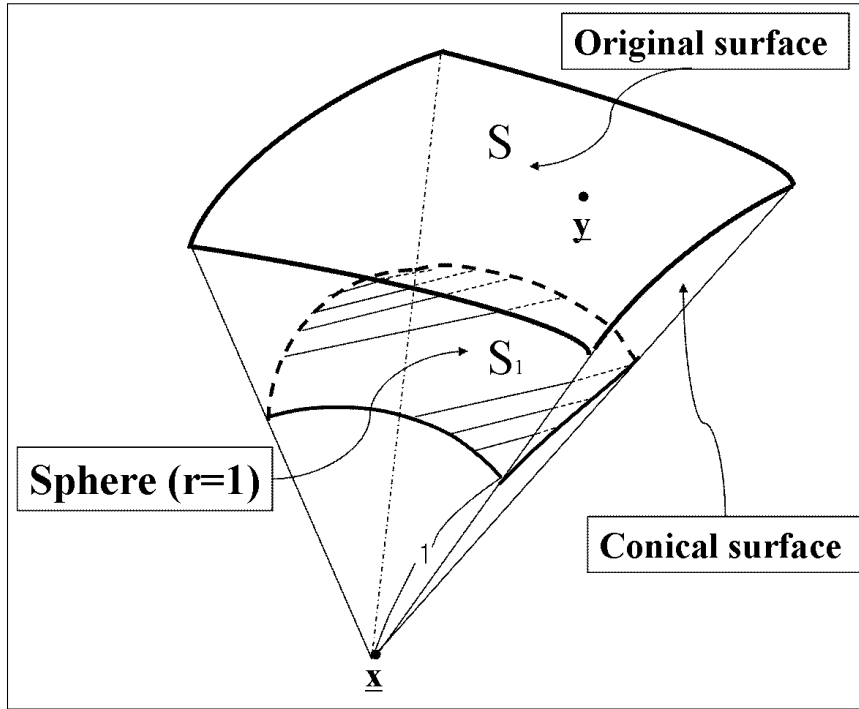
Figure **3.2** Relationship between a constant doublet distribution and the solid angle of the distributed surface.

Because $\underline{x}$ is outside the region, the integral

$$\int_V \nabla^2 \left(\frac{1}{r}\right) dV = 0 \tag{3.31}$$

According to the divergence theorem, the integral becomes

$$\oint_{S+S_1+S_c} \underline{n} \cdot \nabla \left(\frac{1}{r}\right) dS = 0. \tag{3.32}$$

Then the contribution of the conical surface is zero because of $\underline{n} \cdot \nabla \left(\frac{1}{r}\right) = 0$ on S_c, so that

$$\int_S \underline{n} \cdot \nabla \left(\frac{1}{r}\right) dS = -\int_{S_1} \underline{n} \cdot \nabla \left(\frac{1}{r}\right) dS \tag{3.33}$$

Consequently, the integral represents the area of the spherical surface, namely the solid angle of the original surface.

3.2.7 Equivalence of doublet and vortex distributions

For doublets of variable strength $\mu(\underline{y})$ distributed over a patch of surface S, define the induced velocity $\underline{w}$ at a field point $\underline{x}$:

$$\underline{w}(\underline{x}) = \nabla_x\,\phi(\underline{x}) = \frac{1}{4\pi}\int_S \mu(\underline{y})\nabla_x\left(\frac{\underline{n}(\underline{y})\cdot(\underline{x}-\underline{y})}{|\underline{x}-\underline{y}|^3}\right)\,dS_y \qquad (3.34)$$

and for vortices of variable strength $\underline{\gamma}$ distributed over the same patch, define the induced velocity $\underline{u}$ at a field point $\underline{x}$:

$$\underline{u}(\underline{x}) = \frac{1}{4\pi}\int_S \underline{\gamma}(\underline{y})\times\frac{(\underline{x}-\underline{y})}{|\underline{x}-\underline{y}|^3}\,dS_y \qquad (3.35)$$

We seek to determine if these expressions be equivalent in some way. [6]
In our investigation of expansion formulas in Chapter 1, we derived the formula, with $\underline{a} = \underline{n}(\underline{y})$ and $\underline{v} = \dfrac{(\underline{x}-\underline{y})}{|\underline{x}-\underline{y}|^3}$:

$$\nabla_x(\underline{n}\cdot\underline{v}) = \underline{n}\times(\nabla_x\times\underline{v}) + (\underline{n}\cdot\nabla_x)\,\underline{v} = (\underline{n}\times\nabla_x)\times\underline{v} + \underline{n}\,(\nabla_x\cdot\underline{v}) \quad (3.36)$$

We have used the expansion formulas,

$$(\underline{n}\times\nabla_x)\times\underline{v} = n_l\frac{\partial v_l}{\partial x_i} - n_i\frac{\partial v_k}{\partial x_k}, \quad \underline{n}\times(\nabla_x\times\underline{v}) = n_j\frac{\partial v_j}{\partial x_i} - n_j\frac{\partial v_i}{\partial x_j} \quad (3.37)$$

But for $\underline{v} = \dfrac{(\underline{x}-\underline{y})}{|\underline{x}-\underline{y}|^3}$, we have $\nabla_x\cdot\underline{v} = 0$. Also we note the reciprocal property: $\nabla_x|\underline{x}-\underline{y}|^n = -\nabla_y|\underline{x}-\underline{y}|^n$. So that

$$\underline{w}(\underline{x}) = -\frac{1}{4\pi}\int_S \mu(\underline{y})\left\{\underline{n}(\underline{y})\times\nabla_y\right\}\times\frac{\underline{x}-\underline{y}}{|\underline{x}-\underline{y}|^3}\,dS_y \qquad (3.38)$$

---

[6]The derivation was done by Hess, J. L. (1972), "Calculation of Potential Flow about Arbitrary Three-Dimensional Lifting Bodies," Douglas Aircraft Company Report No., MDCJ5679-01, Appendix A.

We now examine the expansion of a term similar to the integrand of this equation:

$$\{\underline{n}(\underline{y}) \times \nabla_y\} \times \{\mu(\underline{y})\,\underline{v}\} = \mu(\underline{y})\,\{\underline{n}(\underline{y}) \times \nabla_y\} \times \underline{v} + \{\underline{n}(\underline{y}) \times \nabla_y\,\mu(\underline{y})\} \times \underline{v}$$
(3.39)

Rearranging this expression, we substitute for the above integrand:

$$\underline{w}(\underline{x}) = -\frac{1}{4\pi}\int_S \left[\{\underline{n}(\underline{y}) \times \nabla_y\} \times \left\{ \mu(\underline{y})\frac{\underline{x}-\underline{y}}{|\underline{x}-\underline{y}|^3} \right\} \right.$$
$$\left. - \{\underline{n}(\underline{y}) \times \nabla_y\,\mu(\underline{y})\} \times \frac{\underline{x}-\underline{y}}{|\underline{x}-\underline{y}|^3} \right]\,dS_y \qquad (3.40)$$

Using the third of Stokes' integral theorem, we can transform the first term in the surface integral to a line integral along a curve C bounding the surface S:

$$\boxed{\begin{aligned}
\underline{w}(\underline{x}) &= \frac{1}{4\pi}\oint_C \mu(\ell)\frac{\underline{x}-\underline{\ell}}{|\underline{x}-\underline{\ell}|^3} \times d\underline{\ell}_y + \frac{1}{4\pi}\int_S \underline{\gamma}(\underline{y}) \times \frac{\underline{x}-\underline{y}}{|\underline{x}-\underline{y}|^3}\,dS_y \quad (3.41)\\
&= \frac{1}{4\pi}\oint_C \mu(\ell)\frac{\underline{x}-\underline{\ell}}{|\underline{x}-\underline{\ell}|^3} \times d\underline{\ell}_y + \underline{u}(\underline{x}) \qquad\qquad\qquad (3.42)
\end{aligned}}$$

where $\underline{\gamma}(\underline{y}) = \underline{n}(\underline{y}) \times \{\nabla_y\,\mu(\underline{y})\}$.

Thus the velocity induced by a distribution of doublets of strength μ is equivalent to the velocity induced by a distribution of vortices of strength $\underline{\gamma} = \underline{n} \times (\nabla\mu)$ over the surface plus a line integral representing a concentrated vortex of strength μ_c at the boundary of the surface as illustrated in Figure **3.3** .
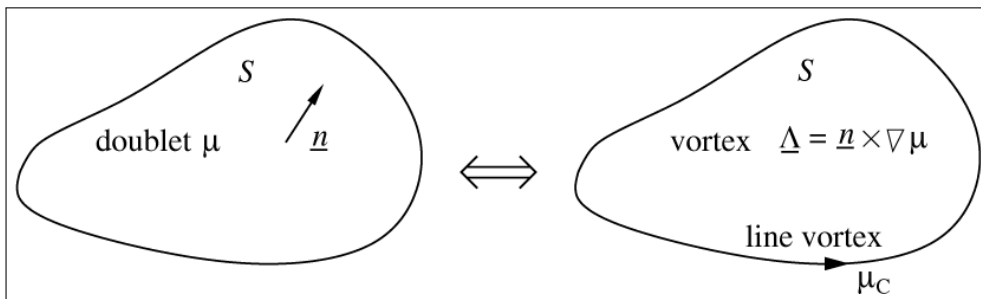
Figure 3.3 Equivalence of doublet and vortex distributions.

If the doublet strength were constant over S, then the induced velocity could be represented as either the direct integral for the doublets distributed over the

surface or the line integral of the vortex of strength $-\mu\,\underline{t}$ where $\underline{t}$ is a unit vector. The result we have derived shows that the vortex lattice procedure commonly used in numerical analysis is equivalent to having panels of constant strength doublets.

3.3   Limiting Form of Expressions

3.3.1   Introduction

We now have several forms that are useful to express the general solution of our fluid flow problem. To find the flow about a given body, the singularity strengths must be selected such that the boundary conditions are satisfied. The singularity solutions already satisfy the Laplace equation in the flow field and tend to zero far from the (non-lifting) body. Hence the solution will be complete once we satisfy the boundary condition on the body surface $(\underline{x} \to \underline{x}_0 \in S_B)$. Thus we need expressions for the integrals as the field point tends to the surface of the body.

We have already looked at this problem from one standpoint for which we found the value of the potential was doubled at the surface and the expression for the integral specifically excluded a circular region around the point $\underline{x}_0$. We can expect that in some way an acceptable approach may result in a surface integral that excludes the region about $\underline{x}_0$ with a nearly circular boundary centered $\underline{x}_0$.

However, in practice it may be convenient to integrate in directions along two axes as illustrated in Figure **3.4** . In this sketch we anticipate that a region about one of the coordinate axes must be exclude to isolate the singular point.

This approach leads to a formulation of the problem such that integration is first along the parametric lines parallel to the one that is excluded, and a second integration that is along the other coordinate direction and having a Cauchy Principle Value Integral. We write the form of the double integral schematically
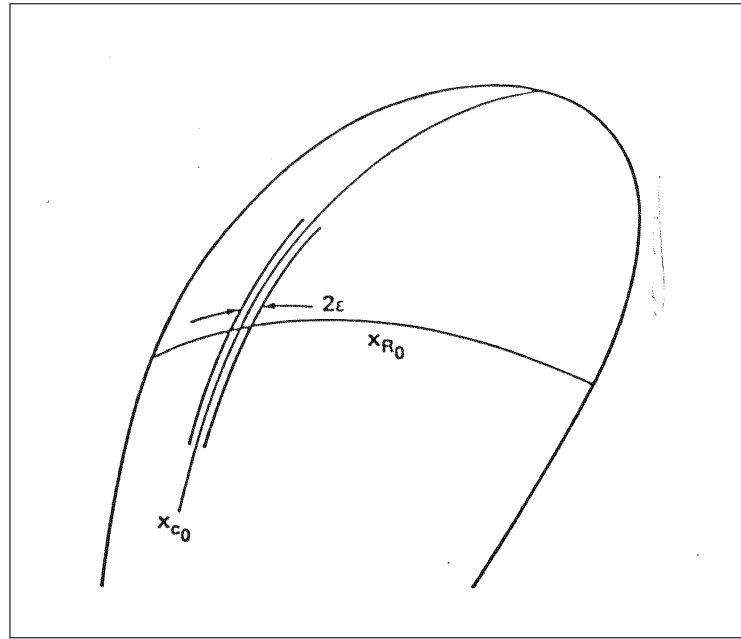
Figure **3.4** Schematic diagram of integration region for singular integrals.

as

$$I(\underline{x}_0) = \lim_{\epsilon \to 0} \left[\left(\int_{\sigma_{1_{min}}}^{\sigma_{1_0} - \epsilon} + \int_{\sigma_{1_0} + \epsilon}^{\sigma_{1_{max}}} \right) d\sigma_1 \int_{a(\sigma_1)}^{b(\sigma_1)} F(\underline{x}_0, \underline{y}(\sigma_1, \sigma_2)) \, d\sigma_2 \right] \quad (3.43)$$

So we seek to find the explicit forms for the limit:

$$I(\underline{x}_0) = \lim_{\underline{x} \to \underline{x}_0} I(\underline{x}) \quad (3.44)$$

where I can be either the scalar or vector arising from the distribution of singularities over the surface. We consider the surface to be the boundary of a 3-D flow field. (Recall we can convert this to the 2-D case by a straightforward integration of the spanwise coordinate x_3 from $-\infty$ to ∞.)

We can divide the surface into two regions, one about the point $\underline{x}_0$ and the other consisting of the remaining area. For the integral over the remaining area, the field point $\underline{x}$ can be set equal to $\underline{x}_0$ directly since no singularity will occur (at leat until $\epsilon \to 0$). Our real task will be to find the integral over the region of small distance to find the limit value. Let the region of S about $\underline{x}_0$ be denoted by $\Sigma(\underline{x}_0, \epsilon)$ where ϵ characterizes the dimensions of Σ; let the distance from $\underline{x}_0$ to $\underline{x}$ be $\eta \underline{e}$, i.e., $\underline{x} - \underline{x}_0 = \eta \, \underline{e}$; and let $F(\underline{x}, \underline{y})$ be the integrand. Then the limit

process can be expressed;

$$\lim_{\underline{x}\to\underline{x}_0} I(\underline{x}) = \lim_{\epsilon\to 0}\left[\lim_{\eta\to 0}\int_{\Sigma(\underline{x}_0,\epsilon)} F(\underline{x}_0 + \eta\,\underline{e}, \underline{y})\,dS_y + \int_{S-\Sigma(\underline{x}_0,\epsilon)} F(\underline{x}_0, \underline{y})\,dS_y\right]$$
(3.45)

In Figure **3.4** , the area $\Sigma(\underline{x}_0, \epsilon)$ is the strip of width 2ϵ centered along the co-ordinate line $\underline{x}_0 = $ constant. The singularity occurs at only one point along the centerline of this region. In the second (or remaining) integral over $S - \Sigma$ we assume the limit as $\epsilon \to 0$ is straightforward and that the integral exists in the limit.

3.3.2   Schematic implementation

A schematic diagram of Σ for a surface with curvature and two coordinate lines (x_1, x_2) is given by Figure **3.5** .
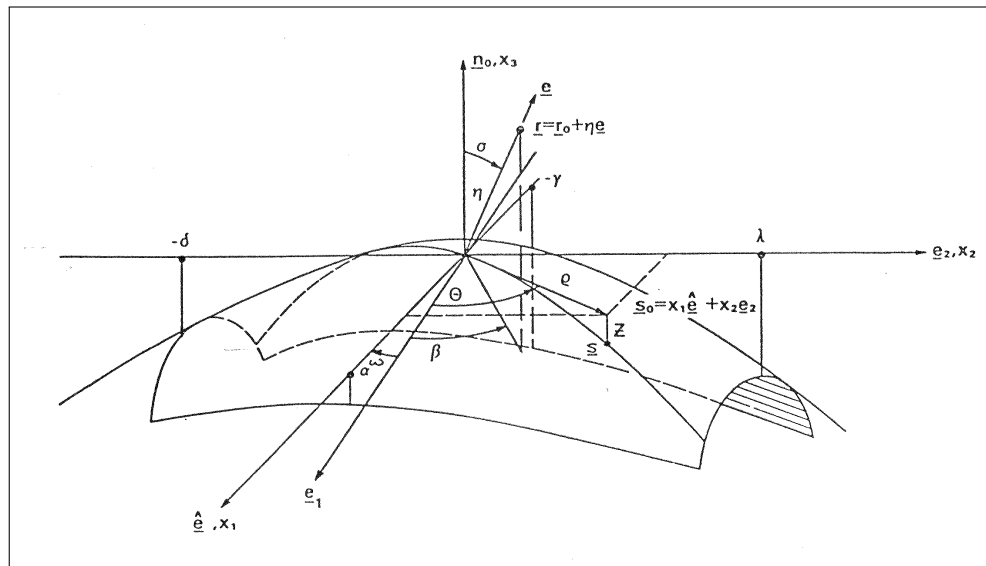
Figure 3.5 Coordinate definition for region surrounding singular point.

These coordinate lines are locally taken as straight lines but are not neces-sarily orthogonal. This illustration is general but since the results are nearly the same as for a surface representation that is planar and the coordinate axes are perpendicular, we will work with the simpler geometry as shown in Figure **3.6** .

The simple form of Σ is a rectangle about $\underline{x}_0$. This is a convenient shape for our work, but we could have selected Σ as a circle or even an ellipse if such a coordinate system were appropriate for the problem. [7] To represent the region of Figure **3.4** , we should let δ and λ be large and $\alpha = \gamma = \epsilon$.
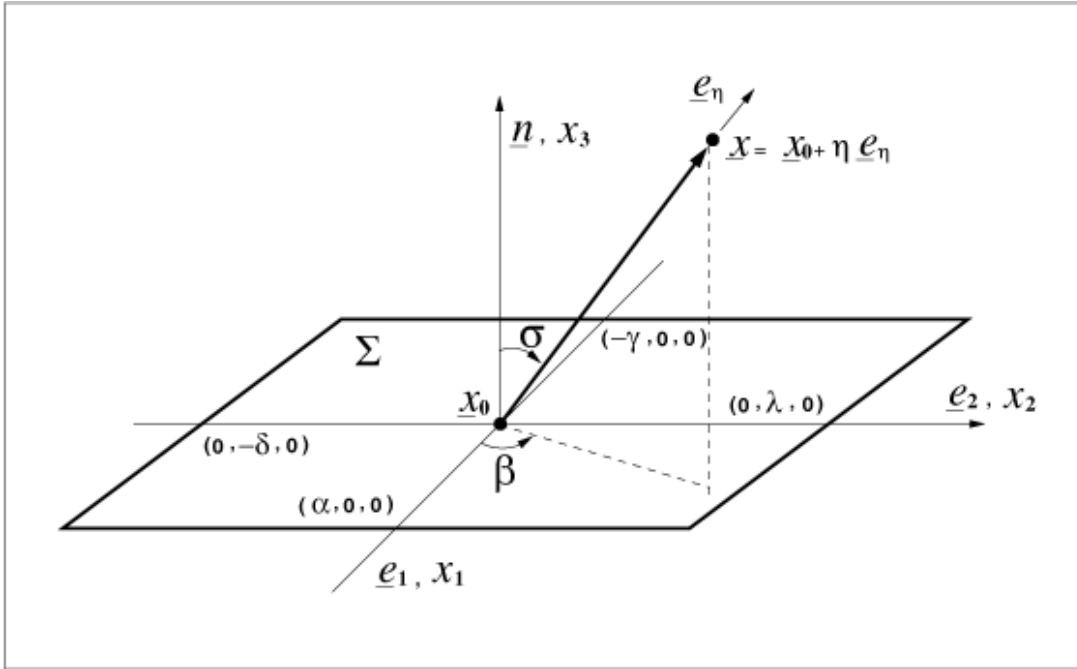
Figure 3.6 Planar approximation of surface surrounding singular point.

3.3.3   Scalar functions

We are concerned here with the approximation to the rectangle excluding the singular point.

$$
\begin{aligned}
\phi(\underline{x}) &= -\frac{1}{4\pi} \oint_S \left[\frac{\partial \phi(\underline{y})}{\partial n} \frac{1}{r} - \phi(\underline{y}) \frac{\partial}{\partial n} \left(\frac{1}{r} \right) \right] dS_y \\
&= -\frac{1}{4\pi} \oint_S \left[\underline{n} \cdot \nabla \phi(\underline{y}) \frac{1}{|\underline{x} - \underline{y}|} - \phi(\underline{y}) \frac{n \cdot (\underline{x} - \underline{y})}{|\underline{x} - \underline{y}|^3} \right] dS_y \quad (3.46)
\end{aligned}
$$

The position vector of the general point in the field is

$$
\underline{x} = \underline{x}_0 + \eta \, \underline{e}_\eta = \underline{x}_0 + \eta \, \cos \sigma \, \underline{n} + \eta \, \sin \sigma \cos \beta \, \underline{e}_1 + \eta \sin \sigma \sin \beta \, \underline{e}_2 \quad (3.47)
$$

[7]See Brockett, T. E. (1972), "Propeller Perturbation Problems", *NSRDC Report*, no. 3880.

and the position vector of the integration point on the planar approximation of the surface is

$$\underline{y} = \underline{x}_0 + x_1 \, \underline{e}_1 + x_2 \, \underline{e}_2 \tag{3.48}$$

So that

$$
\begin{aligned}
\underline{x} - \underline{y} &= \eta \cos \sigma \, \underline{n} + (\eta \sin \sigma \, \cos \beta - x_1) \, \underline{e}_1 + (\eta \sin \sigma \, \sin \beta - x_2) \, \underline{e}_2 \\
|\underline{x} - \underline{y}|^2 &= \eta^2 \cos^2 \sigma + (\eta \sin \sigma \, \cos \beta - x_1)^2 + (\eta \sin \sigma \, \sin \beta - x_2)^2 \\
|\underline{x} - \underline{y}|^3 &= (x_2^2 - 2 \, \eta \, x_2 \sin \sigma \, \sin \beta - 2 \, \eta \, x_1 \sin \sigma \, \cos \beta + \eta^2)^{\frac{3}{2}} \\
dS_y &= dx_1 \, dx_2
\end{aligned}
$$

For the scalar singularity strengths, $\tau \equiv \underline{n} \cdot \nabla \phi(\underline{y})$ and $\mu \equiv \phi(\underline{y})$

$$
\begin{aligned}
\tau(\underline{y}) &= \tau(\underline{x}_0) + (\underline{y} - \underline{x}_0) \cdot \nabla \tau \big|_{\underline{x}_0} + \cdots \tag{3.49} \\
\mu(\underline{y}) &= \mu(\underline{x}_0) + (\underline{y} - \underline{x}_0) \cdot \nabla \mu \big|_{\underline{x}_0} + \cdots \tag{3.50}
\end{aligned}
$$

3.3.3.1   Source distribution

For the source distribution, there is

$$
\begin{aligned}
- \frac{1}{4\pi} \int_\Sigma \tau(\underline{y}) \frac{1}{|\underline{x} - \underline{y}|} \, dS_y &= - \frac{\tau_0}{4\pi} \int_{-\gamma}^{\alpha} \int_{-\delta}^{\lambda} \frac{1}{|\underline{x} - \underline{y}|} \, dx_2 \, dx_1 \tag{3.51} \\
&\quad - \frac{(\nabla \tau_0) \cdot \underline{e}_1}{4\pi} \int_{-\gamma}^{\alpha} \int_{-\delta}^{\lambda} \frac{x_1}{|\underline{x} - \underline{y}|} \, dx_2 \, dx_1 \\
&\quad - \frac{(\nabla \tau_0) \cdot \underline{e}_2}{4\pi} \int_{-\gamma}^{\alpha} \int_{-\delta}^{\lambda} \frac{x_2}{|\underline{x} - \underline{y}|} \, dx_2 \, dx_1
\end{aligned}
$$

These integrals can be easily evaluated using integral tables. The first two integrals are zero with the provision $\alpha \to 0, \gamma \to 0$. The last integral is zero only if $\alpha = \gamma$ and the limit $\gamma \to 0$ is taken. Hence the expression valid for $\underline{x} \to \underline{x}_0$ is

$$
\phi(\underline{x}_0) = - \frac{1}{4\pi} \lim_{\alpha = \gamma \to 0} \oint_{S-\Sigma} \tau(\underline{y}) \frac{1}{|\underline{x}_0 - \underline{y}|} \, dS_y \tag{3.52}
$$

3.3.3.2   Doublet distribution

For the doublet distribution, we have similarly:

$$\frac{1}{4\pi} \int_{\Sigma} \mu(\underline{y}) \frac{\underline{n} \cdot (\underline{x} - \underline{y})}{|\underline{x} - \underline{y}|} \, dS_y = \frac{\mu_0}{4\pi} \int_{-\gamma}^{\alpha} \int_{-\delta}^{\lambda} \frac{\underline{n} \cdot (\underline{x} - \underline{y})}{|\underline{x} - \underline{y}|^3} \, dx_2 \, dx_1 \qquad (3.53)$$

$$+ \frac{(\nabla \mu_0) \cdot \underline{e}_1}{4\pi} \int_{-\gamma}^{\alpha} \int_{-\delta}^{\lambda} x_1 \frac{\underline{n} \cdot (\underline{x} - \underline{y})}{|\underline{x} - \underline{y}|^3} \, dx_2 \, dx_1$$

$$+ \frac{(\nabla \mu_0) \cdot \underline{e}_2}{4\pi} \int_{-\gamma}^{\alpha} \int_{-\delta}^{\lambda} x_2 \frac{\underline{n} \cdot (\underline{x} - \underline{y})}{|\underline{x} - \underline{y}|^3} \, dx_2 \, dx_1$$

As $\eta \to \pm 0$, the first of these integrals goes to $\pm \mu_0/2$ where the (+) sign corresponds one side which the field point appproachs and the (-) sign corresponds the other side. Hence for this integral, it its required only that $\alpha \to 0$ and $\gamma \to 0$. The other two integrals are of the form $(\eta \cdot J)$ where J is bounded and hence the integrals go to zero as $\eta \to 0$. Thus the final expression for the limit of the integral as $\underline{x} \to \underline{x}_0$ is

$$\phi(\underline{x}_0) = \pm \frac{1}{2} \mu(\underline{x}_0) + \frac{1}{4\pi} \lim_{\alpha=\gamma \to 0} \oint_{S-\Sigma} \mu(\underline{y}) \frac{\underline{n} \cdot (\underline{x} - \underline{y})}{|\underline{x} - \underline{y}|^3} \, dS_y \qquad (3.54)$$

3.3.4   Vector functions

Similar procedures applied to the three vector expressions

$$\underline{u}(\underline{x}) = \frac{1}{4\pi} \int_{S} \tau \frac{\underline{x} - \underline{y}}{|\underline{x} - \underline{y}|^3} \, dS_y \qquad (3.55)$$

$$\underline{u}(\underline{x}) = \frac{1}{4\pi} \int_{S} \underline{\gamma} \times \frac{\underline{x} - \underline{y}}{|\underline{x} - \underline{y}|^3} \, dS_y \qquad (3.56)$$

$$\nabla \phi(\underline{x}) = \frac{1}{4\pi} \int_{S} \mu \nabla_x \frac{\underline{n} \cdot (\underline{x} - \underline{y})}{|\underline{x} - \underline{y}|^3} \, dS_y \qquad (3.57)$$

produce the following limits:

$$\underline{u}(\underline{x}_0) = \frac{1}{2}\tau_0\,\underline{n}(\underline{x}_0) + \frac{1}{4\pi}\lim_{\epsilon\to 0}\int_{S-\Sigma}\tau\,\frac{\underline{x}_0-\underline{y}}{|\underline{x}_0-\underline{y}|^3}\,dS_y \tag{3.58}$$

$$\underline{u}(\underline{x}_0) = \frac{1}{2}(\underline{\gamma}\times\underline{n})_{\underline{x}_0} + \frac{1}{4\pi}\lim_{\epsilon\to 0}\int_{S-\Sigma}\underline{\Lambda}\times\frac{\underline{x}_0-\underline{y}}{|\underline{x}_0-\underline{y}|^3}\,dS_y \tag{3.59}$$

$$\nabla\phi(\underline{x}_0) = \frac{1}{2}\left\{(\underline{n}\times\nabla\mu)\times\underline{n}\right\}_{\underline{x}_0}$$
$$+\frac{1}{4\pi}\lim_{\epsilon\to 0}\left[\int_{S-\Sigma}\mu\nabla_x\,\frac{\underline{n}\cdot(\underline{x}_0-\underline{y})}{|\underline{x}_0-\underline{y}|^3}\,dS_y - \frac{4\mu(\underline{x}_0)\,\underline{n}_0}{\epsilon}\right] \tag{3.60}$$

Note that since $\underline{n}$ changes sign across a surface, these forms have the previously discussed discontinuities. When the flow is 2-D and the boundary S is a straight line from a to b, the limit operation in the last equation is the classic expression with replacing $\dfrac{4\mu(\underline{x}_0)\,\underline{n}_0}{\epsilon}$ by $\dfrac{2\mu(\underline{x}_0)\,\underline{n}_0}{\epsilon}$. [8]

3.4   Example : Circular Cylinder in Uniform Flow

So fa we have presented integral formulations for scalar and vector fields. Before we proceed an actual numerical implementation, we consider an analytic example, namely, we solve the boundary value problem for a circular cylinder using the methods based on the aforementioned mathematical backgrounds.

    Let us consider the flow about a circular cylinder in a uniform, ideal stream. (See Figure **3.7**). We apply the various formulations to determine the distribution of sources, dipoles, or vortices.

3.4.1   Point doublet at center

First it is well-known that the velocity potential of the distributed flow is represented as a singularity of a doublet at the center of the circular cylinder with the

---

[8]For self-induced movement of a line vortex, see Batchelor (1967), pp. 509–510 and Brockett, T. E., (2005), "Inviscid duct-rotor interaction elements for a decelerating ducted propulsor," ISP, vol. 52, no. 3, pp. 245–271.
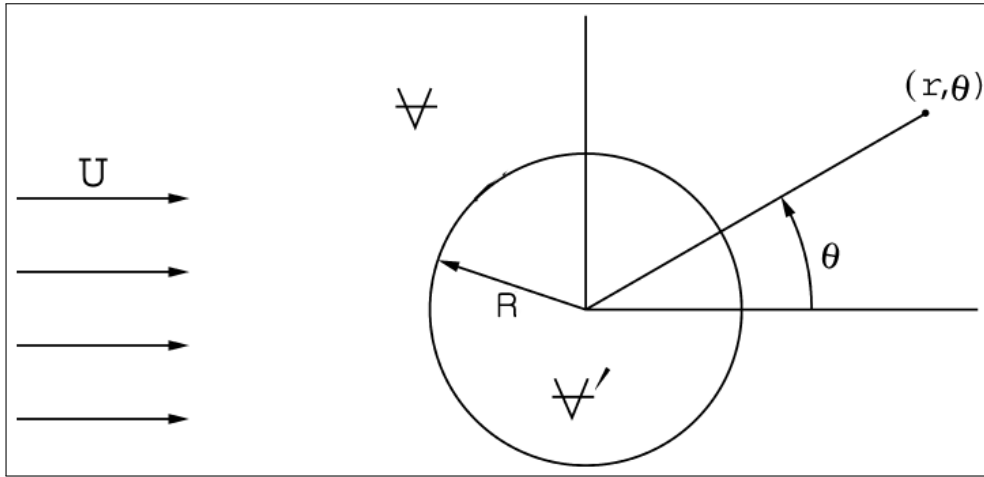
Figure **3.7** Notation for flow about a circular cylinder in a uniform stream.

strength μ in polar coordinate, i.e.,

$$\phi = \frac{\mu}{2\pi} \frac{\cos\theta}{r} \tag{3.61}$$

Thus the total velocity potential is

$$\Phi = \phi_\infty + \phi = Ur\cos\theta + \frac{\mu}{2\pi} \frac{\cos\theta}{r} \tag{3.62}$$

and the velocity becomes

$$\begin{aligned}
\underline{q} &= \nabla\Phi = \frac{\partial\Phi}{\partial r}\underline{e}_r + \frac{\partial\Phi}{r\,\partial\theta}\underline{e}_\theta \\
&= \left(U\cos\theta - \frac{\mu}{2\pi}\frac{\cos\theta}{r^2}\right)\underline{e}_r + \left(-U\sin\theta - \frac{\mu}{2\pi}\frac{\sin\theta}{r^2}\right)\underline{e}_\theta \quad (3.63)
\end{aligned}$$

Now we apply the kinematic (no-penetration) body boundary condition on the cylinder surface, i.e., $\underline{q}\cdot\underline{n}=0$ at $r=R$ where R is the radius of the cylinder

$$U\cos\theta - \frac{\mu}{2\pi}\frac{\cos\theta}{R^2} = 0, \tag{3.64}$$

from which we find the doublet strength

$$\mu = 2\pi R^2 U \tag{3.65}$$

and the distribution of the perturbation velocity potential on the cylinder surface

$$\phi_b = \phi|_{r=R} = UR\cos\theta. \tag{3.66}$$

The subscript b refers to the body surface point. The velocity at any field point in entire domain including the interior and the exterior regions of the cylinder is reduced to

$$\underline{q} = U\cos\left(1 - \frac{R^2}{r^2}\right)\underline{e}_r - U\sin\theta\left(1 + \frac{R^2}{r^2}\right)\underline{e}_\theta \tag{3.67}$$

A typical streamline pattern is illustrated in Figure **3.8** .
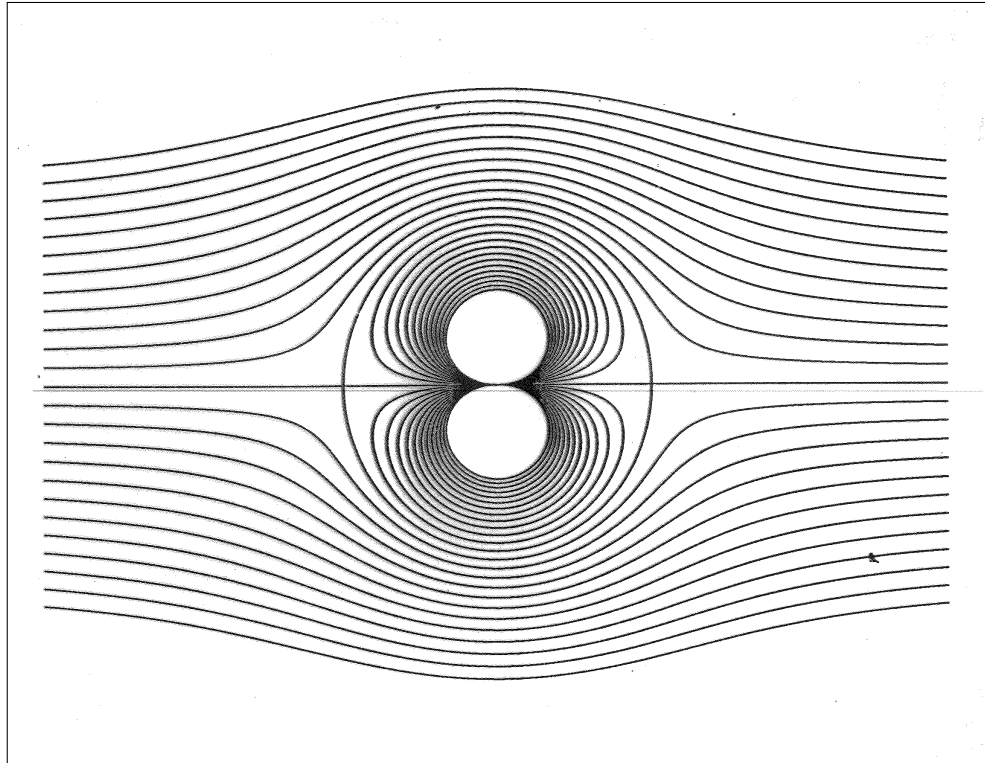
Figure 3.8 Streamlines around/inside a circle (about a doublet) in a uniform stream.

3.4.2 Potential distribution

The Green's scalar identity for the perturbation velocity potential in 2-D fields can be written as

$$\phi = \oint_C \left(\phi \frac{\partial G}{\partial n} - \frac{\partial \phi}{\partial n} G \right) d\ell \qquad (3.68)$$

where the Green function in polar coordinates for a source point $\underline{y}$ on the circular cylinder surface is

$$G = -\frac{1}{2\pi} \ln |\underline{x} - \underline{y}| = \frac{1}{2\pi} \ln \sqrt{r^2 + R^2 - 2rR\cos(\theta - \alpha)} \qquad (3.69)$$

and the normal derivative of G is

$$\frac{\partial G}{\partial n} = \frac{\partial G}{\partial r} = -\frac{1}{2\pi} \frac{R - r\cos(\theta - \alpha)}{r^2 + R^2 - 2rR\cos(\theta - \alpha)}. \qquad (3.70)$$

Use the kinematic body boundary condition to replace $(\frac{\partial \phi}{\partial n})$ by $(-\underline{U} \cdot \underline{n})$ and take the limiting form of the given integral form as a field point approaches a body point (i.e., $r \to R$) in order to establish the integral equation for unknown contour distribution of ϕ :

$$\phi_b = \frac{\phi_b}{2} + \oint_C \left\{ \phi_b \frac{\partial G}{\partial n} + (\underline{U} \cdot \underline{n}) G \right\} d\ell \qquad (3.71)$$

or

$$\frac{\phi_b}{2} - \oint_C \phi_b \frac{\partial G}{\partial n} d\ell = \oint_C (\underline{U} \cdot \underline{n}) G \, d\ell \qquad (3.72)$$

Inserting G and $\dfrac{\partial G}{\partial n}$ obtained previously into this equation gives

$$\frac{\phi_b}{2} + \frac{1}{2\pi} \int_0^{2\pi} \phi_b \frac{R\{1 - \cos(\theta - \alpha)\}}{2R^2\{1 - \cos(\theta - \alpha)\}} R \, d\alpha$$
$$= -\frac{UR}{2\pi} \int_0^{2\pi} \cos \alpha \ln \sqrt{2R^2\{1 - \cos(\theta - \alpha)\}} \, d\alpha \qquad (3.73)$$

Rearrange this equation to obtain

$$\phi_b + \frac{1}{2\pi} \int_0^{2\pi} \phi_b \, d\alpha = -\frac{UR}{2\pi} \int_\theta^{2\pi+\theta} \cos\alpha \, \ln\{1 - \cos(\theta - \alpha)\} \, d\alpha \quad (3.74)$$

Now the integral on the RHS becomes [9]

$$\int_\theta^{2\pi+\theta} \cos\alpha \, \ln\{1 - \cos(\theta - \alpha)\} \, d\alpha = \int_\theta^{2\pi+\theta} \cos\alpha \, \ln\left\{2\sin^2\frac{\theta - \alpha}{2}\right\} d\alpha$$

$$= 2\int_0^1 \cos(\theta + 2\pi x) \, \ln(\sin\pi x) \, 2\pi \, dx$$

$$= -2\pi\cos\theta \quad (3.75)$$

Here, we have put $(\theta - \alpha)/2 = -\pi x$, and used $\displaystyle\int_0^{2\pi} \sin(2\pi x) \, \ln(\sin\pi x) \, dx = 0$ and $\displaystyle\int_0^{2\pi} \cos(2\pi x) \, \ln(\sin\pi x) \, dx = -\frac{1}{2}$. Therefore the integral equation is reduced to

$$\phi_b + \frac{1}{2\pi} \int_0^{2\pi} \phi_b \, d\alpha = UR\cos\theta \quad (3.76)$$

It is easily seen that the solution of this equation is

$$\phi_b = UR\cos\alpha, \quad (3.77)$$

since, for which, $\displaystyle\int_0^{2\pi} \phi_b \, d\alpha = 0$. With the surface distribution of ϕ, the potential at any point either outside or inside the cylinder can be written as [10]

$$\begin{aligned}
\phi(r,\theta) &= \oint_C \left(\phi\frac{\partial G}{\partial n} - \frac{\partial \phi}{\partial n}G\right) d\ell \\
&= -\frac{1}{2\pi}\int_0^{2\pi} (UR\cos\alpha) \frac{R - r\cos(\theta - \alpha)}{r^2 + R^2 - 2rR\cos(\theta - \alpha)} R\,d\alpha \\
&\quad -\frac{1}{2\pi}\int_0^{2\pi} (UR\cos\alpha) \ln\sqrt{r^2 + R^2 - 2\,rR\cos(\theta - \alpha)}\,R\,d\alpha \\
&= UR^2\cos\theta/r \quad (3.78)
\end{aligned}$$

---

[9]Gradshteyn, I. S. and Ryzhik, I. M. (1965), *Table of Integrals, Series and Products*, Academic Press, Inc., New York and London, p. 584.

[10]*Ibid*, pp. 366–367, 593.

Of course, this solution is the same as that presented in the previous case of a point doublet at the center of a cylinder.

3.4.3   Stream function formulation

For comparison to the potential-based formulation, we introduce herein the stream function based formulation. The Green's scalar identity for the perturbation stream function in 2-D fields can be written as

$$\psi = \oint_C \left(\psi \frac{\partial G}{\partial n} - \frac{\partial \psi}{\partial n} G \right) d\ell \tag{3.79}$$

The limiting form as a field point approaches a body point would be, in the same manner as the potential-based formulation,

$$\psi_b = \frac{\psi_b}{2} + \int_C \left\{ \psi_b \frac{\partial G}{\partial n} - \frac{\partial \psi_b}{\partial n} G \right\} d\ell \tag{3.80}$$

Now, the total stream function $\Psi = \psi_\infty + \psi$, where $\psi_\infty = Uy = Ur \sin\theta$, can be set zero at the (closed, non-lifting) body surface, from which

$$\psi_b = -\psi_{\infty b}, \quad \text{i.e.,} \quad \psi_b = -UR \sin\theta \tag{3.81}$$

Insert this relation into the above integral equation

$$-\frac{UR \sin\theta}{2} + \frac{1}{2\pi} \int_0^{2\pi} (-UR \sin\alpha) \frac{R\{1 - \cos(\theta - \alpha)\}}{2R^2\{1 - \cos(\theta - \alpha)\}} R \, d\alpha$$
$$= -\frac{1}{2\pi} \int_0^{2\pi} \frac{\partial \psi_b}{\partial n} \ln \sqrt{2R^2\{1 - \cos(\theta - \alpha)\}} \, R \, d\alpha \tag{3.82}$$

This is the integral equation for unknown distribution of $\dfrac{\partial \psi_b}{\partial n}$ at the contour, in which the solution can be obtained from the same procedure as in the case of the potential-based formulation.

$$\frac{\partial \psi_b}{\partial n} = +U \sin\theta \tag{3.83}$$

Consequently, the total tangential speed at the body surface is the same:

$$V_s = \frac{\partial \Psi_b}{\partial n} = 2U \sin \theta \qquad (3.84)$$

3.4.4   Source distribution

Take the normal component of the gradient of potential and then the limiting form as $\underline{x} \to \underline{x}_b$, noting that $\tau = \left(\dfrac{\partial \phi}{\partial n} - \dfrac{\partial \phi'}{\partial n} \right)$ and $\underline{n} = \underline{e}_r$:

$$\left. \frac{\partial \phi}{\partial n} \right|_{\underline{x}=\underline{x}_b} = +\frac{\tau}{2} - \oint_C \tau \frac{\partial G}{\partial n} \, d\ell \qquad (3.85)$$

Apply the body boundary condition and insert $\partial G / \partial n$ into the resulting equation:

$$-\underline{U} \cdot \underline{n}|_{r=R} = +\frac{\tau}{2} - \int_0^{2\pi} \tau \left(\frac{-1}{2\pi} \frac{R - R\cos(\theta - \alpha)}{R^2 + R^2 - 2RR\cos(\theta - \alpha)} \right) R \, d\alpha \quad (3.86)$$

Namely,

$$U \cos \theta = -\frac{\tau}{2} - \frac{1}{2\pi} \int_0^{2\pi} \tau \frac{1}{2} \, d\alpha \qquad (3.87)$$

Again, by intuition, we can see that the solution for τ is

$$\tau = -2U \cos \theta \qquad (3.88)$$

Similarly, the surface distribution of ϕ over the circle is

$$
\begin{aligned}
\phi_b &= -\oint_C \tau \, G \, d\ell \\
&= \frac{1}{2\pi} \int_0^{2\pi} (-2U \cos \theta) \ln \sqrt{2R^2 (1 - \cos(\theta - \alpha))} R \, d\alpha \\
&= -\frac{UR}{2\pi} (-2\pi \cos \theta) = UR \cos \theta \qquad (3.89)
\end{aligned}
$$

Here we have used the equation (3.75) as in the case of the potential distribution.

3.4.5   Vortex distribution

We take the total velocity formulation for only vortex distribution:

$$\underline{q} = \underline{q}_\infty + \oint_C \underline{\gamma} \times \nabla G \, d\ell \tag{3.90}$$

where the gradient of G in polar coordinates is

$$
\begin{aligned}
\nabla G &= \frac{\partial G}{\partial r} \underline{e}_r + \frac{\partial G}{r \, \partial \theta} \underline{e}_\theta \\
&= \frac{1}{2\pi} \left[\left\{ \frac{R - r\cos(\theta - \alpha)}{r^2 + R^2 - 2rR\cos(\theta - \alpha)} \right\} \underline{e}_r \right. \\
&\qquad \left. + \left\{ \frac{-rR\sin(\theta - \alpha)}{r^2 + R^2 - 2rR\cos(\theta - \alpha)} \right\} \underline{e}_\theta \right]
\end{aligned}
\tag{3.91}
$$

Set $\underline{\gamma} = \gamma\,\underline{k}$ for 2-D cases and then

$$\underline{\gamma} \times \nabla G = \frac{\gamma}{2\pi} \frac{r\sin(\theta - \alpha)\,\underline{e}_r - \{R - r\cos(\theta - \alpha)\}\,\underline{e}_\theta}{r^2 + R^2 - 2rR\cos(\theta - \alpha)} \tag{3.92}$$

Now apply the body boundary condition on the exterior surface:

$$0 = \underline{q} \cdot \underline{n} = \underline{U} \cdot \underline{n} + \underline{n} \cdot \oint_C \gamma\,\underline{k} \times \nabla G \, d\ell \tag{3.93}$$

Recalling $\underline{U} \cdot \underline{n}|_{r=R} = +U\cos\theta$ and $\underline{n} = \underline{e}_r$, we have

$$
\begin{aligned}
U\cos\theta &= \int_0^{2\pi} \frac{\gamma}{2\pi} \frac{-R\sin(\theta - \alpha)}{2R^2\{1 - \cos(\theta - \alpha)\}} R \, d\alpha \\
&= -\int_0^{2\pi} \frac{\gamma}{2\pi} \frac{2\cos\left(\frac{\theta - \alpha}{2}\right)\sin\left(\frac{\theta - \alpha}{2}\right)}{4\sin^2\left(\frac{\theta - \alpha}{2}\right)} \, d\alpha \\
&= -\frac{1}{4\pi} \int_0^{2\pi} \gamma \cot\left(\frac{\theta - \alpha}{2}\right) d\alpha
\end{aligned}
\tag{3.94}
$$

The solution of the above integral equation is, [11]

$$\gamma = 2U\sin\theta \tag{3.95}$$

---

[11] According to Tricomi, F. G. (1957), *Integral Equations*, Interscience Publishers Inc, p. 167.

3.5   Direct Formulation for Surface Speed

3.5.1   Boundary condition for interior flow

To develop a procedure (for 2-D and axisymmetric flow) for which we can directly solve for the surface speed, we have to do a bit more analysis. [12] This approach is not necessarily the best either conceptually or numerically and hence is only illustrative. Consider the past a body with an interior volume. We can represent this flow as a surface distribution of any vortices:

$$q(\underline{x}) = \underline{q}_\infty + \frac{1}{4\pi} \oint_{S_B} \underline{\gamma} \times \frac{\underline{x} - \underline{y}}{|\underline{x} - \underline{y}|^3} \, dS_y \qquad (3.96)$$

Now if we let $\underline{x} \to \underline{x}_0$

$$\underline{q}(\underline{x}_0) = \underline{q}_\infty + \frac{1}{2} \underline{\gamma}(\underline{x}_0) \times \underline{n}^*(\underline{x}_0) + \frac{1}{4\pi} \int_{S_B} \underline{\gamma} \times \frac{\underline{x} - \underline{y}}{|\underline{x} - \underline{y}|^3} \, dS_y \qquad (3.97)$$

If we set $\underline{n}$ to be the exterior normal (pointing from the body into the fluid), then $\underline{n}^* = \underline{n}$ for $\underline{x} \to \underline{x}_0$ from outside the body and $\underline{n}^* = -\underline{n}$ as $\underline{x} \to \underline{x}_0$ from inside the body. The flow external to the body satisfies the B.C.: $\underline{q} \to \underline{q}_\infty$ as $\underline{x} \to \infty$ and also the body B.C. : $\underline{q} \cdot \underline{n} = 0$ (i.e., $\underline{q}(\underline{x}_0)$ is only tangential to S_B).

Our formulation of the problem is such that $\underline{q} \cdot \underline{n}$ is continuous across the body surface, so $\underline{q} \cdot \underline{n} = 0$ inside the surface of the body also. If we require that the flow inside the body be such that $\underline{q} = 0$ for any $\underline{x} = \underline{x}_i$, then $(\underline{q} \cdot \underline{t})_i = 0$ also along the inside of S_B. We will have to see what will require the interior flow to be 0 later. So on the inside,

$$0 = \underline{t}(\underline{x}_0) \cdot \underline{q}_\infty - \frac{1}{2} \underline{t}(\underline{x}_0) \cdot \left[\underline{\gamma}(\underline{x}_0) \times \underline{n}^*(\underline{x}_0) \right] + \frac{\underline{t}(\underline{x}_0)}{4\pi} \cdot \int_{S_B} \underline{\gamma} \times \frac{\underline{x} - \underline{y}}{|\underline{x} - \underline{y}|^3} \, dS_y \quad (3.98)$$

---

[12]Lewis, R. I. and Ryan, P. G. (1972), "Surface vorticity theory for axisymmetric annular aerofoils and bodies of revolution with application to duct cowls," *Journal of Mechanical Engineering Science*, vol. 14, no. 4, pp. 280–291.

and on the outside,

$$\underline{t}(\underline{x}_0){\cdot}\underline{q}(\underline{x}_0) = \underline{t}(\underline{x}_0){\cdot}\underline{q}_\infty - \frac{1}{2}\underline{t}(\underline{x}_0){\cdot}\left[\underline{\gamma}(\underline{x}_0) \times \underline{n}^*(\underline{x}_0)\right] + \frac{\underline{t}(\underline{x}_0)}{4\pi}{\cdot}\oint_{S_B} \underline{\gamma} \times \frac{\underline{x}-\underline{y}}{|\underline{x}-\underline{y}|^3} dS_y \tag{3.99}$$

If we subtract the equation for the inside tangential speed from the equation for the outside tangential speed, then

$$\underline{t}(\underline{x}_0) \cdot \underline{q}(\underline{x}_0) = \underline{t}(\underline{x}_0) \cdot \left[\underline{\gamma}(\underline{x}_0) \times \underline{n}^*(\underline{x}_0)\right] \tag{3.100}$$

Hence for 2-D and axi-symmetric problems, we say $|\underline{\gamma}| = |\underline{q}|$ on the surface. Thus we have only the one scalar γ to find and, except for sign, it will be the surface speed.

Since the tangential component of velocity is zero inside the body, its integral around the contour is also zero. From Stokes theorem, the flow field contained within this volume must be irrotational on average. We have already specified that the flow be irrotational, so nothing new is gained from this information.

The divergence theorem (Gauss theorem) requires that the integral of the normal component of the velocity integrate to zero over the bounding surface for an incompressible fluid. We also have that the value of the potential is constant along the inside of the body since the contour integral of $\underline{q} \cdot d\underline{\ell}$ is zero. Then Green's first identity with $\psi = \phi$ gives

$$\int_{V_i} \left[\phi\nabla^2\phi + \nabla\phi \cdot \nabla\phi\right] dV = \oint_{S_i} \phi\,\underline{n} \cdot \nabla\phi\,dS = \phi \oint_{S_i} \underline{n} \cdot \nabla\phi\,dS \tag{3.101}$$

Since the flow is potential and the RHS is zero, we have only

$$\int_{V_i} \left[\nabla\phi \cdot \nabla\phi\right] dV = 0, \tag{3.102}$$

for which the integral must be zero since it is a positive definite quantity. Thus there is no flow inside the body and hence both $\underline{q}{\cdot}\underline{n}$ and $\underline{q}{\cdot}\underline{t}$ are zero on the inside of the surface and we have established that if the tangential velocity component be zero on the inside of the surface then the normal velocity component must also be zero.

3.5.2   Example: Vortex distribution over a circle

We take, again, the flow problem aorund a circular cylinder in uniform inflow. The velocity formulation for only vortex distribution becomes, as Eq. (3.90) before,

$$q = \underline{q}_\infty + \oint_C \underline{\gamma} \times \nabla G \, d\ell \tag{3.103}$$

where the gradient of G in polar coordinates is given by Eq. (3.91).
For $\underline{\gamma} = \gamma \underline{k}$, use Eq. (3.98), i.e., apply the body boundary condition that the total tangential velocity component on the inside of the body surface is zero:

$$0 = \underline{q} \cdot \underline{t} = \underline{U} \cdot \underline{t} + \underline{t} \cdot \int_C \gamma \, \underline{k} \times \nabla G \, d\ell \tag{3.104}$$

Then, we rearrange this:

$$U \sin \theta = \frac{\gamma}{2} + \int_0^{2\pi} \frac{\gamma}{2\pi} \frac{R \left\{ 1 - \cos(\theta - \alpha) \right\}}{2R^2 \left\{ 1 - \cos(\theta - \alpha) \right\}} R \, d\alpha \tag{3.105}$$

The solution of the above integral equation is the same as the previous one, as expected:

$$\gamma = 2U \sin \theta \tag{3.106}$$

This distribution corresponds to one of the surface speed.

3.6   Numerical Error

3.6.1   Error measures

With an approximation numerical solution, it would be desirable to check the solution for arbitrary point $\underline{x}_0$ in the solution domain; i.e., we seek to find a numerical solution that in some way has converged to a standard or reference value for number of terms (or steps), $M > M_0$, in our numerical solution:

$$|f^S(\underline{x}_0) - f_M(\underline{x}_0)| \le \epsilon \quad \text{all } \underline{x}_0 \in S_B \text{ and all } M > M_0 \tag{3.107}$$

where $f^S(\underline{x}_0)$ is the standard of comparison (perhaps an exact solution for a special case; experimental data judged to be free of viscous effects; or some other numerical solution that one trusts), $f_M(\underline{x}_0) = \sum\limits_{i=1}^{M} f_i(\underline{x}_0)$ and $f_i(\underline{x}_0)$ are the subelements in our numerical analysis that sum to the solution.

Generally numerical solutions are not for arbitrary points in the field of interest but a set of discrete points $\underline{x}_{0_n}, 1 \leq n \leq N$, that may be specified prior to solution. The criterion for convergence for the set $\underline{x}_{0_n}$ may be stated

$$|f^S(\underline{x}_{0_n}) - f_M(\underline{x}_{0_n})| \leq \epsilon \quad \text{all } \underline{x}_{0_n} \in S_B \text{ and all } M > M_0 \qquad (3.108)$$

This criterion is necessary but may not sufficient since the set $\underline{x}_{0_n}$ may not be distributed appropriately. An error measure indicative of this type of convergence is the maximum difference between the standard and our numerical solutions that we find as a result of a search over the entire set of points available ($\underline{x}_{0_j}$). Define the error measure in terms of the relative maximum norm of the local errors:

$$E_\infty = \frac{\left[\max |f^S(\underline{x}_{0_j}) - f_M(\underline{x}_{0_j})|\right]}{\left[\max |f^S(\underline{x}_{0_j})|\right]} \qquad (3.109)$$

Such an error measure defines the maximum non-dimensional error that occurs to the maximum value of the standard.

Perhaps we are more interested in some measure of the average error. Two error measures of the relative cumulative errors are defined:

$$E_1 = \frac{\left[\sum_{j=1}^{N} \left|f^S(\underline{x}_{0_j}) - f_M(\underline{x}_{0_j})\right|\right]}{\left[\sum_{j=1}^{N} \left|f^S(\underline{x}_{0_j})\right|\right]} \qquad (3.110)$$

$$E_2 = \frac{\left[\sum_{j=1}^{N} \left|f^S(\underline{x}_{0_j}) - f_M(\underline{x}_{0_j})\right|^2\right]^{1/2}}{\left[\sum_{j=1}^{N} \left|f^S(\underline{x}_{0_j})\right|^2\right]^{1/2}} \qquad (3.111)$$

The measure E_1 may be representative of the upper bound of error in the computation of the circulation about the foil section. Actually the panel element length should be included if this were to represent the circulation but still this is some measure of it. The measure E_2, the relative square error of the approximation or Euclidean norm, is a popular measure of error in a numerical solution.

It may be representative of the error in the lift coefficient computed from an integration of the pressure over the foil surface. Hence this physical quantity may also be better represented if the local panel length were included. Sometimes a particular point on the surface can be troublesome in terms of convergence. Such may be the case near the trailing edge (although some fixes such as providing rounded trailing edges may be helpful) and near the tips on three-dimensional wings.

4

POTENTIAL BASED METHODS

4.1   Introduction

We have provided the integral formulations for the flow analysis so far. Our
first discussion will be an extended line concerning numerical analysis by panel
methods. The key to this approach is the recognition that the surface integrals
can be represented as a sum of integrals over elementary regions of the surface
with no loss of generality.

We will require the elementary regions to sum to the real surface and make approximations in the calculations. In the limit as the number of elementary regions(or panels) tends to ∞, we expect this procedure to converge to the exact solution since it becomes the Riemann-sum definition of an integral. The utility of this analysis can be assessed by comparison with more exact procedures and with appropriate experimental data. In both analytic and numerical solutions, one seeks to solve a well-posed, or reasonable, problem.

For analytic problems this well-posed condition has been defined as that quality for which a bounded solution exists, the solution is unique, and the solution depends continuously on the data(in particular, small changes in the data produce small changes in the solution).

An extension of these concepts to numerical analysis is given by other researchers who point out that a well-posed computing problem(or algorithm a set of rules specifying the order and kind of arithmetic operations to be used on specific data) is existence, uniqueness in the sense that repeated runs produce the same result, and that the solution depends continuously on the data. In practice there is often more concern with existence than the other two properties of a well-posed problem.

We have a number of representations of the flow field that can be used to derive a solution for the specified boundary conditions. We need satisfy only the body boundary condition since the Laplace equation is already satisfied and the disturbances die off as $\underline{x} \to \infty$(so we have left only the body B.C. to meet).

One of the choices might be to use the results of the formulation in the previous chapter: In particular, we must consider our singularity distribution to be, in 3-D and in 2-D, respectively,

$$\frac{1}{2}\phi(\underline{x}_0) - \frac{1}{4\pi}\int_S \phi(\underline{y})\frac{\underline{n}(\underline{y}) \cdot (\underline{x}_0 - \underline{y})}{|\underline{x}_0 - \underline{y}|^3}\, dS_y \;=\; -\frac{1}{4\pi}\int_S \underline{n} \cdot \nabla\phi(\underline{y})\frac{1}{|\underline{x}_0 - \underline{y}|}\, dS_y$$

$$(4.1)$$

$$\frac{1}{2}\phi(\underline{x}_0) - \frac{1}{2\pi}\int_C \phi(\underline{y})\frac{\underline{n}(\underline{y}) \cdot (\underline{x}_0 - \underline{y})}{|\underline{x}_0 - \underline{y}|^2}\, d\ell_y \;=\; -\frac{1}{2\pi}\int_C \underline{n} \cdot \nabla\phi(\underline{y})\ln\frac{1}{|\underline{x}_0 - \underline{y}|}\, d\ell_y$$

$$(4.2)$$

where $\underline{n}$ is directed from the body into the fluid field, $\underline{n} \cdot \nabla \phi$ is known from the body B.C.: $\underline{n} \cdot \underline{q} = 0 = \underline{n} \cdot (\underline{q}_{\infty} + \nabla \phi) \Rightarrow \underline{n} \cdot \nabla \phi = -\underline{n} \cdot \underline{q}_{\infty}$.

On the RHS we set a known value for a given shape and onset flow and we would select a suitable discretization and approximation of the surface S_B and representation of the unknown ϕ, say ϕ is linear, bilinear, or even constant in each panel.

4.2   Discretization of a Body Surface

For 2-D flows, recall that our formulation would be

$$\boxed{\frac{1}{2}\phi(\underline{x}_0) = \frac{1}{2\pi} \fint_C \left[\phi(\underline{y}) \frac{\underline{n}(\underline{y}) \cdot (\underline{x}_0 - \underline{y})}{|\underline{x}_0 - \underline{y}|^2} - \underline{n} \cdot \nabla \phi(\underline{y}) \ln \frac{1}{|\underline{x}_0 - \underline{y}|} \right] d\ell_y} \quad (4.3)$$

The essence of the panel method approximation is to subdivide the surface into small elements. We can do this without loss of generality by specifying

$$\frac{1}{2}\phi(\underline{x}_0) = \frac{1}{2\pi} \sum_{j=1}^{N} \fint_{C_j} \left[\phi(\underline{y}) \frac{\underline{n}(\underline{y}) \cdot (\underline{x}_0 - \underline{y})}{|\underline{x}_0 - \underline{y}|^2} - \underline{n} \cdot \nabla \phi(\underline{y}) \ln \frac{1}{|\underline{x}_0 - \underline{y}|} \right] d\ell_y$$

$$(4.4)$$

where the C_j are a subdivision of the surface that will be sequentially ordered and one with some sort of formalism such that as N becomes large the maximum length of any C_j becomes arbitrarily fine. As $N \to \infty$, we know that one expression for the integral is the Riemann sum.

In using this representation, our interest is to approximate the integrals over C_j in some manner such that a relatively few number of elements is sufficient to provide an acceptable value for the integral. One of our choices is to consider a portion of the surface of the body. The element is defined to be bounded by the end points of the interval.

With this approach we would find a system of linear equations and solve them for $\phi(\underline{y})$. Once the values of $\phi(\underline{y})$ are known, a differentiation of the values obtained would give the surface speed. We can call such a procedure a

low-order panel method. [1] Such procedures are reported to be cost effective, accurate, and simple to formulate. Note we solve for only the one scalar quantity even for 3-D flow (rather than 3 vector components)

The two-step process required to find the surface speed: that is, first, we must solve for the singularity distribution and then do another step (here taking the gradient) to find one of the quantities of great interest (the surface speed). Recall that once the surface speed is known we can use the Bernoulli equation to obtain the surface pressure and integrate the pressure to find loads.

4.2.1 Evaluation of the integrals for a line element
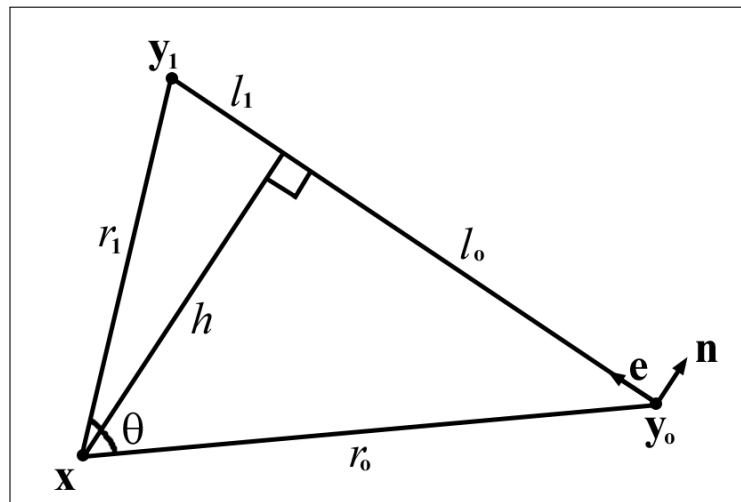
Figure **4.1** Notation for evaluation of induction integrals on a line element.

The symbols shown in Figure (**4.1**) are defined as follows:

$$l = \left| \underline{y}_o - \underline{y}_1 \right| , \quad \underline{r}_o = \underline{y}_o - \underline{x} , \quad \underline{r}_1 = \underline{y}_1 - \underline{x}$$

$$l_o = -\underline{r}_o \cdot \underline{e} , \quad l_1 = \underline{r}_1 \cdot \underline{e} , \quad h = \underline{r}_o \cdot \underline{n} = \underline{r}_1 \cdot \underline{n}$$

$$\theta = \arctan \frac{l_o}{h} + \arctan \frac{l_1}{h} = \arctan \frac{2\,l\,h}{r_o^2 + r_1^2 - l^2}$$

Here, $\underline{x}$ is the point to calculate the value and $\underline{y}$ is defined on the body Panel as $\underline{y} = \underline{y}_o + s\,\underline{e}.$

---

[1] See Maskew, B. (1982), "Prediction of Subsonic Aerodynamic Characteristics of Panel Methods," *J. of Aircraft*, vol. 19, no. 2, pp. 157–163.

The Green function is written as

$$G = \frac{1}{2\pi} \ln r \tag{4.5}$$

$$\nabla G = \frac{1}{2\pi} \frac{r}{r^2} = \frac{1}{2\pi} \frac{s\,\underline{e} + r_o}{(s - l_o)^2 + h^2} \tag{4.6}$$

Then the associated integrals can be evaluated as follows:

(1) Calculation of $\int \underline{n} \cdot \nabla G \, dl$

$$
\begin{aligned}
\int \underline{n} \cdot \nabla G \, dl &= \frac{1}{2\pi} \int_o^l \frac{\underline{n} \cdot (s\,\underline{e} + r_o)}{(s - l_o)^2 + h^2} \, ds \\
&= \frac{h}{2\pi} \int_o^l \frac{ds}{(s - l_o)^2 + h^2} \\
&= \frac{1}{2\pi} \left(\arctan \frac{l_1}{h} + \arctan \frac{l_o}{h} \right) \\
&= \begin{cases} 0 & (\text{if } h = 0) \\[2ex] \dfrac{\theta}{2\pi} & (\text{if } h \neq 0) \end{cases}
\end{aligned}
\tag{4.7}
$$

(2) Calculation of $\int G \, dl$

$$
\begin{aligned}
\int G \, dl &= \frac{1}{2\pi} \frac{1}{2} \int_o^l \ln\left[(s - l_o)^2 + h^2\right] ds \\
&= \begin{cases} \dfrac{1}{2\pi} \left[-l + \dfrac{1}{2} l_o \ln r_o^2 + \dfrac{1}{2} l_1 \ln r_1^2 \right] & (\text{if } h = 0) \\[3ex] \dfrac{1}{2\pi} \left[-l + \dfrac{1}{2} l_o \ln r_o^2 + \dfrac{1}{2} l_1 \ln r_1^2 + h\,\theta \right] & (\text{if } h \neq 0) \end{cases}
\end{aligned}
\tag{4.8}
$$

4.3 Trailing Wake Sheet Behind a Lifting Body

4.3.1 Boundary condtions

Assuming an inviscid fluid, the wake generated by time-varying flow around a lifting body appears as a discontinuity in the tangential flow velocity. In this case the infinitely thin wake sheet must be treated as a physical free boundary of the fluid region, or mathematically as a discontinuity of the domain. From a mathematical standpoint, a difference between two- and three-dimensional flow field disturbed by bodies is that the region occupied by fluid is double-connected in the two-dimensional case and single-connected in the three-dimensional case. [2] To ensure a unique solution, two boundary conditions are required; one is the kinematic boundary condition which states continuity of the velocity component normal to the vortex sheet:

$$(\underline{q}^+ - \underline{q}^-) \cdot \underline{n} = 0. \tag{4.9}$$

The other is the dynamic condition of no net stresses on the vortex sheet; i.e., the vortex sheet is a free surface. For inviscid fluid, this leads to the requirement that pressure be continuous across the sheet:

$$p^+ - p^- = 0. \tag{4.10}$$

4.3.2 Vortex distribution on wake sheet

A wake vortex sheet of vortex strength (γ) is composed of vortices continuously produced at the T. E. according to the Kutta condition. The wake vortex sheet satisfying both the kinematic and the dynamic conditions, is deformed with time as flow conditions change. Let us denote the quantities in two regions separated by the wake sheet with the superscripts $+$ and $-$. Then, from the kinematic condition the relative acceleration vectors on either side of the wake sheet in the

---

[2] See, e.g., Morino, L., Kaprielian, Z. and Sipcic, S. R. (1985), "Free Wake Analysis of Helicopter Rotors," *Vertica*, vol. 9, no. 2, pp. 127–140.

moving frame in the two regions can be written:

$$\underline{a}^+ = \frac{\partial \underline{q}^+}{\partial t} + \underline{q}^+ \cdot \nabla \underline{q}^+ = \frac{\partial \underline{q}^+}{\partial t} + \left(\underline{q}_m - \frac{\gamma}{2}\underline{t}\right) \cdot \nabla \underline{q}^+, \qquad (4.11)$$

$$\underline{a}^- = \frac{\partial \underline{q}^-}{\partial t} + \underline{q}^- \cdot \nabla \underline{q}^- = \frac{\partial \underline{q}^-}{\partial t} + \left(\underline{q}_m + \frac{\gamma}{2}\underline{t}\right) \cdot \nabla \underline{q}^-, \qquad (4.12)$$

where $\underline{q}_m \equiv \dfrac{\underline{q}^+ + \underline{q}^-}{2}$ is the mean velocity on the wake sheet and the vortex strength γ is defined by $\gamma\underline{t} = \underline{q}^- - \underline{q}^+$, the tangential vector being taken as pointing downstream along the vortex sheet. From the Euler equations for the two regions, knowing that the additional acceleration terms resulting from taking the moving frame have the same value across the wake sheet, it follows that

$$(\underline{a}^+ - \underline{a}^-) = -\frac{1}{\rho}(\nabla p^+ - \nabla p^-), \qquad (4.13)$$

where ρ is the (uniform) fluid density. The inner product of (4.13) with the sheet tangential vector gives

$$(\underline{a}^+ - \underline{a}^-) \cdot \underline{t} = 0. \qquad (4.14)$$

This is because $(\nabla p^+ - \nabla p^-) \cdot \underline{t}$ must be zero along the sheet by the dynamic condition of pressure continuity. Therefore, the governing equation for γ from (4.11), (4.12) and (4.14) becomes,

$$\frac{\partial(\gamma\underline{t})}{\partial t} \cdot \underline{t} + \left\{\underline{q}_m \cdot \nabla(\gamma\underline{t})\right\} \cdot \underline{t} + \gamma\left(\underline{t} \cdot \nabla \underline{q}_m\right) \cdot \underline{t} = 0, \qquad (4.15)$$

or

$$\boxed{\frac{\partial\gamma}{\partial t} + \underline{q}_m \cdot \nabla\gamma + \gamma\underline{t} \cdot \frac{\partial \underline{q}_m}{\partial \ell} = 0,} \qquad (4.16)$$

where $\dfrac{\partial}{\partial \ell}$ denotes the differential in the tangential direction ($\underline{t}$) along the sheet. The last term represents the effect of the local stretching of the sheet on the variation of the vortex strength with time.

4.3.3 Doublet distribution (potential jump) on wake sheet

A second alternate wake sheet singularity is that of doublets with strength corresponding to the jump in disturbance potential ($\triangle\phi_v$). This distribution is also governed by the kinematic and dynamic conditions ((4.9) and (4.10)). The subscript v will be used to refer to values at the wake sheet.

If the pressure relation given by (4.74) is applied to the upper and the lower sides of the sheet, respectively, the following two equations are obtained:

$$\frac{p^+}{\rho} + \frac{\partial\phi^+}{\partial t} - \frac{1}{2}\underline{q}_F^2 + \frac{1}{2}\underline{q}^{+^2} + \underline{q}_o \cdot \underline{q}_F = C(t), \qquad (4.17)$$

$$\frac{p^-}{\rho} + \frac{\partial\phi^-}{\partial t} - \frac{1}{2}\underline{q}_F^2 + \frac{1}{2}\underline{q}^{-^2} + \underline{q}_o \cdot \underline{q}_F = C(t). \qquad (4.18)$$

Subtracting (4.18) from (4.17), and knowing that the other terms without a superscript have the same value on the both sides of the sheet under the assumption of zero thickness of the sheet, we have

$$\left(\frac{D(\triangle\phi_v)}{Dt}\right)_m = \left(\frac{D(\phi^+ - \phi^-)}{Dt}\right)_m = \boxed{\frac{\partial(\phi^+ - \phi^-)}{\partial t} + \underline{q}_m \cdot \nabla(\phi^+ - \phi^-) = 0.}$$
$$(4.19)$$

Here the kinematic and dynamic conditions have been used. Equation (4.19) implies that the fixed value of the jump in disturbance potential across the wake vortex sheet is convected with the mean velocity on the sheet. This statement is equivalent to Kelvin's circulation theorem describing the constancy of circulation round any closed material curve. The disturbance potential jump across the sheet corresponding to a doublet distribution with strength $\mu(\underline{x}_v, t)(= \triangle\phi_v = \phi^+ - \phi^-)$ can be replaced by an equivalent vorticity distribution.

4.3.4 Shedding vortex at trailing edge

When including the influence of the wake sheet in the derivation of an analytic solution, the use of (4.19) for the doublet distribution might be easier in manipulation than that of (4.16) for the vorticity distribution on the sheet. The

reason is that we need an extra consideration of the sheet geometry caused by the third term of (4.16) representing the local stretching of the vortex sheet. Another advantage of the numerical implementation of (4.19) is that the value of the potential jump at the T. E. determined by the Kutta condition at each time step can be directly assigned to a fixed value on the wake sheet that just left the T. E.

Meanwhile the position vector $\underline{x}_v(t)$ of a point of fixed $\triangle \phi_v$ value on the shed-vortex sheet that left the T. E. at time t_o $(t_o > 0)$ is given by the non-linear relation:

$$\underline{x}_v(t) = \int_{t_o}^{t} \underline{q}_m(\underline{x}_v(\tau))\, d\tau + \underline{x}_{TE} \,. \tag{4.20}$$

To calculate the mean velocity $(\underline{q}_m)$ in (4.19), the position of the wake sheet must be prescribed by using the integral form given by (4.20). There appears to be a non-linear coupled effect between the mean velocity and the position of the wake sheet.

One of the important features related to the wake sheet in unsteady flow about the foil is a time-varying bound circulation. Applying (4.19) as a point on the wake sheet approaches the T. E. becomes

$$\frac{d\Gamma_B}{dt} = -\underline{q}_m \cdot \underline{t} \bigg|_{TE} \gamma_{TE}, \tag{4.21}$$

where we define the (disturbance) bound circulation by $\Gamma_B = -(\phi^+ - \phi^-)\big|_{TE}$ (with positive taken as counterclockwise) and the shed vorticity at the T. E. by $\gamma_{TE}\,\underline{t} = -\nabla(\phi^+ - \phi^-)_{TE}$. Equation (4.21) is closely related to the unsteady Kutta condition as described in the next section.

4.4   Kutta Condition

4.4.1   Steady Kutta condition

The Kutta condition has been applied originally in the steady two-dimensional flow case for uniqueness of solution mathematically and for regular flow in the

vicinity of the T. E. physically. It eventually implies that the rear stagnation point is at the T. E. for a non-cusped sharp-edged foil in order to satisfy both the pressure-equality condition and the condition of finite velocity at the T. E.
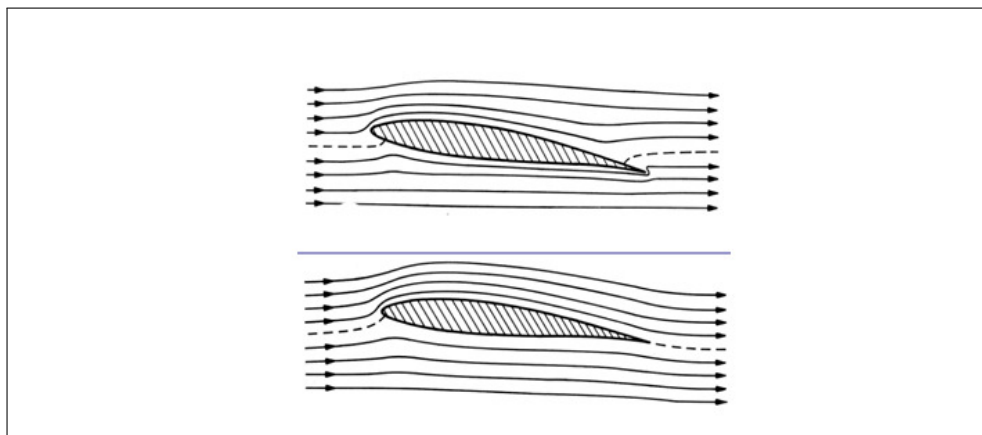
Figure **4.2** Flow past a foil without circulation, and with a properly selected circulation so that a stagnation point is at T.E. From Newman (1977).

There are two commonly used types of the steady (and possibly unsteady) Kutta condition in a panel method. One type, say 'wake-tangency type', consists of selecting a point at a short distance out in the fluid along the wake sheet element attached to the T. E. with a given inclination angle and requiring the flow at that point to be tangent to that element.

The other type, say 'pressure-equality type', consists of requiring equal values of velocity at the control points on the two panel elements adjacent to the T. E. In some cases, significant variations in the overall circulation and local flow properties may result from different choices for the type and/or the location of the application point of the numerical Kutta condition.

4.4.2   Unsteady Kutta condition

But if we applied this interpretation in unsteady flow (in which we have a shed vortex sheet trailing downstream and a time derivative term in the pressure relation), an unacceptable situation will occur; either infinite vortex strength ($\gamma_{TE} = \infty$) or $d\Gamma_B/dt = 0$ at the T. E. as is easily seen in (4.21), whereas shed vorticity (γ_{TE}) as well as the mean velocity ($\underline{q}_m$) at the T. E. should remain finite.

Unlike the steady two-dimensional flow cases, the two conditions of pressure equality and finite velocity can not be applied exactly at the T. E., unless one of the two conditions is sacrificed to save the other one. The reason is that there is inherently a velocity difference (shed-vortex strength) across the sharp T. E.

Following the concepts based on the pressure-equality condition and the finiteness of velocity, Mangler & Smith [3] have investigated the trailing-edge flow for steady three-dimensional lifting problems. The essential result is that the flow leaves the T. E. parallel to either the upper or lower surface depending on the sign of the vorticity in the sheet as it leaves the T. E. The possible orientation of the sheet is limited to be between the tangents of the foil surface at the T. E., otherwise an infinite velocity will occur. As an extension of Mangler and Smith's approach to the unsteady two-dimensional flow case, the so-called 'Maskell' trailing-edge flow is discussed by Basu & Hancock and Morino et al. [4]

There is no rigorous model of the unsteady Kutta condition for general unsteady motions unless the viscous effect is fully investigated. However it is considered acceptable to employ a numerical scheme by which a resulting solution should satisfy nearly the condition of finite velocities and the condition of zero loading in the neighborhood of the T. E. or at the T. E. The unsteady Kutta condition adopted possibly in the numerical method is

(1) to introduce the wake sheet as a 'barrier' for the existence of a single-valued potential function in the fluid region about the foil,

(2) to assume a parabolic form for potential values (ϕ) along the upper and lower foil surfaces so that the potential jump can be extrapolated to the T. E. as points on the foil surface approach the T. E. (the stagnation point can be located at either the upper or the lower trailing edge, depending on the sign of $d\Gamma_B/dt$), and

[3]Mangler, K. W. and Smith, J. H. B. (1970), "Behaviour of the Vortex Sheet at the Trailing Edge of a Lifting Wing," *Aeronautical Journal of the Royal Aeronautical Society*, vol. 74, pp. 906–908.

[4]Basu, B. C. and Hancock, G. J. (1978), "The Unsteady Motion of a Two-Dimensional Aerofoil in Incompressible Inviscid Flow," *Journal of Fluid Mechanics*, vol. 87, pp. 159–178.

Morino, L., Kaprielian, Z. and Sipcic, S. R. (1985), "Free Wake Analysis of Helicopter Rotors," *Vertica*, vol. 9, no. 2, pp. 127–140.

(3) to select a point at a short-distance off the T. E. along a straight-line wake sheet element attached to the T. E. and require the flow at that point to be tangent to the sheet. This model requires an iteration procedure to determine the potential jump and the orientation of the straight-line wake sheet element at the T. E. The iteration process for the orientation of the straight-line element is similar to that of Basu & Hancock. [5] The difference in calculated global forces between the scheme using the 'Maskell' local behavior and the present scheme using the Basu & Hancock procedure for the orientation of the straight-line element is small to negligible (although not illustrated herein) except that if the former is used, the results against time is not smooth at a few time steps near instants at which the sign of the rate of the bound circulation changes. The numerical implementation of the Kutta condition will be described in Appendix A.

4.5 Analytic Solution for Elliptic Section in Steady Uniformly Sheared Flows

4.5.1 Conformal mapping

It is desirable to obtain some exact solutions for steady uniform shear-flow about specific profiles in order to confirm the validity of numerical methods used in the present work. [6] For uniformly sheared onset flow with an inviscid incompressible fluid in 2-D, the disturbance potential exists and its governing equation is the Laplace equation.

A typical solution method is the extension of the classical conformal mapping technique where the foil in the physical plane is mapped into a circle in the complex plane. The known flow about the circle is then transformed to that about the physical shape. Among many available conformal transformations,

---

[5]Basu, B. C. and Hancock, G. J. (1978), "The Unsteady Motion of a Two-Dimensional Aerofoil in Incompressible Inviscid Flow," *Journal of Fluid Mechanics*, vol. 87, pp. 159–178.

[6]The details are refered to Suh (1990).
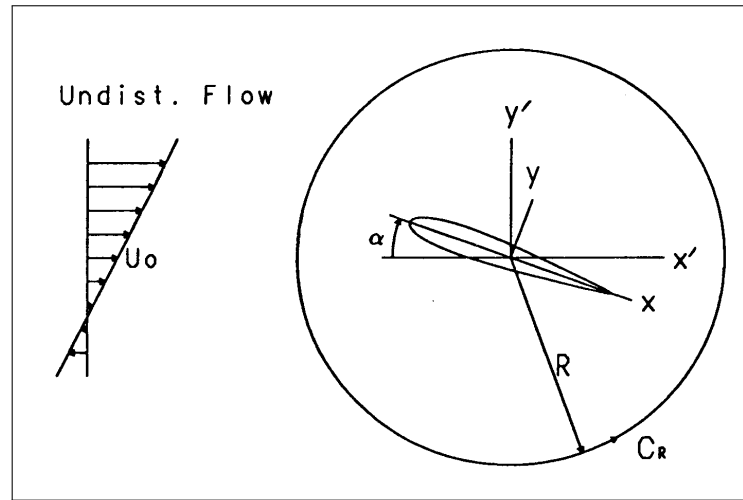
Figure **4.3** Foil configuration for steady uniformly sheared onset flow. U_o is a reference velocity of undisturbed flow at $y' = 0$ parallel to x'-axis. C_R is a control surface of a circle with a radius R.

the Moriya conformal mapping function suggested by Moriya [7] might be used for the purpose of validating the numerical methods developed against analytical results.

The conformal transformation is specified generally as

$$z = x + i\,y = C_{-1}\frac{\zeta}{a} + C_o + \sum_{n=1}^{\infty} C_n \frac{a^n}{\zeta^n}, \tag{4.22}$$

where $z = x + i\,y$ is the complex coordinate of a point in the physical plane (z-plane), $\zeta = \xi + i\,\eta$ is the complex coordinate in the circle plane (ζ-plane), a is a characteristic length dimension (taken as the radius of a circle that is set to 1 for non-dimensionalization), and $C_n = A_n + i\,B_n$ are complex mapping constants. Specially for an ellipse with thickness-chordlength ratio τ, all C_n's are zero except $A_{-1} = (1 + \tau)/4$, $A_1 = (1 - \tau)/4$.

Then the x-coordinates of the surface points can be expressed as $x_s(\theta) = \dfrac{c}{2}\cos\theta$ where θ is polar coordinates in the circle plane where c is chordlength. The y-

---

[7]Moriya, T. (1941), "On the Aerodynamic Theory of an Arbitrary Wing Section," *Journal of the Society of Aeronautical Sciences*, vol. 8, no. 78, pp. 1054–1060, English version: *Selected Scientific and Technical Papers*, University of Tokyo, 1959, pp. 48–59.

coordinates of the points on the upper surface are defined as:

$$y_s(\theta) = \frac{c}{2} \tau \sin \theta \tag{4.23}$$

4.5.2 Mapping coefficients

Now, we assume the complex disturbance potential $F_1(\zeta)$ as, satisfying the Laplace equation and the far-field behavior:

$$F_1(\zeta) = \phi_1 + i\,\psi_1 = -i\,\frac{\Gamma_B}{2\pi}\,\ln\zeta + c_1\,\frac{1}{\zeta} + c_2\,\frac{1}{\zeta^2} + \cdots, \tag{4.24}$$

where ϕ_1 is the disturbance potential and ψ_1 is the disturbance stream function. Here the disturbance bound circulation Γ_B (with positive as counterclockwise) and the complex coefficients $c_n\,(= \alpha_n + i\,\beta_n)$ are to be determined by using the kinematic body boundary condition and the Kutta condition at the T. E.

The kinematic boundary condition on the circle in the ζ-plane becomes

$$\frac{1}{r}\frac{\partial \psi_1}{\partial \theta}\bigg|_{r=1} = -\left(\underline{q}_\infty \cdot \underline{n}\,\left|\frac{dz}{d\zeta}\right|\right)\bigg|_{\zeta=e^{i\theta}}, \tag{4.25}$$

where the undisturbed (sheared onset) velocity $\underline{q}_\infty$ in the z-plane is given by:

$$\underline{q}_\infty = U_o\left\{1 + \frac{K}{c}(y\,\cos\alpha - x\,\sin\alpha)\right\}\underline{i}' \tag{4.26}$$

where K is the gradient of shear inflow velocity. From (4.25), the coefficients α_n and β_n (non-dimensionalized by the chordlength c, the radius of the circle a and the reference speed U_o) are determined (calculation is lengthy but straightforward):

$$
\begin{aligned}
\alpha_1 &= (A_{-1} - A_1)\cos\alpha, \\
\beta_1 &= (A_{-1} + A_1)\sin\alpha, \\
\alpha_2 &= -A_2\cos\alpha - \frac{K}{4}\left(A_{-1}^2 - A_1^2\right)\sin 2\alpha, \\
\beta_2 &= A_2\sin\alpha + \frac{K}{4}\left[(A_{-1} - A_1)^2\cos^2\alpha - (A_{-1} + A_1)^2\sin^2\alpha\right] \tag{4.27}
\end{aligned}
$$

where the coefficients with n greater than 2 in Eq. (4.24) are zero.

Now, to find Γ_B, a stagnation point should be imposed at the T. E. (as the Kutta condition):

$$\left(-\frac{\partial \psi_1}{\partial r} + \underline{q}_o \cdot \underline{t} \left| \frac{dz}{d\zeta} \right| \right) \Bigg|_{\substack{r=1 \\ \theta=0}} = 0. \tag{4.28}$$

Inserting (4.27) for the coefficients α_n and β_n into (4.28) and arranging for Γ_B, we find

$$\frac{\Gamma_B}{2\pi U_o\, c} = - \left[\sum_{n=1}^{2} n\, \beta_n + (A_{-1} - A_1) \left(1 - \frac{K}{2} \sin \alpha \right) \sin \alpha \right]. \tag{4.29}$$

The total surface q_s in the direction of increasing θ is

$$\frac{q_s(\theta)}{U_o} = \left[\{1 + K\, (y\, \cos \alpha - x\, \sin \alpha)\} \left(\frac{dx}{d\theta} \cos \alpha + \frac{dy}{d\theta} \sin \alpha \right) \right.$$
$$\left. + \left\{ \frac{\Gamma_B}{2\pi} + \sum_{n=1}^{2} n(-\alpha_n \sin n\theta + \beta_n \cos n\theta) \right\} \right] \Bigg/ \sqrt{\left(\frac{dx}{d\theta} \right)^2 + \left(\frac{dy}{d\theta} \right)^2} \Bigg|_{r=1} \tag{4.30}$$

Here $\dfrac{dx}{d\theta}\Big|_{r=1}$ and $\dfrac{dy}{d\theta}\Big|_{r=1}$ are the x- and y-component of the surface tangential vector in the direction of increasing θ, respectively:

$$\frac{dx}{d\theta}\Big|_{r=1} = -\, (A_{-1} + A_1)\, \sin \theta, \quad \frac{dy}{d\theta}\Big|_{r=1} = (A_{-1} - A_1)\, \cos \theta. \tag{4.31}$$

4.5.3   Pressure, lift and moment

A Bernoulli equation for two-dimensional steady flow with constant vorticity is given by, [8]

$$\frac{p}{\rho} + \frac{q^2}{2} + \omega_o\, \psi = \text{constant}. \tag{4.32}$$

---

[8]See Yih, C.-S. (1977), *Fluid Mechanics*, McGraw-Hill, p. 70.

where ψ denotes stream function value that depends on streamlines concerned. Then the pressure coefficient along the profile is,

$$C_p \left(\equiv \frac{p - p_\infty}{\frac{1}{2} \rho U_o^2} \right) = (1 + 2KC_\psi) - \frac{q_s^2}{U_o^2}, \tag{4.33}$$

or within an additive constant,

$$C_p = 1 - \frac{q_s^2}{U_o^2}. \tag{4.34}$$

The force components F_x and F_y (in the x- and y- direction of the coordinate system fixed on the foil) and the moment acting on the foil (about the origin) are expressed as an integral of the pressure and velocity distribution on the enclosing circle from the conservation theorem for momentum and angular momentum: [9]

$$
\begin{aligned}
F_x &= -\int_{C_R} p \, dy - \int_{C_R} \rho \, q_x \, (q_x \, dy - q_y \, dx), \\
F_y &= \int_{C_R} p \, dx - \int_{C_R} \rho \, q_y \, (q_x \, dy - q_y \, dx), \\
M_o &= \int_{C_R} p \, (x \, dx + y \, dy) - \int_{C_R} \rho \, (x \, q_y - y \, q_x) \, (q_x \, dy - q_y \, dx),
\end{aligned}
\tag{4.35}
$$

where q_x and q_y are, respectively, the x- and y- component of the total velocity on the contour C_R with a sufficiently large radius (R) in the physical plane. (See Figure **4.3**).

First the inversion of the mapping function is given by

$$\zeta = \frac{z}{A_{-1}} - \frac{A_o}{A_{-1}} - \frac{A_1}{z} - \frac{A_o A_1 + A_2^2}{z^2} + \cdots . \tag{4.36}$$

Then (4.24) for the complex (disturbed) velocity potential is inverted as a power

---

[9]See, for details, Tsien, H.-S. (1943), "Symmetrical Joukowsky airfoils in shear flow," *Quarterly of Applied Mathematics*, vol. 1, pp. 130–148.

series of z:

$$
F_1(z) = -i \frac{\Gamma_B}{2\pi} \ln \frac{z}{A_{-1}} + \left\{ i \frac{\Gamma_B}{2\pi} A_o + (\alpha_1 + i\beta_1) A_{-1} \right\} \frac{1}{z}
$$
$$
+ \left\{ i \frac{\Gamma_B}{2\pi} \left(A_{-1} A_1 + \frac{1}{2} A_o^2 \right) + A_{-1} A_o (\alpha_1 + i\beta_1) + A_{-1}^2 (\alpha_2 + i\beta_2) \right\} \frac{1}{z^2}
$$
$$
+ \cdots . \tag{4.37}
$$

Then, the disturbance velocity $\underline{u}$ can be expressed as

$$
u_x - i\, u_y = \frac{dF_1}{d\zeta} \frac{d\zeta}{dz} \bigg|_{\zeta = re^{i\theta}} \tag{4.38}
$$

Now using (4.36) and (4.37) together with (4.27), (4.32) and (4.38) for the velocity components and the pressure, we find the lift and the moment coefficients (about the mid-chord point):

$$
C_L = 4\pi(a_o - K\, b_1), \tag{4.39}
$$
$$
C_{M_o} = -4\pi(a_1 + K\, b_2), \tag{4.40}
$$

where

$$
a_o = -\frac{\Gamma_B}{2\pi}, \tag{4.41}
$$
$$
a_1 = A_{-1}\, \beta_1 \cos\alpha - A_{-1}\, \alpha_1 \sin\alpha, \tag{4.42}
$$
$$
b_1 = -A_{-1}\, \beta_1 \sin\alpha - A_{-1}\, \alpha_1 \cos\alpha, \tag{4.43}
$$
$$
b_2 = -A_{-1}^2\, \alpha_2 \cos 2\alpha - \left(A_{-1} A_1 \frac{\Gamma_B}{2\pi} + A_{-1}^2\, \beta_2 \right) \sin 2\alpha. \tag{4.44}
$$

Here it is noted that Γ_B, A_n, α_n and β_n have been non-dimensionalized by U_o, c and a.

4.5.4 Summarized results

For an ellipse with the thickness ratio τ, the quantities q_s, C_p, C_L and C_{M_o} can be expressed simply in terms of K, α, τ as:

$$\frac{q_s}{U_o} = \frac{(e_o + e_1 \sin\theta + e_2 \cos\theta + e_3 \sin 2\theta + e_4 \cos 2\theta)}{\sqrt{\sin^2\theta + \tau^2 \cos^2\theta}}, \quad (4.45)$$

$$C_p = \left\{ 1 + \frac{K^2}{8} \left(\tau^2 \cos^2\alpha + \sin^2\alpha \right) \right\} - \frac{q_s^2}{U_o^2}, \quad (4.46)$$

$$C_L = \pi \left\{ 2(1+\tau) \sin\alpha + K\tau \left(\tau \cos^2\alpha - \sin^2\alpha + \frac{1}{2} \right) \right\}, \quad (4.47)$$

$$C_{M_o} = \frac{\pi}{64} (1 - \tau^2) \sin 2\alpha \left\{ 16 + 8K(1+\tau) \sin\alpha \right.$$
$$\left. + K^2(1 + 3\tau) \left(\tau \cos^2\alpha - \sin^2\alpha \right) \right\}, \quad (4.48)$$

where

$$e_o = -(1+\tau) \left\{ \sin\alpha + \frac{K}{4} \left(\tau \cos^2\alpha - \sin^2\alpha \right) \right\}, \quad (4.49)$$

$$e_1 = -(1+\tau) \cos\alpha, \quad (4.50)$$

$$e_2 = (1+\tau) \sin\alpha, \quad (4.51)$$

$$e_3 = \frac{K}{4}(1+\tau)^2 \cos\alpha \sin\alpha, \quad (4.52)$$

$$e_4 = \frac{K}{4}(1+\tau) \left(\tau \cos^2\alpha - \sin^2\alpha \right). \quad (4.53)$$

For uniform onset flows, we can simply set $K = 0$ in the above results to have the solution. The exact value of the surface speed is given, for a general angle of attack α, by

$$\frac{q_s}{U} = (1+\tau) \left[\frac{\sin\theta \cos\alpha + (1 - \cos\theta) \sin\alpha}{\sqrt{\sin^2\theta + \tau^2 \cos^2\theta}} \right] \quad (4.54)$$

The lift coefficient is $\boxed{C_L = 2\pi(1+\tau) \sin\alpha}$.

4.6   Unsteady Lifting Flows for Two-Dimensional Hydrofoils

4.6.1   Equations of motion in a moving frame

Let $\underline{q}(x, y, z, t)$ describe the flow field in a moving coordinate system that is in motion relative to a space fixed system x', y', z'. In general, the relations between coordinates, velocities, and accelerations are those of Eqs. (1.208–1.211);

$$\underline{x}' = \underline{x} + \underline{R} \tag{4.55}$$

$$\underline{q}' = \underline{q} + \underline{\dot{R}} + \underline{\Omega} \times \underline{x} \tag{4.56}$$

$$\frac{d'\underline{q}}{dt} = \frac{d\underline{q}}{dt} + 2\,\underline{\Omega} \times \underline{q} + \underline{\dot{\Omega}} \times \underline{x} + \underline{\Omega} \times (\underline{\Omega} \times \underline{x}) + \underline{\ddot{R}} \tag{4.57}$$

Thus the left-hand side of Eq. (4.57) must be augmented by addition of four new terms, in general, in order to constitute a differential equation for $\underline{q}(x, y, z, t)$.

On the other hand, space derivatives such as grad, div, and curl are unaffected in form by the transformation of axes. The only change in such terms therefore arise from the process of carrying out these operations on quantities, such as $\underline{q}$, which have additional terms. There are no such terms in the scalar quantity p; hence Eq. (4.57) are altered only by addition of the four new left-hand terms mentioned.

Before writing down the new equation of motion, let us consider the equation of continuity. Consider the term $\nabla \cdot '\underline{q}$, and let $\nabla \cdot$ denote the divergence operator in the moving system:

$$\nabla' \cdot \underline{q}' = \nabla \cdot \underline{q}' = \nabla \cdot \left(\underline{q} + \underline{\dot{R}} + \underline{\Omega} \times \underline{x} \right) = \nabla \cdot \underline{q} \tag{4.58}$$

because the divergences of the last two terms are zero (see Eq. (1.67)). The physical meaning of this result should be clear to the reader.

Thus the equations for the general case of fluid motion described in a moving coordinate system are

$$\frac{D\rho}{Dt} + \rho\,\nabla \cdot \underline{q} = 0 \tag{4.59}$$

and

$$\frac{Dq}{Dt} + 2\,\underline{\Omega} \times \underline{q} + \dot{\underline{\Omega}} \times \underline{x} + \underline{\Omega} \times (\underline{\Omega} \times \underline{x}) + \ddot{\underline{R}} = -\frac{1}{\rho}\,\nabla p + \underline{F}_B + \nu\,\nabla^2 \underline{q} \quad (4.60)$$

4.6.2 Representation of unsteady motion of a hydrofoil

A two-dimensional foil of finite thickness and/or camber with a fixed mean angle of attack in uniform onset flow of an incompressible inviscid fluid is assumed to undergo combined unsteady periodic motions (and/or sudden start-up motion).

Since the first effort is concerned with the disturbance velocity field, this section now gives the formulation of the boundary value problem for the unknown disturbance velocity potential.

In most unsteady problems it is convenient to adopt a moving reference frame fixed relative to the body and then to define the flow field relative to the moving body, for which the geometric definition of a rigid body is time-independent.

Figure **4.4** represents a relative configuration of a body in the inertial and moving frames with appropriate notations to be used for the formulation of the boundary value problem. Note that the prime notation $(\prime)$ refers to the quantities expressed in the inertial frame. Here the origin (O) of the moving frame is located at the mid-chord point of the foil and the x-axis is taken as an extension of the chordline.

The vectors $\underline{\rho}_F(t)$ and $\underline{x}_p(= x_p\,\underline{i} + y_p\,\underline{j})$ are the position vector of a reference point (herein taken as the pivot point of a pitching motion) measured in the inertial and the moving frame, respectively.

The vector $\underline{\Omega}(t)$ $(= \Omega(t)\,\underline{k}$ for two-dimensional motion, with positive taken as counterclockwise) is the angular velocity of the moving frame about the reference point. Then $\underline{q}_F(= \dot{\underline{\rho}}_F(t) + \underline{\Omega}(t) \times (\underline{x} - \underline{x}_p))$ represents the velocity (observed in the inertial frame) at a field point $(\underline{x}_p)$ in the moving frame due to its translational and angular motions relative to the inertial frame. We shall call $\underline{q}_F$
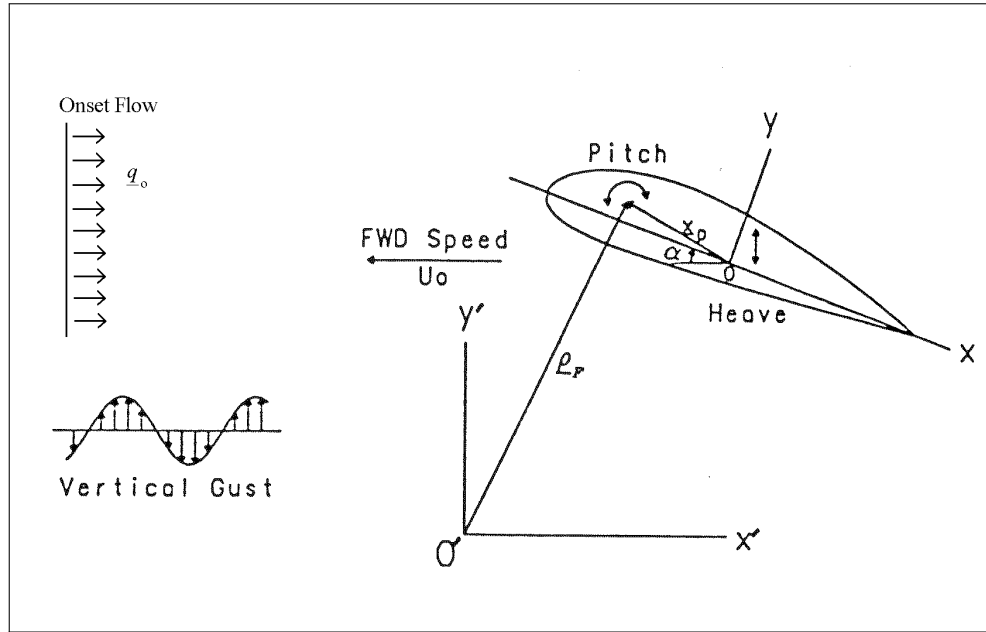
Figure 4.4 The coordinate systems and a combined unsteady flow situation.

frame velocity. Here the overdot $(\cdot)$ in $\dot{\underline{\rho}}_F$ denotes the time derivative. $\alpha(t)$ is the angle of attack at an instant of time related to the pitching motion which can be expressed as

$$\alpha(t) = \alpha_m - \tan^{-1} \frac{r_{LE}\,\sin(\theta_{LE} - \alpha_p) - r_{TE}\,\sin(\theta_{TE} - \alpha_p)}{r_{LE}\,\cos(\theta_{LE} - \alpha_p) - r_{TE}\,\cos(\theta_{TE} - \alpha_p)}. \qquad (4.61)$$

Here r_{LE} and r_{TE} are the distance from the pivot point of the pitching motion (i.e. $\underline{x}_p$) to the leading edge and the trailing edge respectively (hereafter L. E. and T. E. stand for the leading and the trailing edge, respectively). θ_{LE} and θ_{TE} are the angle between the line joining the pivot point to the corresponding edge respectively and the positive Ox-axis, α_m is the angle of attack at the mean position of the foil (fixed in time), and $\alpha_p(t)$ is the instantaneous pitch angle specified by the pitching motion about the pivot point $\underline{x}_p$ (herein $\dot{\alpha}_p(t) = -\Omega(t)$).

Then the coordinates and unit vectors between the two frames can be recovered from the relations:

$$\underline{x}' = \underline{\rho}_F(t) + (\underline{x} - \underline{x}_p), \ \ \underline{i}' = \underline{i}\,\cos\alpha(t) + \underline{j}\,\sin\alpha(t), \ \ \underline{j}' = \underline{j}\,\cos\alpha(t) - \underline{i}\,\sin\alpha(t).$$
$$(4.62)$$

4.6.3 Representation of velocity field in a moving frame

It is important to note that the vorticity is not the same in the two systems. Using the primes as before, we see that, according to Eq. (1.68),

$$\nabla' \times \underline{q}' = \nabla \times \underline{q}' = \nabla \times \left(\underline{q} + \underline{\dot{R}} + \underline{\Omega} \times \underline{x} \right) = \nabla \times \underline{q} + 2\underline{\Omega} \qquad (4.63)$$

We find the physical meaning of this result. An important case is one of flow that is irrotational but is viewed in a rotating coordinate system; it appears to be rotational. The case of a rotating propeller frame is typical.

The total velocity, observed in the inertial frame fixed in space is made up of two parts:

$$\underline{q}'_T(\underline{x}', t) = \underline{q}'_o(\underline{x}') + \underline{u}'(\underline{x}', t), \qquad (4.64)$$

where $\underline{q}'_o(\underline{x}')$ is an onset velocity field that satisfies the continuity equation itself (a steady potential flow when measured in the inertial frame) and $\underline{u}'(\underline{x}', t)$ is the disturbance velocity component to be determined herein.

In the moving frame the total velocity is the sum of the frame velocity ($\underline{q}_F$) and the fluid velocity ($\underline{q}$) measured by an observer in the moving frame:

$$\underline{q}_T(\underline{x}, t) = \underline{q}_F(\underline{x}, t) + \underline{q}(\underline{x}, t), \qquad (4.65)$$

where $\underline{x}$ and $\underline{q}$ are measured relative to the moving frame.

Equating the two different expressions of Eqs. (4.64) and (4.65), the relative velocity ($\underline{q}$) is expressed by

$$\boxed{\underline{q}(\underline{x}, t) = \underline{q}_o(\underline{x}, t) - \underline{q}_F(\underline{x}, t) + \underline{u}(\underline{x}, t)} \qquad (4.66)$$

4.6.4 Formulation of boundary value problems for the disturbance potential.

According to the representation of the foil motion and the velocity field as outlined in the previous subsection, the flow characteristics about a foil can be

determined by solving the boundary value problem for the disturbance velocity ($\underline{u}$) relative to the known undisturbed velocity field ($\underline{q}_o$-$\underline{q}_F$).

Now, let the foil be assumed to undergo unsteady (not necessarily sinusoidal) rigid motions in a uniform, unbounded onset flow field of an inviscid incompressible fluid, with any static effects due to the gravity ignored.

Then the continuity equation applied to the total velocity ($\underline{q}'_T$) in the inertial reference frame becomes (since the differential operators with respect to space coordinates have the same value)

$$\nabla' \cdot \underline{q}'_T = \nabla \cdot (\underline{q}_F + \underline{q}) = 0. \tag{4.67}$$

Since $\nabla \cdot \underline{q}_F = \nabla \cdot (\underline{\dot{\rho}}_F + \underline{\Omega} \times (\underline{x} - \underline{x}_p)) = 0$ and $\nabla \cdot \underline{q}_o = 0$, the continuity equation applied to the relative velocity ($\underline{q}$) in the moving frame is expressed by

$$\nabla \cdot \underline{q} = \nabla \cdot (\underline{u} - \underline{q}_F + \underline{q}_o) = 0. \tag{4.68}$$

Thus the continuity equation in the moving frame for the disturbance velocity reduces to $\nabla \cdot \underline{u} = 0$, which implies that working in a moving frame does not affect the expression of the continuity equation.

For uniqueness, there remain conditions to be imposed on the boundary of the fluid region. The kinematic body boundary condition (tangency condition or no-penetration condition) on the rigid body surface (represented by $B(\underline{x})$) can be expressed in terms of the disturbance velocity ($\underline{u}$) observed in the moving frame:

$$\underline{u} \cdot \underline{n} \left(\equiv \frac{\partial \phi}{\partial n} \right) = -(\underline{q}_o - \underline{q}_F) \cdot \underline{n} \tag{4.69}$$

In the presence of an elastic deformation (which is not considered in the present work), the normal component of the local velocity of deformation is added on the right-hand side of the above equation.

In addition, the far-field condition (i.e., $\underline{u} \to 0$ far away from the body), the Kutta condition at the T. E., and the kinematic and the dynamic conditions on the shed-vortex sheet (represented by $W(\underline{x}, t)$) should be satisfied for the existence of a unique disturbance velocity ($\underline{u}$) or velocity potential (ϕ) for any

lifting problem.

The fluid potential (ϕ) is determined by solving the boundary value problem at discrete time steps in a step-by-step fashion, or at arbitrary time, either analytically or numerically. Once the potential is known, the disturbance velocity field is obtained by taking the gradient of the disturbance potential (ϕ). The velocity field is then obtained by adding the undisturbed velocity field and the disturbance velocity as in (4.66). Finally the surface pressure distributions, and the forces and the moments acting on the foil section can be computed, respectively, by using a Bernoulli-like equation (which is described in the following subsection) and integrating the pressure on the body surface.

4.6.5 Bernoulli-like equation in a moving frame

The Euler equation in an inertial reference frame may be put in the form, neglecting external body force potential terms:

$$\frac{\partial' \underline{q}_T}{\partial t} - \underline{q}_T \times (\nabla' \times \underline{q}_T) = -\nabla' \left(\frac{p}{\rho} + \frac{1}{2} \underline{q}_T^2 \right). \qquad (4.70)$$

Knowing that the gradient operators have the same form in either inertial or non-inertial reference frame, we reduce this equation to

$$\frac{\partial' (\underline{q}_o + \underline{u})}{\partial t} - (\underline{q} + \underline{q}_F) \times (\nabla \times (\underline{q}_o + \underline{u})) = -\nabla \left(\frac{p}{\rho} + \frac{1}{2} (\underline{q} + \underline{q}_F)^2 \right). \qquad (4.71)$$

Because the onset velocity distribution $\underline{q}_o$ is usually a function of only the space position in the inertial reference frame (i.e., $\partial \underline{q}_o'(\underline{x})/\partial t = 0$) and the disturbance velocity ($\underline{u}$) is irrotational (i.e. $\underline{u} = \nabla \phi$), Eq. (4.71) becomes

$$\nabla \left(\frac{\partial' \phi}{\partial t} \right) - (\underline{q} + \underline{q}_F) \times (\nabla \times \underline{q}_o) + \nabla \left(\frac{p}{\rho} + \frac{1}{2} (\underline{q} + \underline{q}_F)^2 \right) = 0. \qquad (4.72)$$

We can convert the operator $\left(\dfrac{\partial'}{\partial t}\right)$ in the inertial frame into $\left(\dfrac{\partial}{\partial t} - \underline{q}_F \cdot \nabla\right)$ in the moving frame. [10] This indicates that the rate of change of a quantity (say ϕ) at a point fixed in the space-fixed frame is measured by an observer in the moving frame. We can then write Eq. (4.72) as

$$\nabla \left(\frac{p}{\rho} + \frac{\partial \phi}{\partial t} + \frac{1}{2}\underline{q}^2 - \frac{1}{2}\underline{q}_F^2 + \underline{q}_o \cdot \underline{q}_F\right) - (\underline{q} + \underline{q}_F) \times (\nabla \times \underline{q}_o) = 0. \quad (4.73)$$

For irrotational onset flow, the pressure equation can be written as

$$\frac{p}{\rho} = -\frac{\partial \phi}{\partial t} + \frac{1}{2}\underline{q}_F^2 - \frac{1}{2}\underline{q}^2 - \underline{q}_o \cdot \underline{q}_F + C(t). \quad (4.74)$$

For the case of marine propellers, we may take $C(t) = \dfrac{p_\infty}{\rho} + \dfrac{1}{2}V_s^2$ and $\underline{q}_F = \underline{\Omega} \times \underline{x} = -2\pi\,n\,r\,\underline{e}_\theta$ for right-hand rotation, where V_s is ship speed and $\underline{e}_\theta$ is the unit vector of the propeller-rotation direction.

The resulting expression for the unsteady pressure coefficient (C_p) non-dimensionalized by a reference speed U_o (which is typically taken as an undisturbed main uniform velocity or the moving speed of a body) is

$$C_p \left(\equiv \frac{p - p_\infty}{\frac{1}{2}\,\rho\,U_o^2}\right) = \frac{\rho\,H_o - p_\infty}{\frac{1}{2}\,\rho\,U_o^2} - \frac{2}{U_o^2}\frac{\partial \phi}{\partial t} + \frac{\underline{q}_F^2}{U_o^2} - \frac{\underline{q}^2}{U_o^2} - \frac{2\,\underline{q}_o \cdot \underline{q}_F}{U_o^2}, \quad (4.75)$$

where H_o is a Bernoulli constant representing total energy-head at the reference point far away from the body, and p_∞ the reference pressure in the inertial frame far away from the body. To within an additive constant, it becomes

$$C_p = -\frac{2}{U_o^2}\frac{\partial \phi}{\partial t} + \frac{\underline{q}_F^2}{U_o^2} - \frac{\underline{q}^2}{U_o^2} - \frac{2\,\underline{q}_o \cdot \underline{q}_F}{U_o^2}. \quad (4.76)$$

---

[10]See Milne-Thomson, L. M. (1968), *Theoretical Hydrodynamics*, fifth ed., Macmillan, London, p. 89, and Kochin, N. E., Kibel, I. A. and Roze, N. V. (1964), *Theoretical Hydrodynamics*, Interscience Publishers Inc., p. 116.

4.6.6   Integral equation for disturbance potential

We will consider two-dimensional lifting flow field for a hydrofoil for our specific examples and general formulation. The problem of defining the velocity field has been reduced to solving the Laplace equation for the disturbance (perturbation) potential (ϕ);

$$\nabla^2 \phi = 0 \;\; \text{in the fluid region,} \tag{4.77}$$

being subject to the no-penetration condition on the body surface;

$$\underline{u} \cdot \underline{n} \left(\equiv \frac{\partial \phi}{\partial n} \right) = -\left(\underline{q}_o - \underline{q}_F \right) \cdot \underline{n} \;\; \text{on} \;\; B(\underline{x}) \tag{4.78}$$

the Kutta condition at the T. E. given by (A.10), the combined kinematic and dynamic conditions on the shed-vortex sheet;

$$\frac{\partial(\phi^+ - \phi^-)}{\partial t} + \underline{q}_m \cdot \nabla(\phi^+ - \phi^-) = 0 \;\; \text{on} \;\; W(\underline{x}) \tag{4.79}$$

and a far-field decay condition;

$$\phi \to \;\; \text{constant as} \;\; r \to \infty. \tag{4.80}$$

The disturbance velocity potential (ϕ) which satisfies the Laplace equation in the fluid region with a 'barrier' representing the wake sheet can be represented in the form of an integral equation based on Green's scalar (second) identity:

$$
\begin{aligned}
\phi(\underline{x}, t) \;=\;& \frac{1}{2\pi} \int_B \left(\frac{\partial \phi(\underline{y}, t)}{\partial n} \ln |\underline{x} - \underline{y}| + \phi(\underline{y}, t) \frac{n(\underline{y}) \cdot (\underline{x} - \underline{y})}{|\underline{x} - \underline{y}|^2} \right) d\ell_y \\
&+ \frac{1}{2\pi} \int_W \triangle \phi_{\mathrm{v}} \frac{n \cdot (\underline{x} - \underline{y})}{|\underline{x} - \underline{y}|^2} \, d\ell_y \, .
\end{aligned}
\tag{4.81}
$$

Here the range of integration of the position vector of the source point ($\underline{y}$) representing the dummy variable of the integrals is the body surface contour $B(\underline{x})$ and the wake sheet $W(\underline{x}_v, t)$. The contribution of the integration along the contour of infinite radius enclosing the body goes to a constant as the radius

of the circuit goes to infinity because the net flux of volume of fluid becomes zero for a closed rigid body. [11]

The unit normal vectors ($\underline{n}$) point outward from the body surface and upward at the wake sheet, and $\triangle\phi_{\mathrm{v}}$ is the jump in the disturbance potential ($\phi^+ - \phi^-$) across the wake sheet of zero thickness. The superscripts $+$ and $-$ indicate the limit on the upper and the lower side, respectively, of the sheet. This integral representation is more efficient in computation time than direct solution of the Euler equation (say, by a finite difference scheme) (since only the surface values of the physical quantities are concerned).

Evaluating the limit of the integral as a field point ($\underline{x}$) approaches a point on the body surface ($\underline{x}_o$) gives the integral equation for the unknown distribution of the disturbance potential (ϕ): [12]

$$
\begin{aligned}
\phi(\underline{x}_o, t) \;=\;& \frac{1}{2\pi} \oint_B \left(\frac{\partial\phi}{\partial n} \ln|\underline{x}_o - \underline{y}| + \phi \frac{n \cdot (\underline{x}_o - \underline{y})}{|\underline{x}_o - \underline{y}|^2} \right) d\ell_y \\
&+ \; \frac{1}{2}\,\phi(\underline{x}_o, t) + \frac{1}{2\pi} \int_W \triangle\phi_{\mathrm{v}} \frac{n \cdot (\underline{x}_o - \underline{y})}{|\underline{x}_o - \underline{y}|^2} \, d\ell_y \,,
\end{aligned}
\qquad (4.82)
$$

where the first integral denotes a Cauchy principal value integral. Also, inserting (4.78) for $\partial\phi/\partial n$ (equivalent source strength) into (4.82) gives a two-dimensional Fredholm integral equation of the second kind for the disturbance potential (ϕ):

$$
\frac{1}{2}\phi(\underline{x}_o, t) - \frac{1}{2\pi} \oint_B \phi \frac{n \cdot (\underline{x}_o - \underline{y})}{|\underline{x}_o - \underline{y}|^2} \, d\ell_y =
$$

$$
\frac{1}{2\pi} \oint_B \left(\underline{q}_F - \underline{q}_o \right) \cdot \underline{n} \ln|\underline{x}_o - \underline{y}| \, d\ell_y + \frac{1}{2\pi} \int_W \triangle\phi_{\mathrm{v}} \frac{n \cdot (\underline{x}_o - \underline{y})}{|\underline{x}_o - \underline{y}|^2} \, d\ell_y.
$$

$$
(4.83)
$$

If the shape of the wake sheet and the potential jump ($\triangle\phi_{\mathrm{v}}$) are specified

---

[11]It may be chosen arbitrarily without failure of uniqueness of the velocity field. In the present work this constant is taken to be zero as the far-field value along the circuit far away from the body. See also Batchelor, G. K. (1967), *An Introduction to Fluid Dynamics*, Cambridge University Press, Cambridge, p. 126.

[12]For the limiting forms for integral expressions of surface distribution of various singularities (source, vortex and doublet), see Brockett, T. E., Kim, M.-H. and Park, J.-H. (1989), "Limiting Forms for Surface Singularity Distributions When the Field Point is on the Surface," *Journal of Engineering Mathematics*, vol. 23, pp. 53–79.

from the Kutta condition at the T. E. (Eq. (A.10)) and the combined kinematic and dynamic conditions on the shed-vortex sheet ((4.79)), the surface potential distribution can be obtained by solving this integral equation. The velocity field is obtained by taking the gradient of the disturbance potential (ϕ) to find the disturbance velocity and then adding the undisturbed velocity ($\underline{q}(\underline{x}, t) = \underline{q}_o(\underline{x}, t) - \underline{q}_F(\underline{x}, t) + \nabla\phi(\underline{x}, t)$). Equation (4.83) is non-linear in the sense that the normal component of the undisturbed velocity on the actual body surface (($\underline{q}_o - \underline{q}_F) \cdot \underline{n}$)) is included (geometric non-linearity), and the jump in the disturbance potential on the shed-vortex sheet ($\triangle\phi_v$) and the sheet position ($\underline{x}_v(t)$) depend on the disturbance potential ($\phi(\underline{x}_o, t)$) distribution on the body surface (solution non-linearity and memory effect).

In practice the integral equation (4.83) can rarely be solved analytically, thus an appropriate numerical evaluation of the integral and an appropriate representation of the body surface and the wake sheet are required. One possible approach is that a panel-method approximation is used just as in the steady flow case and a suitable model is employed to represent the wake sheet. Then the boundary value problem is solved at discrete time steps with a small time increment during which the quantities of interest are assumed to be constant in time.

4.6.7   Vortex model of shed wake sheet: Typical example

To include the influence of the shed-vortex sheet, the singularity strengths and the sheet geometry should be known. Among various computational schemes, the series of vortices can be used to represent the sheet geometry and to evaluate the equivalent potential on the body surface induced by a doublet distribution (potential jump across the sheet) on the shed vortex sheet. Giesing (1968a) [13] presented comparisons of the calculated location of the vortex sheet with photographs by Bratt (1953). [14]

---

[13]Giesing, J. P. (1968a), "Nonlinear Two-Dimensional Unsteady Potential Flow with Lift," *Journal of Aircraft*, vol. 5, no 2, pp. 135–143.

[14]Bratt, J. B. (1953), "Flow Patterns in the Wake of an Oscillating Aerofoil," *Aeronautical Research Council, Reports and Memoranda*, no. 2773.

The comparisons show that this model for the shed-vortex sheet produces remarkably good predictions of sheet position. Thus it is reasonable to adopt a concentrated vortex model because our approach here is aimed at a satisfactory solution rather than a rigorous one. In order to include more precisely the wake influence in the near region of the T. E., a small straight-line element attached to the T. E. is introduced exceptionally, over which a potential jump (doublet strength) is linearly distributed.

The potential and the velocity induced by a linear variation of doublet distribution ($\mu^{(k)} = \mu_o^{(k)} + \delta_o^{(k)}\lambda$ where λ is the projected coordinate onto Ox-axis, the mid-point being an origin as depicted in Figure **4.5**) over the straight-line element are given by (with the same notation as in the previous sections),
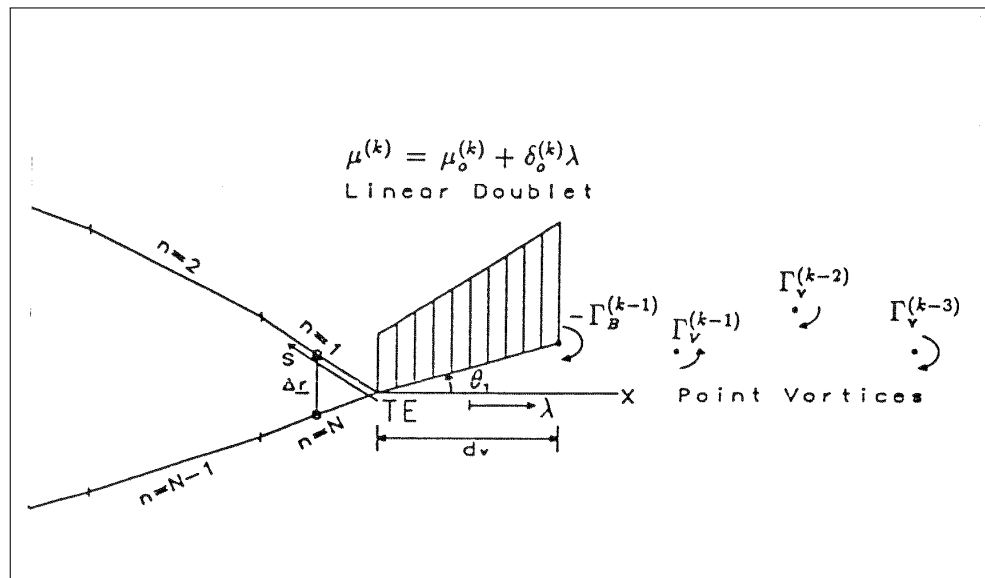
Figure **4.5** A doublet straight-line element attached to the trailing edge and a series of concentrated vortices. The superscripts denote the time steps, (k) referring to the present time step.

The orientation of the element leaving the foil at the time of solution is unknown. For fixed values of the element length ($\triangle v_1$) as an input parameter, the time increment ($\triangle t^{(k)}$) between $t^{(k)}$ and $t^{(k-1)}$ and the inclination of the element to Ox-axis ($\theta_1^{(k)}$) are to be determined as a part of the solution by an iteration procedure described in the next section. The vorticity on the straight-line wake

element attached to the T. E, (γ_{TE}) is given by

$$\gamma_{TE}^{(k)} = \frac{\Gamma_B^{(k-1)} - \Gamma_B^{(k)}}{\triangle v_1} \tag{4.84}$$

where $\triangle v_1 = \dfrac{d_v}{\cos \theta_1}$ as indicated in Figure **4.5** .

A downstream wake of concentrated vortices is formed from the vorticity shed at earlier times, which is assumed to be concentrated into discrete vortices whose strength is given by $\Gamma_v^{(k)} = \gamma_{TE}^{(k)} \triangle v_1$. These discrete vortices are convected with unchanged strengthes from the previous position according to the (total) resultant velocities calculated at the center of each vortex at each successive time interval. The time increment $\triangle t^{(k)}$ is calculated approximately by dividing by $\triangle v_1$ the local total velocity at the mid-point of the straight-line wake element attached to the T. E.

The orientation of the straight-line element is determined such that it is parallel to the local resultant velocity at the mid-point of that element. This model is shown pictorially in Figure **4.5** .

Now the last integral of (4.83) leads equivalently to the potential induced by the series of concentrated vortices, which is written down as the sum of the potential induced by each concentrated vortex. This equivalent replacement demands a determination of reference value of the angle involved in the vortex-potential.

The reference orientation of each vortex potential is taken as a line parallel to the Ox-axis. The difference of phase does not affect directly the velocity and the time derivative because all values of $\phi_j^{(k)}$ differs uniformly in the amount of the phase difference as an additive constant and the pure effect of the total vortex system becomes eventually the phase of the cut extending from the end of the wake sheet to far downstream which may initially be taken as zero. It is easily seen that the phase difference leads to the increment of constant values of ϕ over the closed body surface, from the identity

$$\frac{1}{2\pi} \int_B \frac{n(x_v) \cdot (x - x_v)}{|x - x_v|^2} \, dl_x = 0, \tag{4.85}$$

for a point $\underline{x}_v$ outside a closed body. It should be noticed that the contribution of the point vortex at the downstream end point of the doublet straight-line element (labelled '$-\Gamma_B^{(k-1)}$' in Figure **4.5**) should be included in the equivalent replacement of this concentrated vortex model.

As the number of point vortices shed increases with time steps, the computations for induction between them grow with the square of their number. To reduce the computation time, one can simply ignore the vortices beyond a given number or distance behind the T. E. (about 10 times of the chordlength), since their influence on the body decreases with distance. Another way is, although it is still an approximation, that the two of the oldest shedding vortices beyond a given number (say 250 herein) are amalgamated to reduce the number of point vortices (actually in a computer code it keeps the same number after this time step).

For this operation, two point vortices of strengths Γ_1 and Γ_2 at $\underline{x}_1$ and $\underline{x}_2$, respectively, are replaced by one point vortex of strength $\Gamma_1 + \Gamma_2$ at the position given by $(\underline{x}_1|\Gamma_1| + \underline{x}_2|\Gamma_2|)/(|\Gamma_1| + |\Gamma_2|)$. However in most calculations with moderately reasonable input parameters, it is better to avoid this amalgamation possibly because of lack of its physical equivalence.

4.6.8   Solution procedures

The numerical solution procedures are similar to that in the steady panel method approximation except that there is an another contribution due to a series of concentrated vortices (equivalent to the potential jump (doublet distribution) on the geometrically time-varying vortex sheet). The solution for the unsteady flow about a body is calculated starting at $t = 0$ and continuing the process at successive time steps.

The unsteadiness of the flow is assumed to start from the mean position for harmonic motions of a foil or with zero circulation for a sudden start-up problem.

At successive time steps a shed vortex is defined and is convected with the local mean velocity without change of its strength. Hence this will induce a

known potential back on the body and this effect must be included in the solution of the integral equation.

This approach is carried out as follows. At time $t^{(k)}$, the basic set of equations for $N + 1$ unknowns ($\phi_j^{(k)}, j = 1, \cdots, N$ and $\theta_1^{(k)}$) can be formulated. First the N algebraic equations associated with the integral equation (4.83) can be written down in a matrix form with unknowns ϕ_j :

$$[A_{mj}] \left\{ \phi_j^{(k)} \right\} = \left\{ B_m^{(k)} \right\} + \left[C_{ml}^{(k)} \right] \{(\Gamma_v)_l\} + \left\{ D_m^{(k)} \right\}, \qquad (4.86)$$
$$\text{for } m, j = 1, \cdots, N \ \& \ l = 1, \cdots, (k-1),$$

where $[A_{mj}]$ is the coefficient matrix of the set of linear equation which approximates the integral equation and each of which represents the induced potential at the m-th control point due to the unit density doublet distribution on the j-th panel, $\{B_m^{(k)}\}$, $[C_{ml}^{(k)}]$, $\{(\Gamma_v)_l\}$ and $\{D_m^{(k)}\}$ represent the effect due to the equivalent source distribution with strength $(\underline{q}_F - \underline{q}_o) \cdot \underline{n}$ on the body surface, the effect due to the series of concentrated vortices with strength Γ_v on the downstream wake and the effect due to the doublet distribution with a linear variation over the straight-line wake sheet element attached to the T. E. (with unknown $\theta_1^{(k)}$), respectively.

Another condition to determine $\theta_1^{(k)}$ is that the local resultant velocity at the mid-point of the straight-line wake sheet element attached to the T. E. is parallel to its orientation. This requires an iteration process together with an allowable tolerance, using the previously updated $\phi_j^{(k)}$ and $\triangle \phi_v|_{TE}$ to calculate the local resultant velocity.

The initially guessed values for starting this iterative process are taken as those obtained at the previous time step to reduce the iteration process time. Thus with these guessed values, the N linear equations are solved to obtain $\phi_j^{(k)}, (j = 1, \cdots, N)$.

Once the temporary values of $\phi_j^{(k)}$ are known during the iteration process, $\triangle \phi_v|_{TE}$ and the local resultant velocity can be calculated, from which the newly updated value $\theta_1^{(k)}$ is found. Such a procedure is repeated until $\theta_1^{(k)}$ and $\triangle \phi_v|_{TE}$ have converged within the desired allowance. This results in a relatively rapid

convergence, for example, requiring usually 2-5 iterations for convergence within 1 % change relative to the previously updated value for $\triangle\phi_{\mathrm{v}}|_{TE}$ and 0.1^o change for $\theta_1^{(k)}$.

Once the final values after the iteration procedure have been determined, the tangential component of the disturbance velocity at the body surface is computed (in the moving frame). The disturbance tangential speed can be obtained by numerical differentiation of the surface potential in the local tangential direction at the actual surface point at which the constant value of $\phi_j^{(k)}$ over the panel is assumed to be representative.

A piecewise constant representation of ϕ must be fitted with a polynomial form over several nearby panels before being differentiated. Here for improvement of the numerical accuracy (especially near the L. E.) in the calculation of the disturbance surface speed ($\nabla\phi \cdot \underline{t}$), the cubic spline (e.g., the B-spline or the tension cubic spline) [15] might be used for curve-fitting of the discrete values of the disturbance potential.

If the discrete values of $\phi_j^{(k)}$ versus the angular parameter φ (that is the transformed variable used for 'cosine-spacing' previously) instead of the coordinate x were fitted, the disturbance surface speed is obtained by the chain rule; $\dfrac{d\phi}{ds} = \dfrac{d\phi}{d\varphi} \cdot \dfrac{d\varphi}{ds}$. The reason for the choice of the parametric spline with φ is that we can avoid fitting the rapid change of ϕ near the L. E. and the T. E. from the use of the x-coordinate of the discrete points. Therefore the discrete values of ϕ are fitted smoothly with higher-order accuracy when using a uniform spacing (i.e., $\triangle\varphi = 2\pi/N$) over the interval of the parameter (2π).

Now the total tangential speeds are obtained by adding the tangential component of the undisturbed velocity ($\underline{q}_o - \underline{q}_F$). In the unsteady pressure relation (4.74), the time derivative term $\dfrac{\partial\phi}{\partial t}$ is approximated as

$$\frac{\partial\phi_j^{(k)}}{\partial t} = \frac{\phi_j^{(k)} - \phi_j^{(k-1)}}{t^{(k)} - t^{(k-1)}}. \tag{4.87}$$

---

[15]The tension cubic spline was suggested by McCartin, B. J. (1983), "Applications of Exponential Splines in Computational Fluid Dynamics," *AIAA Journal*, vol. 21, no. 8, pp. 1059-1065.
It is used to get rid of unwanted wiggles (extraneous inflection points), that might occur in some intervals when fitting the discrete values by the original cubic spline, by applying local tensions additionally to those intervals.

By direct integration of the pressure coefficient distribution, the force and moment coefficients are obtained. The integration is also performed after fitting the integrand of the integral expressions ((4.89) and (4.90)) for the forces and moment coefficients by integrating the fitting values by the spline. It is noted that the required slopes at the end points of the spline interval are estimated by parabolically fitting of three points—each end point and two neighboring points. Once the solution at time $t^{(k)}$ has been determined, the model is set up for time $t^{(k+1)}$ with the wake pattern as calculated from the solution at time $t^{(k)}$.

The distributed vorticity on the straight-line wake sheet element attached to the T. E. at time $t^{(k)}$ is now assumed to be concentrated into a vortex of strength $\gamma_{TE}^{(k)} \triangle \mathrm{v}_1$ at time $t^{(k+1)}$ situated at the next moving point convected with the local mean velocity at the mid-point of the wake element. The resultant velocity at the center of each of the other concentrated vortices in the wake is calculated from the solution at time $t^{(k)}$ and then the position of that vortex at time $t^{(k+1)}$ follows directly.

Especially for a 2-D foil, the force components in the x- and y-direction, of the moving frame and the moment about $\underline{x}_m$ (positive is taken as counterclockwise) acting on the foil are given by, respectively,

$$F_x\,\underline{i} + F_y\,\underline{j} = - \oint_B C_p\,(\underline{x}, t)\,\underline{n}\,dl_x\,, \qquad (4.88)$$

and

$$C_M\,\underline{k} = - \oint_B (\underline{x} - \underline{x}_m) \times C_p\,(\underline{x}, t)\,\underline{n}\,dl_x\,. \qquad (4.89)$$

These are non-dimensionalized by the chordlength c, the fluid density ρ and the reference speed (U_o) with a factor 1/2. F_x and F_y are the force components in x- and y-direction, respectively, in the moving frame (see Figure **4.6**). Lift and drag coefficients are resolved relative to an orientation usually specified in the inertial frame at a given instant:

$$C_L = F_y\,\cos\alpha(t) - F_x\,\sin\alpha(t), \qquad (4.90)$$

$$C_D = F_x\,\cos\alpha(t) + F_y\,\sin\alpha(t), \qquad (4.91)$$

where $\alpha(t)$ is an angle of attack at an instantaneous time.
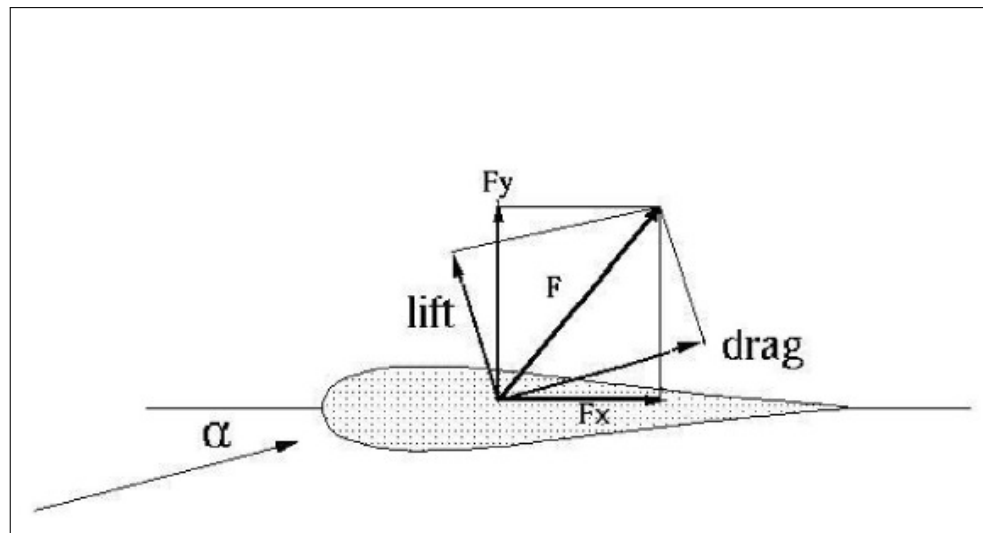
Figure 4.6 Force diagram of 2-D foil.

Each individual step of the numerical solution process is outlined as follows:

(1) Read the body geometry, the mean angle of attack, the type of unsteady motions and/or flows. For application of the combined flow situation, the motions and/or flows are decomposed into harmonic components specified by amplitude, frequency and phase of each component. Also the number of discretized panels on the body surface, the number of the time steps to be performed and the length of the straight-line wake sheet element attached to the T. E. are input parameters.

(2) Discretize the body surface by 'cosine-spacing' to generate the panel geometry and each geometrical parameter such as control point, (approximate) representative surface point and tangential vector.

(3) Calculate the influence coefficients at the control points induced by the flat panels representing the body surface.

(4) Calculate the results of the steady flow case at the mean position or at an ultimate time which will be used as the initial starting value or for normalization.

(5) Guess initially at the (k)-th time step the orientation of the wake sheet element, the shed vorticity at the T. E. and the potential jump at the T. E. by assigning those values computed at the previous time step.

(6) Calculate the undisturbed velocity specified by the unsteady motion and/or the flows observed in the moving frame, from which the no-penetration condition is imposed at each control point.

(7) Calculate the right-hand side of the matrix system of the linear algebraic equations, including the effect of the concentrated vortex system newly updated in position from the previous time step.

(8) Solve the $N \times N$ matrix system of linear equations for the N unknowns $\phi_j^{(k)}(j = 1, 2, \cdots, N)$ by using the inversion by the decomposition of the matrix.

(9) Compute the orientation of the straight-line wake sheet element, the shed vorticity strength and its associated potential jump at the T. E.

(10) Repeat steps (6) through (9) until the converged values of the above quantities are obtained within a given allowance or until a prescribed allowable number of iteration are processed.

(11) Calculate the convective velocities at the vortex cores at the present time step to update their positions for process at the next step. An amalgamation of two distant vortices is carried out at this stage if desired.

(12) Find the surface speed and pressure distribution, the force components and the moment about a given point, by using the exponential spline to differentiate the values of the surface potential and to evaluate the associated integrals.

(13) Repeat steps (5) through (12) until a given or enough number of time steps are executed to achieve the steady-state solution or to carry the solution far downstream.

4.6.9 Numerical results: Steady flow cases

Numerical and analytical surface (disturbance) potentials on an ellipse of 10% thickness-chord ratio at 10° angle of attack in steady uniform ($K = 0$) and shear ($K = 1$) onset flow are compared in Figure **4.7** . The total surface speeds in the same flow situation are also compared in Figure **4.8** .
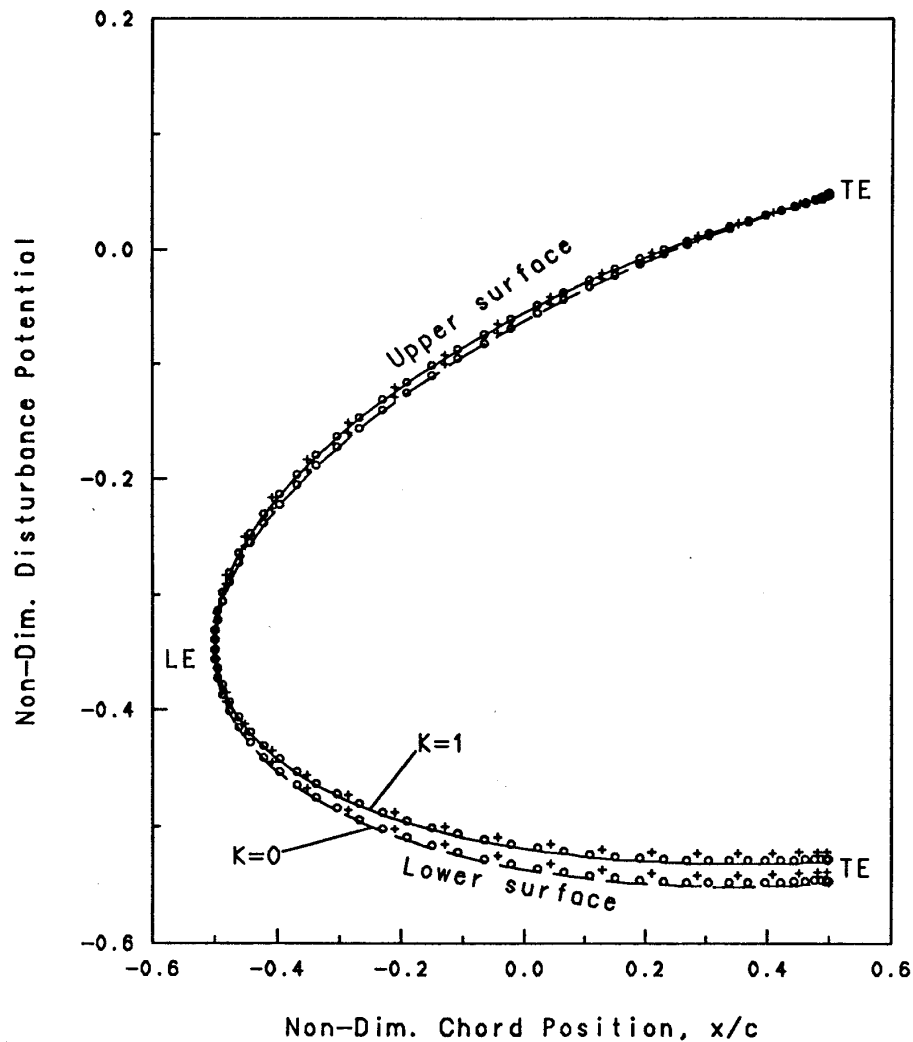
Figure 4.7 Comparison of numerical and analytical disturbance potentials on the surface of an ellipse ($\tau = 10\%$) in steady uniform ($K = 0$) and shear ($K = 1$) flow (at $\alpha = 10^o$). The broken and the solid lines denote the analytical results for $K=0$ and for $K=1$, respectively. The symbols denote the numerical results, using two different number of panels ($+, N = 36$; $\circ, N = 72$).

For the convergence check of the numerical model, two different number of panels ($N = 36, 72$) have been chosen. Good convergence of the solution is
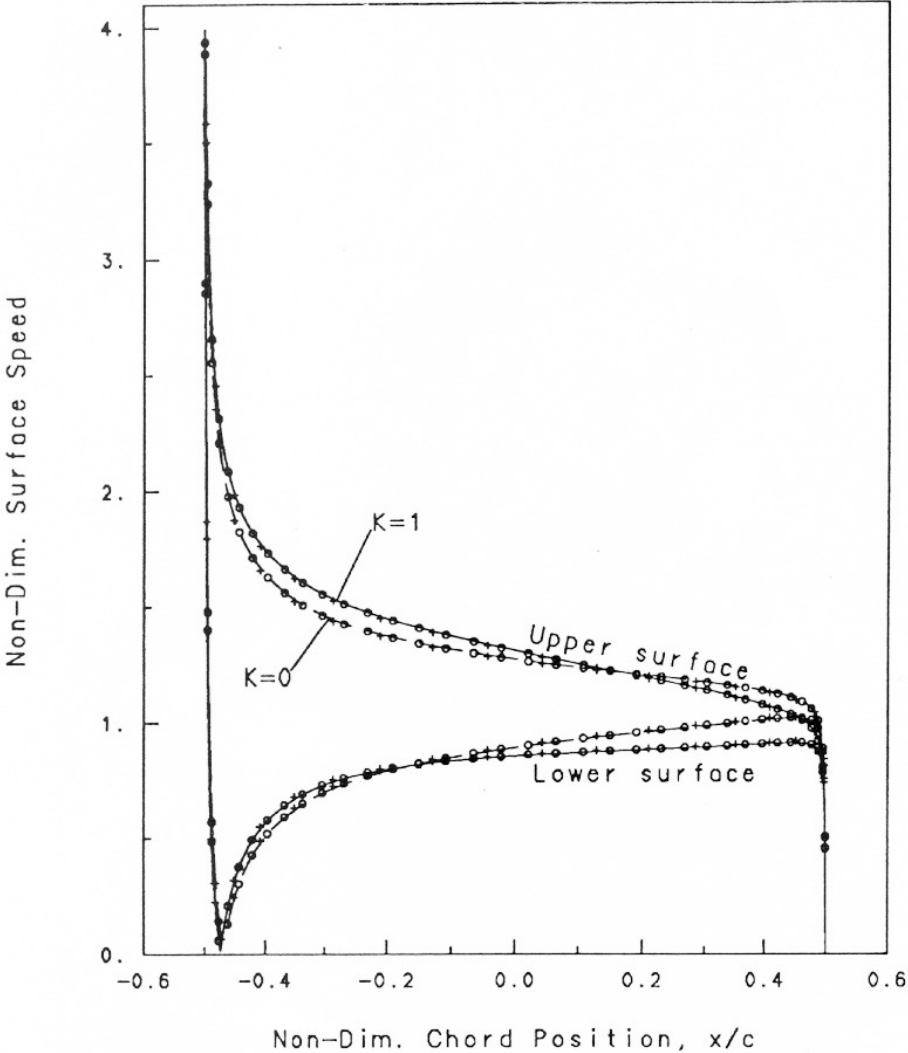
Figure 4.8 Comparison of numerical and analytical total surface speeds on the surface of an ellipse in steady uniform and shear flow. Legends are the same as those in Figure 4.7 .

observed over the entire foil surface. It is seen that the numerical results are locally in good agreement with the analytical ones obtained by the conformal transformation, even when using a moderate number of straight-line elements for representation of foil geometry.

Figure **4.7** shows that the circulation ($\triangle\phi|_{TE}$) for the case $K = 1$ is less than that of the case $K = 0$. Increased speed on the upper surface in the case of $K = 1$ tends to stimulate the flow downstream toward to the T. E. so as to satisfy the Kutta condition with the reduced value of Γ_B than that in the uniform flow case.

Figure **4.8** shows a difference in shape of the surface speed distribution between the uniform and shear flow cases. This figure compares velocities rather than pressure coefficients to look directly at the shear-flow effect on velocity distribution and to avoid uncertainty about the reference pressure for shear-flow case. The velocity curve of the shear flow case ($K = 1$) seems to be obtained by rotating that of the uniform flow case ($K = 0$) in the rotational direction of the shear flow.

In Figure **4.9** , numerical and analytical lift and moment (about the midchord) coefficients versus angle of attack for various velocity gradient values (K) are compared for a Moriya foil ($\epsilon = 0.05, \delta = 0.1$) whose profile shape is symmetric conventional with thickness-chord ratio of 10 % (see Moriya (1941) or Suh (1990) for details). It is seen that the numerical results agree well with the analytical ones, which expected since there is good agreement of surface speed as shown in Figure **4.8** . The results indicate that lift coefficient is fairly linearly proportional to angle of attack over its moderate range.

4.6.10   Numerical results: Unsteady flow cases

4.6.10.1   Start-up problems

There are two non-linear aspects to be considered when employing numerical methods for combined flow situations proposed herein— finite thickness of a foil and distortion of the wake sheet (both of which have been neglected in
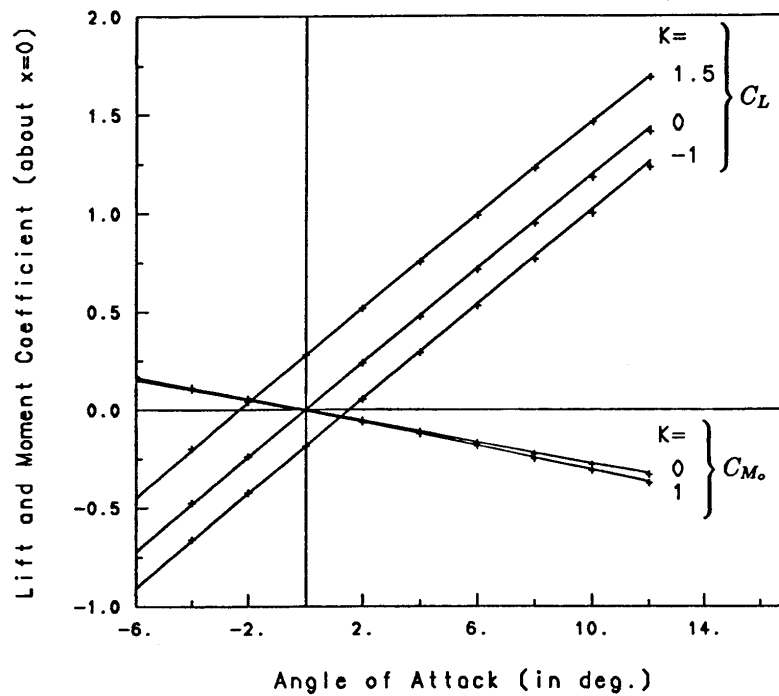
Figure **4.9** Comparison of numerical and analytical lift and moment coefficients (about the mid-chord point) versus angle of attack for a Moriya (1941) foil ($\epsilon = 0.05$, $\delta = 0.1$) in steady shear flow. ——, analytical; +, numerical.

the derivation of the classical linear analytical solutions). Figures **4.10** shows, with varying thickness of a foil, numerical lift growths for start-up problems of NACA 4-digits foil sections, [16] together with the linearized analytic solution (i.e., Wagner function, $W(\sigma)$). These test cases have been chosen to emphasize the non-linear aspects. The effect of foil thickness on growth of lift seems to be more significant quantitatively than that of the angle of attack from the viewpoint of realistic flow situations.

To see the distorted shedding vortex sheet, Figure **4.11** shows the calculated positions of vortex cores for an NACA0012 foil at $\alpha = 10^o$. It is seen that the roll-up behavior occurs together with stretching near the end of the vortex sheet.

---

[16]To generate closed round shape at the T. E. instead of originally defined blunt shape (Abbott & Doenhoff (1959), p. 113), we have used a modified thickness distribution near the T. E. with a parabola of the form specified by matching the conditions of the offset and slope at $x = 0.492404$: $Y_t/t_o = \pm\sqrt{0.5 - x}\,(0.231902 - 1.316268\,(0.5 - x))$, $x > 0.492404$.
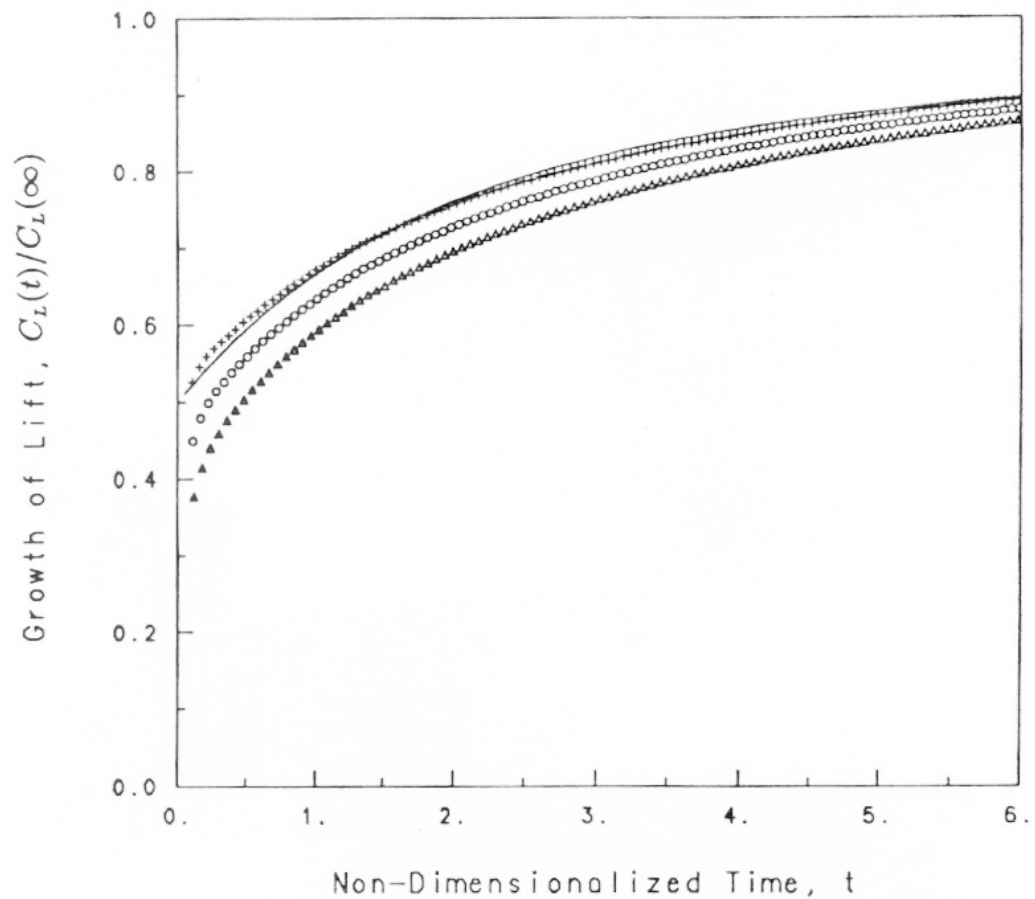
Figure 4.10 Growth of lift for sudden start-up of NACA0006, NACA0012 and NACA 0018 foils in uniform onset flow (at $\alpha = 10^o$). The solid line denotes the linearized analytical solution for a flat plate (Wagner (1925)). The symbols denote the present numerical results with $N = 36, \triangle v_1 = 0.05$ (+, NACA0006; ∘, NACA0012; △, NACA0018).
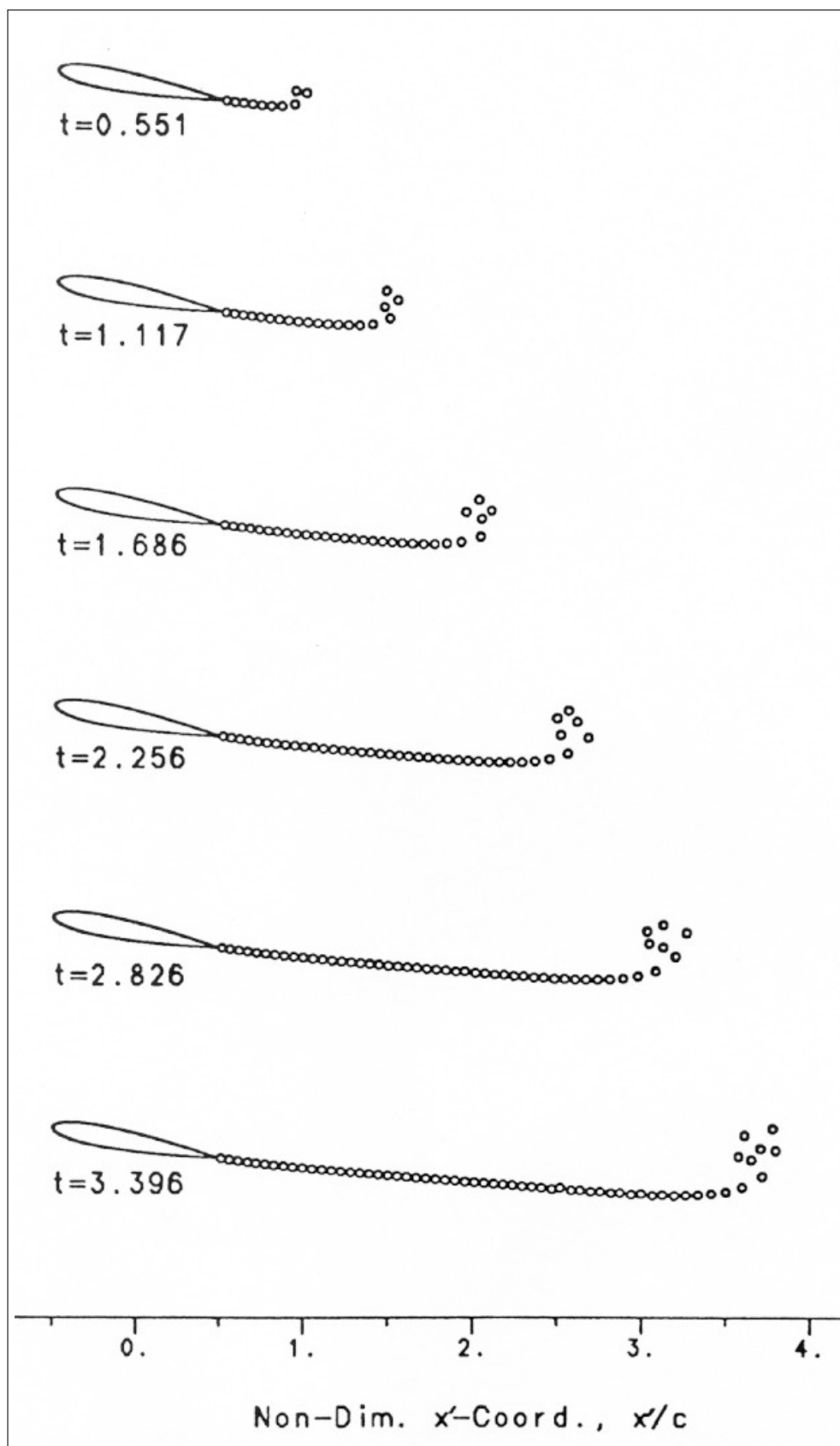
Figure 4.11 Calculated location of vortex cores for start-up of an NACA0012 foil at $\alpha = 10^o$ with $\triangle v_1 = 0.05$. The non-dimensionalized time $t's$ correspond to the time steps $(k) = 10, 20, 30, 40, 50, 60$.

4.6.10.2   Harmonic heave motion

Figure **4.12** presents the calculated location of the vortex cores representing the shed-vortex sheet for harmonic heave motion (with a reduced frequency $k = 2.15$ and a heave amplitude $h_o = 0.018$) of an NACA0015 foil in uniform flow. It shows that the numerical model for calculation of position of the sheet predicts a shape similar to that calculated by Giesing (1968a) and similar to that observed by Bratt (1953). Therefore this distortion of wake sheet shape may affect significantly on the flow characteristics of an interferance problem (like that between two moving foils).
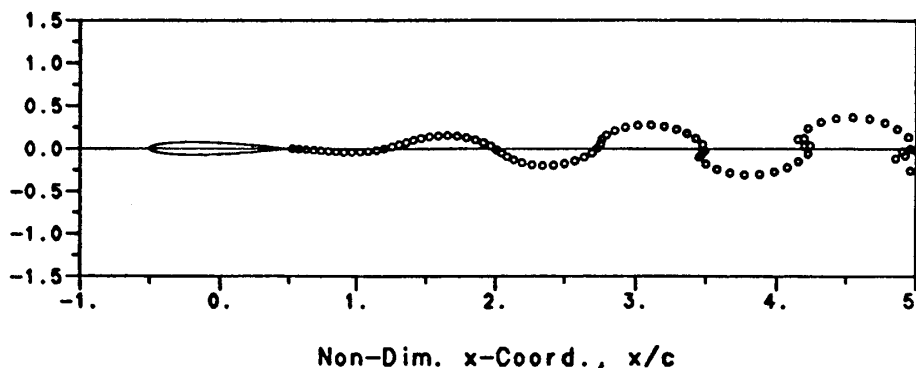
Figure **4.12** Calculated location of vortex cores for harmonic heave motion of an NACA0015 foil in uniform flow (for $\alpha = 0^o, k = 2.15, h_o = 0.018$).

With varying thickness of an NACA 4-digits foil section, time variation of lift coefficient and its fluctuation magnitude for various reduced frequencies k for heave motion are shown in Figure **4.13** . For a comparison purpose, the linearized analytical solution is also presented: [17]

$$C_L(t) = -4\pi h_o\, k \left[Re(C(k))\, \cos(2\, kt + \varphi) - \{ Im(C(k)) + 0.5\, k \} \sin(2\, kt + \varphi) \right]$$

$$(4.92)$$

where $C(k)$ is the Theodorsen function, h_o is an amplitude of heave motion and φ is a phase of heave motion. The magnitude of fluctuating lift decreases with increasing thickness of a foil. This thickness effect becomes larger as k increases, but a relative difference is mostly the same over a wide range of k.

---

[17] Küssner (1960), Hewson-Browne (1963), and van de Vooren & van de Vel (1964) have addresed second-order corrections by considering the separate influence of finite foil thickness at zero mean angle of attack.

For the case of an NACA0012 foil, there is about 7% change of the magnitude of fluctuating lift relative to the magnitude for an NACA0006 foil.
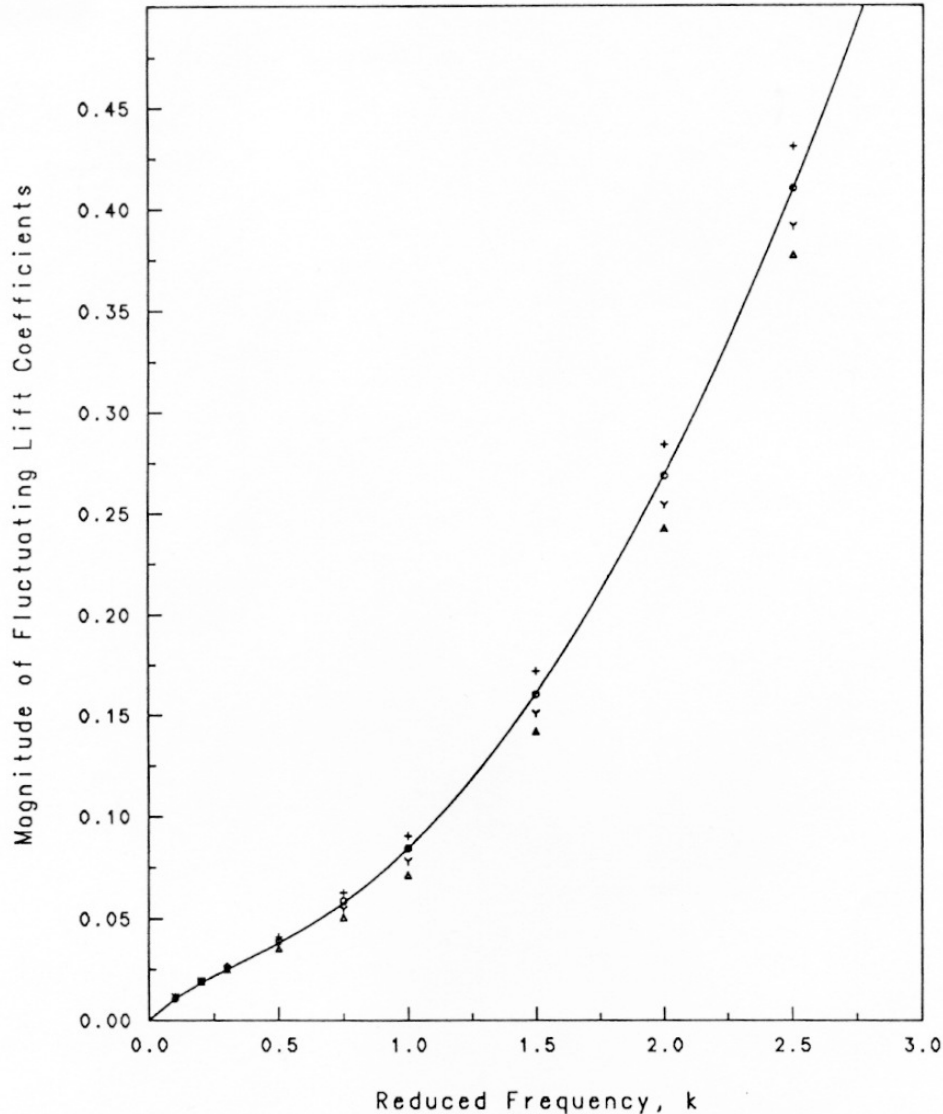
Figure **4.13** Magnitude of fluctuating lift with various reduced frequencies for heave motion of NACA0006, NACA0012, NACA0018 and NACA0024 foils in uniform flow ($K = 0$) (for $\alpha = 0^o, h_o = 0.01$). +, NACA0006; o, NACA0012; Y, NACA0018 △, NACA0024. The solid line denotes the linearized analytical solution (Theodorsen (1935)).

4.6.10.3   Concluding remarks on combined motions

Although not presented herein, the present numerical algorithm can be exten-
sive to arbitrary combined flow situations that is usually composed of heave,

pitch motions and vertical gusts. This combined flow situation can be modeled as that of a foil moving with a forward speed and undergoing the assumed periodic motion in uniform onset flow and the vertical gust. The lift coefficient obtained by superposition of each classical linearized analytic solution plus the numerical steady value at the mean flow condition (i.e., $\alpha_m = 0^o$) is available. The superposed linearized solution gives fairly good agreement in trend of the overall forces with the non-linear numerical results.

This flow situation may be considered as that about the blade section of a marine propeller, for which there is a large multiple blade-order frequency component of non-uniformity in ship wake flow. Therefore a superposition (of multiple gusts) of fluctuating lift coefficient (which has been used in many practical propeller problems) might be appropriate in combined flow case.

4.7 Formulation in Three-dimensions

4.7.1 Extension to 3-D wing

Like 2-D foils, Figure **4.14** represents a relative configuration of a wing in the inertial and moving frames with appropriate notations to be used for the formulation of the boundary value problem. The coordinate system is the same as the 2-D system, but we add the z-axis in third (vertical) direction.

Recall that the continuity equation for the disturbance velocity reduces to $\nabla \cdot \underline{u}$. The present concern is one whether the disturbance velocity is irrotational in the moving frame when the total velocity is irrotational and then the present procedure for solving the potential flow can be applied extensively. The vorticity of the inherent irrotational flow can be expressed by, in the inertial frame,

$$0 = \nabla' \times \underline{q}'_T = \nabla' \times (\underline{q}_F + \underline{q}) = 2\,\underline{\Omega} + \nabla \times \underline{q}, \qquad (4.93)$$

or

$$\nabla \times \underline{q} = -2\,\underline{\Omega} \qquad (4.94)$$

This indicates that the vorticity of a flow in the non-inertial (moving) reference
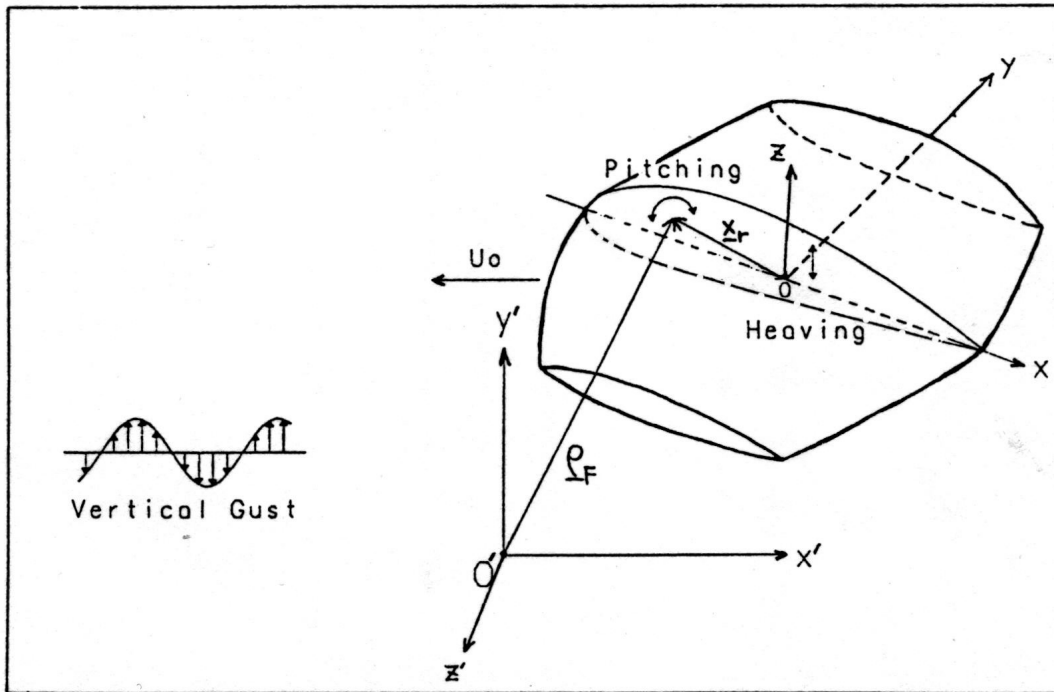
Figure **4.14** The coordinate systems and a combined unsteady flow situation for a 3-D wing.

frame is different from that of a flow in the inertial frame.

However, let us express $\underline{q}$ in terms of the disturbance caused by a body, then the expression reduces to

$$\nabla \times \underline{q} = \nabla \times (\underline{q}_o - \underline{q}_F + \underline{u}) = -2\underline{\Omega} + \nabla \times \underline{u} \qquad (4.95)$$

From Eqs. (4.94) and (4.95), $\nabla \times \underline{u} = 0$ must be statisfied which means that the disturbance velocity field measured in the moving frame is also irrotational. Hence we can introduce a disturbance velocity potential ($\underline{u} = \nabla \phi$) which is governed by the Laplace equation:

$$\nabla^2 \phi = 0 \qquad (4.96)$$

The computational procedures for solving a related problem are similar to those for 2-D foil.

4.7.2   Velocity components at a panel surface

Suppose that the velocity components in direction of two non-orthogonal coordinates (s_1, s_2) on a panel surface have been computed.

$$v_1 = \frac{\partial \phi}{\partial s_1}, \quad v_s = \frac{\partial \phi}{\partial s_2} \tag{4.97}$$

Now we should know the orthogonal velocity components from these non-
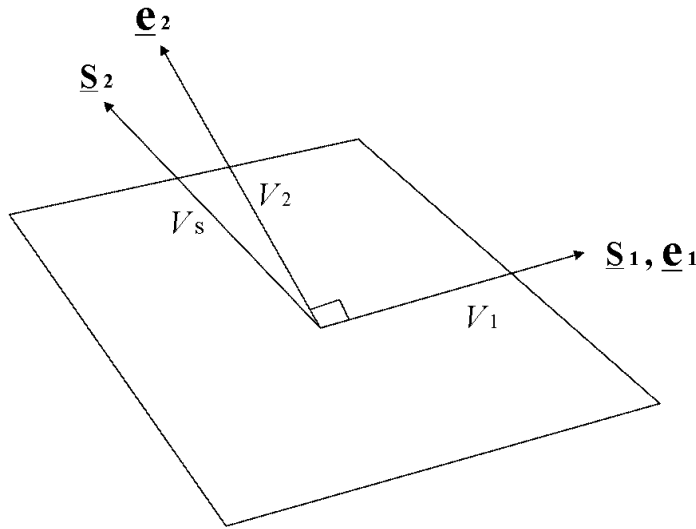
Figure **4.15** Velocity component calculation for local non-orthogonal coordinates of panel surface.

orthogonal components. Take an orthogonal coordinate system (e_1, e_2) where $e_1 = s_1$ with the corresponding unit vectors. (See Figure **4.15**). Then

$$
\begin{aligned}
v_s \, \underline{s}_2 &= v_1 \, \underline{e}_1 + v_2 \, \underline{e}_2 \\
v_s \, \underline{s}_2 \cdot \underline{s}_2 &= v_1 \, (\underline{e}_1 \cdot \underline{s}_2) + v_2 \, (\underline{e}_2 \cdot \underline{s}_2) \\
v_2 &= \frac{v_s - v_1 \, (\underline{e}_1 \cdot \underline{s}_2)}{(\underline{e}_2 \cdot \underline{s}_2)}
\end{aligned}
\tag{4.98}
$$

4.7.3 Non-lifting flow about an ellipsoid

The analytic solution of the disturbance potential about an ellipsoid at zero angle of attack are given in Milne-Thomson (1968). [18] By superposing the analytic solutions at zero angle of attack relative to the different axes, we obtain the analytic solution for an oblique onset flow $\underline{q}_0 = (U, V, W)$. Then the surface speeds are found by differentiating the potential along the surface. For an ellipsoid whose geometry is specified as $(x/a)^2 + (y/b)^2 + (z/c)^2 = 1$ where a, b, c are the length of the semi-axes, respectively, the surface speed $\underline{q}_s$ is given by

$$
\begin{aligned}
\underline{q}_s &= \left(\frac{x^2}{a^4} + \frac{y^2}{b^4} + \frac{z^2}{c^4}\right)^{-1} \cdot \\
&\cdot \Bigg[\, U\left(1 + \frac{\alpha_0}{2 - \alpha_0}\right) \left\{\left(\frac{y^2}{b^4} + \frac{z^2}{c^4}\right)\underline{i} - \frac{x\,y}{a^2\,b^2}\underline{j} - \frac{z\,x}{c^2\,a^2}\underline{k}\right\} \\
&\quad + V\left(1 + \frac{\beta_0}{2 - \beta_0}\right) \left\{\left(\frac{z^2}{c^4} + \frac{x^2}{a^4}\right)\underline{j} - \frac{y\,z}{b^2\,c^2}\underline{k} - \frac{x\,y}{a^2\,b^2}\underline{i}\right\} \\
&\quad + W\left(1 + \frac{\gamma_0}{2 - \gamma_0}\right) \left\{\left(\frac{x^2}{a^4} + \frac{y^2}{b^4}\right)\underline{k} - \frac{z\,x}{c^2\,a^2}\underline{i} - \frac{y\,z}{b^2\,c^2}\underline{j}\right\}\Bigg] \quad (4.99)
\end{aligned}
$$

where

$$
\begin{aligned}
\alpha_0 &= a\,b\,c \int_0^\infty (a^2 + \lambda)^{-3/2}\,(b^2 + \lambda)^{-1/2}\,(c^2 + \lambda)^{-1/2}\,d\lambda \\
\beta_0 &= a\,b\,c \int_0^\infty (b^2 + \lambda)^{-3/2}\,(c^2 + \lambda)^{-1/2}\,(a^2 + \lambda)^{-1/2}\,d\lambda \quad (4.100) \\
\gamma_0 &= a\,b\,c \int_0^\infty (c^2 + \lambda)^{-3/2}\,(a^2 + \lambda)^{-1/2}\,(b^2 + \lambda)^{-1/2}\,d\lambda
\end{aligned}
$$

Figure **4.16** shows the chordwise distributions of the surface speed of an ellipsoid in an oblique onset flow. The numerical results at the three diffreent spanwise positions have good agreement with the analytic solutions. Some discrepancy is observed near the leading edge anf the trailing edge where the numerical resolution does not fairly follow the rapid change in the potemtial. In the numerical calculation, the bilinear distribution over each quadrilateral panel

---

[18] See, for details, Suh, J.-C., Lee, J.-T. and Suh, S.-B. (1992), "A bilinear source and doublet distribution over a planar panel and its application to surface panel methods," *Proc. 19th Symp. Naval Hydro.*, pp. 102–112.

was used to specify the singularity distribution on the surface. No-penetration condition (kinematic boundary condition) was applied at the *nodes of the panels* as the collocation points in the potential-based panel emthod. The resulting linear system of equations forms for the unknown nodal values of the disturbance potential. The surface speeds are calculated numerically using a second order fitting of the potential.
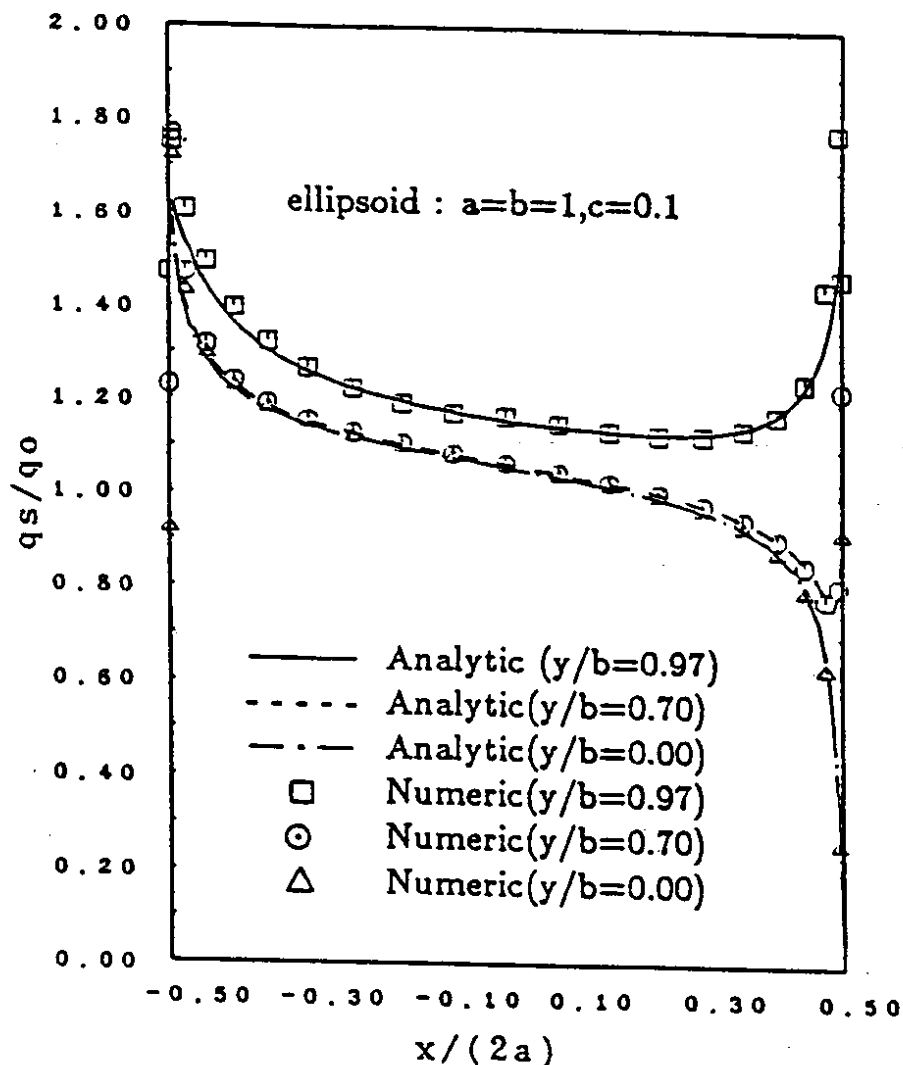
Figure **4.16** The surface speed of an ellipsoid $a = b = 1, c = 0.1$ in an oblique onset flow by using the quadrilateral panels with the bilinear singularity distribution. The onset flow velocity $\underline{q}_0 = (1, 0, 0.1736)$; The number of chordwise and spanwise panels: $N \times M = 40 \times 40$.

4.7.4 Lifting flow about a circular wing

In numerical implementation of the potential-based panel method for solving the potential flow around the lifting body, the trailing wake sheet is represented approximately as the doublet distribution of potential jump. One possible way to include the effect of the local variation of these doublet strengths is to use a bilinear distribution over each wake panel which is uniquely determined from imposed potential jump values at its four vertices.

The use of the bilinear distribution over the quarilateral panels eliminates the discontinuity problem of singularity that is associated with the piecewise constant distribution. Then the singularity strength will be chosen to vary bilinearly across the panel. Therfore it is necessary to derive explicit and elegant closed forms of the induced potential and velocity due to the bilinear distribution. The closed forms are much computer-oriented and explicit so that we can obtain, with easier implementation, the matrix element of the linear system of algebraic equations in application of the surface panel methods. Chapter 5 presents the closed forms for computing the induced potential and velocity due to the bilinear distibution of source and/or doublet singularities over a planar panel. [19] The bilinear distribution cases includes, of course, both the constant and/or the linear distribution cases.

We calculated the circulation distribution for a circular wing, for which the linearized analytic solutions are available. [20] Numerical and analytical circulation distributions for a circular wing with NACA 4-digits section at 5° angle of attack are compared in Figure **4.17** . For the implementation of the Kutta condition described previously, the constant sigularity density was used for wing panels and the bilinear distribution for the trailing wake sheet elements extending on the xy-plane.

It is seen that the numerical method gives fair values compared to the linearized analytic solution using the moderate number of panels. Particularly the numarical results are in good agreement with the analytic ones near the tip

---

[19]See also Suh, J.-C., Lee, J.-T. and Suh, S.-B. (1992), "A bilinear source and doublet distribution over a planar panel and its application to surface panel methods," *Proc. 19th Symp. Naval Hydro.*, pp. 102–112.

[20]See Jordan, P. F. (1972), "Exact solutions for lifting surfaces," *AFOSR Scientic Report*, AFOSR-TR-72-1737.

where the circulation changes raplidly. The bilinear representation of the wake sheet singularity in the numerical method would be appropriate to include this local variation. Figure **4.17** shows that the circulation decreases as the thickness chord ratio increases. This feature is also found in the results provided by Lee, J.-T. (1987).
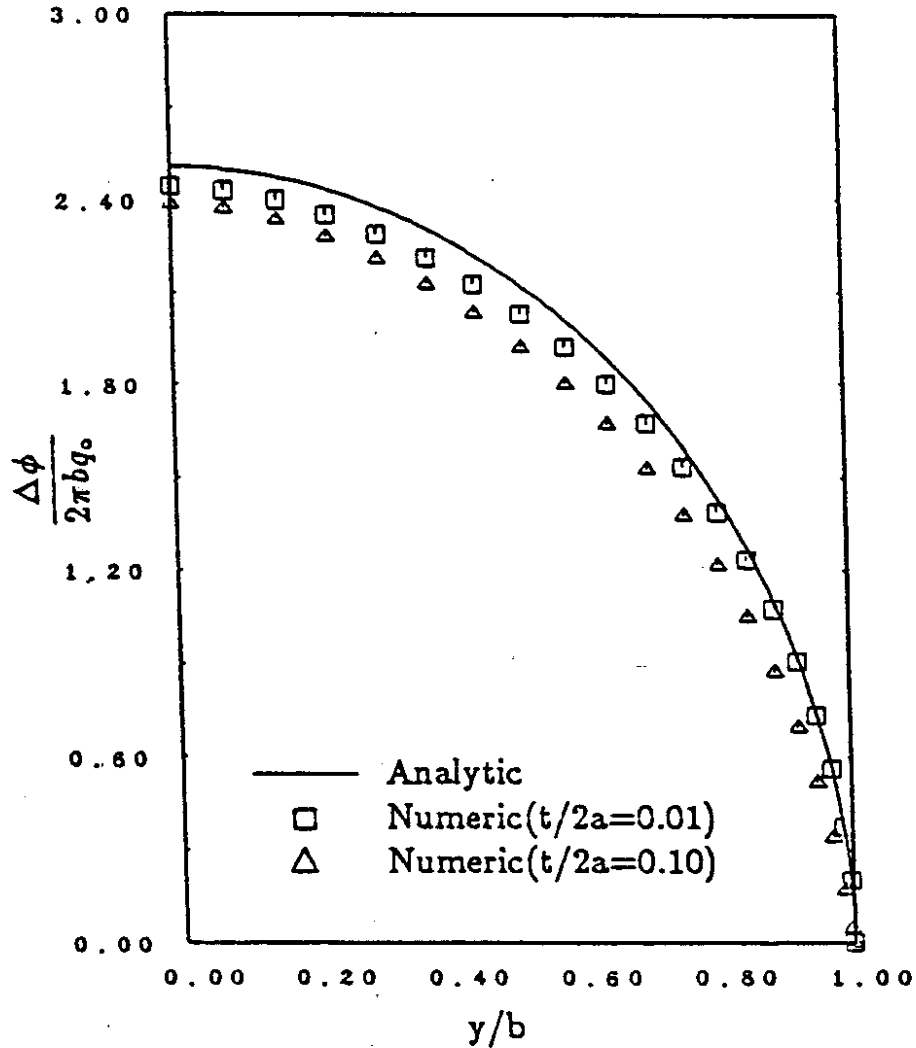
Figure **4.17** Circulation distribution of a circular wing at $\alpha = 5^o$ angle of attack. The number of chordwise and spanwise panels: $N \times M = 40 \times 40$.

5

ANALYTICAL EVALUATION OF BOUNDARY INTEGRALS

5.1   Introduction

The fundamental problem of fluid mechanics for inviscid incompressible flow is to determine velocity potential ϕ in simply connected fluid domain V bounded by the boundary S (S is composed of a body surface and non-realistic surface). The governing equation of the velocity potential becomes the Laplace equation,

$$\nabla^2 \phi = 0, \tag{5.1}$$

satisfying certain proper conditions on S.

With the Green's scalar identity, the potential ϕ within the domain V is expressed in terms of the proper value of ϕ and its normal derivative $\underline{n} \cdot \nabla \phi$ on the boundary S;

$$\phi(\underline{x}_p) = -\frac{1}{4\pi} \left\{ \int_S \frac{1}{r} \underline{n} \cdot \nabla \phi - \phi \, \underline{n} \cdot \nabla \left(\frac{1}{r} \right) \, dS \right\}. \tag{5.2}$$

Here r is a distance between an integration point $\underline{x}_\xi$ on S and a field point $\underline{x}_p$ located in V. Namely, $\underline{r} = \underline{x}_\xi - \underline{x}_p$.

The first surface integral is interpreted as the potential by surface distribution of source-type singularities with density $\sigma \equiv \underline{n} \cdot \nabla \phi$, the second surface integral as the potential by surface distribution of doublet-type singularities, $\mu \equiv -\phi$. [1]

---

[1]Recall that the doublet strength is defined as $\mu \equiv \phi$ in the preceding chapters.

Such a singularity method can be applied for solution of this problem. In numerical implementation, the integration over the bounding surface S is approximately performed by summing up each contribution in terms of the proper value of ϕ and its normal derivative $\underline{n} \cdot \nabla\phi$ on each panel element of the discretized boundary surface S;

$$\phi(\underline{x}_p) = -\frac{1}{4\pi} \sum_j \int_{S_j} \left\{ \frac{1}{r}\, \underline{n} \cdot \nabla\phi - \phi\, \underline{n} \cdot \nabla\left(\frac{1}{r}\right) \right\} dS \qquad (5.3)$$

Applying the boundary condition at collocation points to this equation results in a linear system of algebraic equations for unknown doublet strengths on each panel. [2]

Evaluations of the associated integrals at the collocation points should be performed to obtain the matrix elements. The fast and accurate computation of these elements is very important in the numerical solution.

The velocity components can be derived by differentiation of Eq. (5.3) with respect to the coordinates of the field point. We may take without loss of generality one planar panel as the integration region concerned herein, which can be regarded as a part of the discretized boundary surface.

5.2   Transformation of the Surface Integrals to Contour Integrals

As will be shown in the followings, using the integral theorems, the surface integrals of the singularity method can be transformed into contour integrals for planar facets. Furthermore, for a planar polygon element with the uniform or linear or bilinear or higher-order density distribution of singularities, the analytical evaluation is possible. The numerical integration is then very precise at less calculation cost.

This section is especially prepared to show all the mathematical derivations

---

[2]The basic idea of the singularity method has been introduced by Hess, J. L. and Smith A. M. O. (1966), "Calculation of potential flow about arbitrary bodies," *Progress in Aeronautical Science Series*, vol. 8, pp. 1–138.

and proofs of the related equations. A few of test calculations will show the superiority of these analytic evaluations to numerical integrations. A subroutine program based on the analysis is also provided in Appendix C for computations of the influence coefficients in applications of the panel method.

Cantaloube & Rehbach (1986) [3] show that the surface integrals for constant and/or linear distributions of sources and doublets over a planar facet can be transformed into line integrals along contour of the panel: [4]

(1) for source distributions,

$$
\begin{aligned}
\phi^{(\sigma)} &= -\frac{1}{4\pi}\left[\underline{n}\cdot\oint_C \sigma\frac{\underline{r}}{r}\times d\underline{l} - (\underline{n}\cdot\underline{r})\oint_C \sigma\,\underline{A}\cdot d\underline{l} + (\underline{n}\cdot\underline{r})(\underline{n}\cdot\underline{e})\,\underline{n}\cdot \right.\\
&\qquad\left.\cdot\left\{\nabla\sigma\times\oint_C \ln(r+\underline{e}\cdot\underline{r})\,d\underline{l}\right\} - \underline{n}\cdot\left(\nabla\sigma\times\oint_C r\,d\underline{l}\right)\right] \qquad (5.4)\\
\underline{q}^{(\sigma)} &= -\frac{1}{4\pi}\left[\underline{n}\oint_C \sigma\,\underline{A}\cdot d\underline{l} + \underline{n}\times\oint_C \frac{\sigma}{r}\,d\underline{l} - \underline{n}(\underline{n}\cdot\underline{e})(\underline{n}\times\nabla\sigma)\cdot\right.\\
&\qquad\left.\cdot\oint_C \ln(r+\underline{e}\cdot\underline{r})\,d\underline{l} + \nabla\sigma\left\{\underline{n}\cdot\oint_C \frac{\underline{r}\times d\underline{l}}{r} - (\underline{n}\cdot\underline{r})\oint_C \underline{A}\cdot d\underline{l}\right\}\right] \quad (5.5)
\end{aligned}
$$

(2) for doublet distributions,

$$
\begin{aligned}
\phi^{(\mu)} &= -\frac{1}{4\pi}\left\{-\oint_C \mu\underline{A}\cdot d\underline{l} + (\underline{n}\cdot\underline{e})(\underline{n}\times\nabla\mu)\cdot\oint_C \ln(r+\underline{e}\cdot\underline{r})\,d\underline{l}\right\} \quad (5.6)\\
\underline{q}^{(\mu)} &= -\frac{1}{4\pi}\left\{\oint_C \mu\nabla\left(\frac{1}{r}\right)\times d\underline{l} - \nabla\mu\oint_C \underline{A}\cdot d\underline{l} - (\underline{n}\times\nabla\mu)\times\right.\\
&\qquad\left.\times\left(\underline{n}\times\oint_C \frac{d\underline{l}}{r}\right)\right\} \qquad\qquad\qquad (5.7)
\end{aligned}
$$

---

[3]Cantaloube, B. and Rehbach, C. (1986), "Calcul des Integrales de la Methode des Singularites," *Recherche Aerospatiale*, n° 1, pp. 15–22, English Title: "Calculation of the Integrals of the Singularity Method," *Aerospace Research*, no. 1, pp. 15–22.

[4]See Appendix B for derivation in detail, and also Suh, J.-C. (1990b), *Review of the Paper; Calculation of the Integrals of the Singularity Method by Cantaloube and Rehbach*, KRISO Propulsor Technology Laboratory Report, 22-90. Suh, J.-C. (1990c) *Analytic Evaluations of the Induction-Integrals for Distributions of Sources and Doublets over a Planar Polygon Element*, KRISO Propulsor Technology Laboratory Report, 23-90.

where the vector

$$\underline{A} = \frac{\underline{e} \times \underline{r}}{r(r + \underline{e} \cdot \underline{r})}, \tag{5.8}$$

is introduced by Guiraud (1978), [5] the distance vector $\underline{r} = \underline{x}_\xi - \underline{x}_p$ and $\underline{e} = \pm \underline{n}$. Note that the distance vector is the position vector of the source point relative to the field point, whose direction is opposite to direction of conventionally defined position vectors. The contour integrals are performed along the perimeter of the element in counterclockwise sense.

The details on the derivation of the transformation of the surface integral is given in Appendix B.

For a planar polygon element, the line integrals can be reduced to closed-form expressions. Derivation of these analytic evaluations is the main scope of Appendix B. The computer program based on the analytic evaluation of the contour integrals as outlined in the following section is provided in Appendix C.

5.3   Constant Density Distributions over a Planar Polygon

5.3.1   Source distribution: Potential

The potential at a field point $\underline{x}_p(x, y, z)$ induced by a distribution of sources with unit density (i.e. $\sigma = 1$) over a planar element is, from Eq. (5.4),

$$\phi^{(\sigma)} = -\frac{1}{4\pi} \left\{ \underline{n} \cdot \oint_C \frac{\underline{r}}{r} \times d\underline{l} - (\underline{n} \cdot \underline{r}) \oint_C \underline{A} \cdot d\underline{l} \right\}. \tag{5.9}$$

Rearrange Eq. (5.9) to yield

$$
\begin{aligned}
\phi^{(\sigma)} &= -\frac{1}{4\pi} \left\{ \underline{n} \cdot \oint_C \frac{\underline{r}}{r} \times d\underline{l} - (\underline{n} \cdot \underline{r}) \oint_C \left(\frac{1}{r} - \frac{1}{r + \underline{e} \cdot \underline{r}} \right) \frac{\underline{e} \times \underline{r}}{\underline{e} \cdot \underline{r}} \cdot d\underline{l} \right\} \\
&= -\frac{1}{4\pi} \oint_C \frac{\underline{n} \times \underline{r}}{r + \underline{e} \cdot \underline{r}} \cdot d\underline{l} = -\frac{1}{4\pi} \oint_C \frac{\underline{r} \cdot (d\underline{l} \times \underline{n})}{r + \underline{e} \cdot \underline{r}}. \tag{5.10}
\end{aligned}
$$

---

[5] Guiraud, J. P. (1978), "Potential of Velocities Generated by a Localized Vortex Distribution," *Aerospace Research*, English Translation-ESA-TT-560, pp. 105–107.

Because $\underline{r} \cdot (d\underline{l} \times \underline{n})/dl$ and $\underline{e} \cdot \underline{r}$ are constant for the respective side lines (each of which is a straight-line), it can be written as

$$\phi^{(\sigma)} = -\frac{1}{4\pi} \sum_{i=1}^{N_s} b_i \int_{C_i} \frac{1}{r+a}\, dl, \tag{5.11}$$

where N_s is the number of sides of the polygon element, for example, $N_s = 3$ for triangular elements, $a = \underline{e} \cdot \underline{r}$ is a positive constant value for all sides, and $b_i = \underline{r} \cdot (\underline{e}_{l_i} \times \underline{n})$ is constant for one side whose directional vector $\underline{e}_{l_i} = d\underline{l}/dl$ is chosen counterclockwise direction. The vertices composed of the element and the side of directional vector $\underline{e}_{l_i}$ are numbered in counterclockwise order. The field point is at an arbitrary position except on the side lines. It is seen that each integral for the respective side is related to the relative position of the field point.
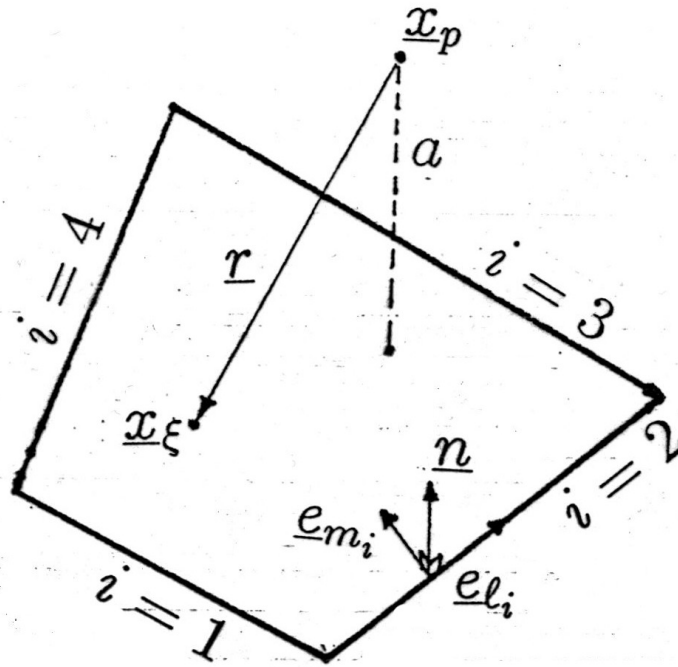
Figure 5.1 Schematic diagram of a planar element.

In the self-induction case that the field point is just above or below the element, we take $\underline{n} \cdot \underline{r} = 0$ in Eq. (5.9) and then the second term of Eq. (5.9) vanishes:

$$\phi^{(\sigma)} = -\frac{1}{4\pi}\underline{n} \cdot \oint_C \frac{\underline{r}}{r} \times d\underline{l}. \tag{5.12}$$

It is reduced to, by setting $a = 0$ in Eq. (5.11)

$$\phi^{(\sigma)} = -\frac{1}{4\pi} \sum_{i=1}^{N_s} b_i \int_{C_i} \frac{1}{r} \, dl. \tag{5.13}$$

This expression is also applied for the case that the field point is on the extension plane of the planar element.

5.3.2 Source distribution: Velocity

The velocity at a field point $\underline{x}_p(x, y, z)$ induced by a distribution of sources with unit density (i.e. $\sigma = 1$) over a planar element is, from Eq. (5.5),

$$\underline{q}^{(\sigma)} = -\frac{1}{4\pi} \left\{ \underline{n} \oint_C \underline{A} \cdot d\underline{l} + \underline{n} \times \oint_C \frac{1}{r} d\underline{l} \right\}. \tag{5.14}$$

Rearrange this equation to yield

$$
\begin{aligned}
\underline{q}^{(\sigma)} &= -\frac{1}{4\pi} \left\{ \underline{n} \oint_C \frac{\underline{e} \times \underline{r}}{r(r + \underline{e} \cdot \underline{r})} \cdot d\underline{l} + \underline{n} \times \oint_C \frac{1}{r} d\underline{l} \right\} \\
&= -\frac{1}{4\pi} \left\{ \underline{n}(\underline{n} \cdot \underline{e}) \oint_C \frac{\underline{n} \times \underline{r}}{r(r + \underline{e} \cdot \underline{r})} \cdot d\underline{l} + \underline{n} \times \oint_C \frac{1}{r} d\underline{l} \right\} \\
&= -\frac{1}{4\pi} \left\{ \underline{n}(\underline{n} \cdot \underline{e}) \oint_C \frac{\underline{r} \cdot (d\underline{l} \times \underline{n})}{r(r + \underline{e} \cdot \underline{r})} + \underline{n} \times \oint_C \frac{1}{r} d\underline{l} \right\} \\
&= -\frac{1}{4\pi} \left\{ \underline{n}(\underline{n} \cdot \underline{e}) \sum_{i=1}^{N_s} b_i \int_{C_i} \frac{1}{r(r + a)} \, dl + \sum_{i=1}^{N_s} \underline{e}_{m_i} \int_{C_i} \frac{1}{r} \, dl \right\} \tag{5.15}
\end{aligned}
$$

where $\underline{e}_{m_i} = \underline{n} \times \underline{e}_{l_i}$.

In the self-induction case that the field point is just above the element, the first integral of Eq. (5.14) is reduced to, with $\underline{e} = -\underline{n}$ (representing the approach of the field point toward the upper surface) and $a = 0$,

$$\oint_C \underline{A} \cdot d\underline{l} = \oint_C \frac{-\underline{n} \times \underline{r}}{r^2} \cdot d\underline{l} = \oint_C \frac{-\underline{n} \times r \, \underline{e}_r}{r^2} \cdot (\underline{e}_r \, dr + r \, \underline{e}_\theta \, d\theta) = -2\pi \tag{5.16}$$

Here we have introduced the unit vectors $\underline{e}_r$ and $\underline{e}_\theta$ of the local polar coordinates,

$\underline{x}_p$ being its origin, to define the line segment $d\underline{l}$. Therefore Eq. (5.15) is reduced to

$$q^{(\sigma)} = \frac{1}{2}\,\underline{n} - \frac{1}{4\pi}\sum_{i=1}^{N_s}\underline{e}_{m_i}\int_{C_i}\frac{1}{r}\,dl \qquad (5.17)$$

On the other hand, when $\underline{x}_p$ approaches toward the lower surface of the element, the sign of the first term of Eq. (5.17) is opposite. If $\underline{x}_p$ is on the (outside) extension plane of the planar panel, the first term in Eq. (5.17) vanishes.

5.3.3   Doublet distribution: Potential

The potential at a field point $\underline{x}_p(x, y, z)$ induced by a distribution of doublets with unit density (i.e. $\mu = 1$) over a planar element is, from Eq. (5.6),

$$\phi^{(\mu)} = +\frac{1}{4\pi}\oint_C \underline{A}\cdot d\underline{l}, \qquad (5.18)$$

where μ is defined as $\mu \equiv -\phi$. Rearrange Eq. (5.18) to yield

$$\begin{aligned}
\phi^{(\mu)} &= +\frac{1}{4\pi}\oint_C \frac{\underline{e}\times\underline{r}}{r(r + \underline{e}\cdot\underline{r})}\cdot d\underline{l} = \frac{1}{4\pi}\oint_C\left(\frac{1}{r} - \frac{1}{r + a}\right)\frac{\underline{e}\times\underline{r}}{\underline{e}\cdot\underline{r}}\cdot d\underline{l} \\
&= \frac{1}{4\pi}\frac{1}{\underline{n}\cdot\underline{r}}\oint_C\left(\frac{1}{r} - \frac{1}{r + a}\right)\underline{r}\cdot(d\underline{l}\times\underline{n}) \\
&= \frac{1}{4\pi}(\underline{n}\cdot\underline{e})\sum_{i=1}^{N_s}b_i\int_{C_i}\frac{1}{r(r + a)}\,dl \qquad (5.19)
\end{aligned}$$

In the self-induction case that the field point is just above the element, we take $\underline{e} = -\underline{n}$ and the same manner as in derivation of Eq. (5.16) for $\oint_C \underline{A}\cdot d\underline{l}$. It follows that

$$\phi^{(\mu)} = -\frac{\mu}{2} \qquad (5.20)$$

For the case that the field point is on the (outside) extension plane of the planar element, this expression is replaced by $\phi^{(\mu)} = 0$.

5.3.4 Doublet distribution: Velocity

The velocity at a field point $\underline{x}_p(x, y, z)$ induced by a distribution of doublets with unit density (i.e. $\mu = 1$) over a planar element is, from Eq. (5.7),

$$\underline{q}^{(\mu)} = -\frac{1}{4\pi} \oint_C \nabla(\frac{1}{r}) \times d\underline{l} \tag{5.21}$$

Rearrange this equation to yield

$$\underline{q}^{(\mu)} = +\frac{1}{4\pi} \oint_C \frac{\underline{r}}{r^3} \times d\underline{l} = +\frac{1}{4\pi} \sum_{i=1}^{N_s} \underline{d}_i \int_{C_i} \frac{1}{r^3}\, dl, \tag{5.22}$$

where $\underline{d}_i = \underline{r} \times \underline{e}_{l_i}$.

Either in the self-induction case that the field point $\underline{x}_p$ is just above the element or in the case that $\underline{x}_p$ is on the (outside) extension plane of the planar element, Eq. (5.22) becomes, with $\underline{d}_i = d_i \underline{n}$,

$$\underline{q}^{(\mu)} = +\frac{1}{4\pi}\underline{n} \sum_{i=1}^{N_s} d_i \int_{C_i} \frac{1}{r^3}\, dl \tag{5.23}$$

5.3.5 Basic integrals

In the preceding sections, we have derived closed-form expressions for the simpler cases, in terms of only the geometric parameters for each side of a polygon i.e., Eqs. (5.11), (5.15), (5.19), (5.22) for field points off the element surface and Eqs. (5.13), (5.17), (5.20), (5.23) for field points on the element surface (for the self-induction cases). There are four types of basic integrals to be evaluated; $\int_{C_i} \frac{1}{r}\, d\xi$, $\int_{C_i} \frac{1}{r+a}\, d\xi$, $\int_{C_i} \frac{1}{r(r+a)}\, d\xi$ and $\int_{C_i} \frac{1}{r^3}\, d\xi$. For the purpose of these evaluations, we define local relative coordinates (X', Z'), as shown in Figure 5.2 , for each side of the polygon in the plane through the field point $\underline{x}_p$ and that side, such that without loss of generality the side line corresponds to the X'-axis and the path of the line integral becomes the positive X'-direction.

First the end points of the side of length l are denoted with $Q_1(x_1, y_1, z_1)$ and
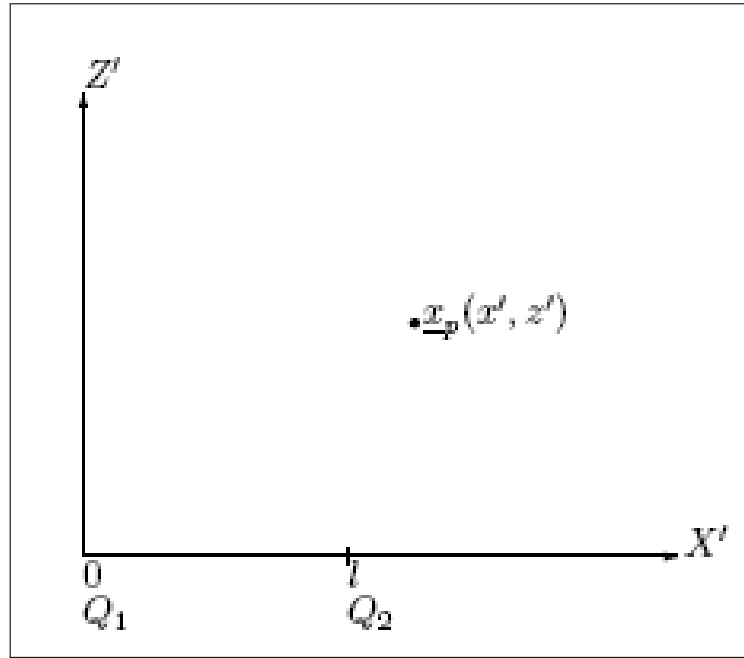
Figure 5.2 A local plane coordinate system for integral over the respective side of a panel. Q_1 and Q_2 denote two vertices of the side with length l.

$Q_2(x_2, y_2, z_2)$ in the global coordinate system, or with $Q_1(0, 0)$ and $Q_2(l, 0)$ in the local plane coordinate system. The field point is also defined by $\underline{x}_p(x_p, y_p, z_p)$ or $\underline{x}_p(x', z')$. The local coordinates (x', z') are related to the global coordinates as follows. The vectors $\underline{Q_1 Q_2}$ and $\underline{Q_1 x_p}$ are written as

$$\underline{Q_1 Q_2} = (x_2 - x_1)\,\underline{i} + (y_2 - y_1)\,\underline{j} + (z_2 - z_1)\,\underline{k} \qquad (5.24)$$

$$\underline{Q_1 x_p} = (x_p - x_1)\,\underline{i} + (y_p - y_1)\,\underline{j} + (z_p - z_1)\,\underline{k}. \qquad (5.25)$$

Then magnitude of cross product of the two vectors is given by

$$|\underline{Q_1 Q_2} \times \underline{Q_1 x_p}| = |\underline{Q_1 Q_2}|\,|\underline{Q_1 x_p}|\,|\sin(\angle x_p Q_1 Q_2)| = |\underline{Q_1 Q_2}|\,|z'|. \qquad (5.26)$$

Thus

$$|z'| = |d_i| = \frac{|\underline{Q_1 Q_2} \times \underline{Q_1 x_p}|}{|\underline{Q_1 Q_2}|} = |\underline{e}_l \times \underline{Q_1 x_p}|. \qquad (5.27)$$

Similarly, from dot product of the two vectors

$$\underline{Q_1 Q_2} \cdot \underline{Q_1 x_p} = |\underline{Q_1 Q_2}|\,|\underline{Q_1 x_p}|\,\cos(\angle x_p Q_1 Q_2) = |\underline{Q_1 Q_2}|\,x'. \qquad (5.28)$$

Then

$$x' = \underline{e}_l \cdot \underline{Q}_1 x_p. \tag{5.29}$$

Now the basic integrals can be expressed in terms of x' and z'. For simplicity, we drop the prime $(\prime)$ in x' and z' in the following analysis. [6]

(1) For the integral $I_1 = \int_0^l \frac{1}{r} \, d\xi$,

$$
\begin{aligned}
I_1 &= \int_0^l \frac{1}{\sqrt{(x-\xi)^2 + z^2}} \, d\xi = \int_0^l \frac{1}{\sqrt{\xi^2 - 2x\xi + x^2 + z^2}} \, d\xi \\
&= \ln \left\{ 2\sqrt{(\xi - x)^2 + z^2} + 2(\xi - x) \right\} \Big|_0^l \\
&= \ln \frac{\sqrt{(l-x)^2 + z^2} + l - x}{\sqrt{x^2 + z^2} - x} \\
&\left(\text{or,} \quad I_1 = \ln \frac{\sqrt{x^2 + z^2} + x}{\sqrt{(l-x)^2 + z^2} - (l-x)} \right)
\end{aligned}
\tag{5.30}
$$

This expression also includes the cases of $z = 0$.

(2) For the integral $I_2 = \int_0^l \frac{1}{r+a} \, d\xi = \int_0^l \frac{1}{\sqrt{(x-\xi)^2 + z^2} + a} \, d\xi$, change the integration variable ξ into $t = \sqrt{(x-\xi)^2 + z^2} + a$. Then $d\xi = \frac{\sqrt{(x-\xi)^2 + z^2}}{\xi - x} \, dt$. Consider three cases for the sign of the denominator $\xi - x$.

(a) When $\xi - x \geq 0$ in the entire interval $[0, l]$ (i.e., $x \leq 0$), $d\xi = \frac{t-a}{\sqrt{(t-a)^2 - z^2}} \, dt$. With the new integration limits $A = \sqrt{x^2 + z^2} + a$ and $B = \sqrt{(l-x)^2 + z^2} + a$,

$$
\begin{aligned}
I_2 &= \int_A^B \frac{t-a}{t\sqrt{t^2 - 2at + a^2 - z^2}} \, dt \\
&= \int_A^B \frac{1}{\sqrt{t^2 - 2at + a^2 - z^2}} \, dt - a \int_A^B \frac{1}{t\sqrt{t^2 - 2at + a^2 - z^2}} \, dt
\end{aligned}
$$

---

[6] For integral formulas, refer to Gradshteyn, I. S. and Ryzhik, I. M. (1965), *Table of Integrals, Series and Products*, Academic Press, Inc., New York and London, pp. 68, 81, 84.

Namely,

$$
\begin{aligned}
I_2 \;=\;& \ln\left\{2\sqrt{(t-a)^2-z^2}+2(t-a)\right\}\Big|_A^B \\[2mm]
& -a\frac{1}{\sqrt{z^2-a^2}}\;\arcsin\left\{\frac{2(a^2-z^2)-2\,a\,t}{t\sqrt{4\,z^2}}\right\}\Big|_A^B,
\end{aligned}
$$

or

$$
\begin{aligned}
I_2 \;=\;& \ln\left\{\frac{\sqrt{(l-x)^2+z^2}+(l-x)}{\sqrt{x^2+z^2}-x}\right\}-\frac{a}{\sqrt{z^2-a^2}}\;\cdot \\[2mm]
& \cdot\left[\arcsin\left\{\frac{-z^2-a\sqrt{(l-x)^2+z^2}}{|z|(\sqrt{(l-x)^2+z^2}+a)}\right\}\right. \\[2mm]
& \left. -\arcsin\left\{\frac{-z^2-a\sqrt{x^2+z^2}}{|z|(\sqrt{x^2+z^2}+a)}\right\}\right]
\end{aligned}
\qquad (5.31)
$$

(b) When $\xi-x\le 0$ in the entire interval $[0,l]$ (i.e., $x\ge l$), $d\xi=-\dfrac{t-a}{\sqrt{(t-a)^2-z^2}}\,dt$.

$$
\begin{aligned}
I_2 \;=\;& -\int_A^B\frac{t-a}{t\sqrt{t^2-2at+a^2-z^2}}\,dt \\[2mm]
\;=\;& -\int_A^B\frac{1}{\sqrt{t^2-2at+a^2-z^2}}\,dt+\int_A^B\frac{a}{t\sqrt{t^2-2at+a^2-z^2}}\,dt
\end{aligned}
$$

$$
\begin{aligned}
I_2 \;=\;& \ln\left\{\frac{\sqrt{(l-x)^2+z^2}+(l-x)}{\sqrt{x^2+z^2}-x}\right\}+\frac{a}{\sqrt{z^2-a^2}}\;\cdot \\[2mm]
& \cdot\left[\arcsin\left\{\frac{-z^2-a\sqrt{(l-x)^2+z^2}}{|z|(\sqrt{(l-x)^2+z^2}+a)}\right\}\right. \\[2mm]
& \left. -\arcsin\left\{\frac{-z^2-a\sqrt{x^2+z^2}}{|z|(\sqrt{x^2+z^2}+a)}\right\}\right]
\end{aligned}
\qquad (5.32)
$$

(c) When $0<x<l$, the integration interval is divided into two parts to

apply the above two cases:

$$I_2 = \int_0^l \frac{1}{r+a} \, d\xi$$

$$= \int_0^x \frac{1}{\sqrt{(x-\xi)^2 + z^2} + a} \, d\xi + \int_x^l \frac{1}{\sqrt{(x-\xi)^2 + z^2} + a} \, d\xi$$

$$I_2 = -\left[\ln\left\{ 2\sqrt{(t-a)^2 - z^2} + 2(t-a) \right\} \Big|_A^{|z|+a} \right.$$

$$\left. -a \frac{1}{\sqrt{z^2 - a^2}} \arcsin\left\{ \frac{2(a^2 - z^2) - 2at}{t\sqrt{4z^2}} \right\} \Big|_A^{|z|+a} \right]$$

$$+ \ln\left\{ 2\sqrt{(t-a)^2 - z^2} + 2(t-a) \right\} \Big|_{|z|+a}^A$$

$$-a \frac{1}{\sqrt{z^2 - a^2}} \arcsin\left\{ \frac{2(a^2 - z^2) - 2at}{t\sqrt{4z^2}} \right\} \Big|_{|z|+a}^A$$

Finally, we have

$$I_2 = \ln\left\{ \frac{\sqrt{(l-x)^2 + z^2} + (l-x)}{\sqrt{x^2 + z^2} - x} \right\} - \frac{a}{\sqrt{z^2 - a^2}} \cdot$$

$$\cdot \left[\pi + \arcsin\left\{ \frac{-z^2 - a\sqrt{(l-x)^2 + z^2}}{|z|(\sqrt{(l-x)^2 + z^2} + a)} \right\} \right.$$

$$\left. + \arcsin\left\{ \frac{-z^2 - a\sqrt{x^2 + z^2}}{|z|(\sqrt{x^2 + z^2} + a)} \right\} \right] \tag{5.33}$$

If $z^2 = a^2$, the integral should be performed by the simplified form;

$$I_2 = \ln\left\{ \frac{\sqrt{(l-x)^2 + z^2} + (l-x)}{\sqrt{x^2 + z^2} - x} \right\}$$

$$- \left\{ \frac{l-x}{\sqrt{(l-x)^2 + z^2} + a} + \frac{x}{\sqrt{x^2 + z^2} + a} \right\} \tag{5.34}$$

(3) For the integral $I_3 = \int_0^l \dfrac{1}{r(r+a)}\, d\xi$, take partial fraction to use the preceding results:

$$I_3 = \frac{1}{a} \int_0^l \left(\frac{1}{r} - \frac{1}{r+a} \right) d\xi = \frac{1}{a}(I_1 - I_2) \qquad (5.35)$$

But if $a = 0$ for which this expression is not valid, another form should be performed;

$$
\begin{aligned}
I_3 &= \int_0^l \frac{1}{(x-\xi)^2 + z^2}\, d\xi = \int_0^l \frac{1}{\xi^2 - 2x\xi + x^2 + z^2}\, d\xi \\
&= \frac{1}{|z|} \arctan\left(\frac{\xi - x}{|z|} \right) \Big|_0^l = \frac{1}{|z|} \left(\arctan \frac{l-x}{|z|} + \arctan \frac{x}{|z|} \right)
\end{aligned}
$$
$$(5.36)$$

Furthermore if $a = 0$ and $z = 0$, then

$$I_3 = \int_0^l \frac{1}{(x-\xi)^2}\, d\xi = \frac{1}{x-l} - \frac{1}{x}. \qquad (5.37)$$

(4) For the integral $I_4 = \int_0^l \dfrac{1}{r^3}\, d\xi$,

$$
\begin{aligned}
I_4 &= \int_0^l \frac{1}{\sqrt{(x-\xi)^2 + z^2}^3}\, d\xi = \frac{\xi - x}{z^2 \sqrt{(x-\xi)^2 + z^2}} \Bigg|_0^l \\
&= \frac{1}{z^2} \left\{ \frac{l-x}{\sqrt{(l-x)^2 + z^2}} + \frac{x}{\sqrt{x^2 + z^2}} \right\}
\end{aligned}
$$
$$(5.38)$$

If $z = 0$, it should be replaced by

$$
I_4 = \int_0^l \frac{1}{|x-\xi|^3}\, d\xi =
\begin{cases}
+\dfrac{1}{2}\left\{ \dfrac{1}{(l-x)^2} - \dfrac{1}{x^2} \right\} & \text{when } x > l \\[3mm]
-\dfrac{1}{2}\left\{ \dfrac{1}{(l-x)^2} - \dfrac{1}{x^2} \right\} & \text{when } x < 0
\end{cases}
\qquad (5.39)
$$

When the inverse trigonometric functions are implemented in the computational algorithm, their values are evaluated in the interval $[-\pi/2, \pi/2]$ without considering the separate arguments of the functions.

5.3.6   Test calculations for constant distributions

A planar rectangular element of 12×1 is adopted for test calculations herein. It may be assumed that the element is in the plane $z = 0$ with the four vertices located at $(0, 0, 0)$,$(1, 0, 0)$, $(1, 12, 0)$,$(0, 12, 0)$, respectively. To check a sensitivity of the calculation, we take various field points in the vicinity of the element surface or one vertex. The coordinates of the field points are, with labelling, $P1(0.5, 6, 0)$, $P2(0.5, 6, +0.00001)$, $P3(0.5, 6, -0.00001)$, $P4(0, -0.00001, 0)$, $P5(0, 0, +0.00001)$ and $P6(0, 0, -0.00001)$. The points $P1, P2$ and $P3$ are on, just above and below, respectively, of the centroid of the element and $P4, P5$ and $P6$ are points very near one vertex of the origin. The constant densities of source and doublet distributions are taken with 1, (i.e., $\sigma = 1, \mu = -\phi = 1$).

First we will compare numerical integrations and analytical evaluations of the basic integrals described in the preceding subsection. At the field point E, the evaluations are compared in Table **5.1**. The influences of the basic integrals at the field points by the respective sides of the element are listed. The side 1 denotes the line between the vertices $(0, 0, 0)$ and $(1, 0, 0)$ and the other sides are numbered in a counterclockwise order in a similar way. In the numerical calculations, the Gaussian quadrature is used with various quadrature-base points to show numerical convergence. It is seen that for a field point having a numerically singular behavior in line integral, a large number of quadrature-base points are required to reach the same order as the analytical evaluations. It results in large computing time undesirably.

The numerical and analytical evaluations for the induced velocities and potentials at the selected field points due to the uniform source and doublet distributions over the rectangular element are compared in Table **5.2**.

Table 5.1 Comparison of the Basic Integrals by Analytic and Numerical Calculation at Point $P5(0.0,\ 0.0,\ +0.00001)$.

	Side	Gaussian-Quadrature Points, $N=$				Analytic
		20	100	500	2500	
$\int \frac{1}{r}\, d\xi$	1	.7195E+01	.1037E+02	.1224E+02	.1221E+02	.1221E+02
	2	.3180E+01	.3180E+01	.3180E+01	.3180E+01	.3180E+01
	3	.8324E-01	.8324E-01	.8324E-01	.8324E-01	.8324E-01
	4	.7195E+01	.1037E+02	.1356E+02	.1469E+02	.1469E+02
$\int \frac{1}{(r+a)}\, d\xi$	1	.7187E+01	.1018E+02	.1121E+02	.1121E+02	.1121E+02
	2	.3180E+01	.3180E+01	.3180E+01	.3180E+01	.3180E+01
	3	.8324E-01	.8324E-01	.8324E-01	.8324E-01	.8324E-01
	4	.7195E+01	.1036E+02	.1320E+02	.1369E+02	.1369E+02
$\int \frac{1}{r(r+a)}\, d\xi$	1	.8378E+03	.1893E+05	.1025E+06	.1000E+06	.1000E+06
	2	.1488E+01	.1488E+01	.1488E+01	.1488E+01	.1488E+01
	3	.6928E-02	.6928E-02	.6928E-02	.6928E-02	.6928E-02
	4	.6998E+02	.1674E+04	.3636E+05	.9987E+05	.1000E+06
$\int \frac{1}{r^3}\, d\xi$	1	.2211E+06	.1266E+09	.1084E+11	.1000E+11	.1000E+11
	2	.9965E+00	.9965E+00	.9965E+00	.9965E+00	.9965E+00
	3	.5767E-03	.5767E-03	.5767E-03	.5767E-03	.5767E-03
	4	.1536E+04	.8856E+06	.5284E+09	.1004E+11	.1000E+11

Table 5.2 Comparison of Potentials and Velocities by Analytic and Numerical Calculation at Point $P2(0.5,\ 6.0,\ +0.00001)$.

	Gaussian-Quadrature Points, $N=$				Analytic
	20	100	500	2500	
$\phi^{(\sigma)}$	-0.6583E+00	-0.6650E+00	-0.6650E+00	-0.6650E+00	-0.6650E+00
$q_x^{(\sigma)}$	0.0000E+00	0.0000E+00	0.0000E+00	0.0000E+00	0.0000E+00
$q_y^{(\sigma)}$	0.0000E+00	0.0000E+00	0.0000E+00	0.0000E+00	0.0000E+00
$q_z^{(\sigma)}$	0.4681E+00	0.5000E+00	0.5000E+00	0.5000E+00	0.5000E+00
$\phi^{(\mu)}$	-0.4681E+00	-0.5000E+00	-0.5000E+00	-0.5000E+00	-0.5000E+00
$q_x^{(\mu)}$	0.5371E-21	0.2791E-22	0.5166E-21	0.3339E-21	-0.2264E-21
$q_y^{(\mu)}$	-0.5143E-25	0.2006E-25	0.2288E-25	0.2600E-24	0.2309E-24
$q_z^{(\mu)}$	0.5366E+00	0.6388E+00	0.6388E+00	0.6388E+00	0.6388E+00

5.3.7   Extension to linear distributions

The preceding analysis can be extended to include a linear distribution of sources and dipoles on each panel. In order to determine the distribution function uniquely, we take only three points (that are not collinear) of a polygon. Therefore we consider a triangular element of a linear source distribution herein. For the doublet distribution, the following procedure can be applied in a similar manner. A form of the linear varying source strength is specified as

$$\sigma(x, y, z) = A\,x + B\,y + C\,z + D \tag{5.40}$$

The coefficients A, B, C and D are determined from the singularity strength values at the vertices.

Define the unit directional vectors of the respective sides (of length l_i) of the element by $\underline{e}_{l_i}, (i = 1, 2, 3)$ and the vertex positions by (x_i, y_i, z_i). From elementary geometry for a corresponding linear source (or doublet) distribution, we can form a linear equation system for A, B and C;

$$\nabla\sigma\cdot\underline{e}_{l_i} \equiv \frac{\sigma_{i+1} - \sigma_i}{l_i} = \frac{A(x_{i+1} - x_i) + B(y_{i+1} - y_i) + C(z_{i+1} - z_i)}{l_i}, \quad i = 1, 2, 3 \tag{5.41}$$

Here the vertices and sides are defined in a counterclockwise sense and the index 4 corresponds to 1. By the Cramer's rule, A, B, C and D are determined ;

$$
\begin{aligned}
A &= \det\ (\sigma_i - \sigma_{i+1}, y_i - y_{i+1}, z_i - z_{i+1})/\triangle, & (5.42)\\
B &= \det\ (x_i - x_{i+1}, \sigma_i - \sigma_{i+1}, z_i - z_{i+1})/\triangle, & (5.43)\\
C &= \det\ (x_i - x_{i+1}, y_i - y_{i+1}, \sigma_i - \sigma_{i+1})/\triangle, & (5.44)\\
D &= \sigma_1 - (A\,x_1 + B\,y_1 + C\,z_1) & (5.45)
\end{aligned}
$$

where det $(\cdots)$ denotes the determinant of a matrix and $\triangle = \det\ (x_i - x_{i+1}, y_i - y_{i+1}, z_i - z_{i+1})$. For a given distribution shape, we can sum up the contribution of the associated line integrals for each side, as in the constant distribution cases. In the linear variation cases, additionally there are integral forms to be

evaluated:

$$\int_0^l \frac{\xi}{r}\,d\xi, \quad \int_0^l \frac{\xi}{r+a}\,d\xi, \quad \int_0^l \frac{\xi}{r(r+a)}\,d\xi, \quad \int_0^l \frac{\xi}{r^3}\,d\xi,$$

$$\int_0^l r\,d\xi, \quad \int_0^l \ln r\,d\xi, \quad \int_0^l \ln(r+a)\,d\xi. \tag{5.46}$$

These integrals are performed without explicit representation in the following manner, by referring to the integrals described in the preceding section and to some of integral formulas in Gradshteyn & Ryzhik (1965). [7]

(1) For $J_1 = \displaystyle\int_0^l \frac{\xi}{r}\,d\xi$,

$$J_1 = \int_0^l \frac{\xi - x + x}{\sqrt{(x-\xi)^2 + z^2}}\,d\xi = \left.\sqrt{(\xi-x)^2 + z^2}\,\right|_0^l + x\,I_1 \tag{5.47}$$

(2) For $J_2 = \displaystyle\int_0^l \frac{\xi}{r+a}\,d\xi$,

$$\begin{aligned}
J_2 &= \int_0^l \frac{\xi - x + x}{\sqrt{(x-\xi)^2 + z^2} + a}\,d\xi \\
&= \left.\sqrt{(x-\xi)^2 + z^2} - a\ln\left\{\sqrt{(x-\xi)^2 + z^2} + a\right\}\right|_0^l + x\,I_2
\end{aligned} \tag{5.48}$$

Here we have changed the integration variable: $t = \sqrt{(x-\xi)^2 + z^2} + a$.

(3) For $J_3 = \displaystyle\int_0^l \frac{\xi}{r(r+a)}\,d\xi$,

$$\begin{aligned}
J_3 &= \frac{1}{a}\int_0^l \left(\frac{\xi}{r} - \frac{\xi}{r+a}\right)\,d\xi = \frac{1}{a}(J_1 - J_2) \\
&= \left.\ln\left\{\sqrt{(x-\xi)^2 + z^2} + a\right\}\right|_0^l + x\,I_3
\end{aligned} \tag{5.49}$$

[7]Gradshteyn, I. S. and Ryzhik, I. M. (1965), *Table of Integrals, Series and Products*, Academic Press, Inc., New York and London.

But if $a = 0$ for which this expression is not valid, other form should be performed;

$$
\begin{aligned}
J_3 &= \int_0^l \frac{\xi}{r^2} \, d\xi = \int_0^l \frac{\xi - x + x}{(x - \xi)^2 + z^2} \, d\xi \\
&= \frac{1}{2} \ln \left\{ (\xi - x)^2 + z^2 \right\} \big|_0^l + x \int_0^l \frac{1}{r^2} \, d\xi \qquad (5.50)
\end{aligned}
$$

The last integral has been already considered in the preceding section as the special case of the integral I_3.

(4) For $J_4 = \int_0^l \frac{\xi}{r^3} \, d\xi$,

$$
J_4 = \int_0^l \frac{\xi - x + x}{\sqrt{(x - \xi)^2 + z^2}^3} \, d\xi = -\frac{1}{\sqrt{(x - \xi)^2 + z^2}} \bigg|_0^l + x \, I_4 \qquad (5.51)
$$

(5) For $J_5 = \int_0^l r \, d\xi$,

$$
J_5 = \int_0^l \sqrt{(x - \xi)^2 + z^2} \, d\xi = \frac{1}{2} (\xi - x) \sqrt{(\xi - x)^2 + z^2} \bigg|_0^l + \frac{1}{2} z^2 \, I_1
$$
$$
(5.52)
$$

(6) For $J_6 = \int_0^l \ln r \, d\xi$,

$$
\begin{aligned}
J_6 &= \frac{1}{2} \int_0^l \ln \left\{ (x - \xi)^2 + z^2 \right\} \, d\xi \\
&= \frac{1}{2} \left[(\xi - x) \ln \left\{ (\xi - x)^2 + z^2 \right\} - 2\xi + 2|z| \arctan \left(\frac{\xi - x}{|z|} \right) \right] \bigg|_0^l
\end{aligned}
$$
$$
(5.53)
$$

(7) For $J_7 = \int_0^l \ln(r + a) \, d\xi$, take an integration by parts and then the same

procedure as I_2:

$$
\begin{aligned}
J_7 &= \int_0^l \ln\left\{\sqrt{(x-\xi)^2 + z^2} + a\right\} d\xi \\
&= (\xi - x)\,\ln(\sqrt{(x-\xi)^2 + z^2} + a) - \xi \\
&\quad + a\,\ln(\xi - x + \sqrt{(x-\xi)^2 + z^2}) \\
&\quad + \sqrt{z^2 - a^2}\,\arcsin\left\{\frac{-z^2 - a\sqrt{(\xi - x)^2 + z^2}}{|z|(\sqrt{(\xi - x)^2 + z^2} + a)}\right\}\Bigg|_0^l \quad (5.54)
\end{aligned}
$$

5.4 Bilinear Source and Doublet Distribution

5.4.1 Introduction

This section deals with evaluations of the surface integrals in the potential-based panel method, associated with bilinear density distributions of source and/or doublet singularities over a planar panel. The surface integrals can be transformed into contour integrals by using Stokes' formulas after simple manipulation on the integrands. We also present the closed-forms for obtaining the induced potentials and velocities due to those singularity distributions over a polygon panel.

5.4.2 Transformation of the surface integrals for Stokes' theorem

Without loss of generality we will consider the domain of one planar panel for the integration region as a part of the discretized boundary surface in Eq. (5.3). We take an orthogonal coordinate system (ξ, η, ζ) to specify a bilinear form, such that the panel is in the plane $\zeta = 0$ and the direction of ζ-axis is the same as that of the unit normal vector ($\underline{n}$) of the panel, as shown in Figure **5.3**. The unit vectors in the direction of ξ-axis and η-axis are denoted by $\underline{e}_\xi$ and $\underline{e}_\eta$, respectively. These two axes may be chosen arbitrarily in the directions but lying on the panel surface. The coordinates (x, y, z) of the field point $\underline{x}_p$ are relatively measured from the origin of the coordinate system.
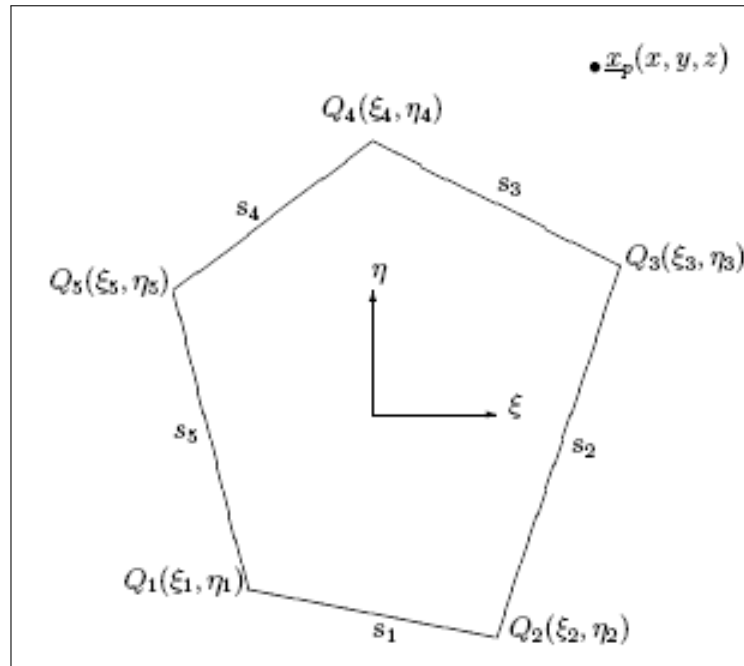
Figure **5.3** A planar panel defined in a local coordinate system. The present derivation can be applied to arbitrary polygons. A pentagon is taken with no loss of generality.

The potentials and the velocities at a field point $\underline{x}_p(x, y, z)$ induced by a bilinear source distribution $\sigma = a_0 + a_1 \xi + a_2 \eta + a_3 \xi \eta$ and by a doublet distribution $\mu = b_0 + b_1 \xi + b_2 \eta + b_3 \xi \eta$, respectively, can be written as,

$$
\begin{aligned}
\phi^{(\sigma)} = -\frac{1}{4\pi} &\left[(a_0 + a_1\,x + a_2\,y + a_3\,x\,y) \int_S \frac{1}{r}\,dS \right. \\
&+ (a_1 + a_3\,y) \int_S \frac{\xi - x}{r}\,dS + (a_2 + a_3\,x) \int_S \frac{\eta - y}{r}\,dS \\
&+ a_3 \int_S \frac{(\xi - x)(\eta - y)}{r}\,dS \Bigg]
\end{aligned} \tag{5.55}
$$

$$
\begin{aligned}
\underline{q}^{(\sigma)} = +\frac{1}{4\pi} &\left[(a_0 + a_1\,x + a_2\,y + a_3\,x\,y) \int_S \nabla\left(\frac{1}{r}\right) dS \right. \\
&+ (a_1 + a_3\,y) \int_S (\xi - x)\nabla\left(\frac{1}{r}\right) dS \\
&+ (a_2 + a_3\,x) \int_S (\eta - y)\nabla\left(\frac{1}{r}\right) dS \\
&+ a_3 \int_S (\xi - x)(\eta - y)\nabla\left(\frac{1}{r}\right) dS \Bigg]
\end{aligned} \tag{5.56}
$$

$$
\begin{aligned}
\phi^{(\mu)} &= -\frac{1}{4\pi}\underline{n}\cdot\left[(b_0 + b_1\,x + b_2\,y + b_3\,x\,y)\int_S \nabla\left(\frac{1}{r}\right)\,dS\right.\\
&\quad + (b_1 + b_3\,y)\int_S (\xi - x)\nabla\left(\frac{1}{r}\right)\,dS \\
&\quad + (b_2 + b_3\,x)\int_S (\eta - y)\nabla\left(\frac{1}{r}\right)\,dS \\
&\quad \left. + b_3\int_S (\xi - x)\,(\eta - y)\nabla\left(\frac{1}{r}\right)\,dS\right] \qquad (5.57)\\
\underline{q}^{(\mu)} &= -\frac{1}{4\pi}\left\{\oint_C \mu\nabla\left(\frac{1}{r}\right)\times d\underline{l}_\xi + \int_S (\underline{n}\times\nabla\mu)\times\nabla\left(\frac{1}{r}\right)\,dS)\right\}\\
&= -\frac{1}{4\pi}\left[\oint_C (b_0 + b_1\,\xi + b_2\,\eta + b_3\,\xi\,\eta)\nabla\left(\frac{1}{r}\right)\times d\underline{l}\right.\\
&\quad + \int_S \left[\{b_1 + b_3\,y + b_3\,(\eta - y)\}\,\underline{e}_\eta\right.\\
&\quad \left.\left. - \{b_2 + b_3\,x + b_3\,(\xi - x)\}\,\underline{e}_\xi\right]\times\nabla\left(\frac{1}{r}\right)\,dS\right] \qquad (5.58)
\end{aligned}
$$

Here Eq. (5.58) has been expressed in the form of the vortex distribution equivalent to the doublet distribution (Lee, J. T. (1987), Brockett (1988)). [8]

In the case of a bilinear singularity distribution, eight different integrands are involved in the surface integrals in Eq. (5.3), which will be described later on. For use of Stokes' formulas, all integrands are changed into equivalent ones either in curl-forms of a vector or in cross product-forms of a vector with the normal $\underline{n}$ as follows:

$$
\frac{1}{r} = \underline{e}\cdot(\nabla\times\underline{B}), \quad \text{with} \quad \underline{B} = \frac{\underline{e}\times\underline{r}}{r + \underline{e}\cdot\underline{r}} \qquad (5.59)
$$

$$
\frac{\xi - x}{r} = \underline{e}_\eta\cdot(\underline{n}\times\nabla r) \qquad (5.60)
$$

$$
\frac{\eta - y}{r} = -\underline{e}_\xi\cdot(\underline{n}\times\nabla r) \qquad (5.61)
$$

$$
\frac{(\xi - x)\,(\eta - y)}{r} = \underline{e}_\eta\cdot[\underline{n}\times\nabla\{(\eta - y)\,r\}] \qquad (5.62)
$$

[8]Lee, J. T. (1987), *A Potential Based Panel Method for the Analysis of Marine Propellers in Steady Flow*, PhD. thesis, Department of Ocean Engineering, MIT, Report no. 87-13.
Brockett, T. E. (1988), *NA 520 Lecture Notes*, (unpublished), Department of Naval Architecture and Marine Engineering, University of Michigan.

$$\nabla\left(\frac{1}{r}\right) = -\nabla \times \underline{A}, \quad \text{with} \quad \underline{A} = \frac{\underline{e} \times \underline{r}}{r(r + \underline{e} \cdot \underline{r})} \quad (5.63)$$

$$(\xi - x)\nabla\left(\frac{1}{r}\right) = \left[\underline{e}_\eta \cdot \left\{\underline{n} \times \nabla\left(\frac{\xi - x}{r}\right)\right\} - \frac{1}{r}\right]\underline{e}_\xi$$

$$- \left[\underline{e}_\xi \cdot \left\{\underline{n} \times \nabla\left(\frac{\xi - x}{r}\right)\right\}\right]\underline{e}_\eta$$

$$- z\left[\underline{e}_\eta \cdot \left\{\underline{n} \times \nabla\left(\frac{1}{r}\right)\right\}\right]\underline{n} \quad (5.64)$$

$$(\eta - y)\nabla\left(\frac{1}{r}\right) = \left[\underline{e}_\eta \cdot \left\{\underline{n} \times \nabla\left(\frac{\eta - y}{r}\right)\right\}\right]\underline{e}_\xi$$

$$- \left[\underline{e}_\xi \cdot \left\{\underline{n} \times \nabla\left(\frac{\eta - y}{r}\right)\right\} + \frac{1}{r}\right]\underline{e}_\eta$$

$$+ z\left[\underline{e}_\xi \cdot \left\{\underline{n} \times \nabla\left(\frac{1}{r}\right)\right\}\right]\underline{n} \quad (5.65)$$

$$(\xi - x)(\eta - y)\nabla\left(\frac{1}{r}\right) = -\underline{e}_\xi \cdot \left[\underline{n} \times \nabla\left\{\frac{(\xi - x)^2}{r}\right\}\right]\underline{e}_\xi$$

$$- \underline{e}_\eta \cdot \left[\underline{n} \times \nabla\left\{\frac{(\eta - y)^2}{r}\right\}\right]\underline{e}_\eta$$

$$+ z\,\underline{e}_\xi \cdot \left[\underline{n} \times \nabla\left\{\frac{(\xi - x)}{r}\right\}\right]\underline{n} \quad (5.66)$$

Equations (5.59) and (5.63) have been introduced by Suh (1992) and Guiraud (1978), respectively, [9] which can be also derived by direct manipulation with starting from the right sides. Of course, these two relations can be simply used if one wants to compute the induced potentials and velocities due to the constant source and doublet distributions.

In the constant distribution cases, although the results are consistent, the present approach using these key relations is considered simpler than those presented by Newman (1986) and by Cantaloube & Rehbach (1986). [10] The re-

---

[9]Suh, J.-C. (1992a), "Analytical evaluation of the surface integral in the singularity methods," *Trans. Soc. Naval Arch. Korea*, vol. 29, no. 1, pp. 1–17.
Guiraud, J. P. (1978), "Potential of velocities generated by a localized vortex distribution," *Aerospace Research*, English Translation-ESA-TT-560, pp. 105–107.
[10]Newman, J. N. (1986), "Distributions of sources and normal dipoles over a quadrilateral panel," *J. Eng. Math.*, vol. 20, pp. 113–126.
Cantaloube, B. and Rehbach, C. (1986), "Calcul des Integrales de la Methode des Singularites," *Recherche Aerospatiale*, n° 1, pp. 15–22, English Title: "Calculation of the integrals of the singularity method," *Aerospace*

maining equations have been derived by a similar deduction, under hypothesis of planarity of the panel. The distance vector $\underline{r}$ is defined as $\underline{x}_\xi - \underline{x}_p$ where the subscripts ξ and p refer to the source point and the field point respectively. While Eqs. (5.59) and (5.63) hold for any $\underline{e}$ independent of the integration point $\underline{x}_\xi$ more generally, the unit vector $\underline{e}$ is taken as $\pm \underline{n}$ for application of Stokes' transformation, where the sign is chosen such that $\underline{e} \cdot \underline{r}$ is not negative.

Using Stokes' formulas of the surface integrals with the alternative forms for a polygon panel, we can express the surface integrals as a sum of the associated line integrals for each side of the panel with independent treatment of the contribution from the side. Each contribution can be written as closed-forms in term of only the geometrical parameters of the side as described in the following section.

5.4.3 Induced potential due to source distribution

The potential at a field point $\underline{x}_p(x, y, z)$ induced by a bilinear source distribution $\sigma = a_0 + a_1\xi + a_2\eta + a_3\xi\eta$, Eq. (5.55) can be written as,

$$
\begin{aligned}
\phi^{(\sigma)} &= -\frac{1}{4\pi} \int_S \frac{\sigma}{r}\, dS \\
&= -\frac{1}{4\pi} \int_S \left\{ c_1 \frac{1}{r} + c_2 \frac{\xi - x}{r} + c_3 \frac{\eta - y}{r} + c_4 \frac{(\xi - x)(\eta - y)}{r} \right\} dS
\end{aligned}
\tag{5.67}
$$

where for shortness of expressions we have defined the constants $c_1 = a_0 + a_1 x + a_2 y + a_3 x y$, $c_2 = a_1 + a_3 y$, $c_3 = a_2 + a_3 x$, $c_4 = a_3$. Using Eq. (5.59) through Eq. (5.63) for the corresponding integrands and then performing Stokes' transformations, we can write Eq. (5.67) as, in terms of line integrals,

$$
\begin{aligned}
\phi^{(\sigma)} &= -\frac{1}{4\pi} \left[c_1 \oint_C \frac{\underline{r} \cdot (d\underline{l} \times \underline{n})}{r + \underline{e} \cdot \underline{r}} + c_2\, \underline{e}_\eta \cdot \oint_C r\, d\underline{l} - c_3\, \underline{e}_\xi \cdot \oint_C r\, d\underline{l} \right. \\
&\qquad\qquad \left. + c_4\, \underline{e}_\eta \cdot \oint_C (\eta - y)\, r\, d\underline{l} \right]
\end{aligned}
\tag{5.68}
$$

Research, no. 1, pp. 15–22.

The term $\underline{r} \cdot (d\underline{l} \times \underline{n})/dl$ represents the projection of the distance vector $\underline{r}$ onto the vector perpendicular to both $d\underline{l}$ and $\underline{n}$. Because it is constant for each side of a straight-line and $\underline{e} \cdot \underline{r}$ ($\equiv a$, that is, the normal distance of the field point from the panel) is a non-negative constant for all sides of the planar panel, Eq. (5.68) can be written as

$$
\phi^{(\sigma)} = -\frac{1}{4\pi} \sum_{i=1}^{N_S} \left[c_1 \, t_i \int_{C_i} \frac{1}{r+a} \, dl + c_2 \, v_i \int_{C_i} r \, dl - c_3 \, u_i \int_{C_i} r \, dl \right.
$$
$$
\left. + c_4 \, v_i \int_{C_i} (\eta - y) \, r \, dl \right] \tag{5.69}
$$

The index i denotes the integer for identification of the side concerned, N_S is the number of sides of the polygon panel (e.g., $N_S = 3$ for triangular panels), $t_i = \underline{r} \cdot (\underline{e}_{l_i} \times \underline{n})$, $u_i = \underline{e}_\xi \cdot \underline{e}_{l_i}$ and $v_i = \underline{e}_\eta \cdot \underline{e}_{l_i}$. The directional vector $\underline{e}_{l_i} = d\underline{l}/dl$ is chosen in a counterclockwise direction as the convention of the contour integral. Rewriting the last integral in Eq. (5.69) in terms of the local coordinates of the nodes, we finally obtain the expression for the source-induced potential:

$$
\boxed{
\begin{aligned}
\phi^{(\sigma)} = -\frac{1}{4\pi} \sum_{i=1}^{N_S} \left[c_1 \, t_i \int_{C_i} \frac{1}{r+a} \, dl + c_2 \, v_i \int_{C_i} r \, dl - c_3 \, u_i \int_{C_i} r \, dl \right. \\
\left. + c_4 \, v_i \, (\eta_i - y) \int_{C_i} r \, dl + c_4 \, v_i^2 \int_{C_i} l \, r \, dl \right]
\end{aligned}
} \tag{5.70}
$$

Here l is the integral variable representing the arc-length along the straight-line of each integration path C_i. The vertices composed of the panel (ξ_i, η_i) and the sides are also defined in a counterclockwise order. It is seen that the integral term for each side is related to the relative position of the field point from the side. Each integral, as will be shown, depends only on the coordinates of the two end points of the corresponding side. Equation (5.70) can be directly used even in the cases of that the field points are just at the panel surface (i.e., in the self-induction cases), by setting $a = 0$ in Eq. (5.70) since $\underline{n} \cdot \underline{r} = 0$. Furthermore, when the field point is just at the side of the panel, the first term vanishes because t_i decays faster than the integral with r approaches zero, while the other terms have finite values.

5.4.4 Induced velocity due to source distribution

The source-induced velocity at the field point, Eq. (5.56) is expressed as

$$
\begin{aligned}
\underline{q}^{(\sigma)} &= +\frac{1}{4\pi} \int_S \sigma \nabla\left(\frac{1}{r}\right) dS \\
&= \frac{1}{4\pi}\left[c_1 \int_S \nabla\left(\frac{1}{r}\right) dS + c_2 \int_S (\xi - x)\nabla\left(\frac{1}{r}\right) dS \right. \\
&\qquad \left. + c_3 \int_S (\eta - y)\nabla\left(\frac{1}{r}\right) dS + c_4 \int_S (\xi - x)(\eta - y)\nabla\left(\frac{1}{r}\right) dS \right]
\end{aligned}
\tag{5.71}
$$

We rearrange the integrand of the first integral in Eq. (5.71):

$$
\nabla\left(\frac{1}{r}\right) = \underline{n}\left\{ \underline{n} \cdot \nabla\left(\frac{1}{r}\right) \right\} - \underline{n} \times \left\{ \underline{n} \times \nabla\left(\frac{1}{r}\right) \right\}
\tag{5.72}
$$

Like Eq. (5.67), using Eq. (5.63) through Eq. (5.66) and rearranging the resulting expressions give us the expression for the source-induced velocity:

$$
\begin{aligned}
\underline{q}^{(\sigma)} = \frac{1}{4\pi}\sum_{i=1}^{N_S} &\left[-c_1 \left\{ \underline{n}(\underline{n}\cdot\underline{e})\, t_i \int_{C_i} \frac{1}{r(r+a)}\, dl + \underline{e}_{m_i} \int_{C_i} \frac{1}{r}\, dl \right\} \right. \\
&+ c_2\, \underline{e}_\xi \left\{ v_i \left\{ (\xi_i - x)\int_{C_i}\frac{1}{r}\,dl + u_i\int_{C_i}\frac{l}{r}\,dl \right\} - t_i\int_{C_i}\frac{1}{r+a}\,dl \right\} \\
&+ c_2\, \underline{e}_\eta(-u_i)\left\{ (\xi_i - x)\int_{C_i}\frac{1}{r}\,dl + u_i\int_{C_i}\frac{l}{r}\,dl \right\} + c_2\,\underline{n}v_i(-z)\int_{C_i}\frac{1}{r}\,dl \\
&+ c_3\,\underline{e}_\xi\, v_i\left\{ (\eta_i - y)\int_{C_i}\frac{1}{r}\,dl + v_i\int_{C_i}\frac{l}{r}\,dl \right\} + c_3\,\underline{n}u_i z\int_{C_i}\frac{1}{r}\,dl \\
&+ c_3\,\underline{e}_\eta\left\{ -u_i\left\{ (\eta_i - y)\int_{C_i}\frac{1}{r}\,dl + v_i\int_{C_i}\frac{l}{r}\,dl \right\} - t_i\int_{C_i}\frac{1}{r+a}\,dl \right\} \\
&+ c_4\,\underline{e}_\xi(-u_i)\left\{ (\xi_i - x)^2\int_{C_i}\frac{1}{r}\,dl + 2(\xi_i - x)u_i\int_{C_i}\frac{l}{r}\,dl + u_i^2\int_{C_i}\frac{l^2}{r}\,dl \right\} \\
&+ c_4\,\underline{e}_\eta\, v_i\left\{ (\eta_i - y)^2\int_{C_i}\frac{1}{r}\,dl + 2(\eta_i - y)v_i\int_{C_i}\frac{l}{r}\,dl + v_i^2\int_{C_i}\frac{l^2}{r}\,dl \right\} \\
&\left. + c_4\,\underline{n}\, u_i\, z\left\{ (\xi_i - x)\int_{C_i}\frac{1}{r}\,dl + u_i\int_{C_i}\frac{l}{r}\,dl \right\} \right]
\end{aligned}
\tag{5.73}
$$

5.4.5 Induced potential and velocity due to doublet distribution

For a bilinear doublet distribution $\mu = b_0 + b_1\,\xi + b_2\,\eta + b_3\,\xi\,\eta$, the induced potentials and velocities can be obtained in a straight-forward manner similar to one in the case of the source distribution. The final results can be written as, for the induced potentials,

$$
\phi^{(\mu)} = -\frac{1}{4\pi}\sum_{i=1}^{N_S}\left[-d_1(\underline{n}\cdot\underline{e})\,t_i\int_{C_i}\frac{1}{r(r+a)}\,dl + d_2\,v_i(-z)\int_{C_i}\frac{1}{r}\,dl\right.
$$
$$
\left. +d_3\,u_i\,z\int_{C_i}\frac{1}{r}\,dl + d_4\,u_i\,z\left\{(\xi_i-x)\int_{C_i}\frac{1}{r}\,dl + u_i\int_{C_i}\frac{l}{r}\,dl\right\}\right] \quad (5.74)
$$

and, for the induced velocities,

$$
\underline{q}^{(\mu)} = \frac{1}{4\pi}\sum_{i=1}^{N_S}\left[(\underline{r}\times\underline{e}_{l_i})\left\{b_0\int_{C_i}\frac{1}{r^3}\,dl + b_1\left(\xi_i\int_{C_i}\frac{1}{r^3}\,dl + u_i\int_{C_i}\frac{l}{r^3}\,dl\right)\right.\right.
$$
$$
+b_2\left(\eta_i\int_{C_i}\frac{1}{r^3}\,dl + v_i\int_{C_i}\frac{l}{r^3}\,dl\right)
$$
$$
\left.+b_3\left(\xi_i\,\eta_i\int_{C_i}\frac{1}{r^3}\,dl + (\xi_i\,v_i + \eta_i\,u_i)\int_{C_i}\frac{l}{r^3}\,dl + u_i\,v_i\int_{C_i}\frac{l^2}{r^3}\,dl\right)\right\}
$$
$$
+d_2\left\{\underline{e}_\xi(\underline{n}\cdot\underline{e})\,t_i\int_{C_i}\frac{1}{r(r+a)}\,dl + (\underline{e}_\eta\times\underline{e}_{m_i})\int_{C_i}\frac{1}{r}\,dl\right\}
$$
$$
+d_3\left\{\underline{e}_\eta(\underline{n}\cdot\underline{e})\,t_i\int_{C_i}\frac{1}{r(r+a)}\,dl - (\underline{e}_\xi\times\underline{e}_{m_i})\int_{C_i}\frac{1}{r}\,dl\right\}
$$
$$
+d_4\left\{\underline{n}\left\{(v_i(\eta_i-y)-u_i(\xi_i-y))\int_{C_i}\frac{1}{r}\,dl + (v_i^2 - u_i^2)\int_{C_i}\frac{l}{r}\,dl\right\}\right.
$$
$$
\left.\left.-\underline{e}_\xi\,u_i\,z\int_{C_i}\frac{1}{r}\,dl + \underline{e}_\eta\,v_i\,z\int_{C_i}\frac{1}{r}\,dl\right\}\right] \quad (5.75)
$$

For shortness of expressions, we have also defined the constants $d_1 = b_0 + b_1\,x + b_2\,y + b_3\,x\,y$, $d_2 = b_1 + b_3\,y$, $d_3 = b_2 + b_3\,x$, $d_4 = b_3$. It is easily found that the expression for the induced potential $\phi^{(\mu)}$ has the same form as the normal component of $\underline{q}^{(\sigma)}$ except notation of the singularity distribution.

5.4.6   Closed-forms of the basic integrals

In the preceding subsections, we have expressed the induced potentials and velocities in forms of a sum of the more simplified line integral given in Eqs. (5.70), (5.73), (5.74) and (5.75). We will derive here closed-forms of the following line integrals involved in those expressions:

$$
I1_i = \int_{C_i} \frac{1}{r}\, dl, \quad I2_i = \int_{C_i} \frac{1}{r+a}\, dl, \quad I3_i = \int_{C_i} \frac{1}{r(r+a)}\, dl, \quad I4_i = \int_{C_i} \frac{1}{r^3}\, dl
$$

$$
J1_i = \int_{C_i} \frac{l}{r}\, dl, \quad J2_i = \int_{C_i} \frac{l}{r^3}\, dl, \quad\quad J3_i = \int_{C_i} r\, dl,
$$

$$
K1_i = \int_{C_i} \frac{l^2}{r}\, dl, \quad K2_i = \int_{C_i} lr\, dl, \quad\quad K3_i = \int_{C_i} \frac{l^2}{r^3}\, dl \tag{5.76}
$$

The line integrals for each side of the polygon can be treated independently by the geometric parameters of that side. It is sufficient, therefore, to consider only one side of the panel, say $i = 1$, for the purpose of these evaluations. For simplicity of the presentation, we drop the subscript i used for identifying the side. We take, without loss of generality, a local plane coordinate system (x', z') in the plane through the field point $\underline{x}_p$ and the side concerned, such that the side lies on the x'-axis, one end point of the side is at the origin and the integration path is performed along the positive x'-axis, as shown in Figure **5.2** . Then the local coordinates (x', z') can be expressed, in terms of the global coordinates, as $|z'| = |\underline{e}_l \times \underline{Q_1 x_p}|$. and $x' = \underline{e}_l \cdot \underline{Q_1 x_p}$.

In the following development, we define the distances between the end points and the field point by $R_1 \equiv |\underline{Q_1 x_p}| = \sqrt{x'^2 + z'^2}$ and $R_2 \equiv |\underline{Q_2 x_p}| = \sqrt{(\ell - x)'^2 + z'^2}$. Expressing the integrals in terms of the local coordinates x' and z' and performing the integration (Gradshteyn & Ryzhik 1965), [11] we

---

[11] Gradshteyn, I. S. and Ryzhik, I. M. (1965), *Table of Integrals, Series and Products*, Academic Press, Inc., New York and London.

get the following results for the integrals.

$$I1 = \ln \frac{R_2 + \ell - x'}{R_1 - x'} \tag{5.77}$$

$$I2 = I1 - \frac{a}{\sqrt{z'^2 - a^2}} \sin^{-1}(H) \tag{5.78}$$

$$\text{with } H = \frac{\sqrt{z'^2 - a^2} \left\{z^2 \ell + a \left(\ell - x'\right) R_1 + a\,x'\,R_2\right\}}{z'^2 (R_1 + a)(R_2 + a)}$$

$$\left(I2 = I1 - \frac{a}{\sqrt{z'^2 - a^2}} \left\{\pi - \sin^{-1}(H)\right\},\right.$$

$$\left. \text{if } (R_1 + a)^2 \left(z'^2 + aR_2\right)^2 + (R_2 + a)^2 \left(z'^2 + a\,R_1\right)^2 \le z'^2 \left(R_1 + a\right)^2 (R_2 + a)^2\right)$$

$$I3 = \frac{1}{a}(I1 - I2) \tag{5.79}$$

$$I4 = \frac{1}{z'^2}\left\{\frac{\ell - x'}{R_2} + \frac{x'}{R_1}\right\} \tag{5.80}$$

$$J1 = R_2 - R_1 + x'\,I1 \tag{5.81}$$

$$J2 = \frac{1}{R_1} - \frac{1}{R_2} + x'\,I4 \tag{5.82}$$

$$J3 = \frac{1}{2}\left\{(\ell - x')\,R_2 + x'\,R_1 + z'^2\,I1\right\} \tag{5.83}$$

$$K1 = \frac{1}{2}\left\{(\ell - x')\,R_2 + x'\,R_1 - z'^2\,I1\right\} + 2x'\,J1 - x'^2\,I1 \tag{5.84}$$

$$K2 = \frac{1}{3}\left(R_2^3 - R_1^3\right) + x'\,J3 \tag{5.85}$$

$$K3 = -\left(\frac{\ell - x'}{R_2} + \frac{x'}{R_1}\right) + I1 + 2x'\,J2 - x'^2\,I1 \tag{5.86}$$

In the cases of $a = 0$ and/or $z = 0$, we can take the limit forms of the above expressions.

The closed-forms of Eq. (5.70) through Eq. (5.75) can be written as, in terms

of the basic integrals retaining the index i for the side and vertex:

$$\phi^{(\sigma)} = -\frac{1}{4\pi} \sum_{i=1}^{N_S} \left[c_1 \, t_i \, \text{I2}_i + \left\{ c_2 \, v_i - c_3 \, u_i + c_4 \, v_i \, (\eta_i - y) \right\} \text{J3}_i + c_4 \, v_i^2 \, \text{K2}_i \right]$$

$$(5.87)$$

$$
\begin{aligned}
\underline{q}^{(\sigma)} = \frac{1}{4\pi} \sum_{i=1}^{N_S} \Big[& -c_1 \left\{ \underline{n}(\underline{n} \cdot \underline{e}) \, t_i \, \text{I3}_i + \underline{e}_{m_i} \text{I1}_i \right\} \\
& + c_2 \left\{ -\underline{e}_\xi \, t_i \, \text{I2}_i + (\underline{e}_\xi \, v_i - \underline{e}_\eta \, u_i) \left\{ (\xi_i - x) \, \text{I1}_i + u_i \, \text{J1}_i \right\} - \underline{n} \, v_i \, z \, \text{I1}_i \right\} \\
& + c_3 \left\{ -\underline{e}_\eta \, t_i \, \text{I2}_i + (\underline{e}_\xi \, v_i - \underline{e}_\eta \, u_i) \left\{ (\eta_i - y) \, \text{I1}_i + v_i \, \text{J1}_i \right\} + \underline{n} \, u_i \, z \text{I1}_i \right\} \\
& + c_4 \left\{ \underline{e}_\xi(-u_i) \left\{ (\xi_i - x)^2 \, \text{I1}_i + 2(\xi_i - x) \, u_i \, \text{J1}_i + u_i^2 \, \text{K1}_i \right\} \right. \\
& \qquad + \underline{e}_\eta \, v_i \left\{ (\eta_i - y)^2 \, \text{I1}_i + 2(\eta_i - y) \, v_i \, \text{J1}_i + v_i^2 \, \text{K1}_i \right\} \\
& \qquad \left. + \underline{n} \, u_i \, z \left\{ (\xi_i - x) \, \text{I1}_i + u_i \, \text{J1}_i \right\} \right\} \Big]
\end{aligned}
$$

$$(5.88)$$

$$
\begin{aligned}
\phi^{(\mu)} = \frac{1}{4\pi} \sum_{i=1}^{N_S} \Big[& d_1 (\underline{n} \cdot \underline{e}) \, t_i \, \text{I3}_i + d_2 \, v_i \, z \, \text{I1}_i - d_3 \, u_i \, z \, \text{I1}_i \\
& - d_4 \, u_i \, z \left\{ (\xi_i - x) \, \text{I1}_i + u_i \, \text{J1}_i \right\} \Big]
\end{aligned}
$$

$$(5.89)$$

$$
\begin{aligned}
\underline{q}^{(\mu)} = \frac{1}{4\pi} \sum_{i=1}^{N_S} \Big[& (\underline{r} \times \underline{e}_{l_i}) \left\{ b_0 \, (\xi_i \, \text{I4}_i + u_i \, \text{J4}_i) + b_1 \, (\eta_i \, \text{I4}_i + v_i \, \text{J4}_i) \right. \\
& \qquad \left. + b_2 \left\{ \xi_i \, \eta_i \, \text{I4}_i + (\xi_i \, v_i + \eta_i \, u_i) \, \text{J4}_i + u_i \, v_i \, \text{K3}_i \right\} + b_3 \, \text{I4}_i \right\} \\
& + d_2 \left\{ \underline{e}_\xi(\underline{n} \cdot \underline{e}) \, t_i \, \text{I3}_i + (\underline{e}_\eta \times \underline{e}_{m_i}) \, \text{I1}_i \right\} \\
& + d_3 \left\{ \underline{e}_\eta(\underline{n} \cdot \underline{e}) \, t_i \, \text{I3}_i - (\underline{e}_\xi \times \underline{e}_{m_i}) \, \text{I1}_i \right\} \\
& + d_4 \left\{ \underline{n} \left\{ v_i \, (\eta_i - y) \, \text{I1}_i + v_i^2 \, \text{J1}_i - u_i \, (\xi_i - y) \, \text{I1}_i - u_i^2 \, \text{J1}_i \right\} \right. \\
& \qquad \left. - \underline{e}_\xi \, u_i \, z \, \text{I1}_i + \underline{e}_\eta \, v_i \, z \, \text{I1}_i \right\} \Big]
\end{aligned}
$$

$$(5.90)$$

We found the newly useful relation of Eq. (5.59) which can be applied directly to calculation of the volumetric integral of vorticity distributions given by the Biot-Savart integral. This integral would often require to be evaluated when the vorticity-velocity formulation is used in inviscid rotational flow problems involving shear-flow interaction. For piecewise constant vorticity distribution within a volumetric element with planar faces, we can first transform the volume integral into the surface integrals on the enclosed faces by using Gauss

theorem. The integrand of the transformed surface integrals becomes $1/r$ and then Eq. (5.59) (with $\underline{e} = \pm\underline{n}$) can be used to transform each surface integral into the line integrals expressed in a form analogous to the first integral term in Eq. (5.70). The evaluation of the Biot-Savart integral is presented in Appendix D.

6

VORTICITY BASED METHODS

6.1   Introduction

In this chapter, we will explain the vorticity-based methods as a tool for the numerical simulation of unsteady incompressible viscous flows. We will deal with various numerical methods based on the vorticity-velocity-pressure formulation for solving the Navier-Stokes equations. Specially, the finite volume method and the vortex particle method are comparatively used for temporal evolution of a vorticity field. The velocity, vorticity and pressure field is calculated in the time marching process.

In general, there are three separate types of approach in the solution procedure for the velocity field:

(a) to use the Biot-Savart integral for a presumably given vorticity field,

(b) to solve directly the kinematic relation between the velocity and the vorticity, and

(c) to solve the Poisson equation for the stream function potential.

In this course, the schemes based on the differential approaches (a) and (c) will be employed. The advantage in employing the integral approach (a) is based on its stability. Integral operators are bounded and smoothing, so that discrete approximations would be stable even if the discretized mesh is refined. The approach (c) corresponds to the VIC (Vortex-In-Cell) method.

The present formulation includes the pressure calculation while most of the existing vorticity-based methods have not treated the pressure field. The main feature of the formulation is the use of an integral approach for obtaining the velocity and pressure fields, in conjunction with a finite volume scheme and the vortex particle method for solving the vorticity transport equation. The integral approach may reflect more easily the global coupling among vorticity, velocity and pressure when imposed the boundary condition for vorticity at a solid surface.

The numerical schemes for computing the vorticity evolution and the integral approach for solving the velocity and the pressure are given in Chapter 7 and

Chapter 8. We will take, as test problems, vorticity dominant flows around a simple geometry such as a circular cylinder, driven cavity and hydrofoil, in which certain special features are apparent, notably concerned with the vorticity distribution on the body surface.

Our numerical schemes could be judged by a comparison with the existing analytical solution and experimental/numerical results provided by other researchers. The demonstrated results indicate that the present integral approach can be incorporated into the finite volume scheme and the Lagrangian vortex method from the viewpoint that the evolution of vorticity in the fluid and on the boundary is accurately predicted and are found to be in good agreement with the comparable solutions.

6.1.1   Various vortical flows

Some vortical flows are natural and essential for movement of fluid (Lugt 1983). The vortical flow behavior at a point in space can be related to a vortex definition. Vorticity is related to the angular velocity of matter at a point in continuum space. Such a vortical motion is composed of a basic mode of motion due to deformation along with rigid motion (Batchelor 1967). Figures **6.1** through **6.3** show typical patterns that may be observed in nature and laboratory.

In some aspects, it is convenient to represent the fluid motion in terms of vorticity together with velocity and pressure. The advantages of the vorticity interpretation and computation rely on the fundamental difference between fluid and solid. Shearing process of fluid at solid surface can be precisely represented by vorticity variable as the skew-symmetric part of the velocity gradient. Moreover, a knowledge of vorticity implies knowing not only the fluid motion at a single spatial point, but also the relation of that motion with those of neighbouring points. Thus, the vorticity reflects the dynamic mechanism of the shearing process more directly than velocity variable (Wu & Wu 1993).
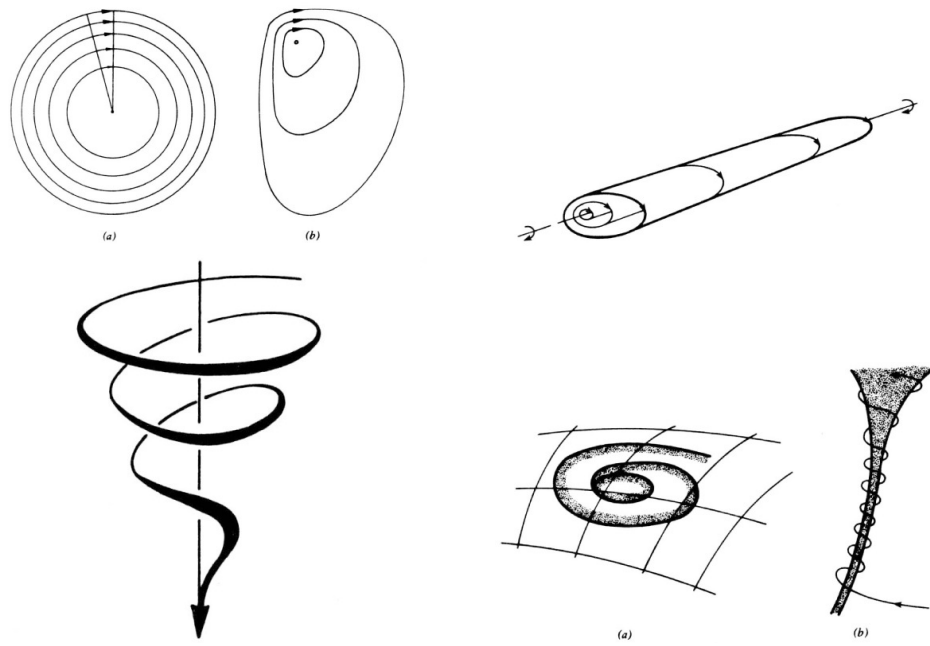
Figure **6.1** Various vortex patterns. Concentric circular vortex and asymmetrical vortex; Cylindrical vortex (perspective view); Spiral vortex; Disk-like and columnar vortices. From Lugt (1983).
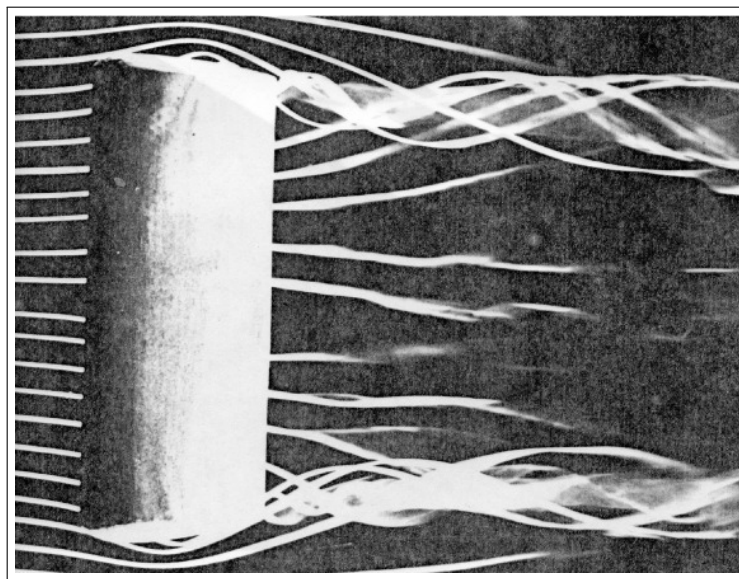
Figure **6.2** Trailing vortices from a rectangular wing. From Van Dyke (1982).
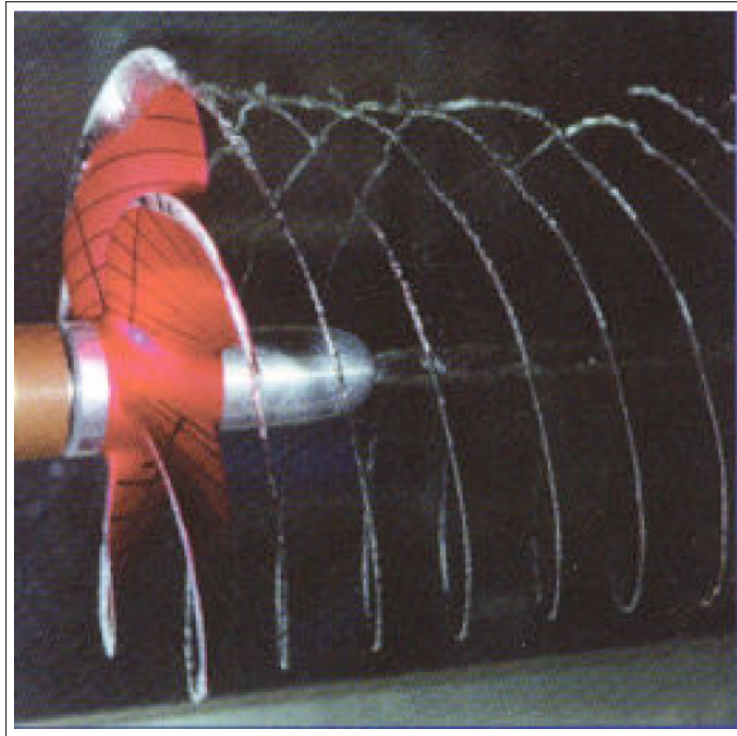
Figure **6.3** Tip vortex cavitation of a marine propeller.

6.1.2 Recent developments

6.1.2.1 CFD modeling

Application of Computational Fluid Dynamics (CFD) might cover the range from the automation of well-established engineering design methods to the use of detailed solutions of the Navier-Stokes (referred to as 'N-S' below) equations as substitutes for experimental research into the nature of complex flows (Ferziger & Perić (1996)). In recent, the advancement in computer hardware technology has made it possible to perform numerical treatment of complex flow fields.

There is yet to be found the most appropriate mathematical formulation of the Navier-Stokes equations to simulate these flows is still open, considering the fact that the choice is strictly dependent on the problem domain and the boundary conditions. For suitable dynamical, spatial and steadiness approximations of Navier-Stokes equations for incompressible viscous flow, there exist

so many mathematical models or discretization techniques. The computational procedures are shown in Figure **6.4** .
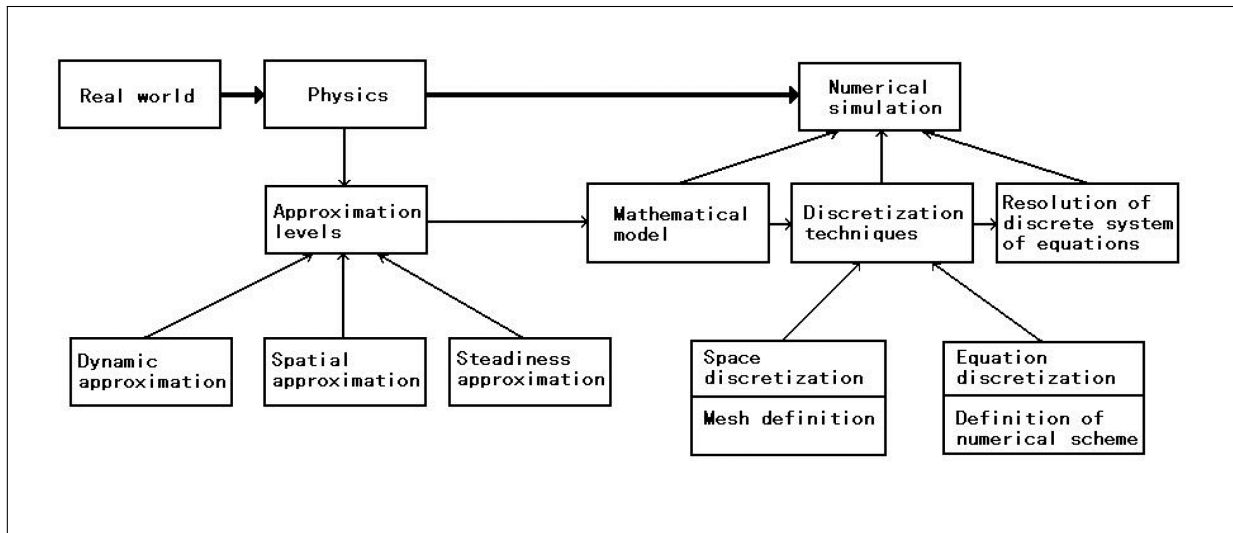
Figure **6.4** Computational procedure for solving Navier - Stokes equations. From Hirsch (1988).

As one candidate for solving Navier-Stokes equations , many researchers have introduced various numerical methods based on the vorticity-velocity formulation. The vorticity-velocity formulation has a few advantages over the primitive variable formulation. A particular numerical algorithm developed for the solution of the vorticity transport equation in an inertial reference frame may be applied to that in a moving frame with correspondingly redefined boundary and initial conditions without any extra consideration of stability problems caused by the additional source terms (Speziale 1987).

6.1.2.2   Physical interpretation

Since the physical interpretation by Lighthill (1963) and Batchelor (1967) of the vorticity dynamics, many researchers have introduced various numerical methods based on the vorticity-velocity formulation for solving the Navier-Stokes equations as an alternative to the primitive variable formulation.

The vorticity-velocity formulation has a few advantages over the primitive variable formulation. The vorticity-velocity formulation is mathematically

natural since the inertia force (including the external body force) term in the Navier-Stokes equations can be expressed as a Helmholtz decomposition form. Then, the pressure and the vorticity become a pair of potentials of the inertia force term (Wu & Wu 1993).

In externally attached flow problems where the viscous region occupies only the boundary layer and wake, a computational region for vorticity evolution can be confined to this region of the entire flow field (Wu 976).

Furthermore, the use of the vorticity field may be desirable to understand certain features of established vortical flows. A particular numerical algorithm developed for the solution of the vorticity transport equation in an inertial reference frame may be applied to that in a non-inertial frame with correspondingly redefined boundary and initial conditions without any extra consideration of stability problems caused by the additional source terms (Speziale 1987).

The fluid around a solid body adheres to the body surface at any instant in time. This no-slip characteristics for fluid velocity must produce a proper quantity of vorticity at the surface. This vorticity then enters and is distributed throughout the fluid by convection and diffusion. The production and redistribution of the vorticity is governed by the vorticity transport equation. One of the most difficult problems encountered in the vorticity-velocity formulation is the introduction of the proper value of vorticity or vorticity flux at the solid surface (Gresho 1991).

Mathematical identity for a vector or scalar field is used to define field values of a quantity of interest, which involves an integral of singularities distributed over a surface and over a field. This concept that was well established for the potential flow analysis have been extensively introduced to solve viscous flow problems (see Morino (1990) for general description). This approach has been recognized to accompany a large amount of computational time, not to ensure a reasonable accuracy in numerical implementation.

Anderson (1989) was the first to present dynamic boundary conditions appropriate for the vorticity formulation of the two-dimensional 'N-S' equations. The boundary conditions do not reveal the inherent vorticity-pressure coupling due to an additional compatibility condition, implying a special force balance

on a solid wall through the N-S equations.

The dynamic mechanism of the viscous shearing process at the solid body surface must be interpreted in terms of the vorticity and the pressure variables together (Wu & Wu 1993). From a different approach, Wu *et al.* (1994) presented a systematic theoretical analysis for these dynamic boundary conditions. They proposed a fully decoupled scheme based on fractional step methods (in which the vorticity transport equation is separated into convection and diffusion equations) applicable for high Reynolds numbers.

6.1.2.3   Vortex particle method

In recent times, great efforts have been made towards solving this problem especially in two-dimensional flow cases by Koumoutsakos & Leonard (1995). In their work, a fractional two-step algorithm is employed in a similar way to the work of Wu *et al.* (1994).

In the first step, discrete point-vortices updated at previous time steps in the time-marching procedure are convected during a time interval ($\triangle t$) via the Biot-Savart integral with smoothed integral kernels (see Figure **6.5**) and their strength is modified based on the scheme of the particle strength exchange scheme. In the second step, a spurious vortex sheet (γ) which is observed on the surface of a body at the end of the first step is computed and related to a vorticity flux (σ) generating from the solid wall in the fluid: $\sigma = \gamma/\triangle t$. In order to reveal dynamical interaction between the vorticity and the pressure, a tangential gradient of the pressure on the right-hand side of this equation should be added.

Essentials of the vortex methods are

(1) one of numerical techniques to solve the N.-S. equations,

(2) suitable simulation for vortical flows,

(3) use of vorticity as a variable,

(4) Lagrangian concept computation,
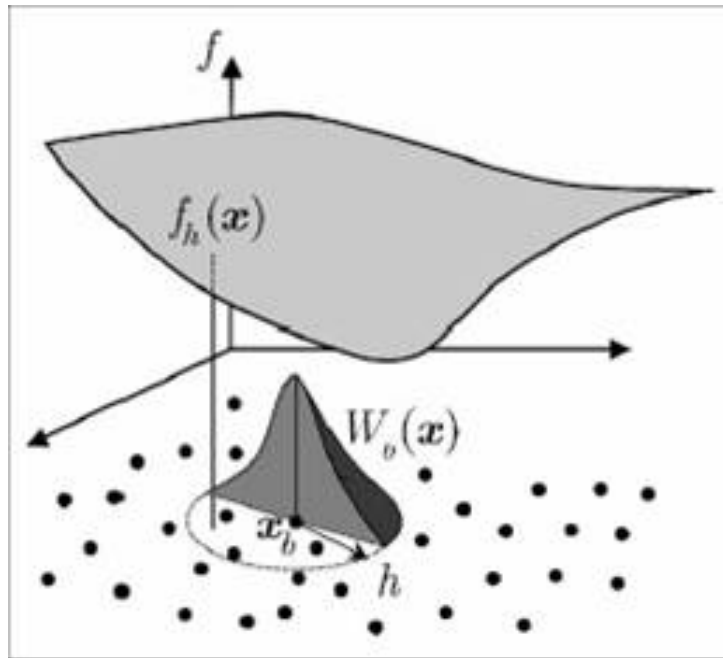
Figure 6.5 Smoothed integral kernel function in particle methods.

(5) confined computational region of non-zero vorticity,

(6) gridless or regular grid system in flow field, and

(7) automatically satisfied far-field boundary condition.

6.1.2.4   Vortex-In-Cell method

The major category of vortex method is distinguished by the scheme of calculation of the velocity field. Generally the vortex method can be divided into grid free method based on the Biot-Savart law (Ploumhans et al (2002)) and vortex-in-cell method where a grid is used for the velocity calculation but particles are used to track the vorticity (Cottet & Poncet (2003)). Vortex-in-cell method has been considered computationally efficient for the evaluation of velocity.

Table **6.1** reproduces the comparison, introduced in Cottet (1999), of the run parameters used for a VIC(Vortex-In-Cell) code and a second order compact finite-difference scheme for 2-D driven cavity flow. The table shows that the VIC method can have economic cost due to the less restrictive time step.

As extentive work, Cottet & Poncet (2003) designed an immersed boundary

vortex-in-cell method for the investigation of a cylinder wake. They computed the velocity and the vorticity strain based on grid Poisson solver.

Table **6.1** Comparison of CPU times between vortex-in-cell method and finite difference method for 2-D driven cavity flow for various Reynolds numbers.

Reynolds number	100	2000	10000
N_{FDM}	64	128	256
N_{VIC}	64	128	256
Δt_{FDM}	0.01	0.008	0.004
Δt_{VIC}	0.01	0.02	0.04
CPUtime$_{\text{FDM}}$	3	24	225
CPUtime$_{\text{VIC}}$	5	16	32

6.2   Vorticity-Velocity-Pressure Formulation

6.2.1   Navier-Stokes equations in Helmholz decomposition

In Chapter 2, we have described the equations of motion, being a relation between the rate of change of momentum of a material volume of a fluid and all forces acting on that portion of fluid,

$$\frac{d}{dt} \int_V \rho \, \underline{q} \, dV \;=\; \int_V \rho \, \underline{f} \, dV \;+\; \oint_S \underline{\tau} \, dS \tag{6.1}$$

where $\underline{f}$ is the external body force per unit mass of fluid and $\underline{\tau}$ is the stress vector (the surface force per unit area).

For incompressible Newtonian fluid, the stress tensor is related to the pressure and the strain rate linearly.

$$\tau_{ij} = -p \, \delta_{ij} + 2\mu \, D_{ij} \tag{6.2}$$

where

$$D_{ij} = \frac{1}{2} \left(\frac{\partial q_i}{\partial x_j} + \frac{\partial q_j}{\partial x_i} \right) \tag{6.3}$$

Then, substitution of Eq. (6.2) in Eq. (6.1) gives

$$\rho \frac{Dq_i}{Dt} = \rho\, f_i - \frac{\partial p}{\partial x_i} + \mu\, \frac{\partial^2 q_i}{\partial x_j \partial x_j} \tag{6.4}$$

Eq. (6.4) becomes, in vector notation,

$$\rho \frac{D\underline{q}}{Dt} = \rho\, \underline{f} - \nabla p + \mu\, \nabla^2 \underline{q} \tag{6.5}$$

Alternatively, for an incompressible flow, Eq. (6.2) can be reduced to

$$\tau_{ij} = -p\, \delta_{ij} + \mu \left(\frac{\partial q_i}{\partial x_j} - \frac{\partial q_j}{\partial x_i} \right) + 2\mu\, \frac{\partial q_j}{\partial x_i} \tag{6.6}$$

As represented by the surface integral of Eq. (6.1), the stress vector is derived as

$$\begin{aligned} \underline{\tau} = \tau_{ij}\, n_j &= \left\{ -p\, \delta_{ij} + \mu \left(\frac{\partial q_i}{\partial x_j} - \frac{\partial q_j}{\partial x_i} \right) + 2\mu\, \frac{\partial q_j}{\partial x_i} \right\} n_j \\ &= -p\, \underline{n} + \mu\, \underline{\omega} \times \underline{n} + 2\mu\, (\nabla \underline{q}) \cdot \underline{n} \end{aligned} \tag{6.7}$$

The equation of motion Eq. (6.1) then gives

$$\begin{aligned} \int_V \rho \frac{D\underline{q}}{Dt}\, dV &= \int_V \rho\, \underline{f}\, dV + \oint_S \left\{ -p\, \underline{n} + \mu\, \underline{\omega} \times \underline{n} + 2\mu\, (\nabla \underline{q}) \cdot \underline{n} \right\}\, dS \\ &= \int_V \rho\, \underline{f}\, dV + \int_V \left\{ -\nabla p - \nabla \times (\mu\, \underline{\omega}) \right\}\, dV \end{aligned} \tag{6.8}$$

Here we have ignored the contribution of the surface integral $J = \oint_S \nabla \underline{q} \cdot \underline{n}\, dS$ because it becomes zero as outlined below.

Contribution of $J = \oint_S \nabla \underline{q} \cdot \underline{n}\, dS$ in Eq. (6.8)

From the vector expansion,

$$(\underline{n} \times \nabla) \times \underline{q} = \nabla \underline{q} \cdot \underline{n} - (\nabla \cdot \underline{q})\, \underline{n} \tag{6.9}$$

$$J = \oint_S \left\{ (\underline{n} \times \nabla) \times \underline{q} + (\nabla \cdot \underline{q}) \, \underline{n} \right\} \, dS \tag{6.10}$$

For incompressible flow, $\nabla \cdot \underline{q} = 0$. Then, dividing the surface region S into two parts S_u and S_l by introducing a line C,

$$J = \int_{S_u} (\underline{n} \times \nabla) \times \underline{q} \, dS + \int_{S_l} (\underline{n} \times \nabla) \times \underline{q} \, dS \tag{6.11}$$

Use the Stokes theorem for each term,

$$J = \oint_C d\ell \times \underline{q} + \oint_{-C} d\ell \times \underline{q} = 0 \tag{6.12}$$

Thus the contribution of $2\mu \nabla \underline{q} \cdot \underline{n}$ to the surface force becomes zero. ∎∎∎

Consequently, we can introduce the reduced stress vector that has the Helmholtz decomposition form:

$$\underline{\tau}^* = -p \, \underline{n} + \mu \, \underline{\omega} \times \underline{n} \tag{6.13}$$

Figure **6.6** shows the directions of the stresses related to the surface vorticity. Viscous stress makes 45° with principal axes of strain rate tensor.
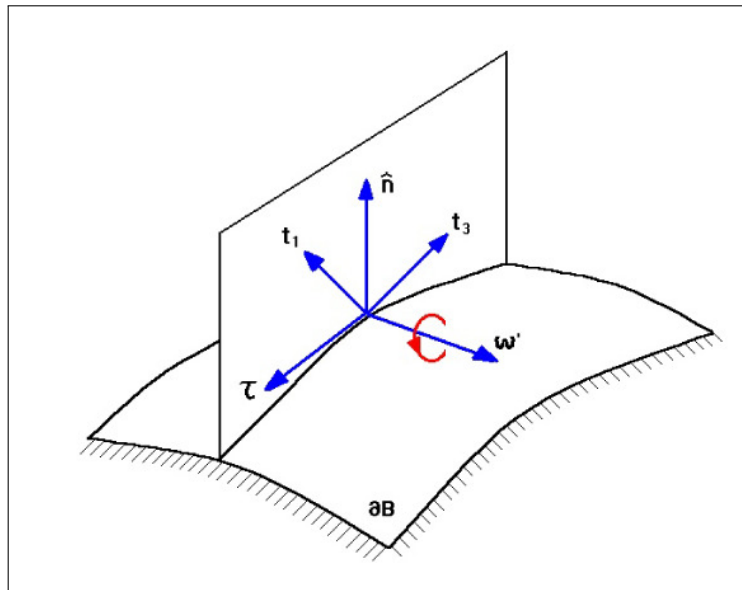
Figure **6.6** Interaction between shearing process and surface vorticity. The principal axes t_1 and t_3 rotate around $\underline{\omega}'$. From Wu *et al.* (1993).

Figure **6.7** shows the erection of the hairpin vortex structures in boundary layers. Vortex stretching (distortion) interacts on vorticity field. Such interaction provides the physiccal background on generation of turbulent flows. Primary hairpin vortex may induce a pressure gradient near the wall surface by which strong secondary or tertiary haipin vortex is ejected and then the multiple breakup of a single turbulent streak occurs.
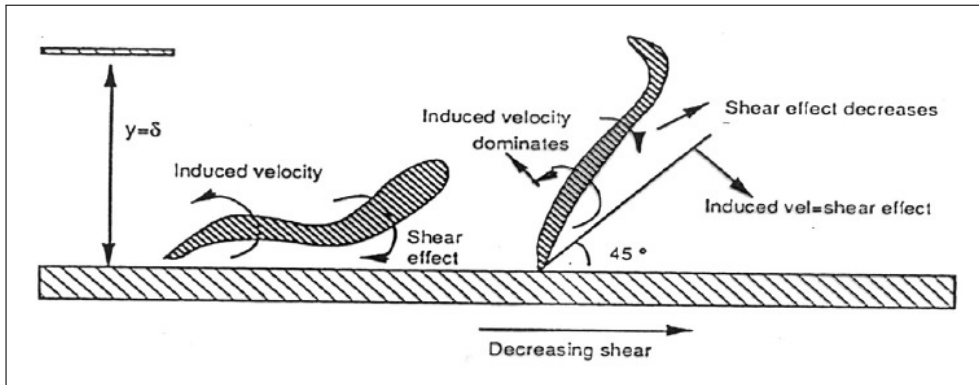
Figure **6.7** Possible effect on the hairpin vortex structures. Adapted from Taylor & Smith (1990).

We also have a natural form of Helmholtz decomposition for the Navier-Stokes equations:

$$\rho \frac{D\underline{q}}{Dt} - \rho \underline{f} = -\nabla p - \nabla \times (\mu \, \underline{\omega}) \tag{6.14}$$

Moreover, the first term in Eq. (6.14) can be rewritten as, by using vector identities:

$$\begin{aligned}
\frac{D\underline{q}}{Dt} &= \frac{\partial \underline{q}}{\partial t} + \underline{q} \cdot \nabla \underline{q} \\
&= \frac{\partial \underline{q}}{\partial t} + \nabla \left(\frac{1}{2} \underline{q} \cdot \underline{q} \right) - \underline{q} \times \underline{\omega}
\end{aligned} \tag{6.15}$$

According to Eqs. (6.14) and (6.15), the Navier-Stokes equations for an incompressible flow of a Newtonian fluid are written as:

$$\frac{\partial \underline{q}}{\partial t} + \nabla \left(\frac{p}{\rho} + \frac{1}{2} \underline{q} \cdot \underline{q} \right) = \underline{f} + \underline{q} \times \underline{\omega} - \nabla \times (\nu \, \underline{\omega}) \tag{6.16}$$

6.2.2   Vorticity transport equation

The vorticity transport equation is obtained by taking the curl of Eq. (6.16):

$$\frac{\partial \underline{\omega}}{\partial t} = \nabla \times \underline{f} + \nabla \times \left(\underline{q} \times \underline{\omega} \right) - \nu \nabla \times (\nabla \times \underline{\omega}) \qquad (6.17)$$

Using the vector expansion formulas:

$$\nabla \times \left(\underline{q} \times \underline{\omega} \right) = \underline{\omega} \cdot \nabla \underline{q} + \underline{q} \left(\nabla \cdot \underline{\omega} \right) - \underline{\omega} \left(\nabla \cdot \underline{q} \right) - \underline{q} \cdot \nabla \underline{\omega} \qquad (6.18)$$

$$\nabla \times (\nabla \times \underline{\omega}) = \nabla \left(\nabla \cdot \underline{\omega} \right) - \nabla^2 \underline{\omega} \qquad (6.19)$$

Since $\nabla \cdot \left(\nabla \times \underline{q} \right) = \nabla \cdot \underline{\omega} = 0$, the vorticity transport equation is equaivalently represented as

$$\frac{\partial \underline{\omega}}{\partial t} + \left(\underline{q} \cdot \nabla \right) \underline{\omega} = \left(\underline{\omega} \cdot \nabla \right) \underline{q} + \nu \nabla^2 \underline{\omega} + \nabla \times \underline{f} \qquad (6.20)$$

The corresponding vorticity transport equation for a compressible fluid with variable viscosity and density is, [1]

$$\begin{aligned}
\frac{\partial \underline{\omega}}{\partial t} = {} & - \left(\underline{q} \cdot \nabla \right) \underline{\omega} + \left(\underline{\omega} \cdot \nabla \right) \underline{q} + \nu \nabla^2 \underline{\omega} + \nabla \times \underline{f} - \underline{\omega} \left(\nabla \cdot \underline{q} \right) \\
& + \frac{1}{\rho^2} \left(\nabla \rho \times \nabla p \right) + \frac{\mu}{\rho} \left\{ \nabla \rho \times (\nabla \times \underline{\omega}) \right\} - \frac{4\mu}{3\rho^2} \left\{ \nabla \rho \times \nabla (\nabla \cdot \underline{q}) \right\} \\
& + \left[\nabla \times \left\{ \frac{1}{\rho} \left(-\frac{2}{3} (\nabla \cdot \underline{q}) \left(\nabla \mu \right) + 2 (\nabla \underline{q}) \cdot (\nabla \mu) + (\nabla \mu) \times \underline{\omega} \right) \right\} \right]
\end{aligned}$$
$$(6.21)$$

The vorticity transport equation in Eulerian and Lagrangian description can be expressed as, respectively, ignoring the body force term,

---

[1]For details, see Zabusky, N. J. (1999), "Vortex paradigm for accelerated inhomogeneous flows: Visiometrics for the Rayleigh-Taylor and Richtmyer-Meshkov environments," *Annual Review of Fluid Mechanics*, vol. 31, pp. 495–536.

(1) *Eulerian Description*

$$\frac{\partial \underline{\omega}}{\partial t} \quad + \quad \underline{q} \cdot \nabla \underline{\omega} \quad = \quad \underline{\omega} \cdot \nabla \underline{q} \quad + \quad \nu \nabla^2 \underline{\omega} \quad + \quad \nabla \times \underline{f}$$

| Local time rate of of vorticity | Convective rate of vorticity | Stretching effect of vorticity | Viscous diffusion | Body force effect |

$$(6.22)$$

(2) *Lagrangian Description*

$$\frac{D\underline{\omega}}{Dt} \quad = \quad \underline{\omega} \cdot \nabla \underline{q} \quad + \quad \nu \nabla^2 \underline{\omega} \quad + \quad \nabla \times \underline{f}$$

| Rate of change of vorticity | Stretching effect of vorticity | Viscous diffusion | Body force effect |

$$(6.23)$$

The vorticity transport equation for 2-D incompressible flow of a viscous fluid, ignoring the external body force, is represented as

$$\frac{\partial \omega}{\partial t} + \left(\underline{q} \cdot \nabla \right) \underline{\omega} = \nu \nabla^2 \underline{\omega} + \nabla \times \underline{f} \tag{6.24}$$

6.2.3   Pressure Poisson equation

The Poisson pressure equation, by taking the divergence of Eq. (6.16) is also derived as

$$\nabla^2 \left(\frac{p}{\rho} + \frac{1}{2} \underline{q} \cdot \underline{q} \right) = \nabla \cdot \left(\underline{q} \times \underline{\omega} \right) + \nabla \cdot \underline{f} \tag{6.25}$$

or equivalently

$$\nabla^2 H = \nabla \cdot \left(\underline{q} \times \underline{\omega} \right) + \nabla \cdot \underline{f} \tag{6.26}$$

Here, the external force is ignored and the pressure p is related to the total pressure H (the static and the dynamic pressure) defined by

$$H = \frac{p - p_\infty}{\rho} + \frac{1}{2} \left(q^2 - q_\infty^2 \right) \tag{6.27}$$

where the constants p_∞ and q_∞ are the reference pressure and velocity at infinity (or at a reference point), respectively. With this definition, the boundary condition at infinity for H is expressed by $H \to 0$ as $|\underline{x}| = r \to \infty$. Thus the contribution due to H at infinity is not considered.

6.2.4 Kinematic boundary condition

Equations (6.24) and (6.26) should be solved in the fluid domain with the boundary, being subject to the boundary conditions for velocity, vorticity and pressure on the surface of a solid body.

At a solid boundary, kinematics dictates that the tangential component of the flow velocity on the wall must be equal to the tangential velocity of the body.

$$\underline{q}(\underline{x}_s, t) \cdot \underline{t} = \underline{U}_B \cdot \underline{t} \tag{6.28}$$

where, if a body translates with a speed $\underline{U}_\infty$ and rotates with angular velocity $\underline{\Omega}_b$ around its center of mass located at $\underline{x}_b$, $\underline{U}_B = \underline{U}_\infty + \underline{\Omega}_b \times (\underline{x}_s - \underline{x}_b)$. This boundary condition results from experimental fact and is valid that the fluid is, to a good approximation, a continuum. This is usually called the *no-slip boundary condition*. Also, the normal component of the velocity of the fluid and the velocity of the body should be the same:

$$\underline{q}(\underline{x}_s, t) \cdot \underline{n} = \underline{U}_B \cdot \underline{n} \tag{6.29}$$

This is usually called the *no-through-flow boundary condition*. Equations (6.28) and (6.29) are the constituents of the kinematic boundary condition:

$$\boxed{\underline{q}(\underline{x}_s, t) = \underline{U}_B} \tag{6.30}$$

Fluid element in contact with the wall is subject to the flow velocity and the motion of the wall. This may result in a net torque onto the fluid element that may in turn impart a rotational motion to the fluid.

6.2.5 Dynamic boundary condition

The boundary condition for the vorticity at the solid surface can be derived by taking the cross product of Navier-Stokes equations Eq. (6.16) with a normal vector $\underline{n}$:

$$\underline{n} \times (\rho\,\underline{a}) + \underline{n} \times \nabla p = -\underline{n} \times (\nabla \times (\mu\,\underline{\omega})) \tag{6.31}$$

where the acceleration is expressed as $\underline{a} = d\underline{q}/dt$ and the external body force $\underline{f}$ is ignored. This condition corresponds to the force equilibrium in the directiontangent to the solid surface. The second term on the right-hand side of Eq. (6.31) also becomes by using vector expansion formulas,

$$\underline{n} \times (\nabla \times (\mu\,\underline{\omega})) = \nabla\left(\mu\underline{\omega}\right) \cdot \underline{n} - \frac{\partial(\mu\,\underline{\omega})}{\partial n} \tag{6.32}$$

Substitution of this relation in Eq. (6.31) then gives

$$\boxed{\frac{\partial(\mu\,\underline{\omega})}{\partial n} = \underline{n} \times (\rho\,\underline{a}) + \underline{n} \times \nabla p + \nabla\left(\mu\,\underline{\omega}\right) \cdot \underline{n}} \tag{6.33}$$

The boundary condition for the pressure at the solid surface can be derived by taking the scalar product of N.-S. equations (6.16) with a normal vector $\underline{n}$:

$$\underline{n} \cdot \frac{\partial \underline{q}}{\partial t} + \frac{\partial}{\partial n}\left(\frac{p}{\rho} + \frac{1}{2}\underline{q} \cdot \underline{q}\right) = \underline{n} \cdot \left(\underline{q} \times \underline{\omega}\right) - \underline{n} \cdot (\nabla \times (\nu\,\underline{\omega})) \tag{6.34}$$

This condition corresponds to the force equilibrium in the direction normal to the solid surface. Equation (6.34) is also expressed by using the total pressure in Eq. (6.27) and ignoring the external force as

$$\boxed{\frac{\partial H}{\partial n} = -\underline{n} \cdot \frac{\partial \underline{q}}{\partial t} + \underline{n} \cdot \left(\underline{q} \times \underline{\omega}\right) - \underline{n} \cdot (\nabla \times (\nu\,\underline{\omega}))} \tag{6.35}$$

6.2.6 Integral approach of formulation

The governing equations for the unsteady flow of a Newtonian incompressible fluid can be written as,

$$\nabla \cdot \underline{q} = 0, \tag{6.36}$$

$$\underline{\omega} = \nabla \times \underline{q}, \tag{6.37}$$

$$\frac{\partial \underline{\omega}}{\partial t} + \underline{q} \cdot \nabla\underline{\omega} = \underline{\omega} \cdot \nabla\underline{q} + \nu\,\nabla^2\underline{\omega} + \nabla \times \underline{f}, \tag{6.38}$$

$$\nabla^2\left(\frac{p}{\rho} + \frac{1}{2}q^2\right) = \nabla \cdot \left(\underline{q} \times \underline{\omega}\right) + \nabla \cdot \underline{f}, \tag{6.39}$$

where $\underline{q}$, $\underline{\omega}$ and p are the velocity, the vorticity and the pressure, respectively, ν is the kinematic viscosity, and ρ is the density of the fluid. The set of Eqs. (6.37), (6.38) and (6.39) is one of the basic differential vorticity-velocity-pressure formulations. In VIC (Vortex-In-Cell) method, a Poisson equation for the stream function $\nabla^2 \underline{\psi} = -\underline{\omega}$, is used instead Eq. (6.37). In the next section, we will describe in detail about the VIC method to be employed.

According to the mathematical vector identity, an equivalent integral formulation of Eq. (6.37) is written as, with use of Eq. (6.36),

$$\underline{q} = \oint_S \left[(\underline{n} \cdot \underline{q}) \, \nabla G + (\underline{n} \times \underline{q}) \times \nabla G \right] \, dS + \int_V \underline{\omega} \times \nabla G \, dV, \qquad (6.40)$$

where $\underline{n}$ is the unit normal pointing into the fluid at the boundary S (C in 2-dimensions) of a fluid domain V (S in 2-dimensions) and ∇ denotes the differential operator with respect to the variable of integration $\underline{\xi}$. Here, G is the fundamental solution of the Laplace equation for an unbounded fluid domain, defined by $G = -\dfrac{1}{4\pi r}$ in 3-dimensions and $G = +\dfrac{1}{2\pi} \ln r$ in 2-dimensions, where r is the distance between a field point $\underline{x}$ and an integration point $\underline{\xi}$.

The velocity field $\underline{q}$ is considered as the sum of two components: the velocity of undisturbed onset flows and the disturbance velocity due to the existence of a solid body. The first integral of Eq. (6.40) represents the contribution from the irrational component of the flows (i.e., $\underline{q}_o + \nabla \phi$ plus the motion of a moving reference frame if introduced). The second one known as the Biot-Savart law represents the disturbance velocity field ($\underline{u}_\omega$) induced by a vorticity field. The use of the Biot-Savart law in computing the velocity field guarantees the enforcement of the boundary condition for the velocity at infinity.

Correspondingly, an integral formulation of Eq. (6.39) can be written as:

$$H = \oint_S \left[H \frac{\partial G}{\partial n} - \frac{\partial H}{\partial n} G \right] \, dS + \int_V \left\{ \nabla \cdot (\underline{q} \times \underline{\omega}) + \nabla \cdot \underline{f} \right\} G \, dV. \quad (6.41)$$

6.2.6.1 Two-dimensional formulation

Ignoring the external body force $\underline{f}$, the two-dimensional version of the system of Eqs. (6.38), (6.40) and (6.41) can be written as, in non-dimensional form,

$$\frac{\partial \omega}{\partial t} + \nabla \cdot (\underline{q}\,\omega) = \frac{1}{Re}\,\nabla^2\omega, \tag{6.42}$$

$$\underline{q} = \underline{q}_\infty + \nabla\phi - \frac{1}{2\pi}\int_S \underline{\omega} \times \nabla(\ln r)\,dS, \tag{6.43}$$

$$H = -\frac{1}{2\pi}\oint_C \left[H\frac{\partial(\ln r)}{\partial n} - \frac{\partial H}{\partial n}(\ln r) \right] dl$$
$$+ \frac{1}{2\pi}\int_S \nabla \cdot (\underline{q} \times \underline{\omega})\,(\ln r)\,dS, \tag{6.44}$$

where Re is the Reynolds number and ω is the scalar plane component of the vorticity vector ($\underline{\omega} \equiv \omega\,\underline{k}$). All non-dimensional quantities are defined based on the characteristic length of a body (e.g., the diameter of a circular cylinder (D) for our test problems) and the velocity of oncoming inflows (q_∞).

The system of Eqs. (6.42), (6.43) and (6.44) must be solved in the fluid domain with a boundary, being subject to the boundary conditions for the velocity, the vorticity and the pressure on the surface (C_B) of a solid body. The no-slip velocity condition states that the velocity of the fluid ($\underline{q}$) is equal to the velocity of the body ($\underline{U}_B$) at the surface points ($\underline{x}_B$) of the body:

$$\underline{q}(\underline{x}_B, t) = \underline{U}_B \quad \text{on } C_B. \tag{6.45}$$

The two-dimensional version of Eq. (6.33) is represented by

$$\frac{\partial(\mu\,\underline{\omega})}{\partial n} = \underline{n} \times (\rho\,\underline{a}) + \underline{n} \times \nabla p \tag{6.46}$$

or equivalently

$$\nu\frac{\partial \underline{\omega}}{\partial n} = \underline{s} \cdot \frac{\partial \underline{q}}{\partial t} + \frac{1}{\rho}\frac{\partial p}{\partial s} \tag{6.47}$$

where $\underline{s}$ is a tangential vector and ν is the kinematic viscosity. This represents an explicit expression of the process of vorticity production described only verbally by Lighthill (1963). This quantity of the vorticity flux diffuses into the fluid

from the body surface.

The boundary vorticity flux (σ) at the solid body for two-dimensional incompressible flow is

$$\sigma \equiv -\frac{1}{Re}\frac{\partial \omega}{\partial n} = -\underline{k} \cdot \left\{ \underline{n} \times \frac{d\underline{U}_B}{dt} + \underline{n} \times \nabla \left(\frac{p}{\rho} \right) \right\} \quad \text{on } C_B. \tag{6.48}$$

This essential boundary condition for the vorticity at the solid surface can be derived by taking the cross product of the N-S equations with $\underline{n}$, with use of the velocity adherence condition. It represents an explicit expression of the process of vorticity production described only verbally by Lighthill (1963). This quantity of the vorticity flux diffuses into the fluid from the body surface. The above expression applies for $t = 0^+$ as well, and is therefore applicable immediately after a solid body is accelerated impulsively. Similarly, the scalar product of the N-S equations with $\underline{n}$ gives an expression for $\partial H / \partial n$ as:

$$\frac{\partial H}{\partial n} = -\underline{n} \cdot \frac{\partial \underline{q}}{\partial t} + \underline{n} \cdot (\underline{q} \times \underline{\omega}) - \frac{1}{Re}\underline{n} \cdot (\nabla \times \underline{\omega}) \quad \text{on } C_B. \tag{6.49}$$

It is seen from Eqs. (6.48) and (6.49) that the boundary conditions for the vorticity and the pressure are coupled. A more rigorous and extensive analysis on these pressure and vorticity conditions for two- or three-dimensional incompressible or compressible flows was given by Wu & Wu (1993).

6.2.7   Stream function approach: VIC method

The velocity field can be decomposed into

$$\underline{q} = \underline{U}_\infty + \underline{u}_\omega + \underline{u}_\phi \tag{6.50}$$

where $\underline{U}_\infty$ is incoming velocity, $\underline{u}_\omega$ represents rotational field, and $\underline{v}_\phi$ represents solenoidal field. The velocity vector can also be expressed according to the Helmholtz decomposition due to the incompressibility,

$$\underline{q} = \underline{U}_\infty + \nabla \times \underline{\psi} + \nabla \phi. \tag{6.51}$$

The vector potential $\underline{\psi}$ and the scalar potential ϕ should vanish in the far field so that the velocity field recover the free stream velocity.

$$\underline{q} \to \underline{U}_\infty \ \text{ as } \ |\underline{x}| \to \infty \tag{6.52}$$

where $\underline{x}$ is the spatial coordinate. The vector potential is related to a stream function in two dimension. If we take the curl of the equation (6.51),

$$\underline{\omega} = \nabla \times (\nabla \times \underline{\psi}) = -\nabla^2 \underline{\psi} + \nabla(\nabla \cdot \underline{\psi}) \tag{6.53}$$

If we enforce $\nabla \cdot \underline{\psi} = 0$, the equation results in Poisson equation,

$$\nabla^2 \underline{\psi} = -\underline{\omega} \tag{6.54}$$

and its solution is

$$\underline{\psi} = \frac{1}{4\pi} \int_V \frac{\underline{\omega}}{r} \, dV \tag{6.55}$$

Fially the rotational velocity field is $\underline{u}_\omega = \nabla \times \underline{\psi}$,

$$\underline{u}_\omega = -\frac{1}{4\pi} \int_V \underline{\omega} \times \nabla \left(\frac{1}{r}\right) dV, \tag{6.56}$$

where r is the distance from the volume element dV to the field point. This equation commonly referred to the Biot-Savart formula.

The rotational velocity field can be evaluated using the Biot-Savart law (6.56). But, the direct calculation involves $O(N^2)$ cost for N elements. This is computationally intensive so that fast evaluation method such as multipole expansion has been developed in order to cut down the cost. The VIC method reduces the computational cost to $O(N \log N)$ by employing grid based fast Poisson solvers. The VIC method is composed of three basic steps. First, the vorticity field is projected to the grid using the interpolation kernel. The Poisson equation for vector potential (6.54) is solved on the grid with the boundary value of $\underline{\psi}$. The velocity on the grid is computed from the definition $\underline{u}_\omega = \nabla \times \underline{\psi}$ with the finite difference formula, and then the velocity is interpolated back to the particles.

6.2.8   Particle method in solving the vorticity transport equation

Let us start with a simplified conservative form of the vorticity transport equation, $L\omega = f$ with a suitable differential operator L:

$$L\,\omega = \frac{\partial \omega}{\partial t} + \nabla \cdot (\underline{q}\,\omega) + c_0\,\omega = f \qquad (6.57)$$

For a material volume $V(t)$, the integral form would be

$$\frac{d}{dt}\int_{V(t)} \omega\, dV + \int_{V(t)} c_0\,\omega\, dV = \int_{V(t)} f\, dV \qquad (6.58)$$

where we have used the Reynolds transport theorem. Here we introduce the idea of particle methods in which mass on points is concentrated:

$$\omega(\underline{x},t) = \alpha(t)\,\delta(\underline{x} - \underline{x}_p(t)) \qquad (6.59)$$

With such particle representation, the above integral becomes discrete values, and then the vorticity transport equation reduces to a set of ordinary differential equations. As example, for the homogeneous equation $L\omega = 0$, we have the general solution form:

$$\frac{d\alpha}{dt} + c_0(\underline{x}_p(t), t)\,\alpha = 0, \quad \text{with} \quad \frac{d\underline{x}_p}{dt} = \underline{q}(\underline{x}_p, t) \qquad (6.60)$$

Now, the extension of this concept to the vorticity transport equation in 3-D gives us following govering equations in the vortex particle methods:

$$\underline{\omega} = \sum_p \underline{\alpha}_p\, \delta(\underline{x} - \underline{x}_p(t)) \qquad (6.61)$$

$$\frac{d\underline{x}_p}{dt} = \underline{q}(\underline{x}_p, t) \qquad (6.62)$$

$$\frac{d\underline{\alpha}_p}{dt} = \nabla \underline{q}(\underline{x}_p, t)\,\underline{\alpha}_p + \text{diffusion term} \qquad (6.63)$$

The effects of the diffusion term can be employed by the PSE(Particle Strength Exchange) scheme and the integral formula for the wall no-slip condition. The overall insights on the PSE scheme and the wall viscous diffusion will be ex-

plined in Chapter 8.

6.2.9 Hydrodynamic Forces

The force exerted by the fluid on the body can be separated into the hydrostatic force and the hydrodynamic force. The hydrodynamic force $\underline{F}$ on the body due to the motion is defined as

$$\frac{\underline{F}}{\rho} = -\frac{d\underline{I}}{dt} \tag{6.64}$$

The quantity $\underline{I}$ is called the *hydrodynamic impulse* that needs to be applied to the body to set it in motion against the inertia of the fluid (Lamb 1932). Thus,

$$\underline{I} = \frac{1}{d-1} \int_V \underline{x} \times \underline{\omega} \, dV \tag{6.65}$$

with d the dimension of the space ($d = 3$ in 3-D, $d = 2$ in 2-D). [2] In two-dimensional case, the position $(\tilde{x}, \tilde{y})$ of vorticity are related to the components (I_x, I_y) of hydrodynamics impulse

$$
\begin{aligned}
I_x &= \int y\,\underline{\omega}\,dS \approx \sum_i y_i \Gamma_i \\
I_y &= -\int x\,\underline{\omega}\,dS \approx -\sum_i x_i \Gamma_i
\end{aligned}
\tag{6.67}
$$

and then the components of the force (F_x, F_y) is

$$F_x = -\rho \frac{dI_x}{dt}, \qquad F_y = -\rho \frac{dI_y}{dt} \tag{6.68}$$

where $\dfrac{d\underline{I}}{dt} = \dfrac{\underline{I}(t + \triangle t) - \underline{I}(t - \triangle t)}{2\triangle t}$. The x-component of the hydrodynamic force is called the *drag* and the y-component is the *lift*.

---

[2]In Eq. (1.113), we set $\underline{f} = \underline{q}$ to find

$$\underline{I} \equiv \int_V \underline{q}\,dV = \frac{1}{d-1} \int_V \underline{x} \times (\nabla \times \underline{q})\,dV - \frac{1}{d-1} \oint_S \underline{x} \times (\underline{n} \times \underline{q})\,dS \tag{6.66}$$

and then the second integral term would vanish from the no-slip boundary condition ($\underline{q} = \underline{U}_B$) for a stationary body (also for steadily moving bodies) and the far-field boundary condition($\underline{q} = \underline{U}_\infty$). Accordingly, the second term on the right-hand side of Eq. (6.66) does not contribute the hydrodynamic forces.

Extensively, if we take $\underline{q} = \nabla p$ in Eq. (6.66) and the divergence theorem for the first volume integral, then the pressure forces can be written as, since the second volume integral term must vanish (i.e., identically $\nabla \times \nabla p = 0$),

$$\underline{F}_p \equiv -\oint_{S_B} p\,\underline{n}\,dS = \frac{1}{d-1}\oint_{S_B} \underline{x} \times (\underline{n} \times \nabla p)\,dS \qquad (6.69)$$

Using Eq. (6.46), the 2-D version of the pressure forces is represented by, in terms of the vorticity flux on body surface and the body acceleration,

$$\underline{F}_p^{(2D)} \equiv -\oint_{S_B} p\,\underline{n}\,dS = \oint_{S_B} \underline{x} \times \left\{ \frac{\partial(\mu\,\underline{\omega})}{\partial n} - \underline{n} \times (\rho\,\underline{U}_B) \right\}\,dS \qquad (6.70)$$

For the 2-D case of an impulsively started body, the result reduces to, in terms of vorticity flux distribution on the body surface,

$$\underline{F}_p^{(2D)} = -\oint_{S_B} p\,\underline{n}\,dS = \oint_{S_B} \underline{x} \times \frac{\partial(\mu\,\underline{\omega})}{\partial n}\,dS \qquad (6.71)$$

In derived Eq. (1.113), we have noted that the left-hand side of Eq. (1.112) and Eq. (1.113) is independent of the choice of the origin of $\underline{x}$, so must be the right-hand side. Namely, if we remove $\underline{x}$ from the right-hand side of these equations, the remaining integrals must vanish.

7

FINITE VOLUME METHODS

7.1   Introduction

In this chapter, we focus on a vorticity-based integro-differential formulation for the numerical solution of the 2-D incompressible Navier-Stokes equations. A finite volume scheme is implemented to solve the vorticity transport equation with a vorticity boundary condition. The Biot-Savart integral is evaluated to compute the velocity field from a vorticity distribution over a fluid domain. The Green's scalar identity is employed to solve the total pressure in an integral approach. The global coupling between the vorticity and the pressure boundary conditions is considered when this integro-differential approach is employed. For the early stage development of the flow about an impulsively started circular cylinder, the computational results with our numerical method are compared with known analytical solutions in order to validate the present formulation.

A finite volume scheme is implemented to solve the vorticity transport equation with a vorticity boundary condition. The Biot-Savart integral is evaluated to compute the velocity field from a vorticity distribution over a fluid domain. The Green's scalar identity is employed to solve the total pressure in an integral approach. The global coupling between the vorticity and the pressure boundary conditions is considered when this integro-differential approach is employed. For the early stage development of the flow about an impulsively started circular cylinder, the computational results with our numerical method are compared with known analytical solutions in order to validate the present formulation.

We have mentioned in the previous chapter that the governing equations as well as the boundary conditions are globally coupled. The present method is im-

plemented in a time-stepping algorithm that proceeds by generating, convecting and diffusing the vorticity, by computing the corresponding velocity and by calculating the pressure with the vorticity and velocity field. Computationally, in order to recover the global coupling between the vorticity and the pressure for their discrete time-dependent solutions, two separate iterative procedures are required: one for solving the vorticity transport equation and the other for solving the total pressure equation.

7.2 Numerical Implementation

7.2.1 Vorticity transport equation

In solving the vorticity transport equation, we seek to advance the solution to the next time step with the velocity and the vorticity fields computed at the present time step. The vorticity field is then changed via the vorticity evolution mechanism.

The no-slip boundary condition is enforced in this stage by the production of a proper amount of vorticity at the body surface. This vorticity production is expressed in terms of the vorticity flux. The vorticity flux on the body surface is iteratively corrected until the no-slip condition is achieved within a preset criterion for the final vorticity field.

During the iteration, only the slip velocity is computed by the Biot-Savart integration, without computing the whole velocity field. The task is then to determine the vorticity distribution over a fluid domain at each instant in time, so that the no-slip condition is satisfied at the solid surface, the vorticity satisfies the vorticity transport equation, and the total vorticity of the field is conserved.

A finite volume discretization is applied to Eq. (6.42) which results in a consistent approximation to the conservation law, where the time rate of change of the vorticity within the domain is balanced by the net fluxes of the convective and the diffusive terms across the boundary surface of the domain. A physical domain is divided into a finite number of small elements, each element

serving as a computational cell. The vorticity field is considered as a discrete sum of the individual vorticity fields over the cells. The discretized solution to Eq. (6.42) results in a set of cell-averaged vorticity variables which is in balance with the face-averaged fluxes across the cell sides. Integrating the vorticity transport equation over an arbitrary but a stationary cell A with a cell boundary C and then applying the divergence theorem yields an integral form:

$$\frac{\partial}{\partial t} \int_A \omega \, dS + \oint_C \left((\underline{q} \cdot \underline{n}) \, \omega - \frac{1}{Re} \underline{n} \cdot \nabla \omega \right) \, dl = 0, \qquad (7.1)$$

where $\left((\underline{q} \cdot \underline{n}) \, \omega - \dfrac{1}{Re} \underline{n} \cdot \nabla \omega \right)$ is the outward flux of ω across the cell boundary.

7.2.1.1   Numerical schemes

Let us assume that at the nth time step (corresponding to time t), the vorticity field has been computed (respecting the no-slip condition), then we seek to advance the solution to the $n + 1$th time step (time $t + \triangle t$). We approximate Eq. (7.1) as a discrete integral form for both time and space coordinates, by replacing the boundary integral with the sum of the flux on the sides of the cell and using an explicit scheme in time-stepping:

$$\omega^{n+1} = \omega^n - \frac{\triangle t}{A} \sum_k F_k, \qquad (7.2)$$

where ω^n is considered the average value of ω at the nth time stage over the cell whose area is A, and F_k represents the value of the flux outgoing through the kth side of the cell.

The diffusive flux term is approximated in its mean value sense in a similar fashion to the central differential scheme (Hoffman & Chiang 1993). For the convective term, the second-order TVD (total variation diminishing) scheme with the flux limiter suggested by Roe (1985) is used (see also Hirsch 1990). Time is advanced by an explicit forward Euler time stepping scheme during the time interval $\triangle t$. In fact, this is performed by several sub-steps with a smaller

time interval δt that satisfies the stability condition for this explicit scheme:

$$\delta t \leq \frac{d^2}{\dfrac{4}{Re} + \sqrt{2}\, q_s\, d}. \tag{7.3}$$

Here, d is the longer diagonal of a cell and q_s is the speed at the cell centroid. For global stability, we take actually a sub-step time increment smaller than the minimum value of such permissible values for all cells.

As the solution for the vorticity is advanced in time, the no-slip is presumably enforced at the beginning of each time increment. At the end of a time step, the distribution for ω would be changed eventually through the integration of Eq. (6.42). One must then calculate a new slip velocity at the surface. In order to reduce the slip velocity to zero, we require that the vorticity be produced at the surface acting as a source of vorticity (Lighthill 1963). The new vorticity would enter the fluid through the surface as represented by Eq. (6.48) and then would be allowed to diffuse and convect into the fluid over a finite time interval $\triangle t$. The task is to relate the vorticity flux on the surface of the body to this no-slip condition at the same time considering its coupling effect with the pressure.

7.2.1.2 No-slip boundary condition with vorticity flux

According to Eq. (6.47), vorticity is transferred to the fluid due to the tangential component of the pressure gradient and an acceleration of the body surface.

Wu et al. (1994) suggested that this pressure gradient is manifested by a spurious slip velocity observed on the body surface and this slip velocity is considered as an acceleration equivalent to a vorticity flux generated at the wall. The vortex sheet on the body surface should account for the modification of the circulation of the flow field.

$$\left(\nu \frac{\partial \omega}{\partial n}\right)^{(k+1)} = \left(\nu \frac{\partial \omega}{\partial n}\right)^{(k)} + \frac{V_s^{(k)}}{\Delta t} \tag{7.4}$$

where V_s is spurious slip velocity at the wall.
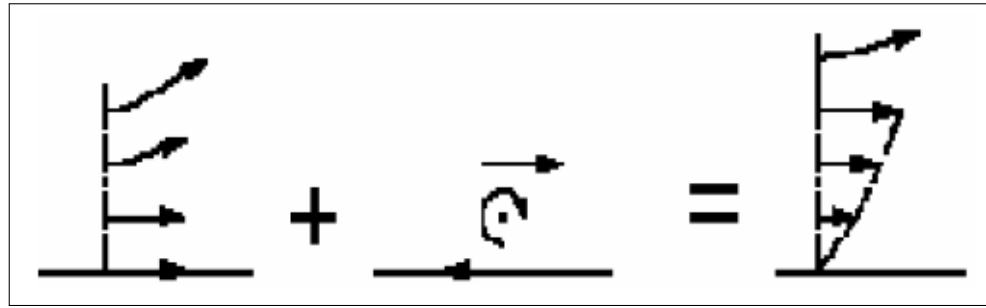
Figure 7.1 Iterative adjustment of vorticity flux for vorticity boundary condition. Adpated from Cottet & Poncet (2003).

In a discrete sense, the vorticity flux may be determined so that the no-slip condition is satisfied at the end of the time step. The spurious slip velocity (V_s) that would appear at the end of the time step can be regarded as the coupling term corresponding to the tangential gradient of the surface pressure in Eq. (6.48). The newly computed V_s can be then used to absorb the coupling term and consequently to update a time-averaged vorticity flux:

$$\bar{\sigma}^{(k+1)} = \bar{\sigma}^{(k)} + \frac{V_s^{(k)}}{\triangle t},\qquad(7.5)$$

where the overbar in $\bar{\sigma}$ denotes the time-averaged values of σ during a small time step $\triangle t$ and the superscript notation refers to the iterative step. The iteration continues until the no-slip condition is satisfied, namely, until V_s reduces to a value within a preset allowance. Although there are practical considerations which must be observed during the specified time interval $\triangle t$, Eq. (7.5) implies that the integrated amount of vorticity flux is produced and remains unchanged during the time interval.

Now the vorticity (ω_b) at the body surface can be obtained from the definition of the vorticity flux, in a discrete differential sense,

$$\omega_b = Re\, d_1\, \sigma + \omega_1,\qquad(7.6)$$

where d_1 is the normal distance of the centroid of a cell adjacent to the body surface from the surface and ω_1 is the cell-centered vorticity value of the cell (see Figure 7.2).
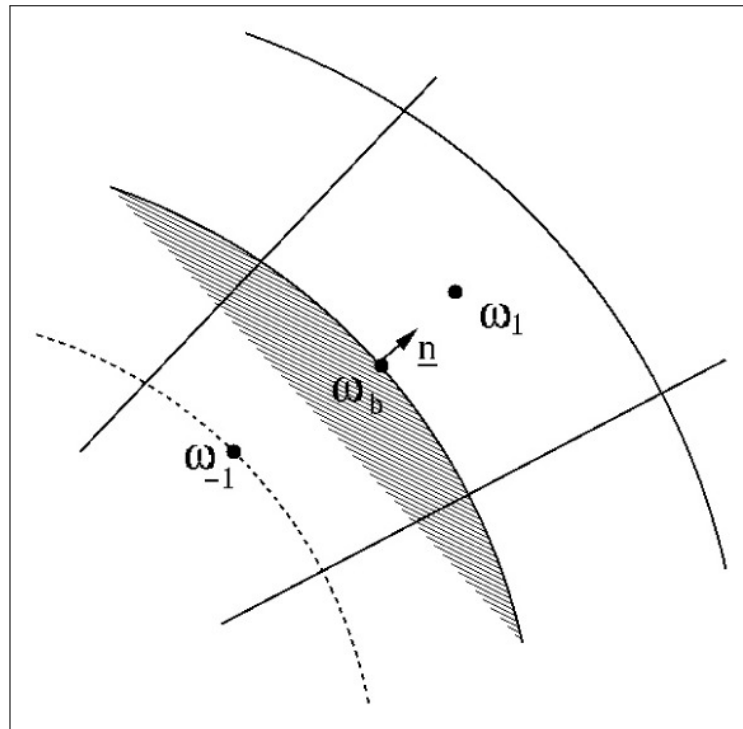
Figure 7.2 Notations for calculating the vorticty at the body surface.

7.2.2 Biot-Savart integral

In the vorticity-velocity integro-differential formulation, the Biot-Savart integral must be evaluated at appropriate field points within the discretized fluid domain. With N elements used in discretizing the fluid domain over which vorticity is distributed, we may require $O(N^2)$ evaluations of the Biot-Savart integral in order to calculate the velocity field. The evaluation of the Biot-Savart integral is, therefore, an important task in numerical implementations.

We will herein summarize the content described in Appendix D. See also Suh (2000) for the more detailed explanation and the extension of the present derivation to three-dimensions.

7.2.2.1 Evaluation of line integrals

The resulting expressions for the velocity field include the line integrals only along the boundary contour of the element. Let the value of the line integral

along each straight edge of the element be $\underline{I}_i$. Then, it follows that

$$\underline{u} = -\frac{\underline{k}}{2\pi} \times \left(\sum_{i=1}^{4} \underline{I}_i \right), \tag{7.7}$$

where the subscript i is denoted by the integer of the vertex associated with the first end point of the individual sides, ℓ_i denotes the length of i-th side and

$$\underline{I}_i = \frac{1}{2}\underline{n}_i \int_0^{\ell_i} \omega \left(\ln r^2 + 1 \right) dl - \frac{1}{4}\nabla\omega \left(\underline{n}_i \cdot \underline{r} \right) \int_0^{\ell_i} \ln r^2 \, dl. \tag{7.8}$$

It is seen that the line integral for each side can be treated independently. After a substantial amount of algebraic manipulations, one may obtain the following result for $\underline{I}_i$:

$$\underline{I}_i = \frac{1}{2}\,\underline{n}_i \left\{ \omega_i \left(\ell_i + I^{(1)} \right) + (\nabla\omega \cdot \underline{s}_i) \left(\frac{1}{2}\ell_i^2 + I^{(2)} \right) \right\} - \frac{1}{4}\nabla\omega \left(\underline{n}_i \cdot \underline{r} \right) I^{(1)}, \tag{7.9}$$

where

$$\underline{r}_i = \underline{\xi}_i - \underline{x}, \quad x' = -\underline{r}_i \cdot \underline{s}_i, \quad y' = (\underline{r}_i \times \underline{s}_i) \cdot \underline{k}, \tag{7.10}$$

$$I^{(1)} = (\ell_i - x') \ln r_{i+1}^2 + x' \ln r_i^2 - 2\,\ell_i + 2|y'|\,\theta_i, \tag{7.11}$$

$$I^{(2)} = \frac{1}{2} \left(r_{i+1}^2 \ln r_{i+1}^2 - r_i^2 \ln r_i^2 \right) - \frac{\ell_i^2}{2} + \ell_i x' + x'\, I^{(1)}, \tag{7.12}$$

and

$$\theta_i = \tan^{-1} \frac{|y'|\,\ell_i}{r_i^2 - \ell_i\, x'} \qquad \text{(see Figure 7.3)} \tag{7.13}$$

7.2.2.2   Computational enhancement

Although this analysis deals with cases of linear distributions, the integration is much simpler, as a result of this construction, if ω is assumed to be constant over the cell. The actual numerical implementation in the present work is performed under the assumption that the vorticity density is piecewise uniform over discretized cell elements of a fluid domain.
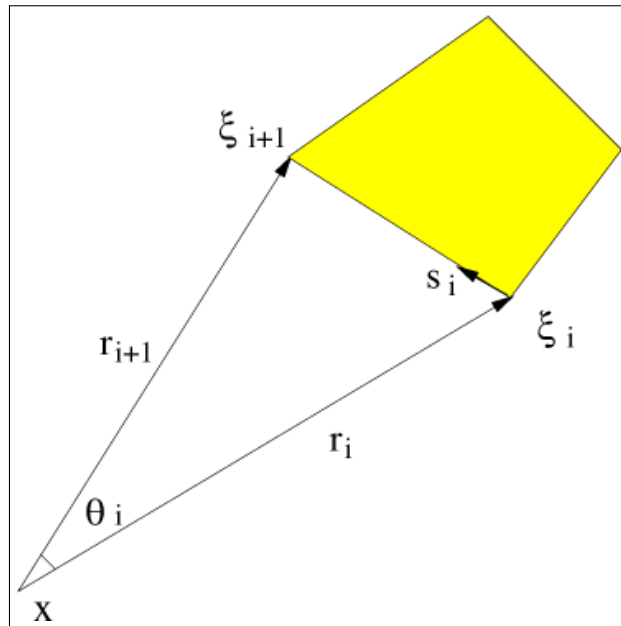
Figure **7.3** Notations for the contour integral of the quadrilateral element. Here, ω_i denotes the vorticity value at the i-th vertex, $\underline{s}_i$ is the unit directional vector of the line integral path, and we denote the distances between the two end points of the side and the field point by r_i and r_{i+1}, respectively.

The present procedure is believed to be quite accurate, but it is nevertheless time-consuming to apply computationally because of a few of the transcendental functions involved in closed-forms. In the present numerical implementation, therefore, for a vorticity distribution with unit density over each cell element, we compute once the induced velocities at desired field points (namely, at centroids of neighboring cell elements) and then save them (within the limit of computer memory capacity) so that such time-consuming calculations can be avoided. Furthermore, when the distance r is sufficiently large (say, more than five times the diagonal dimension of the fluid element), Eq. (6.43) is applied directly without such integrations. That is, the vorticity within the region of area A is treated as a point vortex of strength ωA located at the centroid of the element. The sum of all of the induced velocities from the vorticity is then added to the contribution from the onset flow. In this manner, we can calculate the whole velocity field as well as the slip velocity at the surface.

7.2.3   Pressure Poisson equation

7.2.3.1   Formulation

Once the vorticity and the velocity field are updated, the integral equation for the total pressure must be solved to provide a complete set of solutions at the $n + 1$th time step. Substituting Eq. (6.49) for $\dfrac{\partial H}{\partial n}$ into Eq. (6.44) yields the limiting form for H as a field point approaches the surface points $(\underline{x}_B)$ of a solid body:

$$
\begin{aligned}
\frac{1}{2}H + \frac{1}{2\pi} \oint_{C_B} H \frac{\partial(\ln r)}{\partial n}\, dl = \\
-\frac{1}{2\pi} \oint_{C_B} \left[\underline{n} \cdot \frac{\partial \underline{q}}{\partial t} - \underline{n} \cdot (\underline{q} \times \underline{\omega}) + \frac{1}{Re}\, \underline{n} \cdot (\nabla \times \underline{\omega}) \right] \ln r\, dl \\
+\frac{1}{2\pi} \int_{S} \nabla \cdot (\underline{q} \times \underline{\omega})\, \ln r\, dS,
\end{aligned}
\tag{7.14}
$$

where the integrals over C_B is evaluated on the surface of a body in the sense of the Cauchy principal value integral. Using the vector operation for the integrand of the surface integral in Eq. (7.14), namely, $\nabla \cdot (\underline{q} \times \underline{\omega}) \ln r = \nabla \cdot (\underline{q} \times \underline{\omega}\, \ln r) - (\underline{q} \times \underline{\omega}) \cdot \nabla(\ln r)$ and applying the divergence integral theorem to the resultant expression, yield a Fredholm integral equation of the second kind for H:

$$
\begin{aligned}
\frac{1}{2}H + \frac{1}{2\pi} \oint_{C_B} H \frac{\partial(\ln r)}{\partial n}\, dl \;=\; & -\frac{1}{2\pi} \oint_{C_B} \left[\underline{n} \cdot \frac{\partial \underline{q}}{\partial t} + \frac{1}{Re}\, \underline{n} \cdot (\nabla \times \underline{\omega}) \right] \ln r\, dl \\
& -\frac{1}{2\pi} \int_{S} (\underline{q} \times \underline{\omega}) \cdot \nabla(\ln r)\, dS.
\end{aligned}
\tag{7.15}
$$

Furthermore, if we assume the body to be either fixed or impulsively started as in our test problem later on, the equation reduces to a simpler one:

$$
\begin{aligned}
\frac{1}{2}H + \frac{1}{2\pi} \oint_{C_B} H \frac{\partial(\ln r)}{\partial n}\, dl \;=\; & -\frac{1}{2\pi} \oint_{C_B} \frac{1}{Re} \frac{\partial \omega_B}{\partial s} \ln r\, dl \\
& -\frac{1}{2\pi} \int_{S} (\underline{q} \times \underline{\omega}) \cdot \nabla(\ln r)\, dS.
\end{aligned}
\tag{7.16}
$$

7.2.3.2 Application of panel methods

Accordingly, we base our pressure calculation on an integral equation formation of the pressure-Poisson equation. One possible approach for solving Eq. (7.16) numerically for the total pressure is to use a panel-method approximation in a similar fashion to a one in potential flow analysis. Among the full variety of the numerical implementation of the panel methods, we use herein a straight-line element for the body contour subdivision representation, and a uniform density distribution of singularity strength on each panel at the boundary and over each cell in the fluid domain. This low-order panel-method approximation is relatively robust in the numerical implementation and thus the computing time can be reduced in comparison with other higher-order panel methods without significant loss of accuracy in numerical results.

The body is defined by a set of points on the surface and the body surface is subdivided into N (normally an even number) straight-line elements (flat panels or interior facets). This approximate representation for the body surface enables us to replace the two integrals over C_B in Eq. (7.16) by the sum of the individual integral form for the contribution of each straight-line panel.

The surface integral term on the right-hand side of Eq. (7.16) is similar in form to the Biot-Savart integral in Eq. (6.43) if we replace $(\underline{q} \times \underline{\omega}) \cdot \nabla(\ln r)$ by $\underline{\omega} \times \nabla(\ln r)$. In order to include the influence of the field distribution of $(\underline{q} \times \underline{\omega})$, we can use the algorithm for evaluation of the Biot-Savart integral described in Section 3.2 under the assumption that the distribution is piecewisely constant over each cell element.

Although we have already used the pressure boundary condition Eq. (6.49) when we derived Eq. (7.16), the term $-\dfrac{1}{Re}\dfrac{\partial \omega_B}{\partial s}$ must be evaluated in order to actually impose the boundary condition on the equation. At this stage, we need the iteration procedure to specify the value, which will be described later on.

Consequently Eq. (7.16) deduces a set of algebraic expressions with unknown values of the total pressure head $(H_i, 1 = 1, \cdots, N)$ on the panels. With H_i being solutions of this linear system, the total pressure field can be obtained by integrating Eq. (7.16). The pressure field, as well as the surface

pressure distribution, can be determined by subtracting the dynamic pressure term in Eq. (6.27) from the total pressure.
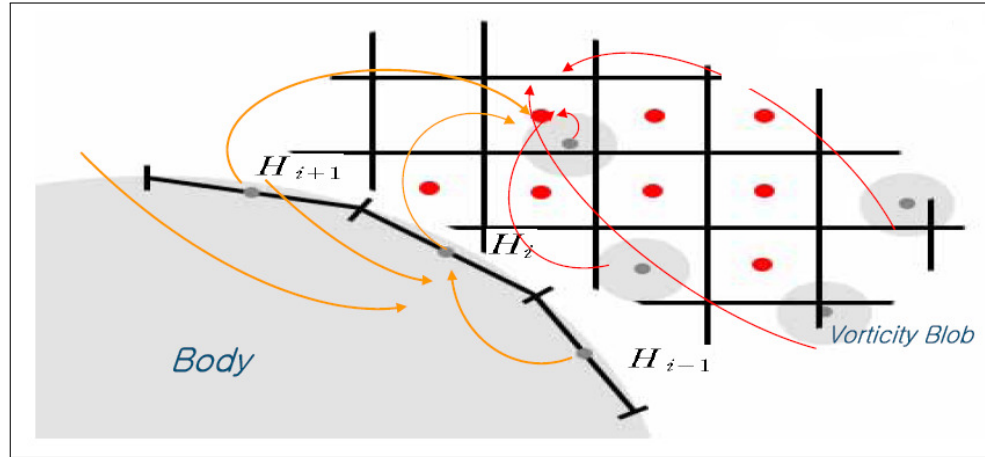
Figure **7.4** Schematic diagram for calculation of pressure field.

7.2.4   Computational procedure

The above considerations can be summarized in the following algorithm of the solution of a system of the governing equations.

(1) Integrate the vorticity transport equation, Eq. (6.42), in time with enforcement of the no-slip condition. At the nth time step (corresponding to time t) the velocity and the vorticity fields are assumed to be computed and we seek to advance the solution to the $n + 1$ time step (time $t + \triangle t$). Given $\underline{q}^n$ and ω^n, the vorticity field ω^{n+1} at the $n + 1$th time step is changed via the vorticity evolution mechanism. The no-slip boundary condition is enforced in this stage by assigning the vorticity flux at the solid surface. The vorticity flux at the surface is assigned as its time-averaged value during a small time interval as given by Eq. (7.5). We need an iterative process to introduce a proper amount of the time-averaged vorticity flux in order to ensure the no-slip condition and accordingly update ω^{n+1}. The spurious slip velocity is computed by performing the Biot-Savart integration for the vorticity field obtained at the present iterative stage.

(2) Evaluate the Biot-Savart integral by using the integration scheme proposed in Section 7.2.2 in order to obtain the velocity field $\underline{q}^{n+1}$ corresponding to

the currently updated vorticity field ω^{n+1}. The vorticity is assumed to be distributed with a uniform strength over an individual cell element. Since the job of the Biot-Savart integration is repeated for all time steps, it is desirable to save computing time by storing the results of the Biot-Savart integral for a unit vorticity-distribution over an individual cell. Because of limited storage in a computer, it applies for field points within a certain distance away from the cell for which we use the exact integration.

(3) Solve the integral equation for H^{n+1} by using $\underline{q}^{n+1}$ and ω^{n+1} obtained in steps (1) and (2). The term $-\dfrac{1}{Re}\dfrac{\partial \omega_B}{\partial s}$ in Eq. (7.16) must be evaluated where the differentiation performs in the direction s tangent to the surface of the body. To obtain the vorticity (ω_B) at the body surface given by Eq. (7.6), the vorticity flux must be evaluated in this stage at the end of the time interval while in step (1), the rate of vorticity production was taken to be uniform over the time t to $t + \triangle t$.

Since the vorticity flux is related to the tangential gradient of the pressure along the body surface and the normal gradient of the total pressure is incorporated with the tangential gradient of the body vorticity at the current time, we employ the iterative calculation between the vorticity flux and the pressure on the surface. With the time-averaged vorticity flux obtained in step (1), we obtain the body vorticity via Eq. (7.6). Then we use this body vorticity value as an initial guess and $\underline{q}^{n+1}$ and ω^{n+1} in order to solve Eq. (7.16) for H and thus to find the pressure at the surface. The tangential gradient of this surface pressure is used to update the vorticity flux at the $(n + 1)$th time step by Eq. (6.48). With this updated vorticity flux at the end of a time step, we update the body vorticity via Eq. (7.6) again.

This iterative procedure is continued until the surface pressure and the vorticity flux reach a converged state. The convergence of the iteration process is measured with the difference in their values between two successive iterations. The typical tolerance is taken as 10^{-4} in our test problem later on. Up to this point, the principle of conservation of vorticity can be invoked by integrating Eq. (6.48).

When the pressure gradient is then integrated around the closed contour of

the a solid body, the result must be zero because the pressure is inherently a single-valued function. It is the argument leading to the principle of the vorticity conservation that the total vorticity in the infinite unlimited space occupied jointly by the fluid and the solid bodies is always zero.

(4) Advance the calculation to the next time step by repeating steps (1), (2) and (3).

The reconstruction of the surrounding cell-averaged data to a common vertex or node is performed by a weighted averaging procedure based on an inverse-distance weighted averaging of the variables from the cell centroid to the cell vertices.

The above solution procedure is summarized in Figure **7.5** .
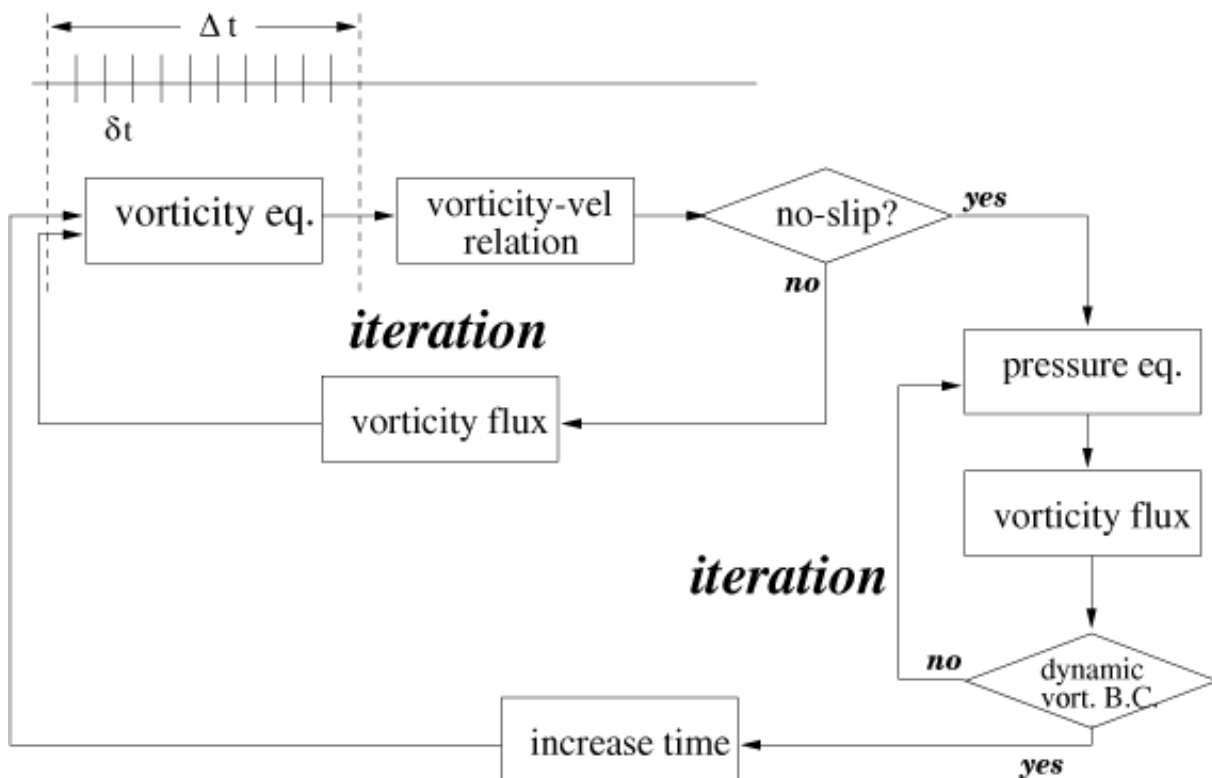
Figure **7.5** Flow chart for solution procedure of the present FVM in the vorticity-velocity-pressure formulation.

7.3 Lid-driven Cavity Flows

7.3.1 Formulation

As an application of the present scheme, we consider a vorticity-based integro-differential formulation for the numerical solution of a two dimensioanl cavity flow driven by shear and body forces (see Figure **7.6**) (Rida et al. 1997, Shih et al. 1989).
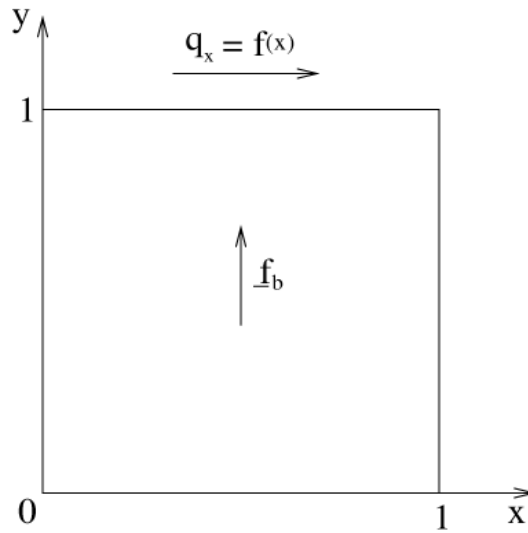
Figure 7.6 Coordinates and geometry for driven cavity.

The shear motion of the lid of the cavity and the body force are prescribed as, respectively,

$$f(x) = x^4 - 2x^3 + x^2 \tag{7.17}$$

$$\underline{f}_b = 8\mu \left[24\, F(x) + 2f'(x)\, g''(y) + f'''\, g(y) \right] \underline{j}$$
$$+ 64 \left[F_2(x)\, G_1(y) - g(y)\, g'(y)\, F_1(x) \right] \underline{j}, \tag{7.18}$$

where

$$g(y) = y^4 - y^2, \quad F(x) = \int_0^x f(x)\, dx, \quad F_1(x) = f(x)\, f''(x) - [f'(x)]^2,$$

$$F_2(x) = 0.5\, f^2(x), \quad G_1(y) = g(y)\, g'''(y) - g'(y)\, g''(y). \tag{7.19}$$

This lid-driven square cavity flow is a standard benchmark for testing numerical

schemes in the context of computational fluid dynamics because of its simplicity
and the availability of the analytical solution.

The governing equations for the unsteady flow of an incompressible Newto-
nian fluid can be written as,

$$\nabla \cdot \underline{q} = 0, \tag{7.20}$$

$$\underline{\omega} = \nabla \times \underline{q}, \tag{7.21}$$

$$\frac{\partial \underline{\omega}}{\partial t} + \underline{q} \cdot \nabla \underline{\omega} = \underline{\omega} \cdot \nabla \underline{q} + \nu \nabla^2 \underline{\omega} + \nabla \times \underline{f}_b, \tag{7.22}$$

$$\nabla^2 \left(\frac{p}{\rho} + \frac{1}{2} q^2 \right) = \nabla \cdot \left(\underline{q} \times \underline{\omega} + \underline{f}_b \right), \tag{7.23}$$

The corresponding integro-differential vorticity-velocity formulation is given,
in non-dimensional form, by,

$$\frac{\partial \omega}{\partial t} + \nabla \cdot (\underline{q}\,\omega) = \frac{1}{Re} \nabla^2 \omega + \nabla \times \underline{f}_b, \tag{7.24}$$

$$\underline{q} = \underline{q}_o - \frac{1}{2\pi} \int_S \underline{\omega} \times \nabla(\ln r)\, dS, \tag{7.25}$$

$$H = -\frac{1}{2\pi} \oint_C \left[H \frac{\partial(\ln r)}{\partial n} - \frac{\partial H}{\partial n} \ln r \right] dl$$
$$+ \frac{1}{2\pi} \int_S \nabla \cdot \left(\underline{q} \times \underline{\omega} + \underline{f}_b \right) \ln r\, dS, \tag{7.26}$$

where p is the pressure, ν the kinematic viscosity, ρ the density of the fluid, Re
the Reynolds number and ω the scalar plane component of the vorticity vector
($\underline{\omega} \equiv \omega \underline{k}$). The velocity term $\underline{q}_o$ in Eq. (7.25) represents the contribution from
the velocity distributions over the boundary(C) of the cavity, namely:

$$\underline{q}_o = \oint_C \left[(\underline{n} \cdot \underline{q}) \nabla G + (\underline{n} \times \underline{q}) \times \nabla G \right] dl, \tag{7.27}$$

where $\underline{n}$ is the unit normal pointing into the fluid at the boundary C. The pres-

sure p is related to the total pressure defined by

$$H = \frac{p - p_r}{\rho} + \frac{1}{2}\left(q^2 - q_r^2\right),\qquad(7.28)$$

where the constants p_r and q_r are the reference pressure and velocity, respectively. In such a formulation, we deal with the Biot-Savart integral in order to compute the velocity from a vorticity distribution in the square cavity and to solve the total pressure in a boundary integral approach.

The boundary conditions for the velocity, the vorticity and the pressure supplement the system of Eqs. (7.24), (7.25) and (7.26). The no-slip velocity condition states that the velocity of the fluid ($\underline{q}$) is equal to the moving velocity($\underline{U}_B$) of the boundary($\underline{x}_B$) of the cavity:

$$\underline{q}(\underline{x}_B, t) = \underline{U}_B \quad \text{on } C.\qquad(7.29)$$

The boundary condition for the vorticity flux (σ) at the boundary can be derived by taking the cross product of the Navier-Stokes equations with $\underline{n}$ and by using the velocity adherence condition:

$$\sigma \equiv -\frac{1}{Re}\frac{\partial \omega}{\partial n} = -\underline{k}\cdot\underline{n}\times\left(\frac{d\underline{U}_B}{dt} + \nabla p - \underline{f}_b\right)\quad\text{on } C.\qquad(7.30)$$

Similarly, the scalar product of the Navier-Stokes equations with $\underline{n}$ gives an expression for $\partial H/\partial n$ as:

$$\frac{\partial H}{\partial n} = -\underline{n}\cdot\left(\frac{\partial \underline{q}}{\partial t} - \underline{q}\times\underline{\omega} + \frac{1}{Re}\nabla\times\underline{\omega} - \underline{f}_b\right)\quad\text{on } C.\qquad(7.31)$$

7.3.2 Comparison with analytic solution

For purposes of comparison with the exact steady-state solution, the calculations are advanced to steady-state. As the initial condition in the time evolution of the flow, an impulsive start was formulated. A uniform grid of equal size that divides the cavity flow region was used. The vorticity, the vorticity flux, and the pressure distributions along the cavity wall for $Re = 100$ with variation of the

time interval and the grids are shown in Figs. **7.7** and **7.8** , where the agreement with the exact solution is excellent.
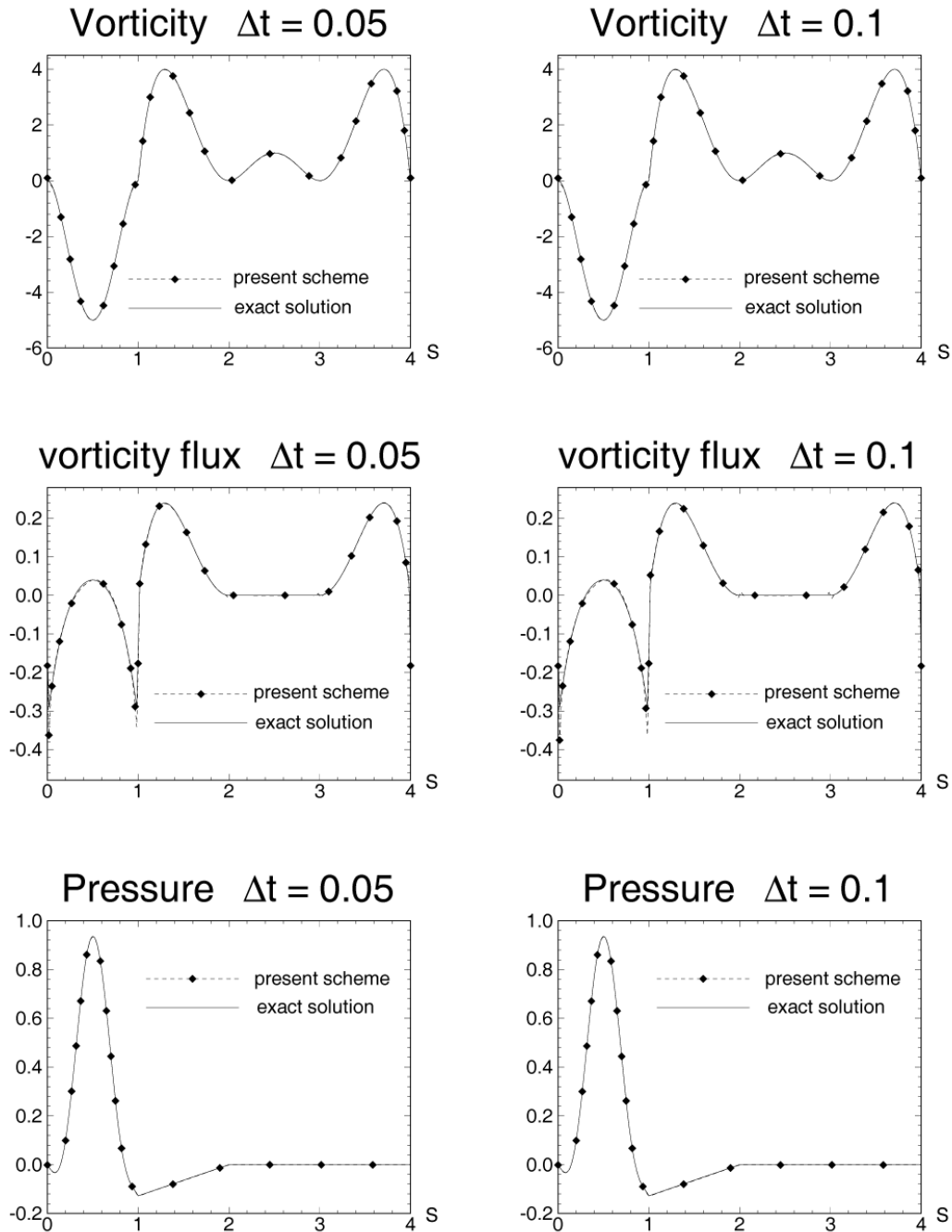
Figure **7.7** Sensitivity of time interval on vorticity, vorticity flux and pressure along the driven cavity wall for $Re = 100$ with the 61×61 grid. The perimeter(S) along the cavity wall has the clockwise direction from the origin at the upper left corner of the cavity.
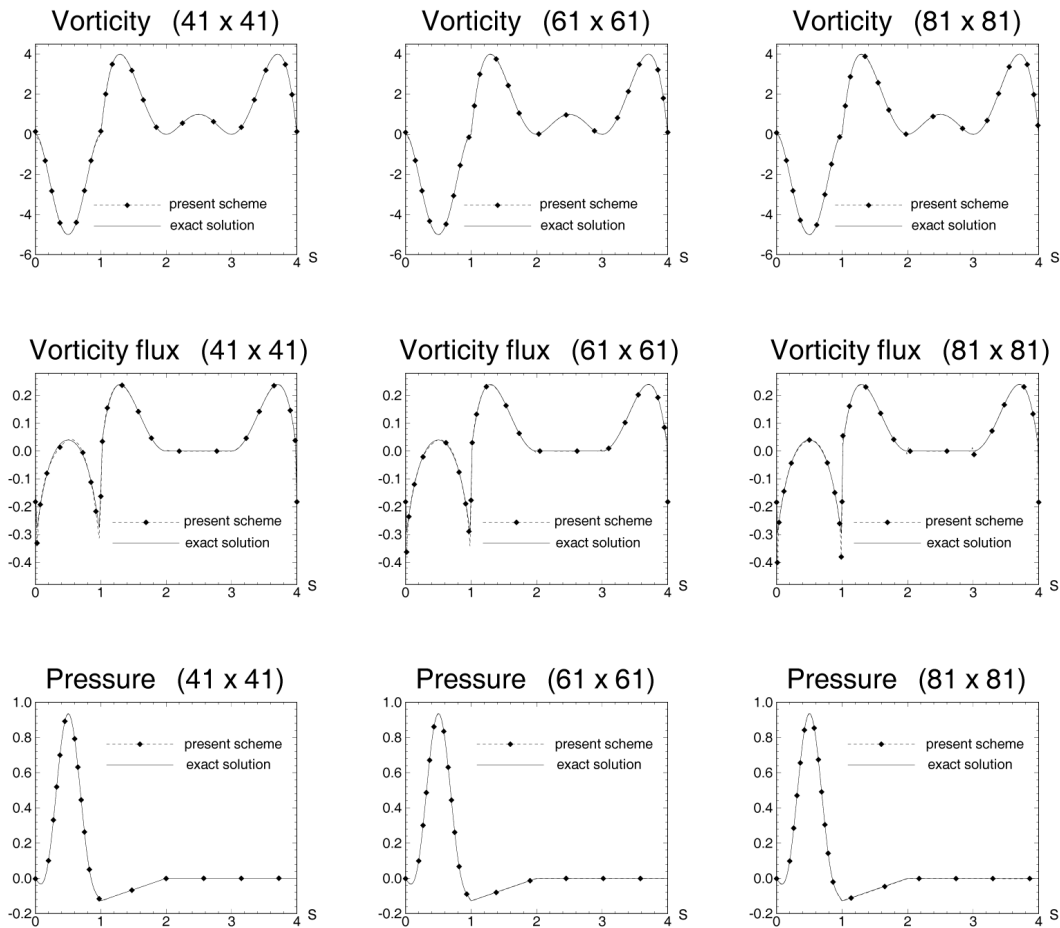
Figure **7.8** Sensitivity of mesh size on vorticity, vorticity flux and pressure along the driven cavity wall for $Re = 100$ with $\triangle t = 0.05$.

Figure **7.9** shows that the time evolution of the velocity along the vertical and the horizontal center lines of the cavity at $Re = 100$ with $\triangle t = 0.05$ and the 61×61 grid. Figure **7.10** shows the time evolution of kinetic energy for cavity flow in this case. This is compared with the exact steady-state value $1216/33075(= 0.0367650)$. The streamline pattern, the vorticity contour, and the pressure contour in the steady-state are shown in Figure **7.11** , where the agreement is again very good. (It is difficult to distinguish between the exact solution and the numerical solution with the present scheme.)
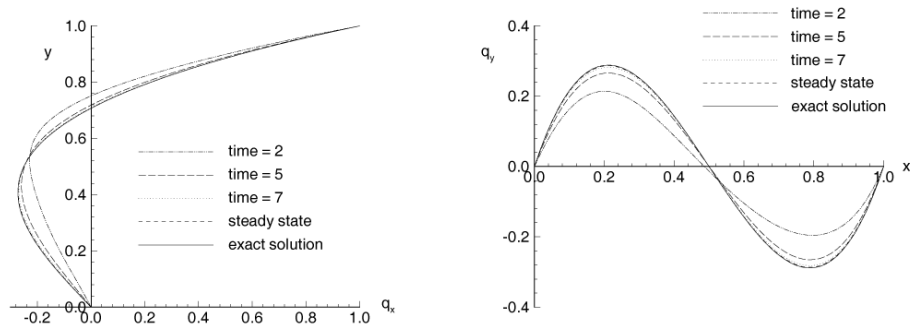
Figure **7.9** Time evolution of the velocity along the center lines of the driven cavity for $Re = 100$ with $\triangle t = 0.05$ and the 61×61 grid.
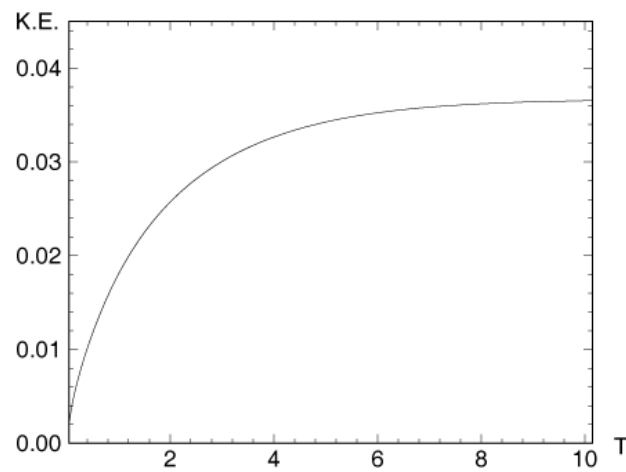
Figure **7.10** Time evolution of kinetic energy of the driven cavity for $Re = 100$ with $\triangle t = 0.05$, and the 61×61 grid.
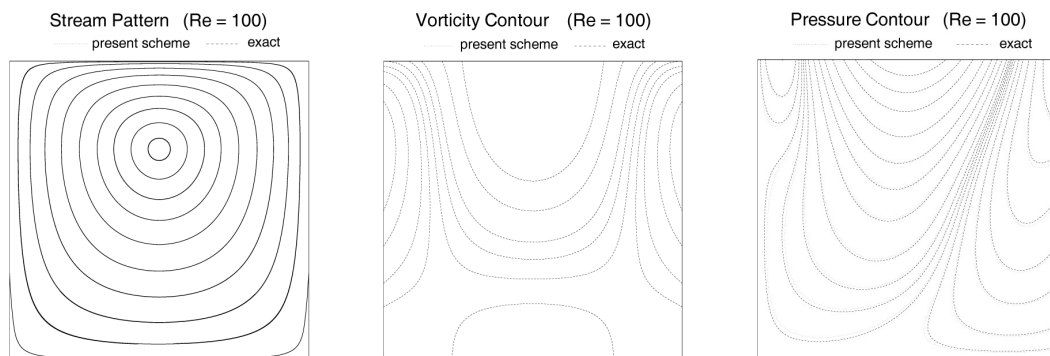
Figure **7.11** Streamline pattern, vorticity contour and pressure contour of the driven cavity for $Re = 100$ with $\triangle t = 0.05$ and the 61×61 grid.

The above comparison implies that the evaluation of the Biot-Savart integral works well. In the present numerical implementation, for a vorticity distribution with unit density over each cell element, we compute the induced velocities at desired field points once (namely, at centroids of neighboring cell elements) and then save them (within the limit of computer memory capacity) so that the time-consuming calculations at successive time steps can be avoided.

7.4   Impulsively Started Circular Cylinder

7.4.1   General aspects

As a numerical example we consider the case of an impulsively started circular cylinder at certain Reynolds numbers. The numerical simulation for the development of two-dimensional, incompressible flow past an impulsively started circular cylinder has been a challenge to computational fluid dynamicists for years. Although the geometry is simple, the flow pattern in the proximity of the circular cylinder is in full variety. Treatment of these special flow problems requires complex numerical procedures to be applied and often validation is defined by comparisons with analytical solutions.

A notable theoretical investigation of the initial flow over an impulsively started circular cylinder was given by Bar-Lev & Yang (1975). They solved the vorticity transport equation by the method of matched asymptotic expansions to the third order of a small quantity of non-dimensional time. Their analytical solution would be reasonably valid for $t < 0.25, Re > 50$. Only for the purpose of comparison with the analytical solution, no attempt is made to advance the calculations to large time values. Rather, the intent is only to provide sufficient results in the early time stage after the impulsive start, from which the validity of the present formulation can be demonstrated. Our calculations are concentrated on those of the vorticity and vorticity flux distribution, the pressure distribution and the drag coefficient.

As the initial condition in the evolution of the flow, an impulsive start may be formulated using the potential flow field although there cannot experimentally

be such a thing as a truly impulsive start. At time $t = 0^+$ the slip velocity distribution $(2 \sin \theta)$ obtained from the potential flow analysis is imposed on the surface of the body. In fact, numerical schemes encounter difficulties in resolving the initially developed thin boundary layers associated with impulsive starts. There exists inherently the singular behavior (having infinity value) on the (drag) force at the time immediately after the impulsive start.

7.4.2   Computational grids

An O-type regular pattern of quadrilateral cells that divides the fluid region about a circular cylinder is used, but we believe a C-type grid will work as well. Our computational domain is described by a set of grid points taken as $\theta_i = 2\pi i/N_I$ and $r_j = R_o - (R_o - 0.5)\, cos(\pi j/2N_J)$, where N_I is the number of cells in the circumferential direction, N_J in the radial direction and R_o is the outer radius of the boundary of the computational domain. Since the first i-index coincides with the last i-index, a periodic boundary condition is applied along the interface corresponding to that index. On the cylinder surface $(r = 0.5)$ which corresponds to $j = 1$, we set the vorticity flux (vorticity production) to a suitable value determined iteratively from the no-slip boundary condition. On the outer boundary, we convect purely ω out of the computational domain in a naturally upwind sense (i.e., without the diffusion term in Eq. (7.2), $\omega^{n+1} = \omega^n - \dfrac{\triangle t}{A} \sum_k \left\{ (\underline{q} \cdot \underline{n})\, \omega^n \right\}_k$.

7.4.3   Numerical results

7.4.3.1   Analytic solution in early time stage

In Figures. **7.12** through **7.14** , the effect of numerical parameters on the pressure drag, the friction drag and the total drag coefficients as computed by the present method is presented for Reynolds number $Re = 60, 3000$ and 9500. The analytical solutions given by Bar-Lev and Yang (1975) are also presented

for the purpose of comparison. The frictional and the pressure drag were calculated by integrating the vorticity and the pressure, respectively, over the surface of the cylinder. The drag coefficients are normalized by $\frac{1}{2}\rho\, q_\infty^2\, D$.

7.4.3.2 Time step

In Figure **7.12** we plot the sensitivity of the time interval $\triangle t$ on the drag for each Reynolds number. For the convergence check, three different time intervals ($\triangle t = 0.0025, 0.005, 0.01$) have been chosen. The grid used in these calculations was 600×80 and the outer radius of the computational domain was taken as $R_o = 1.5$. The present results are shown to give good convergence with respect to $\triangle t$ to the analytical solutions, especially near the immediate time region (near $t = 0^+$) after impulsive start. The inherently singular behavior of the solution is precisely captured as $\triangle t$ becomes smaller. We observe that the numerical results are in good agreement with the analytical solutions for $t < 0.25$, even when using a moderate time interval of $\triangle t = 0.01$.

7.4.3.3 Computational domain

In Figure **7.13** the effect of the size of the computational domain on the drag is presented. Note that it is difficult to make distinctions between all the symbols in the figures. It seems that the effect is negligible if the computational domain contains entirely the fluid domain with non-zero vorticity values like the present cases. But it is apparent that, as time advances, the computational domain should become larger in order to contain the region with non-zero vorticity values.

Figure **7.14** shows the corresponding effect with respect to a measure of the mesh size. We see that the grid dependence on the solutions is small enough to ignore unless grid resolutions for capturing a complicated vortex structure are required. At the early stage in time for the present cases, the complicated vortex structure is not exhibited yet. In the following computations, $\triangle t = 0.005$, the 600×80 grid, and $R_o = 1.5$ are used, from the viewpoint that these choices would not greatly affect our numerical results.
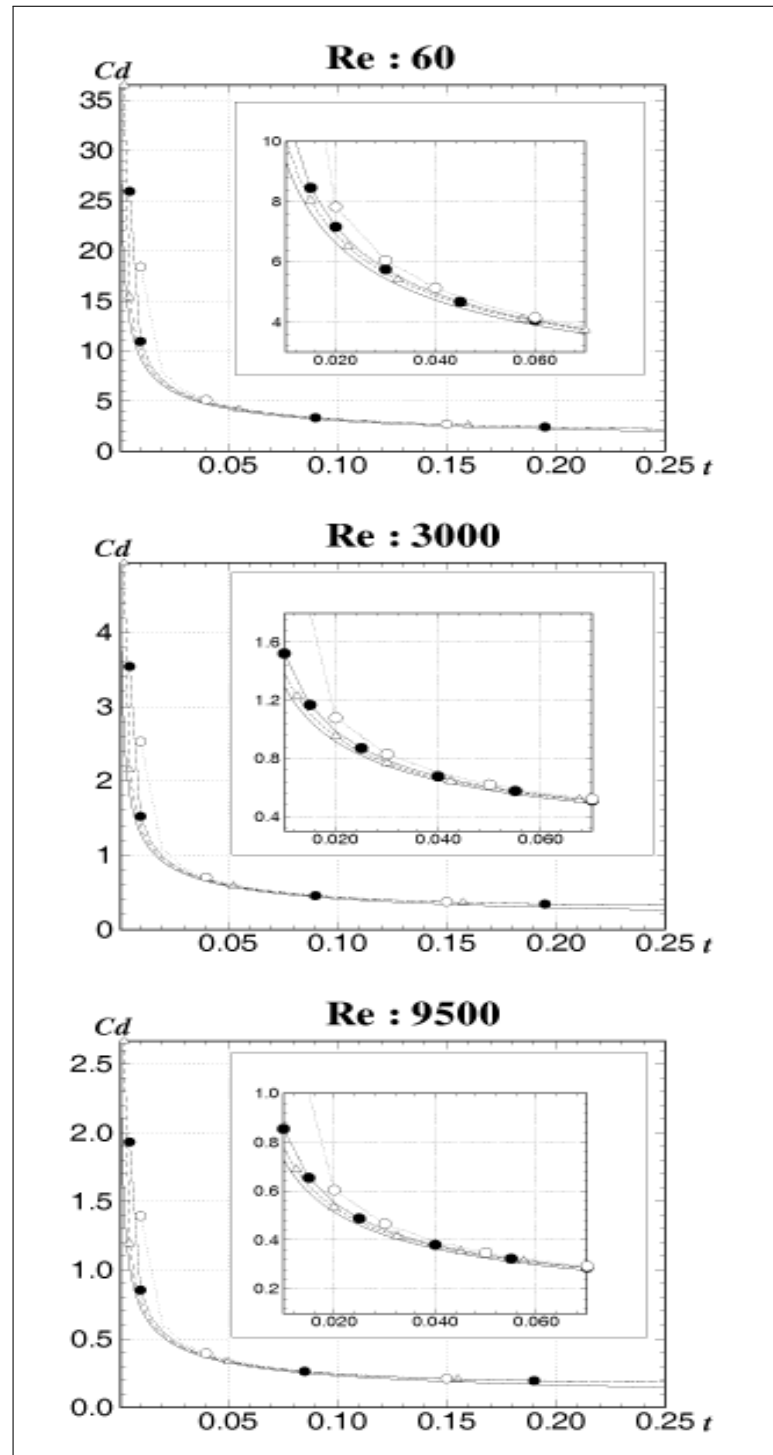
Figure 7.12 Sensitivity of the time interval on the drag coefficients of the impulsively started circular cylinder at $Re = 60, 3000$ and 9500 with $R_o = 1.5$ and the 600×80 grid.
——, analytical (Bar-Lev & Yang (1975)); $\triangle$, $\triangle t = 0.0025$; •, $\triangle t = 0.005$; ○, $\triangle t = 0.01$
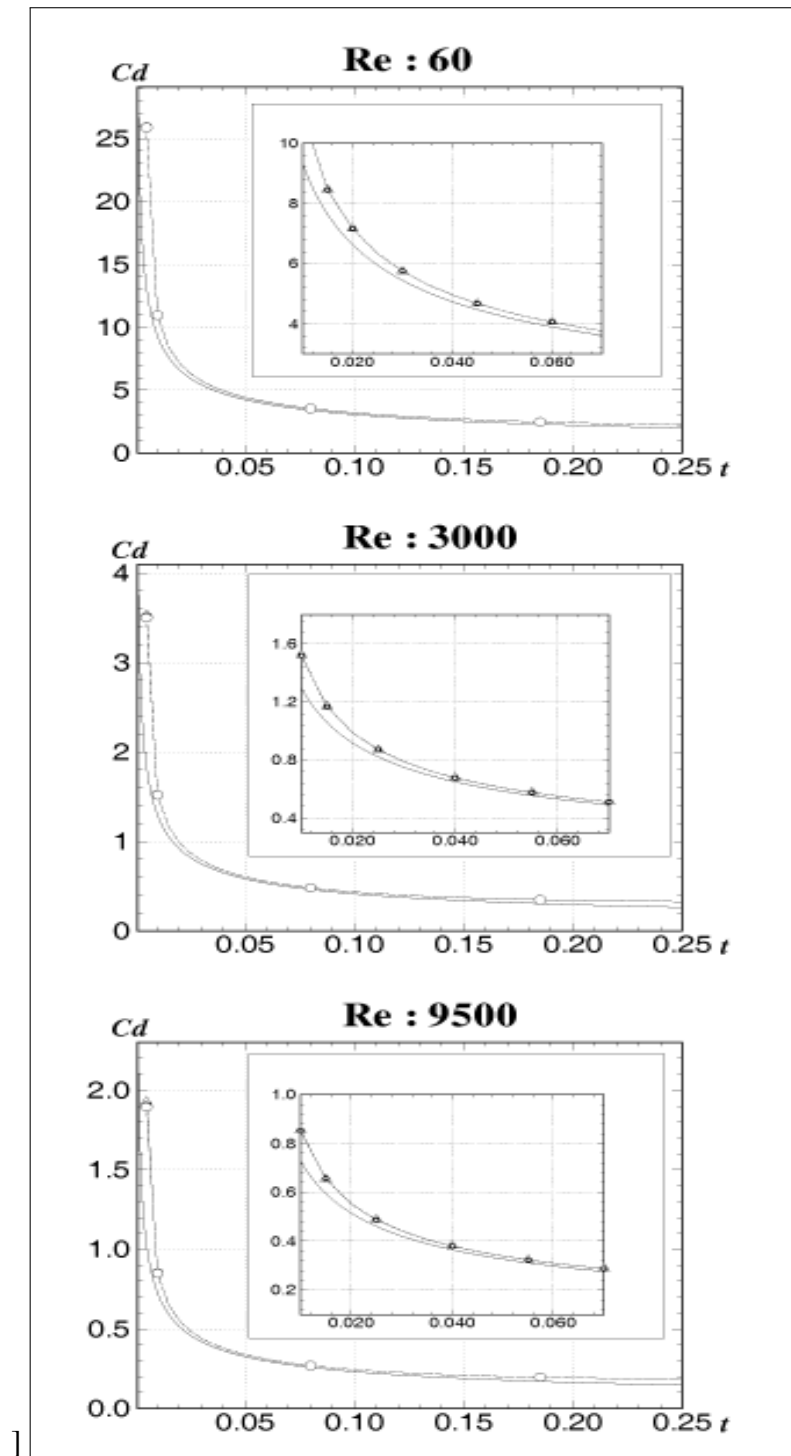
Figure **7.13** Sensitivity of the outer radius on the drag coefficients of the impulsively started circular cylinder at $Re = 60, 3000$ and 9500 with $\triangle t = 0.005$ and the 600×80 grid. ——, analytical (Bar-Lev & Yang (1975)); $\triangle$, $R_o = 1.5$; $\bullet$, $R_o = 2.5$; $\circ$, $R_o = 3.5$
Note: The results corresponding to $R_o = 2.5$ are not detectable because of the nearly same values as the others.
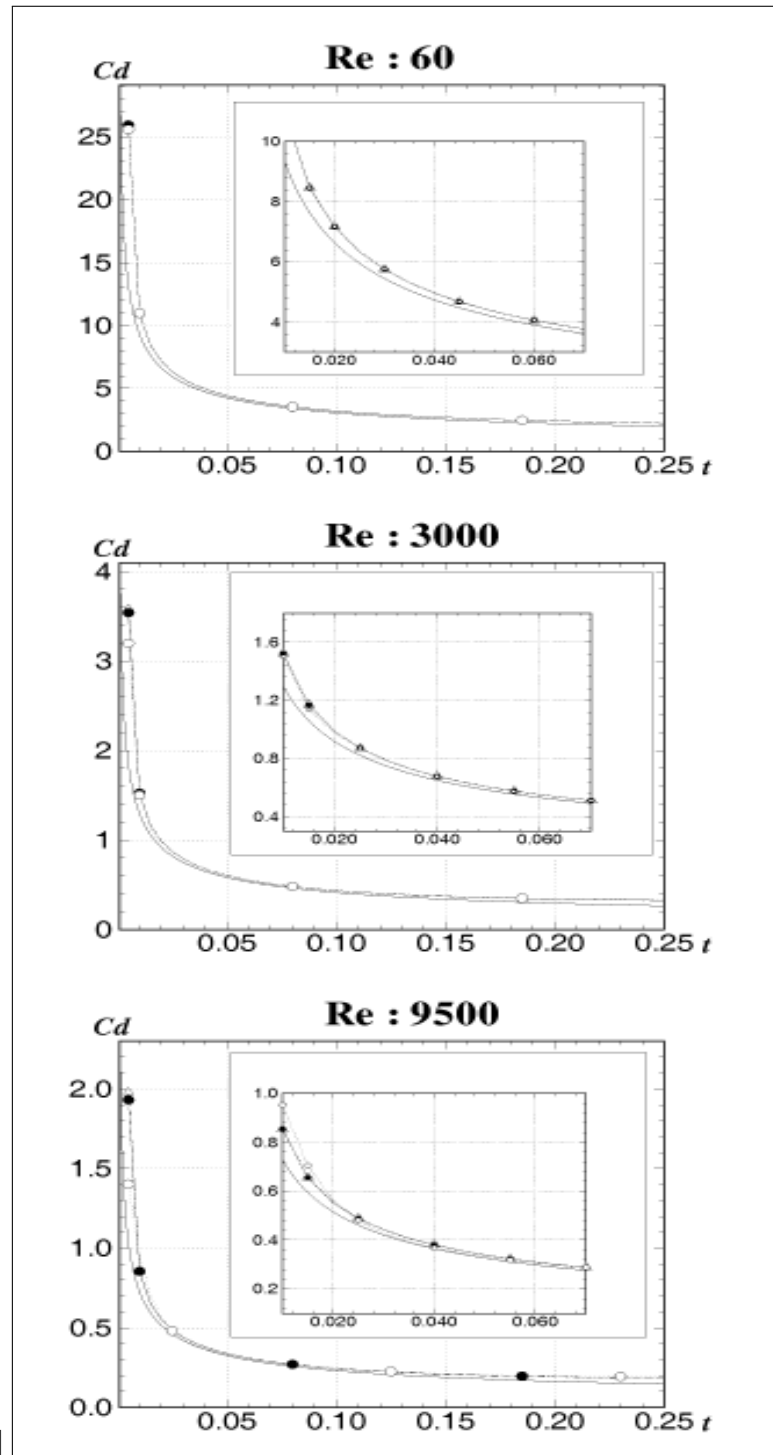
Figure **7.14** Sensitivity of the mesh size on the drag coefficients of the impulsively started circular cylinder at $Re = 60, 3000$ and 9500 with $\triangle t = 0.005$ and $R_o = 1.5$.
——, analytical (Bar-Lev & Yang (1975)); $\triangle$, grid 800×100; •, grid 600×80; ○, grid 300×40

7.4.3.4 Reynolds number

In Figure **7.15** we plot the vorticity distribution on the cylinder surface at $t = 0.2$ and $t = 0.4$ for $Re = 3000$. By comparing these results with the analytical solutions, we find that the body vorticity obtained is satisfactory. Since this measure is directly related to the frictional drag, we guarantee the agreement of the frictional drag with the analytical solution as shown in Figures. **7.12** through **7.14** .
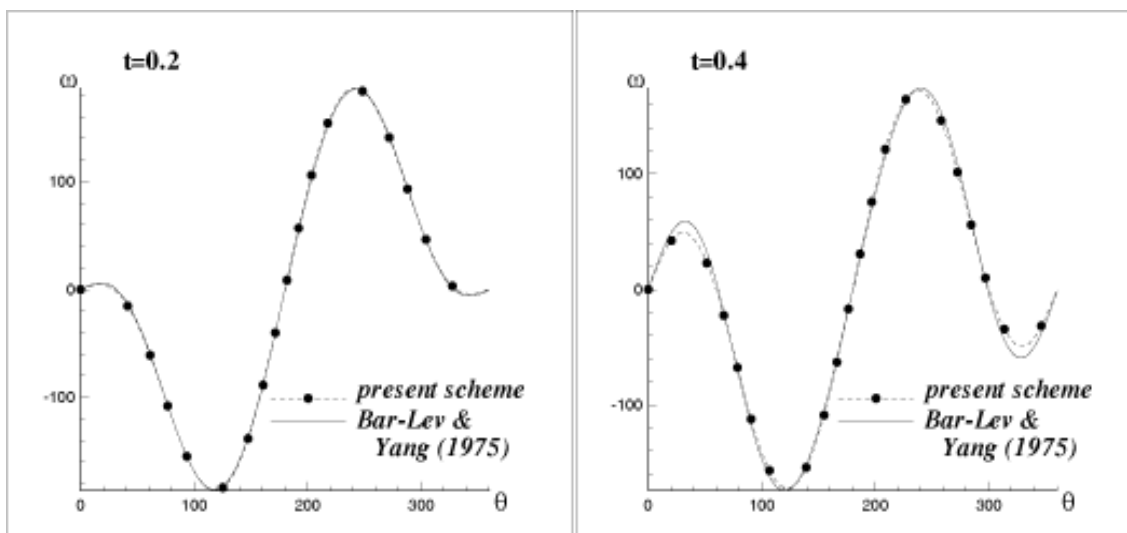
Figure 7.15 Comparison of the computed surface vorticity with the analytical solution of the impulsively started circular cylinder at $Re = 3000$ with the 600×80 grid, $\triangle t = 0.005$ and $R_o = 1.5$.

Figure **7.16** shows the time evolution of the primary separation position for $Re = 9500$. The position is determined in such a way that the body vorticity is zero. The separation angle θ_s is measured from the rear stagnation point. We observe a rapid development of the separation region at about $t = 0.16$ and a reasonable agreement of the present results with those obtained from the analytical solution.

7.4.3.5 Pressure, velocity and vorticity fields

The pressure distribution on the cylinder surface is shown in Figure **7.17** at several instants.
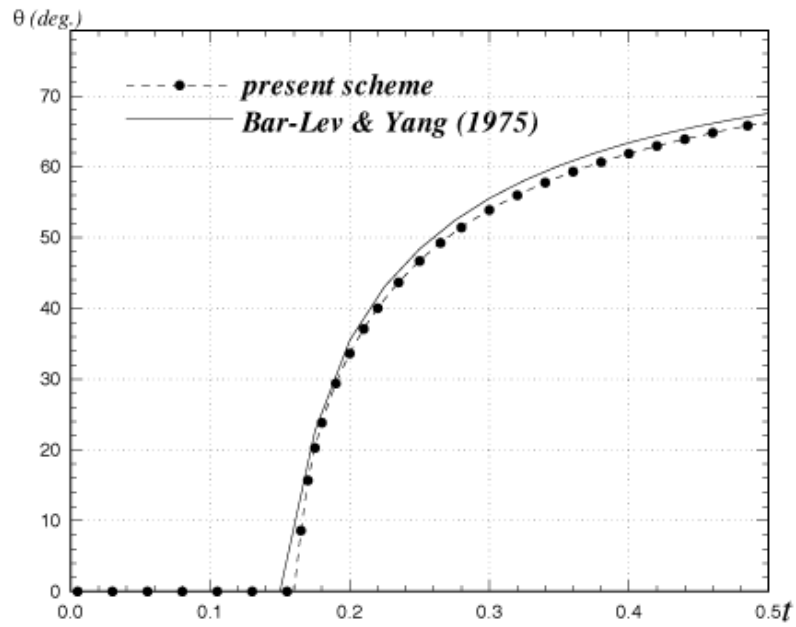
Figure **7.16** Time evolution of the primary separation position of the impulsively started circular cylinder at $Re = 9500$ with $\triangle t = 0.005$, the 600×80 grid and $R_o = 1.5$.
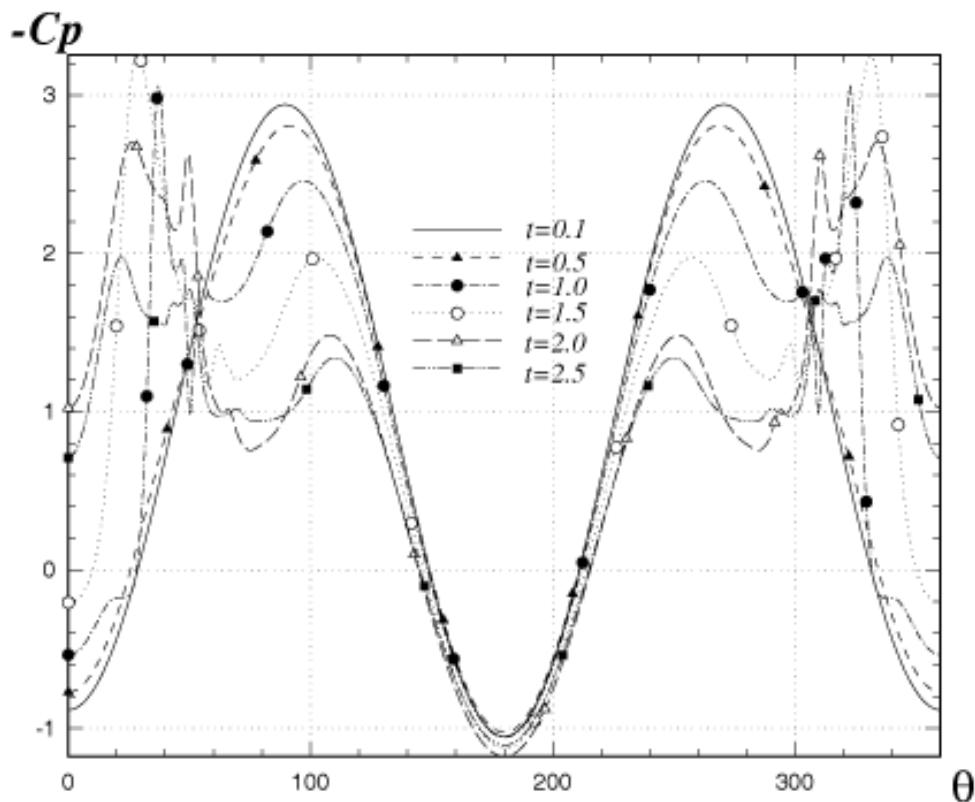
Figure 7.17 Surface pressure distribution of the impulsively started circular cylinder at several

At the early time the pressure distributions represents nearly the distribution obtained from the potential flow analysis, because we can regard a very thin layer of vorticity formed around the cylinder as an equivalent vortex sheet. As this thin layer continues to grow, the pressure distributions are rapidly modified near the strong vortical flow structures. While the change of pressure near the front portion of the cylinder surface is not so great, the pressure distribution near the rear portion is greatly changed. This feature is associated with the complicated flow experimentally observed or numerically simulated in the wake region behind the cylinder at such a high Reynolds number.

Figure **7.18** shows the computed streamline pattern at some instants for $Re = 9500$. Although their results are not presented herein, the pattern reveals good agreement with the experiment by Bouard and Coutanceau (1980) and the computation by Koumoutsakos and Leonard (1995).

In Figure **7.19** , the vorticity contours at several instants for $Re = 9500$ are presented. These contours are reasonably compared to other available results (e.g. those in figure 26 in Koumoutsakos and Leonard, 1995). The complicated interaction between the vortical structures developed at the cylinder surface is expected to appear as time advances. This deduction can be also drawn from the corresponding pressure fields shown in Figure **7.20** . The strong vortical flow forms a lower pressure region moving downstream and the vorticity strength is slightly weaker by the viscous diffusion as time advances.

The comparison between the time-averaged vorticity flux and the vorticity flux at the end of the time interval is presented in Figure **7.21** . It is observed that their difference is negligible except in their high peak value region. The vorticity flux defined in the time-averaged sense when we solved the vorticity transport equation reflects well the global coupling of the vorticity flux with the pressure. However, in the present method, the calculation of the vorticity flux at the end of the time step was separately done because we need the calculation of the pressure drag.

By applying the present numerical algorithm for the impulsively started circular cylinder problems, we have validated the present formulation.
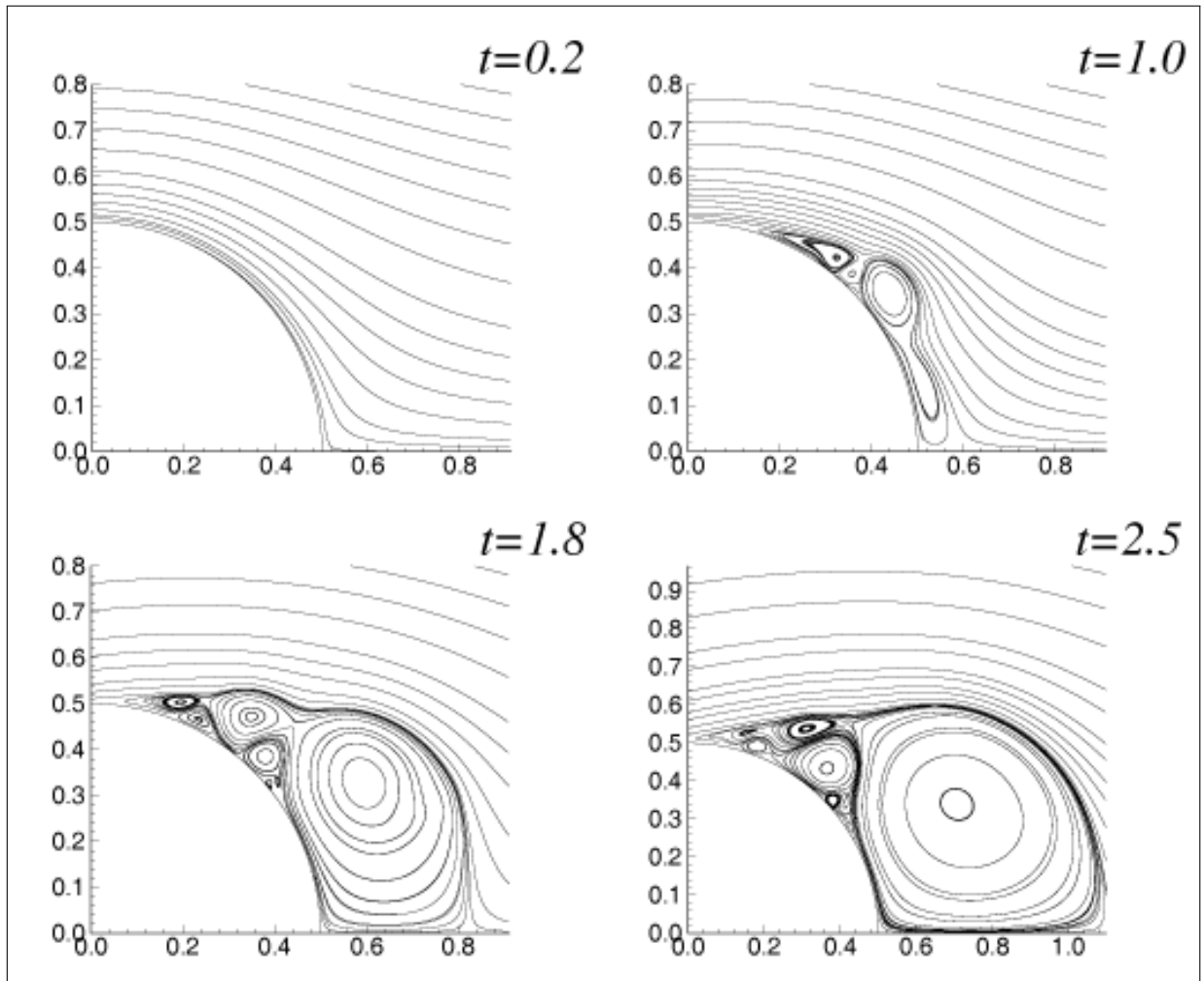
Figure **7.18** Streamline patterns of the impulsively started circular cylinder for $Re = 9500$ with $\triangle t = 0.005$, the 600×80 grid and $R_o = 1.5$.
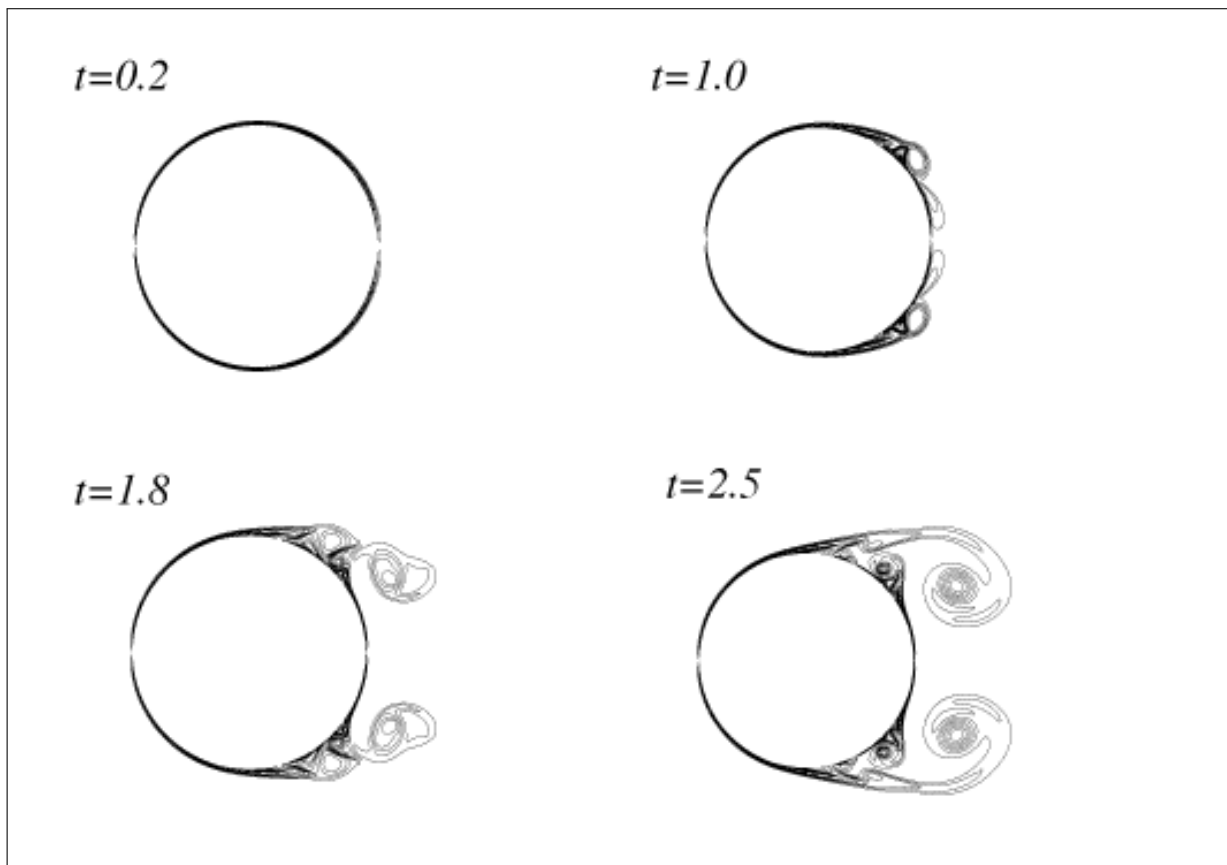
Figure **7.19** Vorticity contours of the impulsively started circular cylinder for $Re = 9500$ with $\triangle t = 0.005$, the 600×80 grid and $R_o = 1.5$.
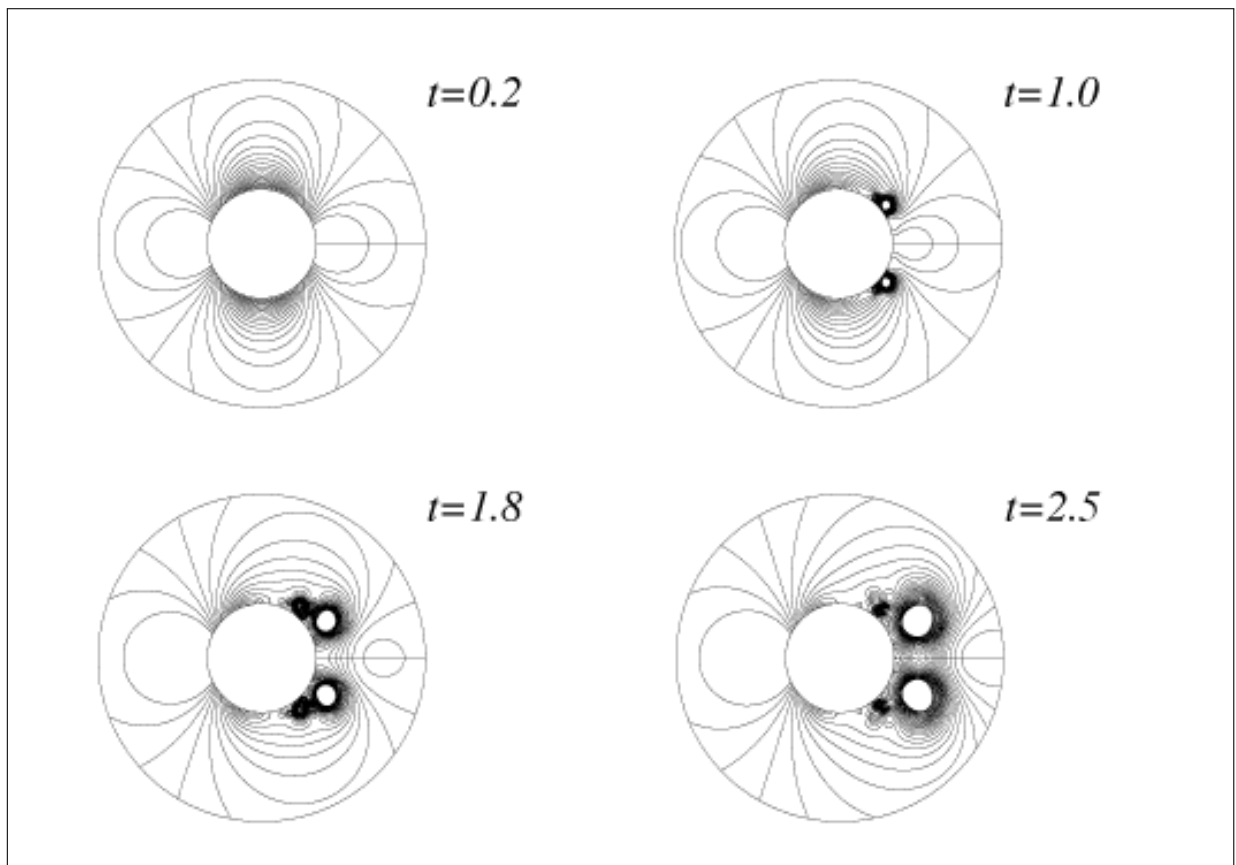
Figure **7.20** Pressure contours of the impulsively started circular cylinder for $Re = 9500$ with $\triangle t = 0.005$, the 600×80 grid and $R_o = 1.5$.
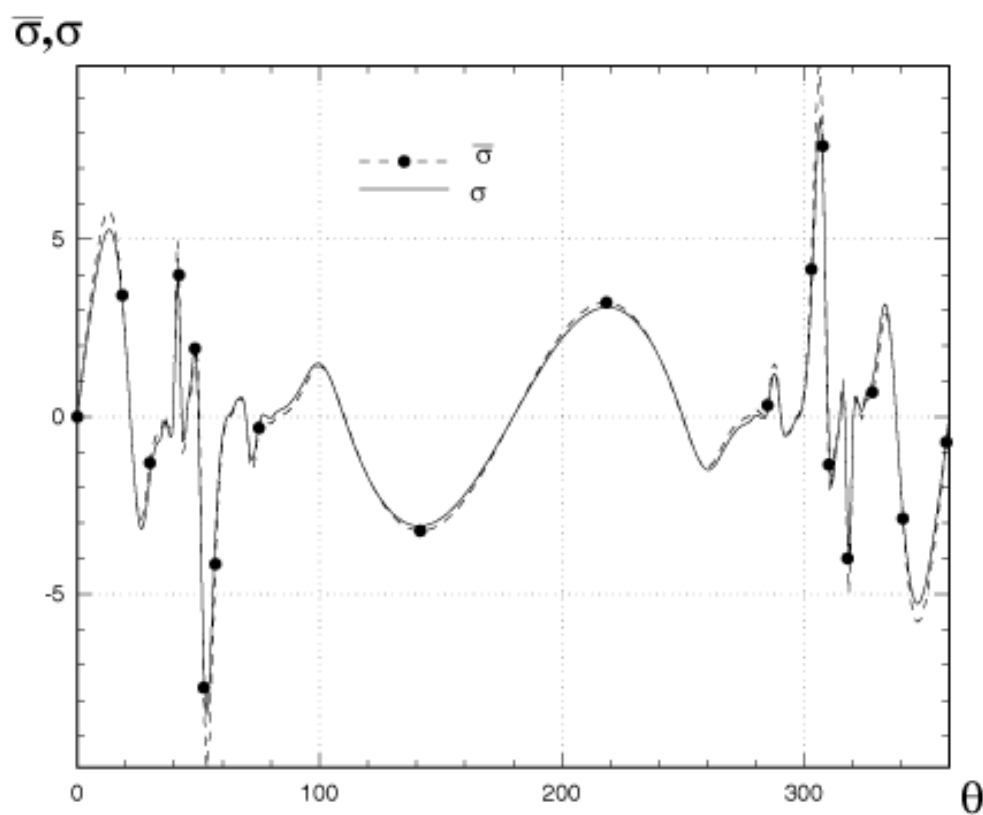
Figure **7.21** Time-averaged vorticity fluxes ($\overline{\sigma}$) of the impulsively started circular cylinder in $t_1 - \triangle t < t < t_1$ and vorticity flux (σ) at $t = t_1$, where $t_1 = 2.5$ for $Re = 9500$ with $\triangle t = 0.005$, the 600×80 grid and $R_o = 1.5$.

7.5 Oscillating Circular Cylinder Problems

7.5.1 Key parameters

The motion of circular cylinders in a fluid at rest is especially of interest in fields of offshore and civil engineering, such as marine risers, subsurface pipelines, etc. An overall review is given by Williamson (1996) and by Sumer and Fredsøe (1997).

When the relative flow past a cylinder is undergoing sinusoidal oscillations, the structure of the flow generated by the cylinder depends mainly on two parameters, namely, the Keulegan-Carpenter number, KC and the Reynolds number, Re. The KC number is defined by

$$KC = \frac{U_m T}{D} = \frac{2\pi A_0}{D} \tag{7.32}$$

in which U_m is the maximum velocity, T is the period of the oscillatory flow, and A_0 is the amplitude of the motion. The Reynolds number is defined as

$$Re = \frac{U_m D}{\nu} \tag{7.33}$$
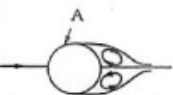
where ν is the kinematic viscosity of the fluid. The ratio

$$\beta = \frac{Re}{KC} = \frac{D^2}{\nu T}, \tag{7.34}$$

being the *Stokes parameter* is a viscous scale parameter(Sarpkaya 1986). Many researchers measured forces acting on a circular cylinder in oscillatory flow as a function of KC and β.

Table 7.1 Regimes of flow around a circular cylinder in oscillatory flow at $Re = 10^3$. Source for $KC < 4$ is from Sarpkaya (1986), and for $KC > 4$ from Williamson (1985).

KC<1.1	a)	No Separation Creeping flow
1.1<KC<1.6	b)	Separation with Honji vortices
1.6<KC<2.1	c)	A pair of symmetric vortices
2.1<KC<4	d)	A pair of symmetric vortices Turbulence over the cylinder
4<KC<7	e)	A pair of asymmetric vortices
7<KC	f)	Vortex shedding

7.5.2 Flow characteristics

Investigating the physical meaning of the KC number , the numerator of the right-hand side of the Eq. (7.32) is proportional to the stroke of the motion, namely $2A_0$, while the denominator of the diameter of the cylinder D, represents the width of the cylinder. Small KC numbers therefore mean that the orbital motion of the fluid particles is small relative to the total width of the cylinder. When KC is very small, separation behind the cylinder may not even occur. Large KC numbers imply that the fluid particles travel quite large distance relative to the total width of the cylinder, resulting in separation and probably vortex shedding. For very large KC numbers ($KC \to \infty$), it is expected that the flow for each half period of the motion resembles that experienced in a steady current(Sumer & Fredsøe 1997).

Experimental investigations of the oscillatory flow around a circular cylinder at small KC have shown that the flow can be classified into a number of different flow regimes governed mainly by KC and with a weak dependency on Re(Bearman *et al.* 1985, Williamson 1985, Sarpkaya 1986). At $KC \ll 1$, the

flow remains symmetrical, attached, and two-dimensional. As KC is increased, the flow becomes asymmetrical ($KC = 4 \sim 5$). At $KC = 10$, a transverse vortex street appears. Table **7.1** summarizes the changes of the flow pattern as the KC number is increased at $Re = 10^3$. Notice that limits of KC regimes are dependent on Re(Justesen 1991, Summer & Fredsøe 1997). By further increasing the KC number, the so-called *vortex-shedding regimes* ($KC > 7$, $Re = 10^3$) appear. According to the description of the vortex trajectory patterns in a systematic manner by Williamson (1985), in the vortex shedding regimes the vortex shedding occurs during the course of each half period of the oscillatory motion. There are several such regimes, each of which has different vortex flow pattern, observed for different ranges of the KC number. These KC ranges include $7 < KC < 15$, $15 < KC < 24$, $24 < KC < 32$, etc.

Figure **7.22** illustrates the time development of vortex motions in the regime at $7 < KC < 15$. The major portion of the KC range, namely $7 < KC < 13$ (Figure **7.22** a), is known as the transverse vortex street regime. The arrows in Figure **7.22** refer to cylinder motion. The wake consists of a series of vortices convecting out to one side of the cylinder in the form of a street. Figure **7.22** b shows the vortex shedding patterns in the regime at $13 < KC < 15$. The wake consists of a series of pairs convecting away each cycle in the direction of about $45°$ to the flow oscillation direction, from only one side of the cylinder. In Figure **7.22** a and Figure **7.22** b, shown is always one pair of vortices which convect away from the cylinder. It is called *"the single pair regime"*.

Figure **7.23** shows the time development of vortex motions in the case of $15 < KC < 24$, that corresponding to *"double pair regime"*. The resultant wake is due to two vortices shed during each half cycle. Two trails of vortex pairs convect away from the cylinder in opposite directions and from opposite sides of the cylinder.

Figure **7.24** depicts the vortex motions in the case of $24 < KC < 32$, namely *"the three pairs regime"*. The wake of three vortices shed during a half cycle becomes three vortex pairings in a cycle. By varying both β and KC (correspondingly Re) , flow patterns may be classified into several regimes according to their structure. The KC and β regimes are plotted in Figure **7.25** . Eight regimes are labelled by A^* through G based on experimental results by
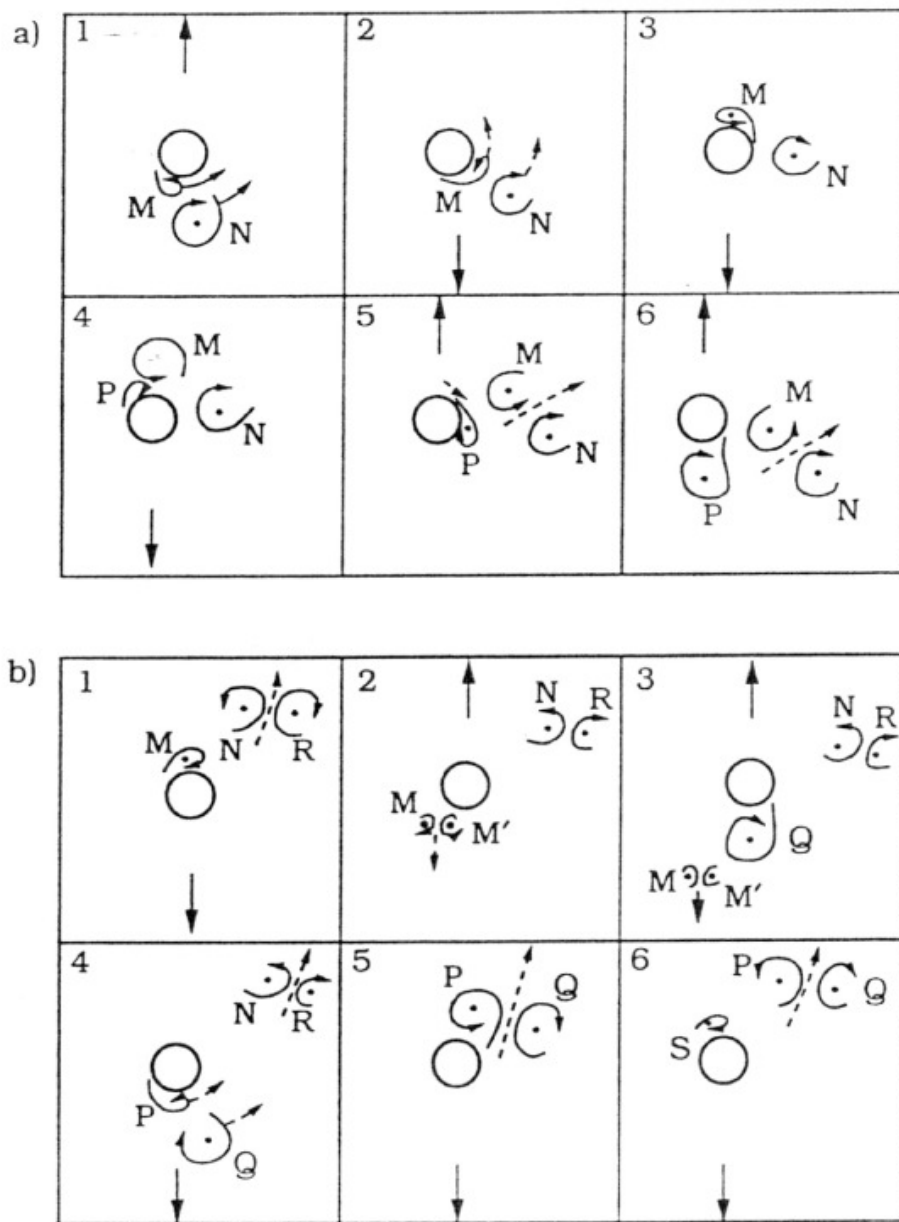
Figure **7.22** Single pair regime of flow around a circular cylinder in oscillatory motion for $7 < KC < 15$. (a) $7 < KC < 13 <$; (b) $13 < KC < 15$. From Williamson (1985).
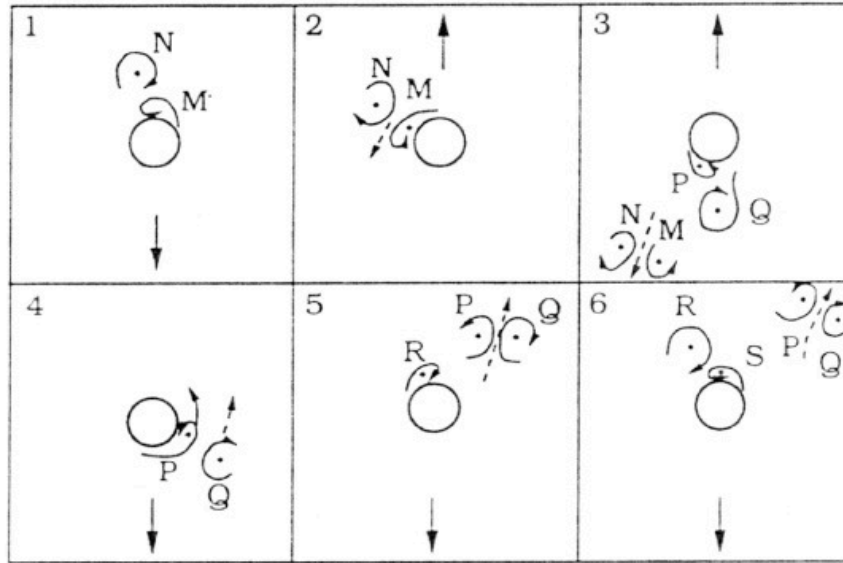
Figure **7.23** Double-pair regime of flow around a circular cylinder in oscillatory motion for $15 < KC < 24$. From Williamson (1985).
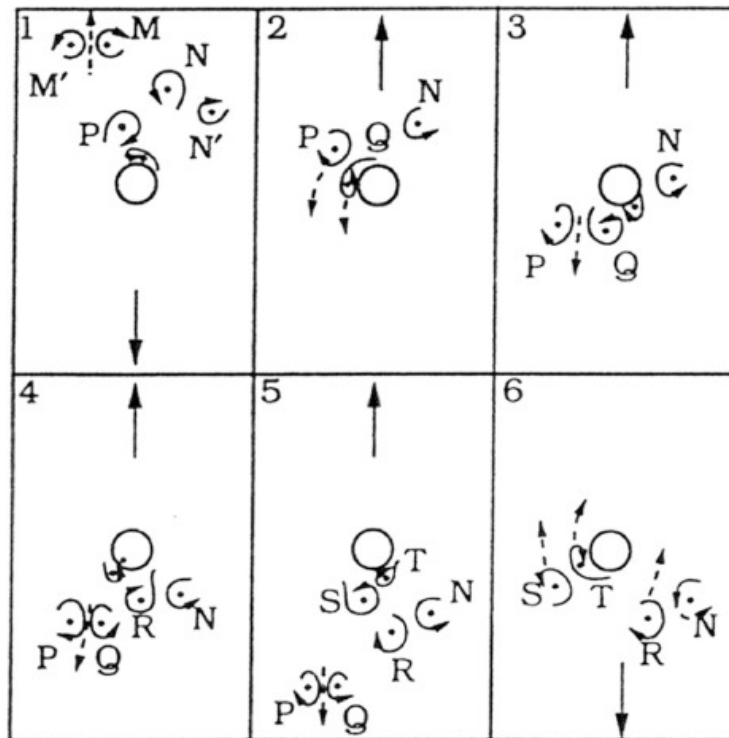
Figure **7.24** Three-pair regime of flow around a circular cylinder in oscillatory motion for $24 < KC < 32$. From Williamson (1985).
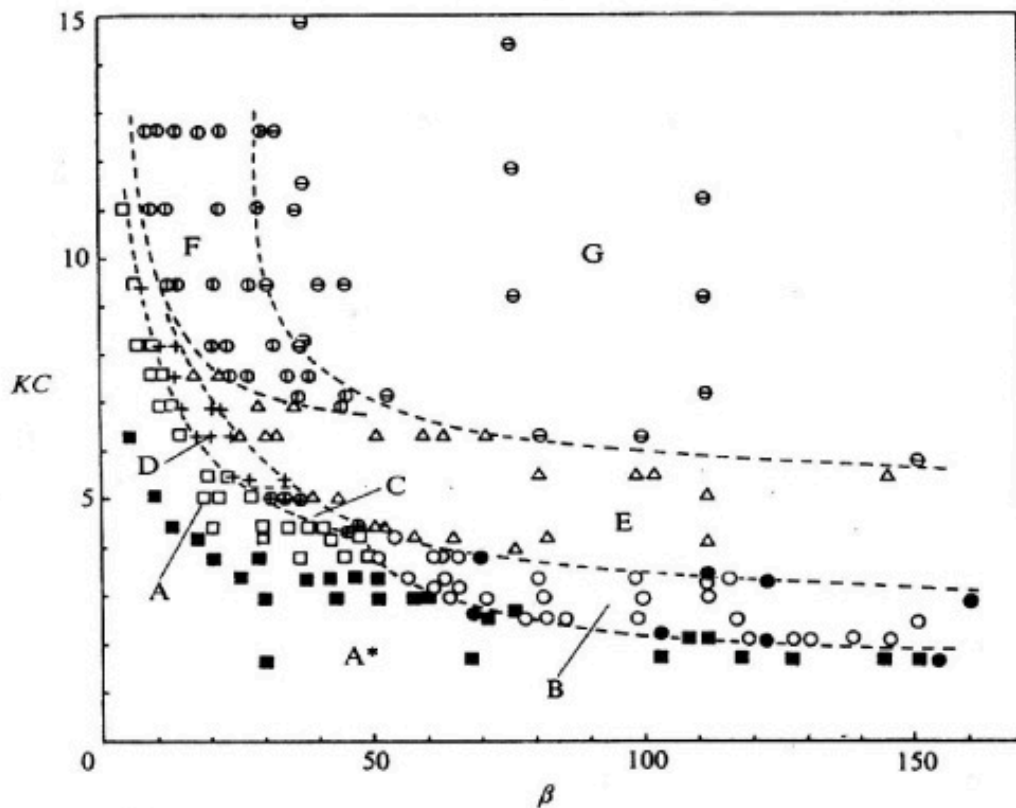
Figure 7.25 Classification of flows around a circular cylinder in oscillatory motion. Flow patterns are identified within eight regimes indicated $A^* - G$. ■ , A^* ; □ , A ; ◯ , B ; ⊕ , C ; + , D; △ , E ; ◐ , F; ⊖ , G ; ● , critical values for appearance of a streaked flow. From Tatsuno & Bearman (1989).

Tatsuno & Bearman (1989). Principal features of the oscillating flow in the eight regimes are summarized in Table **7.2**.

Table **7.2** Principal features of the flows classified in eight regimes of flow around a circular cylinder in oscillatory motion with KC and β. From Tatsuno & Bearman (1989).

flow regimes	principal features
A*	No flow separation; secondary streaming two-dimensional
A	Two vortices shed symmetrically per half cycle two-dimensional
B	Three-dimensional instability longitudinal vortices
C	Rearrangement of large vortices three-dimensional
D	Flow convected obliquely to one side of the axis of oscillation; three-dimensional
E	Irregular switching of flow convection direction three dimensional
F	Flow convected diagonally three dimensional
G	Transverse vortex street three dimensional

Another main feature of the oscillating cylinder is the relation between the vortex shedding frequency and lift frequency. It appears that the peak of the lift force occurs immediately after the reversal motion of the cylinder is associated with the return of the most recently shed vortex to the cylinder, while the other peaks in the lift variation are associated with the vortex shedding. Thus, it is evident that, in oscillatory flows, the lift force frequency is not identical to the vortex shedding frequency(Sumer & Fredsøe 1997). One way for determining lift frequency is by using power spectrum of the lift force and identifying the fundamental frequency. Williamson (1985)'s work, where the ratio of Re to KC was kept constant at $\beta = Re/KC \approx 255$ in one series of the experiments and at $\beta \approx 730$ in the other, has indicated that the fundamental lift frequency increases with increasing KC, as shown in Table **7.3**.

Table 7.3 Fundamental lift frequencies of the observed flow around a circular cylinder in oscillatory motion. From Williamson (1985).

KC regime	KC regime	Reynolds number Re	Normalized fundamental lift frequency (= Number of oscillation in the lift per flow-cycle) $N_L = \dfrac{f_L}{f_\omega}$
Single pair	$7 < KC < 15$	$1.8 - 3.8 \times 10^3$	2
Double pair	$15 < KC < 24$	$3.8 - 6.1 \times 10^3$	3
Three pairs	$24 < KC < 32$	$6.1 - 8.2 \times 10^3$	4
Four pairs	$32 < KC < 40$	$8.2 - 10 \times 10^3$	5

7.5.3 Formulation for moving frame fixed to cylinder

The present calculation provides solutions obtained by the Eulerian FVM method for the problem of the oscillating cylinder. It is expected to provide the simulations of vortex shedding from the cylinder. In addition, when investigating the characteristic of lift frequency, the vortex shedding frequencies are investigated with the variety of the flow regimes with each other KC and β.

Let us consider the harmonic in-line motion of the cylinder in a fluid at rest. Position, velocity and acceleration of the local moving coordinate at the center of the circular cylinder are defined, respectively, as

$$\underline{x} = A_0 \sin(f\,t)\,\underline{i}, \tag{7.35}$$
$$\dot{\underline{x}} = \underline{q}_F = A_0\,f\,\cos(f\,t)\,\underline{i}, \tag{7.36}$$
$$\dot{\underline{q}}_F = -A_0\,f^2\,\sin(f\,t)\,\underline{i}. \tag{7.37}$$

The relative velocity to the local moving frame is $\underline{q} = -\underline{q}_F + \underline{u}$ where $\underline{u}$ is the velocity in the inertia frame. Assume the acceleration of the local moving frame is not zero, then Navier- Stokes equation at the local moving frame is represented as

$$\frac{D\underline{q}}{Dt} + \dot{\underline{q}}_F = -\nabla\left(\frac{p}{\rho}\right) - \nabla \times (\nu\,\underline{\omega}) \tag{7.38}$$

Vorticity transport equation and pressure equation derived from Eq. (7.38) are not changed at the local moving frame. The vorticity-velocity relation with the Biot-Savart integral(Eq. (6.43)), however, should be included with the velocity on the local moving frame. Dynamic vorticity boundary condition and pressure boundary condition (Eqs. (6.48) through (6.49)), are modified.

The main parameters are non-dimensionalized as

$$Re = \frac{U_0 D}{\nu}, \quad t^* = \frac{U_0 t}{D}, \quad U_0 = A_0 f, \quad KC = \frac{2\pi A_0}{D} \tag{7.39}$$

where U_0 is the maximum velocity , D is cylinder diameter, and A_0 is the amplitude of the cylinder. With the non-dimension parameters, the governing equations are expressed as

$$\frac{\partial \omega}{\partial t} + \nabla \cdot (\underline{q}\, \omega) = \frac{1}{Re} \nabla^2 \omega, \tag{7.40}$$

$$\underline{q} = -\underline{U}_0 \cos\left(\frac{2\pi}{KC} t^*\right) \underline{i} + \oint_C (\omega\,\underline{k}) \times \nabla G\, dl. \tag{7.41}$$

$$\nabla^2 \left(\frac{1}{2}\underline{q}^2 + \frac{p}{\rho}\right) = \nabla \cdot (\underline{q} \times \omega\,\underline{k}), \tag{7.42}$$

These equations are equivalent to Eqs. (6.42) through (6.44). The boundary conditions of vorticity and pressure with no-slip condition are

$$\frac{1}{Re} \frac{\partial \omega}{\partial n}\,\underline{k} = \underline{n} \times \left\{ \left(\frac{D\underline{q}}{Dt} + \nabla p\right) - \frac{2\pi}{KC} \sin\left(\frac{2\pi}{KC} t^*\right) \underline{i} \right\} \tag{7.43}$$

$$\frac{\partial H}{\partial n} = \underline{n} \cdot \left\{ \left(\underline{q} \times \omega\,\underline{k} - \frac{1}{Re} \nabla \times \omega\,\underline{k}\right) + \frac{2\pi}{KC} \sin\left(\frac{2\pi}{KC} t^*\right) \underline{i} \right\} \tag{7.44}$$

These are comparable to Eqs. (6.48) and (6.49). (See also Kim *et al.* (2003).)

7.5.4 Numerical simulation

The calculation for three different conditions of KC and β is performed, each of which is characterized with the different flow regimes.

7.5.4.1 Case 1: $KC = 7, \beta = 143\,(Re = 1000)$

According to Tatsuno and Bearman (1989), the regime of the present parameters ($KC = 7$, $\beta = 143$) is the regime named **G**, as shown in Figure **7.25** and Table **7.2**. The principal feature in this regime has transverse vortex street, i.e., the vortex is shedding in direction perpendicular to the in-line motion of the cylinder. The feature of vortex shedding by the present calculation is shown in Figure **7.26** .
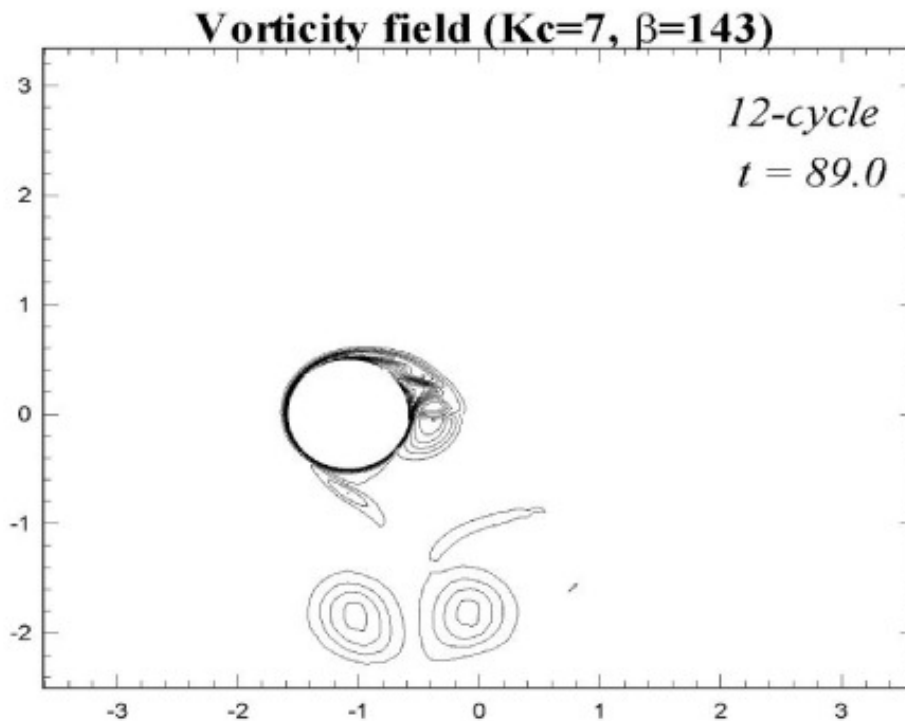
Figure **7.26** Transverse vortex street pattern of flow around a circular cylinder in oscillatory motion at $T = 89$ for $KC = 7,\ \beta = 143$.

In this figure, the single vortex pair is captured at time $t = 89$. The single vortex pair is convecting out perpendicular to one side of the cylinder. This result shows a good agreement with the flow pattern of the regime named G.

Figure **7.27** represents the time history of drag and lift coefficients. In order to analyze the periodic physics of the drag and lift forces, the time domain is converted into the frequency domain by the Fourier transformation.
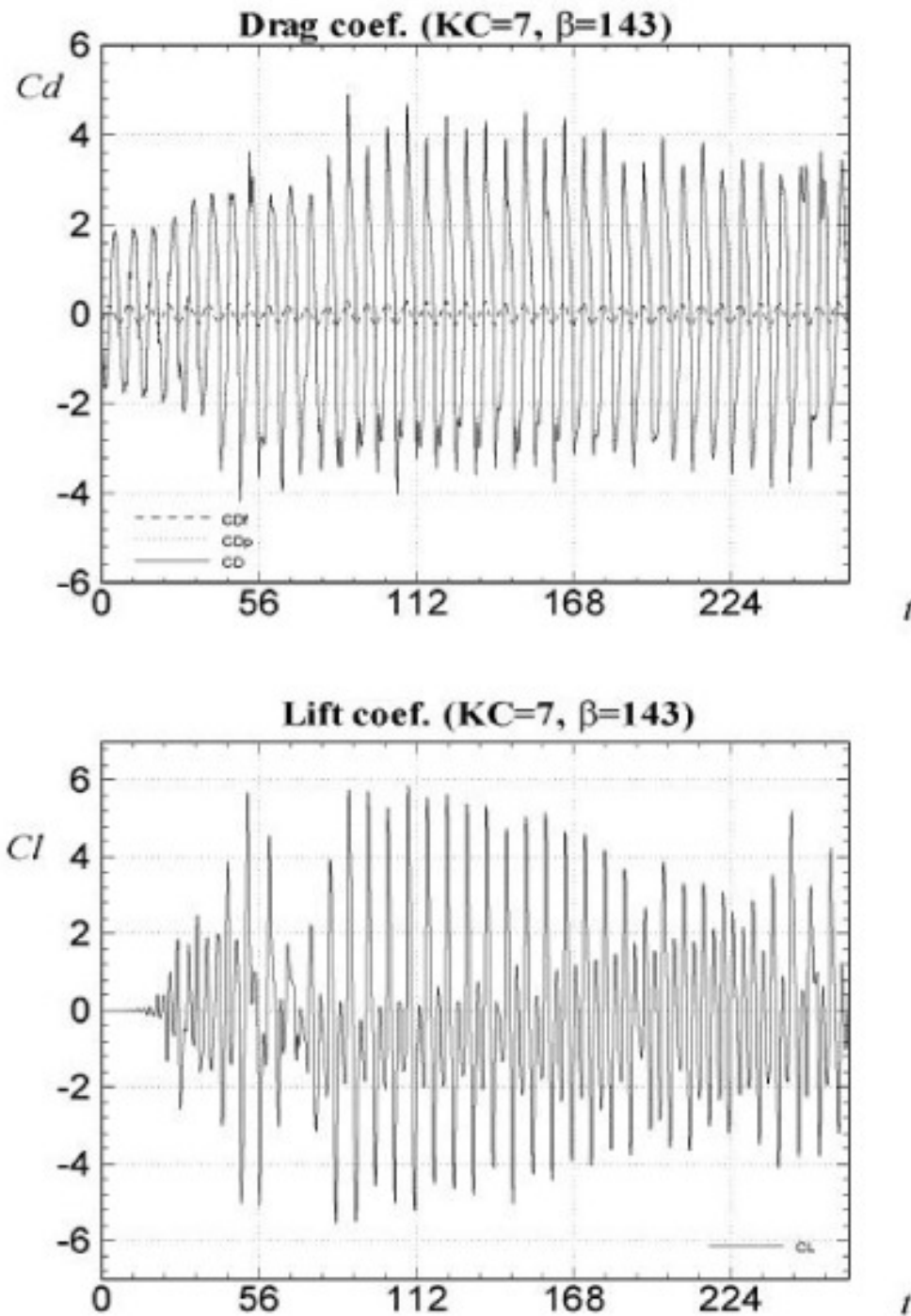
Figure **7.27** Time history of drag and lift forces of flow around a circular cylinder in oscilla-tory motion for $KC = 7$, $\beta = 143$.

As shown in Figure **7.28** , the peak of drag forces in frequency domain occurs only once at $\omega \approx 0.92$.
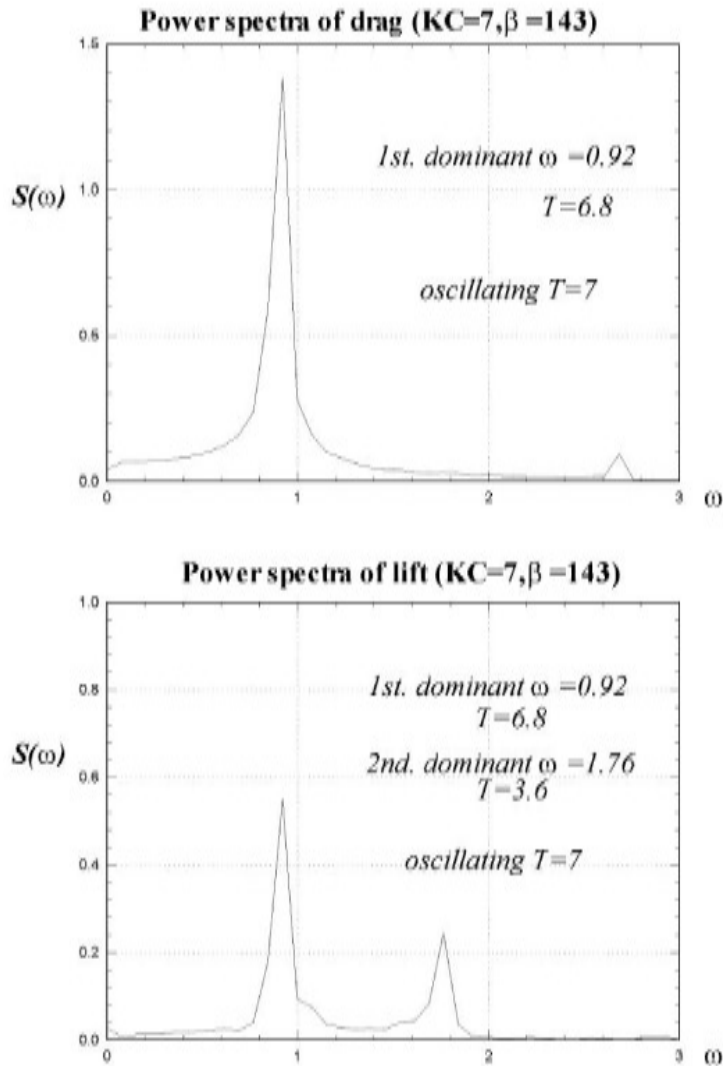
Figure 7.28 Power spectra of drag and lift forces of flow around a circular cylinder in oscillatory motion for $KC = 7$, $\beta = 143$.

The time cycle of cylinder motion is about 7, and the dominant time cycle of drag force shown in Figure **7.28** is about 6.8. The cycle of drag force coincides with the cycle of motion. On the other hand, the peaks of lift forces in frequency are appeared twice. The first fundamental frequency is $\omega = 0.92$ and the second one is $\omega = 1.76$, which corresponding to $T = 6.8$ and $T = 3.6$, respectively. The maximum lift force is appeared twice during one cycle motion of the cylinder. This fact coincides with the characteristic of the fundamental lift frequency observed by other researchers which is described with Table **7.3** in the previous section.

7.5.4.2   Case 2: $KC = 10, \beta = 20$ $(Re = 200)$

In Figure **7.25** and Table **7.2**, the regime of the present parameters($KC = 10$, $\beta = 20$) corresponds to F. The principal feature in this regime is the flow convected diagonally, i.e., when the cylinder moves from right to left, a large clockwise vortex is formed on the upper side of the cylinder and a smaller counterclockwise vortex on the lower side of the cylinder. As the clockwise vortex becomes stronger, a transverse flow appears behind the two vortices. When the cylinder reverses, the stronger clockwise vortex is convected back to the cylinder which induces a new vortex. The transverse flow developed behind the cylinder distorts the trail of flow away from the oscillation axis. This causes one vortex pair of diagonal pattern to shed. In the half cycle from left to right, a strong clockwise vortex and a flow crossing the axis of oscillation are developed in the same manner as in the previous half cycle.

Figure **7.29** shows diagonally pattern formed by single-pair vortex. This result shows a good agreement with the flow pattern of the regime named F. Figure **7.30** shows the time history of drag coefficient and lift coefficient. In
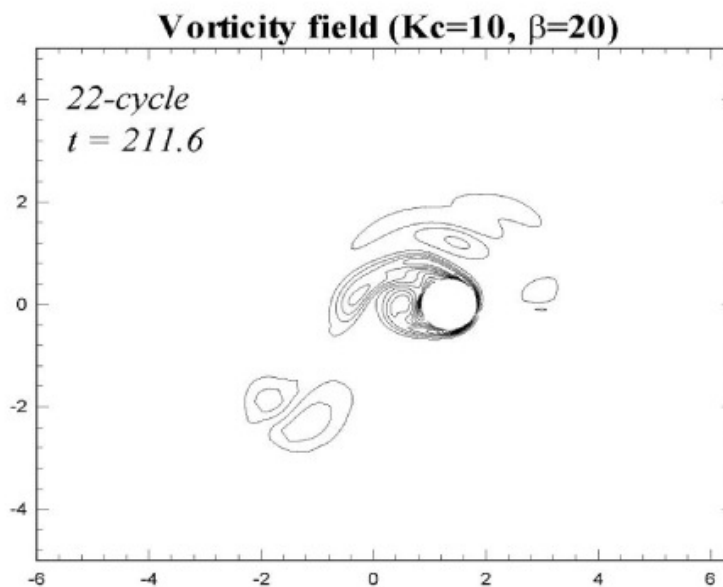
Figure **7.29** Diagonally convected single-pair vortex pattern of flow around a circular cylinder in oscillatory motion at $T = 211.6$ for $KC = 10$, $\beta = 20$.

Figure **7.31** , the peak of drag forces in frequency domain is seen to appear only

once at $\omega \approx 0.61$.
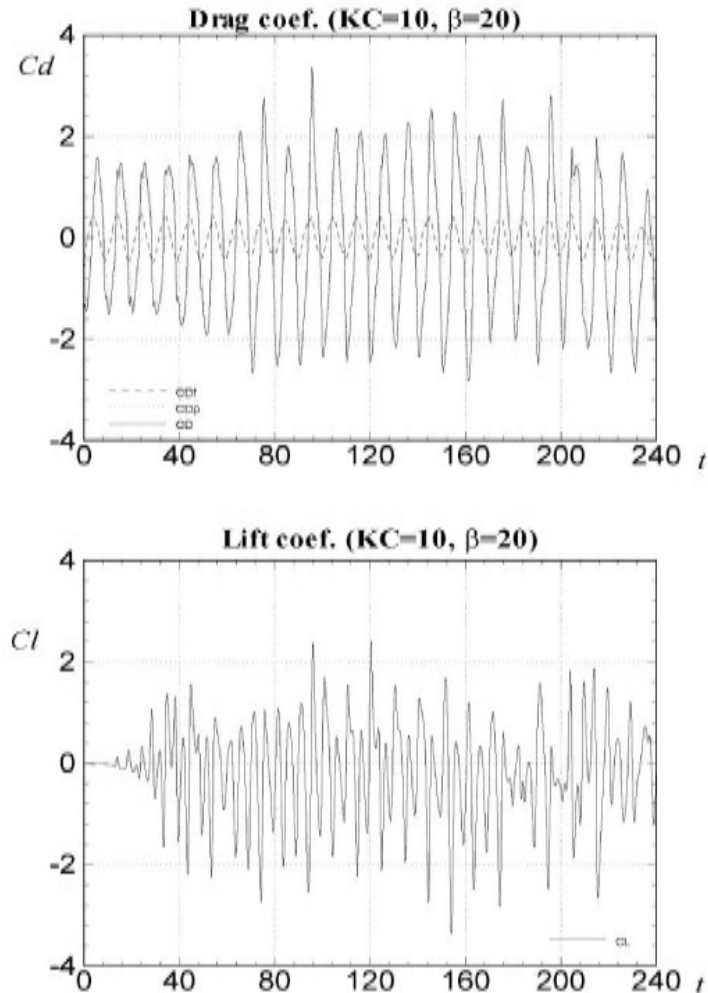
Figure 7.30 Time history of drag and lift forces of flow around a circular cylinder in oscillatory motion at $T = 211.6$ for $KC = 10, \ \beta = 20$.

The time cycle of cylinder motion is about 10, and the dominant time cycle of drag force observed in Figure **7.31** is about 10.3. The cycle of drag force coincides with the cycle of motion. The peak of lift forces in frequency is seen to appear only once. However, the dominant frequency is $\omega = 1.23$, which means that the dominant time cycle of lift force is $T = 5.1$. The maximum lift force is appeared twice during one cycle motion of the cylinder. This fact coincides with the characteristics of the fundamental lift frequency observed by other researchers (Table **7.3**).
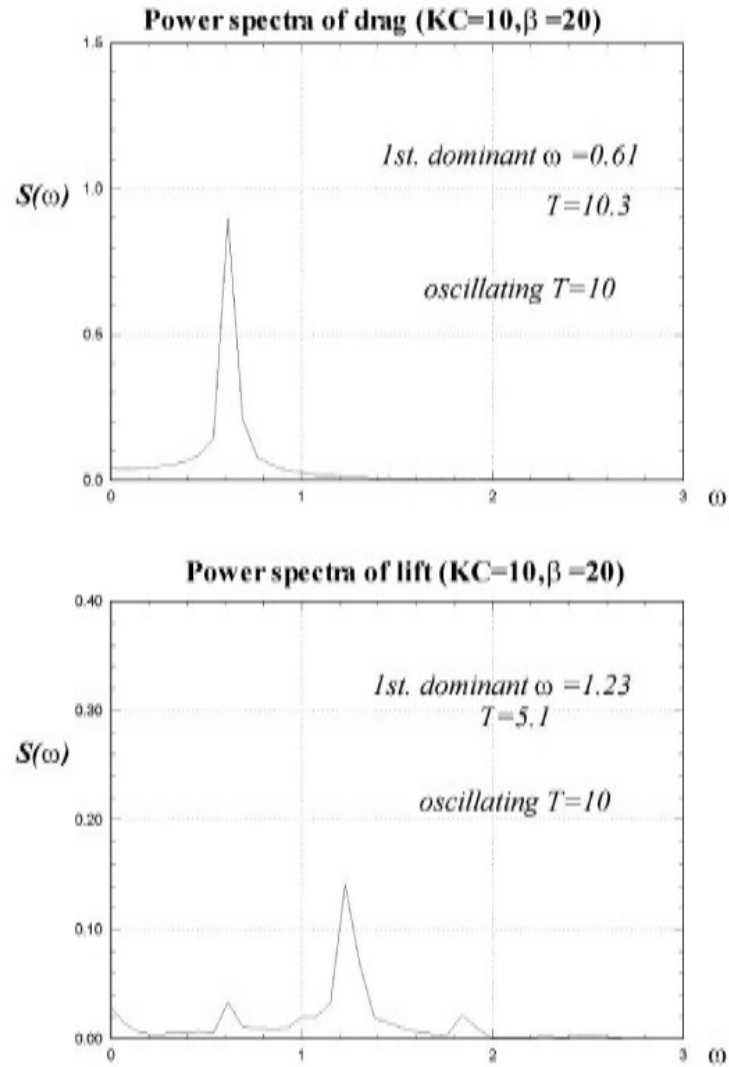
Figure 7.31 Power spectra of drag and lift forces of flow around a circular cylinder in oscillatory motion for $KC = 10$, $\beta = 20$.

7.5.4.3 Case 3: $KC = 16$, $\beta = 62.5$ ($Re = 1000$)

In this case, the vortex shedding mechanism is similar to one in the previous cases, but the resulting flow around the oscillating cylinder is more complex due to the larger KC. According to Williamson (1985)(Table **7.1**), the remarkable feature of the flow is that double-pair vortex is shedding. The regime of the present parameters is between the regime F and the regime G as shown in Figure **7.25** . This regime appears to be similar to the transverse vortex street, but the direction of the flow may change intermittently, into longitudinal, oblique, and transverse direction.

Figure **7.32** shows irregular switching of flow convection pattern formed by double-pair vortex. Figure **7.33** shows the time history of drag coefficient and lift coefficient. With the Fourier transformation, the results are shown in Figure **7.34** . In this figure, the peak of drag forces in frequency domain appears once at $\omega \approx 0.38$. The time cycle of cylinder motion is about 16, and the dominant time cycle of drag force in Figure **7.34** is about 16.5. The cycle of drag force coincides with the cycle of motion. The peak of lift forces in frequency appears once. The fundamental frequency is $\omega = 1.15$, namely, the dominant time cycle of lift force is $T = 5.46$. The maximum lift force appears three times in one cycle motion of the cylinder. This fact coincides with the characteristics of the fundamental lift frequency (see Table **7.3**).
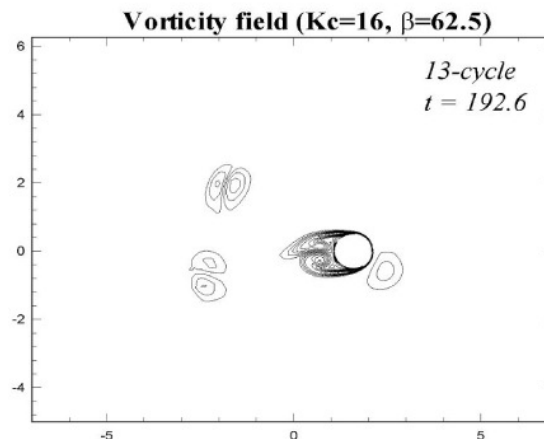
Figure **7.32** Double-pair vortex convection pattern of flow around a circular cylinder in oscillatory motion at $T = 192.6$ for $KC = 16$, $\beta = 62.5$.
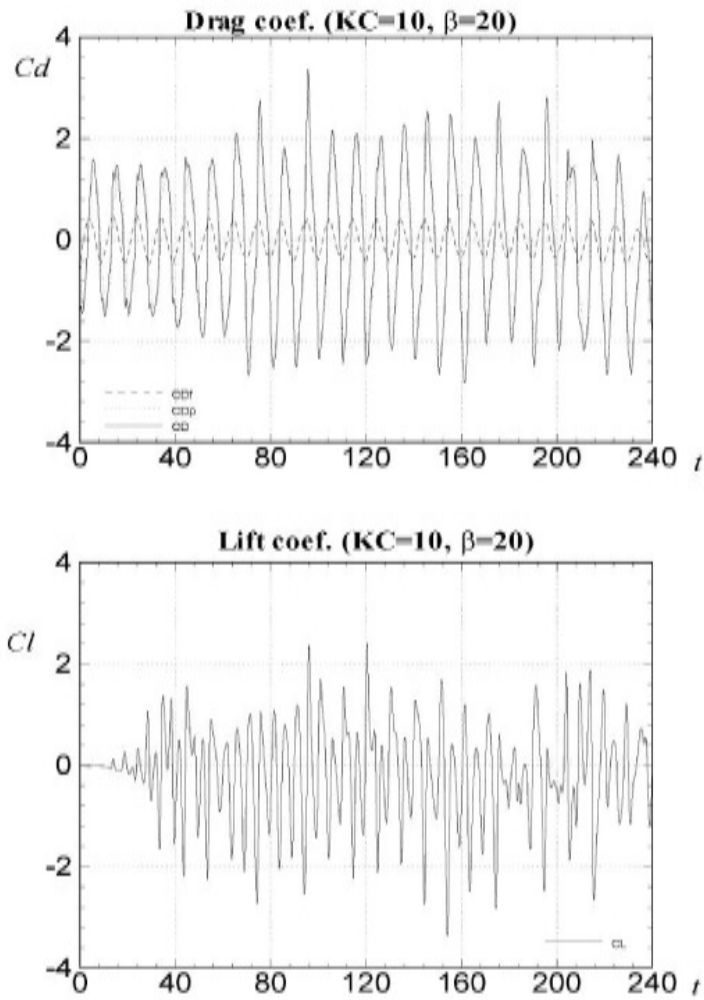
Figure **7.33** Time history of drag and lift forces of flow around a circular cylinder in oscillatory motion for $KC = 16,\ \beta = 62.5$.

Power spectra of drag (KC=10,β =20)

1st. dominant ω =0.61

T=10.3

oscillating T=10

$S(\omega)$

Power spectra of lift (KC=10,β =20)

1st. dominant ω =1.23

T=5.1

oscillating T=10

$S(\omega)$
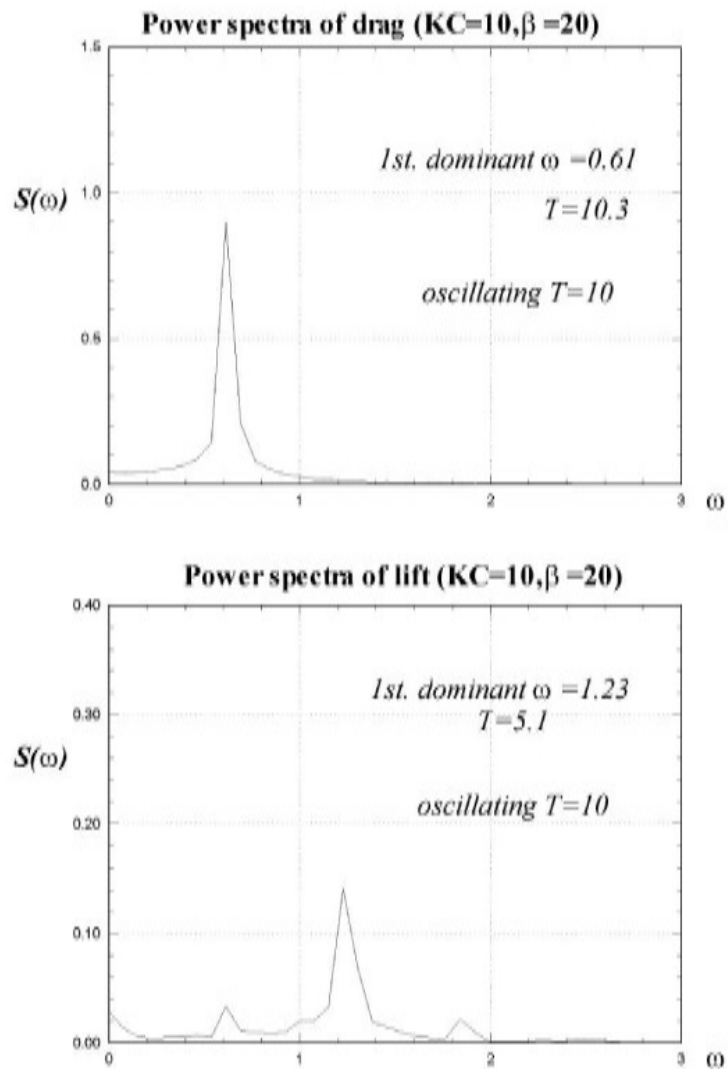
Figure **7.34** Power spectra of drag and lift forces of flow around a circular cylinder in oscil-latory motion for $KC = 16$, $\beta = 62.5$.

8

VORTEX PARTICLE METHODS

8.1   Introduction

This chapter describes a vortex particle method for the solution of the incompressible Navier-Stokes equations. In the early stages of development of flows around a circular cylinder, a hydrofoil section, a sphere and a rectangular wing undergoing an impulsively started motion, the computational results obtained by the vortex particle method (including the vortex-in-cell method) are compared with those obtained by the Eulerian finite volume method. The comparison is performed separately for the pressure fields as well. The results obtained by these methods give a better understanding of the vorticity-based methods.

The vortex method is based on the Lagrangian description of the vorticity field. Its the main idea is one that a vortical flow field is represented by vortex particles. This representation is very attractive for numerical simulations of viscous flow around a body with complex geometry. It is then possible to

avoid the nonlinear convection term of the vorticity transport equation, which involves difficulties associated with numerical diffusion for its discretization in grid-based methods.

We will focus on the two-dimensional formulation but partly some extension of the formulation to three-dimensions will be made.
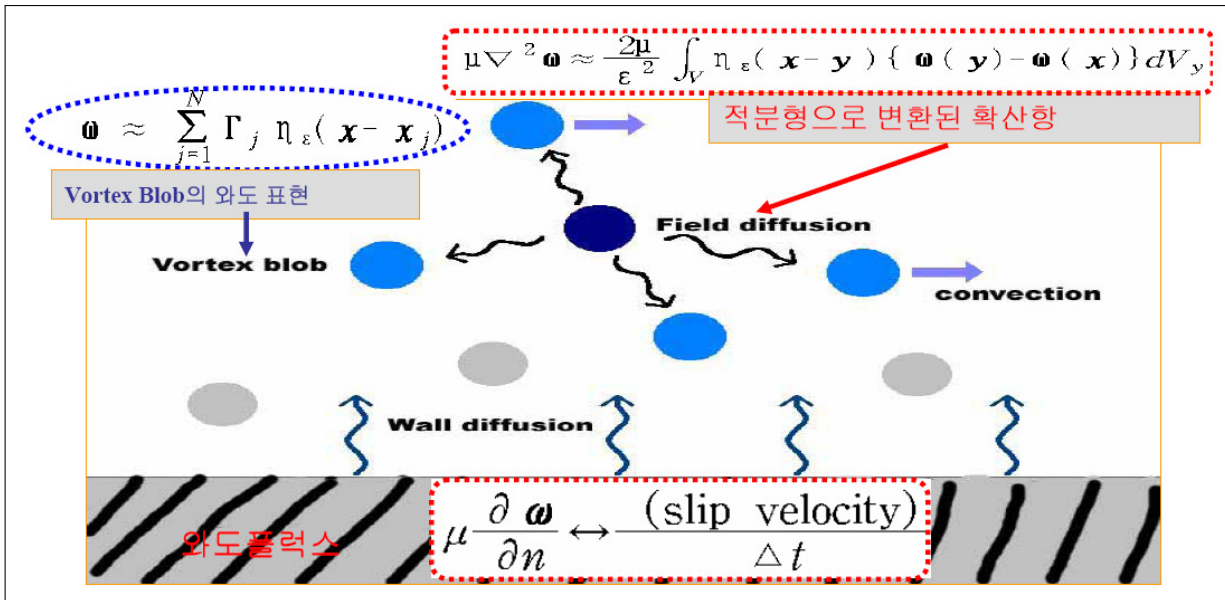
Figure **8.1** Schematic diagram of the vortex particle method in two-dimensions.

8.2   Numerical Implementation

8.2.1   Particle representation of vorticity field

There are several kinds of Lagrangian elements to discretize the vorticity field in vortex methods, such as particles(blobs), sheets, and filaments. In this work, a set of N vortex particles is introduced, of strength $\underline{\alpha}_i$ and position $\underline{x}_i(t)$, to represent the vorticity field

8.2.1.1 Two-dimensions

In the case of two-dimensional flows, a Lagrangian form of Eq. (6.38) is represented as

$$\frac{D\omega}{Dt} = \nu \, \nabla^2 \omega, \tag{8.1}$$

where ω is the scalar plane component of the vorticity vector ($\underline{\omega} \equiv \omega \, \underline{k}$). The vorticity field is represented by N scalar-valued particles:

$$\omega(\underline{x}, t) = \sum_{i=1}^{N} \zeta_\epsilon(\underline{x} - \underline{x}_i) \, \alpha_i. \tag{8.2}$$

Each particle is characterized by its position, $\underline{x}_i(t)$, and its strength, $\underline{\alpha}_i(t) = \alpha_i(t)\underline{k}$, i.e., its *circulation*, $\alpha_i = \int_{S_i} \omega dS \approx \omega_i S_i$, with S_i the area of fluid associated with the particle i. The regularized particle representation of the vorticity field has been used by various researchers (Leonard 1980, Winckelmans 1989,1993). The distribution functions ζ_ϵ associated with each particle are defined by

$$\zeta_\epsilon(\underline{r}) = \frac{1}{\epsilon_i{}^2} \, \zeta\left(\frac{|\underline{r}|}{\epsilon_i}\right), \tag{8.3}$$

where ϵ_i is the smoothing parameter denoting the blob (particle) size which is usually taken as the grid size. In the present study, we choose Gaussian smoothing as the distribution function for its physically appealing properties:

$$\zeta(\rho) = \frac{1}{2\pi} \exp\left(-\frac{\rho^2}{2}\right). \tag{8.4}$$

8.2.1.2 Three-dimensions

In a similar way to two-dimensions, a set of N vortex particles is introduced to represent the vorticity field:

$$\underline{\omega}(\underline{x}, t) = \sum_{i=1}^{N} \zeta_\epsilon(\underline{x} - \underline{x}_i) \, \underline{\alpha}_i, \tag{8.5}$$

where the strength $\underline{\alpha}_i = \int_{V_i} \underline{\omega} \, dV = \underline{\omega}_i V_i$ and V_i is the volume associated with the particle i. The regularization function, ζ_ϵ, associated with each particle is defined by

$$\zeta_\epsilon(\underline{r}) = \frac{1}{\epsilon_i^3} \zeta \left(\frac{|\underline{r}|}{\epsilon_i} \right) \tag{8.6}$$

where ϵ_i is the smoothing parameter. The function ζ is usually taken to be radially symmetric with normalization to conserve circulation. The Gaussian distribution can be used, for instance,

$$\zeta(\rho) = \frac{1}{(2\pi)^{3/2}} \exp \left(-\frac{\rho^2}{2} \right) \tag{8.7}$$

8.2.2   Velocity field

In three dimensional flow, Eq. (6.40) is expressed as

$$\underline{q} = \frac{1}{4\pi} \oint_S \left[(\underline{n} \cdot \underline{q}) \frac{\underline{r}}{|\underline{r}|^3} + (\underline{n} \times \underline{q}) \times \frac{\underline{r}}{|\underline{r}|^3} \right] dS + \frac{1}{4\pi} \int_V \underline{\omega} \times \frac{\underline{r}}{|\underline{r}|^3} \, dV, \tag{8.8}$$

where, $\underline{r} = \underline{x} - \underline{y}$. The second integral term of Eq. (8.8) corresponds to the rotational part($\underline{u}_\omega$) of the velocity field induced by the vorticity field.

Vortex particle positions $\underline{x}_i(t)$ are governed by the equation,

$$\frac{d\underline{x}_i}{dt} = \underline{q}(\underline{x}_i, t) \tag{8.9}$$

Recall that the velocity field is based on the Helmholtz decomposition:

$$\underline{q} = \underline{U}_\infty + \nabla\phi + \underline{u}_\omega \tag{8.10}$$

The term $\nabla\phi$ is equivalent to the surface integral of Eq. (6.40) that is the irrotational part of the velocity field. According to Green's scalar identity, the potential ϕ at arbitrary points on the body surface is written as

$$\frac{1}{2}\phi(\underline{x}) = \oint_{S_B} \left\{ \phi(\underline{y}) \left(\underline{n}(\underline{y}) \cdot \nabla G \right) + \left(\underline{n}(\underline{y}) \cdot \nabla\phi(\underline{y}) \right) G \right\} dl_y. \tag{8.11}$$

The integral equation of Eq. (8.11) is discretized as

$$\frac{1}{2}\phi_i(\underline{x}) = \sum_{j=1}^{M} A_{ij}\,\phi_j + \sum_{j=1}^{M} B_{ij}\,\sigma_j, \qquad (8.12)$$

where

$$A_{ij} = \int_{C_j} \underline{n}(\underline{y}) \cdot \nabla G\,dl_y, \qquad B_{ij} = \int_{C_j} G\,dl_y, \qquad (8.13)$$

$$\sigma_j \equiv \underline{n} \cdot \nabla\phi_j = \underline{n} \cdot \underline{U}_B - \underline{n} \cdot (\underline{U}_\infty + \underline{u}_\omega)\,. \qquad (8.14)$$

By solving the linear system of equations with A_{ij}, B_{ij}, we obtain ϕ_i at collocation points on the surface. Then $\nabla\phi$ on the body surface can be approximated in the sense of the finite difference of ϕ_i. $\nabla\phi$ at field points can be directly computed by using Eq. (3.5) for 3-D and Eq. (3.5) for 2-D.

8.2.2.1   Regularized velocity field

Note that one can view the mollified velocity field as the exact velocity associated with a vorticity $\underline{\omega}$ consisting of vortex particles, in two-dimensions,

$$
\begin{aligned}
\underline{u}_\omega &= \int_S \underline{K} \times \left[\sum_{i=1}^{N} \Gamma_i\,\zeta_\epsilon\,(|\underline{x} - \underline{x}_i|)\right]\,dS \\
&= \sum_{i=1}^{N}\left[\int_{S_i} \underline{K}\,\zeta_\epsilon\,(|\underline{x} - \underline{x}_i|)\,dS\right] \times \Gamma_i \\
&= \sum_{i=1}^{N} \underline{K}_\epsilon\,(|\underline{x} - \underline{x}_i|) \times \Gamma_i \qquad (8.15)
\end{aligned}
$$

Here, with the smooth function η_ϵ, the kernel $\underline{K}_\epsilon$ in (8.15) is expressed as

$$
\begin{aligned}
\underline{K}_\epsilon(r) &= \int_S \underline{K}(r)\,\zeta_\epsilon(r)\,dS \\
&= \underline{K}(r)\int_0^r \int_0^{2\pi} \zeta_\epsilon(r)\,r\,dr\,d\theta \\
&= \underline{K}(r)\left[1 - \exp\left(-\frac{r^2}{2\epsilon^2}\right)\right] \qquad (8.16)
\end{aligned}
$$

where $r = |\underline{x} - \underline{y}|$, $\quad \underline{K} = \nabla G = -\dfrac{1}{2\pi}\dfrac{r}{|r|^2}$.

$$
\underline{K}_\epsilon(\underline{x} - \underline{y}) = -\frac{1}{2\pi}\frac{\underline{x} - \underline{y}}{|\underline{x} - \underline{y}|^2}\left[1 - \exp\left(-\frac{|\underline{x} - \underline{y}|^2}{2\epsilon^2}\right)\right] \qquad (8.17)
$$

The term $\underline{u}_\omega$ of Eq. (8.10) which is equivalent to the volume integral (Biot-Savart integral) of Eq. (6.40), may be discretized by Eq. (8.2) for 2-D:

$$
\underline{u}_\omega(\underline{x}, t) = -\frac{1}{2\pi}\sum_{i=1}^N \underline{K}_\epsilon \times (\alpha_i(\underline{x}_i)\,\underline{k}), \quad \text{in 2-D} \qquad (8.18)
$$

where

$$
\underline{K}_\epsilon = \frac{r_i}{|r_i|^2}\left[1 - \exp\left\{-r_i^2/(2\epsilon_i^2)\right\}\right], \quad \text{with} \quad \underline{r}_i = \underline{x} - \underline{x}_i \qquad (8.19)
$$

Similarly, the regularized velocity for 3-D can be expressed as:

$$
\underline{u}_\omega(\underline{x}, t) = -\frac{1}{4\pi}\sum_{i=1}^N \underline{K}_\epsilon^{(3D)} \times \underline{\alpha}_i(\underline{x}_i), \quad \text{in 3-D} \qquad (8.20)
$$

where

$$
\underline{K}_\epsilon^{(3D)} = \frac{r_i}{|r_i|^3}\left\{\operatorname{erf}\left(\frac{\rho}{\sqrt{2}}\right) - \rho\sqrt{\frac{2}{\pi}}\exp\left(-\frac{\rho^2}{2}\right)\right\}, \quad \rho = |\underline{r}_i|/\epsilon_i \qquad (8.21)
$$

where $\mathrm{erf}(x) = \dfrac{2}{\sqrt{\pi}} \displaystyle\int_0^x \exp(-t^2)\, dt$.

The efficiency of vortex particle method is conditioned in particular by the choice of the cutoff function η_ϵ and the location and strength of particles are initially set. The right hand side of Eq. (8.15) is computed using a fast algorithm, proposed by Greengard and Rohklin (1987), that has an operation count of $\mathcal{O}(N \log N)$ and with active error control based on accurate error bounds. The numerical time-advancing scheme required for solving the location of particles is an additional important factor. In practice it is important to use schemes that are at least second order (Adam-bashforth or Runge-Kutta schemes are commonly used).

Note that the term $\underline{u}_\omega$ has been included when we apply the no-penetration condition $\underline{q}\cdot\underline{n} = \underline{U}_B\cdot\underline{n}$ on the body surface. In fact, the no-penetration condition is numerically imposed by Eq. (8.14).

The vector potential (stream function) corresponding to the 3-D velocity field would be

$$\underline{\psi}(\underline{x},t) = \frac{1}{4\pi} \sum_{i=1}^N \frac{1}{\rho\,\epsilon_i} \,\mathrm{erf}\left(\frac{\rho}{\sqrt{2}}\right) \underline{\alpha}_i \tag{8.22}$$

A simpler algebraic function can be used rather than such a Gaussian function, especially for the calculation of the stream function at the boundary:

$$\begin{aligned}
\underline{\psi}(\underline{x}_B,t) &= \frac{1}{4\pi} \sum_{i=1}^N \frac{1}{\epsilon_i} \frac{1}{\sqrt{|\underline{x}-\underline{x}_i|^2/\epsilon_i^2 + 1}} \,\underline{\alpha}_i \\
&= \frac{1}{4\pi} \sum_{i=1}^N \frac{1}{\sqrt{|\underline{x}-\underline{x}_i|^2 + \epsilon_i^2}} \,\underline{\alpha}_i
\end{aligned} \tag{8.23}$$

8.2.3 Field viscous diffusion: PSE scheme

The treatment of the diffusion equation Eq. (8.1) is based on a technique related to the PSE (Particle Strength Exchange) scheme introduced by Degond & Mas-Gallic (1989). The Laplacian operator ∇^2 is approximated by an integral

operator, which is discretized over the particles.

$$\nu\nabla^2\omega \approx \frac{2\nu}{\epsilon^2} \int_S \eta_\epsilon(|\underline{x} - \underline{y}|)\,(\omega(\underline{y}) - \omega(\underline{x}))\,dS_y. \qquad (8.24)$$

Then, the evolution equation for the particle strength becomes

$$\frac{d\alpha_i}{dt} = \frac{2\nu}{\epsilon^2} \sum_{j=1}^{N} (S_i\,\alpha_j - S_j\,\alpha_i)\,\eta_\epsilon(\underline{x}_i - \underline{x}_j), \qquad (8.25)$$

where

$$\eta_\epsilon(\underline{x}_i - \underline{x}_j) = \frac{1}{2\pi\,\epsilon^2}\,\exp\left(-\frac{|x_i - x_j|^2}{2\epsilon^2}\right) \qquad (8.26)$$

This function is the same as one given in Eq. (8.4). Herein, ϵ is taken to be constant for all particles.

The three-dimensional version would be

$$\frac{d\underline{\alpha}_i}{dt} = \frac{2\nu}{\epsilon^2} \sum_{j=1}^{N} \left(V_i\,\underline{\alpha}_j - V_j\,\underline{\alpha}_i\right)\,\eta_\epsilon(\underline{x}_i - \underline{x}_j) \qquad (8.27)$$

8.2.3.1   Image layer method in two-dimensions

If Eq. (8.25) is used for wall-bounded computations, particles close to the wall are not completely surrounded by other particles. Consequently, a spurious vorticity flux appears at the wall while the total vorticity is conserved (Ploumhans 2000, Cottet 2000).

We use an image particle layer to complete the PSE for particles close to the wall. Solid walls are approximated as discretized panels. The images are placed along a layer inside the body close to the panel, as shown in Figure **8.3** .
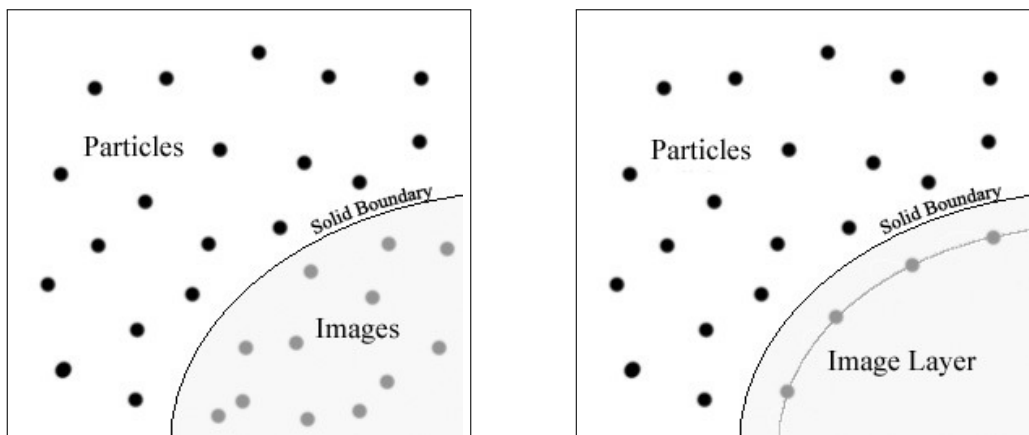
Figure 8.2 Comparison of the image vortex layer of the present method with the image vortex system in Ploumhans & Wickelmans (2000).
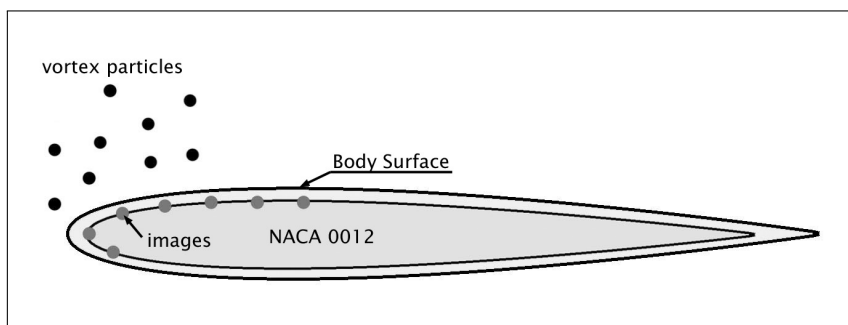
Figure 8.3 Example of the image vortex layer around an NACA 0012 hydrofoil.

The extended vorticity of the image layer adds to the vorticity on the body,

$$
\underline{\omega}\left(\underline{x}\right) \;=\; \sum_{i=1}^{N} \alpha_i \, \zeta_{\epsilon i}\left(\underline{x} - \underline{x}_i\right) \;+\; \sum_{m=1}^{M} \alpha_m^* \, \zeta_{\epsilon m}^*\left(\underline{x} - \underline{x}_m^*\right) \quad \text{for} \quad \underline{x} \in \partial\mathcal{D}, \quad (8.28)
$$

where the superscript '$*$' refers to quantities of images. Then the vorticity flux on the body is expressed as

$$
\frac{\partial \underline{\omega}}{\partial n} \;=\; \sum_{i=1}^{N} \alpha_i \, \frac{\partial \zeta_{\epsilon i}\left(\underline{x} - \underline{x}_i\right)}{\partial n} \;+\; \sum_{m=1}^{M} \alpha_m^* \, \frac{\partial \zeta_{\epsilon m}^*\left(\underline{x} - \underline{x}_m^*\right)}{\partial n} \quad \text{for} \quad \underline{x} \in \partial\mathcal{D}, \quad (8.29)
$$

where $\underline{n}$ is the normal vector of the particle $\underline{x}$ and the zero vorticity-flux condition means $\partial\underline{\omega}/\partial n = 0$ at the body surface. The normal derivative of the

smoothing function is found to be

$$
\frac{\partial \zeta_{\epsilon i}\left(\underline{r}\right)}{\partial n} = -\frac{1}{2\pi\,\epsilon^4}\exp\left(-\frac{r^2}{2\epsilon^2}\right)\left(\underline{r}\cdot\underline{n}\right). \tag{8.30}
$$

Denoting the radius of the image blob by ϵ^*, Eq. (8.29) is expressed as

$$
\begin{aligned}
\frac{\partial\underline{\omega}(\underline{x}_p)}{\partial n} &= \frac{1}{2\pi\epsilon^{*4}}\sum_{m=1}^{M}\alpha_m^*\exp\left(-\frac{r^{*2}}{2\epsilon^{*2}}\right)\left(\underline{r}^*\cdot\underline{n}\right) \\
&+\frac{1}{2\pi\,\epsilon^4}\sum_{i=1}^{N}\alpha_i\exp\left(-\frac{r^2}{2\epsilon^2}\right)\left(\underline{r}\cdot\underline{n}\right)=0. \tag{8.31}
\end{aligned}
$$

where $\underline{r} = \underline{x}_p - \underline{x}_i$ and $\underline{r}^* = \underline{x}_p - \underline{x}_m$. With the image layer, Eq. (8.24) is replaced by

$$
\begin{aligned}
\frac{d\alpha_i}{dt}\frac{1}{S_i} &= \frac{2\nu}{\epsilon^2}\sum_{j=1}^{N}\left[\frac{\alpha_j}{S_j}-\frac{\alpha_i}{S_i}\right]\zeta_\epsilon\left(|\underline{x}_i-\underline{x}_j|\right)\,S_j \\
&+\frac{2\nu}{\epsilon^2}\sum_{m=1}^{M}\left[\frac{\alpha_m^*}{S_m}-\frac{\alpha_i}{S_i}\right]\zeta_\epsilon\left(|\underline{x}_i-\underline{x}_m|\right)\,S_m, \tag{8.32}
\end{aligned}
$$

where $S_m = \epsilon^{*2}$ for the image. This technique is insensitive to the local shape of a body. That is, because one image layer in the body is used, it may be suitable in the case of a thin body, e.g., foils with cusped trailing edges.

8.2.3.2   Image layer method in three-dimensions

For particle i close to the boundary, the computation of the PSE involves two subsets of particles: $\mathcal{P}_i$(the subset of particles close enough to $\underline{x}_i$) and $\mathcal{P}_i'$ (the set of images of the particles in $\mathcal{P}_i$). The position of image particle $\underline{x}_i'$ is computed using symmetry, the plane of symmetry being the plane tangent to body surface closest to $\underline{x}_i$. The volume and smoothing parameter of an image particle are taken equal to those of the original particle. The two components of the strength $(\underline{\alpha}_i')$ parallel to the tangential plane are taken equal to those of $\underline{\alpha}_i$. The normal component is taken with the opposite sign. If (ξ, η, n) are the local orthogonal

coordinates,

$$\underline{\alpha}_i' = (\underline{\alpha}_i \cdot \underline{\xi})\,\xi + (\underline{\alpha}_i \cdot \underline{\eta})\,\eta - (\underline{\alpha}_i \cdot \underline{n})\,n \qquad (8.33)$$

Lee (2005) pointed out that the position and strength of an image are not easily determined for a slender body such as NACA0012 hydrofoil, if the technique outlined above is used. He suggested a more general treatment for the image, and applied successfully to the 2-D flow simulation around NACA0012 at arbitrary angles of attack, as well as around a circular cylinder. He positioned images just below the control points of the discretized body panels (the total number of image particles becomes the number of panels). The strength of an image particle can be determined from the zero vorticity flux condition on the control point of a panel,

$$\frac{\partial \underline{\omega}}{\partial n} = \sum_{i=1}^{N} \underline{\alpha}_i \frac{\partial \zeta_\epsilon (\underline{x} - \underline{x}_i)}{\partial n} + \sum_{m=1}^{M} \underline{\alpha}_m' \frac{\partial \zeta_\epsilon'(\underline{x} - \underline{x}_m')}{\partial n} \qquad (8.34)$$

Cottet & Poncet (2003) demonstrated in the immersed boundary VIC method that such particular diffusion formulas are no longer necessary near the boundary. He used plain PSE formulas all over the domain, even near the boundary. The spurious vorticity in the flow, usually introduced with the PSE ignoring the boundary, was supposed to be corrected from the application of vorticity flux formulas, because the evaluation of the slip and the enforcement of the no slip boundary condition are made on the boundary itself. The PSE in this work pursued Cottet's demonstration, but as described in the section 8.4.3 for the potential field calculation, normal flow condition is satisfied on the panel as well as tangential flow. Figure **8.4** compares the differences between the PSE using images and immersed boundary PSE schematically.
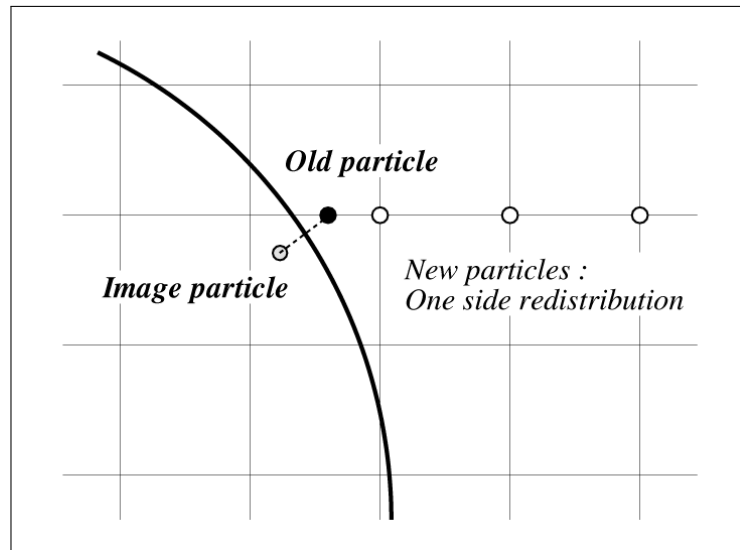
(a) Remeshing and image in vortex method
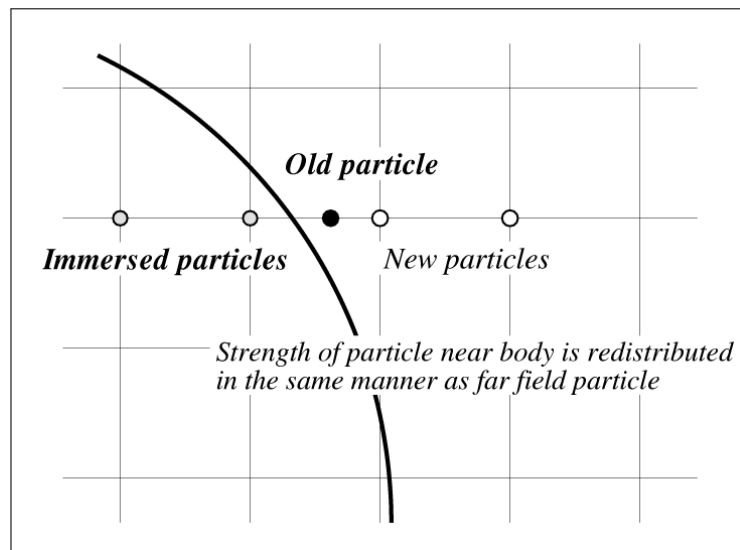
(b) Immersed boundary and particles in VIC

Figure 8.4 Comparison of particle locations between the vortex particle method and the immersed boundary method in VIC.

8.2.4   No-slip condition: Vorticity flux at wall

The solution of the heat equation may be expressed in integral form as: [1]

$$\underline{\omega} \;=\; \nu \int_0^t \int_{\partial\mathcal{D}} H_\epsilon\left(\underline{x}, t; \underline{\xi}\,,\ \tau\right) \frac{\partial\omega\left(\underline{\xi}, \tau\right)}{\partial n} \, d\xi \, d\tau \qquad (8.35)$$

where

$$H_\epsilon \;=\; \frac{1}{4\pi\nu\left(t - \tau\right)} \, \exp\left(-\frac{|\underline{x} - \underline{\xi}|^2}{4\nu\left(t - \tau\right)}\right)$$

Therefore, the Gaussian smoothing meets all these requirements and is a natural choice since it is the kernel of the heat equation. Its associated η_ϵ is also a Gaussian and with the proper normalization, it is found that $H_\epsilon = \eta_\epsilon$ which be of some computational benefit (Raviart 1987, Pepin 1990),

$$H_\epsilon\left(|\underline{x} - \underline{y}|\right) \;=\; \frac{1}{2\pi\epsilon^2} \, \exp\left(-\frac{|\underline{x} - \underline{y}|^{\,2}}{2\epsilon^2}\right) \qquad (8.36)$$

where $2\,\nu\,dt \;=\; \epsilon^2$.

A vorticity flux $(\nu\frac{\partial\omega}{\partial n})$ may be determined on the boundary in such a way that the no-slip condition is satisfied. Wu *et al.* (1994) introduced a relation between a vorticity flux and spurious slip velocity(V_s). If a vorticity flux is constant over a small interval of time (Δt), the spurious slip velocity(V_s) that would appear at the end of the time step can be regarded as the coupling term corresponding to the tangential gradient of the surface pressure in Eq. (6.48). The newly computed V_s, which can be obtained by the Biot-Savart integral, can then used to absorb the coupling term and consequently to update a vorticity flux:

$$\left(\nu\frac{\partial\omega}{\partial n}\right)^{(k+1)} = \left(\nu\frac{\partial\omega}{\partial n}\right)^{(k)} + \left(\frac{V_s}{\Delta t}\right)^{(k)} \qquad (8.37)$$

wher the superscript notation refers to the iterative step.

The iteration continues until the no-slip condition is satisfied, i.e., until V_s

------

[1]See Friedman (1964).

reduces to a value within a preset allowance. Eq. (8.37) indicates the total flux to be emitted into the flow for the diffusion process during a time Δt. This elegant decoupled scheme was introduced by Wu *et al.* (1994), through which we can efficiently recover the global coupling between the vorticity and the pressure boundary condition instead of the implementation of the fully coupled schemes.

The vorticity flux is distributed to neighboring particles by discretizing the Green's integral for the inhomogeneous Neumann problem corresponding to the diffusion equation. For diffusion within the schemes to work properly, the spatial distribution of the particles must remain as uniform as possible. To re-mesh the distorted particles, we overlaid a uniform rectangular grid. This is necessary in order to accurately interpolate the current vorticity field onto the new grid of initially uniformly spaced particle location that replaces the distorted particle locations (as suggested by Ploumhans and Winckelmans (2000)).

8.2.4.1 Wall viscous diffusion in two-dimensions

The total flux to be emitted into the flow for the diffusion process must be emitted during a time Δt. In effect, the vortex sheet V_s must be distributed to neighboring particles by discretizing the Green's integral for the inhomogeneous Neumann problem corresponding to the diffusion equation. As shown in Figure 8.5 , consider a panel of uniform strength V_s located along the x-axis, and diffusing to the right side. The vortex sheet does not diffuse toward the interior of the body. The amount of circulation, $\Delta\alpha_i$, that will be imposed on the particle located at (x_i, y_i) $(y_i > 0 , \ x_i \ (any \ sign))$, is given by

$$\Delta\alpha_i = \int_{x_i-h_i/2}^{x_i+h_i/2} \int_{y_i-h_i/2}^{y_i+h_i/2} \Delta\omega \, dx \, dy \tag{8.38}$$

where $h_i{}^2 = S_i$ is the fluid area associated with particle i. The change in vorticity $\Delta\omega$ is due to the flux from the panel acting over a time Δt, which reduced t.

$$\Delta\omega = \int_0^{\Delta t} \frac{d\omega}{dt} \, dt \tag{8.39}$$
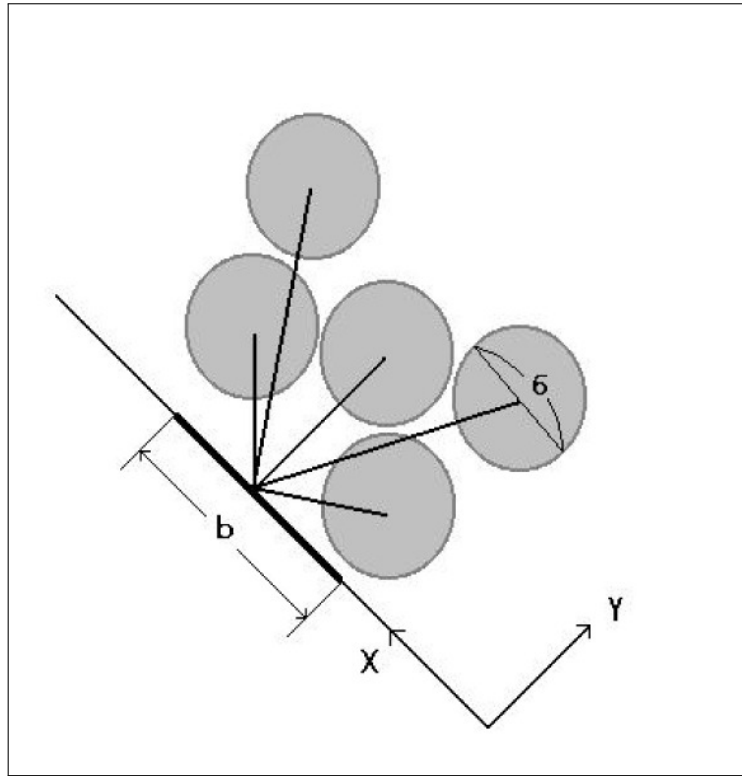
Figure 8.5 Particles with respect to a panel for viscous wall diffusion.

Then,

$$\frac{d\alpha_i}{dt} = \iint \frac{d\omega}{dt}\, dx\, dy \tag{8.40}$$

$$\Delta\alpha_i = \int_0^{\Delta t} \frac{d\alpha_i}{dt}\, dt \approx \frac{d\alpha_i}{dt}\, \Delta t \tag{8.41}$$

Eq (8.41) is integrated numerically using mid-point rule:

$$\Delta\alpha_i = h_i{}^2\, V_s \left(1 - \kappa\sqrt{\pi\nu\Delta t}\right)^{-1} \frac{1}{\sqrt{2\pi\,\nu\,\Delta t}} \times$$
$$\times\ \exp\left(-\frac{y_i{}^2}{2\,\nu\,\Delta t}\right) [\mathrm{erfc}(s)]_{(x_i + h_i/2)/\sqrt{2\,\nu\,\Delta t}}^{(x_i - h_i/2)/\sqrt{2\,\nu\,\Delta t}} \tag{8.42}$$

where $\mathrm{erfc}(s) = \dfrac{2}{\sqrt{\pi}}\displaystyle\int_s^{\infty} \exp(-v^2)\, dv = 1 - \mathrm{erf}(s)$. To resolve the non con-
servation problem caused by numerical integration, the integral of Eq. (8.40) is

performed as follows (Ploumhans & Winckelmans 2000)

$$
\begin{aligned}
\frac{d\alpha_i}{dt} &= \iint \frac{d\omega}{dt}\, dx\, dy = \frac{\Delta\gamma}{\Delta t}\left([\mathrm{erfc}(s)]_{(y_i+h_l/2)/\sqrt{4\nu t}}^{(y_i-h_{i,l}/2)/\sqrt{4\nu t}}\right)\times \\
&\quad \times \left\{\sqrt{4\,\nu\,t}\,\frac{1}{2}\left([\mathrm{ierfc}(s)]_{x_i-b/2+h_i/2/\sqrt{4\nu t}}^{x_i-b/2-h_i/2/\sqrt{4\nu t}} - [\mathrm{ierfc}(s)]_{x_i+b/2+h_i/2/\sqrt{4\nu t}}^{x_i+b/2-h_i/2/\sqrt{4\nu t}}\right)\right\}
\end{aligned}
\tag{8.43}
$$

where $\mathrm{ierfc}(s) = \int_s^\infty (u)\, du = \dfrac{1}{\sqrt{\pi}}\exp(-s^2) - s\,\mathrm{erfc}(s)$, and $h_{i,l}/2 = x_i$ if $0 \le x_i < h_i$ and $h_{i,l}/2 = h_i/2$ otherwise.

If particles are on a regular lattice aligned with the panel, Eq.(8.43) is always conservative. Thus, it could also be used to perform under resolved computations, where the value of $h^2/(4\nu\Delta t)$ would be very high. The large value of $h^2/(4\nu\Delta t)$ is equivalent to $h^2/\sigma^2 \gg 1$, which means the violation of the blob overlap condition($h/\sigma < 1$). In practice, however, the spatial distribution of the particles is not well aligned with the vortex panel. Therefore, in order to enforce conservation, the correction is made as follows (Ploumhans & Winckelmans 2000):

$$
\Delta\alpha_{i,conserv.} = \Delta\alpha_i + \frac{(\Delta\alpha_i)^2}{\sum_j (\Delta\alpha_j)^2}\left(b\,V_s - \sum_j \Delta\alpha_j\right),
\tag{8.44}
$$

where j runs over all particles concerned by the panel V_s. This scheme minimizes

$$
\sum_i (\Delta\alpha_i - \Delta\alpha_{i,conserv.})^2/(\Delta\alpha_i)^2
\tag{8.45}
$$

with the constraint that $(b\,V_s) - \left(\sum_i \Delta\alpha_{i,conserv.}\right) = 0$.

For diffusion with the above schemes to work properly, the spatial distribution of the particles must remain fairly uniform as long as possible. This is one reason why particle redistribution procedure must be performed every 5 to 10 time steps.

8.2.4.2   Wall viscous diffusion in three-dimensions

The process that the vorticity created at the boundary shed on to the particles has been accounted for by the diffusion, and the solution to the diffusion equation for the voricity with homogeneous initial condition and the Neumann type boundary condtion has been implemented in an appropriate discretized form. The solution may be expressed in integral form using Green's function for the diffusion equation.

The 3-D version of the discretization is well explained in Ploumhans (2002). Consider a retangular panel of uniform strength $\Delta\underline{\gamma}(=\underline{n}\times\underline{u}_s)$ and size $b\times f$, located on the XY plane, and diffusing toward the positive Z direction. A particle located at (x_i, y_i, z_i), $(z_i > 0)$, receives, from that panel, an amount of 'vorticity$\times$volume' given by

$$\Delta\underline{\alpha}_i = \int_0^{\Delta t} \frac{d\underline{\alpha}_i}{dt}\, dt \tag{8.46}$$

with

$$\frac{d\underline{\alpha}_i}{dt} = \int_{x_i-h_i/2}^{x_i+h_i/2} \int_{y_i-h_i/2}^{y_i+h_i/2} \int_{z_i-h_i/2}^{z_i+h_i/2} \frac{d\underline{\omega}}{dt}\, dx\, dy\, dz \tag{8.47}$$

The rate of change of the vorticity owing to the panel is equal to

$$
\begin{aligned}
\frac{d\underline{\omega}}{dt} =& \frac{\Delta\underline{\gamma}}{\Delta t} \frac{1}{2\sqrt{\pi}} \frac{1}{\sqrt{4\,\nu\,t}} \exp\left(-\frac{z^2}{4\,\nu\,t}\right) \times \\
& \times \left[\mathrm{erfc}(s)\right]_{(x-b/2)/\sqrt{4\,\nu\,t}}^{(x+b/2)/\sqrt{4\,\nu\,t}} \times \left[\mathrm{erfc}(s)\right]_{(y-f/2)/\sqrt{4\,\nu\,t}}^{(y+f/2)/\sqrt{4\,\nu\,t}}
\end{aligned}
\tag{8.48}
$$

Equation (8.48) is then integrated exactly, giving

$$
\begin{aligned}
\frac{d\underline{\alpha}_i}{dt} =& \frac{\Delta\underline{\gamma}}{\Delta t} \left(\left[\mathrm{erfc}(u)\right]_{(z_i+h_i/2)/\sqrt{4\nu t}}^{(z_i-h_{i,l}/2)/\sqrt{4\nu t}}\right) \\
& \times \left\{\sqrt{\nu t}\left(\left[\mathrm{ierfc}(u)\right]_{(x_i-h_i/2-b/2)/\sqrt{4\,\nu\,t}}^{(x_i+h_i/2-b/2)/\sqrt{4\,\nu\,t}} - \left[\mathrm{ierfc}(u)\right]_{(x_i-h_i/2+b/2)/\sqrt{4\,\nu\,t}}^{(x_i+h_i/2+b/2)/\sqrt{4\,\nu\,t}}\right)\right\} \\
& \times \left\{\sqrt{\nu t}\left(\left[\mathrm{ierfc}(u)\right]_{(y_i-h_i/2-f/2)/\sqrt{4\nu t}}^{(y_i+h_i/2-f/2)/\sqrt{4\,\nu\,t}} - \left[\mathrm{ierfc}(u)\right]_{(y_i-h_i/2+f/2)/\sqrt{4\nu t}}^{(y_i+h_i/2+f/2)/\sqrt{4\,\nu\,t}}\right)\right\}
\end{aligned}
\tag{8.49}
$$

where $\text{ierfc}(s) = \int_s^\infty \text{erfc}(x)\,dx$. Notice that $h_{i,l}/2 = z_i$ if $0 \leq z_i < h_i$ and $h_{i,l}/2 = h_i/2$ otherwise. Even though Eq. (8.49) is exact for a rectangular panel of size $b \times f$, the equation is still applicable to triangular panels, if each triangular panel is considered as a square centered at the triangle centroid.

In the intial setting of the vortex particles, the vortex particles with zero strength are first distributed on a regular mesh and several iterations of wall diffusion and slip velocity calculation are carried out to achieve no slip on the surface. The procedure is repeated at the end of each time marching step.
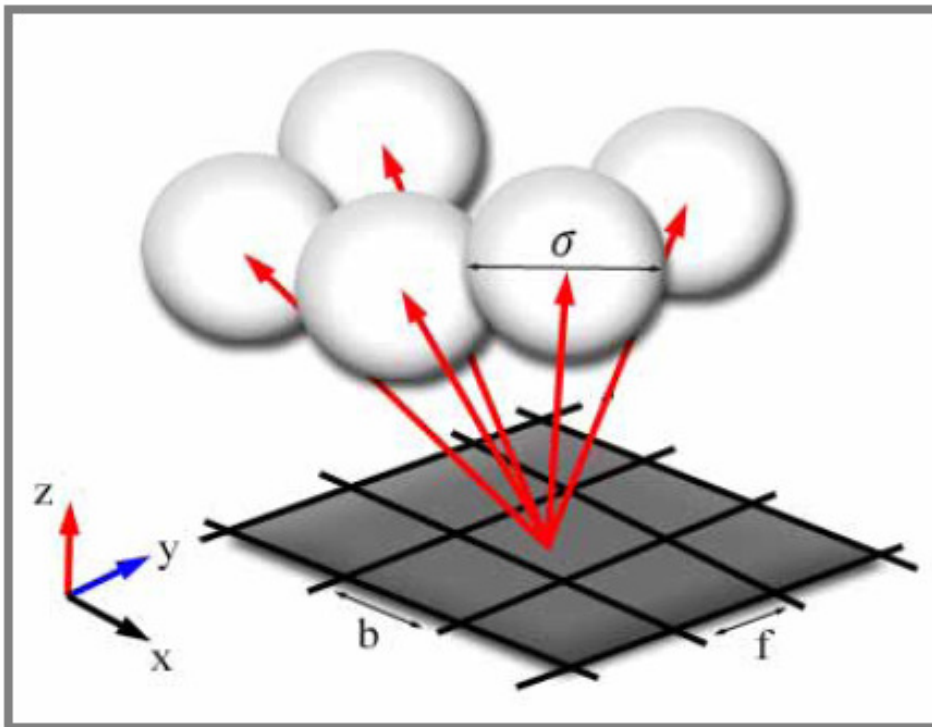
Figure **8.6** Diffusion of vorticity from body boundary. Vorticity correction is performed in the iterative way for satisfying the boundary condition at the surface.

8.2.5   Pressure equation

Once the vorticity and the velocity fields are updated, the integral equation for the total pressure may be solved. Basically, the process for calculating the pressure in a Lagrangian frame is similar to one in an Eulerian frame. Substituting Eq. (6.49) for $\partial H/\partial n$ into Eq. (6.44) yields the limiting form for H as a field

point approaches the surface points ($\underline{x}_B$) of a solid body:

$$
\frac{1}{2}H \; + \; \frac{1}{2\pi}\oint_{C_B} H\,\frac{\partial(\ln r)}{\partial n}\,dl =
$$

$$
-\frac{1}{2\pi}\oint_{C_B}\left[\underline{n}\cdot\frac{\partial\underline{u}}{\partial t} - \underline{n}\cdot(\underline{q}\times\underline{\omega}) + \underline{n}\cdot(\nabla\times(\nu\,\underline{\omega}))\right]\ln r\,dl
$$

$$
+\frac{1}{2\pi}\int_S \nabla\cdot(\underline{q}\times\underline{\omega})\,\ln r\,dS, \tag{8.50}
$$

where the integrals over C_B are evaluated on the surface of a body in the sense of the Cauchy principal value integral. Using the vector operation for the integrand of the surface integral in Eq. (8.50), namely, $\nabla\cdot(\underline{q}\times\underline{\omega})\,\ln r = \nabla\cdot\{(\underline{q}\times\underline{\omega})\,\ln r\} - (\underline{q}\times\underline{\omega})\cdot\nabla(\ln r)$ and applying the divergence integral theorem to the resultant expression, yield a Fredholm integral equation of the second kind for H:

$$
\frac{1}{2}H + \frac{1}{2\pi}\oint_{C_B} H\,\frac{\partial(\ln r)}{\partial n}\,dl \;=\; -\frac{1}{2\pi}\oint_{C_B}\left[\underline{n}\cdot\frac{\partial\underline{u}}{\partial t} + \underline{n}\cdot(\nabla\times(\nu\,\underline{\omega}))\right]\ln r\,dl
$$

$$
-\frac{1}{2\pi}\int_S(\underline{q}\times\underline{\omega})\cdot\nabla(\ln r)\,dS. \tag{8.51}
$$

Furthermore, if we assume that the body will be either fixed, or impulsively started, as in the test problem, the equation reduces to a simpler form:

$$
\frac{1}{2}H + \frac{1}{2\pi}\oint_{C_B} H\,\frac{\partial(\ln r)}{\partial n}\,dl \;=\; -\frac{1}{2\pi}\oint_{C_B}\nu\,\frac{\partial\omega_B}{\partial s}\,\ln r\,dl
$$

$$
-\frac{1}{2\pi}\int_S(\underline{q}\times\underline{\omega})\cdot\nabla(\ln r)\,dS. \tag{8.52}
$$

The two integrals over C_B in Eq. (8.52) may be replaced by the sum of the individual integral form for the contribution of each straight-line body panel. This can then be solved using the panel method in a way similar to that used in potential flow analysis (as mentioned before).

The surface integral term on the right-hand side of Eq. (8.52) may be solved with distorted vorticity particles, unlike the well aligned cell elements in an Eulerian description. The discretization of Eq. (8.52) (except the last surface

integral term) is expressed as

$$
\frac{1}{2} H_i \;+\; \frac{1}{2\pi} \sum_{j=1}^{M} H_j \int_{C_j} \nabla (\ln r)\, dl_j = -\frac{1}{2\pi} \sum_{j=1}^{M} \left\{ \underline{n} \cdot (\nabla \times (\nu\,\underline{\omega}))_j \right\} \int_{C_j} \ln r\, dl_j
$$

$$
-\frac{1}{2\pi} \int_{S} (\underline{q} \times \underline{\omega}) \cdot \nabla (\ln r)\, dS. \tag{8.53}
$$

Body vorticities on the body panels may be calculated from the distribution function of Eq. (8.2). The second term on the right-hand side of Eq. (8.53), (source-like strength, $\underline{n} \cdot \nabla \times (\nu\,\underline{\omega})$) is calculated by numerically differentiating the body vorticities in the tangential direction of the body surface panel. With the vorticity field of Eq. (8.2), the last integral term in Eq. (8.53) is discretized as

$$
\frac{1}{2\pi} \int (\underline{q} \times \underline{\omega}) \cdot \nabla (\ln r)\, dS \;=\; \frac{1}{2\pi} \sum_{k=1}^{N} \left[\underline{q}_k \times (\alpha_k\, \underline{k}) \cdot \frac{\underline{r}_k}{|\underline{r}_k|^2} \int_{S_k} \zeta_{\epsilon_k}\, dS \right]
$$

$$
= \frac{1}{2\pi} \sum_{k=1}^{N} \left[\frac{(x - x_k)\, q_y\, \alpha_k - (y - y_k)\, q_x\, \alpha_k}{|\underline{r}_k|^2} \right] \times
$$

$$
\times \left[1 - \exp\left(-\frac{|\underline{r}_k|^2}{2\,\epsilon^2} \right) \right] \tag{8.54}
$$

Consequently, the total pressure H_i ($i = 1, 2, \cdots, M$) on the body panels is calculated by using the following equation (see Appendix B):

$$
\sum_{j=1}^{M} \left(\frac{1}{2} \delta_{ij} \;+\; A_{ij} \right) H_i \;=\; -\left(\sum_{j=1}^{M} C_{ij} + \sum_{k=1}^{N} S_{ik} \right) \tag{8.55}
$$

where

$$
A_{ij} \;=\; \int_{C_j} \underline{n}_j \cdot \nabla G \left(|\underline{x}_i - \underline{x}_j| \right)\, dl
$$

$$
C_{ij} \;=\; \int_{C_j} \underline{n}_j \cdot \left(\nabla \times (\nu\,\underline{\omega}_j) \right) G \left(|\underline{x}_i - \underline{x}_j| \right)\, dl
$$

$$
S_{ik} \;=\; \left(\underline{q}_k \times \underline{\Gamma}_k \right) \cdot \underline{K}_\epsilon \left(|\underline{x}_i - \underline{x}_k| \right)
$$

Then the total pressure at the field is explicitly calculated with the total pressure on the body surface :

$$H_i = -\sum_{j=1}^{M} A_{ij} H_j - \left(\sum_{j=1}^{M} C_{ij} + \sum_{k=1}^{N} S_{ik} \right) \tag{8.56}$$

where $i = 1, 2, \cdots, N$.

8.2.6   Computational procedure

As shown in Figure **8.7** , the numerical implementation for two dimensional Lagrangian formulation can be summarized in the following sub-steps of the solution of the system of governing equations. The overall procedure is similar
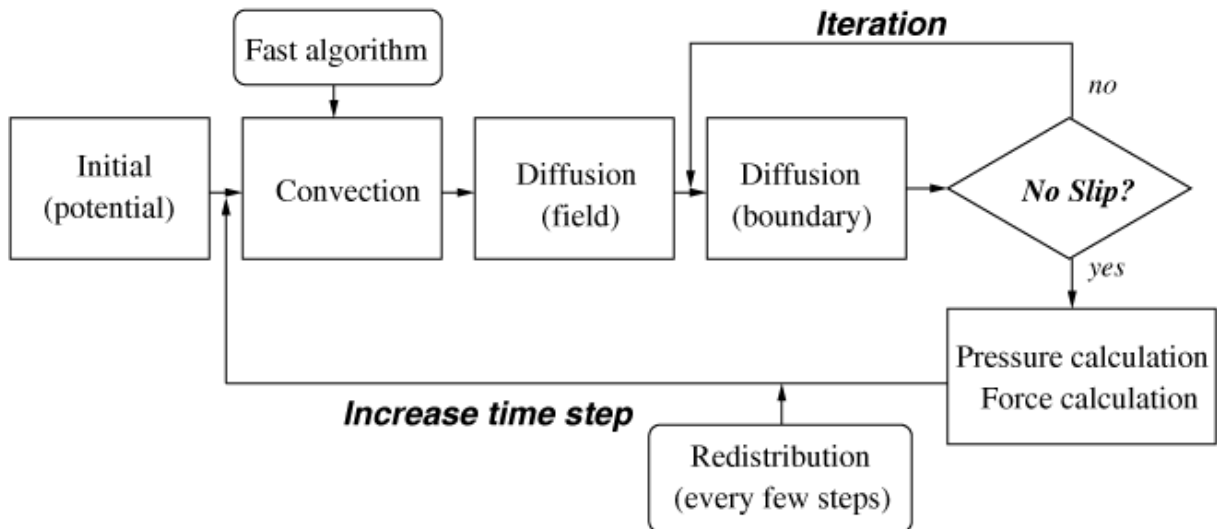
Figure 8.7 Numerical procedure of the vortex particle method.

to those of Koumoutsakos *et al.* (1994) and Ploumhans *et al.* (2000). In the present method, however, the irrotational (potential field) part of the velocity field is calculated by using the well-established panel method and the iterative process is used for more physically suitable creation of vorticity flux in order to ensure the no slip condition, which was taken on the previous vorticity-based method in the Eulerian description (Suh and Kim 1999). A typical time step, Δt, of the Lagrangian vortex method is divided into two substeps.

(1) The local velocity ($\underline{q} = \underline{u}_\omega + \nabla\phi + \underline{U}_\infty$) is computed as follows: $\underline{u}_\omega$ calculated by the Biot-Savart integral (Eq. (8.18)), $\nabla\phi$ calculated by the panel method (Eqs. (8.11)). Then, the velocity is integrated with a second-order Adam-Bashforth scheme (or a second-order Runge-Kutta method immediately after the redistribution process is applied) to convect the particle. Their strengths are updated with the PSE scheme (Eq. (8.32)) that is integrated with an Euler explicit scheme. Algorithmically, this step is expressed as

$$
\underline{x}_i^{n+1} = \underline{x}_i^n + \Delta t\left(\frac{3}{2}\underline{q}_i(\underline{x}^n, \underline{\alpha}^n) - \frac{1}{2}\underline{q}_i(\underline{x}^{n-1}, \underline{\alpha}^{n-1})\right) \tag{8.57}
$$

$$
\underline{\alpha}_i^* = \underline{\alpha}_i^n + \Delta t\left.\frac{d\underline{\alpha}_i}{dt}\right|_{PSE}(\underline{x}^n, \underline{\alpha}^n). \tag{8.58}
$$

(2) The vorticity flux $\nu\dfrac{\partial\omega}{\partial n}$ necessary on the body surface to cancel the slip velocity computed by sub-step (1), is computed (Eq. (8.18)). However, recalculation of the slip velocity on the body boundary may reveal that the no slip condition is not satisfied. Vorticity flux due to the remaining slip velocity is then re-calculated. The iteration continues until the no-slip condition is satisfied, i.e., until the spurious slip velocity reduces to a value within a preset allowance. The vorticity strength corresponds to a vorticity flux that must be emitted during a time Δt:

$$
\underline{\alpha}_i^{n+1} = \underline{\alpha}_i^* + \Delta t\left.\frac{d\underline{\alpha}_i}{dt}\right|_{wall}(\underline{x}^{n+1}, \underline{\alpha}^*). \tag{8.59}
$$

(3) The redistribution scheme is applied every few steps(herein every 5 to 10 time steps) to maintain spatial uniformity of the particle distribution. Once the vorticity and velocity are updated after two substeps are taken, the pressure equation (i.e., Eqs.(8.53) through (8.54)), is solved.

8.2.6.1 Redistribution

Vortex methods have been guaranteed on its convergence by the condition that particle cores overlap at all times. Redistribution is an essential operation to

maintain a good representation of the vorticity field. The vortex-in-cell method is characterized by the information exchange between particles and grid, as is explained in section 8.4.2. As a good quality scheme to bring the particles information to grid, and the grid information to the particles, the M_4' scheme was introduced. The formula is also used for the redistribution of every few time steps. The scheme is continuous and so is the first derivative. It is known as a second order scheme. In summary, the M_4' formula is used at three stages of the method. First, when particle vorticity is interpolated on a regular Cartesian grid where velocity are evaluated, second, when the grid values are interpolated back to particles, and finally to redistribute the disorted particles onto uniform rectangular grid. In order to avoid for the number of particles to grow at a too high rate, a newly generated particle having strength $|\underline{\alpha}| < \epsilon_\alpha |\underline{\alpha}|$ and $Re_h = |\underline{\omega}| \, h^2 / \nu < Re_{h,trsh}$ is deleted after redistribution. The particluar choice for the cutoff parameters is different with application.

In order to remesh on the distorted Lagrangian particles, we overlay a uniform rectangular grid as shown in Figure **8.8** . It is necessary to accurately interpolate the current vorticity field onto the new grid initially uniform-spaced particle location ($\underline{\tilde{x}}$) that replaces the distorted particle location ($\underline{x}$). After redistribution, the uniform grid cell centers become the location of the new particles.

(a) Before redistribution   (b) After redistribution
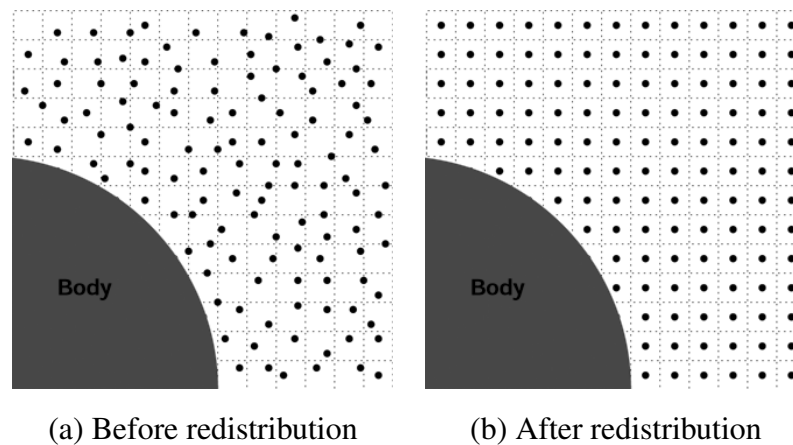
Figure **8.8** Redistribution scheme for a general boundary in two-dimensions.

The new particle strengths are determined using an appropriate interpolation

kernel Λ so that:

$$\tilde{\Gamma}_i(\tilde{x}) \approx \sum_{j=1}^{N} \Gamma_j(x_j) \, \Lambda_p(\tilde{x}_i - x_j) \tag{8.60}$$

where $\tilde{\Gamma}, \Gamma$ denote the new and old particle strength respectively, Λ_p interpolation kernel of p-th order. The process is not of the usual interpolation type as it is complicated by the fact that the particles are disordered. The basic analysis of interpolation of this type is given by Schoenberg (1973).

Consider first the normalized 1-D problem with unit spacing, $u = (x - \tilde{x}) / h$. In the $\Lambda_3(u)$ scheme, an old particle located at $-1/2 \leq u \leq 1/2$ gives

$$\Lambda_3(u) = \begin{cases} (3 - 2u)\,(4u^2 - 1)/48 & \text{to the new particle located at} & -3/2 \\ (1 - 2u)\,(9 - 4u^2)/16 & \text{to the new particle located at} & -1/2 \\ (1 + 2u)\,(9 - 4u^2)/16 & \text{to the new particle located at} & 1/2 \\ (3 + 2u)\,(4u^2 - 1)/48 & \text{to the new particle located at} & 3/2 \end{cases}$$

If a wall is present, the redistribution of particles close to the wall must be modified so that particles are prevented from penetrating the body. This is achieved by using $\Lambda_p{'}$ schemes. Two such schemes are detailed here, considering that an old particle is located at $-1/2 \leq u \leq 1/2$ and that the wall is at $u = -\frac{1}{2}$ for the $\Lambda_2{'}$ scheme and $u = -1$ for the $\Lambda_3{'}$ scheme:

$$\Lambda_2{'}(u) = \begin{cases} (u - 2 - 1/2)\,(u - 1 - 1/2)/2 & \text{at } 1/2 \\ (u - 1/2)\,(2 - u + 1/2) & \text{at } 3/2 \\ (u - 1/2)\,(u - 1 - 1/2)/2 & \text{at } 5/2 \end{cases}$$

$$\Lambda_3{'}(u) = \begin{cases} (1 - 2u)\,(2u - 5)\,(2u - 3)/48 & \text{at } -1/2 \\ (2u - 5)\,(2u - 3)\,(1 + 2u)/16 & \text{at } 1/2 \\ (1 - 2u)\,(2u - 5)\,(1 + 2u)/16 & \text{at } 3/2 \\ (1 - 2u)\,(3 - 2u)\,(1 + 2u)/48 & \text{at } 5/2 \end{cases}$$

In the present approach, a Λ_3 scheme is used for particle located more than $3/2$ from the wall, a $\Lambda_3{'}$ scheme for particles with distance between $1/2$ and $3/2$, and a $\Lambda_2{'}$ scheme for particles less than $1/2$ from the wall (Λ_3, $\Lambda_3{'}$ and

$\Lambda_2{}'$ schemes is suggested by Ploumhans and Winckelmans (2000) for general boundary).

The 2-D redistribution formulas are Cartesian products of their 1-D counterparts. In this case, the interpolation kernel is defined as

$$\Lambda(x, y) = \Lambda(x)\,\Lambda(y)$$

We use two steps. First, an old particle is redistributed in the x-direction and temporary particles are created. This redistribution in the x-direction has created three or four temporary particles. Each temporary particle is then redistributed in the y-direction. Figure **8.9** gives an example of the redistribution scheme.

(a) Before redistribution

(b) Redistribution in the x-direction

(c) Redistribution in the y-direction

(d) After redistribution
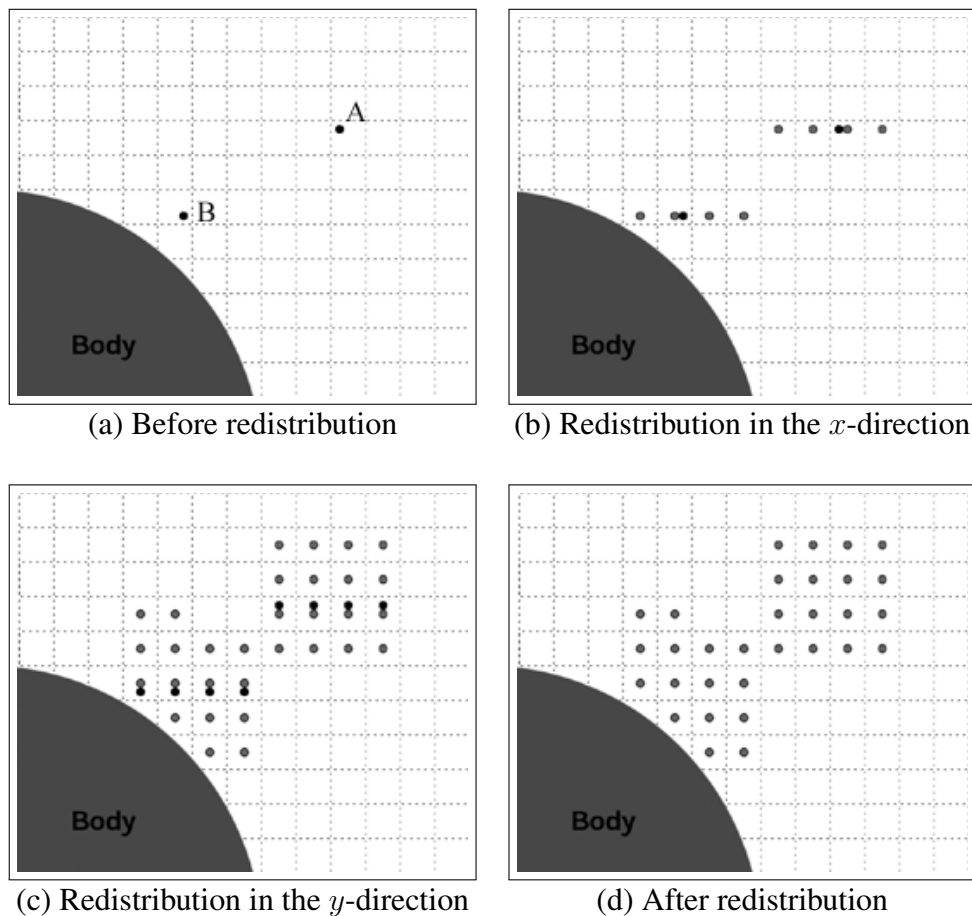
Figure **8.9** Two-dimensional redisribution scheme for a particle near a boundary. Λ_3 scheme for point A, and $\Lambda_3\,\Lambda_3{}'$ and $\Lambda_2{}'$ schemes for point B are used.

8.2.6.2 Force calculation

Hydrodynamic forces on the solid bodies can be computed either (1) by integration of the pressures on the boundaries, or (2) from integral expression of the system momentum balance. In vortex method, the second approach is very robust and has an almost zero computational cost. The total force $\underline{F}$ on a solid body can be computed from the time change of the linear impulse in the domain,

$$\underline{F} = -\rho \frac{d\underline{I}}{dt} \tag{8.61}$$

where ρ is the density and $\underline{I}$ is the first order moment of vorticity,

$$\underline{I} = \frac{1}{d-1} \int_V \underline{x} \times \underline{\omega}\, dV \tag{8.62}$$

with d the dimension of the space ($d = 3$ in 3-D, $d = 2$ in 2-D), and V the volume occupied by the fluid. The discretization of the equation is straight forward as it needs just summation running over all particles.

$$
\begin{aligned}
I_x &= \frac{1}{2} \int_V (y\,\omega_z - z\,\omega_y)\, dV \approx \sum_p (y_p\,\alpha_z - z_p\,\alpha_y) \\
I_y &= \frac{1}{2} \int_V (z\,\omega_x - x\,\omega_z)\, dV \approx \sum_p (z_p\,\alpha_x - x_p\,\alpha_z) \\
I_z &= \frac{1}{2} \int_V (x\,\omega_y - y\,\omega_x)\, dV \approx \sum_p (x_p\,\alpha_y - y_p\,\alpha_x)
\end{aligned}
\tag{8.63}
$$

The coefficient for the drag and lift, when the flow direction generates drag in x direction and lift in y respectively, with the surface area A,

$$C_D = \frac{F_x}{\frac{1}{2}\rho U_\infty^2 A} = -\frac{2}{U_\infty^2 A} \frac{dI_x}{dt} \tag{8.64}$$

$$C_L = \frac{F_y}{\frac{1}{2}\rho U_\infty^2 A} = -\frac{2}{U_\infty^2 A} \frac{dI_y}{dt} \tag{8.65}$$

8.3   Some Comparative Results

8.3.1   Impulsively started cylinder

The time development of an incompressible viscous flow around an impulsively started circular cylinder is a classical problem in fluid mechanics. Despite the simplicity of its geometry, the flow structure is complicated and all possible flow phenomena occur (Ta Phouc Loc and Bouard 1985). In this section, comparative studies of this problem are performed with the results of the Eulerian formulation (Suh and Kim 1999) and other researchers' work, including theoretical (Bar-Lev and Yang 1975), and numerical (Koumoutsakos and Leonard 1995, Ploumhans and Winckelmans 2000) investigations of the validity of the Lagrangian formulation.

Input parameters for the present comparison are as follows: $Re = U_\infty D/\nu$ = 550 , $T = t\,U_\infty/D$, $\Delta t = 0.05$, blob size $\epsilon = 0.005$, surface panel size $d = \pi/600 \approx 0.0052$. These parameters are chosen to satisfy the stability condition $\nu\,\Delta t/h^2 = \mathcal{O}(1)$ for the diffusion term, and to satisfy the stability conditions of the second-order Adam-Bashforth scheme for the convection term, and the explicit Euler scheme for time marching. N particles (or blobs) result in the so-called 'N-body problem' in the evaluation of the Biot-Savart integral. Therefore, the convection and diffusion terms are treated with the fast algorithm (Greengard 1987) to reduce computing time. Computational parameters used for the present comparison are tabulated in Table 8.1.

Figure 8.10 gives the comparison of vortex sheet strength with the results by Ploumhans and Winckelmans (2000).

Table **8.1** Parameters used in the numerical simulation of the flow around an impulsively started circular cylinder.

	Finite Volume Method	Vortex Particle Method
Reynolds number	550	550
Time step, Δt	0.01	0.01
Radius	0.5	0.5
Number of surface panels	600	600
Panel size	about 0.005	about 0.005
Grid meshes	600×40	.
Particles	.	$9000 \sim 70000$
Computational domain	$2.5 \times$ diameter	no limit
Computational time	about 6 hours	about 8 hours
(pentium IV)	(400 time steps)	(400 time steps)
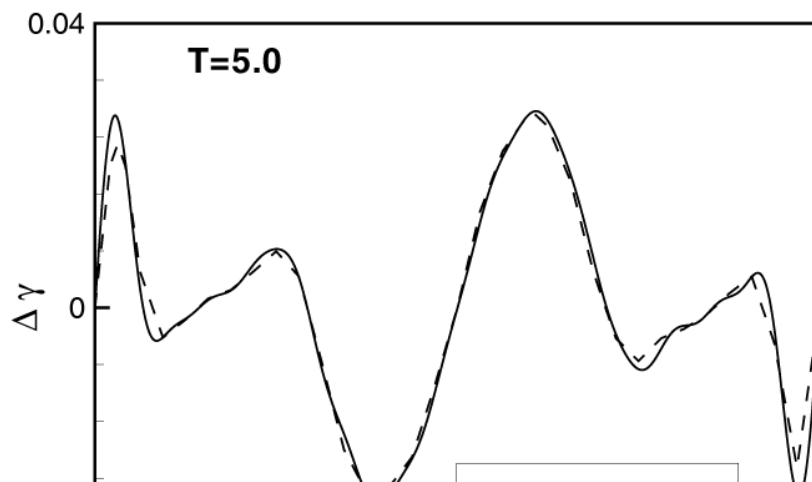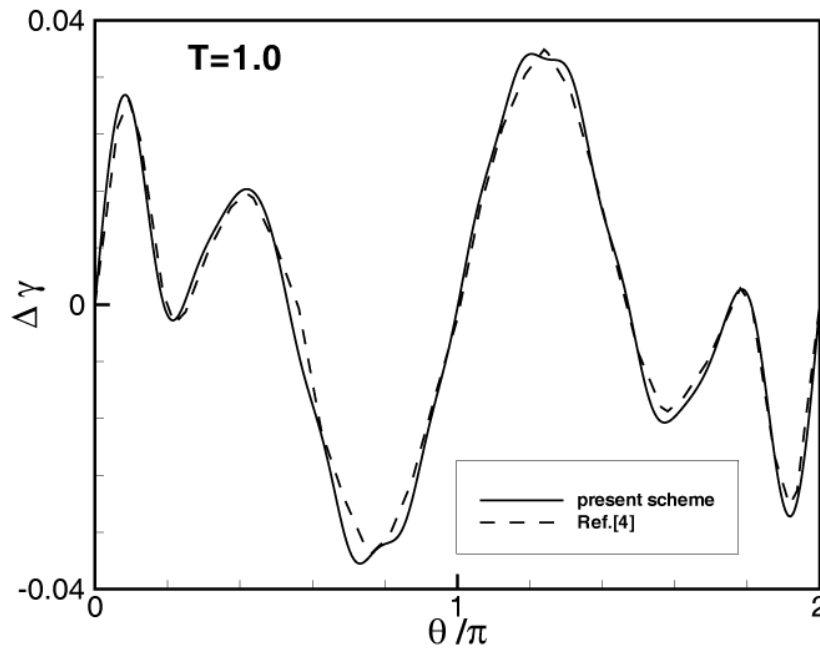
The vortex sheet strength(V_s) is equivalent to the accumulation of spurious slip velocity on the body boundary, which is calculated during the iterative process for the no-slip condition. The results of Ploumhans and Winckelmans are obtained in a manner such that vortex singularities are distributed on the body surfaces, and the no-slip condition is conferred to the interior boundary surfaces, which is equivalent to a no-penetration condition. Figure **8.10** shows that the distribution of V_s is in good agreement, except for some peak values. This implies that the iterative process for the body boundary condition imposed in FVM is also applicable to the vortex particle method.

A comparison is made in Figure **8.11** of I_x as a function of $T = t\,U_\infty/D$ for the x-component of momentum $\left(\underline{I} = \int_S \underline{x} \times \underline{\omega}\,dS\right)$, $I_x = \int_S y\,\omega\,dS = \sum_p y_p\,\alpha_p$, and Figure **8.11** includes the analytical solution for early developing flows ($T < 0.25$).
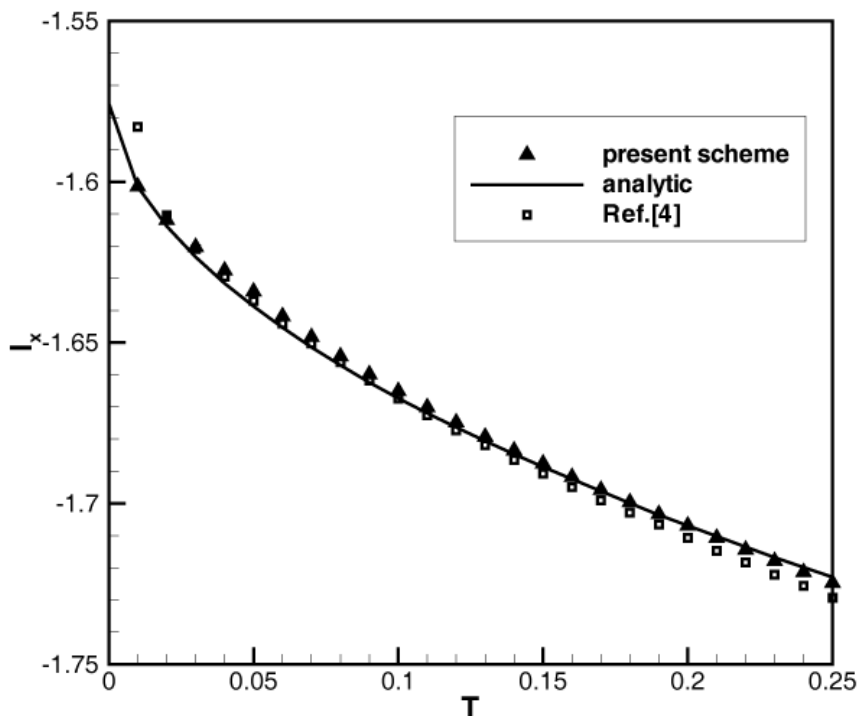
Figure **8.11** Comparison of I_x for the impulsively started cylinder problem ($0 < T < 0.25$). Solid line ($-$): analytical solution (Bar-Lev & Yang (1975)); ▲: Lagrangian vortex method (present scheme); □: Lagrangian vortex method (Ploumhans & Winckelmans (2000)).

The numerical and analytical results are in good agreement. As shown in Figure **8.12** , for a longer time interval, the two numerical methods give indistinguishable results.
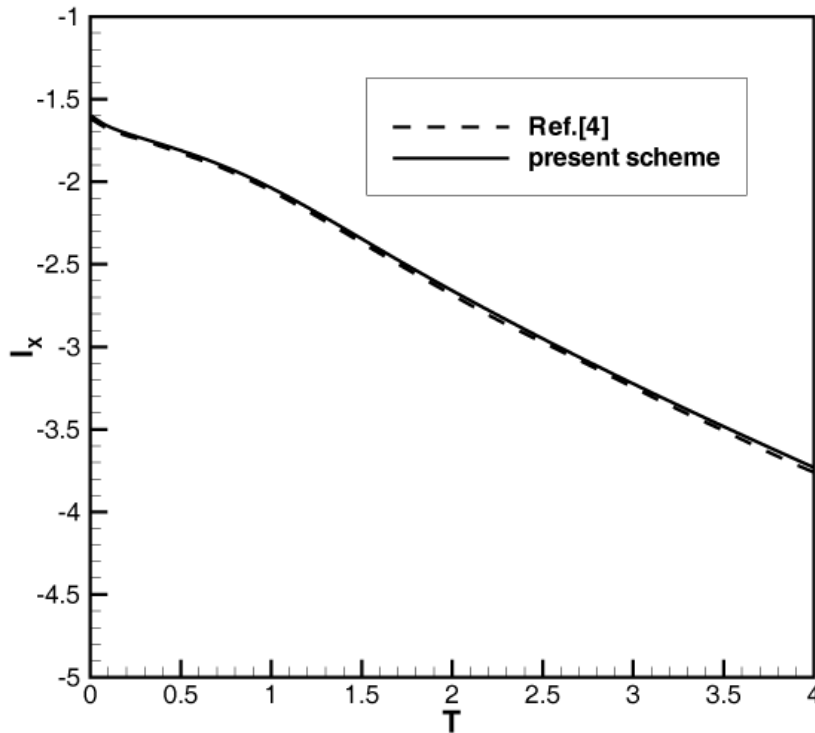
Figure **8.12** Comparison of I_x for the impulsively started cylinder problem $(0 < T < 4)$. Solid line $(-)$: Lagrangian vortex method (present scheme); dashed line $(--)$: Lagrangian vortex method (Ploumhans & Winckelmans (2000)).

The same comparison for the drag coefficient, $C_D = F_x / \frac{1}{2} \rho U_\infty^2 D$ with $F_x = -\rho \, dI_x/dt$, is shown in Figure **8.13** and Figure **8.14** . Here, the result obtained by FVM is included. Figure **8.13** shows that, of the two methods, the present Lagrangian scheme produces results somewhat closer to the analytical results.
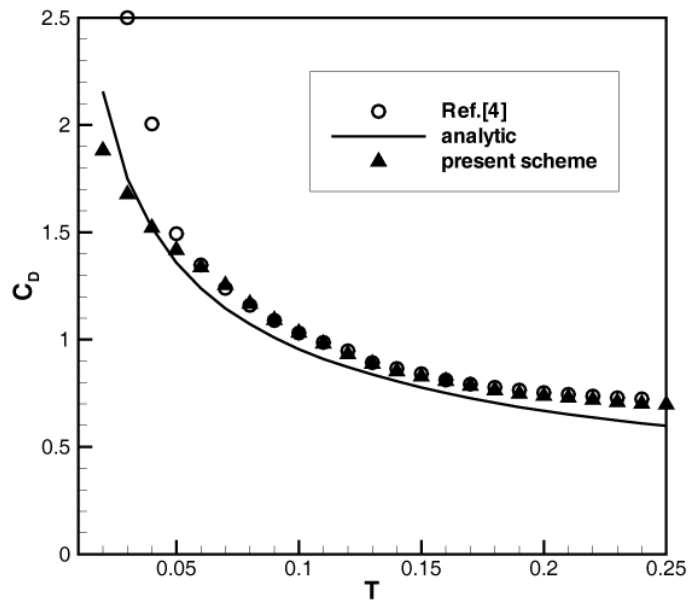
Figure **8.13** Comparison of C_D for the impulsively started cylinder problem ($0 < T < 0.25$). Solid line ($-$): analytical solution (Bar-Lev & Yang (1975)); ▲: Lagrangian vortex method (present scheme); □: Lagrangian vortex method (Ploumhans & Winckelmans (2000)).
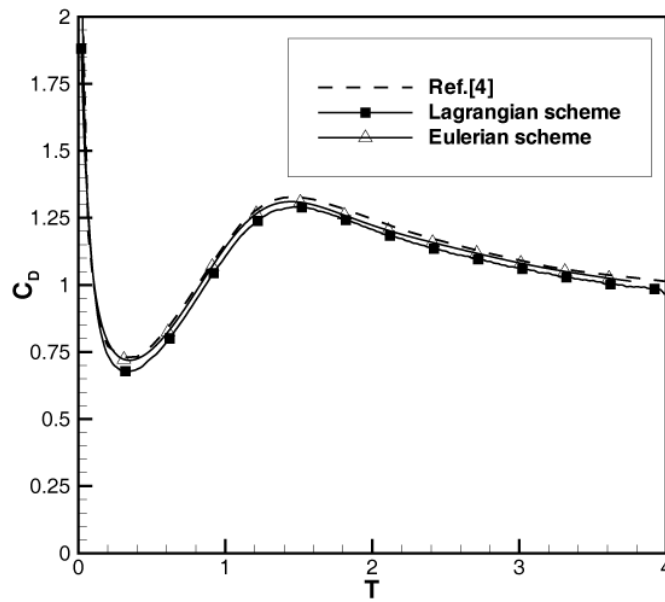
Figure **8.14** Comparison of C_D for the impulsively started cylinder problem ($0 < T < 4$). ■: Lagrangian vortex method; △: Eulerian FVM; dashed line($--$): Lagrangian vortex method (Ploumhans & Winckelmans (2000)).

Figure **8.15** represents the comparison of the body vorticity between the Eulerian FVM and the Lagrangian vortex method.
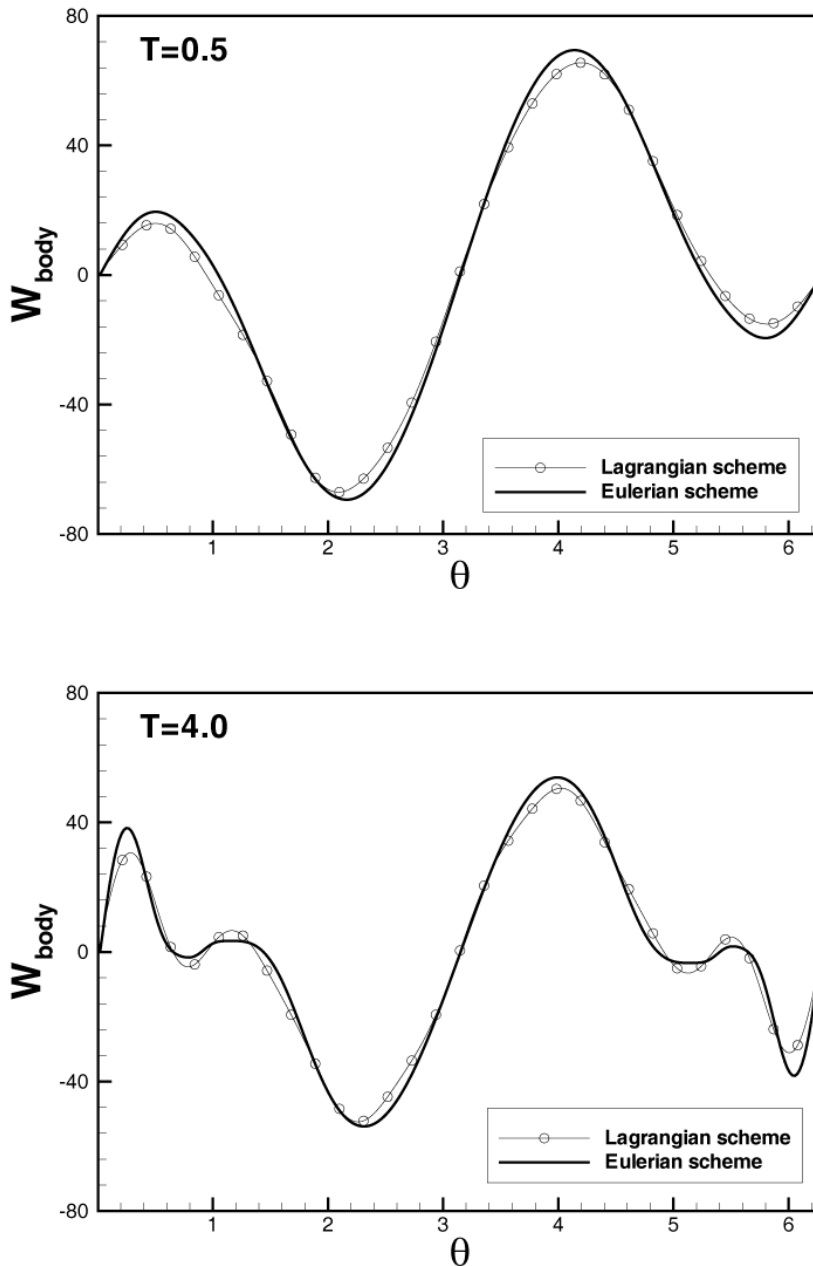
Figure 8.15 Comparison of the surface vorticity for the impulsively started cylinder problem for $Re = 550$ at $T = 0.5$ and $T = 4.0$. Solid line$(-)$: Eulerian FVM; $\circ$: Lagrangian vortex method.

The front stagnation point of the cylinder corresponds to the angular position of $\theta = \pi$ measured from the positive x-axis. The body vorticity obtained by the

Lagrangian vortex method is the 'filtered' (smoothed) value. The Lagrangian scheme has high-frequency noise in the values due to dispersed particles, so the filtered value is taken by an inverse Fourier transformation of the 16 first modes. The agreement between the two methods is seen to be quite satisfactory, but with small differences at local extrema. It is observed that, as time progresses, the local peaks of body vorticity become large. These local peaks occur at the instant the vortical wake behind the cylinder develops.

Figure **8.16** shows the streamline patterns. It is found that the wake length behind the cylinder is half the diameter of the cylinder at $T = 2$, and almost the same as the diameter at $T = 4$. At $T = 2$, a secondary vortex is generated at a position of about $\theta = 60°$. The results obtained from the Lagrangian vortex method and the Eulerian FVM are found to be almost identical, but the Lagrangian scheme produces short wavelength oscillations at regions where there are few nearby particles.

Figure **8.17** presents a comparison of iso-contours of vorticity between the Lagrangian and Eulerian approaches. The agreement between the two is shown to be very good, except that the minimum and maximum values of ω differ slightly.

Figure **8.18** shows the pressure contours in the computational domain. The results from the two methods are almost identical. As time advances, the pressure distributions are rapidly changed near strong vortical flow structures. It is seen that a low pressure region is formed at the core of the downstream wake.

Figure **8.19** presents a comparison of pressure coefficients $C_P\left(\equiv \dfrac{p - p_\infty}{\rho\, q_\infty^2}\right)$ on the body surface at several instants. It is observed that the agreement between these results is satisfactory.
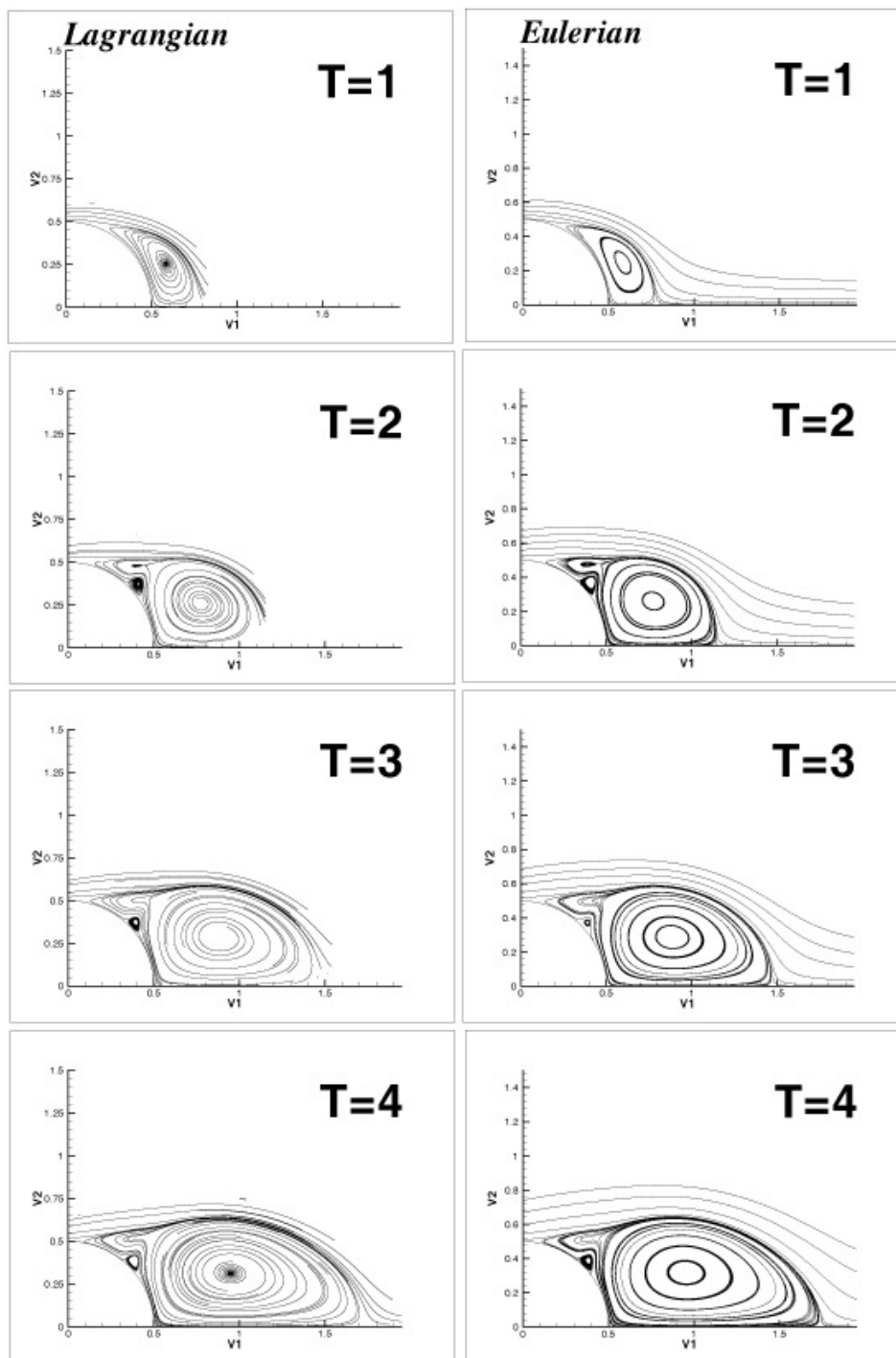
Figure **8.16** Comparison of the streamline patterns for the impulsively started cylinder problem for $Re = 550$ at $T = 1, T = 2, T = 3$ and $T = 4$. (left) Lagrangian vortex method; (right) Eulerian FVM.
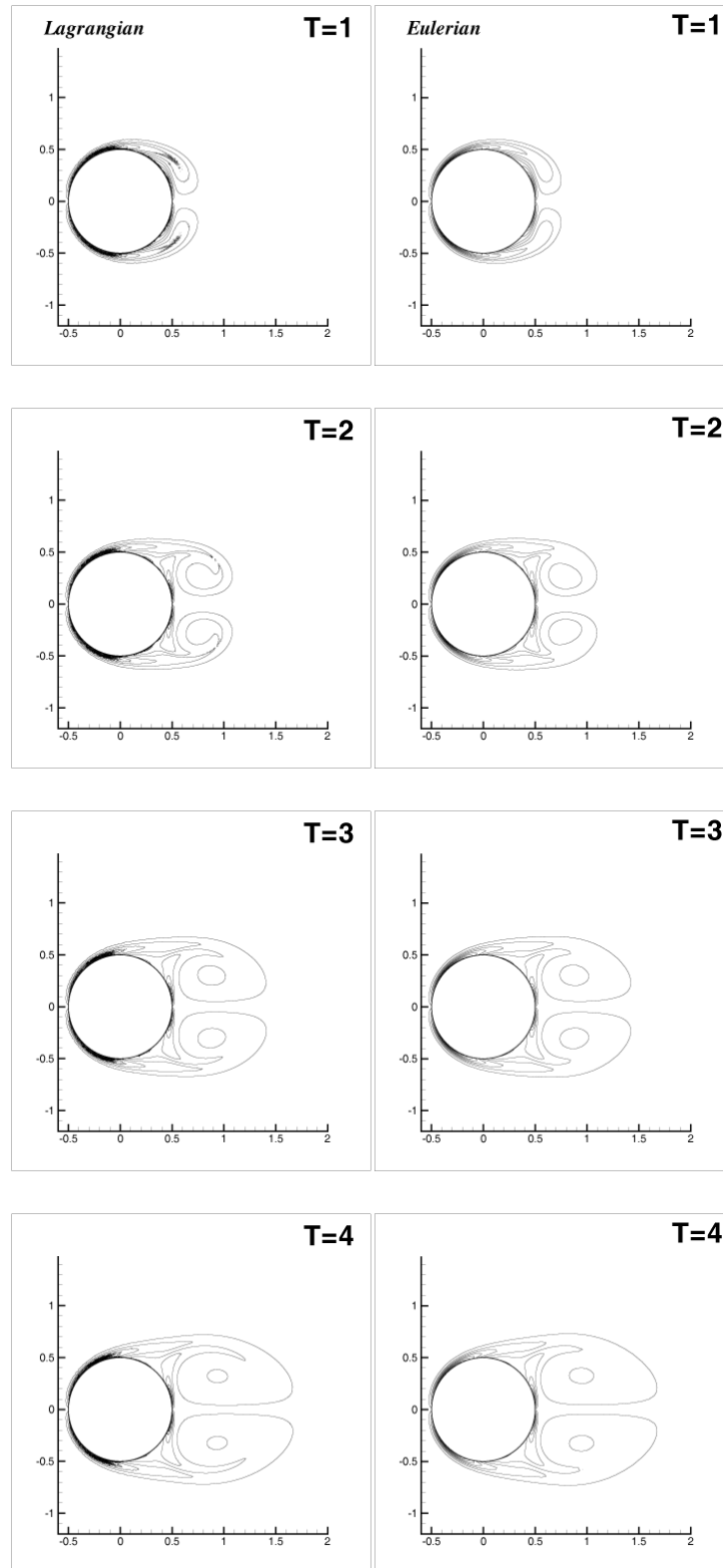
Figure **8.17** Comparison of the vorticity contours for the impulsively started cylinder problem for $Re = 550$ at $T = 1$, $T = 2$, $T = 3$ and $T = 4$. (left) Lagrangian vortex method; (right) Eulerian FVM.
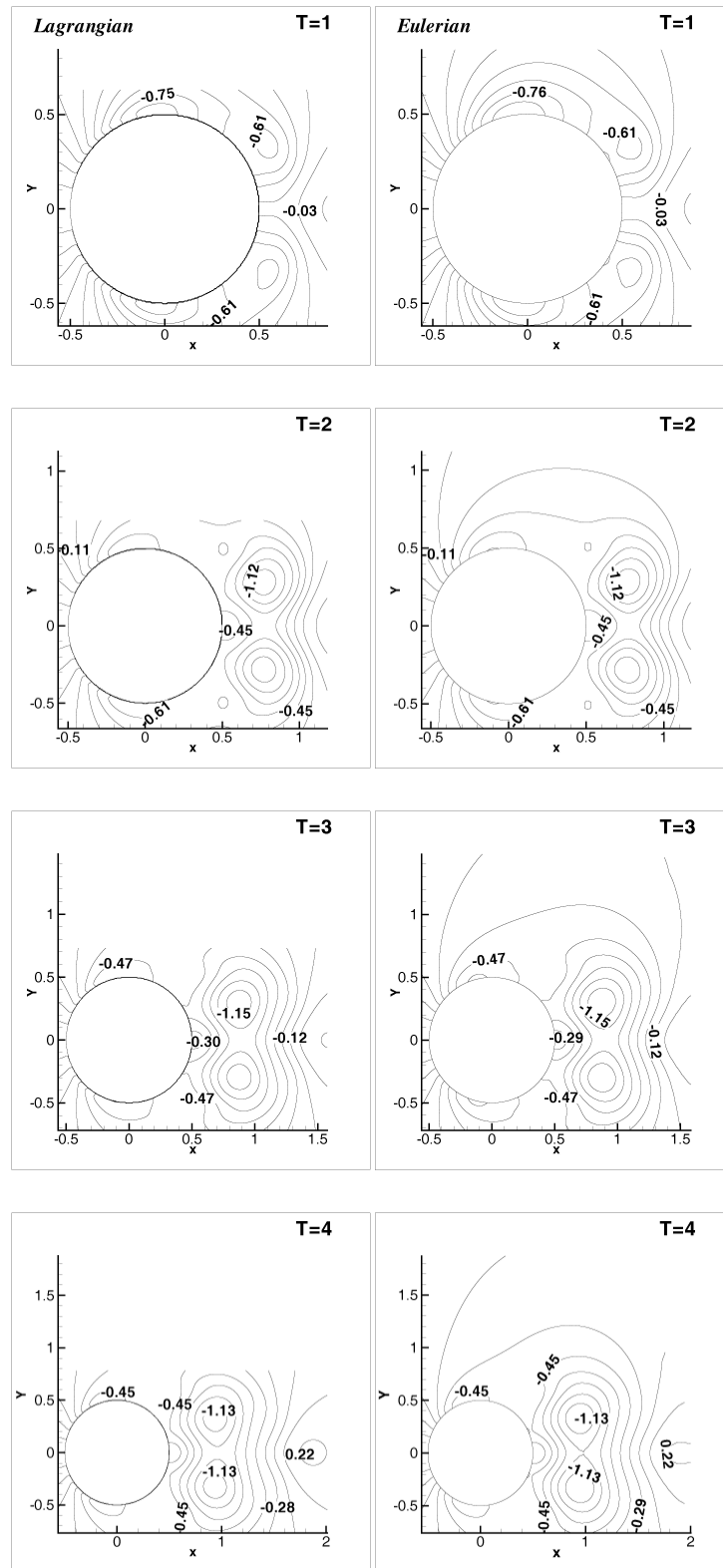
Figure **8.18** Comparison of the pressure contours for the impulsively started cylinder problem for $Re = 550$ at $T = 1.0$, $T = 2.0$, $T = 3.0$ and $T = 4.0$. (left) Lagrangian vortex method; (right) Eulerian FVM.
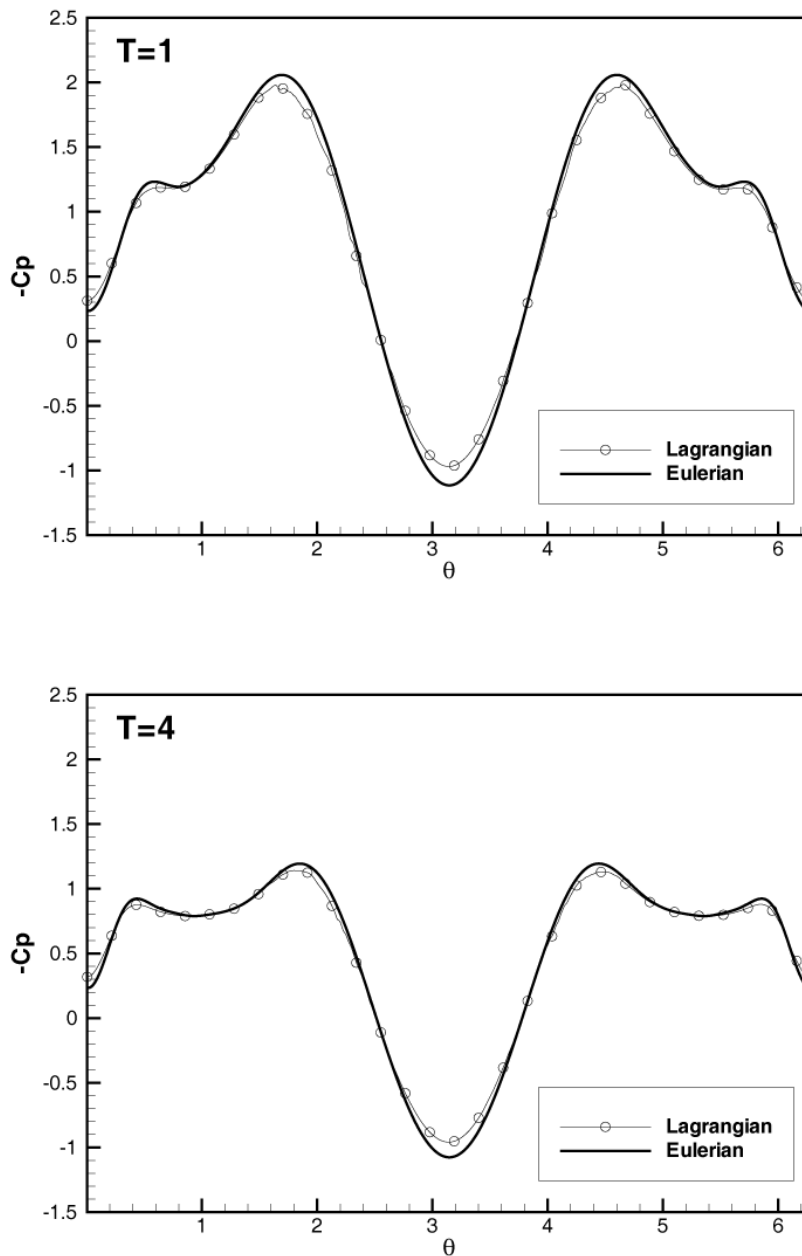
Figure **8.19** Comparison of C_p for the impulsively started cylinder problem for $Re = 550$ at $T = 1$ and $T = 4.0$. Solid line($-$): Eulerian FVM; Circle($\circ$): Lagrangian vortex method.

8.3.2 Impulsively started foil with varying angles of attack

We now take the case of the impulsively started NACA0021 with varying angles of attack. The present image particle layer scheme is suitable for this case. The

parameters used in the calculation are similar to the case of the impulsively started cylinder (see Table **8.2**).

Table 8.2 Parameters used in the numerical simulation of the flow around an impulsively started NACA 0021 hydrofoil.

	Eulerian FVM	Lagrangian vortex method
Reynolds number	550	550
Time step,Δt	0.01	0.01
Thickness ratio	0.21	0.21
Number of surface panels	408	408
Angle of attack	$5°,10°$	$5°,10°$
Grid meshes	408×60	.
Particles	.	$13000 \sim 40000$
Computational domain	$3\times$ chord	no limit
Computational time	about 31 hours	about 50 hours
(pentium IV)	(400 time steps)	(400 time steps)

A hydrofoil section of NACA0021 is chosen for the computation. It is a symmetrical hydrofoil whose thickness ratio is 21%. The thickness distribution for the NACA0021 is given in Abbott and Doenhoff (1958).

The parameters used in the simulation are $\Delta T = 0.01$ and $Re = 550$. The Reynolds number is based on the uniform flow velocity and chord length of the hydrofoil. There are 408 panels at body surface. The radius of all vortex particles has used with $\epsilon = 0.0025$. Image particles are located underneath body panels. Redistribution is done every five time steps. If new particle has $|\alpha| < 0.001 |\alpha|_{max}$, it is deleted and the loss of circulation is redistributed equally among the remaining particles. The integration scheme for convection is a second order Adam-Bashforth (second order Runge-Kutta for the first step just after each redistribution). For diffusion, a first order Euler explicit scheme is used. A fast algorithm proposed by Greengard and Rohklin (1987), is used for both convection and diffusion substeps. After vorticity and velocity are updated through two fractional steps, the pressure equation is solved when needed.

Some experimental results were provided by Huang *et al.* (2001). His experiments were conducted in a towing water tank. The particle tracking flow

visualization (PTFV) and the particle image velocimetry (PIV) were used to obtain a picture of vortex evolution on the suction surface of an impulsively started NACA 0012 hydrofoil. Five characteristic vortex evolution regimes are identified in the parameter domain of angle of attack.

The computing time is longer than in the case of the cylinder. The reason may be that the number of iterations required for canceling the spurious slip velocity and generating the vorticity flux on the body boundary is larger than that in the case of the cylinder problem. As the angle of attack is higher, the computing time is much longer. We applied the present scheme to the foil with two angles of attack, $5°$ and $10°$.

Figure **8.20** shows the streamline patterns, the vorticity contours and the pressure contours at Reynolds number 550 around the foil with angle of attack $5°$. The two results are shown to be in good agreement. In the streamline patterns, the reverse flows are captured near the trailing edge of the foil. As observed in the results of the Lagrangian vortex method, the fields of velocity and pressure are confined to the viscous region around the foil, because we consider only the field where the vorticity evolves and exists.

Figure **8.21** shows the streamline patterns, the vorticity contours and pressure contours at Reynolds number of 550 at $T = 4.0$ for the angle of attack of $10°$. This shows aspects similar to those of the previous case.

Figure **8.22** and Figure **8.23** show the comparison of the drag coefficients and the lift coefficients. In the case of angle of attack $5°$, the results of Lagrangian vortex and Eulerian FVM methods are nearly identical.

On the other hand, in the case of angle of attack $10°$, there is a small difference between the results, especially at about $T = 3.0$. This may be due to the strong starting vortex. When the angle of attack of the foil is higher, the strength of the starting vortex is larger. Each scheme may reflect the evolution of the vorticity on the body in a different manner. In fact, we only focus on the unsteady flow simulation at an early stage. We may expect to obtain the same steady-state characteristics.
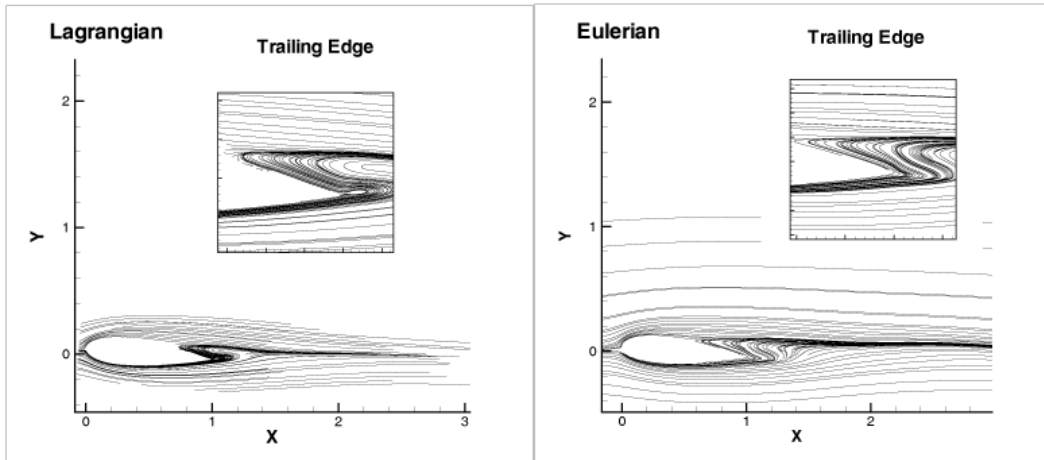
(a) Streamlines
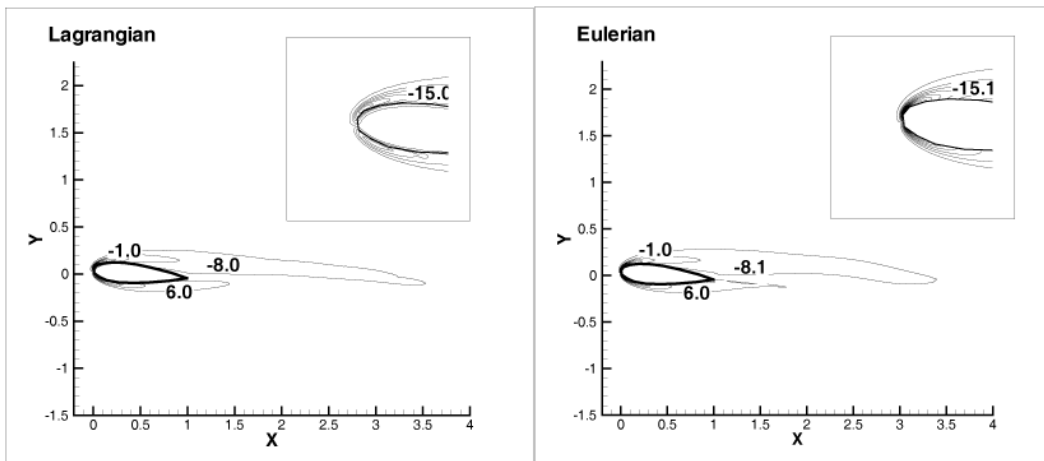
(b) Vorticity
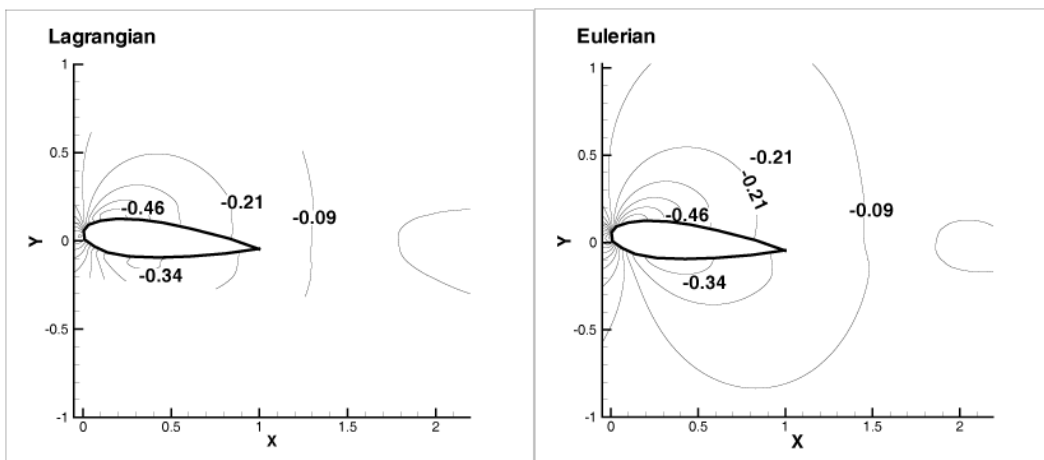
(c) Pressure

Figure **8.20** Streamline patterns, vorticity contours and pressure contours for the impulsively started NACA0021 at $Re = 550$, $\alpha = 5°$ and $T = 4.0$. (left) Lagrangian vortex method; (right) Eulerian FVM.
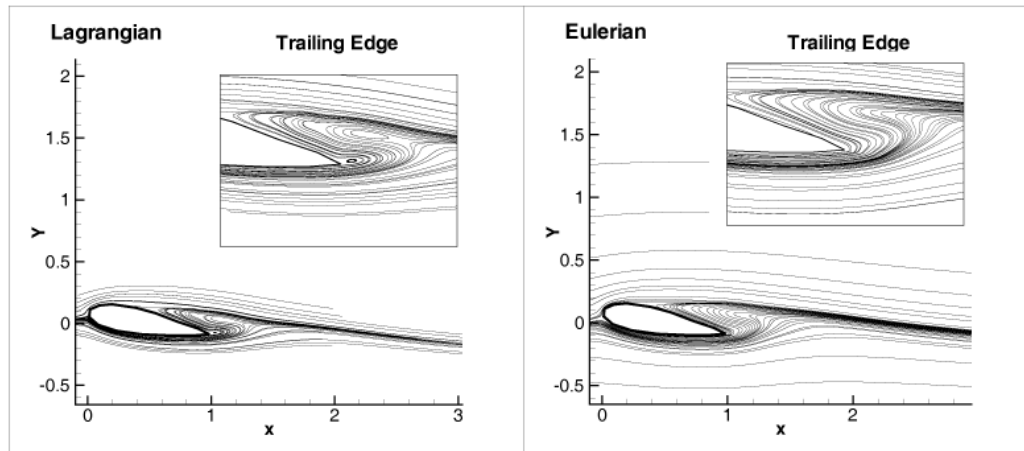
(a) Streamlines
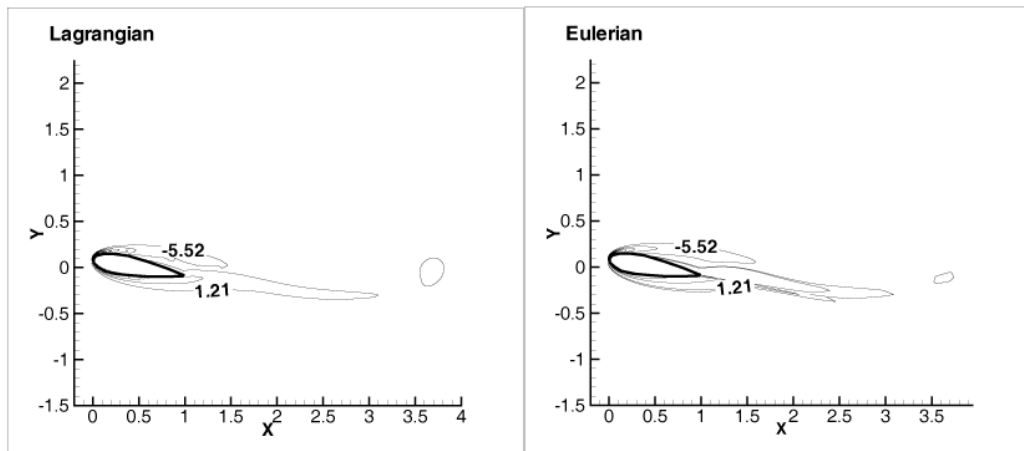
(b) Vorticity
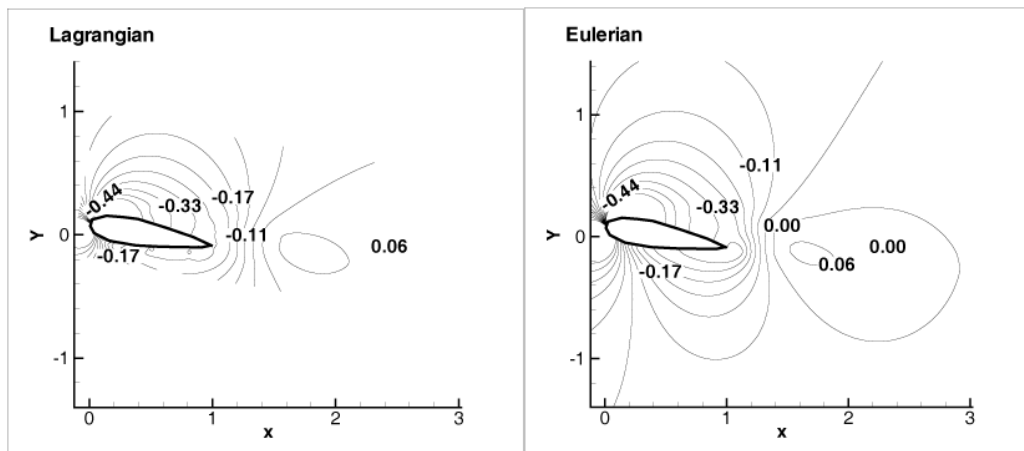
(c) Pressure

Figure **8.21** Streamline patterns, vorticity contours and pressure contours for the impulsively started NACA0021 foil at $Re = 550$, $\alpha = 10°$ and $T = 4.0$. (left): Lagrangian vortex method; (right): Eulerian FVM.
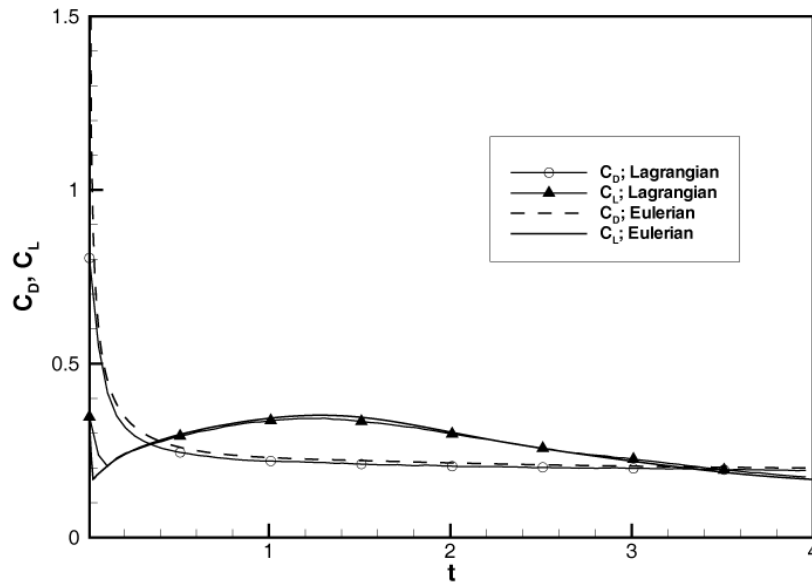
Figure **8.22** Comparison of drag and lift for the impulsively started NACA0021 foil at $Re = 550$ and $\alpha = 5$. $\circ$: C_D by Lagrangian vortex method; $\blacktriangle$: C_L by Lagrangian vortex method; dashed line($--$): C_D by Eulerian FVM; solid line($-$): C_L by Eulerian FVM.
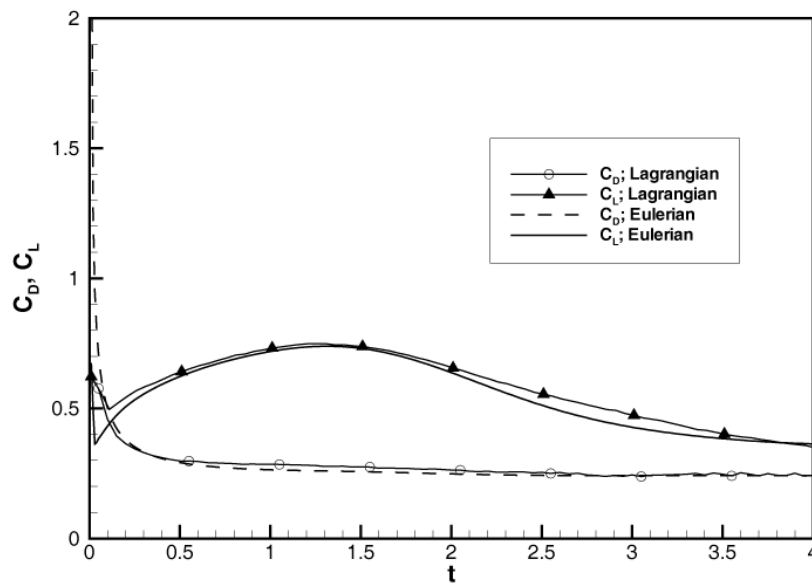
Figure **8.23** Comparison of drag and lift for the impulsively started NACA0021 foil at $Re = 550$ and $\alpha = 10$. $\circ$: C_D by Lagrangian vortex method; $\blacktriangle$: C_L by Lagrangian vortex method; dashed line($--$): C_D by Eulerian FVM; solid line($-$): C_L by Eulerian FVM.

8.3.2.1   Angle of attack : 90 deg.

At very large angles of attack, the bluff body effect becomes dominant. The starting vortex is generated from both the leading and the trailing edges. The vortex evolving from the sharp trailing edge appears to be a little larger than one from the leading edge. The corresponding results are shown in Figures **8.24** , **8.25** , and **8.26** .
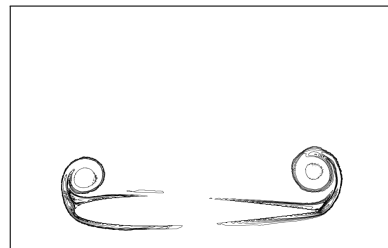
(a) $T = 0.250$
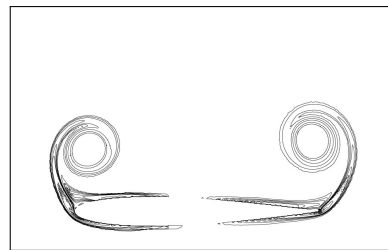
(b) $T = 0.500$
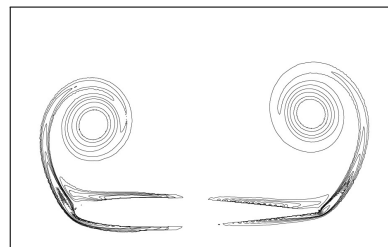
(c) $T = 0.750$
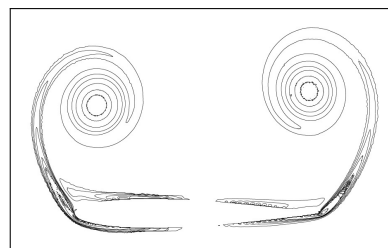
(d) $T = 1.000$

Figure **8.24** Iso-contours of vorticity around NACA 0012 hydrofoil at $\alpha = 90^o$ and $Re = 1200$.
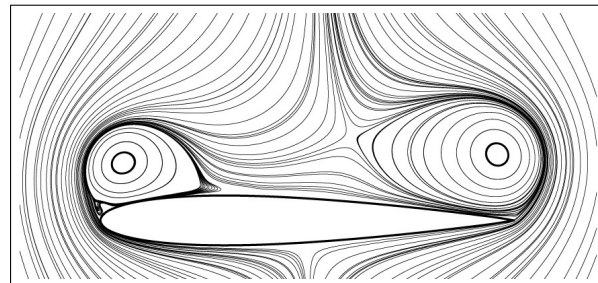
(a) $T = 0.250$
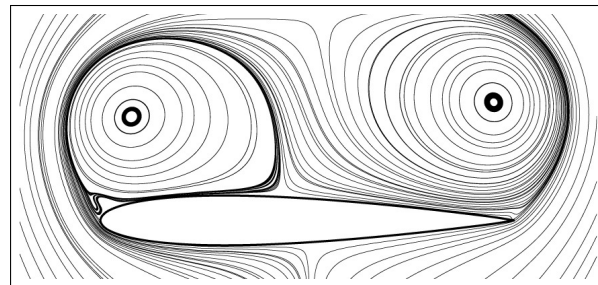
(b) $T = 0.500$
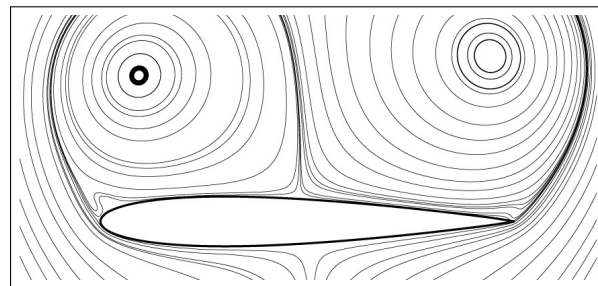
(c) $T = 0.750$
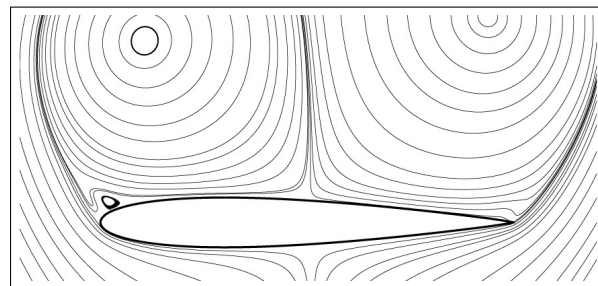
(d) $T = 1.000$

Figure **8.25** Streamlines around NACA 0012 hydrofoil at $\alpha = 90^o$ and $Re = 1200$.

(a) $T = 0.786$

(b) $T = 0.750$

(c) $T = 1.048$

(d) $T = 1.000$
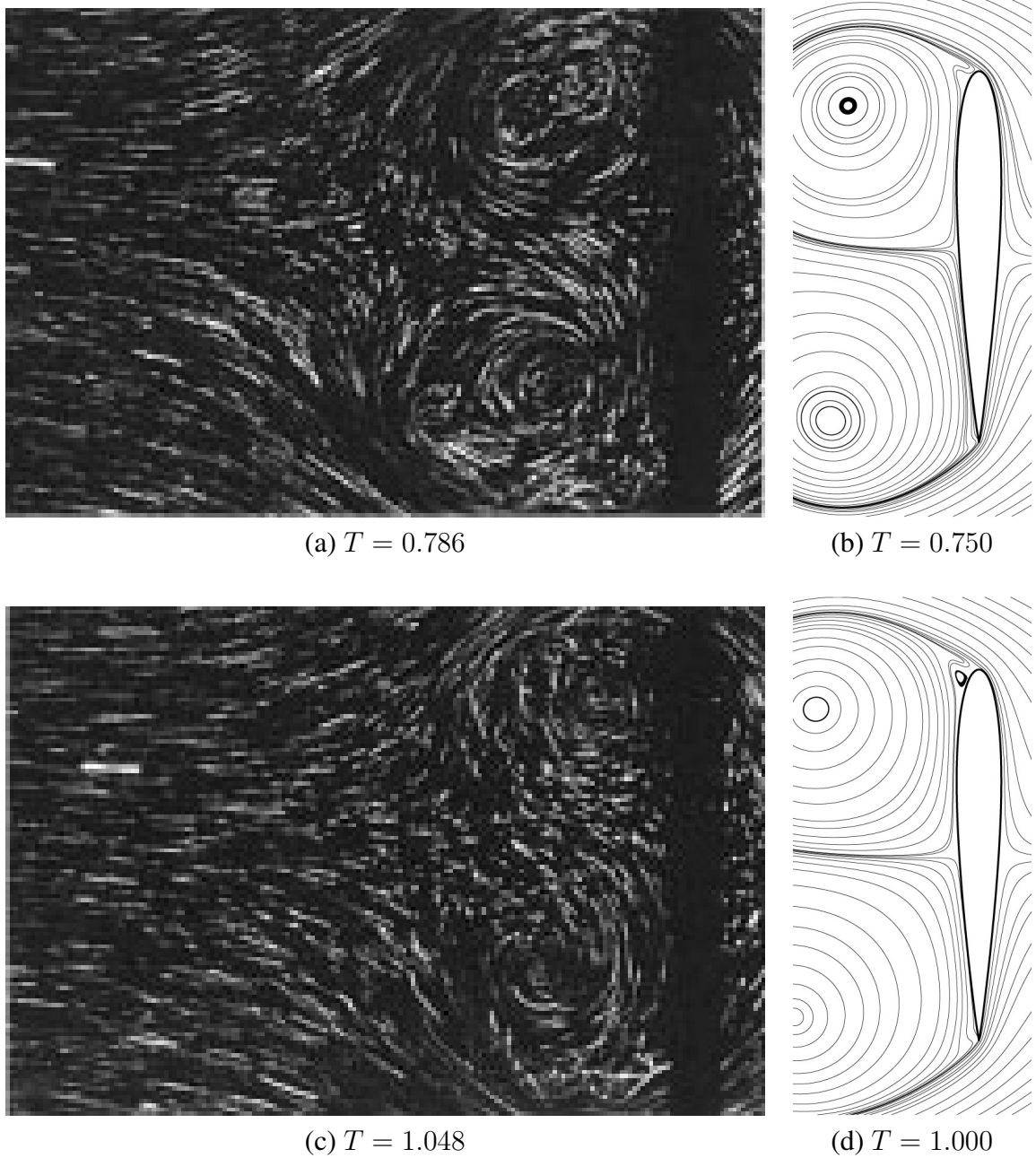
Figure **8.26** Comparison of the streamlines around NACA 0012 hydrofoil with the experimetal result (Huang *et al.* 2001) at $\alpha = 90^o$ and $Re = 1200$.

8.4   Vortex-In-Cell Methods

8.4.1   Introduction

The computation of velocity and stretching is realized through the vector potential and vorticity formulation on the immersed Cartesian grid. The present method is similar to the immersed boundary vortex-in-cell method by Cottet and Poncet (2003) in terms of the use of unified interpolation formulas. But, the use of panel method makes it possible to impose both the no through flow condition and no slip condition on the body surface. The vorticity flux from the panel satisfies the no slip condition and the singularity distribution over the panel does not make the flow across the body surface. The panel method is set up on the triangular discretization of the body surface and linear distribution of the singularities on the panel. The implementation has advantages over constant strength method that eliminates the discontinuities of singularities between panels and reduces the size of matrix elements as well. In the present method, the panel method is also utilized for the calculation of pressure field. The inversion result of the influence coefficient matrix can be adopted without any modification due to the integral equation formulation for the pressure.
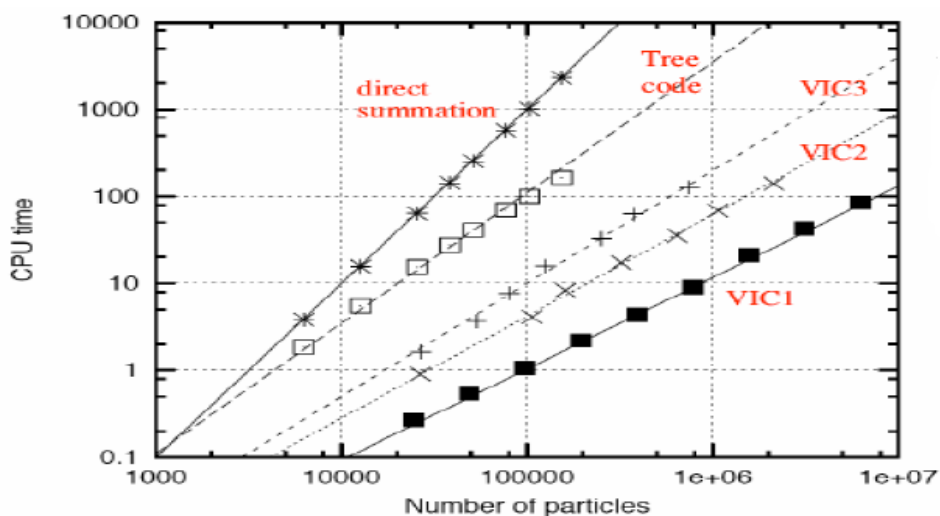
Figure **8.27** Comparison of CPU times for velocity evaluations in 3-D. Krasny tree-code vs. VIC with Fishpack and 64 points interpolation formulas. VIC1: Cartersian grid with 100 % particles; VIC2: Polar grid with 65 % particles; VIC3: Polar grid with 25 % particles. From Cottet (1999).

8.4.2   Rotational velocity component: FFT scheme based on regular grid
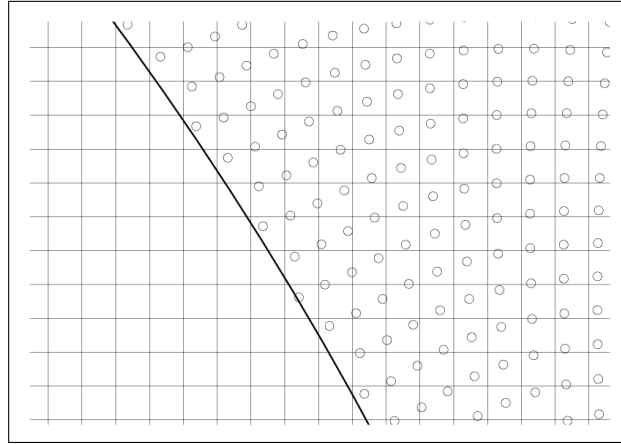
(a) Before particle strength assignment on the grid
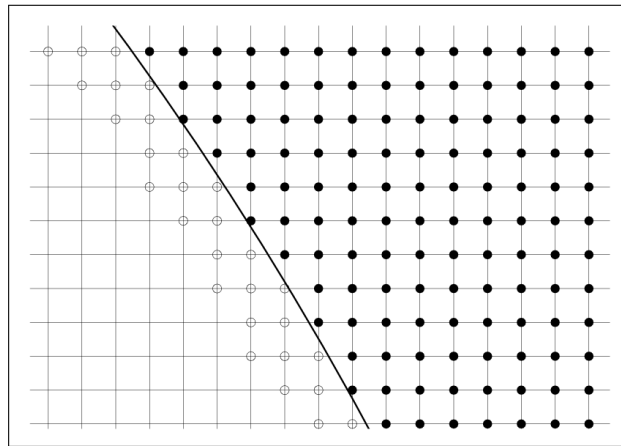
(b) After assignment, strengths assigned onto hollow circle inside body are reserved for PSE

Figure 8.28 Regular immersed grids for FFT.

The present work uses FFT based Poisson solver to calculate rotational velocity field. A regular Cartesian grid is placed so that the grid compactly encloses the vortex particles including the body. The grid is immersed in the body, and the vorticity field is extended so that vorticity has zero value on the grid inside the body. The vorticity of the particles is distributed to the Cartesian grid by the interpolation formula,

$$\underline{\omega}_g = \frac{1}{V_p} \sum_p^N \underline{\alpha}_p \, W\left(\frac{x_p - x_g}{h}\right) \, W\left(\frac{y_p - y_g}{h}\right) \, W\left(\frac{z_p - z_g}{h}\right) \qquad (8.66)$$

where g and p are subscripts for grid and particle quantities, respectively, and $W(x)$ is the interpolation kernel. In the present work the third order M_4' kernel is chosen. The kernel is defined by

$$
W(x) = M_4'(x) = \begin{cases} 1 - \frac{5}{2}|x|^2 + \frac{3}{2}|x|^3, & \text{for} \quad |x| \le 1 \\ \frac{1}{2}(2 - |x|)^2(1 - |x|), & \text{for} \quad 1 < |x| < 2 \\ 0, & \text{for} \quad |x| \ge 2 \end{cases} \qquad (8.67)
$$

The kernel preserves the first three moments of the distribution, the total, linear and angular impulse of the fields, twice continuously differentiable and symmetric. The VIC method needs regridding of particles on regular locations on occasion to preserve the accuracy, and the kernel is also used for the regular distribution of the distorted particles.

After the interpolation step the Poisson equation for vector potential is solved by following the procedure which is introduced as Fourier transform method in the book "*Numerical Recipes in C*". Here the procedure is briefly recited for the two dimensional Poisson equation $\nabla^2 \psi = -\omega$ with Dirichlet boundary condition. The finite difference representation of the equation is, approximating the Laplacian via the second order central difference scheme,

$$
\frac{\psi_{i+1,j} - 2\psi_{i,j} + \psi_{i-1,j}}{h^2} + \frac{\psi_{i,j+1} - 2\psi_{i,j} + \psi_{i,j-1}}{h^2} = -\omega_{i,j} \qquad (8.68)
$$

where $\psi_{i,j}$ represents function value at a point (x_i, y_j) and h is grid spacing. If we substitute the discrete inverse sine transforms,

$$
\psi_{i,j} = \frac{2}{IJ} \sum_{m=1}^{I-1} \sum_{n=1}^{J-1} \hat{\psi}_{m,n} \sin\frac{\pi i m}{I} \sin\frac{\pi j n}{J} \qquad (8.69)
$$

$$
\omega_{i,j} = \frac{2}{IJ} \sum_{m=1}^{I-1} \sum_{n=1}^{J-1} \hat{\omega}_{m,n} \sin\frac{\pi i m}{I} \sin\frac{\pi j n}{J} \qquad (8.70)
$$

in the finite difference equation (8.68), we can get the relation between Fourier

coefficients,

$$\hat{\psi}_{m,n} = \frac{h^2 \hat{\omega}_{m,n}}{2 \left(\cos \dfrac{\pi m}{I} + \cos \dfrac{\pi n}{J} - 2 \right)} \tag{8.71}$$

We can get $\psi_{i,j}$ on the regular grid by the inverse sine transform (8.69).

In 3-D, the inverse sine transform has one more term and the relation between Fourier coefficients becomes similar form,

$$\hat{\psi}_{l,m,n} = \frac{h^2 \hat{\omega}_{l,m,n}}{2 \left(\cos \dfrac{\pi l}{I} + \cos \dfrac{\pi m}{J} + \cos \dfrac{\pi n}{K} - 3 \right)} \tag{8.72}$$

Above procedure was explained for homogeneous Dirichlet condition at boundary. As the grid is set up so that it tightly includes the particles, the values of ψ on the sides of the VIC grid become non trivial. When the boundary values of ψ are known, the procedure can be simply modified by taking them over to the right-hand side. If we write the solution as $\psi = \psi' + \psi^B$, where $\psi' = 0$ on the boundary, while ψ^B has nonzero values only on the boundary, which is the given boundary value, the finite difference equation (8.68) becomes equivalent to the case of zero boundary condition. The equation for a boundary takes the form, say for $i = I - 1$,

$$\psi'_{I,j} + \psi'_{I-2,j} + \psi'_{I-1,j+1} + \psi'_{I-1,j-1} - 4\,\psi'_{I-1,j} = h^2\,\omega_{I-1,j} - \psi^B_{I,j} \tag{8.73}$$

so whenever the boundary value is non-zero, the source term $h^2\,\omega_{I-1,j}$ (be careful that one grid inside from boundary) is replaced by

$$h^2\,\omega_{I-1,j} - \psi^B_{I,j} \tag{8.74}$$

The values on the boundary is evaluated using the expression (8.23) by fast algorithm developed by Kim (2003). If the boundary is located far from the particle positions, the homogeneous boundary condition may be used, but this approach involves too much grid and the advantage of using compact grid cannot be taken.

The velocity on the grid is computed by fourth order finite difference method

from the definition $\underline{u}_\omega = \nabla \times \underline{\psi}$, for example, the component u is

$$
\begin{aligned}
u &= \frac{\partial \psi_z}{\partial y} - \frac{\partial \psi_y}{\partial z} \\
&= \frac{\psi_{z_{i,j-2,k}} - 8\,\psi_{z_{i,j-1,k}} + 8\,\psi_{z_{i,j+1,k}} - \psi_{z_{i,j+2,k}}}{12\,h} \\
&\quad - \frac{\psi_{y_{i,j,k-2}} - 8\,\psi_{y_{i,j,k-1}} + 8\,\psi_{y_{i,j,k+1}} - \psi_{y_{i,j,k+2}}}{12\,h}
\end{aligned}
\tag{8.75}
$$

The velocity on the particle position is then interpolated from the velocities of the grid. The same interpolation formula M_4' is used. The velocity on the grid very close to the body can have singular behavior since sub-grid scale can have a significant effect when applying finite difference formula. The velocity at such a point is directly evaluated using the Biot-Savart formula. The points are found by a criteria that the distance from the body is less than half of the grid size.

8.4.3 Potential velocity component: Panel method with linearly varying singularity distribution

For the solution of the Laplace equation $\nabla^2 \phi = 0$, the identity with a distribution of singularities on the surface is applied to the discretized surface so that the strengths of them determined by the boundary condition. This technique is known as the popular 'panel method'. The no through flow condition is employed to points on the surface, unlike Cottet & Poncet (2003)'s method. Figure **8.29** shows the difference between Cottet & Poncet (2003) and the present work in handling no through flow condition.
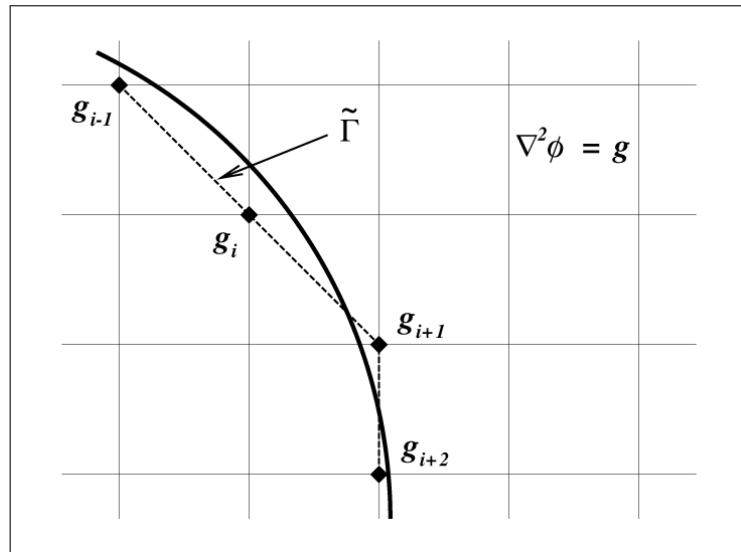
(a) Immersed boundary VIC, Cottet & Poncet (2003)
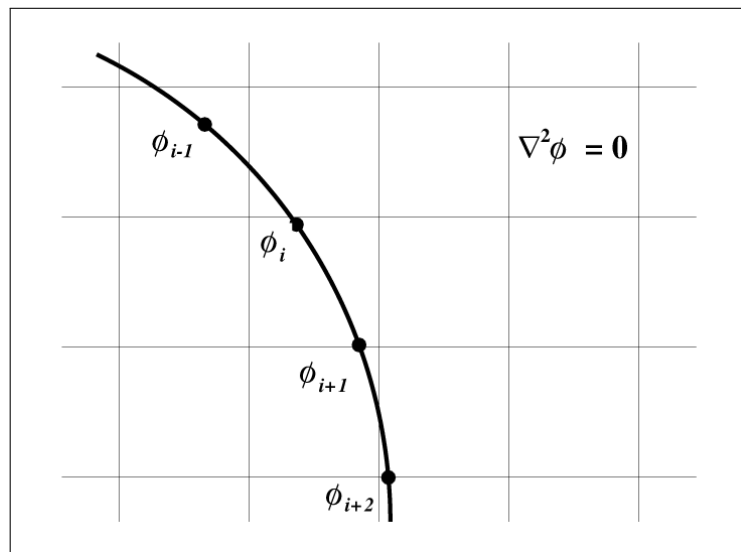
(b) Present work

Figure **8.29** Two types for enforcement of the no-penetration flow condition in the regular grid system.

The present method is extended in the context of the VIC of this work to a linear distribution of singularities on a triangular panel. This choice is more flexible, since surface of a complex geometry can be more uniformly discretized with triangular elements. Furthermore, the discontinuity of the singularities, which is present between panels in constant strength panel method, can be avoided with the linear variation. And, as the number of panels becomes approximately twice that of the vertices, it would be a great benefit that the un-

knowns in the resulting system of linear equations can be notably decreased with the unknowns defined on the panel vertices.

The Green's scalar identity expresses the potential ϕ within the fluid domain as a sum of each contribution in terms of the surface value of ϕ and its normal derivative $\underline{n} \cdot \nabla \phi$ on each panel of the discretized boundary surface S_i,

$$\phi(\underline{x}) = -\frac{1}{4\pi} \sum_i \iint_{S_i} \left\{ \frac{1}{r} \underline{n} \cdot \nabla_\xi \phi - \phi(\underline{\xi}) \, \underline{n} \cdot \nabla_\xi \left(\frac{1}{r} \right) \right\} dS_\xi \qquad (8.76)$$

where $\phi(\xi)$ is the surface distribution of doublets, and $\underline{n} \cdot \nabla_\xi$ is that of sources. The strength of source σ corresponds to the no through flow boundary condition,

$$\sigma = \underline{n} \cdot \nabla_\xi \phi = -\underline{n} \cdot (\underline{U}_\infty + \underline{u}_\omega) \qquad (8.77)$$

If the equation (8.76) is discretely applied for each vertex with the surface integrals evaluated assuming that the source and doublet are linearly distributed on each panel, we can get the linear system of algebraic equations.

$$(1 + D_{kk}) \, \phi_k - \sum_{m=1}^{N-(k)} \phi_m \, D_{km} = \sigma_k \, E_{kk} + \sum_{m=1}^{N-(k)} \sigma_m \, E_{km} \qquad (8.78)$$

$$D_{km} = \sum_{n=1}^{L_m} \frac{1}{4\pi} \iint_{S_m} \underline{n} \cdot \nabla \left(\frac{1}{r} \right) dS_\xi$$

$$E_{km} = \sum_{n=1}^{L_m} \frac{1}{4\pi} \iint_{S_m} \frac{1}{r} \, dS_\xi$$

where L_m is the number of panels which have the vertex m in common. D_{kk} and E_{kk} are the special case that the field point coincides with the source point. Due to the linear distribution of the singularities, it should sum up all the contributions from each panel when the surface integral is calculated. As shown in Figure 8.30 , when the induced potential is calculated at the point k by the unit strength on m, all the panels filled with gray should be involved with the other nodes having value zero.
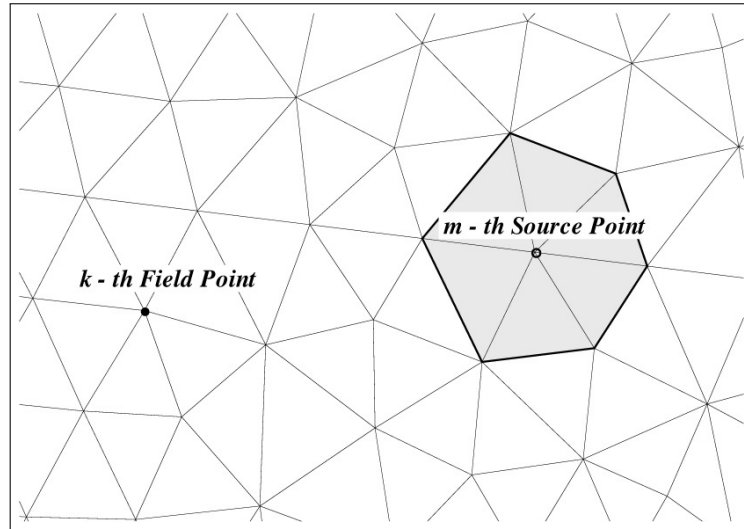
Figure **8.30** Schematic arrangement of a field point k due to a singularity distribution element composed of several triangular panels. There is a linear variation of the singularity density over each panel with unit strength at a source point m and zero strength on other neighboring points of the element.

The surface integrations are evaluated using explicit simple analytic expressions for the linear distributions derived by Suh (1992). The expressions are line integrals along the contour of the panel, which can be easily evaluated with global coordinates.

The slip velocity induced by the singularity distribution exist on the surface of the body. This component equivalently becomes the strength of the vortex sheet, which will be diffused in the field for the satisfaction of the no slip condition.

$$\Delta\underline{\gamma} = \underline{n} \times \underline{q}_s = \underline{n} \times (\underline{U}_\infty + \underline{u}_\omega + \nabla\phi) \tag{8.79}$$

The velocity field is finally corrected by superimposing the potential component, $\underline{u}_\phi(\underline{x}) = \nabla\phi(\underline{x})$, which can be calculated by the similar integration formula, with the solution of linear system (8.78),

$$\underline{u}_\phi(\underline{x}) = \frac{1}{4\pi} \sum_i \iint_{S_i} \left\{ \phi(\underline{\xi}) \left(\frac{\underline{n}}{r^3} - 3\frac{\underline{n} \cdot \underline{r}}{r^5}\underline{r} \right) + (\underline{n} \cdot \nabla_\xi\phi)\,\frac{\underline{r}}{r^3} \right\}\, dS_\xi \tag{8.80}$$

One advantage can be obtained that the pressure field can be computed with the similar procedure when the panel method is selected as a method to satisfy no through flow condtion. As it will be described in the subsequent section, the

integral equation for pressure Eq. (6.41) is very similar to the scalar identity, except with the one additional term that involves a volume integral of the cross product of velocity and vorticity. In system of the resulting linear equations, the right hand side only would be different, so we can directly use the inversion result of the same matrix.

8.4.4   Stretching term in 3-D

In a VIC method the grid values of velocities and vorticities can be directly used for finite differencing in the stretching when they are interpolated onto the grid. Furthermore, a VIC method can have an advantage of being conservative on the grid, if the conservative form $\nabla \cdot (\underline{\omega}\, \underline{u})$ of the stretching term is implemented.

In order to treat the stretching term, the vorticity and velocity are first multiplied on the grid, the divergence is then computed by 4th order finite difference formula and interpolated on the particle locations along with the velocity.

8.4.5   Stability issue

Although the vortex method demands more loose stability condition than classical CFL type condition due to the Lagrangina advection of the particle, there exist stability criteria constrained by the explicit diffusion solver with PSE ($\nu\,\delta t \le C\,h^{-2}$) and by the strain of the flow ($\Delta t \le C\,|\nabla u|^{-1}$). Even though these conditions are fulfilled, the current study experienced an unstable behavior of solution, when the method is applied to the simulation of flow past a rectangular wing, if the particle core size(smoothing parameter) or time step does not meet the condition for the conservation of vortex strength in wall diffusion,

$$\epsilon < \sqrt{2\,\nu\,\Delta t} = \sqrt{\frac{2\Delta t}{Re}}, \tag{8.81}$$

where $Re = \dfrac{U\,L}{\nu}$ ($U = L = 1$). The particle size should be made small as the Reynolds number of the flow increases. Figure **8.31** shows the behavior of

the maximum residual slip when the vortex sheet diffusion to the initial parti-
cle layer is iterated with the change of the particle strength. The vortex sheet
is firstly evaluated from the potential flow of the impulsive start. As shown
in the figure, the residual slip increases with the parameters $\epsilon = 0.008633$,
$\Delta t = 0.005$ when the Reynolds number is $Re = 200$. This choice of paramters
resulted eventually in unstable solution, as $0.008633 > \sqrt{2 \times 0.005 \times 0.005} =$
0.007071. The computations of flow past a rectangular wing are performed with
the appropriate selection of the parameters. However, the condition does not
necessarily need to be satisfied for the simulation of flow past a sphere.
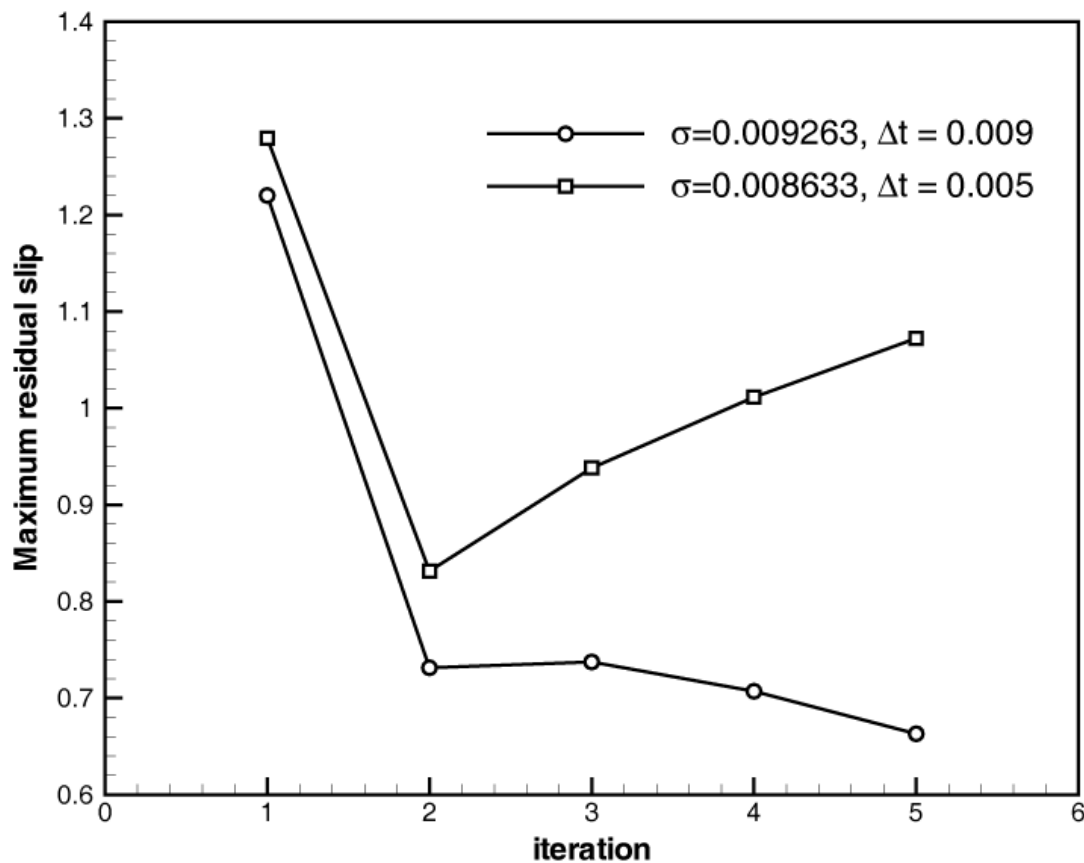
Figure **8.31** Behavior of the maximum residual slip velocity during the iteration. Here $\sigma = \epsilon$.

8.4.5.1   Stability criterion

To gauge the quality of a numerical simulation, one has to consider the *mesh*
Reynolds number. In vortex methods, it is natural to use the mesh Reynolds

number based on vorticity:

$$Re_h = \frac{|\underline{\omega}|\, h^2}{\nu}$$

A well-resolved simulation is one such that

$$Re_h = \mathcal{O}(1). \tag{8.82}$$

as this ensures that the relevant viscous scales presented in the flow are resolved. To accurately resolve the diffusion phenomena, it is required to have

$$\frac{\nu\, \Delta t}{h^2} = \mathcal{O}(1). \tag{8.83}$$

Multiplying (8.82) by (8.83), one finds that (Ploumhans & Winckelmans 2000)

$$|\underline{\omega}|\, \Delta t \; = \; \mathcal{O}(1)$$

Also, in the PSE the algorithm is stable under the condition (Cottet & Koumoutsakos 2000)

$$\frac{\nu\, \Delta t}{\epsilon^2} < \frac{1}{\lambda}$$

It was done by an analysis of the stabiblity of the PSE by Ploumhans and Winckelmans (2000). For the Gaussian smoothing function, one finds $1/\lambda = 0.595$ for the Euler explicit scheme.

8.4.6 Outline of the VIC scheme

With each building block of the VIC scheme described in the previous sections, one time step of the algorithm can be outlined as follows.

1. Create the grid used to solve the Poisson equation. It is chosen so that it tightly includes the vortex particles, and has regular Cartesian shape immersed in the body. The maximum and minimum particle position are first located and the VIC grid boundary is set up at several grid size apart from the extreme particle positions to ensure that the grid is not changed too often.

2. Interpolate the strengths of the particles onto the grid, to obtain the vorticity field $\underline{\omega} = \underline{\alpha}/V$ on the grid. The M_4' high order interpolation scheme was introduced for this purpose. The vorticity field is extended into the body, inside which the vorticity value is assigned by zero. The vorticity values replaced by zero are saved at another array for the PSE to be performed with including them.

3. Obtain the Dirichlet boundary condition for $\underline{\psi}$ on the sides of the VIC grid, using the fast algorithm by Kim (2003).

4. Solve the Poisson equation $\nabla^2 \underline{\psi} = -\underline{\omega}$ on the VIC grid using an FFT Poisson solver. The solver uses the grid with $\underline{\psi}$ provided on the boundaries and with $\underline{\omega}$ known inside. From the manipulation of the Fourier coefficients $\hat{\underline{\psi}}$ and $\hat{\omega}$, the $\underline{\psi}$ field on the grid is constructed.

5. Evaluate the rotational velocity field, $\underline{u}_\omega$, from $\underline{\psi}$, using finite differences (the fourth order scheme used here). Evaluate the potential field with the resulting residual normal component of the rotational velocity plus free stream plugged into the boundary condition for the integral equation(no through flow condition). Superimpose the potential velocity field on the rotational field. Finally, the grid values are interpolated on to the particle locations.

6. Evaluate the stretching term, $\nabla \cdot (\underline{q}\ \underline{\omega})$, using finite differences on the grid. The conservative form leads to better results than the other form like $(\nabla \underline{q}) \cdot \underline{\omega}$. The stretching on the mesh is also sent back to particle positions.

7. Update the vortex strengths due to the stretching and diffusion. The particle strength exchange for diffusion includes the strengths interpolated into the grid inside the body.

$$\frac{\underline{\alpha}_i^{n+1} - \underline{\alpha}_i^n}{\Delta t} = h^3 \nabla \cdot (\underline{\omega}\, \underline{q}) + \left.\frac{d\underline{\alpha}_i}{dt}\right|_{PSE}$$

8. Convect the particle with the interpolated velocity information on it. The

time integration of the ordinary differential equation

$$\frac{D\underline{x}_i}{Dt} = \underline{U}_\infty + \nabla \times \underline{\psi} + \nabla \phi$$

is treated differently according to whether the particles are redistributed on regular location or not. In the case particle redistribution has been done prior to the time step, the second order Runge-Kutta scheme is used to convect particles.

$$\underline{x}_i^{*,n+1} = \underline{x}_i^n + \Delta t \, \underline{q}_i(\underline{x}^n, \, \underline{\alpha}^n)$$
$$\underline{x}_i^{n+1} = \underline{x}_i^n + \frac{1}{2} \Delta t \left(\underline{q}_i(\underline{x}^n, \, \underline{\alpha}^n) + \underline{q}_i(\underline{x}^{*,n+1}, \, \underline{\alpha}^{*,n+1}) \right)$$

After the first explicit Euler step, the velocity field is evaluated once more with the induced residual slip and wall diffusion due to the location change. In the case particle redistribution has not been done prior to the time step, as we have the velocity of a particle from the previous time step, the second order Adams-Bashforth scheme is used for update of particle positions.

$$\underline{x}_i^{n+1} = \underline{x}_i^n + \Delta t \left(\frac{3}{2} \underline{q}_i(\underline{x}^n, \, \underline{\alpha}^n) - \frac{1}{2} \underline{q}_i(\underline{x}^{n-1}, \, \underline{\alpha}^{n-1}) \right)$$

9. After the convection substep, a slip velocity comes to be present at the body boundary. The slip velocity $\underline{q}_s$ is translated into vortex sheet by $\Delta\gamma = \underline{n} \times \underline{q}_s$, and the vortex sheet is diffused by the wall diffusion formula to cancel the slip velocity. This algorithm is an immersed boundary method. Its schematic diagram is shown in Figure **8.32** . The normal component of the residual slip makes up the source strength in the integral equation for the potential field correction.
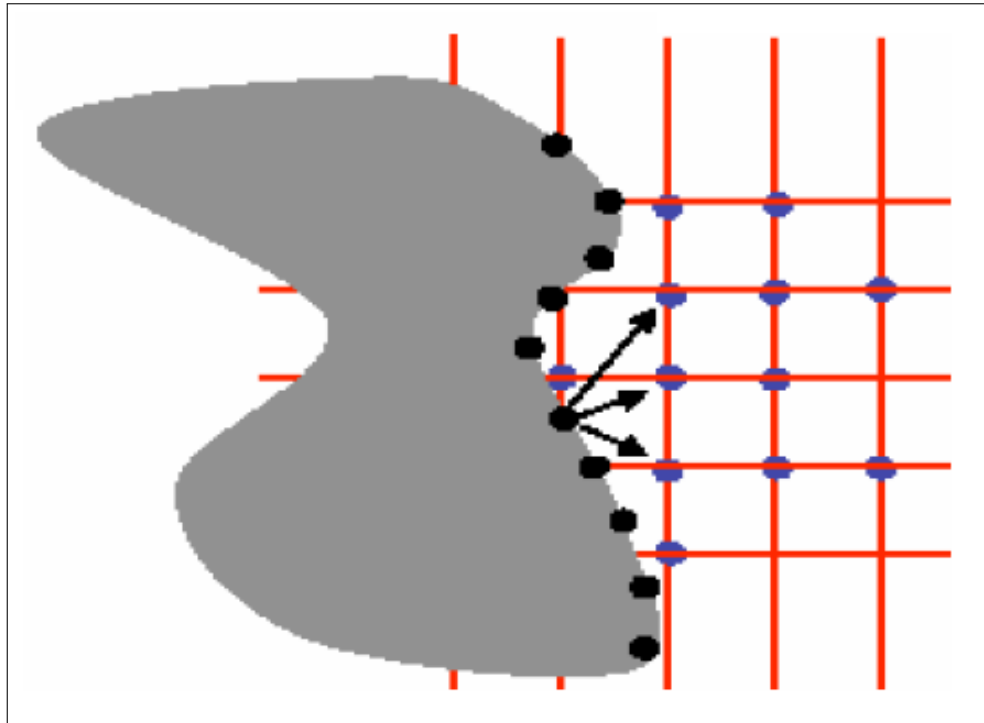
Figure **8.32** Diffusion of vorticity on a regular Cartesian grid in VIC methods. Vorticity correction is performed in the iterative way for satisfying the boundary condition at the surface. From Cottet & Poncet (2003).

8.4.7   Pressure calculation by panel method with a linearly varying singularity

The method of solving the pressure equation (6.26) with the boundary condition (6.35), when the integral equation (6.41) is formulated, is very similar to the procedure of finding potential field for the no through flow correction. The surface integral term can be discretized in the exactly same manner as the distribution of the potential on the triangular panel. The volume integral term, which is similar in form to Biot-Savart integral, must be manipulated with the Lagrangian particle representations.

$$\frac{\partial H}{\partial n} = -\frac{1}{Re}\underline{n}\cdot(\nabla\times\underline{\omega}) = -\frac{1}{Re}\left(\underline{t}\cdot\nabla\omega\right) = -\frac{1}{Re}\frac{\partial\omega}{\partial t} \tag{8.84}$$

where $\underline{t}$ is the unit tangential vector along the axis of symmetry on the body surface in axisymmetric flow. The source term can be evaluated in a general

case by using the Stokes's theorem,

$$\int_S \underline{n} \cdot (\nabla \times \underline{\omega})\, dS = \int_C \underline{\omega} \cdot d\underline{l} \tag{8.85}$$

The value of $\underline{n} \cdot (\nabla \times \underline{\omega})$ for the node point i, is obtained by the approximation of the line integral,

$$\underline{n} \cdot (\nabla \times \underline{\omega})_i \approx \frac{1}{S} \sum_j \underline{\omega}_j \cdot d\underline{l}_j \tag{8.86}$$

where $\underline{l}_j$ is the line connecting the center of the panels, which has node i as one of their vertices. $\underline{\omega}_j$ is the mean value of the vorticities at the ends of a line, and S is the area of the polygon made up by the lines. Figure **8.33** illustrates the polygon for the evaluation of the source term. The surface value of the vorticity is obtained by just switching a surface point into the particle representation of the vorticity field. The value of vorticity at the center of each panel is computed from applying the inverse distance weight to the vorticity at the vertices of the panel.
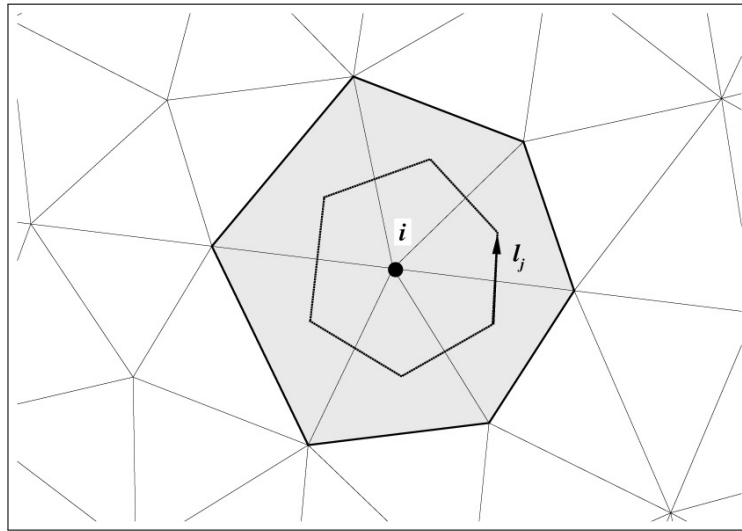
Figure 8.33 Schematic arrangement for boundary condition of the pressure head H.

By using the vector relation $\nabla \cdot (\underline{u} \times \underline{\omega})\, G = \nabla \cdot ((\underline{u} \times \underline{\omega})\, G) - (\underline{u} \times \underline{\omega}) \cdot \nabla G$, the integrand of the volume integral can be modified as

$$\int_V \nabla \cdot (\underline{u} \times \underline{\omega})\, G\, dV = \oint_S \underline{n} \cdot (\underline{u} \times \underline{\omega})\, G\, dS - \int_V (\underline{u} \times \underline{\omega}) \cdot \nabla G\, dV \tag{8.87}$$

The first integral in the right-hand side vanishes because the velocity on the body boundary is zero and the vorticity becomes zero at far field. Substituting the particle representation of the vorticity field for $\underline{\omega}$ in the above equation, we can get the discretized volume integral as follows.

$$
\int_V \nabla \cdot (\underline{u} \times \underline{\omega})\, G\, dV = -\int_V (\underline{u} \times \underline{\omega}) \cdot \nabla G\, dV
$$

$$
= -\sum_{k=1}^N \underline{u}_k \times \underline{\alpha}_k \cdot \nabla G \int_{V_k} \zeta_k\, dV \tag{8.88}
$$

$$
= -\sum_{k=1}^N (\underline{u}_k \times \underline{\alpha}_k) \cdot \frac{\underline{x} - \underline{x}_k}{|\underline{x} - \underline{x}_k|^3}\, q\left(\frac{\underline{x} - \underline{x}_k}{\epsilon_k}\right)
$$

where

$$
q(\rho) = \left\{ \mathrm{erf}\left(\frac{\rho}{\sqrt{2}}\right) - \rho\sqrt{\frac{2}{\pi}} \exp\left(-\frac{\rho^2}{2}\right) \right\} \tag{8.89}
$$

The use of cutoff function can avoid the singularity in the gradient of the Green function. The final form of the discretization reduces to the similar one in (8.78) with the volume integral having on the right hand side.

8.5   Numerical Results by VIC Methods

In this section, the present VIC method is applied to the flow simulation around several 2-D and 3-D bodies. The flow field around impulsively started two dimensional bodies are firstly simulated, for a circular cylinder and a NACA0012 hydrofoil section. For 3-D, the flow around a sphere is simulated as a typical example of wake flow behind a bluff body. The VIC algorithm then is also applied to the rectangular wing of finite span.

8.5.1 Two dimensional flows

In the case of two dimensional flow the vorticity is a scalar variable and the governing equation for it does not carry the stretching term,

$$\frac{D\omega}{Dt} = \nu \nabla^2 \omega \tag{8.90}$$

The diffusion is the only process to change strengthes of particles. Moreover, the vector potential becomes scalar field known as stream function. The Poisson equations for the vector potential and the vorticity reduce to one component,

$$\nabla^2 \psi = -\omega \tag{8.91}$$

The velocity components (u, v) are given by,

$$u = \frac{\partial \psi}{\partial y}, \quad -v = \frac{\partial \psi}{\partial x} \tag{8.92}$$

The stream function can be obtained on the boundaries using two dimensional Green's function

$$\psi = -\frac{1}{2\pi} \int \omega \ln r \, dS \tag{8.93}$$

8.5.1.1 Impulsively started circular cylinder

In this section the result of computation is provided for the flow over a circular cylinder impulsively set into motion with a constant speed U_∞ in the direction negative x coordinate. For this problem, a large number of experimental and numerical results has been available in the literature. The Reynolds number is defined as $Re = DU_\infty/\nu$, where D is the diameter of the cylinder and ν is the kinematic viscosity. The computational results are presented for a Reynolds number 550.

The computational parameters are given in the Table **8.3**. The cylinder surface is discretized by 600 line panels with even length. The particle size is balanced with the panel size and, at the same time, is chosen to meet the stability restriction.

Table 8.3 Parameters used in the numerical simulation of the flow around an impulsively started circular cylinder.

Reynolds number	550
Number of panels	600
Blob size, σ	0.00521
Time step, Δt	0.01
Cutoff parameter, ϵ_Γ	0.001

Figure **8.34** shows a comparison between the analytical expression of impulse I_x for short times by Bar-Lev and Yang (1975) and I_x computed by the present scheme. The comparison includes the result computed by Ploumhans and Winckelmans (2000). The present scheme gives slightly different values for the very earlier time ($t < 0.10$).

The time history of the drag coefficent is compared in Figure **8.35** for short times and **8.36** for longer times. For the early developed flows, the present scheme predicts the drag coefficients close to the analytical results. The comparison for longer times with Ploumhans and Winckelmans (2000) in Figure **8.36** does not show distinguishable results, while the impulse shows slightly different longer time behavior as presented in Figure **8.34** . This means that the absolute values of the impulses are slightly different between the two method, but the changes of the impulse are revealed to have similar time rates. The difference seems to be caused by the parameters chosen by each scheme.

The profiles of streamwise centerline velocity in the wake is shown in Figure **8.37** with the experimental results by Bouard & Coutanceau (1980). Their results are provided with the time nondimensinalized by the radius of cylinder, whereas the present scheme uses the diameter as the characteristic length. The time in the figure represents nondimensional time by the diameter of the cylinder. There is good qualitative agreement, but the length of the wake(distance to the point the velocity profile crosses the x axis) is computed somewhat shorter than the experiment. Due to the use of compact grid for velocity computation, the profiles of the present scheme are not presented beyond the extent of the grid.
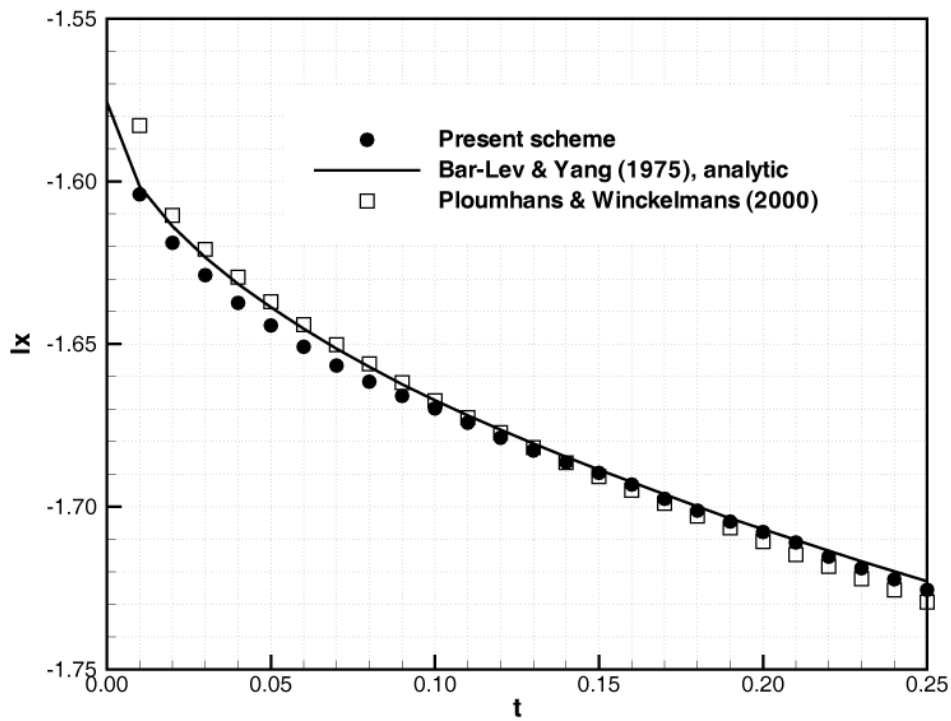
(a) Short time
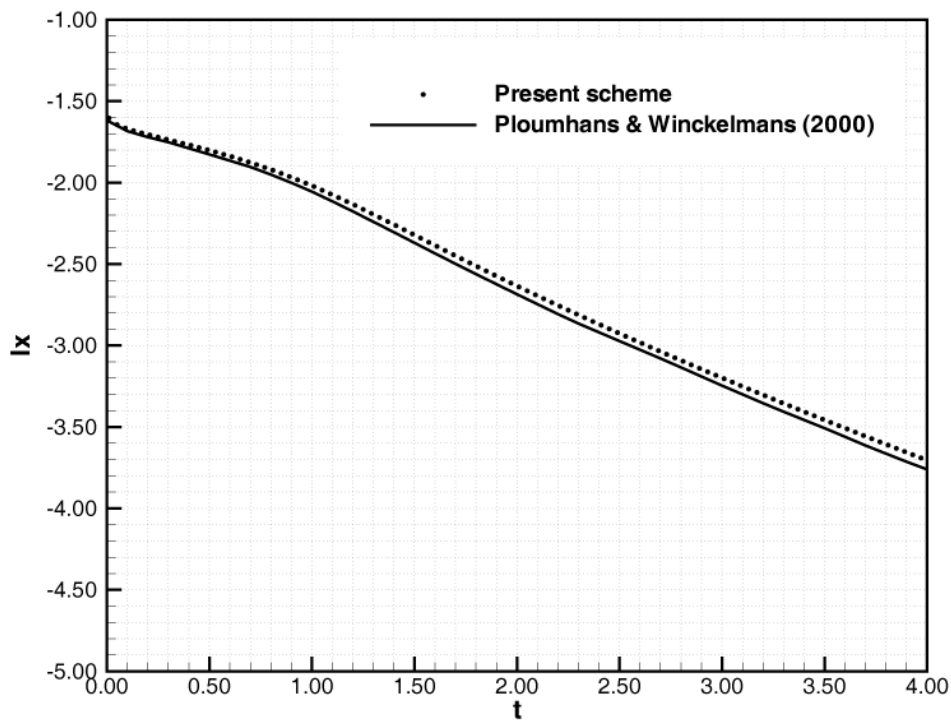
(b) Long time

Figure **8.34** Comparison of I_x for an impulsively started circular cylinder at $Re = 550$.
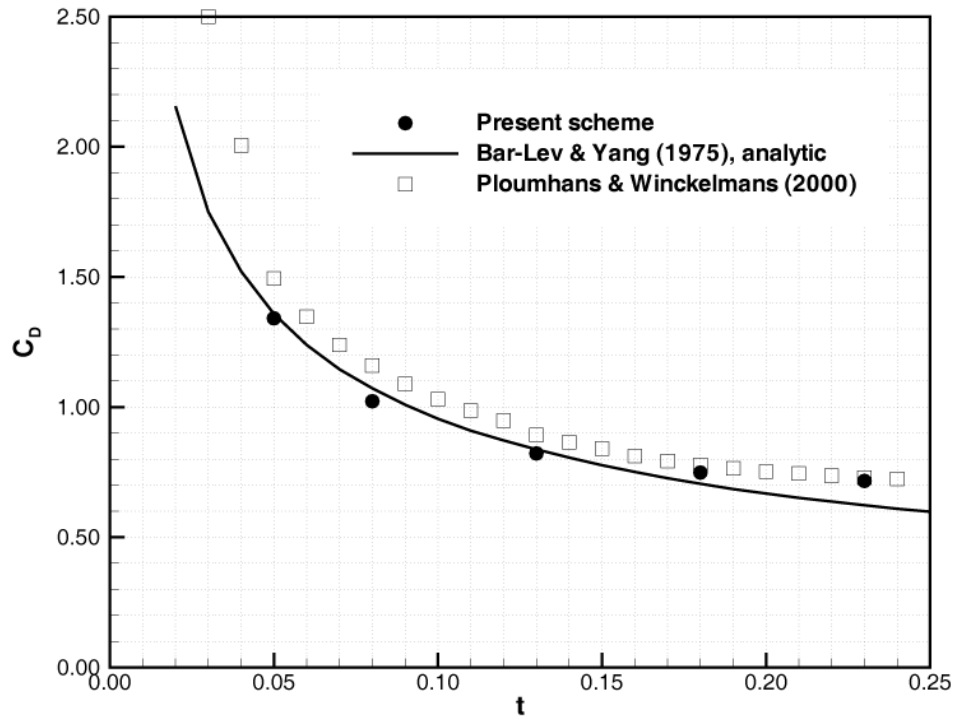
Figure **8.35** Drag coefficient of an impulsively started circular cylinder at early stage of times for $Re = 550$.
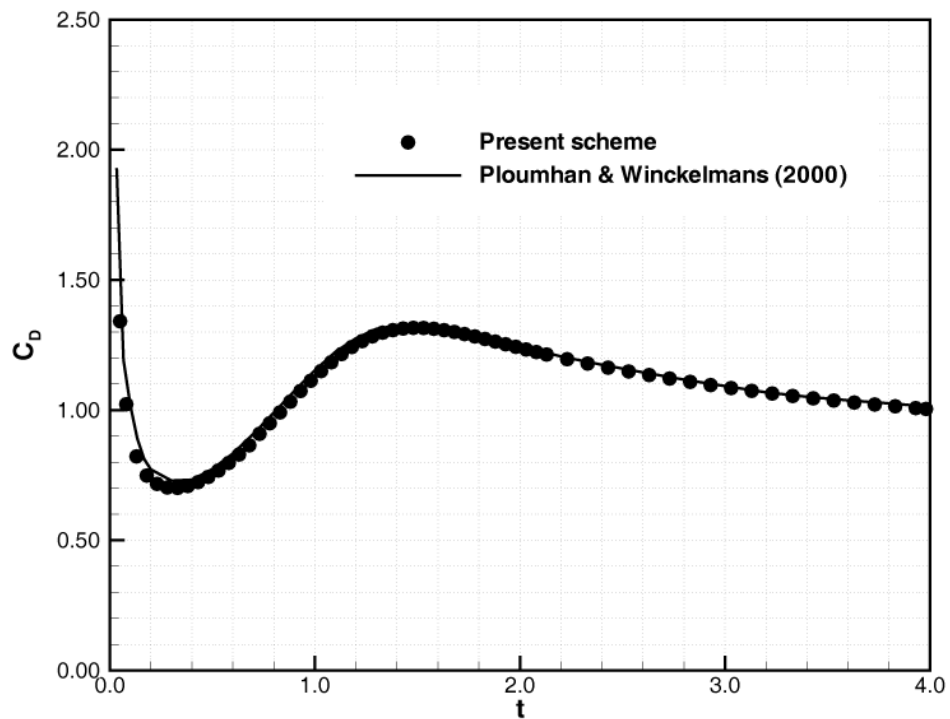
Figure **8.36** Drag coefficient of an impulsively started circular cylinder for $Re = 550$.
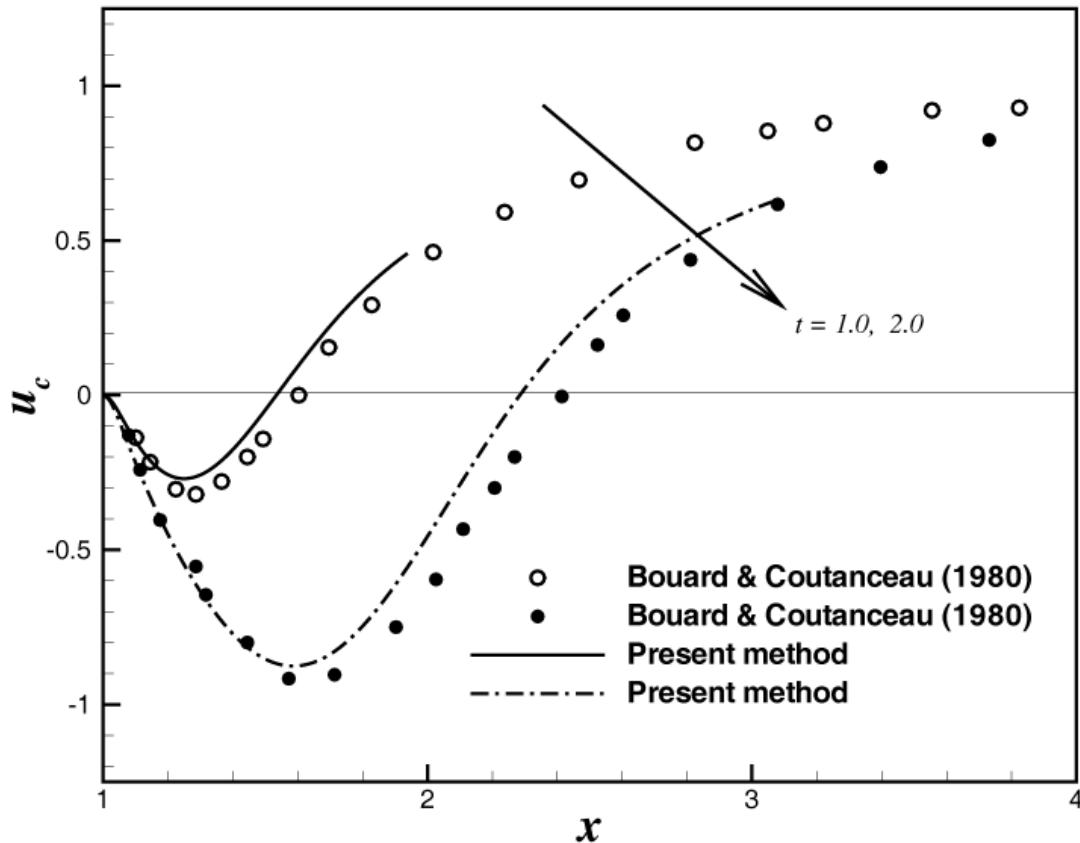
Figure **8.37** Velocity distribution along wake centerline for an impulsively started circular cylinder for $Re = 550$.

Computed streamlines are shown in Figure **8.38** . Note that the cylinder moves to the left. A large recirculating flow region of closed streamlines is clearly captured behind the cylinder. The streamwise length of this recirculating region grows in time. The region is also called as the separation bubble.

The streamline at $t = 3.0$ is compared with the results obtained in the experiment of Bouard and Coutanceau (1980) in Figure **8.39** . The computed streamline in the large recirculating flow region are in good visual agreement with those of the experiment. Along with the large recirculating regions, smaller secondary recirculation zones between rear half of the cylinder and the separation bubbles are observed in the computation, as well as in the experiment.
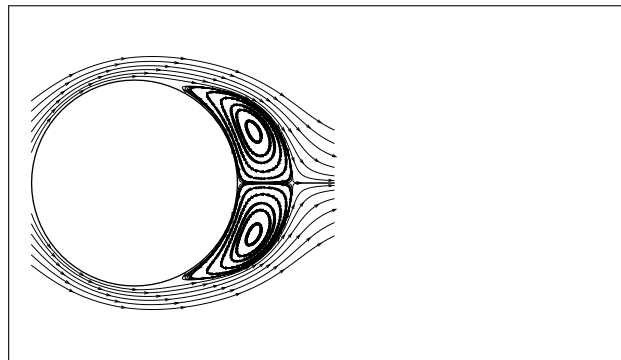
(a) $t = 1.0$
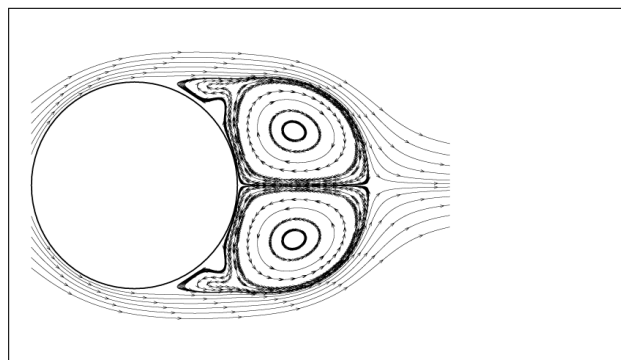
(b) $t = 2.0$
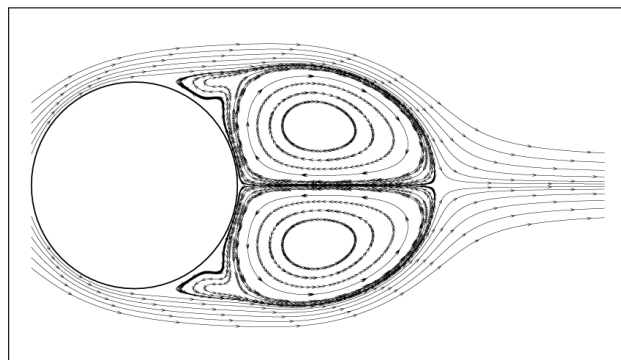
(c) $t = 3.0$
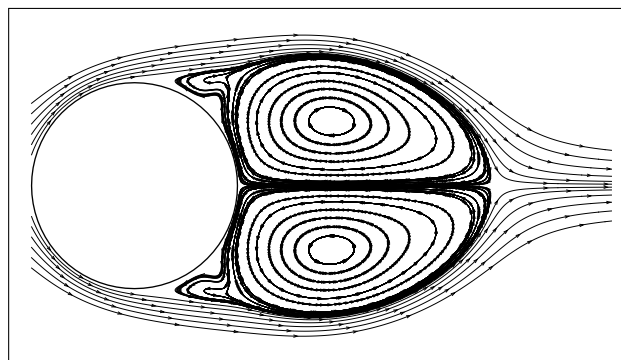
(d) $t = 4.0$

Figure **8.38** Instantaneous streamlines around impulsively started circular cylinder at $Re = 550$.
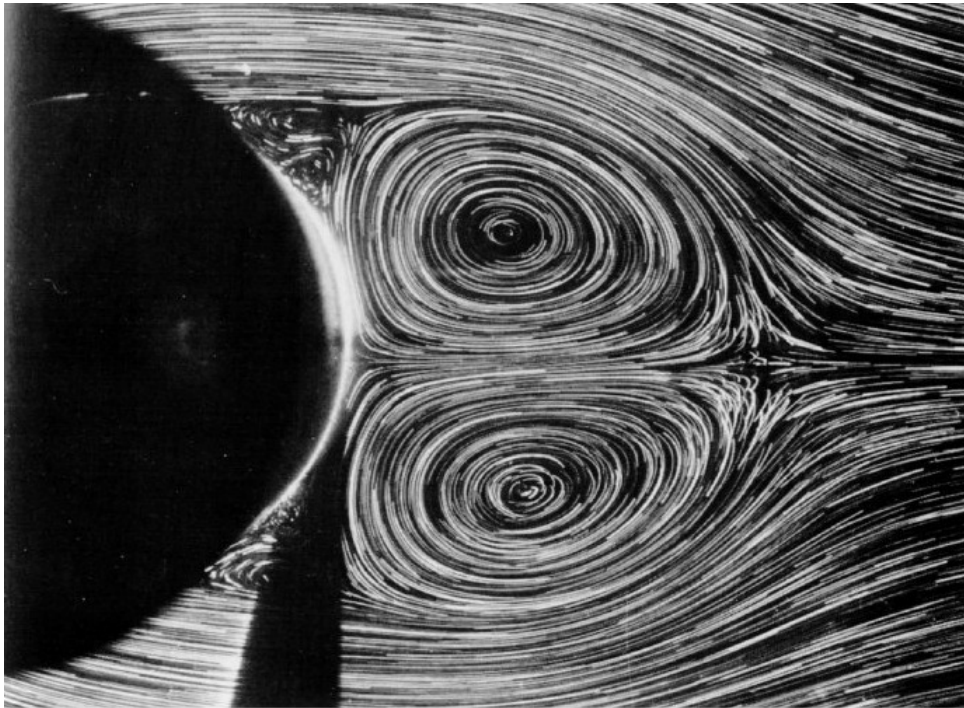
(a) Streamlines from experiment, Bouard & Coutanceau
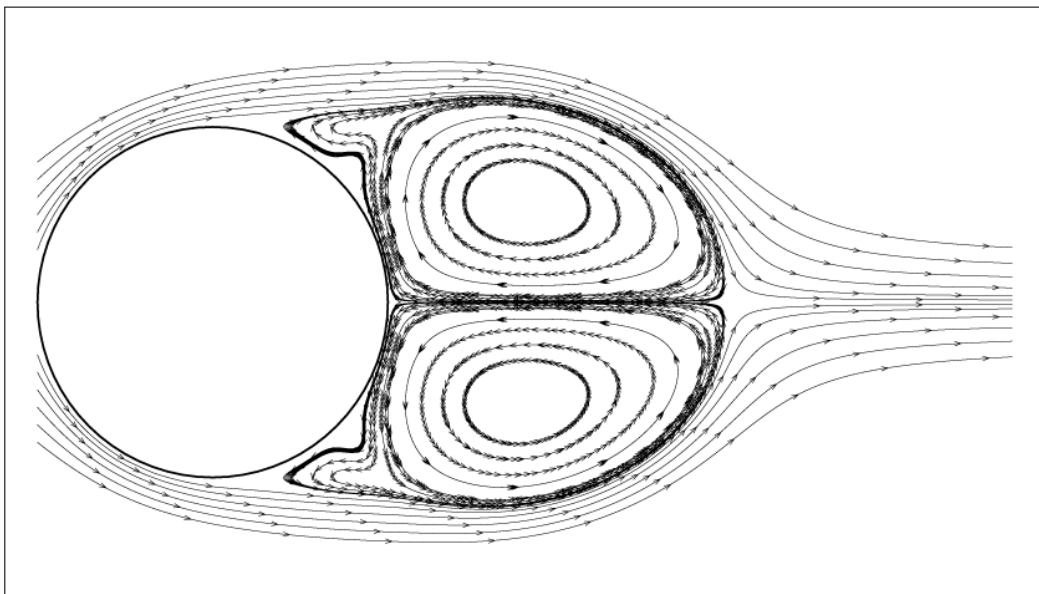
(b) Streamlines from the present method

Figure **8.39** Comparison of streamlines for an impulsively started circular cylinder for $Re = 550$.

8.5.1.2   Impulsively started NACA0012 hydrofoil

As a second representative for simulation in two dimension, an impulsively started NACA0012 section hydrofoil is selected in order to examine suitability of the method for the analysis of thin streamlined body with sharp edge. The Reynolds number is 1200, based on the chord length of the section. The parameters used in the simulation are listed in Table **8.4**. The computations are performed at two angles of attack, $\alpha = 0°$ and $30°$.

Table 8.4 Parameters used in the numerical simulation of the flow around an impulsively started NACA 0012 hydrofoil.

Reynolds number	1200
Number of panels	800
Blob size, σ	0.00249
Time step, Δt	0.005
Cutoff parameter, ϵ_Γ	0.001

Figure **8.40** compares impulse I_x with the result of Lee (2005) for zero angle of attack. In his vortex method, a fast algrithm is used for the convection velocity and image particles are located underneath body panels to correct PSE diffusion. As shown in the figure, the impulses are in good agreement for long times as well as for short times.

The method is applied next to the flow at angle of attack $\alpha = 30°$. After the impulsive start, the starting vortex is formed from the trailing edge and shed into the wake as shown in Figure **8.41** . At the same time, the flow is separated from the leading edge and a vortex is generated. The leading edge vortex rolls downstream along the suction side and convects slowly near the surface. Two secondary vortices can be seen to have been formed upstream of the separated vortex. The computed streamlines are compared with the experimental results by Huang et al. (2001). Figures **8.42** and **8.43** show the observation results using the particle tracking flow visualization along with the streamlines from the present scheme. The large separation vortex from leading edge and the two secondary vortices are clearly seen in the figures.
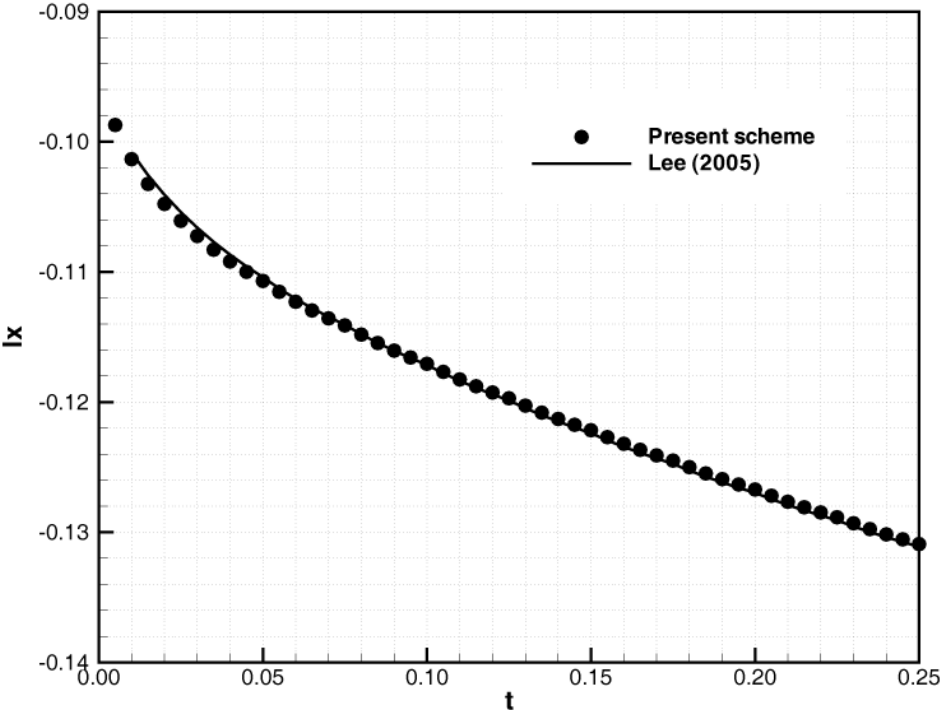
(a) Short time
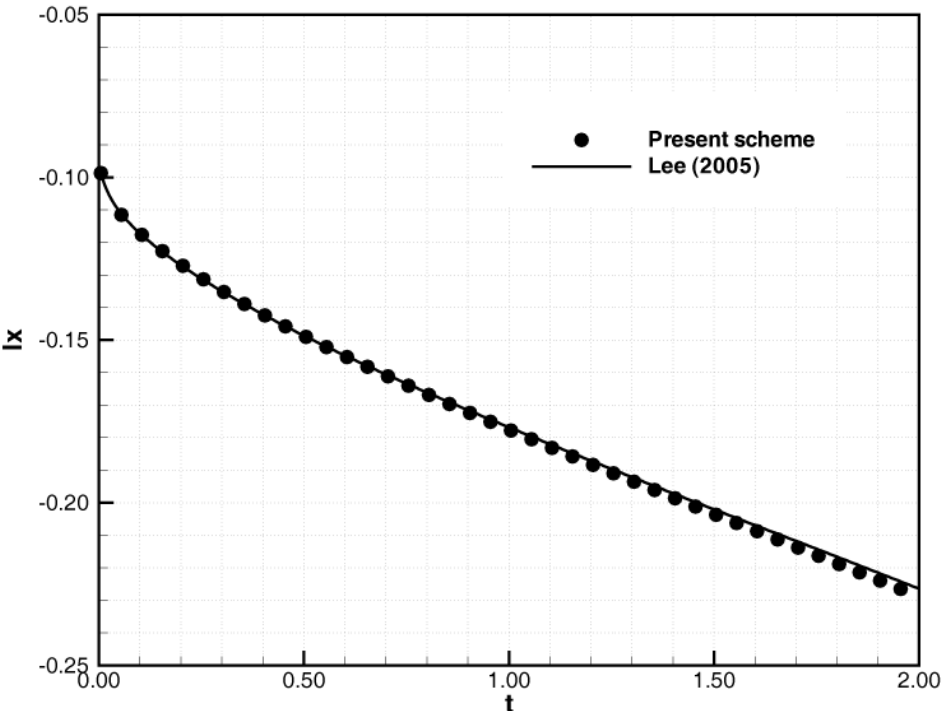
(b) Long time

Figure **8.40** Comparison of I_x for an impulsively started NACA0012 hydrofoil at zero angle of attack for $Re = 1200$.
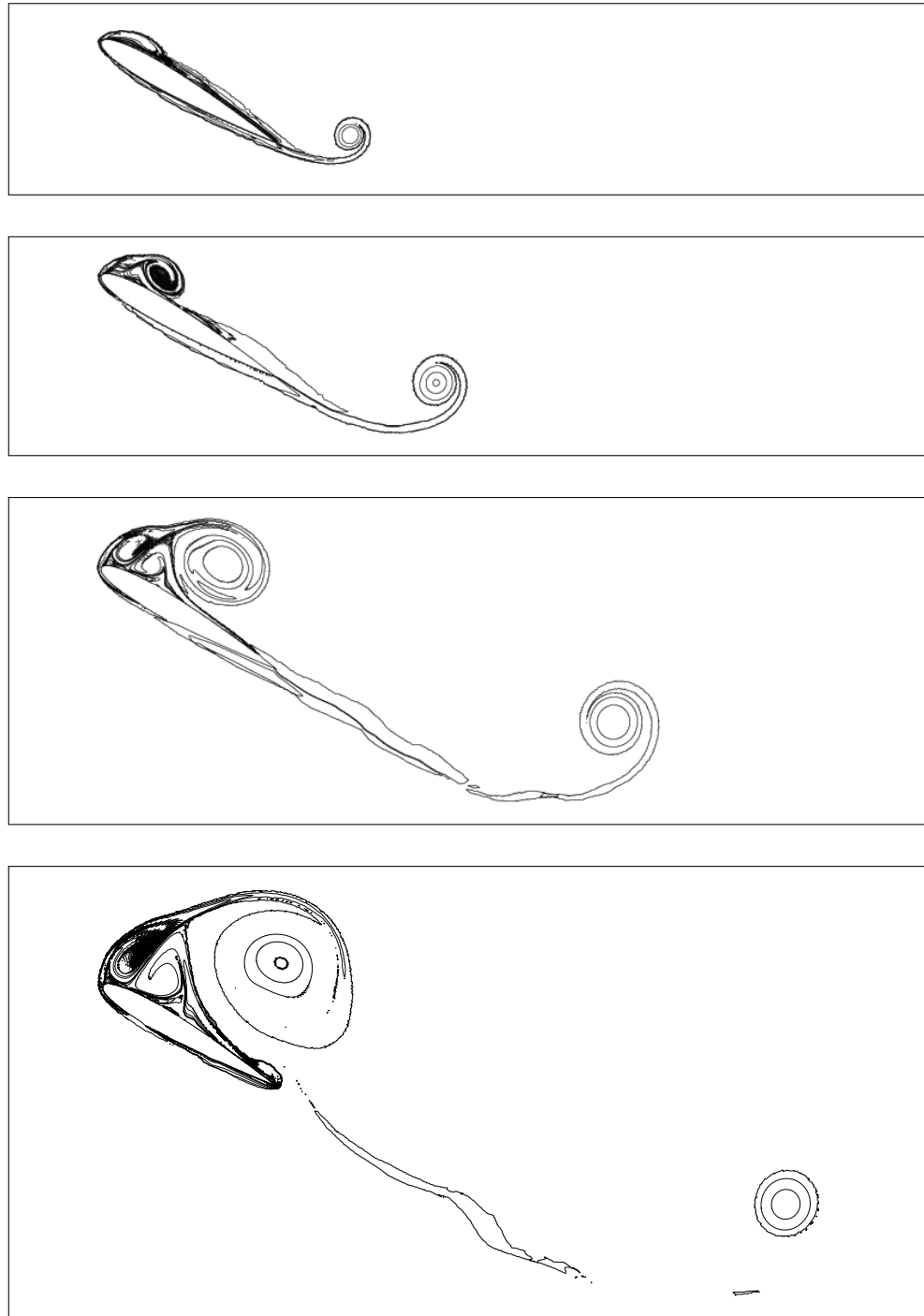
Figure **8.41** Vorticity contours for an impulsively started NACA0012 hydrofoil for $\alpha = 30°$ and $Re = 1200$. The time is at $T = 0.5, 1.0, 2.0, 3.0$ from top.

(a) Streamlines from experiment, Huang et al (2001), $t = 1.043$
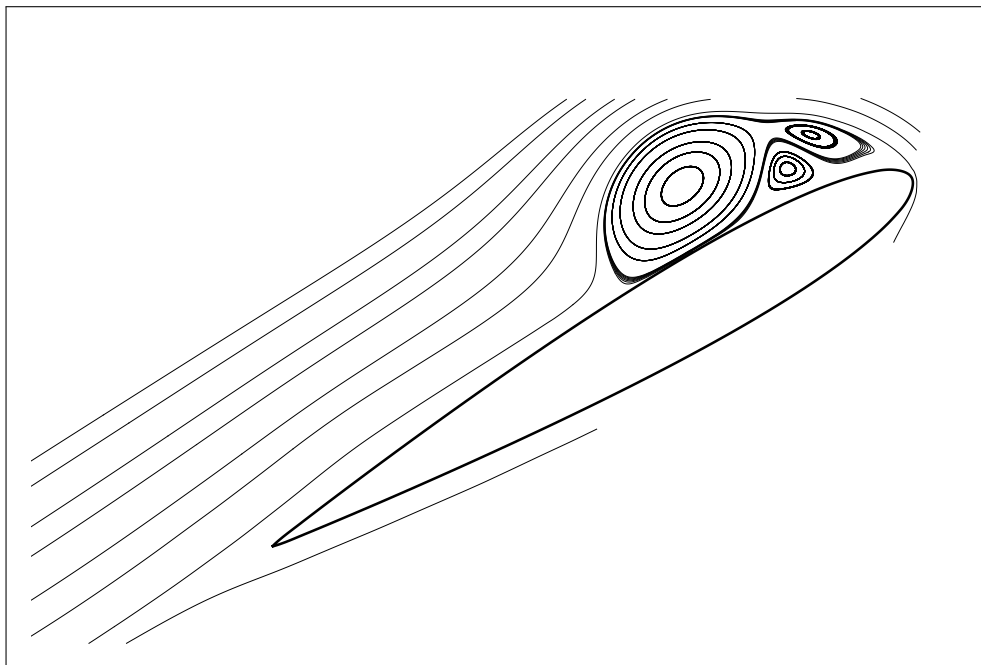
(b) Streamlines from the present method, $t = 1.0$

Figure **8.42** Comparison of streamlines at $T = 1.0$ with the experimental snapshot for an impulsively started NACA 0012 hydrofoil at $\alpha = 30°$ for $Re = 1200$.

(a) Streamlines from experiment, Huang et al (2001), $t = 2.348$
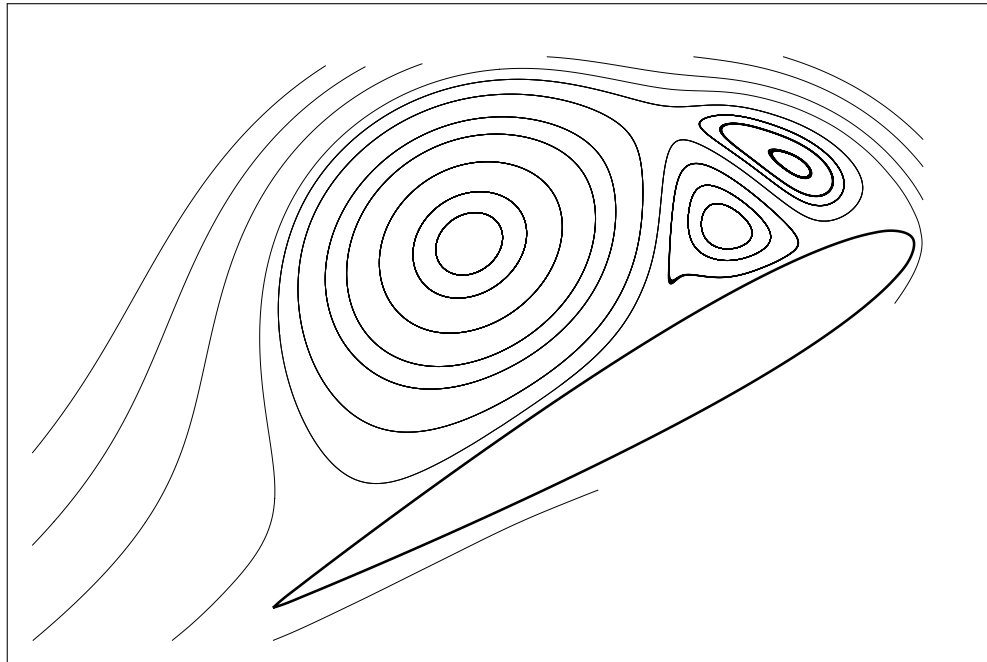
(b) Streamlines from the present method, $t = 2.0$

Figure **8.43** Comparison of streamlines at $T = 2.0$ with the experimental snapshot for an impulsively started NACA 0012 hydrofoil at $\alpha = 30°$ for $Re = 1200$.

8.5.2   Three dimensional flows

8.5.2.1   Sphere

The flow past a sphere is considered as an example for three dimensional bluff body flow analysis. It has been investigated numerically and experimentally at Reynolds number $Re = U_\infty D/\nu$ between about 0.5 and several thousand by many authors. From the experimental work of Taneda (1956), it is found that a recirculating zone develops close to the rear stagnation point at about $Re = 30$. This recirculating zone or wake expands toward streamwise direction as well as along the surface of the sphere with further increase in the Reynolds number. The flow remains steady and axisymmetric up to $Re = 210 \sim 212$. Defining locations on the surface by the angle from the front stagnation point, the separation point moves forward from about $130°$ at $Re = 100$ to about $115°$ at $Re = 300$.

In this work, the flows at $Re = 50, 100$ are simulated and compared with the numerical solution of Johnson & Patel (1999). The sphere of radius 0.5 is discretized into triangular panels, and the number of panels is 10,008. Figure 8.44 shows the discretization of the sphere.
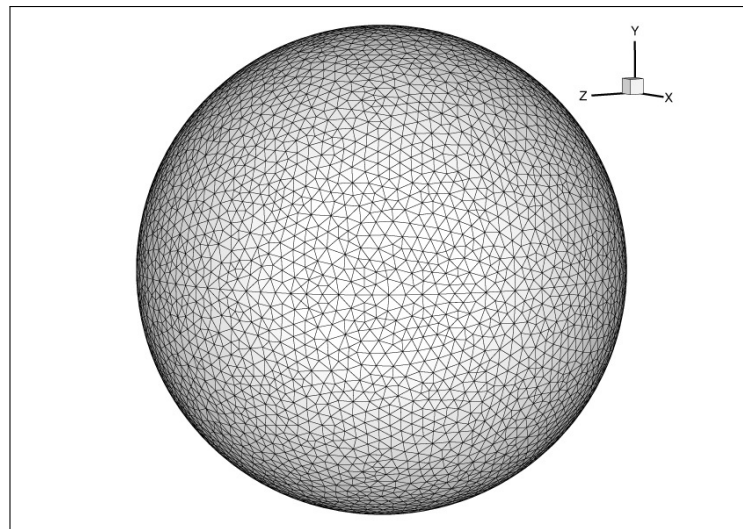
Figure 8.44 Surface panel discretization of a sphere.

The number of vertices is about half of the panels. The grid size h is selected to be square root of mean area of the panels $h = \sqrt{A_{mean}}$, where $A_{mean} =$

$\sum A_i/N$. The time step for the simulation is $\Delta t = 0.02, 0.015$ for the Reynolds number of 50, 100, respectively. The value of $\epsilon_\alpha = 10^{-4}$ and $Re_{h,trsh} = 10^{-4}$ are used.

The drag coefficients from the derivative of the linear impulse are plotted in Figure **8.45** along with the classical curve of $C_d = C_d(Re)$ for the flow past a sphere. The drag coefficient C_d is calculated at the final stage of the computation when the change of the linear impulse is thought to come into a steady phase and shows good agreement with the curve. The drag coefficients are made further comparison with the computation by Johnson & Patel (1999) in Figure **8.46** , and also show good agreement with their results.
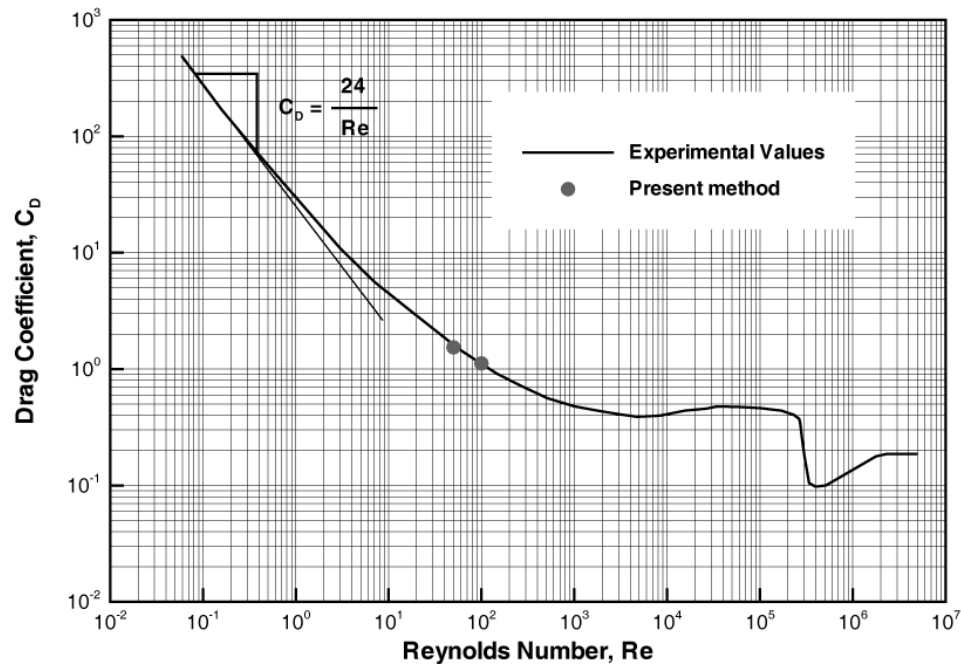
Figure 8.45 Comparison of drag coefficient of a sphere with experiments.

The streamline patterns, vorticity contours and pressure fields at several early moments for $Re = 100$ are provided in Figures **8.47** , **8.48** , and **8.49** , respectively.

The streamlines, vorticity contours and contours of pressure coefficients are also compared with the numerical results of Johnson & Patel (1999), in Figures **8.50** $\sim$ **8.53** . The length of the separation bubble in the flow direction(left to right) seems to be in good agreement.
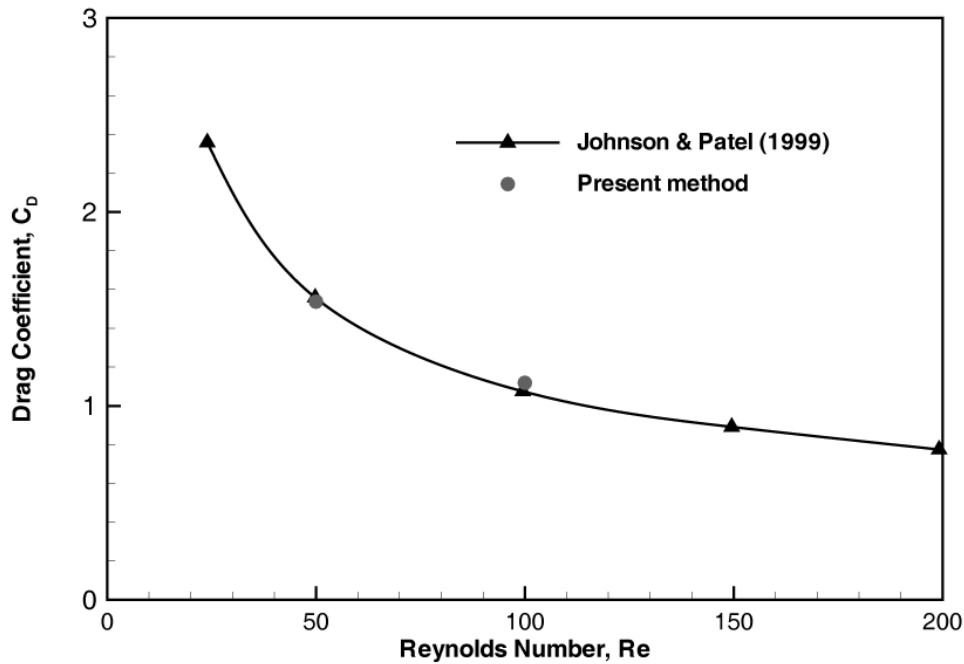
Figure 8.46 Comparison of drag coefficient of a sphere with the numerical one by Johnson & Patel (1999).

Figure **8.51** compares the length and position of the vortex center, and shows good agreement with the results of Johnson & Patel. The downstream extensions of vorticity contour of $\pm\,0.5$ from the present method show slightly shorter than the results by Johnson & Patel. Figure **8.54** compares the streamline of the present scheme with the visualization by Taneda (1956). As the Reynolds number of the expmeriment is 118, which is larger than the present computation, the recirculating zone expands more downstream. But, the general appearance of the flow including separation point looks very similar to the computed result.
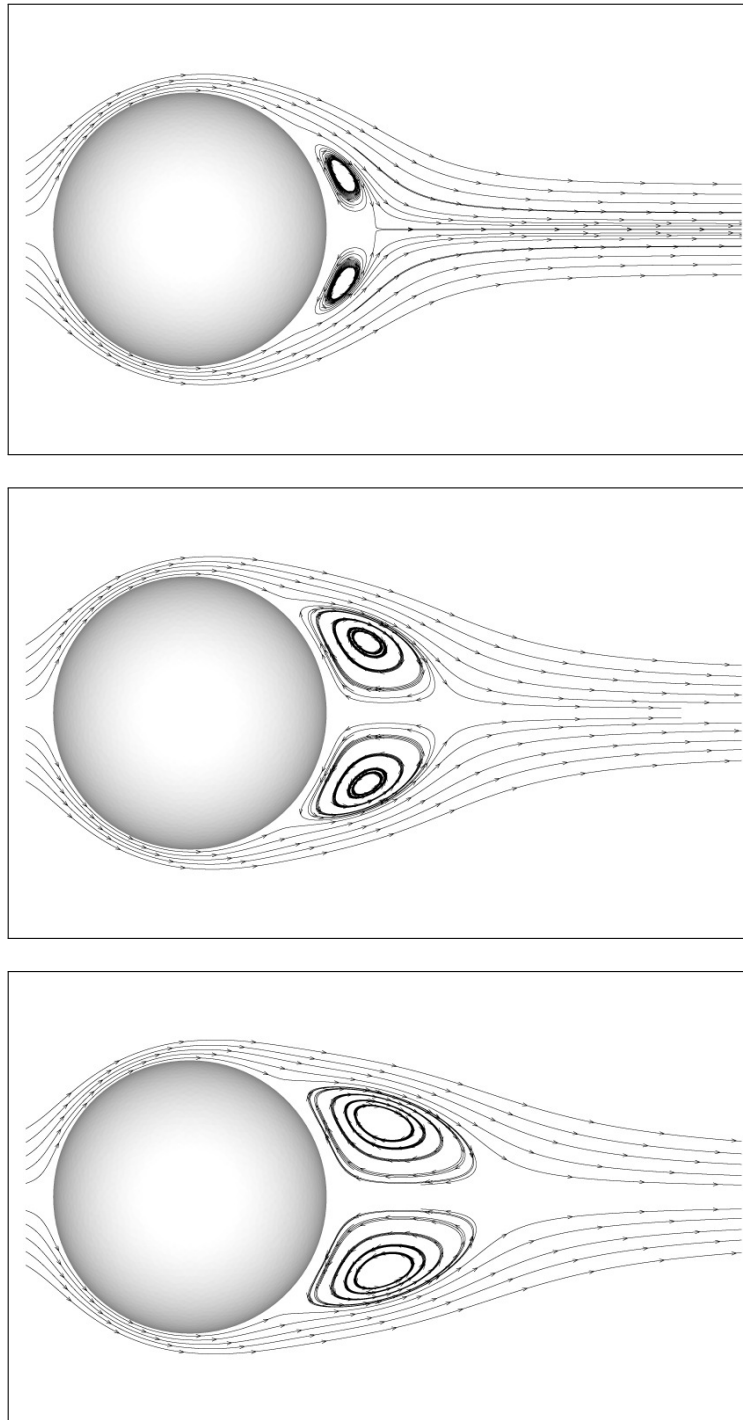
Figure **8.47** Streamlines about an impulsively started sphere for $Re = 100$. The time is at $T = 1.0, 2.0, 3.0$ from top.
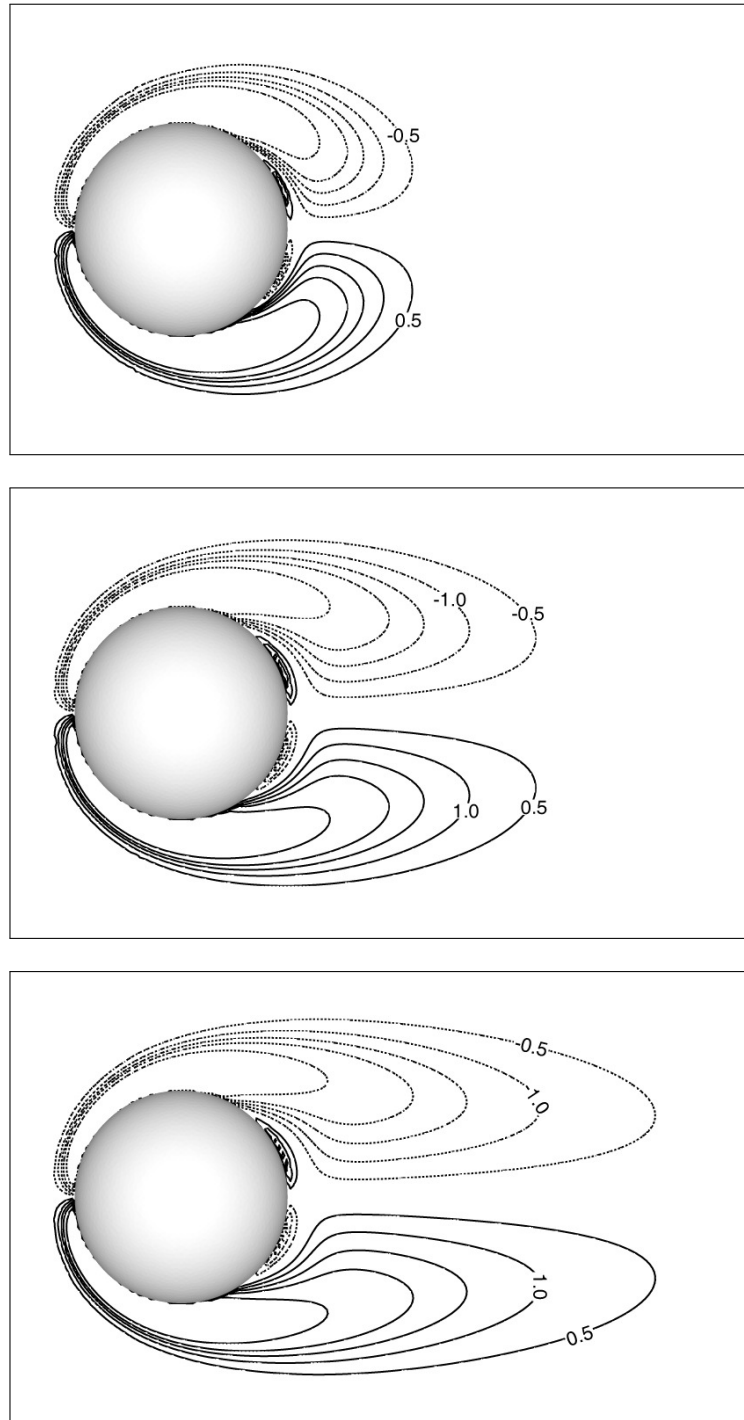
Figure **8.48** Vorticity contours for an impulsively started sphere for $Re = 100$. The time is at $T = 1.0, 2.0, 3.0$ from top.
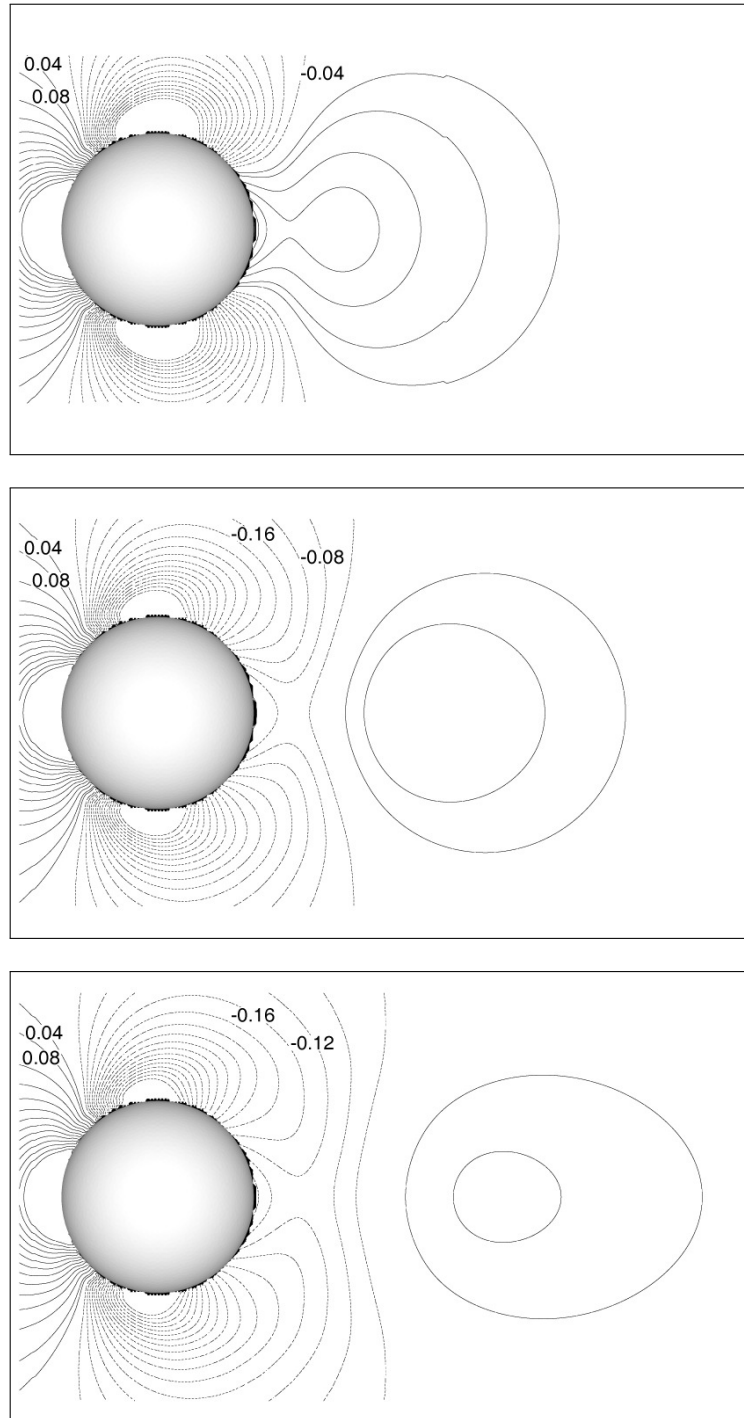
Figure **8.49** Pressure coefficient contours for an impulsively started sphere for $Re = 100$. The time is at $T = 1.0, 2.0, 3.0$ from top.
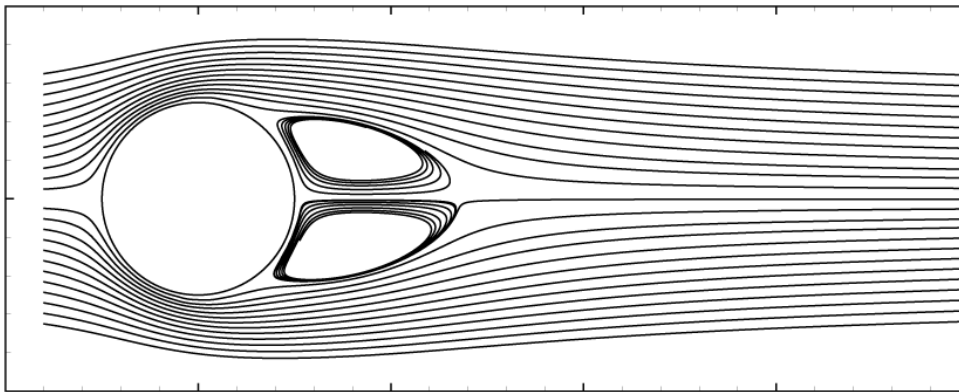
(a) Streamlines from the present method ($t = 7.5$)
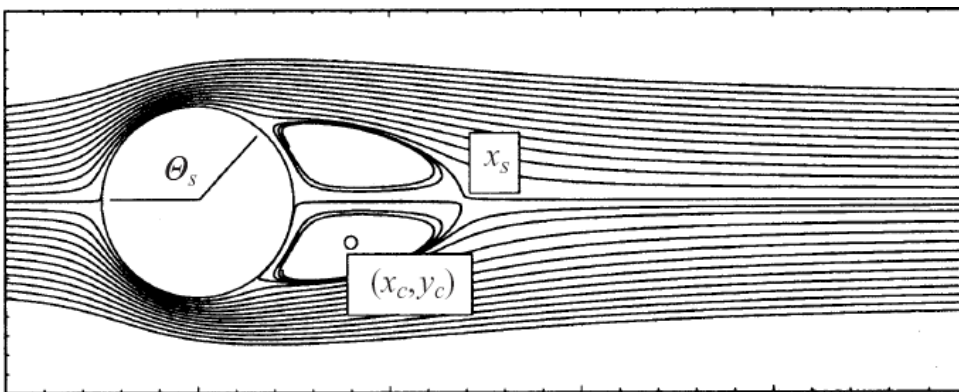
(b) Streamlines computed by Johnson & Patel (1999)

Figure **8.50** Comparison of streamlines about a sphere for $Re = 100$ with the numerical ones by Johnson & Patel (1999).
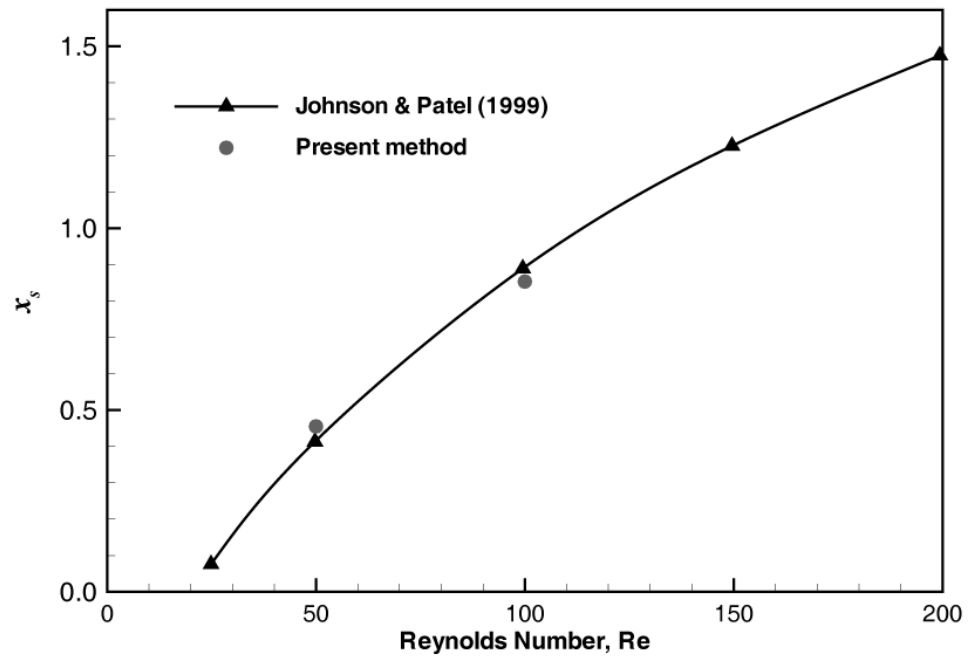
(a) Separation length, x_s
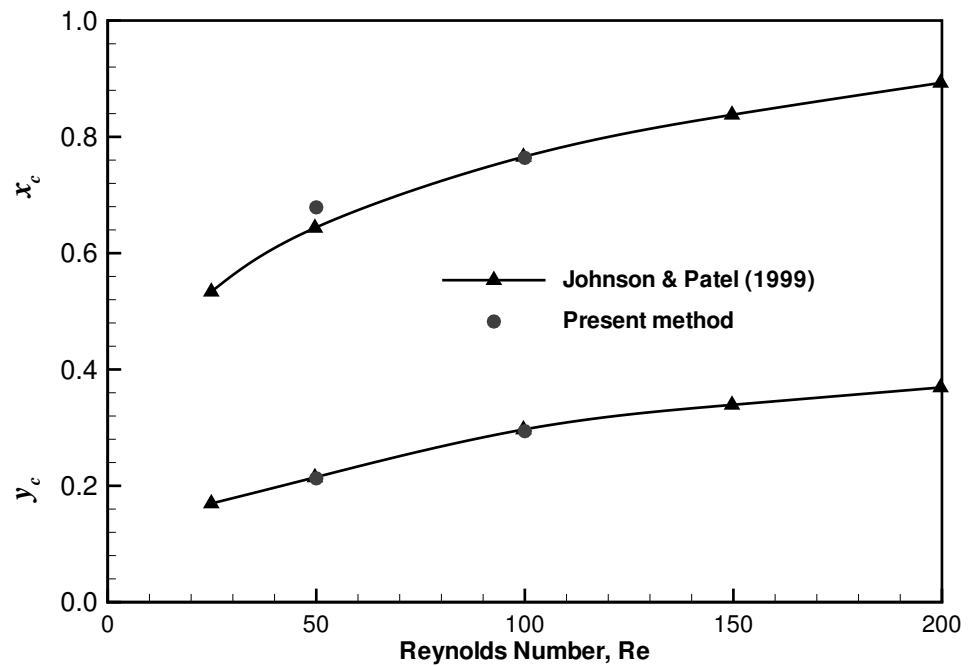
(b) Vortex position, (x_c, y_c)

Figure **8.51** Comparison of wake pattern for a sphere with the numerical one by Johnson & Patel (1999). x_s denotes the distance from the sphere of the end point of the wake. x_c and y_c are the center position of the vortical shedding wake.
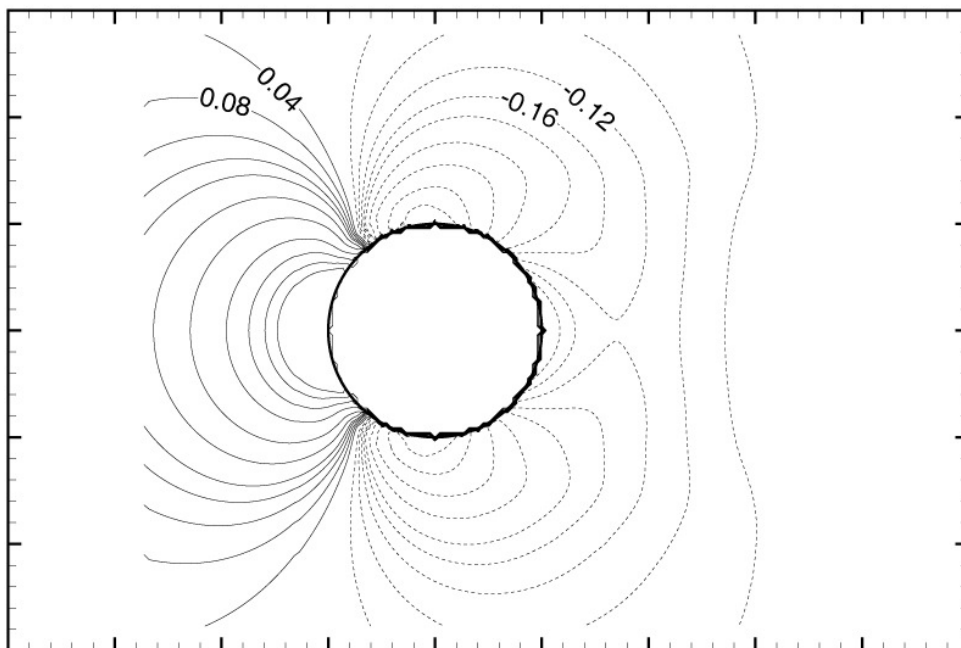
(a) C_p from the present method ($t = 7.5$)
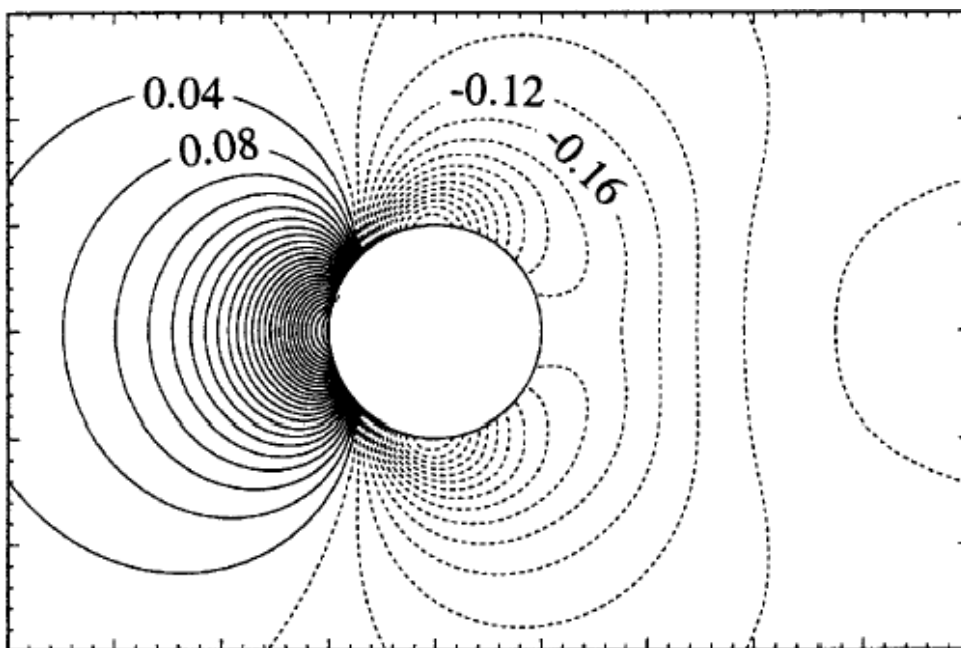
(b) C_p computed by Johnson & Patel (1999)

Figure **8.52** Comparison of pressure contours for a sphere for $Re = 100$ with the numerical one by Johnson & Patel (1999).
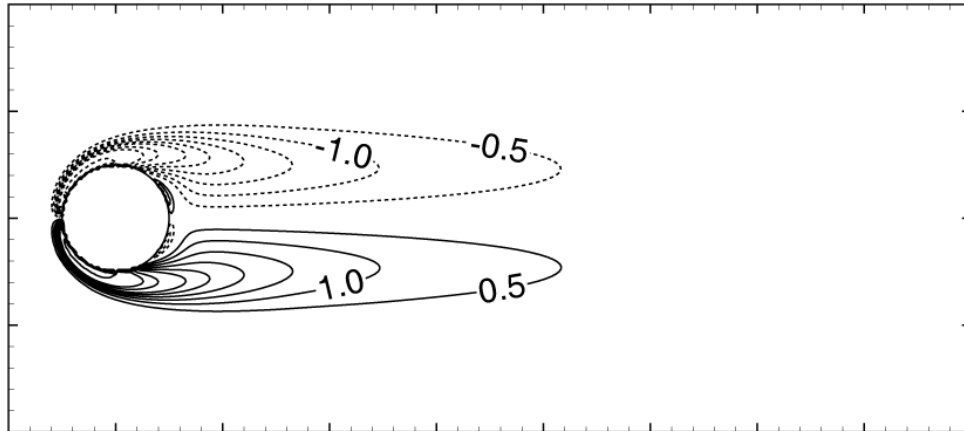
(a) Contours from the present method ($t = 7.5$)
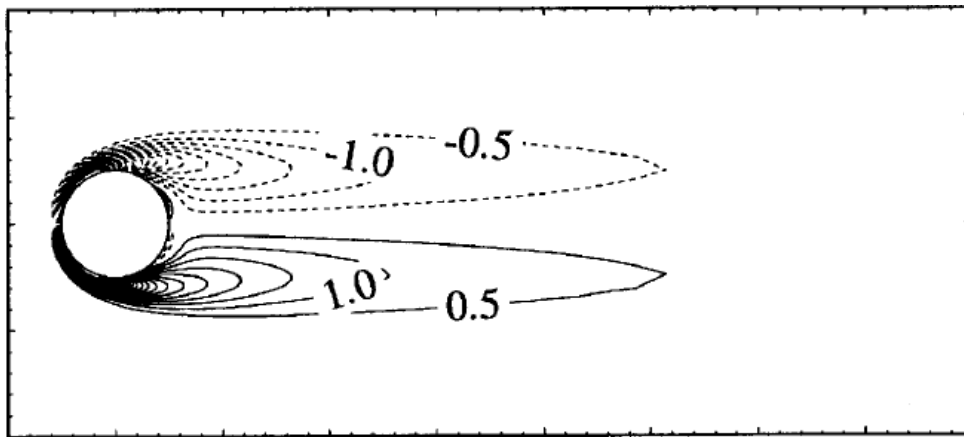
(b) Contours computed by Johnson & Patel (1999)

Figure **8.53** Comparison of vorticity contours for a sphere for $Re = 100$ with the numerical one by Johnson & Patel (1999).
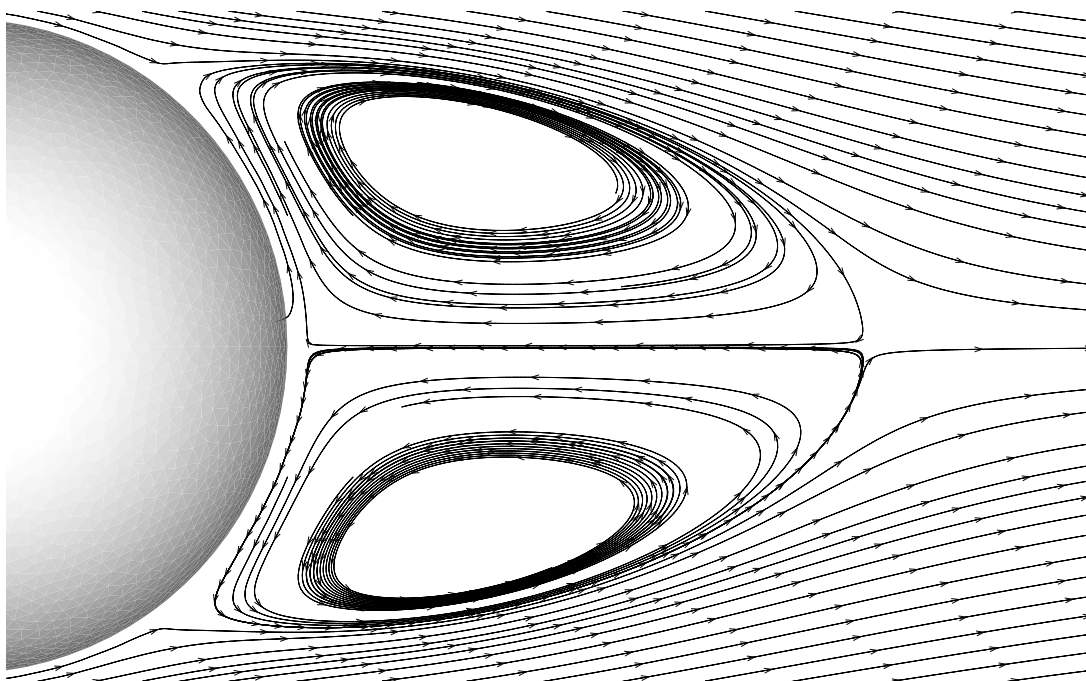
(a) Streamlines from the present method

(b) Visualization from experiment ($Re = 118$), Taneda

Figure 8.54 Comparison of streamlines for a sphere for $Re = 100$ with the experimental ones by Taneda (1956).

Figures **8.55** $\sim$ **8.57** show the streamlines, vorticity contours, and contours of the pressure coefficient at $Re = 50$ and 100. For the two Reynolds

numbers the general characteristic feature of the flow remains the same with the changes only in separation location, the center of recirculating flow, and the length of wake. The separation point moves upstream with the increase of Reynolds number. At Reynolds number of 100, the opposite sign of vorticity exists between the surface of the sphere and the separation vortex.
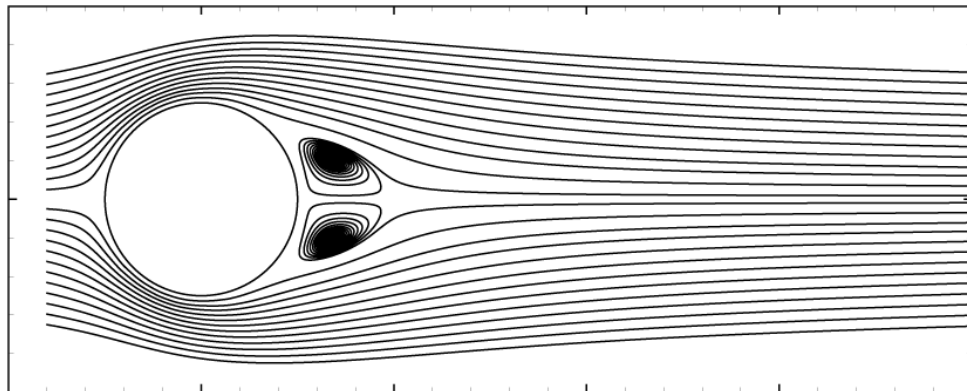
(a) $Re = 50$
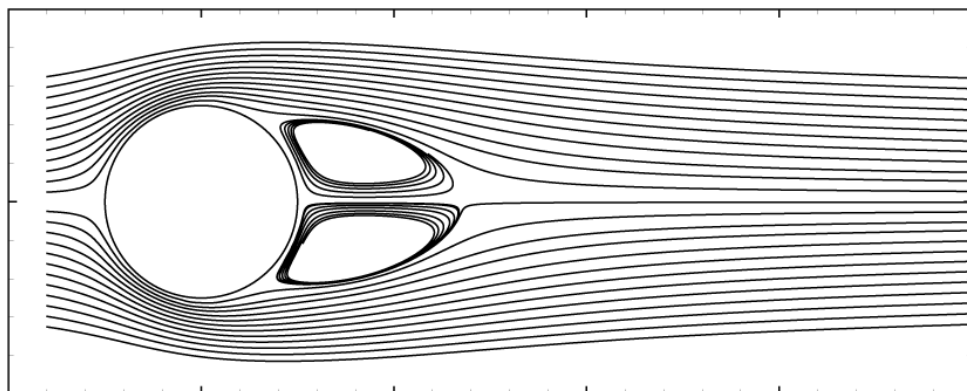
(b) $Re = 100$

Figure **8.55** Comparison of streamlines between two Reynolds numbers.
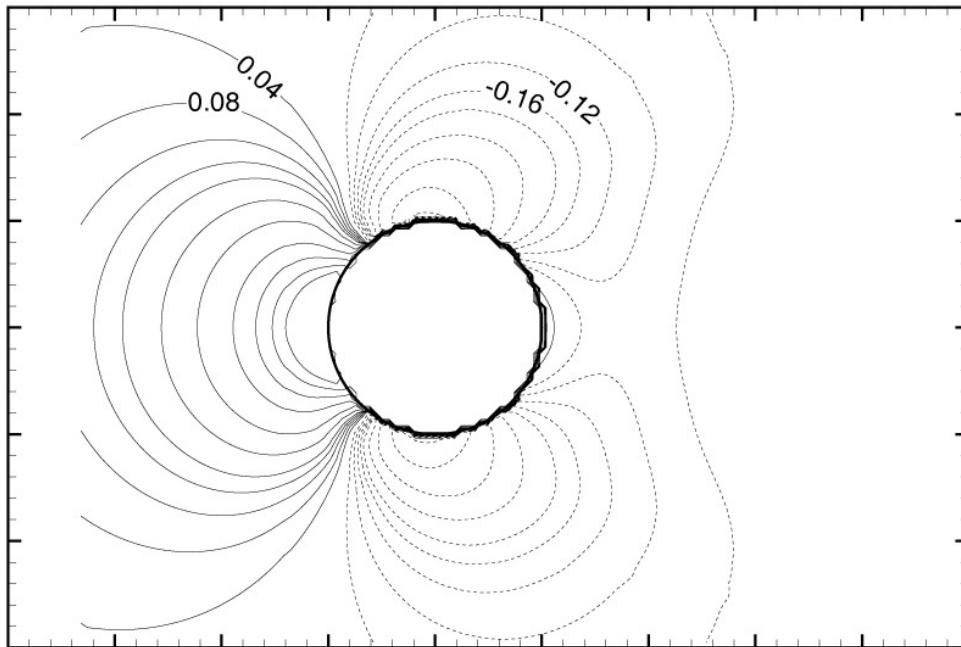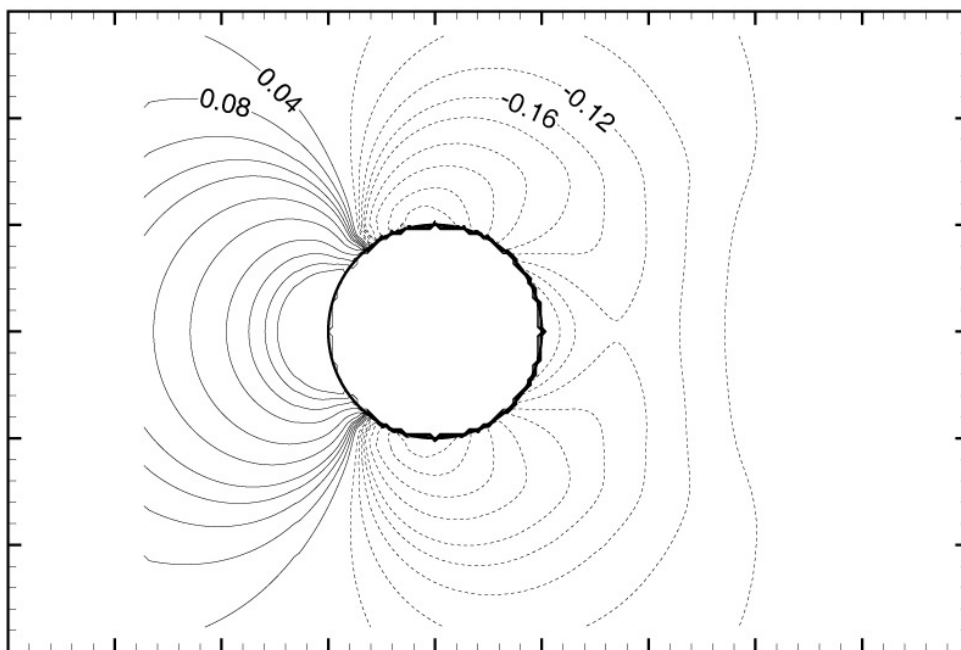
(a) $Re = 50$

(b) $Re = 100$

Figure **8.56** Comparison of pressure coefficient contours between two Reynolds numbers.
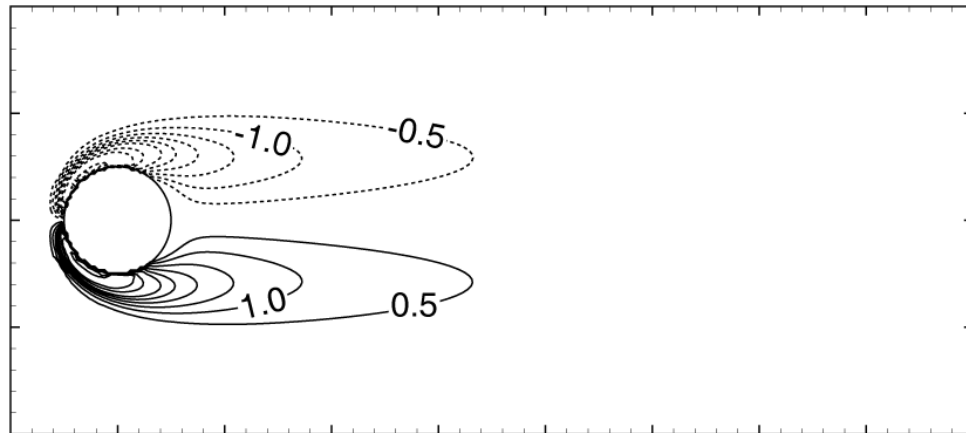
(a) $Re = 50$
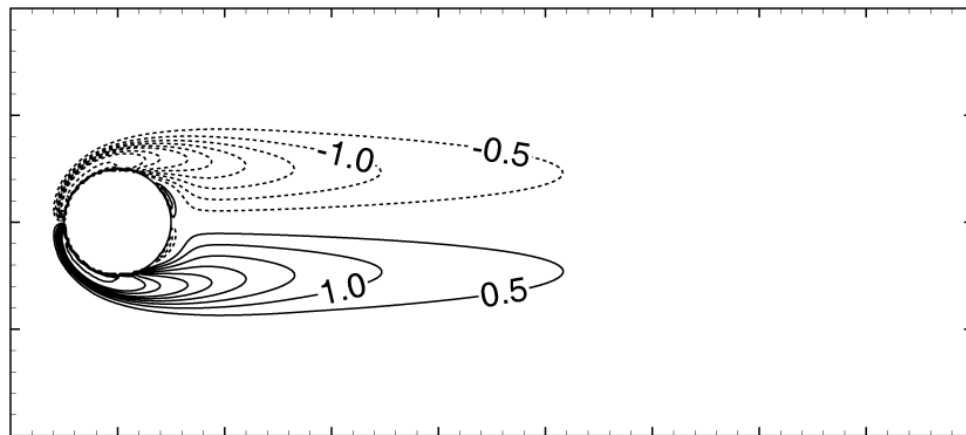
(b) $Re = 100$

Figure 8.57 Comparison of vorticity contours between two Reynolds numbers.

8.5.2.2   Rectangular wing

The present method is finally demonstrated on the flow past a three dimensional wing of rectangular planform. The NACA0012 section profile is employed for the illustration of the method. Figure **8.58** shows discretization of the rectangular wing. The ratio of span to chord is 1:1 for the figure. The panels on the side surfaces are constructed in the fully unstructured manner, where as the upper and lower surfaces of the wing have regular shape of triangles. The surfaces are firstly discretized into square rectangles, then the respective rectangles are divided into two triangles.

The simulation is performed for the rectangular wing with aspect ratio of 2 at angle of attack $\alpha = 7°$. The Reynolds number is 100 based on the wing chord length. The time step for the simulation is $\Delta t = 0.012$. The streamtraces around the tip and the pressure coefficient in the center plane of the wing are compared with the FLUENT results in Figure **8.59** . A stream trace starting below of the pressure side turns around the wing side, and forms into swirling flow downstream of the wing. It is clearly seen that the four stream traces are turning around each other by the tip vortex formation. It is seen from the pressure field in the center plane that the stagnation point is constituted near the leading edge of the wing. The pressure drop on the suction side is also illustrated in the figure.

Figure **8.60** shows the streamwise component of the vorticity, ω_x at several sreamwise planes, $x = 0.67, 0.8, 1.0$. The trailng edge is positioned at $x = 0.5$ when the angle of attack is zero. Figure **8.61** shows the tip vortex core position at the same streamwise planes plotted in Figure **8.60** . The coordinates of the core are extracted from the figure in such a manner that ω_x has a maximum value in each plane. The tip vortex core moves downward vertically and inside horizontally.

8.5.3   Features of vortex-in-cell method

An algorithm of VIC and panel method combination is developed and applied to the simulation of the viscous flow around impulsively started 2-D and 3-D objects. The main features of the present method are summarized as follows:

- The convection velocity of the vortex particles is efficiently computed on a regular Cartesian grid using an FFT based Poisson solver. The boundary of the grid compactly encloses the particles so as to reduce the domain size of the computation.

- The boundary conditions are enforced on the surface of the body for the tangential and normal components of the velocity. The tangential component of the slip is cancelled by the diffusion of vortex sheet, and the normal component is suppressed by the singularity which is linearly distributed
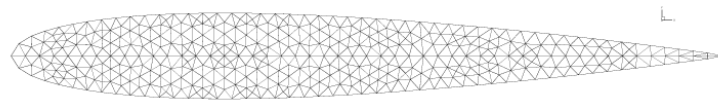
(a) Wing side discretization
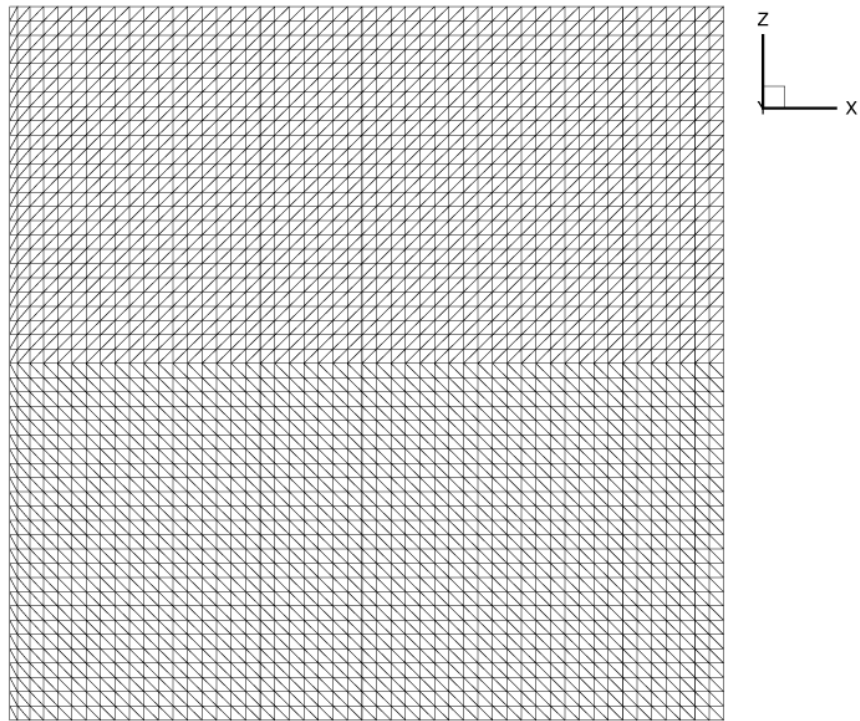
(b) Wing upper and lower surface discretization

Figure **8.58** Surface panel discretization of a rectangular wing. Number of the panels is 11,416.
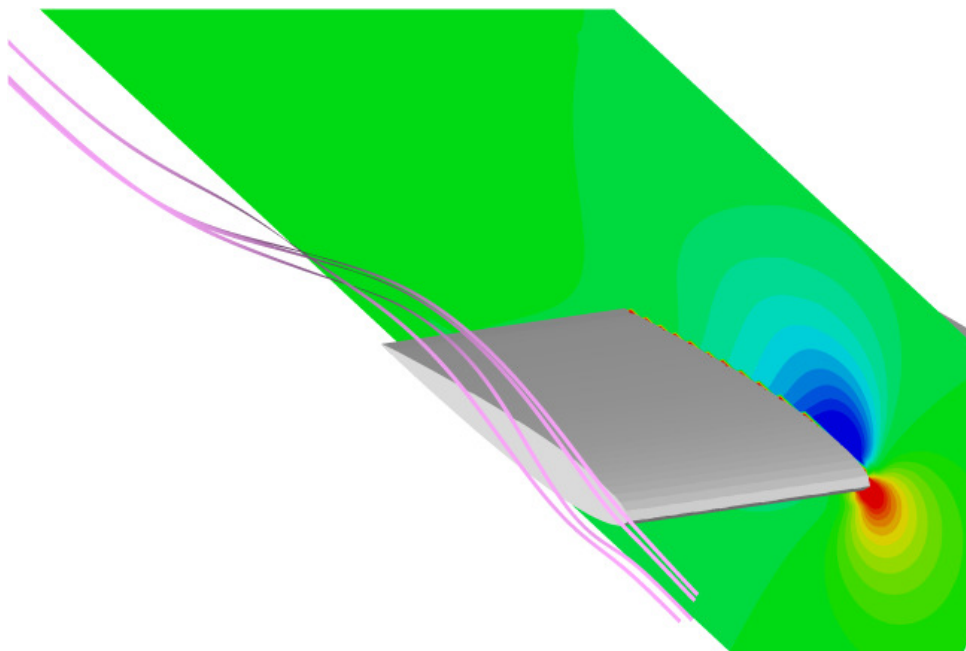
(a) Streamtraces and pressure coefficient, the present method
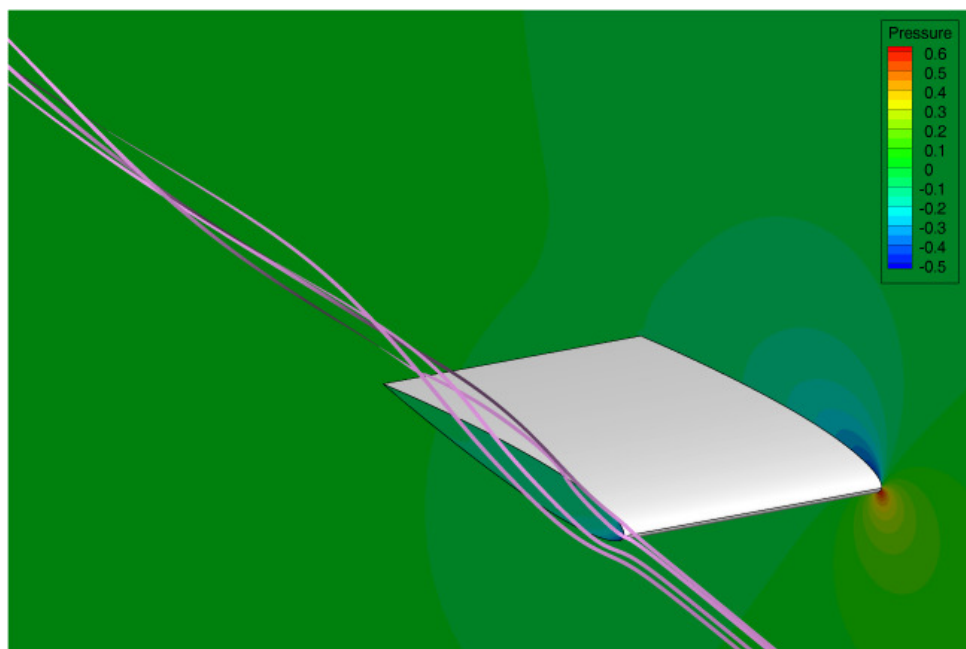
(b) Streamtraces and pressure coefficient, FLUENT

Figure **8.59** Comparison of streamtraces and pressure coefficient for a rectangular wing for $Re = 100$ with the results obtained by FLUENT.
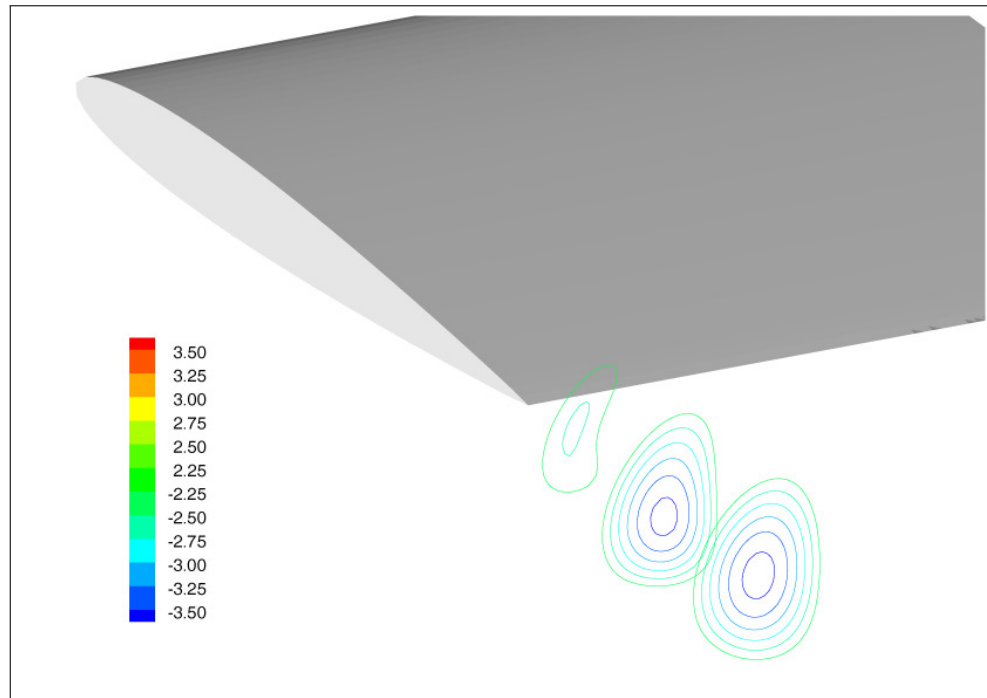
Figure **8.60** Streamwise vorticity contours at downstream locations $x = 0.67, 0.8$, and 1.0 at $t = 1.92$.

over a panel on the body. The use of panel method makes it possible for the application points of the two components of the boundary conditions to coincide on the center of the panel.

- The particle strength exchange (PSE) is modified to include the particles positioned inside of the body in the spirit of the immersed boundary nature of the method. The spurious slip resulting from the symmetric treatment near the body is corrected in the wall diffusion step for the no slip condition.

- The calculation of the pressure field is designed to use the solution method of integral equation approach, which is the same as the singularity distribution method for the no through flow condition. The matrix elements constructed and inverted once in the early stage of the method can be used throughout the method.

- The applicability of the present scheme is illustrated on the flow past 2-D and 3-D bodies in impulsive start. The method is in good agreement with other vortex method computation or the experimental work.
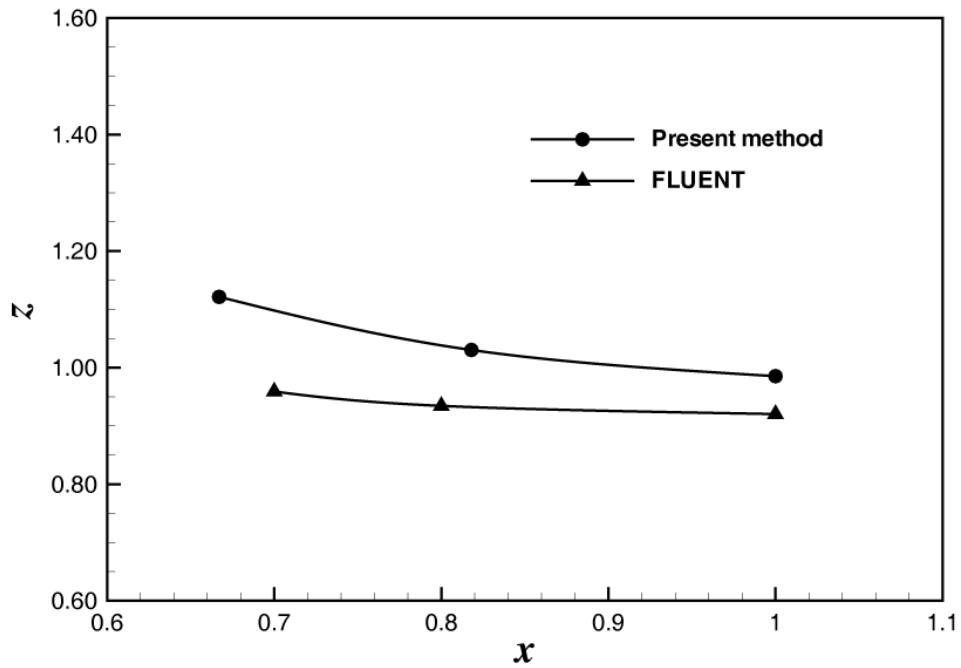
(a) Spanwise location of the center
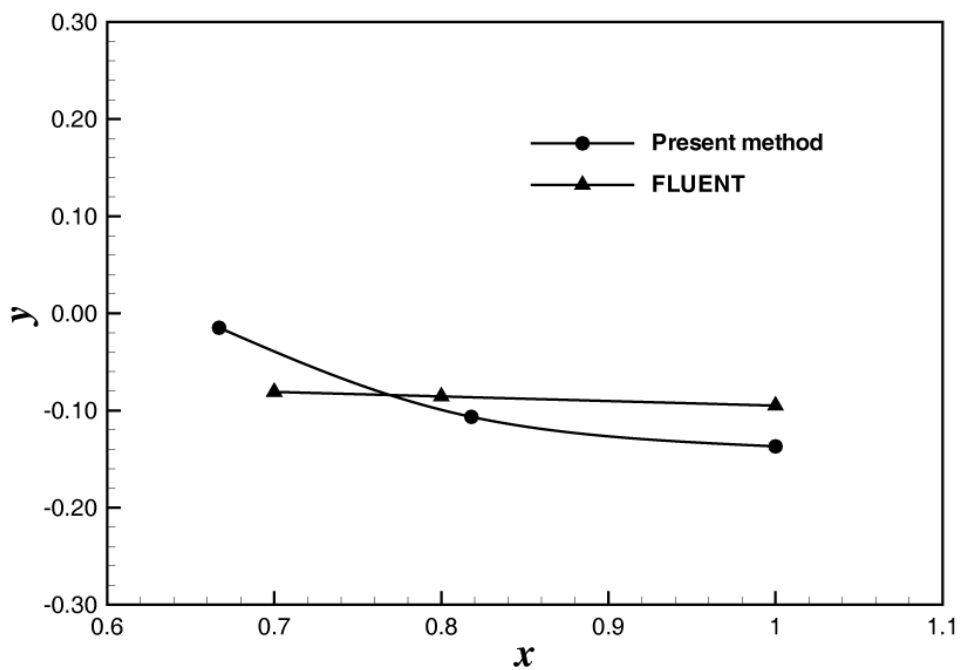
(b) Vertical location of the center

Figure 8.61 Location of the tip vortex center along downstream.

The proposed method is regarded as one possible solution of overcoming the leakage problem across a body boundary in the Cottet & Poncet (2003)'s method by the combination of vortex in cell method with a panel method. The panel method is formulated on the discretized surface panel in orde not to generate through flow component. This approach has an advantage in the computation of surface pressure as well as pressure field. The linear system of equations, constituted in the course of making normal boundary condition to be satisfied, can be applicable to the pressure calculation with the only change in the right hand side of the system.

8.6   Concluding Remarks

This course presents a vorticity-based integro-differential formulation for the numerical solution of unsteady incompressible flows. The integral approach that is a fundamental part of the present formulation is directly applicable for solving the integral equation for the pressure field as well. The present scheme includes a pressure calculation which is a distinctive feature, not previously treated in most vorticity-based methods. These aspects have been adapted for the vorticity-velocity-pressure formulation by an Eulerian description.

For the kinematics of flow and the physical interpretation of the velocity field ($\underline{q} = \underline{u}_w + \nabla\phi + \underline{U}_\infty$), a Lagrangian vortex method connected with the panel method has been presented. An iterative process was used in order to enforce the no-slip condition through the vorticity flux at the body boundary. For a thin body, we suggest the use of an image particle layer for the zero-vorticity flux condition on the solid boundary.

By applying the present scheme for the impulsively-started cylinder and the impulsively-started NACA0021 foil with angles of attack, we performed comparisons with existing results, and with the results of an Eulerian FVM.

Although the present work has mainly focused on comparative studies, future work would address (i) the treatment of turbulence models, (ii) the extension of the vortex method to three-dimensional flow problems, and (iii) the development of efficient numerical schemes associated with the solution procedure.

8.6.1 LES in vortex methods

The direct numerical simulation of turbulent flows is possible for low Reynolds number. Number of elements required for large Reynolds number of practical application is very large so that the actual simulation is restricted. With the current computer resource, the large eddy simulation is possible in which we take modeling for the small-scale (subgrid-scale) turbulence in the viscous wake and in the boundary layers.

The vortex method has been thought of as a natural approach to the simulation of turbulent flows. The use of vortex particles that convect with the flow in a Lagrangian manner has been considered as a way of minimizing numerical diffusion, which is an important matter in turbulent flow solution. The discretization of the vorticity field using a smoothing function

$$\underline{\omega}(\underline{x}, t) = \sum_{i=1}^{N} \zeta_\epsilon(\underline{x} - \underline{x}_i)\,\underline{\alpha}_i \tag{8.94}$$

can be considered to be some kind of filtering (normally, particle filtering) operation in LES. The filtered voriticity transport equation

$$\frac{D\overline{\omega}}{Dt} = \overline{\underline{\omega}} \cdot \nabla \overline{\underline{u}} + \nu\,\nabla^2 \overline{\underline{\omega}} - \nabla \cdot \underline{\underline{T}} \tag{8.95}$$

differs from the laminar version in that vorticity stress term $\nabla \cdot \underline{\underline{T}}$ is added, where $T_{ij} = (\overline{\omega_i\,u_j} - \overline{\omega}_i\,\overline{u}_j) - (\overline{u_i\,\omega_j} - \overline{u}_i\,\overline{\omega}_j)$ is the subfilter scale vorticity stress.

If we take the vorticity version of the Smagorinsky model for that term, $-\nabla \cdot \underline{\underline{T}} = \nabla \cdot (\nu_t\,\nabla \overline{\underline{\omega}})$, the turbulent diffusion can be treated in a similar way to the particle strength exchange of the laminar diffusion. Cottet (1999) suggested a simple selective model that the eddy diffusivity ν_t comes into action in region of intense vortex activity, where the flow is strongly three dimensional.

$$\nu_t = \begin{cases} C_s^2\,\Delta^2\,|\overline{\omega}|, & \text{for} \quad \beta_0 < \beta_m < \pi - \beta_0 \\ 0, & \text{otherwise} \end{cases} \tag{8.96}$$

The region of nonzero eddy diffusivity is where the angle β_m between the vorticity at a given grid point and the average neighboring vorticity becomes antialigned. The turbulent diffusion then becomes particle strength exchange with average eddy diffusivity,

$$\nabla \cdot (\nu_t \nabla \overline{\omega}) = \frac{1}{2\,\epsilon^2} \sum_j (\nu_{t_i} + \nu_{t_j})\,(\underline{\alpha}_j - \underline{\alpha}_i)\,\eta_\epsilon(\underline{x}_i - \underline{x}_j) \tag{8.97}$$

The extension of the VIC algorithm developed in this work to the turbulent flow analysis is expected to be realized in future work.
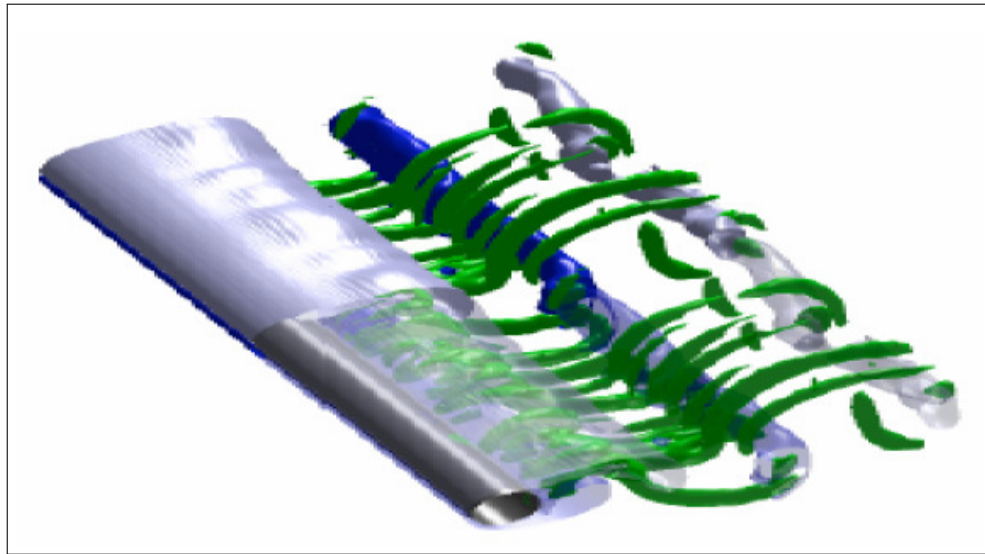
Figure **8.62** Turbulent flow past a cylinder by VIC method. Cylindrical grid: $256 \times 128 \times 128$ in a domain $4\pi \times 2\pi \times 2\pi$ filled with 25 % particles; CPU time: 8 min/RK4 iteration on alpha single processor, 3 hours/shedding cycle. From Cottet & Poncet (2003).

8.6.2 Interaction between flow and bubble

The vorticity transport equation for two-dimensional incompressible flow of a viscous fluid can be rewritten, without ignoring the external force, as

$$\frac{D\underline{\omega}}{Dt} = \nu\,\nabla^2\underline{\omega} + \nabla \times \underline{f} \tag{8.98}$$

where $\underline{f}$ is the external force caused by all the bubbles in fluid. The external force is accounted for here the total force $\underline{f}_B$ acting on the bubble; $\underline{f} = -\underline{f}_B$.

Equation of motion for a single bubble yields the following trajectory equation for a bubble of changing volume:

$$
\begin{aligned}
m_B \frac{d\underline{u}_B}{dt} \;=\;& \rho\,V_B\,\frac{D\underline{u}}{Dt} - \frac{1}{2}\rho\,V_B\left(\frac{d\underline{u}_B}{dt} - \frac{D\underline{u}}{Dt}\right) + \frac{1}{2}\rho\left(\underline{u} - \underline{u}_B\right)\frac{dV_B}{dt} \\
& + \frac{1}{2}\rho\,\pi\,R^2\,C_D\,\left|\underline{u} - \underline{u}_B\right|\left(\underline{u} - \underline{u}_B\right)
\end{aligned}
\tag{8.99}
$$

where the forces with the gravitational acceleration are neglected in this study; the gravity and the buoyant force.

Recall that the force acting on the bubble is

$$
\underline{f}_B \;=\; \underline{F}_U \;+\; \underline{F}_M \;+\; \underline{F}_V \;+\; \underline{F}_D
\tag{8.100}
$$

where

$$
\begin{aligned}
\underline{F}_U &= \text{Unsteady force due to the acceleration of the undisturbed flow} \\
\underline{F}_M &= \text{Convential added mass force} \\
\underline{F}_V &= \text{Additional added mass force due to the volume variation} \\
\underline{F}_D &= \text{Drag force}
\end{aligned}
$$

The hydrostatic forces, *i.e.* the bouyancy and graivity force, are accounted for without directly producing any disturbace. Because the forces that are included Du/Dt term are not produced by the bubble motion, they must be negligible. Hence, Equation (8.99) is rewritten as

$$
\rho\,V_B\,\frac{d\underline{u}_B}{dt} \;=\; \rho\left(\underline{u} - \underline{u}_B\right)\frac{dV_B}{dt} \;+\; \rho\,\pi\,R^2\,C_D\,\left|\underline{u} - \underline{u}_B\right|\left(\underline{u} - \underline{u}_B\right)
\tag{8.101}
$$

where ρ_B is neglected due to $\rho_B \ll \rho$. With the drag force $\underline{F}_D$ and the additional added mass force $\underline{F}_V$ due to volume variation, (8.101) accounted for the force acting on the fluid element which occupies the same volume and velocity of the bubble. These external forces can be considered as the disturbance exerted by the motion of the bubble.

Suppose now that the disturbance is separated into two parts, the disturbance induced by the translational motion of the bubble and the distubance induced
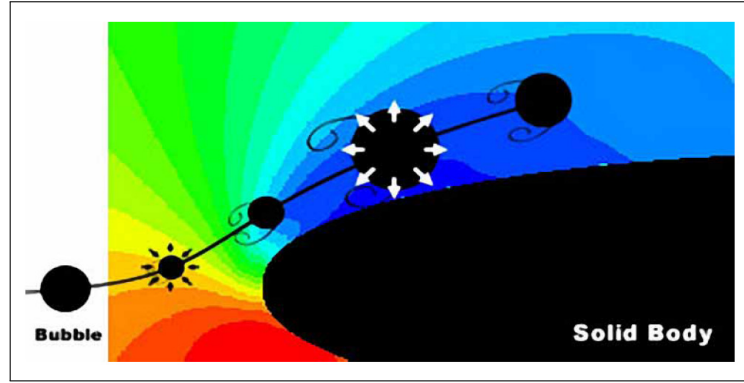
Figure **8.63** Schematic diagram of interaction between the motion of a single bubble and the ambient viscous flow.

by the volumetric motion as shown in Figure **8.63** .

$$\underline{f} = \underline{F}_V + \underline{F}_D \tag{8.102}$$

8.6.2.1   Disturbance by volumetric motion

The disturbance which is induced by the *pure* volumetric motion of the bubble, can be considered as mass source/sink in flow according to Eq. (8.101). According to *Lagally Theorem*, that is, the force on the bubble is proportional to the source strength and to the magnitude of the velocity $(\underline{u} - \underline{u}_B)$ induced at the location of the source by all mechanisms other than the source itself. The direction of the force coincides with that of the relative velocity vector. Thus, the force which is the volumetric motion of the bubble is defined as

$$\underline{F}_V = \rho \left(\underline{u} - \underline{u}_B \right) \frac{dV_B}{dt} = \rho \, \mathcal{Q} \left(\underline{u} - \underline{u}_B \right) \tag{8.103}$$

The strength of the mass source/sink becomes

$$\mathcal{Q} = \frac{dV_B}{dt} = 4\pi R^2 \dot{R} \tag{8.104}$$

Recall that the velocity potential ϕ is used to enforce the no-through-flow boundary condition,

$$\underline{u}' = U_\infty + \underline{u}_\omega + \nabla\phi \tag{8.105}$$

and that the velocity potential for the pure radial motion of the bubble is defined by

$$\phi_B = -\frac{1}{4\pi}\frac{Q}{r} = -\frac{R^2\dot{R}}{r} \qquad (8.106)$$

Hence, with the velocity induced by the radial motion of the bubble, the flow velocity is rewritten as

$$\underline{u}'' = U_\infty + \underline{u}_\omega + \nabla\phi + \nabla\phi_B \qquad (8.107)$$

where

$$\nabla\phi_B = \frac{R^2\dot{R}}{r^2}\underline{e}_r \qquad (8.108)$$

The symbol $\underline{e}_r$ denotes the unit vector in the outward radial direction from the bubble.

Owing to the no-through-flow boundary condition, the normal component of the velocity on the body surface becomes zero as

$$\underline{n}\cdot\underline{u}'' = \underline{n}\cdot(U_\infty + \underline{u}_\omega + \nabla\phi + \nabla\phi_B) = 0 \qquad (8.109)$$

Then, substituting Eqn. (8.109) into Eqn. (4.2), it is found that

$$\frac{1}{2}\phi - \oint_C \phi\,(\underline{n}\cdot\nabla G)\,d\ell = -\oint_C (\underline{n}\cdot(U_\infty + \underline{u}_\omega + \nabla\phi_B))\,G\,d\ell \qquad (8.110)$$

The velocity potential on the body surface is implicitly computed. The velocity at the field is adjusted by the velocity potential obatained by the above equation.

8.6.2.2 Disturbance by translational motion

Previous to computing the disturbance induced by the pure translational motion of the bubble, consider the definition of the hydrodynamic force $\underline{F}$ with the hydrodynamic impulse $\underline{I}$ (Lamb 1932, Saffman 1992); thus,

$$\underline{F} = -\rho\frac{\Delta\underline{I}}{\Delta t} \qquad (8.111)$$

In two-dimensional case, the components of the hydrodynamic impulse (I_x, I_y) are defined as

$$I_x = \sum y_i \, \Gamma_i \,, \qquad I_y = -\sum x_i \, \Gamma_i \tag{8.112}$$

and then the components of the force (F_x, F_y) are

$$F_x = -\rho \frac{\Delta I_x}{\Delta t} \,, \qquad F_y = -\rho \frac{\Delta I_y}{\Delta t} \tag{8.113}$$
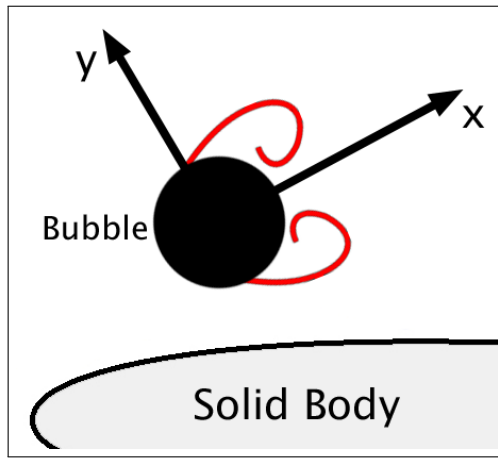
Figure **8.64** Local coordinates for the hydrodynamic impulse of the bubble

Also, the drag force $\underline{F}_D$ acting on a sphere in creeping flow at very low Reynolds numbers is defined as (Batchelor 1973)

$$\underline{F}_D \;=\; -\rho \frac{\Delta I_x}{\Delta t} \;=\; 12 \, \pi \mu R \, (\underline{u} - \underline{u}_B) \tag{8.114}$$

or equivalently

$$\Delta I_x \;=\; -12 \, \pi \nu R \, (\underline{u} - \underline{u}_B) \, \Delta t \tag{8.115}$$

From these definitions, it is considered that the vorticity generated by the translational motion of the bubble, which is exerted by the only drag force (the effect exerted by the lift force is neglected in this study). Then, it can be modeled that a symmetrical pair of two-dimensional vorticity of finite size on the bubble surface is generated monotonically during Δt.

$$y_{up} \, \Gamma_{up} \,+\, y_{dn} \, \Gamma_{dn} \;=\; -12 \, \pi \, \nu \, R \, (\underline{u} - \underline{u}_B) \, \Delta t \tag{8.116}$$

The vorticity strength is obtained as $|\Gamma| = 6\pi\nu\,|\underline{u} - \underline{u}_B|\,\Delta t$ at $|y| = R$. The magnitude of the induced vorticity is rewritten with with non-dimensional value as

$$|\Gamma^*| = \frac{6\pi}{Re}\,|\underline{u}^* - \underline{u}_B^*|\,\Delta t^* \tag{8.117}$$

with Reynolds number $Re = U_\infty L/\nu$ for the flow. The vorticity induced by the bubble (Figure **8.65**) is computed by differentiating directly over the Lagrangian control points, without requiring the interpolation onto the grid. In
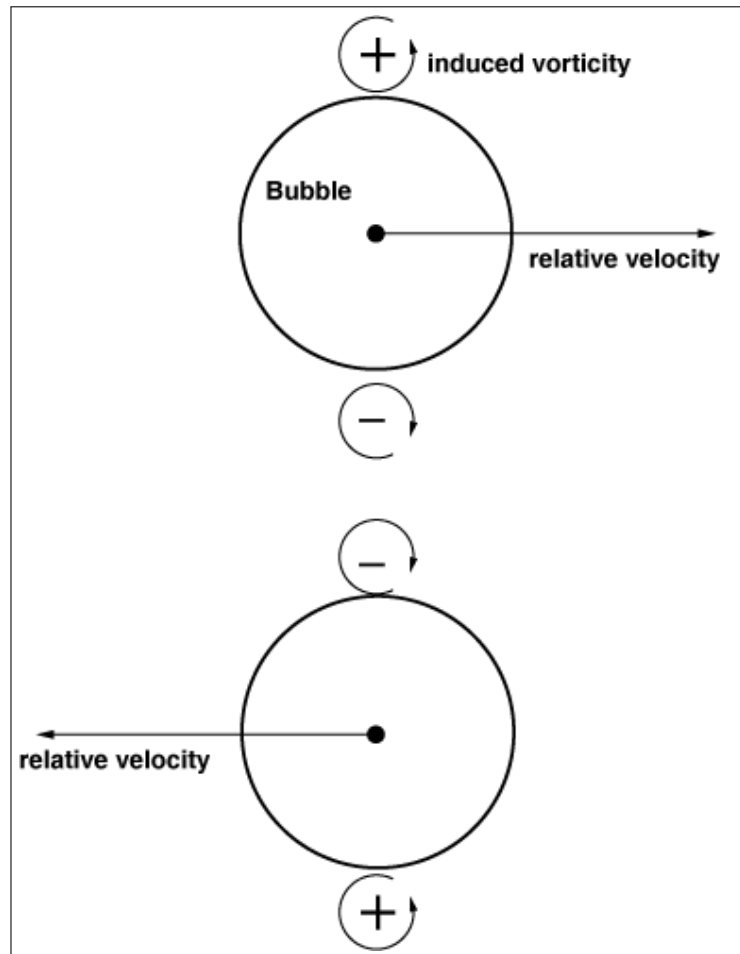
Figure 8.65 Schematic of the vorticity generation

fact, the actual vortices shedding behind a sphere would be of ring type. Therefore an axisymmetric ring vortex model equivalent to the drag forces is more realistic than the present model taken herein. Such a three dimensional numeric modelling is beyond of the present workscope, even through there still exists inconsistency on the bubble interactions, in the respect of overall two dimensional analysis.
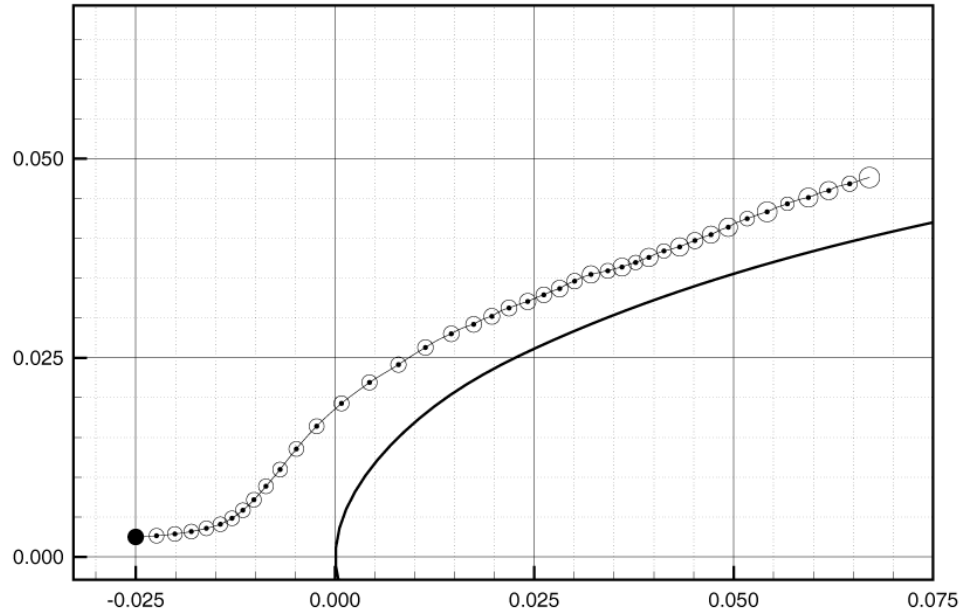
(a) Cavitation number $C_a = 1.0$
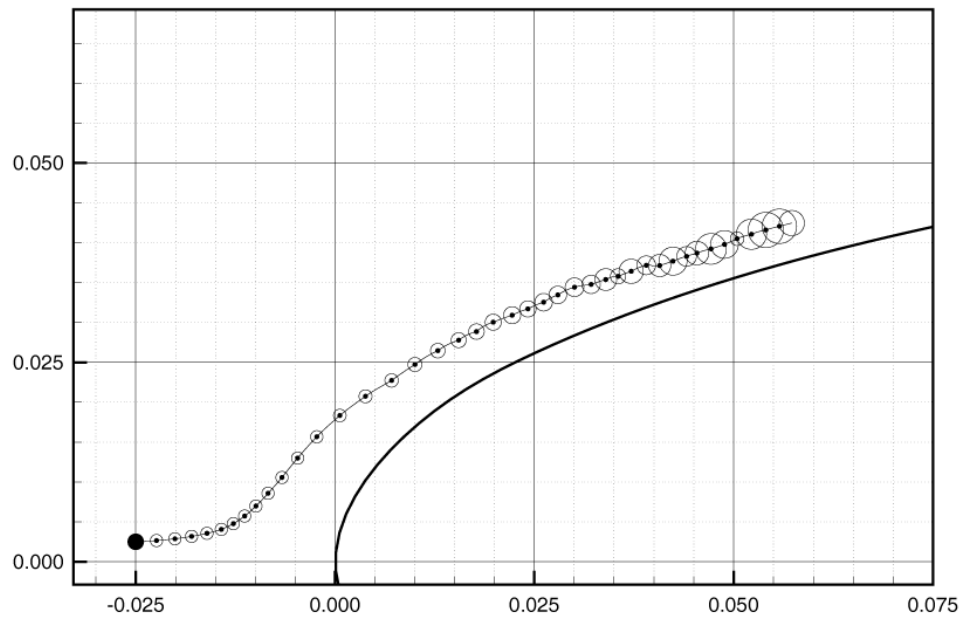
(b) Cavitation number $C_a = 0.1$

Figure **8.66** Bubble behavior for two different cavitation numbers. Initial bubble radius $R_o = 1,000 \mu m$

A

NUMERICAL IMPLEMENTATION OF KUTTA CONDITION

A.1 Implementation of Kutta Condition in Two-Dimensions

The physical features behind the Kutta condition, although the interpretation is not complete, are complex as explained before. The object of the numerical implementation of the Kutta condition here is to determine the jump in the

disturbance potential ($\triangle\phi_v$) at the T. E. for which acceptable results may be obtained.

Following the feature of the 'Maskell' trailing-edge flow for the velocity at the T. E., we can define the tangential velocities (i.e., shed vorticity) on both the upper and lower surfaces at the T. E. by imposing a stagnation point at either the upper or the lower trailing-edge point. Then the difference of the velocity there is assigned to the shed vorticity.

Accordingly we can evaluate the jump in disturbance potential at the T. E. ($\triangle\phi_v|_{TE}$) such that a surface potential distribution near the T. E. satisfies the behavior of the tangential velocities corresponding to the local flow characteristics near the T. E.

In practice, the Kutta condition is implemented first by attaching the wake to the T. E. (or by specifying a point where the vorticity leaves the body surface) and evaluating $\triangle\phi_v|_{TE}$ from the values of the disturbance potential of the panels (ϕ_j).

Let us approximate the disturbance potential distributions (ϕ) on the upper and the lower surfaces near the T. E. as a parabolic form of the parameter s:

$$\phi_u\left(s\right) = a_u\,s^2 + b_u\,s + c_u\,, \tag{A.1}$$

$$\phi_\ell\left(s\right) = a_\ell\,s^2 + b_\ell\,s + c_\ell\,, \tag{A.2}$$

where the parameter s is arc-length along the body surface contour from the T. E. with positive taken as counterclockwise (see Figure **4.5**) and the subscripts u and ℓ refer to the upper and the lower surface, respectively. The coefficients b_u, b_ℓ, c_u and c_ℓ are to be determined by imposing the Kutta condition, but the coefficients a_u and a_ℓ (which have been kept in the following derivation) are ignored in the final expression (A.10) for $\triangle\phi_v|_{TE}$ by assuming their contribution to be higher order.

Similar procedure has been presented by Ingham et al. (1981) [1] for the problems with two regions of different physical features, in which the two analytical

---

[1] Ingham, D. B., Heggs, P. J. and Manzoor, M. (1981), "The Numerical Solution of Plane Potential Problems by Improved Boundary Integral Equation Methods," *Journal of Computational Physics*, vol. 42, pp. 77–98.

solution forms of the Laplace equation for the two regions in the neighborhood of the discontinuity are introduced and then the appropriate physical matching conditions at the common interface are enforced to determine the coefficients associated with those forms. Another simple application of this procedure has been introduced by Batchelor (1967) to flow problem near a stagnation point. [2]

Then taking the gradient of (A.1) and (A.2) and then including the undisturbed velocity $\underline{q}_\infty (\equiv \underline{q}_o - \underline{q}_F)$ give the total tangential components (positive as counterclockwise) on the upper and the lower surface near the T. E. can be expressed as, respectively,

$$q_{tu}(s) = (\underline{q}_\infty + \nabla\phi_u) \cdot \underline{t}_u = \underline{q}_\infty \cdot \underline{t}_u + 2a_u\, s + b_u \,, \qquad (A.3)$$
$$q_{t\ell}(s) = (\underline{q}_\infty + \nabla\phi_\ell) \cdot \underline{t}_\ell = \underline{q}_\infty \cdot \underline{t}_\ell + 2a_\ell\, s + b_\ell \,. \qquad (A.4)$$

Then the potential jump at the T. E. from (A.1) and (A.2) can be written as

$$\triangle\phi_{\mathrm{v}}|_{TE} = \phi_u(0) - \phi_\ell(0) = c_u - c_\ell \,. \qquad (A.5)$$

This potential jump is expressed in terms of quantities in the panel-method approximation as:

$$\triangle\phi_{\mathrm{v}}|_{TE} = c_u - c_\ell = (\phi_1 - a_u\, s_1^2 - b_u\, s_1) - (\phi_N - a_\ell\, s_N^2 - b_\ell\, s_N), \qquad (A.6)$$

where ϕ_1 and ϕ_N are the (unknown) disturbance potential, respectively, on the two adjacent panels to the T. E. (i.e., the 1st panel from the T. E. on the upper surface and the N-th panel on the lower surface) (see Figure 4.5). But we specify the coefficients a_u, b_u, a_ℓ and b_ℓ by applying the Kutta condition at the T. E.

A.1.1 Steady flow cases

As a special case, first let us consider <u>steady flow</u> for which a stagnation point (for non-cusped foils) should be located at the T. E. Then it means $q_{tu}(0) = 0$

---

[2] See Batchelor, G. K. (1967), *An Introduction to Fluid Dynamics*, Cambridge University Press, Cambridge, p. 105.

and $q_{t\ell}(0) = 0$. Applying these constraints to (A.3) and (A.4) gives

$$b_u = -\underline{q}_\infty \cdot \underline{t}_u \Big|_{TE} \quad \text{and} \quad b_\ell = -\underline{q}_\infty \cdot \underline{t}_\ell \Big|_{TE} . \tag{A.7}$$

With these coefficients, (A.6) reduces to

$$
\begin{aligned}
\triangle\phi_{\mathrm{v}}\big|_{TE} &= c_u - c_\ell \\
&= \phi_1 - a_u\, s_1^2 + \underline{q}_\infty \cdot \underline{t}_u \Big|_{TE} s_1 - \phi_N + a_\ell\, s_N^2 - \underline{q}_\infty \cdot \underline{t}_\ell \Big|_{TE} s_N \\
&= \phi_1 - \phi_N + a_\ell\, s_N^2 - a_u\, s_1^2 - \underline{q}_\infty \cdot (\underline{t}_N\, s_N) + \underline{q}_\infty \cdot (\underline{t}_1\, s_1) \\
&= \boxed{\phi_1 - \phi_N + \underline{q}_\infty \cdot \triangle\underline{r}} ,
\end{aligned}
\tag{A.8}
$$

where the term $(a_\ell s_N^2 - a_u s_1^2)$ has been neglected, being of higher order compared with other terms and $\triangle\underline{r}(= \underline{r}_1 - \underline{r}_N)$ represents difference of position vectors of the control points of the two adjacent panels (Figure **4.5**).

Equation (A.8) is the same as the Kutta condition for steady two-dimensional lifting flow suggested first by Lee (1987). [3] He pointed out that the 'implicit' Kutta condition imposed just as $\triangle\phi_{\mathrm{v}}\big|_{TE} = \phi_1 - \phi_N$, [4] may lead to inaccurate results for extreme cases such as for a circular cylinder at 90° angle of attack (for which the lift calculated by using this 'implicit' Kutta condition is incorrectly about half of the analytical one).

A.1.2   Unsteady flow cases

Next, we can follow a similar procedure for <u>unsteady flow</u>. First the tangential speed at the T. E. either on the upper or the lower surface, depending on the sign of $d\Gamma_B/dt$ as mentioned previously, should be specified in order to determine the unknown coefficients b_u and b_ℓ in (A.6). According to the behavior of the 'Maskell' trailing edge flow, the tangential speeds at the T. E. on both the upper and the lower surfaces are expressed in terms of a vortex strength at the T. E.

---

[3]Lee, J. T. (1987), *A Potential Based Panel Method for the Analysis of Marine Propellers in Steady Flow*, Department of Ocean Engineering, MIT, Report no. 87-13.

[4]For example, see Maskew, B. (1982), "Prediction of Subsonic Aerodynamic Characteristics: a Case for Low-Order Panel Methods," *Jounal of Aircraft*, vol. 19, no. 2, pp. 157–163.

(γ_{TE}) as:

$$
\begin{cases}
q_{t\ell} = \gamma_{TE} \,, \; q_{tu} = 0, & \text{if } d\Gamma_B/dt < 0 \\
q_{t\ell} = 0, \quad\quad q_{tu} = \gamma_{TE} \,, & \text{if } d\Gamma_B/dt > 0 \\
q_{t\ell} = 0, \quad\quad q_{tu} = 0, & \text{if } d\Gamma_B/dt = 0
\end{cases}
\tag{A.9}
$$

Substituting these relations into (A.3) and (A.4) in order find b_u and b_ℓ, then neglecting the term $(a_\ell \, s_N^2 - a_u \, s_1^2)$ as the steady flow cases and recalling $\underline{q}_\infty \equiv \underline{q}_o - \underline{q}_F$, we obtain the following expression for $\triangle\phi_{\mathrm v}|_{TE}$:

$$
\triangle\phi_{\mathrm v}|_{TE} =
\begin{cases}
\phi_1 - \phi_N + (\underline{q}_o - \underline{q}_F)_{TE} \cdot \triangle\underline{r} + \gamma_{TE}\, s_N, & \text{if } d\Gamma_B/dt < 0 \\
\phi_1 - \phi_N + (\underline{q}_o - \underline{q}_F)_{TE} \cdot \triangle\underline{r} - \gamma_{TE}\, s_1, & \text{if } d\Gamma_B/dt > 0 \\
\phi_1 - \phi_N + (\underline{q}_o - \underline{q}_F)_{TE} \cdot \triangle\underline{r} \,, & \text{if } d\Gamma_B/dt = 0
\end{cases}
\tag{A.10}
$$

In a numerical code, from two circulation values at successive time steps an approximation for γ_{TE} may be used:

$$
\gamma_{TE} = \frac{\Gamma_B^{(k-1)} - \Gamma_B^{(k)}}{\triangle\mathrm{v}_1}
\tag{A.11}
$$

Here $\triangle\mathrm{v}_1$ (that is given as an input parameter in a numerical code) is the length of the straight-line element of the wake sheet leaving the T. E. Consequently an iteration procedure is required to obtain unknown $\Gamma_B^{(k)}$ at the present instant of time, which is equal to the negative value of $\triangle\phi_{\mathrm v}|_{TE}$.

A.2 Implementation of Kutta Condition in 3-D Steady Flows

The Kutta condition has been applied originally in the steady two-dimensional flow case for uniqueness of solution mathematically and for regular flow in the vicinity of the trailing edge (T. E.) physically. It eventually implies that the rear stagnation point is at the T. E. for a non-cusped sharp-edged foil in order to satisfy both the pressure-equality condition and the condition of finite velocity at the T. E.. But if we applied this interpretation in steady three-dimensional flow, the two conditions of pressure equality and finite velocity can not be satisfied

exactly at the T. E., since there is inherently a velocity difference across the sharp T. E.. and (iii) to satisfy the pressure equality condition at the T. E..

Let us approximate the disturbance potential distributions (ϕ) on the upper and the lower surfaces near the T. E. as a linear form of the local coordinates (geometrical parameters) ξ and η: [5]

$$\phi_u(\xi_u, \eta) = a_u\,\xi_u + b_u\,\eta + c_u\,, \tag{A.12}$$

$$\phi_\ell(\xi_\ell, \eta) = a_\ell\,\xi_\ell + b_\ell\,\eta + c_\ell\,, \tag{A.13}$$

where the parameter η is arclength along the T. E. positive taken as spanwise direction (see Fig. 2 in reference Mangler & Smoth (1970)) and the parameters ξ_u and ξ_ℓ are arclength along the upper surface and the lower surface, respectively, measured from the T. E. and normal to the T. E.. Here the subscripts u and ℓ refer to the upper and the lower surface, respectively. Then the potential jump at the T. E. from (A.12) and (3.8) can be written, including its spanwise variation term,

$$\triangle\phi = \phi_u\,(0, \eta) - \phi_\ell\,(0, \eta) = c_u - c_\ell + (b_u - b_\ell)\,\eta \tag{A.14}$$

This potential jump is expressed in terms of unknown quantities in the panel-method approximation as:

$$\triangle\phi = (\phi_1 - \phi_N) - (a_u\xi_{u1} - a_\ell\xi_{\ell N}) - (b_u\eta_1 - b_\ell\eta_N) + (b_u - b_\ell)\eta \tag{A.15}$$

where ϕ_1 and ϕ_N are the (unknown) disturbance potential, respectively, at the control points of the two adjacent panels to the T. E. (i.e., the 1st panel from the T. E. on the upper surface and the N-th panel on the lower surface). $\xi_{u1}, \xi_{\ell N}, \eta_1, \eta_N$ are the local coordinates of the control points. Then taking the gradient of (A.12) and (3.8) and then including the undisturbed velocity $\underline{q}_o$ give

---

[5]Similar procedure has been presented by Ingham et al. (1981) for the problems with two regions of different physical features, in which the two analytical solution forms of the Laplace equation for the two regions in the neighborhood of the discontinuity are introduced and then the appropriate physical matching conditions at the common interface are enforced to determine the coefficients associated with those forms. Also this procedure has been applied to irrotational solenoidal flow near a stagnation point (Batchelor (1967)).

the total tangential speeds on the upper and the lower surface near the T. E.:

$$q_u^2 = (\underline{q}_o \cdot \underline{e}_{\xi u} + a_u)^2 + (\underline{q}_o \cdot \underline{e}_\eta + b_u)^2 \qquad (A.16)$$

$$q_\ell^2 = (\underline{q}_o \cdot \underline{e}_{\xi \ell} + a_\ell)^2 + (\underline{q}_o \cdot \underline{e}_\eta + b_\ell)^2 \qquad (A.17)$$

where $\underline{e}_{\xi u}$, $\underline{e}_{\xi \ell}$ and $\underline{e}_\eta$ are the unit vectors of the local coordinate system at the trailing edge point.

According to the Mangler and Smith's analysis, vanishing the tangential speed at the T. E. either on the upper or the lower surface allows us to determine the unknown coefficients a_u and a_ℓ in (A.15):

$$\begin{cases} a_u = -\underline{q}_o \cdot \underline{e}_{\xi u} + \sqrt{-D} \, , \; a_\ell = -\underline{q}_o \cdot \underline{e}_{\xi \ell}, & \text{if } D < 0 \\ a_u = -\underline{q}_o \cdot \underline{e}_{\xi u} \, , \; a_\ell = -\underline{q}_o \cdot \underline{e}_{\xi \ell} + \sqrt{D}, & \text{if } D > 0 \\ a_u = -\underline{q}_o \cdot \underline{e}_{\xi u} \, , \; a_\ell = -\underline{q}_o \cdot \underline{e}_{\xi \ell}, & \text{if } D = 0 \end{cases} \qquad (A.18)$$

where $D = 2(\underline{q}_o \cdot \underline{e}_\eta)(b_u - b_\ell) + (b_u^2 - b_\ell^2)$. Here b_u and b_ℓ are still unknown representing variation of the perturbation potential in η-direction on the upper surface and the lower surface at the T. E. panels. Consequently this model requires an iteration procedure to determine these coefficients by fitting the potential values at the T. E. panels in that direction.

As a special case of two-dimensional steady flow, (for which a stagnation point should be located at the T. E.) it holds $q_u = 0$ and $q_\ell = 0$. Applying these constraints to (A.16) and (A.17) gives

$$a_u = -\underline{q}_o \cdot \underline{e}_{\xi u} \quad \text{and} \quad a_\ell = -\underline{q}_o \cdot \underline{e}_{\xi \ell} \qquad (A.19)$$

With these coefficients, (A.15) reduces to

$$\triangle \phi = \phi_1 - \phi_N + \underline{q}_o \cdot \triangle \underline{r} \qquad (A.20)$$

where $\triangle \underline{r} (= \underline{r}_1 - \underline{r}_N)$ denotes difference of position vectors of the control points of the two adjacent panels. Lee, J. T. (1987) suggested this equation as the Kutta condition for steady two-dimensional lifting flows, by which he has shown significant improvement on accuracy of numerical solutions compared to those

obtained by the so-called Morino's Kutta condition. Accordingly Eq. (A.15) contains the Kutta condition Eq. (A.8) for two-dimensional flows.

B

INTEGRATION FOR SINGULARITY DISTRIBUTIONS

Using Stokes' formulas, Cantaloube & Rehbach (1986) show that the surface integrals of the singularity method can be transformed into contour integrals for

planar facets. The numerical integration is then very precise at less calculation cost.

This Appendix is especially prepared to show all the mathematical derivations and proofs of the equations in the original paper by Cantaloube & Rehbach. A subroutine program based on the analysis is also provided in the Appendix C for computations of the influence coefficients in applications of the panel method.

B.1   Introduction

The fundamental problem of fluid mechanics for inviscid incompressible flow is to determine velocity potential ϕ, whose governing equation becomes the Laplace equation,

$$\nabla^2 \phi = 0, \tag{B.1}$$

satisfying certain proper conditions on the boundary S.

The singularity method is applied for solution of this problem. This basic idea of the singularity method has been introduced by Hess & Smith (1966), using the surface distribution of sources. With the Green's scalar identity, the potential ϕ within the domain V is expressed in terms of the proper value of ϕ and its normal derivative $\underline{n} \cdot \nabla \phi$ on the boundary S;

$$\phi = -\frac{1}{4\pi} \left(\int_S \frac{1}{r} \left(\underline{n} \cdot \nabla \phi \right) dS_\xi - \int_S \phi \, \underline{n} \cdot \nabla \left(\frac{1}{r} \right) dS_\xi \right). \tag{B.2}$$

Here r is a distance between an integration point ξ on S and a field point p located in V. The first surface integral is interpreted as the potential by surface distribution of source-type singularities with density $\sigma \equiv \underline{n} \cdot \nabla \phi$, the second surface integral as the potential by surface distribution of doublet-type singularities, $\mu \equiv -\phi$. [1]

For a planar polygon element with the uniform or linear density distributions of singularities, the closed-forms for obtaining the influence coefficients in the

---

[1] We follow herein the definition given in the original paper: $\mu \equiv -\phi$.

panel method are derived.

The analytic evaluations of the associated integrals may improve a solution accuracy in the panel method with much reduced computing time. A few of test calculations show the superiority of these analytic evaluations to numerical integrations.

B.1.1 Related work for closed-form expressions

The closed-form expressions of the surface integrals for constant source distributions over flat quadrilateral panels have been introduced by Hess & Smith (1966). [2] They expressed the surface integrals as a superposition of line integrals for each side of the panels, with independent treatment of the contribution from the side.

Webster (1975) [3] has extended the Hess and Smith analysis to a triangular panel in order to eliminate the discontinuity problem for a flat quadrilateral source panel by allowing a linear variation of the source strength across the triangular panel. These two approaches are concerned with only the source distributions and the resultant expressions are considerably complicated to employ a computer code.

A simpler and more unified derivation has been provided by Newman (1986) [4] for computing the potential due to a constant doublet or source distribution. His analysis is based on the elementary plane geometry related to the solid angle of a panel. He defined four infinite sectors (for a quadrilateral panel), bounded by semi-infinite extensions of the two adjacent sides of the panel with respect to the corresponding vertices, such that the difference between the domains of the four sectors is the domain of the panel. Then the surface integral over each infinite sector is evaluated in terms of the included angle of the corresponding vertex projected onto the unit sphere with center at the field point. He has also

---

[2]Hess, J. L. and Smith A. M. O. (1966), "Calculation of Potential Flow about Arbitrary Bodies," *Progress in Aeronautical Science Series*, vol. 8, Pergamon Press, pp. 1–138.

[3]Webster, W. C. (1975), "The flow about arbitrary, three-dimensional smooth bodies," *J. Ship Res.*, vol 19, no. 4, pp. 206–218.

[4]Newman, J. N. (1986), "Distributions of sources and normal dipoles over a quadrilateral panel," *J. Eng. Math.*, vol. 20, pp. 113–126.

described the more general recursive scheme for computing the potential due to a source or doublet distribution of linear, bilinear or higher order form, using the base results for the case of the constant distribution.

Another elegant approach based on mathematical formulations has been presented by Cantaloube & Rehbach (1986), [5] by which they introduced more explicit expressions of the surface integrals for the source or doublet distribution. With vector operations of the integrands for using Stokes' formulas, they show that the surface integrals for the constant or linear distributions of sources and doublets over a planar facet can be transformed into line integrals along the contour of the panel. The major advantages of their study are that the formulations are valid for a planar curve-sided panel and that the resultant equations are expressed in a global coordinate system while the aforementioned analysis requires the transformation of the local coordinate system. Thus the expressions derived by Cantaloube & Rehbach may be regarded as a more computer-oriented form.

They have proposed the use of direct numerical integrations of the line integrals by an integration quadrature (e.g. Simpson rule or Gaussian quadrature), illustrating the numerical consistency and accuracy for a linear doublet distribution on a quadrilateral panel. However when a field point is very close to the sides or vertices of a panel, a large number of the quadrature base points and considerable effort to choose these points suitably would be needed in order to achieve good comparisons with the known values. Such numerical implementation in a computer code may lead to a large amount of extra-computer time. Any attempt for finding closed form expressions of the line integrals for a polygon panel does not appear in their study.

Suh (1992a) [6] obtained, as an extension of Cantaloube & Rehbach's work (with some corrections in sign), the closed-forms for computing the induced potentials and velocities due to constant and/or linear distributions of the singularities. He expressed them as a sum of contribution from each side of the

[5]Cantaloube, B. and Rehbach, C. (1986), "Calcul des Integrales de la Methode des Singularites," *Recherche Aerospatiale*, n° 1, pp. 15–22, English Title: "Calculation of the Integrals of the Singularity Method," *Aerospace Research*, no. 1, pp. 15–22.

[6]Suh, J. C. (1992a), "Analytical evaluation of the surface integral in the singularity methods," *Trans. Soc. Naval Arch. Korea*, vol. 29, no. 1, pp. 1–17.

panel, in terms of appropriate basic integrals.

As an another extension but by a different approach the present section deals with a *bilinear* distribution over *a planar polygonal panel*. In numerical implementation of the potential-based panel method for solving the potential flow around a lifting body, the trailing wake sheet is represented approximately as the doublet distribution of potential jump. One possible way to include the effect of the local variation of these doublet strengths is with the use of a bilinear distribution over each wake panel (which is uniquely determined from imposed potential jump values at its four vertices). The use of the bilinear distribution over quadrilateral panels (or the linear distribution over triangular panels) eliminates the discontinuity problem for the piecewise constant distribution. Then the singularity strength will be chosen to vary bilinearly (or linearly) across the panel. The main scope of this section is therefore to derive explicit and elegant closed-forms of the induced potential and velocity due to a bilinear distribution. The bilinear distribution case includes, of course, both the constant and the linear distribution cases.

In order to transform the associated surface integrals into line integrals along contour of the panel by using Stokes' formulas, alternative forms of the associated integrands for the bilinear distribution of sources and doublets over a planar panel are presented. For a planar polygon panel, the derived line integrals can be reduced to closed-form expressions for the potential and velocity. The closed-form expressions of the line integrals for the induced potential and velocity are presented. They are expressed compactly as a sum of contribution from each side of the panel, in terms of appropriate basic integrals. It will be shown that each contribution depends on the relative position of a field point from the side.

B.1.2   Stokes' theorem

The general form of Stokes' formulae is

$$\int_S (d\underline{S} \times \nabla) X = \int_C d\underline{l}\, X \tag{B.3}$$

where S is the surface enclosed by a curve C, $d\underline{S} \equiv \underline{n}\, dS$ is the oriented surface element and $d\underline{l} \equiv \underline{t}\, dl$ is the integration element along the curve C. X is a scalar or vector function of space coordinates.

If we choose X as scalar f, then it becomes

$$\int_S \underline{n} \times \nabla f \, dS = \oint_C f \, d\underline{l}. \tag{B.4}$$

Identifying X as vector $\underline{f}$ reduces it to

$$\int_S (d\underline{S} \times \nabla) \cdot \underline{f} = \oint_C \underline{f} \cdot d\underline{l}, \tag{B.5}$$

or vector transformation of the first part gives

$$\int_S (\nabla \times \underline{f}) \cdot d\underline{S} = \oint_C \underline{f} \cdot d\underline{l}. \tag{B.6}$$

B.1.3   Basic vector operations

For the purpose of derivations of some relations, often-used vector expansion formulas are presented as follows.

$$\underline{a} \cdot (\underline{b} \times \underline{c}) = \underline{b} \cdot (\underline{c} \times \underline{a}) = \underline{c} \cdot (\underline{a} \times \underline{b}) \tag{B.7}$$

$$\underline{a} \times (\underline{b} \times \underline{c}) = \underline{b}\, (\underline{a} \cdot \underline{c}) - \underline{c}\, (\underline{a} \cdot \underline{b}) \tag{B.8}$$

$$\nabla \times (\underline{a} \times \underline{b}) = \underline{a}\, (\nabla \cdot \underline{b}) + (\underline{b} \cdot \nabla)\, \underline{a} - \underline{b}\, (\nabla \cdot \underline{a})\, (\underline{a} \cdot \nabla)\, \underline{b} \tag{B.9}$$

$$\nabla(\underline{a} \cdot \underline{b}) = (\underline{a} \cdot \nabla)\, \underline{b} + (\underline{b} \cdot \nabla)\, \underline{a} + \underline{a} \times (\nabla \times \underline{b}) + \underline{b} \times (\nabla \times \underline{a}) \tag{B.10}$$

$$\nabla \cdot (\phi\, \underline{a}) = \underline{a} \cdot \nabla\phi + \phi\, \nabla \cdot \underline{a} \tag{B.11}$$

$$\nabla \times (\phi\, \underline{a}) = (\nabla\phi) \times \underline{a} + \phi\, \nabla \times \underline{a} \tag{B.12}$$

$$\nabla r = \frac{\underline{r}}{r} \tag{B.13}$$

$$\nabla \left(\frac{1}{r}\right) = \frac{-\underline{r}}{r^3} \tag{B.14}$$

$$\nabla \cdot \underline{r} = 3 \tag{B.15}$$

$$\nabla \times \underline{r} = 0 \tag{B.16}$$

B.2   Induced Potential Due to Source Distribution

The potential and velocity induced by surface distribution of source density σ over the surface S are

$$\phi = -\frac{1}{4\pi} \int_S \frac{\sigma}{r} \, dS_\xi \tag{B.17}$$

with $\underline{r} = \underline{x}_\xi - \underline{x}_p$, $r \equiv |\underline{r}|$.

For the indices of variables of differentiation and integration, the reciprocal relation holds: $\nabla_p(\frac{1}{r}) = -\nabla(\frac{1}{r})$. For the integration variable $\underline{x}_\xi$, the distribution surface S is represented hypothetically as collection of planar surfaces. Then $\underline{n}$ is independent of $\underline{x}_\xi$. Equation (B.17) for the potential is reduced to,

$$
\phi = -\frac{1}{4\pi} \left[\int_S \underline{n} \cdot \left\{ \nabla \times \left(\sigma \underline{n} \times \frac{\underline{r}}{r} \right) \right\} dS + \int_S (\underline{n} \cdot \underline{r}) \left\{ (\sigma \underline{n}) \cdot \nabla \left(\frac{1}{r} \right) \right\} dS \right.
$$
$$
\left. - \int_S \underline{n} \cdot \left\{ \nabla \sigma \times \left(\underline{n} \times \frac{\underline{r}}{r} \right) \right\} dS \right] \tag{B.18}
$$

<u>Proof of Eq. (B.18)</u>

The detailed derivation is performed reversely from Eq. (B.18) into Eq. (B.17) as follows:

(1) The integrand of the first surface integral becomes

$$
\begin{aligned}
I_1 &= \underline{n} \cdot \nabla \times \left(\sigma \underline{n} \times \frac{\underline{r}}{r} \right) \quad : \text{using Eq. (B.9)} \\
&= \underline{n} \cdot \left[\sigma \underline{n} \left\{ \nabla \cdot \left(\frac{\underline{r}}{r} \right) \right\} + \left(\frac{\underline{r}}{r} \cdot \nabla \right) (\sigma \underline{n}) - \frac{\underline{r}}{r} \left\{ \nabla \cdot (\sigma \underline{n}) \right\} - (\sigma \underline{n} \cdot \nabla) \frac{\underline{r}}{r} \right] \\
&= \underline{n} \cdot \left[\sigma \underline{n} \left\{ \underline{r} \cdot \nabla \left(\frac{1}{r} \right) + \frac{1}{r} \nabla \cdot \underline{r} \right\} \quad : \text{using Eq. (B.9)} \right. \\
&\quad \left. + \underline{n} \left(\frac{\underline{r}}{r} \cdot \nabla \sigma \right) - \frac{\underline{r}}{r} (\underline{n} \cdot \nabla \sigma) - (\sigma \underline{n} \cdot \nabla) \frac{\underline{r}}{r} \right] \quad : \text{since } \underline{n} \text{ is constant}
\end{aligned}
$$
$$\tag{B.19}$$

Here the last term is rearranged by tensor operation,

$$
\begin{aligned}
\underline{n} \cdot (\sigma \, \underline{n} \cdot \nabla) \frac{\underline{r}}{r} &= n_i \left\{ \sigma \, n_j \frac{\partial}{\partial \xi_j} \left(\frac{\xi_i - x_i}{r} \right) \right\} \\
&= n_i \frac{1}{r} \sigma \, n_j \frac{\partial}{\partial \xi_j} (\xi_i - x_i) + n_i \, (\xi_i - x_i) \, \sigma \, n_j \frac{\partial}{\partial \xi_j} \left(\frac{1}{r} \right) \\
&= n_i \frac{1}{r} \sigma \, n_j \, \delta_{ij} + n_i \, (\xi_i - x_i) \, \sigma \, n_j \frac{-(\xi_j - x_j)}{r^3} \\
&= \frac{\sigma}{r} - \frac{\sigma \, (\underline{n} \cdot \underline{r})^2}{r^3} \qquad\qquad\qquad\qquad\qquad \text{(B.20)}
\end{aligned}
$$

Then,

$$
I_1 = \frac{2}{r} \sigma + \frac{\underline{r}}{r} \cdot \nabla \sigma - \frac{(\underline{n} \cdot \underline{r})}{r} (\underline{n} \cdot \nabla \sigma) - \frac{\sigma}{r} + \frac{\sigma (\underline{n} \cdot \underline{r})^2}{r^3} \qquad \text{(B.21)}
$$

(2) The integrand of the second surface integral in Eq. (B.18) becomes:

$$
\begin{aligned}
I_2 &= (\underline{n} \cdot \underline{r}) \left\{ \sigma \, \underline{n} \cdot \nabla \left(\frac{1}{r} \right) \right\} = (\underline{n} \cdot \underline{r}) \left\{ \sigma \, \underline{n} \cdot \left(\frac{-\underline{r}}{r^3} \right) \right\} \quad : \text{using Eq. (B.14)} \\
&= -\frac{\sigma \, (\underline{n} \cdot \underline{r})^2}{r^3} \qquad\qquad\qquad\qquad\qquad\qquad\qquad\qquad \text{(B.22)}
\end{aligned}
$$

(3) The use of Eq. (B.8) reduces the integrand of the third surface integral to

$$
\begin{aligned}
I_3 &= \underline{n} \cdot \left\{ \nabla \sigma \times \left(\underline{n} \times \frac{\underline{r}}{r} \right) \right\} \\
&= \underline{n} \cdot \left\{ \underline{n} \left(\nabla \cdot \frac{\underline{r}}{r} \right) - \frac{\underline{r}}{r} (\nabla \sigma \cdot \underline{n}) \right\} \\
&= \nabla \sigma \cdot \frac{\underline{r}}{r} - \frac{\underline{n} \cdot \underline{r}}{r} (\nabla \sigma \cdot \underline{n}) \qquad\qquad\qquad \text{(B.23)}
\end{aligned}
$$

Therefore by combining the three items above, Eq. (B.18) can be reduced to Eq. (B.17):

$$
\begin{aligned}
\phi &= -\frac{1}{4\pi} \int_S (I_1 + I_2 - I_3)\, dS \\
&= -\frac{1}{4\pi} \int_S \left\{ \frac{\sigma}{r} + \frac{\underline{r}}{r} \cdot \nabla\sigma - \frac{(\underline{n}\cdot\underline{r})}{r}(\underline{n}\cdot\nabla\sigma) + \frac{\sigma(\underline{n}\cdot\underline{r})^2}{r^3} \right. \\
&\quad\left. -\frac{\sigma(\underline{n}\cdot\underline{r})^2}{r^3} - \nabla\sigma\cdot\frac{\underline{r}}{r} + \frac{(\underline{n}\cdot\underline{r})}{r}(\nabla\sigma\cdot\underline{n}) \right\} dS \\
&= -\frac{1}{4\pi} \int_S \frac{\sigma}{r}\, dS
\end{aligned}
\tag{B.24}
$$

∎∎∎

B.2.1 Transformation of Eq. (B.18) into line integrals

Now the surface integrals of Eq. (B.18) can be transformed as follows:

(1) The first one becomes, using Eq. (B.5)

$$
\begin{aligned}
\int_S \underline{n} \cdot \left\{ \nabla \times \left(\sigma\,\underline{n} \times \frac{\underline{r}}{r} \right) \right\} dS &= \oint_C \sigma\left(\frac{\underline{n}\times\underline{r}}{r} \right) \cdot d\underline{l} \\
&= \underline{n} \cdot \oint_C \sigma\,\frac{\underline{r}\times d\underline{l}}{r}
\end{aligned}
\tag{B.25}
$$

(2) For the second one, let us introduce the relation [7]

$$
\nabla\left(\frac{1}{r} \right) = -\nabla \times \underline{A}
\tag{B.26}
$$

with

$$
\underline{A} = \frac{\underline{e}\times\underline{r}}{r\,(r + \underline{e}\cdot\underline{r})}
\tag{B.27}
$$

where $\underline{e}$ is a unit vector, being a function of $\underline{x}_p$, chosen such that the de-

---

[7] Proof is given below and see also Guiraud, J. P. (1978), "Potential of velocities generated by a localized vortex distribution," *Aerospace Research*, English Translation-ESA-TT-560, pp. 105–107.

nominator is not zero, and use the vector operation

$$\sigma \, \nabla \left(\frac{1}{r} \right) = -\sigma \, \nabla \times \underline{A} = -\nabla \times (\sigma \, \underline{A}) - \underline{A} \times \nabla \sigma. \tag{B.28}$$

Then, by Eq. (B.5)

$$
\begin{aligned}
& \int_S (\underline{n} \cdot \underline{r}) \left\{ (\sigma \, \underline{n}) \cdot \nabla \left(\frac{1}{r} \right) \right\} dS \\
& = \int_S (\underline{n} \cdot \underline{r}) \, \underline{n} \cdot \{ -\nabla \times (\sigma \, \underline{A}) - \underline{A} \times \nabla \sigma \} \, dS \\
& = -(\underline{n} \cdot \underline{r}) \oint_C \sigma \, \underline{A} \cdot dl + (\underline{n} \cdot \underline{r}) \, \underline{n} \cdot \int_S \nabla \sigma \times \underline{A} \, dS \tag{B.29}
\end{aligned}
$$

(3) The third integral becomes

$$-\int_S \underline{n} \cdot \left\{ \nabla \sigma \times \left(\underline{n} \times \frac{\underline{r}}{r} \right) \right\} dS = -\int_S \underline{n} \cdot \{ \nabla \sigma \times (\underline{n} \times \nabla r) \} \, dS. \tag{B.30}$$

Consequently, the expression (B.18) is replaced by

$$
\begin{aligned}
\phi = \ & -\frac{\underline{n}}{4\pi} \cdot \left\{ \oint_C \sigma \frac{\underline{r}}{r} \times d\underline{l} - \underline{r} \oint_C \sigma \, \underline{A} \cdot d\underline{l} + (\underline{n} \cdot \underline{r}) \int_S \nabla \sigma \times \underline{A} \, dS \right. \\
& \left. - \int_S \nabla \sigma \times (\underline{n} \times \nabla r) \, dS \right\} \tag{B.31}
\end{aligned}
$$

Now the double integral in Eq. (B.31) can be transformed into contour integral if we suppose $\nabla \sigma$ to be constant over S and if we choose $\underline{e} = \pm \underline{n}$:

$$
\begin{aligned}
\phi = \ & -\frac{1}{4\pi} \left[\underline{n} \cdot \oint_C \sigma \frac{\underline{r}}{r} \times d\underline{l} - (\underline{n} \cdot \underline{r}) \oint_C \sigma \, \underline{A} \cdot d\underline{l} \right. \\
& + (\underline{n} \cdot \underline{r}) \, (\underline{n} \cdot \underline{e}) \, \underline{n} \cdot \left\{ \nabla \sigma \times \oint_C \ln(r + \underline{e} \cdot \underline{r}) d\underline{l} \right\} \\
& \left. - \underline{n} \cdot \left(\nabla \sigma \times \oint_C r \, d\underline{l} \right) \right] \tag{B.32}
\end{aligned}
$$

For this transformation taking account of Eq. (B.4), another form for the vector function $\underline{A}$, has been used $\underline{A} = \underline{e} \times \nabla R$ with $R = \ln(r + \underline{e} \cdot \underline{r})$. Namely the

second integral in Eq. (B.31) can be written as, with $\nabla \sigma = \text{const.}$ and $\underline{e} = \pm \underline{n}$,

$$
\begin{aligned}
(\underline{n} \cdot \underline{r}) \int_S \nabla \sigma \times \underline{A} \, dS &= (\underline{n} \cdot \underline{r}) \nabla \sigma \times \int_S (\underline{n} \cdot \underline{e}) \, (\underline{n} \times \nabla R) \, dS \\
&= (\underline{n} \cdot \underline{r}) \, (\underline{n} \cdot \underline{e}) \nabla \sigma \times \oint_C \ln(r + \underline{e} \cdot \underline{r}) \, d\underline{l} \quad \text{(B.33)}
\end{aligned}
$$

Accordingly, the following relation holds for $\underline{e} = \pm \underline{n}$,

$$
\int_S \underline{A} \, dS = (\underline{n} \cdot \underline{e}) \oint_C \ln(r + \underline{e} \cdot \underline{r}) \, d\underline{l}. \tag{B.34}
$$

Proof of Eq (B.26)

Now let's prove Eq. (B.26) by showing that the right-hand side reduces to the left hand side. For simplicity, dropping out the subscript ξ of the operator ∇,

$$
\begin{aligned}
\nabla \times \underline{A} &= \nabla \times \left\{ \frac{1}{r(r + \underline{e} \cdot \underline{r})} (\underline{e} \times \underline{r}) \right\} \\
&= \nabla \left\{ \frac{1}{r(r + \underline{e} \cdot \underline{r})} \right\} \times (\underline{e} \times \underline{r}) + \frac{1}{r(r + \underline{e} \cdot \underline{r})} \nabla \times (\underline{e} \times \underline{r}) \quad : \text{using (B.12)} \\
&= \frac{-\nabla \{r(r + \underline{e} \cdot \underline{r})\}}{r^2(r + \underline{e} \cdot \underline{r})^2} \times (\underline{e} \times \underline{r}) + \frac{1}{r(r + \underline{e} \cdot \underline{r})} \nabla \times (\underline{e} \times \underline{r}) \quad \text{(B.35)}
\end{aligned}
$$

Knowing that $\underline{e}$ is chosen as a function of $\underline{x}_p$, independent of $\underline{x}_\xi$ and using (B.10), (B.13) and (B.16),

$$
\begin{aligned}
\nabla \{r(r + \underline{e} \cdot \underline{r})\} &= (r + \underline{e} \cdot \underline{r}) \nabla r + r \nabla (r + \underline{e} \cdot \underline{r}) \\
&= (r + \underline{e} \cdot \underline{r}) \frac{\underline{r}}{r} + r \left\{ \frac{\underline{r}}{r} + (\underline{e} \cdot \nabla)\underline{r} + (\underline{r} \cdot \nabla)\underline{e} + \underline{e} \times (\nabla \times \underline{r}) + \underline{r} \times (\nabla \times \underline{e}) \right\} \\
&= \left(2 + \frac{\underline{e} \cdot \underline{r}}{r} \right) \underline{r} + r\underline{e} \quad \text{(B.36)}
\end{aligned}
$$

Recall that the following relation is used while deriving the above expression:

$$
(\underline{e} \cdot \nabla) \underline{r} = e_i \frac{\partial x_j}{\partial x_i} = e_i \, \delta_{ij} = e_j = \underline{e}. \tag{B.37}
$$

Then use Eq. (B.8) for the triple vector product

$$
\begin{aligned}
&\nabla \left\{ r(r + \underline{e} \cdot \underline{r}) \right\} \times (\underline{e} \times \underline{r}) \\
={}& \left(2 + \frac{\underline{e} \cdot \underline{r}}{r} \right) \left\{ r^2 \underline{e} - \underline{r}(\underline{e} \cdot \underline{r}) \right\} + r \left\{ (\underline{e} \cdot \underline{r})\underline{e} - \underline{r} \right\} \\
={}& \left\{ 2r^2 + 2r(\underline{e} \cdot \underline{r}) \right\} \underline{e} - \left\{ \left(2 + \frac{\underline{e} \cdot \underline{r}}{r} \right)(\underline{e} \cdot \underline{r}) + r \right\} \underline{r} \\
={}& 2r \left\{ r + (\underline{e} \cdot \underline{r}) \right\} \underline{e} - \left\{ r + (\underline{e} \cdot \underline{r}) \right\}^2 \frac{\underline{r}}{r} \qquad \text{(B.38)}
\end{aligned}
$$

Therefore, one can derive Eq. (B.26):

$$
\begin{aligned}
\nabla \times \underline{A} ={}& -\frac{2\underline{e}}{r(r + \underline{e} \cdot \underline{r})} + \frac{\underline{r}}{r^3} \\
&+ \frac{1}{r(r + \underline{e} \cdot \underline{r})} \left\{ \underline{e}(\nabla \cdot \underline{r}) + (\underline{r} \cdot \nabla)\underline{e} - \underline{r}(\nabla \cdot \underline{e}) - (\underline{e} \cdot \nabla)\underline{r} \right\} \\
={}& -\frac{2\underline{e}}{r(r + \underline{e} \cdot \underline{r})} + \frac{\underline{r}}{r^3} + \frac{1}{r(r + \underline{e} \cdot \underline{r})}(3\underline{e} - \underline{e}) \\
={}& \frac{\underline{r}}{r^3} = -\nabla \left(\frac{1}{r} \right) \qquad \text{(B.39)}
\end{aligned}
$$

Remark: The vector $\underline{A}$ is evidently related to an explicit expression for the velocity potential for the volumetric distribution of vorticity. We define the solid angle ψ_p subtended at a point $\underline{x}_p$ by the surface S (is not necessarily a plane) (Milne-Thomson (1968)):

$$
\begin{aligned}
\psi_p ={}& \int_S \underline{n} \cdot \nabla \left(\frac{1}{r} \right) dS \\
={}& -\oint_C \frac{\underline{e} \times \underline{r}}{r(r + \underline{e} \cdot \underline{r})} \cdot d\underline{l} \qquad \text{(B.40)}
\end{aligned}
$$

■■■

B.3   Induced Velocity Due to Source Distribution

Expression for the velocity induced by the sources distribution is given by

$$\underline{q} = \nabla_p \phi = \frac{1}{4\pi} \int_S \sigma \, \nabla \left(\frac{1}{r} \right) \, dS_\xi \qquad \text{(B.41)}$$

Equation (B.41)) is transformed into, applying the triple vector product (Eq. (B.9)) to $\underline{n} \times \left\{ \underline{n} \times \nabla \left(\frac{1}{r} \right) \right\}$,

$$\underline{V}_p = \frac{1}{4\pi} \left[\int_S \sigma \left\{ \underline{n} \cdot \nabla \left(\frac{1}{r} \right) \right\} \underline{n} \, dS - \int_S \sigma \, \underline{n} \times \left\{ \underline{n} \times \nabla \left(\frac{1}{r} \right) \right\} \, dS \right].$$
$$\text{(B.42)}$$

For the first surface integral, use Eq. (B.28)

$$\int_S \sigma \left\{ \underline{n} \cdot \nabla \left(\frac{1}{r} \right) \right\} \underline{n} \, dS = - \int_S \left[\underline{n} \cdot \left\{ \nabla \times (\sigma \, \underline{A}) \right\} \underline{n} + \left\{ \underline{n} \cdot (\underline{A} \times \nabla \sigma) \right\} \underline{n} \right] \, dS$$
$$\text{(B.43)}$$

and then apply Eq. (B.6) for a plane surface S

$$- \underline{n} \oint_C \sigma \, \underline{A} \cdot d\underline{l} - \underline{n} \int_S \left\{ \underline{n} \cdot (\underline{A} \times \nabla \sigma) \right\} \, dS. \qquad \text{(B.44)}$$

The second surface integral of Eq. (B.42) is decomposed into two parts:

$$- \int_S \sigma \, \underline{n} \times \left\{ \underline{n} \times \nabla \left(\frac{1}{r} \right) \right\} \, dS \; = \; - \int_S \underline{n} \times \left\{ \underline{n} \times \nabla \left(\frac{\sigma}{r} \right) \right\} \, dS$$
$$+ \int_S \frac{\underline{n}}{r} \times (\underline{n} \times \nabla \sigma) \, dS. \qquad \text{(B.45)}$$

For the plane S, apply Eq. (B.6) for the first part to yield:

$$- \underline{n} \times \oint_C \frac{\sigma}{r} \, d\underline{l} + \int_S \frac{\underline{n}}{r} \times (\underline{n} \times \nabla) \, dS \qquad \text{(B.46)}$$

Either Eq. (B.41) or Eq. (B.42) is replaced by

$$q = \frac{1}{4\pi} \left\{ -\underline{n} \oint_C \sigma \underline{A} \cdot d\underline{l} - \underline{n} \times \oint_C \frac{\sigma}{r} d\underline{l} \right.$$
$$\left. - \underline{n} \int_S \underline{n} \cdot (\underline{A} \times \nabla\sigma) \, dS + \int_S \frac{\underline{n}}{r} \times (\underline{n} \times \nabla\sigma) \, dS \right\} \quad \text{(B.47)}$$

The two surface integrals can be simplified if we suppose $\nabla\sigma$ constant over S and if we pretend $\underline{e} = \pm\underline{n}$. The first one becomes, by Eq. (B.34):

$$- \underline{n} \int_S \underline{n} \cdot (\underline{A} \times \nabla\sigma) \, dS = -\underline{n} (\nabla\sigma \times \underline{n}) \cdot \int_S \underline{A} \, dS \quad : \text{using (B.7)}$$
$$= -\underline{n} (\underline{n} \cdot \underline{e}) (\nabla\sigma \times \underline{n}) \cdot \oint_C \ln(r + \underline{e} \cdot \underline{r}) \, d\underline{l}$$
$$\text{(B.48)}$$

and the second one becomes, using Eq. (B.8) and the fact that $\underline{n} \cdot \nabla\sigma = 0$ over S,

$$\int_S \frac{\underline{n}}{r} \times (\underline{n} \times \nabla\sigma) \, dS = \{\underline{n} (\underline{n} \cdot \nabla\sigma) - \nabla\sigma (\underline{n} \cdot \underline{n})\} \int_S \frac{1}{r} \, dS$$
$$= -\nabla\sigma \int_S \frac{1}{r} \, dS \quad \text{(B.49)}$$

Now applying Eqs. (B.17) and (B.31) for the case of $\sigma = $ const., it becomes

$$-\nabla\sigma \left\{ \underline{n} \cdot \oint_C \frac{\underline{r} \times d\underline{l}}{r} - (\underline{n} \cdot \underline{r}) \oint_C \underline{A} \cdot d\underline{l} \right\} \quad \text{(B.50)}$$

Therefore, the final result is

$$q = -\frac{1}{4\pi} \left[\underline{n} \oint_C \sigma \underline{A} \cdot d\underline{l} + \underline{n} \times \oint_C \frac{\sigma}{r} d\underline{l} \right.$$
$$- \underline{n}(\underline{n} \cdot \underline{e})(\underline{n} \times \nabla\sigma) \cdot \oint_C \ln(r + \underline{e} \cdot \underline{r}) \, d\underline{l}$$
$$\left. + \nabla\sigma \left\{ \underline{n} \cdot \oint_C \frac{\underline{r} \times d\underline{l}}{r} - (\underline{n} \cdot \underline{r}) \oint_C \underline{A} \cdot d\underline{l} \right\} \right] \quad \text{(B.51)}$$

B.4   Induced Potential Due to Doublet Distribution

The potential induced by a surface distribution of doublets with density $\mu(\equiv -\phi)$ is written as

$$\phi = -\frac{1}{4\pi} \int_S \mu\, \underline{n} \cdot \nabla \left(\frac{1}{r} \right) dS \tag{B.52}$$

A variation for expression of doublet-potential (B.52), using Eq. (B.26) and the relation $\nabla \times (\mu\, \underline{A}) = \mu \nabla \times \underline{A} - \underline{A} \times \nabla \mu$ by Eq. (B.12), can be performed:

$$
\begin{aligned}
\mu\, \underline{n} \cdot \nabla \left(\frac{1}{r} \right) &= \mu\, \underline{n} \cdot (-\nabla \times \underline{A}) \\
&= -\underline{n} \cdot \mu \nabla \times \underline{A} = -\underline{n} \cdot \nabla \times (\mu\, \underline{A}) - \underline{n} \cdot (\underline{A} \times \nabla \mu) \\
&= -\underline{n} \cdot \nabla \times (\mu\, \underline{A}) + (\underline{n} \times \nabla \mu) \cdot \underline{A}
\end{aligned} \tag{B.53}
$$

Consequently,

$$\phi = -\frac{1}{4\pi} \left[-\int_S \underline{n} \cdot \{ \nabla \times (\mu\, \underline{A}) \}\, dS + \int_S (\underline{n} \times \nabla \mu) \cdot \underline{A}\, dS \right] \tag{B.54}$$

becomes, with transformation of the first surface integral by Eq. (B.6),

$$\phi = -\frac{1}{4\pi} \left\{ -\oint_C \mu\, \underline{A} \cdot d\underline{l} + \int_S (\underline{n} \times \nabla \mu) \cdot \underline{A}\, dS \right\}. \tag{B.55}$$

For constant $\nabla \mu$ over a plane surface S and $\underline{e} = \pm \underline{n}$, the surface integral is transformed into the contour integral (by Eq. (B.34)).

$$\phi = -\frac{1}{4\pi} \left\{ -\oint_C \mu\, \underline{A} \cdot d\underline{l} + (\underline{n} \cdot \underline{e})\, (\underline{n} \times \nabla \mu) \cdot \oint_C \ln(r + \underline{e} \cdot \underline{r})\, d\underline{l} \right\}. \tag{B.56}$$

B.5   Induced Velocity Due to Doublet Distribution

Differentiation of Eq. (B.52) with respect to $\underline{x}_p$ yields

$$\underline{q} = -\frac{1}{4\pi} \int_S \mu \nabla_p \left\{ \underline{n} \cdot \nabla \left(\frac{1}{r} \right) \right\} dS \tag{B.57}$$

or, alternatively by using a lengthy transformation (see Lee, J. T. (1987) and Brockett (1988))

$$
\underline{q} = -\frac{1}{4\pi} \left\{ \oint_C \mu \nabla \left(\frac{1}{r} \right) \times d\underline{l} + \int_S (\underline{n} \times \nabla \mu) \times \nabla \left(\frac{1}{r} \right) dS \right\} \tag{B.58}
$$

In this form showing the correspondence presented by Hess (1969) for the first part, the velocity can be considered as one induced by two distributions of vorticity:

(1) a first due to a concentrated vorticity $\mu \, d\underline{l}$ over the contour C of the surface cap S, and

(2) a second due to a surface distribution of vorticity density, $\underline{\gamma} \equiv \underline{n} \times \nabla \mu$ over S.

Surface integral, one component of expression (Eq. (B.58)) for the velocity induced by the doublet distribution is transformed to, with the identity (B.8) applied on scalar $\frac{1}{r}$:

$$
\int_S \underline{\gamma} \times \nabla \left(\frac{1}{r} \right) dS = \int_S \underline{\gamma} \times \left[\underline{n} \left\{ \underline{n} \cdot \nabla \left(\frac{1}{r} \right) \right\} \right] dS
$$
$$
- \int_S \underline{\gamma} \times \left[\underline{n} \times \left\{ \underline{n} \times \nabla \left(\frac{1}{r} \right) \right\} \right] dS. \tag{B.59}
$$

For constant γ for a plane surface S, the first integral is reduced to, by Eqs. (B.6) and (B.26)

$$
\int_S \underline{\gamma} \times \left[\underline{n} \left\{ \underline{n} \cdot \nabla \left(\frac{1}{r} \right) \right\} \right] dS = \int_S \underline{\gamma} \times [\underline{n} \{ \underline{n} \cdot (-\nabla \times \underline{A}) \}] \, dS
$$
$$
= -\underline{\gamma} \times \underline{n} \oint_C \underline{A} \cdot d\underline{l} = -(\underline{n} \times \nabla \mu) \times \underline{n} \oint_C \underline{A} \cdot d\underline{l}
$$
$$
= \{ \underline{n} \, (\underline{n} \cdot \nabla \mu) - \nabla \mu \} \oint_C \underline{A} \cdot d\underline{l} = -\nabla \mu \oint_C \underline{A} \cdot d\underline{l}, \tag{B.60}
$$

and the second one becomes, by Eq. (B.5)

$$-\int_S \underline{\gamma} \times \left[\underline{n} \times \left\{ \underline{n} \times \nabla \left(\frac{1}{r} \right) \right\} \right] dS = -\underline{\gamma} \times \left(\underline{n} \times \oint_C \frac{d\underline{l}}{r} \right). \qquad \text{(B.61)}$$

The first expression represents a velocity component tangent to S and the second one a velocity component normal to S.

The velocity induced by a doublet distribution characterized by constant $\nabla \mu$ over a plane surface S is written as

$$
\begin{aligned}
\underline{q} \;=\; & -\frac{1}{4\pi} \left\{ \oint_C \mu \nabla \left(\frac{1}{r} \right) \times d\underline{l} - \nabla \mu \oint_C \underline{A} \cdot d\underline{l} \right. \\
& \left. - (\underline{n} \times \nabla \mu) \times \left(\underline{n} \times \oint_C \frac{d\underline{l}}{r} \right) \right\}. \qquad \text{(B.62)}
\end{aligned}
$$

C

CODE *PRpan* FOR PANEL METHOS

C.1   Introduction

PRpan code provides the calculation of potential and velocity induced by source and doublet distribution on a planar polygon element with linearly varying density.

As input arguments, the number of sides and vertex positions for specifying the element geometry are needed. The source and doublet strengths should be entered. Note that the doublet strength is defined as the negative value of potential: $\mu = -\phi$.

The number of sides is at least 3 and the vertex positions are specified as a pair of x, y, z coordinates. Multiple field points can be entered in a form of (x_p, y_p, z_p) to avoid duplicate calculations for each side of the element when calculating the influence coefficients in the panel method. By assuming that any combination of 3 points among the vertices form a unique planar element, the vector outward normal to the element surface is calculated by cross-product of two vectors connected between the first, the second and the third vertex points.

C.2   Program Lists of Subroutine *PRpan*

```
C------------------- Subroutine PRpan.ftn ----------------------------
C                                                                     |
C      PRpan code provides the calculation of potenial and velocity   |
C      induced by source and doublet distributions with constant plus |
C      linear variation on a planar polygon element, by following the |
C      formulation of Cantaloube and Rehbach ~(1986) and performing the |
C      analytic evaluations of the associated line integrals          |
C      (Suh ~(1990)).                                                 |
C      Before this subroutine is called, the subroutine PRgeom should |
C      be called to generate the geometric parameters of the element  |
C      associated with the analytic evaluations of the line integrals. |
C                                                                     |
C      REFERENCES:                                                     |
C       [1] Cantaloube, B. and Rehbach, C. ~(1986)                    |
C          " Calcul des Integrales de la Methode des Singularites"    |
C            Recherche Aerospatiale, no. 1, pp. 15-22,                 |
C             (English Title: " Calculation of the Integrals of the   |
C             Singularity Method" Aerospace Research, No. 1, pp. 15-22) |
C       [2] Suh, J. C. ~(1990)                                        |
C          " Review of the Paper; Calculation of the Integrals of the |
C             Singularity Method by Cantaloube and Rehbach"           |
C             KRISO Propulsor Technology Laboratory Report, 22-90     |
C       [3] Suh, J. C. ~(1990)                                        |
C          " Analytic Evaluations of the Induction-Integrals for      |
C             Distributions of Sources and Doublets over a Planar     |
C             Polygon Element"                                         |
C             KRISO Propulsor Technology Laboratory Report, 23-90     |
C       [4] Lee, C.-S. ~(1990)                                        |
C          " Treatment of non-planar panel"                           |
```

```
C              Technical Notes (unpublished), 11/29/90          |
C                                                               |
C      Note: The doublet strength is defined as a negative value of  |
C            potential here.                                    |
C                                                               |
C      Programmer: Suh, Jung-Chun                               |
C       Dept. Naval Architecture and Ocean Engineering,         |
C       Seoul National University                               |
C      (Copyright:Korea Research Institute of Ships & Ocean Engineering) |
C                                                               |
C      Version 1.0, December 15, 1990                           |
C      Version 1.1, December 27, 1990                           |
C      Version 1.2, January   3, 1991                           |
C                                                               |
C      Input argument descriptions:                             |
C       NSIDE            = number of sides of a planar element   |
C                          (at least 3)                          |
C       XV(i,N)          = x-, y- and z-coordinates of the       |
C                          NSIDE vertices of the element         |
C                          (two-dimensional arrayed values in a  |
C                           counterclockwise order).             |
C       NFP              = number of field points at which the induced |
C                          potentials and velocities are calculated.  |
C       XFP(i,n)         = x-, y- and z-coordinates of the NFP field   |
C                          points (two-dimensional arrayed values).    |
C       ISELF(n)         = choice of location of each field point to   |
C                          specify a self-induction case         |
C                          (NFP arrayed values).                 |
C                          (If it is just    on surface,    ISELF(n)=+1 |
C                           If it is exactly at surface,    ISELF(n)= 0 |
C                           If it is just    below surface, ISELF(n)=-1 |
C                           If it is away from surface, ISELF(n)=others)|
C       SEGL(N)          = lengths of the NSIDE respective sides, |
C                          computed by the subroutine PRGEOM      |
C                          (NSIDE arrayed values).               |
C       AN(i)            = x-, y- and z-components of the unit outward |
C                          normal vector of the planar element,  |
C                          computed by the subroutine PRGEOM      |
C                          (3 arrayed values).                   |
C       EL(i,N)          = x-, y- and z-components of the unit    |
C                          orientation vector of the NSIDE respective |
C                          sides, computed by the subroutine PRGEOM    |
C                          (two-dimensional arrayed values).     |
```

```
C       EM(i,N)              = x-, y- and z-components of the unit      |
C                              vector lying on the plane and normal to the |
C                              NSIDE respective sides,computed by the    |
C                              subroutine PRGEOM                         |
C                              (two-dimensional arrayed values).         |
C       CG(i)                = x-, y- and z- coordinates of the centroid |
C                              of the element, computed by the subroutine |
C                              PRGEOM (3 arrayed values).                |
C       AREA                 = surface area of the element, computed by the |
C                              subroutine PRGEOM.                        |
C       DIAGNL               = longest diagonal of the element, computed by |
C                              the subroutine PRGEOM.                    |
C       RFAR                 = reference ratio of field-point distance to  |
C                              longest diagonal to apply far-field       |
C                              approximation.                            |
C       ICOMP                = choices of selected calculations         |
C                              (ICOMP=1: only potential calculations;    |
C                               ICOMP=2: only velocity calculations;     |
C                               ICOMP=3: both potential and velocity calc.) |
C       SIGMAX,SIGMAY,       = coefficients to specify the linear variation |
C       SIGMAZ,SIGMA0          of source distribution as                |
C                              sigma=SIGMAX*x+SIGMAY*y+SIGMAZ*z+SIGMA0.   |
C       AMUX,AMUY,           = coefficients to specify the linear variation |
C       AMUZ,AMU0              of doublet distribution as                |
C                              mu=AMUX*x+AMUY*y+AMUZ*z+AMU0.             |
C                                                                        |
C     Output argument descriptions:                                     |
C       SPOT(N)                  = induced potentials at NFP field points |
C                                  due to the linear-source distribution |
C                                  (NFP arrayed values).                 |
C       SVX(N), SVY(N), SVZ(N) = induced velocity componets at field    |
C                                  points due to the linear-source       |
C                                  distribution (NFP arrayed values).    |
C       DPOT(N)                  = induced potentials at field points due |
C                                  to the linear-doublet distribution    |
C                                  (NFP arrayed values).                 |
C       DVX(N), DVY(N), DVZ(N) = induced velocity componets at field    |
C                                  points due to the linear-doublet      |
C                                  distribution (NFP arrayed values).    |
C     Recommendations:                                                  |
C     When one applies this subroutine to the panel method, it may be    |
C     efficient in computing time to separate the subroutine into        |
C     parts for constant and linear distribution cases, and              |
```

```
C      furthermore into potential and velocity calculation parts.       |
C                                                                        |
C------------------------------------------------------------------------
C


      SUBROUTINE PRPAN
     &   (NSIDE,XV,NFP,XFP,ISELF,SEGL,AN,EL,EM,CG,AREA,DIAGNL,RFAR,{input}
     &    ICOMP,SIGMAX,SIGMAY,SIGMAZ,SIGMA0,AMUX,AMUY,AMUZ,AMU0,   {input}
     &    SPOT,SVX,SVY,SVZ,DPOT,DVX,DVY,DVZ)                       {output}
      IMPLICIT REAL*8 (A-H,O-Z)           {high precision is recommended}
C     single precision is used only for calling arguments.
      REAL*4 XV,XFP,SEGL,AN,EL,EM,RINTM,CG,AREA,DIAGNL,RFAR,
     &       SIGMAX,SIGMAY,SIGMAZ,SIGMA0,AMUX,AMUY,AMUZ,AMU0,
     &       SPOT,SVX,SVY,SVZ,DPOT,DVX,DVY,DVZ
      PARAMETER (NSDMAX=4)
      {up to a quadrilateral panel; change 4 to N for an N-side polygon}
      DIMENSION AN(3),R(3,NSDMAX),D(3),CG(3),SEGL(NSDMAX),PQ(NSDMAX),
     &          EL(3,NSDMAX),EM(3,NSDMAX),XV(3,NSDMAX),XFP(3,1),
     &          ISELF(1),GSEM(NSDMAX),GDEM(NSDMAX),SIGMA(NSDMAX),
     &          AMU(NSDMAX),ALPHA(NSDMAX),BETA(NSDMAX),
     &          SPOT(1),SVX(1),SVY(1),SVZ(1),
     &          DPOT(1),DVX(1),DVY(1),DVZ(1)
C     CHECK NUMBER OF SIDES OF A POLYGON
      IF (NSIDE.LT.3 .OR. NSIDE.GT.NSDMAX) THEN
      WRITE(*,*) 'ERROR: NUMBER OF SIDE SHOULD BE AT LEAST 3 ',
     &                   'AND AT MOST ',NSDMAX,'.'
      STOP     {terminate process in the case of out of range for NSIDE}
      END IF
C     DEFINE OFTEN-USED CONSTANTS
      PI=3.141592653589793
      R4PI=0.25D0/PI                                           {1/(4*pi)}
      EPS=1.0D-07    {tolerance for checking that field point is on plane}
C     LINEAR VARIATION OF SIGMA & DOUBLET
      A1=SIGMAX
      A2=SIGMAY
      A3=SIGMAZ
      A4=SIGMA0
      B1=AMUX
      B2=AMUY
      B3=AMUZ
      B4=AMU0
      DO 3 J=1,NSIDE
      SIGMA(J)=A1*XV(1,J)+A2*XV(2,J)+A3*XV(3,J)+A4
```

```
C        {source density at vertex}
         AMU(J)  =B1*XV(1,J)+B2*XV(2,J)+B3*XV(3,J)+B4
C         {doublet density at vertex}
         ALPHA(J)=A1*EL(1,J)+A2*EL(2,J)+A3*EL(3,J)
C         {linear variation along side}
         BETA(J) =B1*EL(1,J)+B2*EL(2,J)+B3*EL(3,J)
C        DOT PRODUCT BETWEEN GRADIENT OF SIGMA (OR DOUBLET) & VECTOR em
         GSEM(J)=A1*EM(1,J)+A2*EM(2,J)+A3*EM(3,J)
       3 GDEM(J)=B1*EM(1,J)+B2*EM(2,J)+B3*EM(3,J)
C
C        CALCULATIONS FOR MULTIPLE FIELD POINTS
C
         DO 100 K=1,NFP                                    {loop for field points}
C
         DO 5 I=1,3
       5 D(I)=CG(I)-XFP(I,K)
         ANR= AN(1)*D(1)+AN(2)*D(2)+AN(3)*D(3)                {define constant a}
C        FAR-FIELD APPROXIMATIONS
         RR=D(1)**2+D(2)**2+D(3)**2
         IF(RR/DIAGNL**2 .GT.RFAR**2) THEN                   {far-field approx.}
            APPR=DSQRT(RR)                               {representative distance}
            AA=R4PI*AREA/(RR*APPR)
            SIGMAR=A1*CG(1)+A2*CG(2)+A3*CG(3)+A4
C            {representative source density}
            AMUR  =B1*CG(1)+B2*CG(2)+B3*CG(3)+B4
C            {representative doublet density}
            IF(ICOMP.EQ.1 .OR. ICOMP.EQ.3) THEN
            SPOT(K)=-R4PI*AREA/APPR*SIGMAR                    {source-potential}
            DPOT(K)=+AA*ANR*AMUR                             {doublet-potential}
            END IF
            IF(ICOMP.EQ.2 .OR. ICOMP.EQ.3) THEN
            SVX(K) =-AA*D(1)*SIGMAR
            SVY(K) =-AA*D(2)*SIGMAR                            {source-velocity}
            SVZ(K) =-AA*D(3)*SIGMAR
            DVX(K) =+AA*(3*ANR*D(1)/RR-AN(1))*AMUR
            DVY(K) =+AA*(3*ANR*D(2)/RR-AN(2))*AMUR           {doublet-velocity}
            DVZ(K) =+AA*(3*ANR*D(3)/RR-AN(3))*AMUR
            END IF
C
         ELSE                                                {if not far-field}
C
C        DEFINE VECTOR r FOR EACH SIDE AND DISTANCE
         DO 20 J=1,NSIDE
```

```
      DO 10 I=1,3
   10 R(I,J)=XV(I,J)-XFP(I,K)    {vector r between vertex and field point}
      PQ(J)=DSQRT(R(1,J)**2+R(2,J)**2+R(3,J)**2)          {its distance}
   20 CONTINUE
C     SIGN OF n.e
      IF(ISELF(K).EQ.+1.OR.ISELF(K).EQ.0.OR.ISELF(K).EQ.-1) THEN
        ENR=0.D0
        ISIGN=-ISELF(K)
      ELSE
        ENR=DABS(ANR)                                           {a=e.r}
        IF(ANR.GT.0.0D0) THEN
          ISIGN=+1
        ELSE                                                {sign of n.e}
          ISIGN=-1
        END IF
      END IF
C     CHECK THAT FIELD POINT IS ON EXTENSION PLANE OF PANEL (IANULL=1).
      IANULL=0
      IF(ENR.LT.EPS) IANULL=1
C     INITIAL SET FOR SUMMING UP CONTRIBUTION OF RESPECTIVE SIDE
      SPT=0.0D0
      DPT=0.0D0
      IF(ICOMP.EQ.2 .OR. ICOMP.EQ.3) THEN     {selection of calculations}
      SVEL1 =0.0D0
      SVEL2X=0.0D0
      SVEL2Y=0.0D0
      SVEL2Z=0.0D0
      SVEL3 =0.0D0
      DVEL1X=0.0D0
      DVEL1Y=0.0D0
      DVEL1Z=0.0D0
      DVEL2 =0.0D0
      DVEL3 =0.0D0
C
      END IF
C     FOR CONTRIBUTION OF EACH SIDE BY ANALYTIC EVALUATIONS
      DO 30 J=1,NSIDE                         {loop for sides of element}
C
      J1=J+1
      IF(J.EQ.NSIDE) J1=1                            {cyclic convention}
      AL=SEGL(J)                                        {length of side}
      IF(AL. LT. EPS) GO TO 30 {skip contribution of side of small length}
      B=-(R(1,J)*EM(1,J)+R(2,J)*EM(2,J)+R(3,J)*EM(3,J))     {constant bi}
```

```
C        CALL CROSS(R(1,J),EL(1,J),D)
         D(1)=R(2,J)*EL(3,J)-R(3,J)*EL(2,J)
         D(2)=R(3,J)*EL(1,J)-R(1,J)*EL(3,J)                    {vector d=r x el}
         D(3)=R(1,J)*EL(2,J)-R(2,J)*EL(1,J)
C        CALCULATIONS OF LOCAL PLANE COORDINATES (x',z')
         X=-(EL(1,J)*R(1,J)+EL(2,J)*R(2,J)+EL(3,J)*R(3,J))
         Z2=D(1)**2+D(2)**2+D(3)**2
         Z=DSQRT(Z2)
C        CHECK THAT FIELD POINT IS ON EXTENSION LINE OF SIDE (IZNULL=1).
         IZNULL=0
         IF(Z.LT.EPS) IZNULL=1                                 {if z' approx. 0}
C        SUPPRESS CALCULATIONS WHEN FIELD POINT IS JUST ON SIDE LINE.
         IF(IZNULL.EQ.1 .AND. (X.GE.0 .AND. X.LE.AL)) THEN
         WRITE(*,2) XFP(1,K),XFP(2,K),XFP(3,K),
       &           XV(1,J),XV(2,J),XV(3,J),XV(1,J1),XV(2,J1),XV(3,J1)
     2 FORMAT('WARNING: NUMERICAL SINGULARITY OCCURS AT FIELD POINT',
       &       ' ( ',3E13.4,' )', /6X,'FOR THE SEGMENT WITH END POINTS',
       &       ' ( ',3E13.4,' ), (', 3E13.4, ' )')
         STOP                      {terminate the process for a singular point}
         END IF
C
C        INTEGRALS WITH INTEGRAND 1/r,1/(r+a),1/r(r+a) AND 1/r**3.
C
C--- EXACT EVALUATIONS ---
C
         ALMX=AL-X                                    {because of often-used one}
         PQ1=PQ(J)           {distances between field point and end points}
         PQ2=PQ(J1)
         IF(IZNULL.EQ.1) THEN
C          {if field pt is on extension line of side, z'=a=0}
             AI1=DLOG(-ALMX/X)
             AI4=0.5D0*(AL*(ALMX-X)/(X*ALMX)**2)
                IF(X.GT.AL) THEN
                    AI1=-AI1
                    AI4=-AI4
                END IF
             AI3=-AL/(ALMX*X)                         {1/r(r+a) becomes 1/r**2}
             AI2=AI1                                  {1/(r+a) becomes 1/r}
         ELSE                                         {if IZNULL.NE.1}
            IF( X.LT. 0.D0-EPS) THEN
                 AI1=DLOG((PQ2+ALMX)/(PQ1-X))         {integral of 1/r}
            ELSE IF( X .GT. AL+EPS) THEN
                 AI1=DLOG((PQ1+X)/(PQ2-ALMX))
```

```
         ELSE IF((PQ1-X).GT.EPS .AND. (PQ2-ALMX).GT.EPS) THEN
             AI1=0.5D0*DLOG((PQ2+ALMX)*(PQ1+X)/((PQ1-X)*(PQ2-ALMX)))
C              {mean}
             ELSE IF((PQ1-X).LE.EPS) THEN
             AI1=DLOG((PQ2+ALMX)*2.D0*X/Z2)
             ELSE IF((PQ2-ALMX).LE.EPS) THEN
             AI1=DLOG((PQ1+X)*2.D0*ALMX/Z2)
             ELSE
             WRITE(*,2) XFP(1,K),XFP(2,K),XFP(3,K),
     &          XV(1,J),XV(2,J),XV(3,J),XV(1,J1),XV(2,J1),XV(3,J1)
             STOP
         END IF
C
         IF(X.GT.0.D0 .AND. X.LT.AL) THEN
         AI4=(AL*PQ1 + X*(PQ2-PQ1))/(Z2*PQ1*PQ2)     {integral of 1/r**3}
         ELSE
         AI4=AL*(ALMX-X)/(PQ1*PQ2*(ALMX*PQ1-X*PQ2))
         END IF
         IF(IANULL.EQ.1) THEN                        {1/r(r+a) becomes 1/r**2}
            AI2=AI1                                   {1/(r+a) becomes 1/r}
            IF(DABS(Z2-X*ALMX).LT.EPS) THEN
             ARG=DATAN(ALMX/Z)+DATAN(X/Z)
             ELSE
             ARG=DATAN(AL*Z/(Z2-X*ALMX))  {combine two inverse functions}
             IF(Z2.LT.X*ALMX .AND. X.LT.AL) ARG=PI+ARG
            END IF
            AI3=ARG/Z
         ELSE
            IF((Z-ENR).LT.EPS) THEN                           {if z'.EQ.a}
               AI3=(AL*(PQ1+ENR)+X*(PQ2-PQ1))/((PQ2+ENR)*(PQ1+ENR)*ENR)
            ELSE                                              {if z'.NE.a}
               AA=(-Z2-ENR*PQ1)/(Z*(PQ1+ENR))
               BB=(-Z2-ENR*PQ2)/(Z*(PQ2+ENR))
               EE=DSQRT(Z2-ENR**2)
                IF(X.GT.0.D0 .AND. X.LT.AL) THEN
                 CC= EE*(Z2*AL+ENR*(ALMX*PQ1+X*PQ2))
     &                  /(Z2*(PQ1+ENR)*(PQ2+ENR))
                 ELSE
                 CC= EE*AL*(1+ENR*(ALMX-X)/(ALMX*PQ1-X*PQ2))
     &                  /((PQ1+ENR)*(PQ2+ENR))
                END IF
               IF(DABS(CC).LT.1.0D0) ASINCC=DASIN(CC)
               IF(CC.GE.1.0D0) ASINCC=0.5D0*PI
```

```
                   IF(CC.LE.-1.0D0) ASINCC=-0.5D0*PI
                    IF(X.LE.0. .OR. X.GE.AL .OR. (AA**2+BB**2).GE.1.) THEN
                     AI3=ASINCC/EE
                     ELSE
                     AI3=(PI-ASINCC)/EE
                    END IF
C
               END IF                          {for special case of z'=a}
               AI2=AI1-ENR*AI3 {by partial fraction, a/r(r+a)=1/r - 1/(r+a)}
            END IF                                   {for extension of plane}
         END IF                                 {for extension of each side}
C    BASIC INTEGRALS FOR LINEAR VARIATION
      AJ1=PQ2-PQ1+X*AI1
      AJ4=(PQ2-PQ1)/(PQ1*PQ2)+X*AI4
      AJ5=0.5D0*(AL*PQ2+X*(PQ1-PQ2))+0.5D0*Z2*AI1
      ALOG1=DLOG(PQ1)
      ALOG2=DLOG(PQ2)
      AJ6=AL*ALOG2+X*(ALOG1-ALOG2)-AL
      IF(IZNULL.NE.1) THEN
            IF(IANULL.NE.1) THEN
            IF(DABS(Z2-X*ALMX).LT.EPS) THEN
             ARG=DATAN(ALMX/Z)+DATAN(X/Z)
             ELSE
             ARG=DATAN(AL*Z/(Z2-X*ALMX))  {combine two inverse functions}
             IF(Z2.LT.X*ALMX .AND. X.LT.AL) ARG=PI+ARG
            END IF
            END IF
            AJ6=AJ6+Z*ARG
      END IF
      IF(IANULL.EQ.1) THEN
      AJ2=AJ1
      AJ7=AJ6
      ELSE
      ALOG1=DLOG(PQ1+ENR)
      ALOG2=DLOG(PQ2+ENR)
      AJ2=PQ2-PQ1-ENR*(ALOG2-ALOG1)+X*AI2
      AJ7=AL*ALOG2+X*(ALOG1-ALOG2)-AL+ENR*AI1
            IF((Z-ENR).GE.EPS) THEN                              {if z'.NE.a}
                IF(X.LE.0. .OR. X.GE.AL .OR. (AA**2+BB**2).GE.1.) THEN
                 AJ7=AJ7+EE*ASINCC
                 ELSE
                 AJ7=AJ7+EE*(PI-ASINCC)
                END IF
```

```
            END IF
        END IF
C

      AJ3=ALOG2-ALOG1+X*AI3
C     MULTIPLY FACTORS AND SUM UP CONTRIBUTION OF EACH SIDE
      IF(ICOMP.EQ.1 .OR. ICOMP.EQ.3) THEN
        IF(IANULL.EQ.1) THEN
        SPT=SPT+B*(SIGMA(J)*AI2+ALPHA(J)*AJ2)
     &        +GSEM(J)*AJ5
        ELSE
        SPT=SPT+B*(SIGMA(J)*AI2+ALPHA(J)*AJ2)
     &        +GSEM(J)*(AJ5-ENR*AJ7)
        END IF
        DPT=DPT+B*(AMU(J)*AI3 +BETA(J)*AJ3)
     &        +GDEM(J)*AJ7
      END IF
      IF(ICOMP.EQ.2 .OR. ICOMP.EQ.3) THEN        {selection of calculations}
          SVEL1=SVEL1+B*(SIGMA(J)*AI3+ALPHA(J)*AJ3)+GSEM(J)*AJ7
          SVEL2X=SVEL2X+EM(1,J)*(SIGMA(J)*AI1+ALPHA(J)*AJ1)
          SVEL2Y=SVEL2Y+EM(2,J)*(SIGMA(J)*AI1+ALPHA(J)*AJ1)
          SVEL2Z=SVEL2Z+EM(3,J)*(SIGMA(J)*AI1+ALPHA(J)*AJ1)
          SVEL3=SVEL3+B*AI2
          DVEL1X=DVEL1X+D(1)*(AMU(J)*AI4+BETA(J)*AJ4)
          DVEL1Y=DVEL1Y+D(2)*(AMU(J)*AI4+BETA(J)*AJ4)
          DVEL1Z=DVEL1Z+D(3)*(AMU(J)*AI4+BETA(J)*AJ4)
          DVEL2=DVEL2+B*AI3
          DVEL3=DVEL3+GDEM(J)*AI1
      END IF
C

   30 CONTINUE                                   {end of side-loop}
C

      DPT=ISIGN*DPT
      IF(ICOMP.EQ.1 .OR. ICOMP.EQ.3) THEN
          SPOT(K)=-R4PI*SPT                       {source-potential}
          DPOT(K)=+R4PI*DPT                       {doublet-potential}
      END IF
      IF(ICOMP.EQ.2 .OR. ICOMP.EQ.3) THEN
          SVX(K) =-R4PI*(ISIGN*AN(1)*SVEL1+SVEL2X+A1*SVEL3)
          SVY(K) =-R4PI*(ISIGN*AN(2)*SVEL1+SVEL2Y+A2*SVEL3)
          SVZ(K) =-R4PI*(ISIGN*AN(3)*SVEL1+SVEL2Z+A3*SVEL3)
          DVX(K) =+R4PI*(DVEL1X+ISIGN*B1*DVEL2-AN(1)*DVEL3)
          DVY(K) =+R4PI*(DVEL1Y+ISIGN*B2*DVEL2-AN(2)*DVEL3)
          DVZ(K) =+R4PI*(DVEL1Z+ISIGN*B3*DVEL2-AN(3)*DVEL3)
```

```
      END IF
C
      END IF                        {end of control of far-field approx.}
  100 CONTINUE                           {end of field-point loop}
      RETURN
      END
C


C------------------- Subroutine PRgeom.ftn -------------------------
C                                                                   |
C     PRgeom code provides the geometric parameters of a planar or  |
C     non-planar element for the calculation of potential and velocity |
C     induced by constant plus linear source/doublet distributions on a |
C     planar polygon element, by adapting the formulation of Lee ~(1990) |
C     to follow the formulation of Cantaloube and Rehbach ~(1986) and to |
C     perform the analytic evaluations of the associated line integrals |
C     (Suh ~(1990)).                                                |
C     This subroutine may be called before the subroutine PRpan for |
C     computing the induced potentials and velocities is called, but |
C     only once for each element.                                   |
C                                                                   |
C     REFERENCES:                                                   |
C      [1] Cantaloube, B. and Rehbach, C. ~(1986)                   |
C         " Calcul des Integrales de la Methode des Singularites"   |
C            Recherche Aerospatiale, no. 1, pp. 15-22,              |
C            (English Title: " Calculation of the Integrals of the  |
C            Singularity Method" Aerospace Research, No. 1, pp. 15-22) |
C      [2] Suh, J. C. ~(1990)                                       |
C         " Review of the Paper; Calculation of the Integrals of the |
C            Singularity Method by Cantaloube and Rehbach"          |
C            KRISO Propulsor Technology Laboratory Report, 22-90     |
C      [3] Suh, J. C. ~(1990)                                       |
C         " Analytic Evaluations of the Induction-Integrals for     |
C            Distributions of Sources and Doublets over a Planar    |
C            Polygon Element"                                       |
C            KRISO Propulsor Technology Laboratory Report, 23-90     |
C      [4] Lee, C.-S. ~(1990)                                       |
C         " Treatment of non-planar panel"                          |
C            Technical Notes (unpublished), 11/29/90                |
C                                                                   |
*-------------------------------------------------------------------|
*                                                                   |
*     Version 1.2, November 16, 1990    by Y.-G. Kim                |
```

```
*       Version 2.2, November 28, 1990    by C.-S. Lee          |
C       (add a control for planar-element case on 1/4/91 by J.-C. Suh)    |
C                                                                |
*-----------------------------------------------------------------------|
*                                                                |
*       INPUT :  Vertex Points:  xv(i,j), where i=1,3 for x,y,z-coords   |
*                                         j=1,...,Nside for sides.   |
*                                                                |
*       OUTPUT:  Panel geometrical data, including               |
*               cg, el, em, an, segl,area,diagnl                 |
*                                                                |
*  ...Panel Geometry.....................................................|
*       1)  Counter-clockwise when              4 *-----* 3        |
*             viewed from fluid                 |     |            |
*       2)  Dipole axis pointing                |     |            |
*             into the fluid                J = 1 *-----* 2        |
*  .....................................................................|
*                                                                |
C       Input argument descriptions:                            |
C       NSIDE            = number of sides of a planar element    |
C                           (at least 3).                         |
C       XV(i,N)          = x-, y- and z-coordinates of the        |
C                           NSIDE vertices of the element         |
C                           (two-dimensional arrayed values in a  |
C                           counterclockwise order).              |
C       IPLANE           = control index for planar or non-planar |
C                           element (if planar element, IPLANE=1) |
C                                                                |
C       Output argument descriptions:                           |
C       SEGL(N)          = lengths of the NSIDE respective sides  |
C                           (NSIDE arrayed values).               |
C       AN(i)            = x-, y- and z-components of the unit outward  |
C                           normal vector of the planar element   |
C                           (3 arrayed values).                   |
C       EL(i,N)          = x-, y- and z-components of the unit     |
C                           orientation vector of the NSIDE respective  |
C                           sides (two-dimensional arrayed values). |
C       EM(i,N)          = x-, y- and z-components of the unit     |
C                           vector lying on the plane and normal to the  |
C                           NSIDE respective sides                |
C                           (two-dimensional arrayed values).     |
C       CG(i)            = x-, y- and z- coordinates of the centroid  |
C                           of the element (3 arrayed values).    |
```

```
C     AREA              = surface area of the element.              |
C     DIAGNL            = longest diagonal of the element.          |
C                                                                   |
C    Notice: Please contact C.-S. Lee at CNU by a letter or by      |
C            a phone call at (042) 821-6623 if there are any problems   |
C            for usage of this subroutine, so that he can give notice   |
C            of them to other users.                                |
C                                                                   |
C-------------------------------------------------------------------
C


      SUBROUTINE PRGEOM (NSIDE,XV,IPLANE,SEGL,AN,EL,EM,CG,AREA,DIAGNL)
              {input arguments}{output to be used in other subroutines}
      PARAMETER (NSDMAX=4)                      {up to a quadrilateral panel}
      DIMENSION AN(3),CG(3),SEGL(NSDMAX),EL(3,NSDMAX),EM(3,NSDMAX),
     &          XV(3,NSDMAX),Xip(3,4),Xgl(3),UL(3),VL(3)
      DATA QUART / 0.25D+00 /, HALF/ .5D+00/
      DATA ZERO/0.D+00/,ONE/1.D+00/,THREE/3.D+00/,FOUR/4.D+00/
C     CHECK NUMBER OF SIDES OF A POLYGON
      IF (NSIDE.LT.3 .OR. NSIDE.GT.NSDMAX) THEN
      WRITE(*,*) 'ERROR: NUMBER OF SIDE SHOELD BE AT LEAST 3 ',
     &                   'AND AT MOST ',NSDMAX,'.'
      STOP      {terminate process in the case of out of range for NSIDE}
      END IF
C
      TOL=1.0D-07
C      {tolerance for checking that neighboring vertices are near}
C
      IF(NSIDE.EQ.3 .OR. IPLANE.EQ.1) THEN
C                     ----------- FOR A PLANAR ELEMENT ---------
C     UNIT OUTWARD VECTOR NORMAL TO THE ELEMENT
      DO 10 I=1,3
      UL(I)=(XV(I,2)-XV(I,1))
   10 VL(I)=(XV(I,3)-XV(I,1))              {with only 3 vertices of polygon}
      CALL CROSS(UL,VL,AN)                                {cross product}
      ANS=SQRT(PRDOT(AN,AN))                              {dot product}
      IF(ANS.LT.TOL) THEN                          {check small magnitude}
      IER=0
      RETURN
      END IF
      DO 20 I=1,3
   20 AN(I)=AN(I)/ANS                              {unit normal vector}
C     DEFINE ASSOCIATED UNIT VECTORS
```

```
      DO 50 J=1,NSIDE                          {loop for sides of element}
      J1=J+1
      IF(J.EQ.NSIDE) J1=1
      DO 30 I=1,3
  30  UL(I)=XV(I,J1)-XV(I,J)
      SEGL(J)=SQRT(PRDOT(UL,UL))
      IF(SEGL(J) .GT. TOL) THEN                {check tiny length of side}
       DO 40 I=1,3
  40   EL(I,J)=UL(I)/SEGL(J)    {el: unit directional vectors along sides}
       CALL CROSS(AN,EL(1,J),EM(1,J))              {unit vector em = n x el}
      ELSE
       IER=1
      END IF
  50  CONTINUE
C     CHARACTERISTIC LENGTH, AREA, CENTROID
      IF(NSIDE.EQ.3) THEN                             {triangular element}
       S=0.5D0*(SEGL(1)+SEGL(2)+SEGL(3))
       AREA=SQRT(S*(S-SEGL(1))*(S-SEGL(2))*(S-SEGL(3)))  {Helon's formula}
       DO 60 I=1,3
  60   CG(I)=(XV(I,1)+XV(I,2)+XV(I,3))/3.D0
       DIAGNL=AMAX1(SEGL(1),SEGL(2))
       DIAGNL=AMAX1(SEGL(3),DIAGNL)
      ELSE                                         {quadrilateral element}
       DIAG1=(XV(1,3)-XV(1,1))**2+(XV(2,3)-XV(2,1))**2
     &      +(XV(3,3)-XV(3,1))**2
       DIAG2=(XV(1,4)-XV(1,2))**2+(XV(2,4)-XV(2,2))**2
     &      +(XV(3,4)-XV(3,2))**2
       DIAGNL=SQRT(DIAG1)                  {separate it into two triangles}
       S=0.5D0*(DIAGNL+SEGL(1)+SEGL(2))                  {first triangle}
       AREA=SQRT(S*(S-DIAGNL)*(S-SEGL(1))*(S-SEGL(2)))
       DO 70 I=1,3
  70   VL(I)=   AREA*(XV(I,1)+XV(I,2)+XV(I,3))/3.D0         {1st moment}
       S=0.5D0*(DIAGNL+SEGL(3)+SEGL(4))                 {second triangle}
       S=SQRT(S*(S-DIAGNL)*(S-SEGL(3))*(S-SEGL(4)))
       DO 80 I=1,3
  80   VL(I)=VL(I)+S*(XV(I,3)+XV(I,4)+XV(I,1))/3.D0
       AREA=AREA+S
       DO 90 I=1,3
  90   CG(I)=VL(I)/AREA
       IF(DIAG2.GT.DIAG1) DIAGNL=SQRT(DIAG2)
      END IF
C
      ELSE                                       {for non-planar element}
```

```
 C
 C                        ----------- FOR A NON-PLANAR ELEMENT ---------
 C (method: projection of non-planar surface
 C                                  onto a mean planar surface)
*----------------------------------------------------------------------
*     EVALUATION OF REFERENCE COORDINATES OF THE ORIGIN OF THE LOCAL
*     COORDINATE SYSTEM.
*     ORIGIN AT AVERAGE POINT; FIRST APPROXIMATION.
*----------------------------------------------------------------------
*
      do 100 i = 1,3
        V12=xv(i,1)+xv(i,2)
        V23=xv(i,2)+xv(i,3)
        V34=xv(i,3)+xv(i,4)
        V41=xv(i,4)+xv(i,1)
        CG(I)=(V12+V34)*QUART
        UL(I)=(V23-V41)*HALF
        VL(I)=(V34-V12)*HALF
  100    continue
      ULS=SQRT(PRdot(UL,UL))
      VLS=SQRT(PRdot(VL,VL))
      IF(ULS.LT.TOL.OR.VLS.LT.TOL) THEN
       IER=0
       RETURN
      END IF
      do 110 i = 1,3
        UL(I)=UL(I)/ULS
        VL(I)=VL(I)/VLS
  110    continue
*----------------------------------------------------------------------
*     EVALUATION OF THE UNIT VECTORS(ul,vl,wl) OF LOCAL FRAME
*----------------------------------------------------------------------
      CALL CROSS(UL,VL,AN)
      ANS = SQRT( PRdot(AN,AN) )
      IF(ANS.LT.TOL) THEN
      IER=0
      RETURN
      END IF
      do 120 i = 1,3
  120      AN(I)=AN(I)/ANS
      CALL CROSS(AN,UL,VL)
*----------------------------------------------------------------------
*     LOCAL COORDINATES OF VERTICES WITH CG AS THE TEMPORARY ORIGIN.
```

```
*      Project onto u-v plane(local planar plane) by dropping Xip(3,j).
*-----------------------------------------------------------------------
       do 140 j = 1,Nside
           do 130 i = 1,3
  130      SEGL(I)=xv(i,j)-CG(I)
         Xip(1,J)=PRdot( SEGL,UL)
         Xip(2,J)=PRdot( SEGL,VL)
  140    continue
*-----------------------------------------------------------------------
*      LOCAL COORDINATES RELATIVE TO CENTROID;
*-----------------------------------------------------------------------
       A1=(Xip(1,2)+Xip(1,3))*HALF
       A2=(Xip(1,3)+Xip(1,4))*HALF
       A3=(Xip(1,3)+Xip(1,1))*HALF
       B1=(Xip(2,2)+Xip(2,3))*HALF
       B2=(Xip(2,3)+Xip(2,4))*HALF
       B3=(Xip(2,3)+Xip(2,1))*HALF
       D0=A1*B2-A2*B1
         area = four * D0
       D1=A1*B3-A3*B1
       D2=A3*B2-A2*B3
       D0I=ONE/(THREE*D0)
*.....Centroid in Temporary Coordinate System.
       Xgl(1)=(D1*A1+D2*A2)*D0I
       Xgl(2)=(D1*B1+D2*B2)*D0I
*.....Xip is now relative to the centroid.
       do 160 j = 1,Nside
           do 150 i = 1,2
  150        Xip(I,J)=Xip(I,J) - Xgl(I)
  160        CONTINUE
*-----------------------------------------------------------------------
*      RE-EVALUATION OF NEW COORDINATES OF CENTROID and VERTICES
*         IN GLOBAL COORDINATE SYSTEM.
*-----------------------------------------------------------------------
       DO 165 I=1,3
  165      cg(I)= CG(I) + UL(I)*Xgl(1) + VL(I)*Xgl(2)
       do 180 j = 1,Nside
         do 170 i = 1,3
  170      xv(i,j)  = cg(i) + UL(i)*Xip(1,j)+VL(i)*Xip(2,j)
  180    continue
C    DEFINE ASSOCIATED UNIT VECTORS
       DO 210 J=1,NSIDE                        {loop for sides of element}
       J1=J+1
```

```
      IF(J.EQ.NSIDE) J1=1
      DO 190 I=1,3
 190  EL(I,J)=XV(I,J1)-XV(I,J)
      SEGL(J)=SQRT(PRDOT(EL(1,J),EL(1,J)))
      IF(SEGL(J) .GT. TOL) THEN
      DO 200 I=1,3
 200  EL(I,J)=EL(I,J)/SEGL(J)    {el: unit directional vectors along sides}
      CALL CROSS(AN,EL(1,J),EM(1,J))           {unit vector em = n x el}
      ELSE
      IER=1
      END IF
 210  CONTINUE
      DIAG1=(XV(1,3)-XV(1,1))**2+(XV(2,3)-XV(2,1))**2
     &      +(XV(3,3)-XV(3,1))**2
      DIAG2=(XV(1,4)-XV(1,2))**2+(XV(2,4)-XV(2,2))**2
     &      +(XV(3,4)-XV(3,2))**2
      DIAGNL=AMAX1(DIAG1,DIAG2)
      DIAGNL=SQRT(DIAGNL)     {longest diagonal as characteristic length}
*.......................
      END IF
C
      RETURN
      END
 C
 C      CALCULATE VECTOR CROSS PRODUCT
      SUBROUTINE CROSS(A,B,C)
       DIMENSION A(1),B(1),C(1)
       C(1)=A(2)*B(3)-A(3)*B(2)
       C(2)=A(3)*B(1)-A(1)*B(3)
       C(3)=A(1)*B(2)-A(2)*B(1)
       RETURN
       END
 C
 C      Calculates vector dot product
      FUNCTION PRdot(A,B)
       DIMENSION A(1),B(1)
       PRdot=A(1)*B(1)+A(2)*B(2)+A(3)*B(3)
       RETURN
       END
C--------------------------------------------------------{end of file}
```

D

EVALUATION OF THE BIOT-SAVART INTEGRAL

D.1   Introduction

In this appendix, a computational method is described for evaluating the Biot-Savart integral. The approach emphasizes the transformation of the involved integrand into suitable forms, from which integral theorems can be used to reduce the volume integral into line integrals. This method is applied to the case where the density of vorticity distributed over a volumetric element bounded by planar surfaces (straight lines in 2-D) is constant and/or linear. The resulting expressions for the volume integral involve closed-form expressions for line integrals along the edges of the element. The evaluation of the line integrals is treated independently for each of the edges as opposed to direct numerical integration. The closed-form formulas are expressed in terms of geometric parameters of the element edges. Vector mathematical identities involving an integral of singularities distributed over a surface and a field can be employed to define field values of a vector variable of interest at a point within a field. For example, the field values of an irrotational and solenoidal vector can be obtained from the integrals over the sole surfaces bounding the field. In boundary-integral methods which were inspired by the work of Hess and Smith (1964, 1966, 1969) for potential flow problems of an incompressible fluid, the surface integrals involved may be evaluated on the boundary by assuming that the bounding surfaces are composed of a set of discrete panels and assuming a certain variation in the boundary values of the dependent variable in space (over the panels) and time.

For other problems related to rotational and solenoidal vector fields, a volume integral exists, the so-called Biot-Savart integral. It is well known that the Biot-Savart integral represents a formula in electromagnetic field theory that relates a field distribution of electric current to the induced magnetic field (see e.g., Bodner (1992)). In a manner analogous with the magnetic field induced by the given distribution of current, this induction law has been also applied to hydro- and aerodynamics by many workers: a distribution of vorticity in a field induces the velocity field whose curl becomes the given value of vorticity everywhere (Batchelor 1967, Saffman 1992).

In vortex methods for viscous flow analyses— especially in the vorticity-velocity integro-differential formulations (see e.g., Gresho (1991)), the Biot-Savart integral must be evaluated at appropriate field points within the discretized fluid domain. With N elements used in discretizing the fluid domain over which vorticity is distributed, $O(N^2)$ evaluations of the Biot-Savart integral may be required in order to calculate the velocity field. The evaluation of the Biot-Savart integral is, therefore, an important task in the numerical implementations associated with computational electromagnetics and fluid mechanics.

D.1.1 Integral representation

For a distributed vorticity field, $\underline{\omega}$, in a fluid region V, the general form of the Biot-Savart law is

$$\underline{q} = \int_V \underline{\omega} \times \nabla G \, dV, \tag{D.1}$$

where $\underline{q}$ is the induced velocity (magnetic) field and G the fundamental function, defined by

$$G = \begin{cases} \dfrac{1}{4\pi r} & \text{in 3-dimensions,} \\[2ex] -\dfrac{1}{2\pi} \ln r & \text{in 2-dimensions.} \end{cases} \tag{D.2}$$

Hereafter, ∇ denotes the gradient, divergence, and curl differential operator with respect to integration variables $\underline{\xi}$, and r the distance between a field point $\underline{x}$ and an integration point $\underline{\xi}$.

In this appendix, efficient numerical analysis schemes for a linear distribution of vorticity over a surface in two-dimensions or over a volume in three-dimensions are presented on the basis of transformations of the integrals. It will be shown that the induced velocity field due to a vorticity distribution with linear strength can be derived from a sum of line integrals along the edges of a subdivided element. The derivation used here employs Stokes's and/or Gauss's theorem, by which the velocity field can be expressed in terms which are dependent only on the properties of each edge: namely, the terms of the position

of a field point relative to each edge. In this manner, an analysis associated with direct calculation of the triple (double in 2-d) integral over the element can be avoided. An additional feature of the present derivation is that it is valid for an arbitrary element bounded by planar surfaces (straight lines in 2-D).

D.2   Biot-Savart Integral in 2-D

D.2.1   Transformation of integral

A quadrilateral element is, without loss of generality, taken for the present analysis. The complete induced field is constructed by superposing the field contributions due to the individual elements. For any polygon, we can easily deduce the corresponding results from the expression, Eq. (D.6) below, by taking into account the number of sides of the polygon in the summation of the contributions for each side. The vertices with coordinates (ξ_i, η_i) are denoted by $\underline{\xi}_i$, as shown in Figure D.1, where each vertex is indicated by the index i. The induced velocity $(\underline{q})$ at an arbitrary field point $P(\underline{x})$ with coordinates (x, y) due to a distribution of vorticity over the domain of the element S is

$$\underline{q} = -\frac{\underline{k}}{2\pi} \times \int_S \omega \, \nabla(\ln r) \, dS, \tag{D.3}$$

where $r = |\underline{r}| = |\underline{\xi} - \underline{x}|$ and ω is the scalar plane component of the vorticity vector, $\underline{\omega} \; (\equiv \omega \, \underline{k})$.

The integrand can be transformed into, through simple vector operations,

$$\omega \, \nabla(\ln r) = \nabla(\omega \, \ln r) - \frac{1}{2} \left\{ \nabla \cdot (\underline{r} \, \ln r) - 1 \right\} \nabla \omega. \tag{D.4}$$

For a vorticity distribution of linear-variation density, we can convert the surface integral in Eq. (D.3) into line integral terms, by applying the Gauss theorem with the transformed integrand given in Eq. (D.4):

$$\int_S \omega \, \nabla(\ln r) \, dS = \frac{1}{2} \oint_C \underline{n} \, \omega \, (\ln r^2 + 1) \, dl - \frac{1}{2} \nabla \omega \oint_C (\underline{n} \cdot \underline{r}) \, \ln r \, dl. \tag{D.5}$$

Here the contour integrals are performed along the perimeter (C) of the element in a counter-clockwise direction, and $\underline{n}$ is the unit normal vector on the boundary of the element in the sense of a right-handed rule, i.e., $\underline{n} = \underline{s} \times \underline{k}$ where $\underline{s}$ is the unit directional vector of the contour integral path. Then $\underline{k}, \underline{n}$ and $\underline{s}$ constitute a right-handed triple of orthogonal unit vectors.
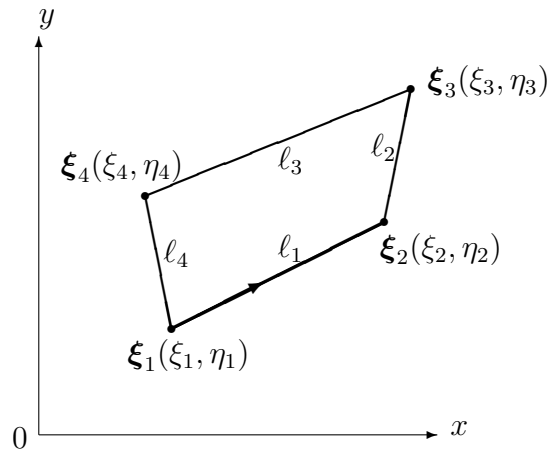
Figure D.1 Definition of a quadrilateral element.

D.2.2 Analytic form of integrals

The resulting expressions for the velocity field include the line integrals only along the boundary contour of the element. Let the value of the line integral along each straight edge of the element be $\underline{I}_i$. It then follows that

$$\underline{q} = -\frac{\underline{k}}{2\pi} \times \left(\sum_{i=1}^{4} \underline{I}_i \right), \tag{D.6}$$

where, with the side of length ℓ_i,

$$\underline{I}_i = \frac{1}{2} \underline{n}_i \int_0^{\ell_i} \omega \left(\ln r^2 + 1 \right) dl - \frac{1}{4} \nabla \omega \left(\underline{n}_i \cdot \underline{r} \right) \int_0^{\ell_i} \ln r^2 \, dl. \tag{D.7}$$

It is seen that the line integral for each side can be treated independently. It is sufficient, therefore, to consider only one side of the polygon for the purpose

of integration. The essential task is to evaluate the line integrals along a straight segment from $\boldsymbol{\xi}_i$ to $\boldsymbol{\xi}_{i+1}$ with linear variation of ω over it.

For the evaluation of the associated integrals, we take a local coordinate system (x', y') in the plane through the field point $\underline{x}$ and the side concerned, such that the side lies on the x'-axis and one end point of the side is at the origin of the coordinates (see Figure **D.2**). The integration is performed along the positive x'-axis. The reason for choosing the local coordinate system as such is because the integration is more compact and systematic than that for the case of the global coordinate system, even though both procedures, in fact, produce identical results. Of course the coordinates of the field point in the global coordinate system must be transformed into the local coordinate systems of the respective sides, and the computed field components must then be defined in the global coordinate system to superpose the contributions due to the respective sides.
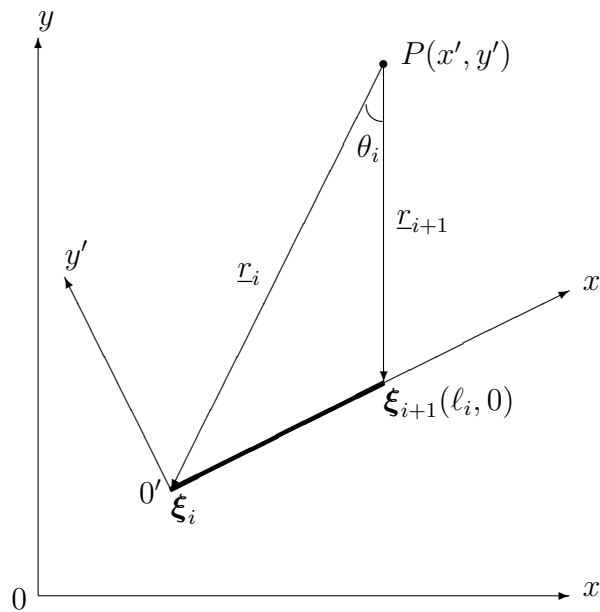
Figure D.2 Definition sketch of the local coordinate system (x', y').

The local coordinates are related to the vectors defined in the global coordinate system as: $x' = -\underline{r}_i \cdot \underline{s}_i$ and $y' = (\underline{r}_i \times \underline{s}_i) \cdot \underline{k}$. This transformation implies the projections of distance vectors between the field point P and the end points of the segment on the x'- and y'-axis. Let us denote the distances between the two end points of the side and the field point by $r_i = \sqrt{x'^2 + y'^2}$

and $r_{i+1} = \sqrt{(\ell_i - x')^2 + y'^2}$, respectively. After a substantial amount of algebraic manipulations (see Gradshteyn and Rhyzik 1980, pp. 81-84) for integral formulae), the following result for $\underline{I}_i$ can be obtained:

$$\underline{I}_i = \frac{1}{2}\underline{n}_i \left\{ \omega_i \left(\ell_i + I^{(1)} \right) + (\nabla\omega \cdot \underline{s}_i) \left(\frac{1}{2}\ell_i^2 + I^{(2)} \right) \right\} - \frac{1}{4}\nabla\omega(\underline{n}_i \cdot \underline{r})I^{(1)}, \quad \text{(D.8)}$$

where ω_i denotes the vorticity value at the i-th vertex,

$$I^{(1)} = (\ell_i - x') \ln r_{i+1}^2 + x' \ln r_i^2 - 2\ell_i + 2|y'|\theta_i, \quad \text{(D.9)}$$

$$I^{(2)} = \frac{1}{2} \left(r_{i+1}^2 \ln r_{i+1}^2 - r_i^2 \ln r_i^2 \right) - \frac{\ell_i^2}{2} + \ell_i x' + x' I^{(1)}, \quad \text{(D.10)}$$

and

$$\theta_i = \tan^{-1} \frac{|y'|\ell_i}{r_i^2 - \ell_i x'}. \quad \text{(D.11)}$$

Here the pair of arctangents appearing in this evaluation have been combined by using the trigonometric formulae. Eventually it is seen that θ_i denotes the included angle between distance vectors of the segment end points as viewed from the field point P (see Figure **D.2**). Thus, the included angle is uniquely measured as a value between 0 and π without considering the separate arguments of the arctangent function, since the numerator of the argument of the arctangent is non-negative. Note that the terms $I^{(1)}$ and $I^{(2)}$ given by Eqs. (**D.9**) and (**D.10**) are determinate when the field point is on the extensions of the side. For example, if the field point approaches one of the end points of the side, we have finite values according to L'Hospital's rule (for the indeterminate form $0 \cdot \infty$).

D.3 Biot-Savart Integral in 3-D

D.3.1 Transformation of integral

The induced velocity due to a vorticity distribution over an element whose boundary is composed of planar panels, can be expressed in a volume form

analogous to Eq. (D.3):

$$
\begin{aligned}
\underline{q} &= \frac{1}{4\pi} \int_V \underline{\omega} \times \nabla \left(\frac{1}{r} \right) dV \\
&= \frac{1}{4\pi} \int_V \left\{ \frac{1}{r} (\nabla \times \underline{\omega}) - \nabla \times \left(\frac{1}{r} \underline{\omega} \right) \right\} dV.
\end{aligned}
\tag{D.12}
$$

The vorticity distribution is assumed to be linear so that $(\nabla \times \underline{\omega})$ is constant. By using the divergence (Gauss) theorem, Eq. (D.12) can be reduced to

$$
4\pi \underline{q} = (\nabla \times \underline{\omega}) \int_V \frac{1}{r} dV - \oint_S \underline{n} \times \left(\frac{1}{r} \underline{\omega} \right) dS,
\tag{D.13}
$$

where S is the surfaces bounding the volume V and $\underline{n}$ is the outward normal unit vector on the bounding surfaces.

In order to evaluate the volume integral term in Eq. (D.13), we use here Green's second identity for a scalar function ϕ such that $\nabla^2 \phi = 1$;

$$
\int_V \frac{1}{r} dV = -\alpha \, \phi(\underline{x}) - \oint_S \left\{ \phi \underline{n} \cdot \nabla \left(\frac{1}{r} \right) - \frac{\underline{n} \cdot \nabla \phi}{r} \right\} dS,
\tag{D.14}
$$

where α is constant. When $\underline{x}$ is inside the volumetric region V, α is 4π. If $\underline{x}$ is on the boundary of V, it is 2π. For $\underline{x}$ outside the volume, this value is zero. Equation (D.13) can then be expressed as a sum of integrals over the bounding planar surfaces as:

$$
\begin{aligned}
4\pi \underline{q} &= -(\nabla \times \underline{\omega}) \left[\alpha \, \phi(\underline{x}) + \oint_S \left\{ \phi \underline{n} \cdot \nabla \left(\frac{1}{r} \right) - \frac{\underline{n} \cdot \nabla \phi}{r} \right\} dS \right] \\
&\quad - \oint_S \underline{n} \times \left(\frac{1}{r} \underline{\omega} \right) dS, \\
&= -(\nabla \times \underline{\omega}) \, \alpha \, \phi(\underline{x}) - \sum_{j=1}^{6} \left\{ (\nabla \times \underline{\omega}) \, K_j + \underline{L}_j \right\}.
\end{aligned}
\tag{D.15}
$$

Here the upper limit 6 in the summation denotes the number of faces of the volumetric cell element taken. Let us consider the surface integral term over one planar panel since the corresponding integral terms for other panels can be evaluated in the same manner. We drop the subscript j in K_j and $\underline{L}_j$ for sim-

plicity of notation. The integral K represents induced potentials due to dipole distributions of the second order in density and source distributions with linearly varying density over the bounding surfaces. The integral has been evaluated in various manners by numerous researchers. Bai and Yeung (1974) have set up the basic framework for treating the potential and the normal potential induced by a source density distribution which varies linearly over a triangular patch element (see also (Webster 1975, Newman 1986). Herein on the basis of Bai & Yeung's procedure, we take the approach described in literature Suh et al. (1992) for consistency with the present work. The analysis schemes are based on transformation of the associated integrals.

Let us take, for example, $\phi = 0.5x^2$ as a simple choice of ϕ in Eq. (D.14). In order to specify the second order variation of dipole density μ and the linear variation of source density σ over the respective planar panels of the bounding surfaces, we take a local coordinate system (ξ, η, ζ) such that the integration surface is in the plane $\zeta = 0$ and the direction of the ζ-axis is the same as that of the normal vector $\underline{n}$. The other two axes are on the surface and their directional unit vectors $(\underline{e}_\xi, \underline{e}_\eta)$ with the normal vector $(\underline{n})$ form a right-handed triple of orthogonal unit vectors. We can specify the dipole distribution as $\mu = 0.5\{x_0 + \xi(\underline{e}_\xi \cdot \underline{i})\}^2$ and the source distribution as $\sigma = \{x_0 + \xi(\underline{e}_\xi \cdot \underline{i})\}(\underline{n} \cdot \underline{i})$, where x_0 is the x-coordinate of the origin of the local coordinate system and $\underline{e}_\xi = \underline{n} \times (\underline{i} \times \underline{n})/|\underline{i} \times \underline{n}|$. The integrands involved in Eq. (D.14) can now be transformed into either the curl form of a vector or the cross product of a vector with the normal $\underline{n}$, as follows (Guiraud 1978, Suh 1992):

$$\underline{n} \cdot \nabla \left(\frac{1}{r}\right) = -\underline{n} \cdot (\nabla \times \underline{A}), \tag{D.16}$$

$$(\xi - x_r)\,\underline{n} \cdot \nabla \left(\frac{1}{r}\right) = -z_r \left\{ \underline{e}_\eta \cdot \underline{n} \times \nabla \left(\frac{1}{r}\right) \right\}, \tag{D.17}$$

$$(\xi - x_r)^2\,\underline{n} \cdot \nabla \left(\frac{1}{r}\right) = z_r \left\{ \frac{1}{r} - \underline{e}_\xi \cdot \nabla \left(\frac{\xi - x_r}{r}\right) \right\}, \tag{D.18}$$

$$\frac{1}{r} = \underline{e}_n \cdot (\nabla \times \underline{B}), \tag{D.19}$$

$$\frac{\xi - x_r}{r} = \underline{e}_\eta \cdot (\underline{n} \times \nabla r), \tag{D.20}$$

with

$$\underline{A} = \frac{\underline{e}_n \times \underline{r}}{r(r + \underline{e}_n \cdot \underline{r})}, \qquad \underline{B} = \frac{\underline{e}_n \times \underline{r}}{(r + \underline{e}_n \cdot \underline{r})}, \tag{D.21}$$

where the coordinates (x_r, y_r, z_r) of the field point are measured with respect to the origin of this local coordinate system, and $\underline{e}_n$ is a constant unit vector, which is independent of the integration variables of the surface integral. Note that Eqs. (D.17), (D.18) and (D.20) have been derived under the hypothesis of planarity of the surfaces. While Eq. (D.19) holds for any $\underline{e}_n$ independent of the integration variables, the unit vector $\underline{e}_n$ is conveniently taken as $\pm\underline{n}$ in order to use Stokes's theorem for Eqs. (D.16) and (D.33) where the sign is chosen such that the term $\underline{e}_n \cdot \underline{r}$ in the numerator of $\underline{A}$ and $\underline{B}$ is non-negative.

D.3.2   Specific line integrals

The integral K can then be written as, with the constants $a_0 = x_0 + x_r(\underline{e}_\xi \cdot \underline{i})$ and $a_1 = \underline{e}_\xi \cdot \underline{i}$ for shortness of expressions,

$$K = (\underline{n} \cdot \underline{i})(a_0\,\phi_\sigma^{(0)} + a_1\,\phi_\sigma^{(1)}) + 0.5\,a_0^2\,\phi_\mu^{(0)} + a_0\,a_1\,\phi_\mu^{(1)} + 0.5\,a_1^2\,\phi_\mu^{(2)}, \tag{D.22}$$

where

$$\phi_\sigma^{(0)} = -\sum_{i=1}^{4} b_i\,K^{(1)}, \quad \phi_\sigma^{(1)} = -\sum_{i=1}^{4} s_{i\eta}\,K^{(2)},$$

$$\phi_\mu^{(0)} = -\sum_{i=1}^{4} b_i\,(\underline{n} \cdot \underline{e}_n)\,\frac{E - K^{(1)}}{e}, \quad \phi_\mu^{(1)} = -z_r \sum_{i=1}^{4} s_{i\eta}\,E,$$

$$\phi_\mu^{(2)} = -z_r \left[\phi_\sigma^{(0)} + \sum_{i=1}^{4} \left\{ \underline{e}_\xi \cdot (\underline{s}_i \times \underline{n})\,K^{(3)} \right\} \right], \tag{D.23}$$

and the upper limit 4 in the summation denotes the number of sides of the panel. Similar to the 2-D cases, the associated line integrals for the sides of the quadrilateral planar surface can be treated independently by using the geometric parameters of each side. Taking the local coordinate system (x', y'), as shown in Figure D.2 for the evaluation of the line integrals, the following closed-form expressions of the associated integrals can be obtained by using the integral

formulae (Grashteyn and Rhyzik 1980, pp. 81-84):

$$
K^{(1)} = \int_0^{\ell_i} \frac{1}{\sqrt{(x'-\xi)^2 + y'^2} + e} \, d\xi = E - \frac{e}{\sqrt{y'^2 - e^2}} \, \beta, \tag{D.24}
$$

$$
K^{(2)} = \int_0^{\ell_i} \sqrt{(x'-\xi)^2 + y'^2} \, d\xi = \frac{1}{2} \left\{ (\ell_i - x') \, r_{i+1} + x' \, r_i + y'^2 \, E \right\}, \tag{D.25}
$$

$$
K^{(3)} = (\xi_i - x_r) \, E + s_{i\xi} \, (r_{i+1} - r_i + x' \, E), \tag{D.26}
$$

$$
E = \ln \frac{r_{i+1} + \ell_i - x'}{r_i - x'}, \tag{D.27}
$$

$$
\beta = \begin{cases} \sin^{-1} H & \text{if } F > 0, \\ \pi - \sin^{-1} H & \text{if } F \le 0, \end{cases} \tag{D.28}
$$

$$
H = \frac{\sqrt{y'^2 - e^2} \left\{ y'^2 \, \ell_i + e \, (\ell_i - x') \, r_i + e \, x' \, r_{i+1} \right\}}{y'^2 (r_i + e)(r_{i+1} + e)}, \tag{D.29}
$$

$$
F = \left(\frac{y'^2 + e \, r_i}{r_i + e} \right)^2 + \left(\frac{y'^2 + e \, r_{i+1}}{r_{i+1} + e} \right)^2 - y'^2, \tag{D.30}
$$

$$
b_i = (\underline{n} \times \underline{r}) \cdot \underline{s}_i, \quad s_{i\xi} = \underline{s}_i \cdot \underline{e}_\xi, \quad s_{i\eta} = \underline{s}_i \cdot \underline{e}_\eta, \quad e = \underline{e}_n \cdot \underline{r}. \tag{D.31}
$$

Recall that $\underline{s}_i$ denotes the unit directional vector along the path of integration. In certain cases, some evaluations require special treatment. While the term $K^{(2)}$ is bounded, the term $K^{(1)}$ might be indeterminate if the field point lies on the same plane as the panel or on one of the lines defining the panel edge. In this respect, let us investigate the behavior of the term $b_i K^{(1)}$ in the vicinity of the panel sides. If $|y'|$ is equal to e, we have $K^{(1)} = E - \frac{x'}{r_i + e} - \frac{\ell_i - x'}{r_{i+1} + e}$ but the factor b_i vanishes and, hence, the term $b_i K^{(1)}$ also vanishes. Furthermore, when y' is very small (accordingly the factor e approaches zero), b_i and $b_i K^{(1)}$ vanish in the same limit. When the field point approaches one of the vertices (i.e., as $x' \to 0$ and $y' \to 0$) $K^{(1)}$ is logarithmically infinite, but $b_i K^{(1)}$ vanishes. Thus the integral K has a finite value even, if the field point is on the same plane as the panel.

Next we will evaluate the second integral term $\underline{L}$ in Eq. (D.15):

$$\underline{L} = -\int_S \underline{n} \times \left(\frac{1}{r}\,\underline{\omega}\right)\,dS = \int_S \frac{\gamma\,\underline{t}}{r}\,dS, \qquad (D.32)$$

where $\gamma\,\underline{t} = -\,\underline{n} \times \underline{\omega}$.

Similar to the integral K, Eq. (D.32) has the same form as the expression for the induced potential due to a source distribution over a surface. For the cases of distributions of vorticity with linearly varying densities within an element domain, γ has a linear variation over the surface being an integration region. With a specified linear distribution $\gamma\,\underline{t} = c_0\,\underline{t}_0 + c_1\,(\xi - x_r)\,\underline{t}_1 + c_2\,(\eta - y_r)\,\underline{t}_2$, we have

$$\underline{L} = c_0\,\underline{t}_0 \int_S \frac{1}{r}\,dS + c_1\,\underline{t}_1 \int_S \frac{\xi - x_r}{r}\,dS + c_2\,\underline{t}_2 \int_S \frac{\eta - y_r}{r}\,dS. \qquad (D.33)$$

Herein the vectors $\underline{t}_0$, $\underline{t}_1$ and $\underline{t}_2$ are brought outside the integral, because they are the constant vectors which are uniquely determined from the linearly varying distribution of vorticity density over the panel. The integrands in Eq. (D.33) can now be transformed, as given in Eqs. (D.19) and (D.20), and

$$\frac{\eta - y_r}{r} = -\underline{e}_\xi \cdot (\underline{n} \times \nabla r). \qquad (D.34)$$

Consequently Eq. (D.33) can be written as

$$\underline{L} = \sum_{i=1}^4 \left\{ c_0\,\underline{t}_0\,b_i\,K^{(1)} + (c_1\,\underline{t}_1\,s_{i\eta} - c_2\,\underline{t}_2\,s_{i\xi})\,K^{(2)} \right\}. \qquad (D.35)$$

For constant distributions of vorticity, we need only the term $-\sum_{i=1}^6 \underline{L}_j$ without the first and the second term in Eq (D.15).

References

Most of material covered in the notes has been adapted from the following sources.

[1] Brockett, T. (1988), *Lecture Notes for NA520 Ship Resistance and Propulsion III*, (informal notes), University of Michigan.

[2] Sears, W. R. (1970), *Theoretical Aerodynamics, Part 1: Introduction to Theoretical Hydrodynamics*, Ithaca, New York.

[3] Suh, J.-C. (1990a), *Unsteady Analysis for a Two-Dimensional Foil in Uniformly Sheared Onset Flow*, PhD. thesis, University of Michigan.

[4] Suh, J.-C. (1990b), *Review of the Paper: Calculation of the Integrals of the Singularity Method by Cantaloube and Rehbach*, KRISO Propulsor Technology Laboratory Report, 22-90.

[5] Suh, J.-C. (1990c), *Analytic Evaluations of the Induction-Integrals for Distributions of Sources and Doublets over a Planar Polygon Element*, KRISO Propulsor Technology Laboratory Report, 23-90.

[6] Suh, J.-C. (1992a), "Analytical evaluation of the surface integral in the singularity methods," *Trans. Soc. Naval Arch. Korea*, vol. 29, no. 1, pp. 1–17.

[7] Suh, J.-C., Lee, J. T. and Suh, S. B. (1992b), "A bilinear source and doublet distribution over a planar panel and its application to surface panel methods," *Proc. 19th Symp. Naval Hydro.*, pp. 102–112.

[8] Suh, J. -C. and Kim, K. -S. (1999), "A vorticity-velocity formulation for solving the two-dimensional Navier-Stokes equations," *Fluid Dynamics Research*, vol. 25, no. 4, pp. 195–216.

[9] Suh, J. -C. (2000), "The evaluation of the Biot-Savart integral," *Journal of Engineering Mathematics*, vol. 37, pp. 375–395.

[10] 김광수(Kim, K. S.) (2003), 비압축성 *Navier-Stokes* 방정식의 수치해법을 위한 와도-속도-압력 정식화 *(A Vorticity-Velocity-Pressure Formulation for Numerical Solutions of the Incompressible Navier-Stokes Equations)*, 서울대 박사학위 논문, 2003. 8.

[11] 이경준 (Lee, K. J.) (2009), 비압축성 점성 유동 해석을 위한 판 요소법과 복합된 가상 경계 보텍스 인 셀 방법 *(An Immersed Boundary Vortex-In-Cell Method Combined with a Panel Method for Incompressible Viscous Flow Analysis)*, 서울대 박사학위 논문, 2009. 2.

[12] 이승재 (Lee, S. J.) (2005), *Lagrangian* 보오텍스 방법을 이용한 단일 기포 거동의 수치 모사 *(Numerical Simulation of Single-bubble Dynamics with Two-way Coupling Using the Lagrangian Vortex Method)*, 서울대 박사학위 논문, 2005. 2.

General References

[1] 김 형 종 (1999), *미적분학*, 총 2권, 서울대학교 출판부.

[2] 이승준 (1992), "재료역학과 고체역학: 유체역학자의 관점에서," *대한 조선학회지*, 제29권, 제3호.

[3] 이창섭, 서정천 (1995), "쌍곡면 패널에의 다이폴 분포," *대한조선학회 논문집*, 제32권, 제2호.

[4] Abdolhosseini, R. and Milane, R. E. (2000), "On the effect of vortex grid density in the vortex-in-cell simulation of mixing layers," *International Journal of Computational Fluid Dynamics*, vol. 13, pp. 161–183.

[5] Abott, I. H. and von Doenhoff, A. E. (1959), *Theory of Wing Sections*, Dover.

[6] Anderson, C. R. (1989), "Vorticity boundary conditions and boundary vorticity generation for two-dimensional viscous incompressible flows," *J. Comp. Physics*, vol. 80, pp. 72–97.

[7] Arfken, G. (1970), *Mathematical Methods for Physicists*, 2nd ed., Academic Press.

[8] Aris, R. (1962), *Vectors, Tensors and the Basic Equations of Fluid Mechanics*, Prentice Hall.

[9] Babic, S. and Gavrilovic, M. M. (1997), "New expression for calculating magnetic fields due to current-carrying solid conductors," *IEEE Trans. Magn.*, MAG-33, no. 5, pp. 4134–4136.

[10] Bai, K. J. and Yeung, R. W. (1974), "Numerical solutions to free-surface flow problems," *Proc. 10th Symp. Naval Hydro.*, pp. 609–647.

[11] Banerjee, P. K. and Morino, L. (ed.) (1990), *Boundary Element Methods in Nonlinear Fluid Dynamics*, Elsevier Applied Science.

[12] Barba, L. A., Leonard, A. and Allen, C. B. (2005), "Vortex method with meshless spatial adaption for accurate simulation of viscous, unsteady vortical flows," *Int. J. Numer. Meth. Fluids*, vol. 47, pp. 841–848.

[13] Bar-Lev, M. and Yang, H. T. (1975), "Initial flow field over an impulsively started circular cylinder," *J. Fluid Mech.*, vol. 72, pp. 625–647.

[14] Barnes, J. and Hut, P. (1986), "A hierarchical $\mathcal{O}(N \log N)$ force calculation algorithm," *Nature*, vol. 324, no. 4, pp. 446–449.

[15] Basu, B. C. and Hancock, G. J. (1978), "The unsteady motion of a two-dimensional aerofoil in incompressible inviscid flow," *Journal of Fluid Mechanics*, vol. 87, pp. 159–178.

[16] Batchelor, G. K. (1967), *An Introduction to Fluid Dynamics*, Cambridge University Press, Cambridge.

[17] Beal, J. T., and Majda, A. (1982), "Vortex methods. I: Convergence in three dimensions," *Math. Comput.*, vol. 39, no. 159, pp. 1–27.

[18] Beal, J. T., and Majda, A. (1982), "Vortex methods. II: Higher order accuracy in two and three dimensions," *Math. Comput.*, vol. 39, no. 159, pp. 29–52.

[19] Beal, J. T., Cottet, G. -H. and Huberson, S.(ed.) (1992), *Vortex Flows and Related Numerical Methods*, Kluwer Academic Publishers, Dordrecht.

[20] Bearman, P. W., Downie, M. J., Graham, J. M. R. and Obasaju, E.D. (1985), "Forces on cylinders in viscous oscillatory flow at low Keulegan-Carpenter numbers," *J. Fluid Mech.*, vol. 154, pp. 337–356.

[21] Benhaddouch, R. (1998), "Treatment of Neumann boundary condition by a particle strength exchange method," *Proc. Third International Workshop*

on Vortex Flows and Related Numerical Methods. Toulose, France, available at http://www.emath.fr/Maths/Proc/Vol.7/.

[22] Bodner, B., K*ö*fler, H. and Sammer, J. (1992), "3-dimensional magnetic field calculation for an arrangement of s.c. coils with an outer magnetic core," *IEEE Trans. Magn.*, MAG-28, 2, pp. 1402–1405.

[23] Boswell, R. J., Kim, K.-H., Jessup, S. D. and Lin, G.-F. (1983), "Practical methods for predicting periodic propeller loads," *Proc. Second International Symposium on Practical Design in Shipbuilding (PRADS)*, Seoul and Tokyo, pp. 321–330.

[24] Bouard, R. and Coutanceau, M. (1980), "The early stage of development of the wake behind an impulsively started cylinder for $40 < Re < 10^4$," *J. Fluid Mech.*, vol. 101, pp. 583–607.

[25] Bratt, J. B. (1953), "Flow patterns in the wake of an oscillating aerofoil," *Aeronautical Research Council, Reports and Memoranda*, no. 2773.

[26] Braverman, E., Israeli, M., Averbuch, A. and Vozovoi, L. (1998), "A fast 3-D Poisson solver of arbitrary order accuracy," *J. Comput. Phys.*, vol. 144, pp. 109–136.

[27] Braverman, E., Israeli, M. and Averbuch, A. (1999), "A fast spectral solver for a 3-D Helmholtz equation," *Siam J. Sci. Comput.*, vol. 20, pp. 2237–2260.

[28] Brennen, C. E. (1995), *Cavitation and Bubble Dynamics*, Oxford University Press.

[29] Brockett, T. E. (1965), "Steady two-dimensional pressure distribution on arbitrary profiles," *U. S. Navy David Taylor Model Basin Report*, no. 1821.

[30] Brockett, T. E. (1972), "Propeller Perturbation Problems", *NSRDC Report*, no. 3880.

[31] Brockett, T. E. (1986), *NA 420 Ship Resistance and Propulsion II Lecture Notes*, University of Michigan.

[32] Brockett, T. E. (1988), *NA 520 Lecture Notes*,(unpublished), University of Michigan.

[33] Brockett, T. E., Kim, M.-H. and Park, J.-H. (1989), "Limiting forms for surface singularity distributions when the field point is on the surface," *Journal of Engineering Mathematics*, vol. 23, pp. 53–79.

[34] Cantaloube, B. and Rehbach, C. (1986), "Calcul des Integrales de la Methode des Singularites," *Recherche Aerospatiale*, n° 1, pp. 15–22, English Title: "Calculation of the integrals of the singularity method," *Aerospace Research*, no. 1, pp. 15–22.

[35] Chatelain, P., Curioni, A., Bergdorf, M., Rossinelli, D., Andreoni, W. and Koumoutsakos, P. (2008), "Billion vortex particle direct numerical simulations of aircraft wakes," *Comput. Methods Appl. Mech. Engrg.*, vol. 197, pp. 1296–1304.

[36] Chen, H. and Marshall, S. (1999), "A Lagrangian vorticity method for two-phase particulate flows with two-way phase coupling," *J. Comput. Phys*, vol. 148, pp. 169–198.

[37] Cheng, H. , Greengard, L. and Rokhlin, V. (1999), "A fast adaptive multipole algorithm in three dimensions," *J. Comput. Phys.*, vol. 155, pp. 468–498.

[38] Chorin, A. J. (1973), "Numerical study of slightly viscous flow," *J. Fluid Mech.* , vol. 57, pp. 785–796.

[39] Chou, M.-H. and Huang, W. (1996), "Numerical study of high-Reynolds-number flow past a bluff object," *Int. J. Numer. Methods Fluids*, vol. 23, pp. 711–732.

[40] Cielak, Z. M. and Kinney, R. B. (1978), "Analysis of unsteady viscous flow past an airfoil: Part II-numerical formulation and results," *AIAA J.*, vol. 16, no. 2, pp. 105–110.

[41] Ciric, I. R. (1987), "New models for current distributions and scalar potential formulations of magnetic filed problems," *J. Appl. Phys.*, vol. 61, no. 8, pp. 2709–2717.

[42] Ciric, I. R. (1991), "Simple analytic expressions for the magnetic field of current coils," *IEEE Trans. Magn.*, MAG-27, no. 1, pp. 669–673.

[43] Cocle, R., Winckelmans, G. and Daeninck, G. (2007), "Combining the vortex-in-cell and parallel fast multipole methods for efficient domain decomposition simulations," *J. Comput. Phys.*, vol. 227, pp. 9091–9120.

[44] Constantinescu, G. and Squires, K. (2004), "Numerical investigations of flow over a sphere in the subcritical and supercritical regimes," *Physics of Fluids*, vol. 16, no. 5, pp. 1449–1466.

[45] Cottet, G.-H. (1999), "3-D vortex methods: achievements and challenges," *Proc. First International Conference on Vortex Methods*, Kobe.

[46] Cottet, G.-H. and Koumoutsakos, P.D. (2000), *Vortex Methods: Theory and Practice*, Cambridge University Press, Cambridge.

[47] Cottet, G.-H. and Poncet, P. (2003), "Advances in direct numerical simulations of 3-D wall-bounded flows by Vortex-in-Cell methods," *J. Comput. Phys.*, vol. 193, pp. 136–158.

[48] Courant, R. and Hilbert, D. (1953), *Methods of Mathematical Physics*, 2 vols., Interscience.

[49] Currie, I. G. (1993), *Fundamental Mechanics of Fluids*, McGraw-Hill Book Co., Singapore.

[50] Dennis, S. C. R. and Hudson, J. D. (1995), "An h^4 accurate vorticity-velocity formulation for calculating flow past a cylinder," *Int. J. Numer. Methods Fluids*, vol. 21, pp. 489–497.

[51] Degond, P. and Mas-Gallic, S. (1989), "The weighted particle method for convection diffusion equations, Part I: The case of an isotropic viscosity; Part II: The anisotropic case," *Mathematics of Computation*, vol. 53, pp. 485–507.

[52] Djojodihardjo, R. H. and Widnall, S. E. (1969), "A numerical method for the calculation of nonlinear, unsteady lifting potential flow problems," *AIAA Journal*, vol. 7, no. 10, pp. 2001–2009.

[53] Draghicescu, C. I. (1994), "An efficient implementation of particle methods for the incompressible Euler equations," *SIAM J. Numer. Anal.*, vol. 31, no. 4, pp. 1090–1108.

[54] Draghicescu, C. I. and Draghicescu, M. (1995), "A fast algorithm for vortex blob interactions," *J. Comput. Phys.*, vol. 116, pp. 69–78.

[55] Dütsch,H., Durst,F., Becker,F. and Lienhart, F. (1998), "Low Reynolds number flow around an oscillating circular cylinder at low Keulegan Carpenter numbers," *J. Fluid Mech.*, vol. 360, pp. 249–271.

[56] E, Weinan and Liu, J.-G. (1997), "Finite difference methods for 3-D viscous incompressible flows in the vorticity-vector potential formulation on nonstaggered grids," *J. Comput. Phys.*, vol. 138, pp. 57–82.

[57] Eldredge, J. D. (2007), "Numerical simulation of the fluid dynamics of 2-D rigid body motion with the vortex particle method," *J. Comput. Phys.*, vol. 221, pp. 626–648.

[58] Ern, A. and Smooke, M. D. (1993), "Vorticity-velocity formulation for three-dimensional compressible flows," *J. Comput. Phys.*, vol. 105, pp. 58–71.

[59] Ferziger, J. H. and Perić, M. (1996), *Computational Methods for Fluid Dynamics*, Springer-Verlag, New York.

[60] Fox, R. W., McDonald, A. T. and Pritchard, P. J. (2004) *Introduction to Fluid Mechanics*, John Wiley & Sons, Inc.

[61] Friedman, A. (1964), *Partial Differential Equations of Parabolic Type*, Prentice-Hall, Englewood Cliffs.

[62] Ghia, U., Ghia, K. N. and Shin, C. T. (1982), "High-Re solutions for incompressible flow using the Navier-Stokes equations and a multigrid Method," *J. Comput. Phys.*, vol. 48.

[63] Ghosal, S. and Moin, P. (1995), "The basic equations for the large eddy simulation of turbulent flows in complex geometry," *J. Comput. Phys.*, vol. 118, pp. 24–37.

[64] Giesing, J. P. (1968a), "Nonlinear two-dimensional unsteady potential flow with lift," *Journal of Aircraft*, vol. 5, no. 2, pp. 135–143.

[65] Giesing, J. P. (1968b), "Nonlinear interaction of two lifting bodies in arbitrary unsteady motion," *Transaction of ASME, Journal of Basic Engineering*, vol. 90, Series D, pp. 387–394.

[66] Giesing, J. P. (1969), "Vorticity and Kutta condition for unsteady multienergy flows," *Transaction of ASME, Journal of Applied Mechanics*, vol. 36, Series E, pp. 608–613.

[67] Giesing, J. P., Roden, W. P. and Stahl, B. (1970), "Sears function and lifting surface theory for harmonic gust fields," *Journal of Aircraft*, vol. 7, no. 2, pp. 252–255.

[68] Gradshteyn, I. S. and Ryzhik, I. M. (1980), *Table of Integrals, Series and Products*, corrected and enlarged edition, Academic Press, Inc., New York and London.

[69] Graglia, R. D. (1983), "On the numerical integration of the linear shape functions times the 3-D Green's function or its gradient on a plane triangle," *IEEE Trans. Antennas Propagat.*, vol. 41, pp. 1448–1455.

[70] Greengard, L and Rokhlin, V. (1987), "A Fast algorithm for particle simulations," *Journal of Computational Physics*, vol. 73, pp. 325–348.

[71] Greengard,L and Strain, J. (1990), "A fast algorithm for the evaluation of heat potentials," *Commun. Pure Appl. Math.*, vol. XLIII, pp. 949–963.

[72] Gresho, P. M. (1991), "Incompressible fluid dynamics: some fundamental formulation issues," *Ann. Rev. Fluid Mech.*, vol. 17, pp. 411–445.

[73] Guiraud, J. P. (1978), "Potential of velocities generated by a localized vortex distribution," *Aerospace Research*, English Translation-ESA-TT-560, pp. 105–107.

[74] Guj, G. and Stella, F. (1993), "A vorticity-velocity method for the numerical solution of 3-D incompressible flows," *J. Comp. Physics*, vol. 106, pp. 286–298.

[75] Hess, J. L. and Smith A. M. O. (1964), "Calculation of non-lifting potential flow about arbitrary three-dimensional bodies," *J. Ship Res.*, vol. 8, no. 2, pp. 22–44.

[76] Hess, J. L. and Smith A. M. O. (1966), "Calculation of potential flow about arbitrary bodies," *Progress in Aeronautical Science Series*, vol. 8, Pergamon Press, pp. 1–138.

[77] Hess, J. L. (1969), "Calculation of potential fow about abitrary three-dimensional lifting bodies," *Douglas Aircraft Company Report*, AD 699615.

[78] Hess, J. L. (1972), "Calculation of potential flow about arbitrary three-dimensional lifting bodies," *Douglas Aircraft Company Report*, no. MDCJ5679-01.

[79] Hess, J. L. (1974), "The problem of three-dimensional lifting potential flow and its solution by means of surface singularity distribution," *Computer Methods in Applied Mechanics and Engineering*, vol. 4, pp. 283–319.

[80] Hess, J. L., Johnson, F. T. and Rubbert, P. E. (1978), *Panel Methods*, AIAA Professional Study Series, a collection of original papers, AIAA.

[81] Hewson-Browne, R. C. (1963), "The oscillation of a thick aerofoil in an incompressible flow," *Quarterly Journal of Mechanics and Applied Mathematics*, vol. 1, no. 16, pp. 79-92.

[82] Hirsch, C. (1990), *Numerical Computation of Internal and External Flows*, John Wiley & Sons Ltd., Chichester.

[83] Hoffman, K. A. and Chiang, S. T. (1993), *Computational Fluid Dynamics for Engineers*, Publication of Engineering Education System, Wichita.

[84] Horlock, J. H. (1968), "Fluctuating lift forces on aerofoils moving through transverse and chordwise gusts," *Transaction of ASME, Journal of Basic Engineering*, vol. 90, Series D, pp. 494–500.

[85] Huang, R. F., Wu, J. Y., Jeng, J. H. and Chen, R. C. (2001), "Surface flow and vortex sheddeing of an impulsively started wing," *J. Fluid Mech.*, vol. 441, pp. 265–292.

[86] Hunt, B. (1980), "The mathematical basis and numerical principles of the boundary integral method for incompressible potential flow over 3-D aerodynamic configurations," *Numerical Methods in Applied Fluid Dynamics*.

[87] Ingham, D. B., Heggs, P. J. and Manzoor, M. (1981), "The numerical solution of plane potential problems by improved boundary integral equation methods," *Journal of Computational Physics*, vol. 42, pp. 77–98.

[88] Johnson, T. A. and Patel, V. C. (1999), "Flow past a sphere up to a Reynolds number of 300," *J. Fluid Mech.*, vol. 378, pp. 19–70.

[89] Jordan, P. F. (1972), "Exact solutions for lifting surfaces," *AFOSR Scientic Report*, AFOSR-TR-72-1737.

[90] Justesen, P. (1991), "A numerical study of oscillating flow around a circular cylinder," *J. Fluid Mech.*, vol. 222, pp. 157–196.

[91] Kaplan, W. (1952), *Advanced Calculus*, Addison-Wesley.

[92] Kaplan, W. (1981), *Advanced Mathematics for Engineers*, Addison-Wesley.

[93] Kármán, von Th. and Sears, W. R. (1938), "Airfoil theory for non-uniform motion," *Journal of the Aeronautical Sciences*, vol. 5, no. 10, pp. 379–390.

[94] Kerwin, J. E. and Lee, C.-S. (1978), "Prediction of steady and unsteady marine propeller performance by numerical lifting-surface theory," *SNAME Trans.*, vol. 86, pp. 218–253.

[95] Kim, K.-S and Suh, J.-C. (1998), "The vorticity based analysis of the viscous flow around an impulsively started cylinder," (in Korean), *J. Soc. Naval Archi. Korea*, vol. 35, no. 4.

[96] Kim, K.-S., Lee, S.-J. and Suh, J.-C. (2003), "Numerical simulation of the vortical flow around an oscillating circular cylinder," (in Korean), *J. Soc. Naval Archi. Korea*, vol. 40, no. 2, pp. 21–27.

[97] Kim, K.-S. (2003), *A Vorticity-Velocity-Pressure Formulation for Numerical Solutions of the Incompressible Navier-Stokes Equations*, PhD. Thesis, Seoul National University.

[98] Kim K.-S., Lee S.-J. and Suh J.-C. (2005), "Numerical simulation of the vortical flow around an oscillating circular cylinder," *Proc. 15th ISOPE 2005*, Seoul, June 19–24, 2005.

[99] Kim, M. J., and Mook, D. T. (1986), "Application of continuous vorticity panels to general unsteady incompressible two-dimensional lifting flows," *Journal of Aircraft*, vol. 23, no. 6, pp. 464–471.

[100] Kinney, R. B. and Cielak, Z. M. (1977), "Analysis of unsteady viscous flow past an airfoil: Part I-theoretical development," *AIAA J.*, vol. 15, no. 12, pp. 1712–1717.

[101] Kirshner, I. N. (1989), *The Bilinear Triangular Vorticity Patch* (unpublished), University of Michigan.

[102] Kochin, N. E., Kibel, I. A. and Roze, N. V. (1964), *Theoretical Hydrodynamics*, (Translation of fifth Russian edition, Moscow, Fizmatgiz, 1963), Interscience Publications Inc.

[103] Koumoutsakos, P. D. (1993), *Direct Numerical Simulations of Unsteady Separated Flows Using Vortex Methods*, PhD. Thesis, California Institute of Technology.

[104] Koumoutsakos, P. D., Leonard, A. and Pépin, F. M. (1994) "Viscous boundary conditions for vortex methods," *Journal of Computational Physics*, vol. 113, pp. 52–56.

[105] Koumoutsakos, P. and Leonard, A. (1995), "High-resolution simulations of the flow around an impulsively started cylinder using vortex methods," *J. Fluid Mech.*, vol. 296, pp. 1–38.

[106] Koumoutsakos, P. and Shiels, D. (1996), "Simulations of the viscous flow normal to an impulsively started and uniformly accerated flat plate," *J. Fluid Mech.*, vol. 328, pp. 177–227.

[107] Kreyszig, E. (1993), *Advanced Engineering Mathematics*, Seventh ed.,Wiley.

[108] Kuethe, A. M. and Chow, C.-Y. (1976), *Foundations of Aerodynamics: Bases of Aerodynamic Design*, Wiley.

[109] Küssner, H. G. (1940), "Das zweidimensionale Problem der beliebig bewegten Tragfläche unter Berücksichtigung von Partialbewegungen der Flüssigkeit," *Luftfahrtforschung*, vol. 17, pp. 355–361.

[110] Küssner, H. G. (1960), "Non-statinary theory of airfoils of finite thickness in incompressible flow," *AGARD Manual on Aeroelasticity*, vol. 2, Chapter 8.

[111] Lamb, H. (1932), *Hydrodynamics*, Sixth Ed., Dover.

[112] Lee, J. T. (1987), *A Potential Based Panel Method for the Analysis of Marine Propellers in Steady Flow*, PhD. thesis, Department of Ocean Engineering, MIT, Report no. 87-13.

[113] Lee, Seung-Jae (2005), *Lagrangian 보오텍스 방법을 이용한 단일 기포 거동의 수치 모사 (Numerical simulation of single-bubble dynamics with two-way coupling using the Lagrangian vortex method)*, 서울대 박사학위 논문, 2005. 2.

[114] Lee, S.-J., Kim, K.-S. and Suh, J.-C. (2005), "A vorticity-velocity formulation for numerical simulations of viscous flows around impulsive started bodies," *Proc. Osaka Colloquium*, March 14-15, 2005.

[115] Leonard, A. (1980) "Vortex methods for flow simulation," *Journal of Computational Physics*, vol. 37, pp. 289–335.

[116] Leonard, A. , Shiels, D., Salmon, J. K., Winckelmans, G. S. and Ploumhans, P. (1997), "Recent advances in high resolution vortex methods for incompressible flows," *AIAA*, 97-2108, pp. 1–17.

[117] Lewis, R. I. and Ryan, P. G. (1972), "Surface vorticity theory for axisymmetric annular aerofoils and bodies of revolution with application to

duct cowls," *Journal of Mechanical Engineering Science*, vol. 14, no. 4, pp. 280–291.

[118] Lighthill, M. J. (1963), "Introduction, boundary layer theory," *Laminar Boundary Layers*, edited by J. Rosenhead, Oxford University Press, New York, pp. 54–61.

[119] Lindsay, K. (1997), *A Three-dimensional Cartesian Tree-code and Applications to Vortex Sheet Roll-up*, PhD. Thesis, University of Michigan.

[120] Lindsay, K. and Krasny, R. (2001), "A particle method and adaptive treecode for vortex sheet motion in three-dimensional flow," *J. Comput. Phys.*, vol. 172, pp. 879–907.

[121] Lingjia, Z. and Hiroshi, T. (2007), "Hybrid vortex method for high Reynolds number flows around three-dimensional complex boundary," *Computers & fluids*, vol. 36, pp. 1213–1223.

[122] Liu, C. H. (2001), "A three-dimensional vortex particle-in-cell method for vortex motions in the vicinity of a wall," *Int. J. Numer. Meth. Fluids*, vol. 37, pp. 501–523.

[123] Lugt H. J. (1983), *Vortex Flow in Nature and Technology*, John Wiley & Sons, New York.

[124] Lurie, E. A. (1996), *Investigation of High Reduced Frequency, Separated Trailing Edge Flows*, Doctoral thesis, Dept. of Ocean Engineering, MIT.

[125] Mangler, K. W. (1952), "Improper integrals in theoretical aerodynamics," *Aeronautical Research Council*, Current Papers 94.

[126] Mangler, K. W. and Smith, J. H. B. (1970), "Behaviour of the vortex sheet at the trailing edge of a lifting wing," *The Aeronautical Journal of the Royal Aeronautical Society*, vol. 74, pp. 906–908.

[127] Mansfield, J. R., Knio, O. M. and Meneveau, C. (1996), "Towards Lagrangian large vortex simulation," *Proc. International Workshop on Vortex Flows and Related Numerical Methods. ESAIM*, available at http://www.emath.fr/Maths/Proc/Vol.1/.

[128] Mansfield, J. R., Knio, O. M. and Meneveau, C. (1998), "A dynamic LES scheme for the vorticity transport equation: Formulation and a priori Tests," *J. Comput. Phys.*, vol. 145, pp. 693–730.

[129] Mansfield, J. R., Knio, O. M. and Meneveau, C. (1999), "Dynamic LES of colliding vortex rings Using a 3-D vortex method," *J. Comput. Phys.*, vol. 152, pp. 305–345.

[130] Marcos, C. F. , Barge, P. and Marcos, R. F. (2002), "Dust dynamics in protoplanetary disks: Parallel computing with PVM," *J. Comput. Phys.*, vol. 176, pp. 276–294.

[131] Maskew, B. (1982), "Prediction of subsonic aerodynamic characteristics: A case for low-order panel methods," *Jounal of Aircraft*, vol. 19, no. 2, pp. 157–163.

[132] McCartin, B. J. (1983), "Applications of exponential splines in computational fluid dynamics," *AIAA Journal*, vol. 21, no. 8, pp. 1059-1065.

[133] Milne-Thomson, L. M. (1968), *Theoretical Hydrodynamics*, fifth edition, Macmillan, London.

[134] Morgenthal, G. (2002), *Aerodynamic Analysis of Structures Using High-resolution Vortex Particle Methods*, PhD. Thesis, University of Cambridge.

[135] Moran, J. (1984), *An Introduction to Theoretical and Computational Aerodynamics*, Wiley.

[136] Morino, L., Kaprielian, Z. and Sipcic, S. R. (1985), "Free wake analysis of helicopter rotors," *Vertica*, vol. 9, no. 2, pp. 127–140.

[137] Morino, L. (1990), "Helmholtz and Poincare potential-vorticity decompositions for the analysis of unsteady compressible viscous flows," *Boundary Element Methods in Nonlinear Fluid Dynamics*, edited by Banerjee, P. K. and Morino, L., Elsevier Applied Science, London and New York, pp. 1–54.

[138] Moriya, T. (1941), "On the aerodynamic theory of an arbitrary wing section," *Journal of the Society of Aeronautical Sciences*, vol. 8, no. 78,

pp. 1054–1060 English version in Selected Scienic and Technical Papers, University of Tokyo, 1959, pp.48–59.

[139] Morsh, P. M. and Feshbach (1953), *Methods of Theoretical Physics*, 2 Vols., McGraw-Hill.

[140] Newman, J. N. (1977), *Marine Hydrodynamics*, MIT Press, Revised (1997).

[141] Newman, J. N. (1986), "Distributions of sources and normal dipoles over a quadrilateral panel," *J. Eng. Math.*, vol. 20, pp. 113–126.

[142] Obasaju, E. D., Bearman, P. W. and Graham, J. M. R. (1988), "A study of forces, circulation and vortex patterns around a circular cylinder in oscillating flow," *J. Fluid Mech.*, vol. 196, pp. 467–494.

[143] O'Neill, B. (1966), *Elementary Differential Geometry*, Academic Press.

[144] Panton, R. L. (1996), *Incompressible Flow*, John Wiley & Sons, New York.

[145] Parsons, M. G. (1984), *NA 420 Ship Resistance and Propulsion II*, (informal notes), University of Michigan.

[146] Pépin, F. M. (1990), *Simulation of the Flow past an Impulsively Started Cylinder Using a Discrete Vortex Method*, PhD. Thesis, California Institute of Technology.

[147] Ploumhans, P. , Winckelmans, G. S. and Salmon, J. K. (1998), "Vortex particles and tree codes.I.Flows with arbitrary crossing between solid boundaries and particle redistribution lattice. II: Vortex ring encountering a plane at an angle," *Proc. Third International Workshop on Vortex Flows and Related Numerical Methods. Toulose, France*, available at http://www.emath.fr/Maths/Proc/Vol.7/.

[148] Ploumhans, P. and Winckelmans, G. S. (2000), "Vortex methods for high-resolution simulations of viscous flow past bluff bodies of general geometry," *Journal of Computational Physics*, vol. 65, pp. 354–406.

[149] Ploumhans, P., Winckelmans, G. S., Salmon, J. K., Leonard, A. and Warren, M. S. (2002), "Vortex methods for direct numerical simulation of three-dimensional bluff body flows: Application to the sphere at Re=300, 500, and 1000," *Journal of Computational Physics*, vol. 178, pp. 427–463.

[150] Prandtl, L. and Tietjens, O. G. (1934), *Fundamentals and Applied Hydro- and Aeromechanics*, Translated by Den Hartog, J. P., 2 Vols., McGraw-Hill (also Dover Publications 1957).

[151] Raviart, P. A. (1985), "An analysis of particle methods, numerical methods in fluid dynamics," *Lecture Notes in Mathematics Series*, Springer-Verlag, Berlin, vol. 1127, pp. 243-324.

[152] Ribeiro, R. S. and Kroo, I. (1992), "Vortex-in-cell analysis of wing wake roll-up," *AIAA Applied Aerodynamics Conference*, Technical Papers. Pt. 2, pp. 753–763.

[153] Rida, S., Mckenty, F., Meng, F. L. and Reggio, M., (1997), "A staggered control volume scheme for unstructured triangular grids," *Int. J. Numer. Meth. Fluids.*, vol. 25, pp. 697–717.

[154] Roe, P. L. (1985), "Some contributions to the modelling of discontinuous flows," *Proc. 1983 AMS-SIAM Summer Seminal on Large Scale Computing in Fluid Mech., Lectures in Applied Math.*, vol. 22, pp. 163–193.

[155] Rosenhead, L. (Ed.) (1963), *Laminar Boundary Layers*, Oxford University Press.

[156] Saffman, P. G. (1992), *Vortex Dynamics*, Cambridge University Press.

[157] Sarpkaya, T. (1975), "Forces on cylinders and spheres in a sinusoidally oscillating fluid," *Trans. ASME E, J. Appl. Mech.*, vol. 42, pp. 32–37.

[158] Sarpkaya, T. (1986), "Force on a circular cylinder in viscous oscillatory flow at low Keulegan-Carpenter number," *J. Fluid Mech.*, vol. 165, pp. 61–71.

[159] Sarpkaya, T. (1989), "Computational methods with vortices - the 1989 Freeman Scholar Lecture," *Transactions of ASME, J. of Fluids Engineering*, vol. 111, pp. 5–52.

[160] Schlichting, H. (1968), *Boundary Layer Theory*, McGraw-Hill.

[161] Sears, W. R. (1941), "Some aspects of non-stationary airfoil theory and its practical application," *Journal of The Aeronautical Sciences*, vol. 8, no. 3, pp. 104–108.

[162] Sears, W. R. (1970), *Theoretical Aerodynamics, Part 1: Introduction to Theoretical Hydrodynamics*, Ithaca, New York.

[163] Shih, T. M., Tan, C. H. and Hwang, B. C. (1989), "Effects of grid staggering on numerical schemes," *Int. J. Numer. Meth. Fluids.*, vol. 9, pp. 193–212.

[164] Speziale, C. G. (1987), "On the advandages of the vorticity-velocity formulation of the equations of fluid dynamics," *J. Comp. Physics*, vol. 73, pp. 476–480.

[165] Stakgold, I. (1979), *Green's Functions and Boundary Value Problems*, John Wiley & Sons Inc.

[166] Stoker, J. J. (1957), *Water Waves*, Interscience.

[167] Streeter, V. L. (1948), *Fluid Dynamics*, McGraw-Hill.

[168] Suh, J.-C. (1990a), *Unsteady Analysis for a Two-dimensional Foil in Uniformly Sheared Onset Flow*, Ph.D thesis, University of Michigan.

[169] Suh, J.-C. (1990b), *Review of the Paper; Calculation of the Integrals of the Singularity Method by Cantaloube and Rehbach*, KRISO Propulsor Technology Laboratory Report, 22-90.

[170] Suh, J.-C. (1990c) *Analytic Evaluations of the Induction-Integrals for Distributions of Sources and Doublets over a Planar Polygon Element*, KRISO Propulsor Technology Laboratory Report, 23-90.

[171] Suh, J.-C. (1992a), "Analytical evaluation of the surface integral in the singularity methods," *Trans. Soc. Naval Arch. Korea*, vol. 29, 1, pp. 1–17.

[172] Suh, J.-C., Lee, J.-T. and Suh, S.-B. (1992b), "A bilinear source and doublet distribution over a planar panel and its application to surface panel methods," *Proc. 19th Symp. Naval Hydro.*, pp. 102–112.

[173] Suh, J. -C. and Kim, K. -S. (1999), "A vorticity-velocity formulation for solving the two-dimensional Navier-Stokes equations," *Fluid Dynamics Research*, vol. 25, no. 4, pp. 195–216.

[174] Suh, J. -C. (2000), "The evaluation of the Biot-Savart integral," *Journal of Engineering Mathematics*, vol. 37, pp. 375–395.

[175] Sumer, B. M. and Fredsøe, J. (1997), *Hydrodynamics around Cylindrical Structures*, World Scientific Publishing, Singapore.

[176] Taneda, S. (1956), "Studies on wake vortices (III): Experimental investigation of the wake behind a sphere at low Reynolds number," *Rep. Res. Inst. Appl. Mech.*, Kyushu University, vol. 4, pp. 99–105.

[177] Tatsuno, M. and Bearman, P. W. (1990), "A visual study of the flow around an oscillating circular cylinder at low Keulegan-Carpenter numbers and low Stokes numbers," *J. Fluid Mech.*, vol. 211, pp. 157–182.

[178] Ta Phouc Loc and Bouard, R. (1985), "Numerical solution of the early stage of the unsteady viscous flow around a circular cylinder: A comparison with experimental visualization and measurements," *Journal of Fluid Mechanics*, vol. 160, pp. 93–117.

[179] Thwaites, B. (Ed.) (1960), *Incompressible Aerodynamics*, Oxford.

[180] Theodorsen, T. (1935), "General theory of aerodynamic instability and the mechanicsm of flutter," *NACA Report*, no. 496.

[181] Ton, Tran-Cong and Blake, J. R. (1984), "General solutions of the Stokes flow equations," *J. of Mathematical Analysis and Applications*, vol. 92, pp. 72–84.

[182] Tricomi, F. G. (1957), *Integral Equations*, Interscience Publishers Inc., London and New York.

[183] Tsien, H.-S. (1943), "Symmetrical Joukowsky airfoils in shear flow," *Quarterly of Applied Mathematics*, vol. 1, pp. 130–148.

[184] Urankar, L. M. (1980), "Vector potential and magnetic field of current-carrying finite arc segment in analytical form, Part I: filament approximation," *IEEE Trans. Magn.*, MAG-16, no. 5, pp. 1283–1288.

[185] Urankar, L. M. (1982a), "Vector potential and magnetic field of current-carrying finite arc segment in analytical form, Part II: thin sheet approximation," *IEEE Trans. Magn.*, MAG-18, no. 3, pp. 911–917.

[186] Urankar, L. M. (1982b), "Vector potential and magnetic field of current-carrying finite arc segment in analytical form, Part III: exact computation for rectangular cross section," *IEEE Trans. Magn.*, MAG-18, no. 6, pp. 1860–1867.

[187] van de Vooren, A. I. and van de Vel, H. (1964), "Unsteady profile theory in incompressible flow," *Archiwum Mechaniki Strosowanej*, vol. 3, no. 16, pp. 709–735.

[188] van Dyke (1982), *An Album of Fluid Motion*, Parabolic press, Stanford.

[189] Wagner, H. (1925), "Über die Entstehung des dynanmischen Auftriebes von Tragflügeln," *Zeitscrift fur Angewandte Mathematik und Mechanik*, vol. 5, no. 1, pp. 17–35.

[190] Walther, J. H. and Koumoutsakos, P. (2001), "Three-dimensional vortex methods for particle-laden flows with two-way coupling," *J. Comput. Phys.*, vol. 167, pp. 39–71.

[191] Warren, M. S. and Salmon, J. K. (1995), "A portable parallel particle program," *Computer Phys. Commun.*, vol. 87, pp. 266–290.

[192] Webster, W. C. (1975), "The flow about arbitray, three-dimensional smooth bodies," *J. Ship Res.*, vol. 19, no. 4, pp. 206–218.

[193] Weggel, C. F. and Schwartz, D. P. (1988), "New analytic formulas for calculating magnetic fields," *IEEE Trans. Magn.*, MAG-24, no. 2, pp. 1544–1547.

[194] White, F. (1974), *Viscous Fluid Flow*, McGraw-Hill.

[195] White, F. (1986), *Fluid Mechanics*, McGraw-Hill.

[196] Williamson, C. H. K. (1985), "Sinusoidal flow relative to circular cylinders," *J. Fluid Mech.*, vol. 155, pp. 141–174.

[197] Williamson, C. H. K. (1996), "Vortex dynamics in the cylinder wake," *Annu. Rev. Fluid Mech.*, vol. 28, pp. 477–539.

[198] Wilton, D. R., Rao, S. M., Glisson, A. W., Schaubert, D. H., Al-Bundak, O. M. and Butler, C. M. (1984), "Potential integrals of uniform and linear source distributions on polygonal and polyhedral domains," *IEEE Trans. Antennas Propagat.*, AP-32, pp. 276–281.

[199] Winckelmans, G. (1989), *Topics in Vortex Methods for the Computation of Three- and Two-dimensional Incompressible Unsteady Flows*, PhD. Thesis, California Institute of Technology.

[200] Winckelmans, G. and Leonard, A. (1989), "Improved methods for three-dimensional flows," *Mathematical Aspects of Vortex Dynamics*, edited by Caflish, R., Society for industrial and applied mathematics, Philadelphia, pp. 25–35.

[201] Winckelmans, G. and Leonard, A. (1993), "Contributions to vortex particle methods for the computation of three dimensional incompressible unsteady flows," *Journal of Computational Physics*, vol. 109, pp. 247–273.

[202] Winckelmans, G., Cocle, R., Dufresne, L. and Capart, R. (2005), "Vortex methods and their application to trailing wake vortex simulations," *C. R. Physique*, vol. 6, pp. 467–486.

[203] Wu, J. C. (1976), "Numerical boundary conditions for viscous flow problems," *AIAA J.*, vol. 14, no. 8, pp. 1042–1049.

[204] Wu, J. C. (1981), "Theory for aerodynamic force and moment in viscous flows," *AIAA J.*, vol. 19, no. 4, pp. 432–441.

[205] Wu, J.-Z. and Wu, J.-M. (1993), "Interactions between a solid surface and viscous compressible flow field", *J. Fluid Mech.*, vol. 254, pp. 183–211.

[206] Wu, J.-Z., Wu, X.-H., Ma, H.-Y. and Wu, J.-M. (1994), "Dynamic vorticity condition: theoretical analysis and numerical implementation," *Int. J. Numer. Meth. Fluids*, vol. 19, pp. 905–938.

[207] Wu, J.-Z, Ma, H.-Y. and Zhou, M.-D. (2006), *Vorticity and Vortex Dynamics*, Springer.

[208] Yih, C.-S. (1977), *Fluid Mechanics*, McGraw-Hill.

[209] Ying, L. -A. and Zhang, P. -W. (1997), *Vortex Methods*, Science Press and Kluwer Academic Publisher, Beijing.

[210] Zabusky, N. J. (1999), "Vortex paradigm for accelerated inhomogeneous flows: Visiometrics for the Rayleigh-Taylor and Richtmyer-Meshkov environments," *Annual Review of Fluid Mechanics*, vol. 31, pp. 495-536.